



JRC CONFERENCE AND WORKSHOP REPORTS

Proceedings of the 23rd Transport and Air Pollution (TAP) conference – Part I

*15th-17th May 2019,
Thessaloniki, Greece*

Editors:
Mamarikas, Sokratis
Ntziachristos, Leonidas
Karamountzou, Georgia
Fontaras, Georgios

2020



This publication is a Conference and Workshop report by the Joint Research Centre (JRC), the European Commission's science and knowledge service. It aims to provide evidence-based scientific support to the European policymaking process. The scientific output expressed does not imply a policy position of the European Commission. Neither the European Commission nor any person acting on behalf of the Commission is responsible for the use that might be made of this publication. For information on the methodology and quality underlying the data used in this publication for which the source is neither Eurostat nor other Commission services, users should contact the referenced source. The designations employed and the presentation of material on the maps do not imply the expression of any opinion whatsoever on the part of the European Union concerning the legal status of any country, territory, city or area or of its authorities, or concerning the delimitation of its frontiers or boundaries.

Contact information

Name: Georgios FONTARAS
Address: European Commission, Joint Research Centre, Via Enrico Fermi, 2749, I - 21027 Ispra (VA) Italy
Email: Georgios.FONTARAS@ec.europa.eu
Tel.: +39 0332 786425

EU Science Hub

<https://ec.europa.eu/jrc>

JRC117559

EUR 30140 EN

PDF ISBN 978-92-76-17328-1 ISSN 1831-9424 doi:10.2760/289885

Luxembourg: Publications Office of the European Union, 2020

© European Union, 2020

The reuse policy of the European Commission is implemented by the Commission Decision 2011/833/EU of 12 December 2011 on the reuse of Commission documents (OJ L 330, 14.12.2011, p. 39). Except otherwise noted, the reuse of this document is authorised under the Creative Commons Attribution 4.0 International (CC BY 4.0) licence (<https://creativecommons.org/licenses/by/4.0/>). This means that reuse is allowed provided appropriate credit is given and any changes are indicated. For any use or reproduction of photos or other material that is not owned by the EU, permission must be sought directly from the copyright holders.

All content © European Union, 2020

How to cite this report: *Proceedings of the 23rd Transport and Air Pollution (TAP) conference – Part I*, EUR 30140 EN, Publications Office of the European Union, Luxembourg, 2020, ISBN 978-92-76-17328-1, doi:10.2760/289885, JRC117559.

Contents

Acknowledgements	2
Abstract	3
1 Introduction	4
1.1 Message of the Chairman.....	5
1.2 Organisation	6
1.2.1 General Information	6
1.2.2 Organisers	6
1.2.3 Contributors	6
1.2.4 Scientific Committee	7
1.2.5 Organising Committee	8
2 Conference Proceedings – Papers	9
2.1 Gaseous and particulate pollutants characterisation	11
2.1.1 Consistent Emission Factors from PEMS and Chassis Dyno Tests for HBEFA 4.1	12
2.1.2 Euro 3 and Euro 5 Diesel vehicles’ particles evolution in ageing chamber ..	25
2.1.3 Real world emission factors based on roadside increment concentrations of NO _x and CO ₂	37
2.1.4 Cold-Start Emissions and Excess Fuel Consumption at Low Ambient Temperatures - 2019 Update and Historic Review	43
2.1.5 Review of Legislative Requirements and Methods for the Estimation of PN/PM Emissions for Advanced Light-duty OBD Applications.....	58
2.1.6 Real-world Vehicle Emission Measurements using PEMS in Hong Kong	70
2.1.7 PEMS accuracies under harsh environmental conditions	81
2.1.8 Trends in Light Duty Gasoline Vehicle Emissions Based on Real-World Measurements.....	91
2.1.9 NO _x Emissions of Heavy-Duty Vehicles with Euro VI Certified Engines.....	104
2.1.10 Measuring real emissions with simplified PEMS	115
2.1.11 Exhaust Gas Temperature and NO _x After-treatment Performance of Euro 6 Passenger Cars.....	132
2.2 Marine and aviation emissions	139
2.2.1 Effects of present (2016) versus future (2030) Baltic Sea ship emissions	140
2.2.2 Shipping fuel consumption and emissions modelling in fourteen port areas	150
2.2.3 Current and future impacts of ship emissions on air quality and human health in the urban area of Gothenburg	161
2.2.4 The impact of port operations on air quality in Piraeus and the surrounding urban areas	166
2.2.5 Impact assessment for a potential emission control area in the Mediterranean Sea	171

2.2.6	An Improved Model for Calculation of Emissions Based on Typical Flight Records.....	178
2.3	Air quality measurement, monitoring and modelling.....	189
2.3.1	Modelling human exposure to urban air quality: Application to Paris megacity	190
2.3.2	Analysis of long term roadside air pollution trends in European cities using ambient data from sparse monitoring networks	198
2.3.3	Mobile air quality measurements using bicycle to obtain spatial distribution and high temporal resolution in and around the city center of Stuttgart	210
2.3.4	NO ₂ measurements in the city centre of Wuppertal	221
2.3.5	NO ₂ Air Quality in German Cities: Trends Forecasts and Scenarios.....	231
2.3.6	Source apportionment of the oxidative potential of ambient fine Particulate Matters: A case study of Athens, Greece.....	245
2.3.7	Emission compliance over the lifespan of a vehicle	257
2.3.8	Air Quality Impacts of New Public Transport Provision: A Causal Analysis of the Jubilee Line Extension in London	266
2.3.9	Investigating the technological impact of European transport research and innovation towards a clean and decarbonised urban landscape	281
2.3.10	On-road heavy-duty truck emission factors for black carbon and nitrogen oxides in China.....	287
2.4	Energy optimization of transportation systems	292
2.4.1	Developing Eco-Driving Strategies Considering City Characteristics.....	293
2.4.2	How automation and connectivity can impact traffic flow and CO ₂ emissions. A microsimulation study on a highway network.	304
2.4.3	Optimization of a Bus Lane with Intermittent Priority dynamically activated by the road traffic.....	314
2.4.4	Well-to-wheel emission factors for future cars in Germany with a focus on fleet composition, new technologies and emissions from energy supplies.....	326
2.4.5	Has the Climate Benefited from the EU "Diesel Boom"? – Assessment of CO ₂ -eq Emissions from EU's Increasing Diesel Car Fleet.....	342
2.4.6	OLYMPUS: An urban emissions model focused on the individual.....	349

Acknowledgements

We would like to thank all the people involved in the successful organisation of the 23rd International Transport and Air Pollution conference, and in particular the members of the Scientific and Organizing Committees for their invaluable efforts. Above all we would like to thank all authors for their high quality contributions to the conference proceedings.

Abstract

This publication contains the proceedings of the 23rd Transport and Air Pollution (TAP) conference that took place in Thessaloniki, Greece, from 15th to 17th of May 2019. The 23rd TAP conference collected the main research developments and policy targets taking place in Europe at the turn of the decade, in the areas of electromobility, clean maritime shipping, fuels and energy decarbonisation, air pollution/climate change trade-offs, low emission engines and vehicles, enhanced air quality modelling tools and their impacts on regulation and decision making.

The publication is addressed to researchers, engineers and policy makers, as well as to all those who are interested in the development of a more efficient and cleaner transportation system.

1 Introduction

The 23rd Transport and Air Pollution (TAP) conference took place in Thessaloniki, Greece, from May 15th-17th, 2019. It was co-organised by the Laboratories of Applied Thermodynamics and Heat Transfer and Environmental Engineering of the Aristotle University (Thessaloniki, Greece) and EMISIA S.A. (Thessaloniki, Greece), with the support of the Joint Research Centre of the European Commission.

The main theme of this year's TAP conference was “**2020-2030: Transport in critical transition**”. The conference accumulated various research contributions in the area of transport and the environment, including the fields of emissions' characterisation, emission modelling, environmental assessment of transportation measures, marine and aviation emissions, electric vehicles, air quality and projections and particulate matter. In the context of the conference sixty-nine (69) scientific papers were presented in the form of oral presentations, sixty-five (65) research poster announcements were performed and three (3) main thematic keynote speeches were given by invited speakers. The conference was attended by two hundred and thirty (230) participants. Selected papers will be considered for further publication at the scientific journal Atmospheric Environment, Elsevier (ISSN: 1352-2310).

The present report includes the proceedings of this 23rd TAP conference (2019), i.e. the collection of all the papers and posters that were presented in the framework of the conference. The remainder of the report is organised as follows:

- Chapter 1 include an introductory message from the Chairman at the 23rdTAP conference (2019), as well as information related to the organisation of the conference,
- Chapter 2 provides the full-text of all the papers presented in the conference,
- Chapter 3 includes all the poster presentations.

1.1 Message of the Chairman

The International Transport and Air Pollution Conference (TAP) has been held since 1986 in Graz (Austria), Zurich (Switzerland), Avignon, Reims, Toulouse and Lyon (France), Boulder (Colorado, USA) and Thessaloniki (Greece) and has turned into a key event of dialogue and networking in the areas of transport and air pollution, between scientists, researchers, transport users and decision makers.

The 23rd TAP conference took place in Thessaloniki, Greece in the period May 15th-17th, 2019. It was co-organised by the Laboratories of Applied Thermodynamics and Heat Transfer and Environmental Engineering at the Mechanical Engineering Department of Aristotle University Thessaloniki and EMISIA SA, with the financial and administrative support of the European Commission's Joint Research Centre.

The main theme of the 23rd TAP Conference was “2020-2030: Transport in critical transition”. Indeed, this decade will be determining whether transport systems will succeed in moving ahead with their sustainability targets. In this direction, specific areas include electromobility in the road sector, clean maritime shipping, fuels and energy decarbonisation, air pollution / climate change trade-offs, low emission engines and vehicles, enhanced air quality modelling tools and their impacts on regulation and decision making. The 23rd TAP conference collected the main research developments and policy targets taking place in Europe at the turn of the decade.

These activities were presented in 69 conference papers, 65 posters and discussed by the 230 participants at the conference. While only time will tell how successful research, science and policy have been in meeting the challenges ahead, the conference clearly showed that a faster technology uptake together with behavioural changes are required to meet the challenging greenhouse gas targets for road transport. With regard to air pollutants, and in the wake of the diesel scandal, some strong positive messages were given on how bold new regulation on emission control of vehicles on the road can deliver technologies that perform as supposed to under their actual use. Finally, maritime emissions receive increasing attention as the result of the global 0.5% sulfur cap, the Tier III NO_x standards lying ahead and the efficiency targets that have been established - clearly an area where the industry and researchers can work together to select the best combinations of fuel, engine, and aftertreatment technology per application.

I sincerely hope the proceedings of the conference will prove useful and a good reference to your studies!

Leonidas Ntziachristos

Chairman at 23rd TAP conference (2019)

1.2 Organisation

1.2.1 General Information

Conference Logo	
Conference Title	23rd International Transport and Air Pollution Conference
Date	15 - 17 May 2019
Venue	Thessaloniki Concert Hall, Thessaloniki, Greece

1.2.2 Organisers

	EMISIA S.A.
	Laboratory of Heat Transfer and Environmental Engineering (LHTEE) of the Aristotle University of Thessaloniki (AUTH)
	Laboratory of Applied Thermodynamics (LAT) of the Aristotle University of Thessaloniki (AUTH)
	with the support of the: European Commission (EC), Joint Research Centre (JRC)

1.2.3 Contributors

	French Institute of Science and Technology for Transport, Development and Networks (IFSTTAR)
	Graz University of Technology (TU GRAZ)
	Swiss Federal Laboratories for Materials Science and Technology (EMPA)

1.2.4 Scientific Committee

The members of the Scientific Committee (SC) of TAP 2019 contributed to the overall organisation of the conference, the review of the received papers, the formulation of the program, the oral sessions' chairing and the in-situ evaluation of the presented papers and posters. The members of the Scientific Committee, as well as their affiliations are provided below:

- Leonidas Ntziachristos (Chairman), Laboratory of Heat Transfer and Environmental Engineering / Aristotle University of Thessaloniki (GR)
- Nicolas Moussiopoulos, Laboratory of Heat Transfer and Environmental Engineering/ Aristotle University of Thessaloniki (GR)
- Zissis Samaras, Laboratory of Applied Thermodynamics / Aristotle University of Thessaloniki (GR)
- Jon Andersson, Ricardo (UK)
- Evangelos Bekiaris, Centre for Research and Technology Hellas / Hellenic Institute of Transport (GR)
- Pierre Bonnel, European Commission, Joint Research Centre
- Jens Borken-Kleefeld, International Institute for Applied Systems Analysis
- Thomas Büttler, Empa (CH)
- Asif Faiz, Faiz & Associates LLC (US)
- Georgios Fontaras, European Commission, Joint Research Centre
- Chris Frey, NC State University (US)
- Stefan Hausberger, IVT TUGraz (AT)
- Jukka-Pekka Jalkanen, Finnish Meteorological Institute (FI)
- Georgios Karavalakis, UC Riverside CERT (US)
- Salah Khaldi, IFSTTAR (FR)
- Norbert Ligterink, Netherlands Organisation for Applied Scientific Research - TNO (NL)
- Federico Millo, Politecnico di Torino (IT)
- Andrés Monzón, Universidad Politecnica de Madrid, (ES)
- Simsoo Park, Korea University (KR)
- Martin Rexeis, IVT TUGraz (AT)
- Constantinos Sioutas, University of Southern California (US)
- Åke Sjödin, IVL (SE)
- Robin Smit, University of Queensland (AU)
- Till Riedel, Karlsruhe Institute of Technology (DE)
- Carol Wong, Hong Kong Environmental Protection Department (HK)
- Ye Wu, Tsinghua University (CN)

1.2.5 Organising Committee

The members of the Organising Committee (OC) of the conference undertook tasks related to the organisation of the conference, the reception, organisation and allocation of the scientific papers for review, the notification of authors, the identification of the thematic areas, the formulation of the program and the in-situ organisation of all conference's aspects. The members of the Organising Committee, as well as their affiliations are provided below:

- Leonidas Ntziachristos (Chairman), Laboratory of Heat Transfer and Environmental Engineering / Aristotle University of Thessaloniki (GR)
- Evi Gouliarou (Conference Secretary), EMISIA S.A. (GR)
- Sokratis Mamarikas, Laboratory of Heat Transfer and Environmental Engineering / Aristotle University of Thessaloniki (GR)
- Chara Tziveli, Laboratory of Applied Thermodynamics / Aristotle University of Thessaloniki (GR)
- Thomas Papageorgiou, EMISIA S.A. (GR)
- Vasilis Kouliaridis, EMISIA S.A. (GR)

2 Conference Proceedings – Papers

The present chapter includes the papers' proceedings of the conference, i.e. the full-text collection of all the papers that were presented during the conference, in the form of oral announcements. Papers of this section are:

- structured based on the thematic sessions of the TAP 2019, as defined in the final program of the conference,
- listed in the order that were presented during the conference,
- included in the version that was submitted by authors to the conference's website before the implementation dates of TAP 2019.

Table 1 provides the thematic sessions of TAP 2019 for papers, as well as the main topics discussed in each session.

Table 1. Thematic sessions of TAP 2019 and main contents.

	Thematic Sessions	Main Contents
2.1	Gaseous and particulate pollutants characterisation	<ul style="list-style-type: none"> • PEMS & dynamometer measurements • Emission factors' development • Vehicle technology compliance with emission standards
2.2	Marine and aviation emissions	<ul style="list-style-type: none"> • Shipping and aviation emissions' modeling & estimation • Impact assessment of traffic conditions and measures' implementation • Future trends
2.3	Air quality measurement, monitoring and modelling	<ul style="list-style-type: none"> • Dispersion and human exposure modeling • Impact assessment of traffic measures on air quality • New methods and techniques on air quality measurements
2.4	Energy optimisation of transportation systems	<ul style="list-style-type: none"> • Measures and strategies for CO₂ and energy consumption reduction • Automation of road transport
2.5	Road transport management and emissions estimation	<ul style="list-style-type: none"> • Measures and strategies for emissions reduction • Road transport emissions' modeling and estimation
2.6	Alternative fuels, new powertrains	<ul style="list-style-type: none"> • PEMS & dynamometer measurements enabling alternative fuels • Air quality effects of alternative fuels • New powertrains, including electrics and hybrids
2.7	Remote sensing of vehicle emissions	<ul style="list-style-type: none"> • Emissions' measurements using remote sensing • New techniques in remote sensing • Remote sensing utilization for emissions' policy enforcement

	Thematic Sessions	Main Contents
2.8	Particulate Matter	<ul style="list-style-type: none"> • Exhaust and non-exhaust particulate matter • Dispersion of particulate matter • Air quality assessment & human exposure to particulate matter
2.9	Special Session on H2020 projects	<ul style="list-style-type: none"> • Results of project funded under the EU H2020 program
2.10	New sensors and techniques	<ul style="list-style-type: none"> • Sensors, methods and techniques in vehicular emissions measurements and air pollution

2.1 Gaseous and particulate pollutants characterisation

This section includes papers presented in the context of the “Gaseous and particulate pollutants characterisation” sessions of the TAP conference. Table 2 provides an overview of these papers, as they are listed in the following sub-sections.

Table 2. Titles and authors of “Gaseous and particulate pollutants” papers

	Paper Title	Authors
2.1.1	Consistent Emission Factors from PEMS and Chassis Dyno Tests for HBEFA 4.1	S. Hausberger, C. Matzer, S. Lipp, K. Weller, M. Dippold, M. Röck, M. Rexeis and G. Silberholz
2.1.2	Euro 3 and Euro 5 Diesel vehicles' particles evolution in ageing chamber	B. Vansevenant, Y. Liu, C. Ferronato, L. Fine, P. Tassel, C. Louis and M. André
2.1.3	Real world emission factors based on roadside increment concentrations of NOx and CO2	C. Johansson, L. Burman, M. Norman and M. Elmgren
2.1.4	Cold-Start Emissions and Excess Fuel Consumption at Low Ambient Temperatures - 2019 Update	J. Laurikko
2.1.5	Review of Legislative Requirements and Methods for the Estimation of PN/PM Emissions for Advanced Light-duty OBD Applications	D. Kontses, S. Geivanidis and Z. Samaras
2.1.6	Real-world Vehicle Emission Measurements using PEMS in Hong Kong	T.S. Lo, K.L. Ng, A.H.L. Wong, C.K.L. Wong, C. Keramydas and G. Papadopoulos
2.1.7	PEMS accuracies under harsh environmental conditions	L. Landl, T. Vuckovic and S. Hausberger
2.1.8	Trends in Light Duty Gasoline Vehicle Emissions Based on Real-World Measurements	H.C. Frey, T. Wei, T. Khan, W. Yuan and N. Rastogi
2.1.9	NOx Emissions of Heavy-Duty Vehicles with Euro VI Certified Engines	R.J. Vermeulen, R.N. van Gijlswijk and S. van Goethem
2.1.10	Measuring real emissions with simplified PEMS	P. Öhlund and L. Eriksson
2.1.11	Exhaust gas temperature and NO _x after-treatment performance of Euro 6 passenger cars	Z. Mera, N. Fonseca, J. Casanova and J.M. López

2.1.1 Consistent Emission Factors from PEMS and Chassis Dyno Tests for HBEFA 4.1

S. Hausberger^{1}, C. Matzer¹, S. Lipp¹, K. Weller¹, M. Dippold¹, M. Röck¹, M. Rexeis¹, G. Silberholz¹*

¹Institute of Internal Combustion Engines and Thermodynamics, Graz University of Technology, Graz, Austria, Hausberger@ivt.tugraz.at

Introduction

The Handbook Emission Factors for Road Transport (HBEFA, www.hbefa.net) is a data base system with additional calculation routines, which provides emission factors (EFs) for 2345 different traffic situations (TS). The TS cover various road categories at different traffic volumes (Levels of service) for different road gradients. EFs give the emissions of exhaust gas components and fuel consumption in [g/km] and the electric energy consumption in [kWh/km]. HBEFA covers mopeds, motorcycles, passenger cars (PCs), light commercial vehicles (LCVs), heavy goods vehicles (HGVs), buses and coaches in different mass classes and with different propulsion technologies and all relevant emission classes (EURO 0 to EURO 6d).

HBEFA users can select combinations of traffic and ambient temperatures, the reference year, defining the mileage shares of the single vehicle segments in the fleet and the level of detail for the results. With these features, HBEFA is a benchmark for data used in all kinds of analysis concerning traffic related emissions.

Since the huge number of combinations of TS and vehicle segments cannot be covered by vehicle measurements, the EFs are simulated based on measured data over a limited number of real-world cycles. This simulation is based on the vehicle emission model PHEM (Passenger car and Heavy duty Emission Model) from TU Graz.

To set up the vehicle models in PHEM, the available emission test data within European labs is collected. Compared to the former version, for HBEFA 4.1 several new boundary conditions had to be considered:

- Approximately 11 times more vehicle tests were available compared to HBEFA 3.3
- More than 50% of the available test data was from tests with portable emission measurement systems (PEMS) (only 10% in HBEFA 3.3)
- The EFs for CO₂ were calibrated with real-world fuel consumption monitoring studies
- Battery electric vehicles (BEVs), Plug-In- and Hybrid electric vehicles (PHEVs and HEVs) were included

These conditions led to many novel approaches, the most important ones are:

- More accurate method for time alignment between emission signals, engine speed and engine power (Weller, 2016)
- New approach to compute the instantaneous engine power in PEMS tests
- Calibration methods to convert vehicle mass and road load from type approval data to average real-world driving conditions
- Extension of the model PHEM for PHEV and BEV simulation
- Automation of calculation routines

Due to a much higher number of vehicle tests used as basis for the vehicle models in PHEM as well as the accurate calibration of real-world driving conditions, the representativeness of the resulting EFs is expected to increase significantly. This fact should provide deeper insights into differences between real-world and type approval emission and fuel consumption levels.

Methods

The hot EFs for the HBEFA 4.1 are simulated for all vehicle categories with the model PHEM for the pre-defined set of driving cycles representing the 2345 different TS.

The Vehicle Emission Model PHEM

PHEM is developed at the Institute of Internal Combustion Engines and Thermodynamics (IVT) of TU Graz since the late 1990s. Development is continuously ongoing to include new technologies and to improve simulation methods. A short description is given below. More details can be found e.g. in (Hausberger, 2003), (Rexeis, 2013), (Hausberger, 2012), (Matzer, 2017).

PHEM calculates the fuel consumption and emissions of road vehicles in 1Hz for a given driving cycle based on the vehicle longitudinal dynamics and emission maps. The engine power demand is calculated for each time step in a cycle from the vehicle's driving resistances, losses in the drivetrain and auxiliary power demand. The engine speed is determined based on tire dimensions and the drivetrain's gear ratios, where an integrated gearshift model operates the transmission. Specific gearshift models for standard test procedures (NEDC, WLTP, etc.) as well as for real-world driving behaviour are included. Base exhaust emissions and fuel flow are then interpolated from engine maps depending on the resulting engine speed and power. To increase the accuracy of the simulated emissions, correction functions applied consider different emission behaviour under transient engine loads. Furthermore, detailed models for the conversion efficiency of different exhaust gas after treatment systems exist. The temperatures of catalytic converters are simulated based on the 0-dimensional heat transfer between exhaust gas and catalyst material as well as between exhaust line and ambient air. This routine is especially important for simulation of SCR (Selective Catalytic Reduction) systems – which cool down at low engine loads – and for simulation of cold start effects.

PHEM Passenger car and Heavy duty Emission Model

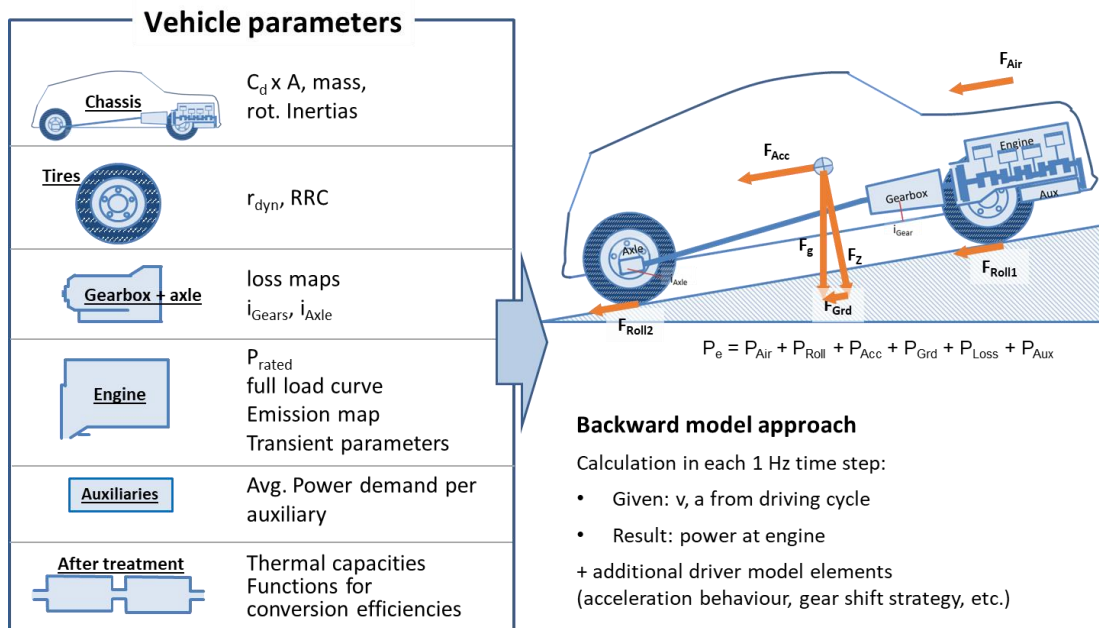


Figure 1: Scheme of the PHEM model

Since the vehicle longitudinal dynamics model calculates the engine power output and speed from physical interrelations, this approach can depict any driving condition. The model can handle different payloads of vehicles in combination with longitudinal road gradients and variable speeds and accelerations as well as effects of different gear shifting behaviour.

For simulation of EFs, a set of “average vehicles” are elaborated for each update of the HBEFA, representing average European vehicles per segment. A segment covers a combination of vehicle category, EURO-class, propulsion system and mass class; e.g. passenger car, EURO 5, diesel, average size.

The engine emission maps and the aftertreatment system parameters are gained from the time-resolved measurement data of all vehicles in the ERMES (European Research on Mobile Emission Sources, www.ermes-group.eu) database (db). To produce the engine emission map for each single vehicle tested, PHEM computes the required engine power from the existing test data and then allocates the measured emissions to the respective range of engine speed and power in the engine map. Here, 3-second moving average values are used for power, rpm and emissions to reduce issues with inaccurate time alignments between these signals.

The maps use normalised formats, for the engine speed between idling (=0) and rated speed (=1) and for the power between 0 kW (=0) and rated power (=1). This allows calculating weighted average engine maps from all vehicles measured within each segment (e.g. all EU 5 diesel cars with the single maps weighted according to the sales numbers per make and model). Similarly, the efficiency maps from after-treatment systems are set up as function of space velocity and temperature. The relevant vehicle data covers the vehicle mass, rated engine power, the loading, air and rolling resistance values, descriptors for the transmission system etc. As a result, a set of input data for PHEM per vehicle segment contains the vehicle properties, engine maps and after-treatment data.

Calibration methods

For the HBEFA 4.1 simulations, we calibrated the vehicle parameters shown in Figure 1 for each vehicle segment to consider all relevant influences in real-world driving:

- Vehicle loading (number of passengers, luggage, goods)
- Vehicle and ambient conditions (different tires and tire pressure, roof boxes, trailers, road surface conditions, side wind, etc.)
- Gear shift behaviour of the drivers
- Power demand from auxiliaries
- Fuel quality

Furthermore, differences in driving cycles (velocity and altitude profile) and ambient temperature levels, start conditions and trip length are considered. The driving cycles are pre-defined representing the different traffic situations of the HBEFA.

We used the chassis dynamometer tests collected in the ERMES db to set up the vehicle input data sets representing typical type approval test conditions. By simulation of these type approval tests (NEDC, WLTC) with PHEM, the uncertain vehicle parameters in this step were calibrated. These are the base auxiliary power demand, the transmission loss maps and the engine fuel consumption maps.

Then we used the input data calibrated for chassis dyno conditions to simulate the on-board real-world tests (RDE PEMS tests). Instead of the chassis dyno cycles the speed and altitude profiles from the PEMS tests were used as input. The altitude profile was generated by matching GPS x-y coordinates with open street map data. In this step again a calibration of the uncertain model input data was done with regard to the air and rolling resistance in real-world driving and the auxiliary power demand due to activated auxiliaries during the tests. After the calibration the measured and simulated fuel consumption in the PEMS tests have a high correlation, as shown in the results later.

In the last step, a final calibration of the vehicle parameters was performed to match representative real-world conditions. Those are different from PEMS tests since for example PEMS tests usually are neither performed with trailers or roof boxes nor in bad weather conditions. Thus, loading, air drag and rolling resistance values and auxiliary power demand - including HVAC (Heating, Ventilation and Air Conditioning) system operation for all seasons - were adjusted in this step.

For this final calibration step, we calculated the fuel consumption values with PHEM for all HBEFA cycles. Then we weighted the results per cycle according to their share of each TS in Germany and added cold start extra fuel consumption. These weighted results were then compared with data from real-world fuel consumption monitoring, such as 'spritmonitor.de' for cars and LCVs.

This calibration exercise was done for a selected sample of four gasoline and four diesel cars to set up calibration functions (CaFs) for converting type approval settings to real-world conditions (Figure 2).

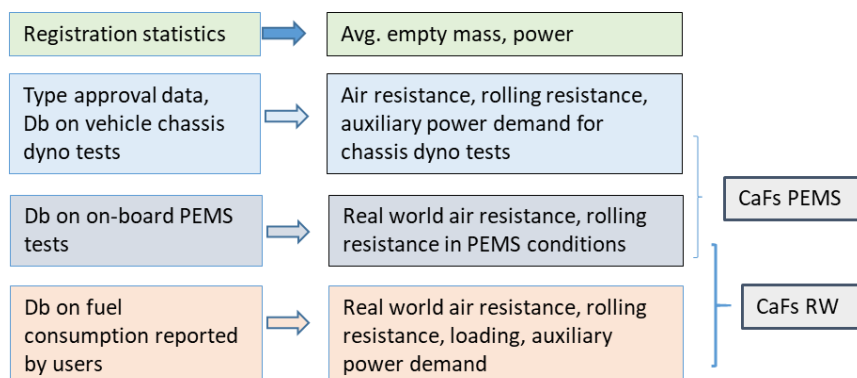


Figure 2: Schematic picture of the workflow in the calibration process

The resulting CaFs are shown in Table 1. The main effects leading to differences compared to the WLTC settings are:

NEDC: Tolerances in vehicle and tire selection for coast down as well as tolerances in coast down time and torque meter calibration of the chassis dyno lead to clearly lower road loads. In addition, the auxiliary power demand to be covered by the engine is low since the alternator is running mostly in idling over the test due to the battery usually being fully charged at test start. An “optimized real speed trajectory” was used to mimic a well-trained driver.

RDE-PEMS: The test mass weighted before PEMS test start was used in the simulation, typically leading to a higher mass compared to the WLTC settings. For air drag, the WLTC_{high} settings were used to consider the additional air drag due to the PEMS system. Furthermore, the difference in air drag due to differences in air density was considered for tests below 20°C.

Real world (HBEFA cycles): The loading was set differently for gasoline and diesel to meet the ‘spritmonitor.de’ data per vehicle model. The difference reflects that diesel cars are usually larger and used more frequently for long distance driving, including holiday trips etc. The increased air drag value reflects side wind effects (+3%), 5% mileage shares of driving with trailers and 5% with roof boxes (+2.5%) and a higher air density at average German temperatures (+2.8%). The increased rolling resistance coefficient can be explained by mileage shares on wet or snowy roads (~+2%) and with winter tires (~ +4.5%). For diesel cars, we assumed that the high share of SUVs (Sport Utility Vehicles) with possibly wider tire dimensions and worse rolling resistance may lead to further increases in the rolling resistance to better match the ‘spritmonitor.de’ data (Figure 3).

Table 1: Calibration functions identified from the EURO 6 PC sample

Test	MRO	C _d x A	Fr ₀	P _{Aux}
NEDC	DIN + 100	0.83*WLTP _{low}	0.80*WLTP _{low}	100
WLTC	WLTC value	WLTC value	WLTC value	600
RDE-PEMS	Test mass	WLTC _{high}	Tire specific ⁽¹⁾	1500
Real world diesel	DIN*1.05 +215	0.5*(WLTC _{high}	+ 1.12*WLTC	1500
Real world gasoline	DIN*1.05 +120	WLTC _{low}) * 1.085		

With: MRO (Mass in running order [kg]); C_d x A (air drag coefficient x frontal area of the vehicle [m²]); Fr₀ (rolling resistance coefficient [N/N]); P_{Aux} (Average auxiliary power demand [W])

(1)Different for winter and summer tires and depending on tire label RRC value

Figure 3 shows the average results for the four gasoline and four diesel cars. The simulation of the WLTC and of the RDE is matching the measured values very well. For the diesel cars analysed, the “real-world” CO₂ emissions simulated for the HBEFA 4.1 cycles are 9% lower than the ‘spritmonitor.de’ data even with the extra increased rolling resistance due to high SUV shares.

It may be, that the sample of the four vehicle models from 'spritmonitor.de' was too small to lead to fuel consumption results representative for average German driving. For the average diesel cars, the simulation with the CaFs met the 'spritmonitor.de' data very well (Figure 4).

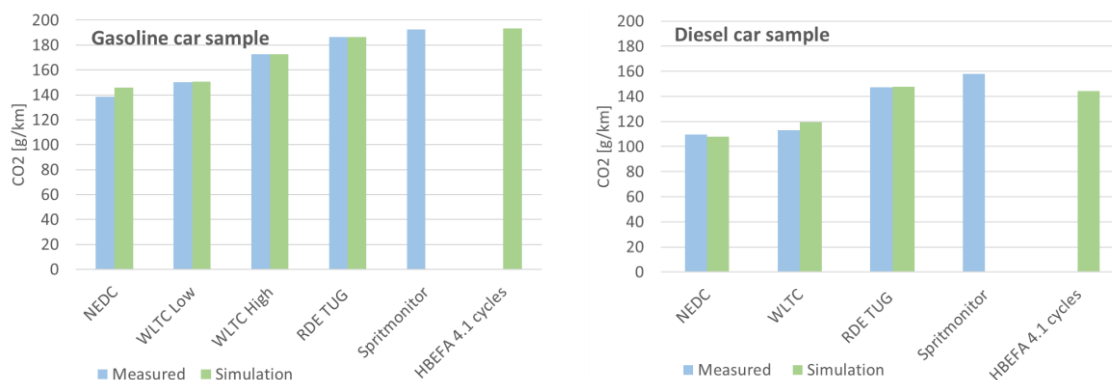


Figure 3: Average measured and simulated CO2 emissions for the 4 EURO 6 gasoline cars (left) and for the 4 EURO 6 diesel cars (right)

To produce the average real-world vehicle data sets for HBEFA 4.1 we applied the calibration functions (CaFs) found for the vehicle sample described above to the average vehicles per segment. The average vehicle masses in running order and the engine rated power of the new vehicle fleet were gained from registration statistics and from CO₂ monitoring data for the EU 28. Rolling resistance and air resistance values in type approval tests were taken from the chassis dyno data in the ERMES db and from an internal data base at TU Graz.

After the application of the calibration functions to the vehicle parameters, the PHEM simulation met the average fuel consumption calculated from the 'spritmonitor.de' data for the single segments quite accurately (Figure 4, Figure 5). The evaluation of the 'spritmonitor.de' data according to model years for the shares of different makes and models in the German fleet was provided by ICCT (International Council on Clean Transportation) in an ongoing project for UBA Germany (German Environment Agency). The simulation also reproduced the gap between real-world driving and NEDC type approval of approximately +35% for the EURO 6 gasoline fleet and of +40% for the EURO 6 diesel fleet, as reported by ICCT e.g. in (Mock, 2014).

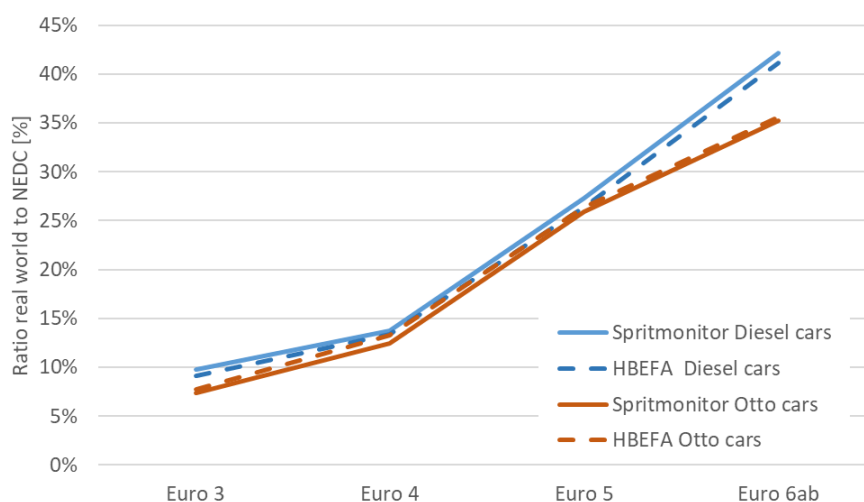


Figure 4: Ratio of real-world CO2 emissions to the type approval values for the average new PC fleets per EURO class simulated with PHEM for the HBEFA 4.1 and reported from the 'spritmonitor.de' data in an update from (Mock, 2014).

For HDVs (Heavy-duty vehicle), the calibration of the models was based on data available from vehicle tests and data collected during the development of the method for determination of CO₂ emissions of HDVs (Regulation (EU) 2017/2400, e.g. (Rexeis, 2017)). From 2020 on, a broader pool of data shall be available also for HDVs from monitoring of the European fleet. For two-

wheelers, no data collection of typical real-world fuel consumption is available yet. However, road load values from coast down tests under real-world conditions were used for these vehicles. Also engine maps and auxiliary power consumption used should represent real-world conditions.

Automation of calculation routines

Due to the huge amount of data available (approx. 700 vehicle tests with instantaneous data), the calculation routines were largely automatized. All tests are stored in the ERMES db. To be able to use PEMS data, which typically does not include an engine torque signal, an efficient method was elaborated to calculate the engine power from engine speed and CO₂ mass flow based on generic CO₂ maps per engine technology, (Matzer, 2016).

With this method, PHEM computes the engine emission map for each vehicle directly from the time-resolved test data exported from the ERMES db. After application of plausibility checks, the single emission maps are merged to an average map for each vehicle segment by weighting them according to their share of total vehicle registration numbers of the segment.

Results

All HBEFA 4.1 cycles were simulated with the calibrated data set. The results presented are preliminary, since the HBEFA 4.1 has not been published at the time of finalising this paper.

Fuel Consumption Values

The real-world CO₂ reductions of the fleet of newly registered vehicles between Euro 0 und EURO 6 were on average 0.14% per year for diesel cars and 0.9% per year for gasoline cars. The lower reduction concerning diesel cars is caused by increasing vehicle sizes and weights (see Table 2). This effect also explains that today's fleet of newly registered diesel cars has higher CO₂ emission values than the gasoline car fleet.

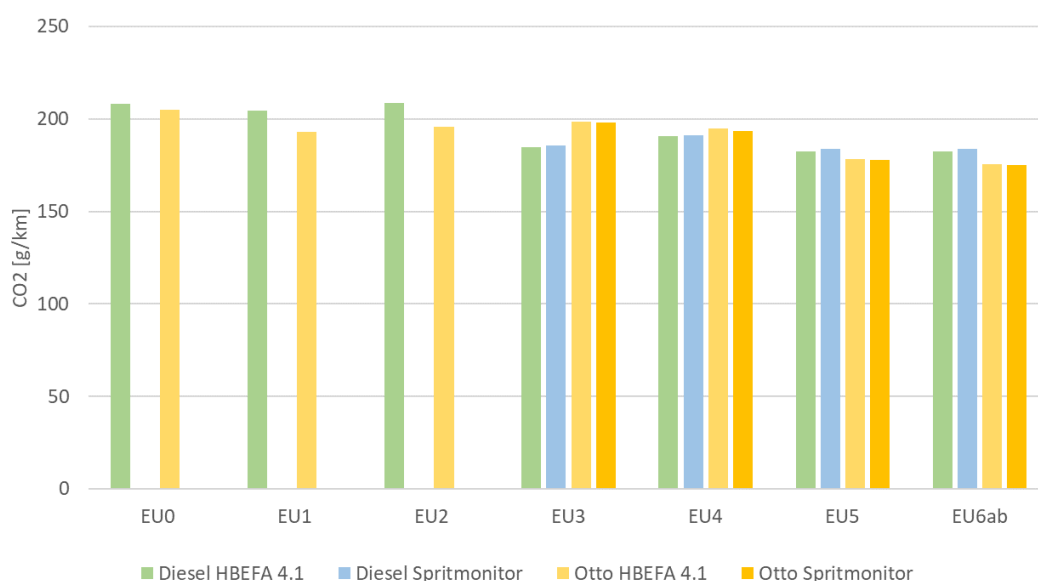


Figure 5: Average CO₂ emissions simulated with PHEM for gasoline and diesel cars compared to the real-world values reported in 'spritmonitor.de'

Also BEVs and PHEVs are included in HBEFA 4.1. While HBEFA 4.1 vehicle data represents the average real-world fleet, a fair comparison of propulsion concepts shall evaluate different propulsion systems in the same vehicle chassis, where just masses, properties of the drivetrain and of the energy storage system are exchanged in the simulation. This comparison was done using also the model PHEM. The main vehicle characteristics used are shown in Table 2.

Figure 6 compares the resulting CO₂ emissions for different propulsion systems. The EURO 6 segment C vehicles were simulated in the "RWC (Real World Cycle)" representing the standard

route driven for RDE measurements by TU Graz. For this comparison the CO₂ emissions from electricity generation were considered with a CO₂-factor of 480 g/kWh for the EU power plant mix.

Table 2: Vehicle masses and rated power for the average EURO 6ab vehicles in HBEFA and for a generic C-segment car with different propulsion systems

	HBEFA 4.1	Segment C Analysis
Diesel	1924 kg, 121 kW	1361 kg, 90 kW
Gasoline	1396 kg, 99 kW	1276 kg, 90 kW
BEV	1721 kg, 99 kW	1496 kg, 90 kW
Diesel PHEV	2180 kg, 121 kW	1578 kg, 90 kW
Gasoline PHEV	1642 kg, 99 kW	1495 kg, 90 kW

Comparing only the C segment chassis, the diesel engine has approximately 17% lower CO₂ emissions compared to the gasoline engine. This is also valid for the PHEV configuration where a 40% share of electric driving was assumed according to the analysis in (Lipp, 2017).



Figure 6: CO₂ emissions simulated with PHEM for EURO 6ab cars with average vehicle data according to HBEFA 4.1 and with vehicle data representing a C-class car

Figure 7 shows results for the HGV category tractor-semi-trailer combination. The relative reduction from EURO 0 to EURO VI was similar to the one for diesel cars, i.e. approx.. 15%.

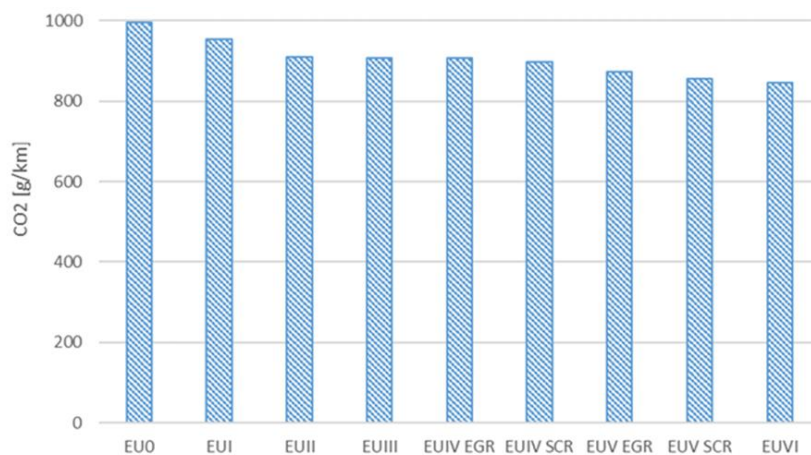


Figure 7: Specific fuel consumption values of 40t tractor-semi-trailer combinations in the HBEFA 4.1 on an average German motorway

Due to the continuous reduction of NO_x emission limits and the introduction of more demanding test procedures from EURO III on, fuel consumption more or less stagnated for several years. With the introduction of SCR systems from EURO V on, fuel consumption values dropped again, since SCR systems allow higher raw exhaust NO_x emissions enabling a more fuel-efficient setting of the combustion parameters. For HDVs also BEVs and HEVs were simulated for HBEFA 4.1 but the results are not presented in this paper.

Emission Factors

HBEFA provides EFs for CO₂, CO, HC, NO_x, NO₂, PM and PN based on PHEM simulations. To limit the size of this paper, we focus here on NO_x emissions and show some results for PN emissions. Results for all components will be available in the HBEFA 4.1.

For simulation of NO_x from diesel engines with SCR, the model considers the dependency of NO_x conversion on temperature and space velocity as well as the effect of suspended AdBlue dosing at low exhaust gas temperatures. The resulting reduction of NH₃ stored in the SCR leads to a reduction of NO_x conversion efficiency. This effect is significant in cycles with longer phases of low engine loads.

For diesel PCs, the real-world NO_x emission levels dropped significantly with EURO 6 and even more drastically with EURO 6d-temp. While diesel cars from EURO 0 to EURO 5 emitted around 800 mg NO_x/km on average, the 11 EURO 6d-temp diesel cars tested so far led to an average hot NO_x level of 44 mg/km simulated for the HBEFA traffic situation mix. The four gasoline EURO 6d-temp cars resulted in 33 mg NO_x/km. It is open yet, to which extent these NO_x levels may change once the entire fleet of newly registered cars has to meet EURO 6d-temp standards. However, a huge reduction in real-world NO_x emissions can be attributed to the new PC type approval system with RDE testing, which is mandatory from EURO 6c on.

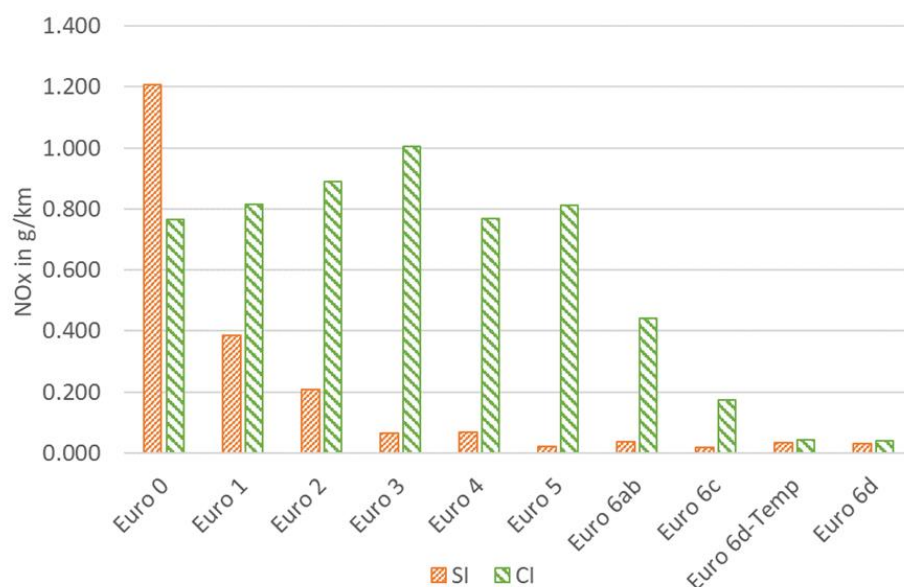


Figure 8: Average hot NO_x EFs of the PC segments for HBEFA (calibrated to German driving and vehicle conditions)

The EFs for HBEFA 4.1 were generated with average vehicle emission maps. For these maps, the single vehicle emission maps were weighted according to the new registrations of PC models in Europe in order to represent the fleet of the 28 member states (EU28). The large number of measured vehicles for HBEFA 4.1 allows to run a sensitivity analysis, using country-specific weightings for Germany, Austria and Sweden as examples. Figure 9 shows the share of new registrations of EURO 6ab PCs by make in the mentioned countries and in EU28 for the diesel car fleet. The registration data, available for the years 2013 to 2017, was taken from (EEA, 2018). The data shows, inter alia, that the share of new registrations vary strongly from country to country, e.g. the share of Volkswagen cars is over 20% in Germany and Austria but only 12% in Europe. The share of new registrations of Volvo diesel cars is over 30% in Sweden, while the share in Europe, Austria and Germany is below 5%.

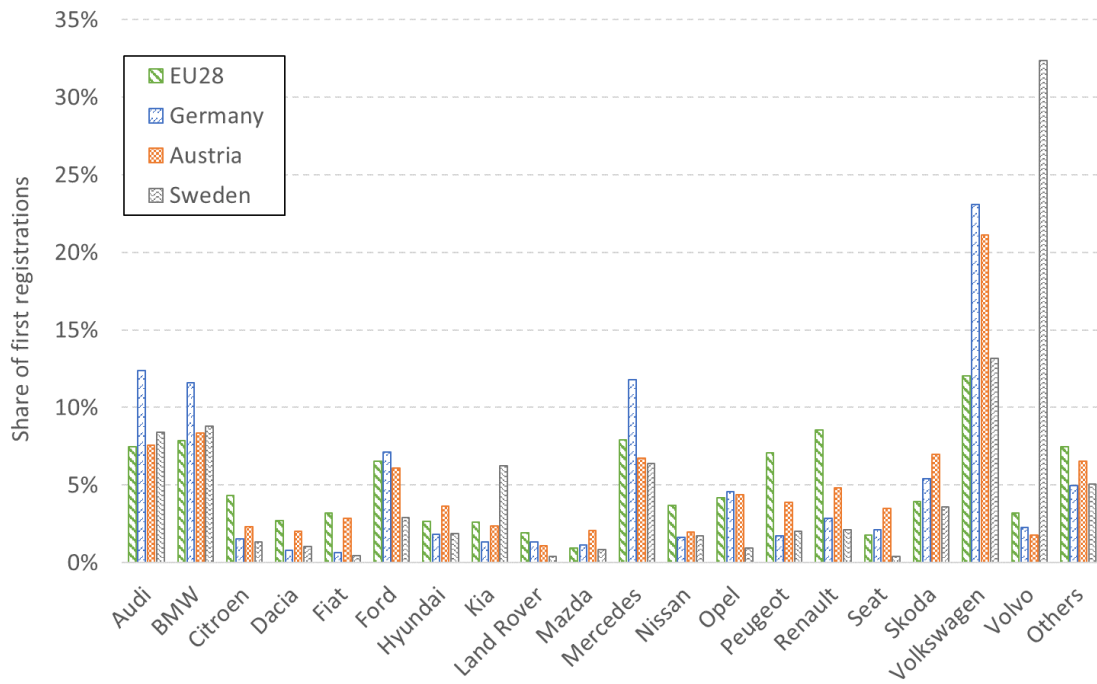


Figure 9: Share of first registrations of EURO 6ab PCs by make for the diesel car fleet

In order to show only the effects due to different weighting of makes and models, the German mix of traffic situations was used as basis for all variants. Thus, the NO_x emissions simulated with the EU28 map are similar to those shown in Figure 8. For the German diesel car fleet NO_x emissions are about 13% lower than the NO_x emissions simulated with the EU28 map. The same applies to the Austrian diesel car fleet. For the weighted map according to the diesel car fleet of Sweden the NO_x emissions are about 2% lower than the ones for the EU28 map.

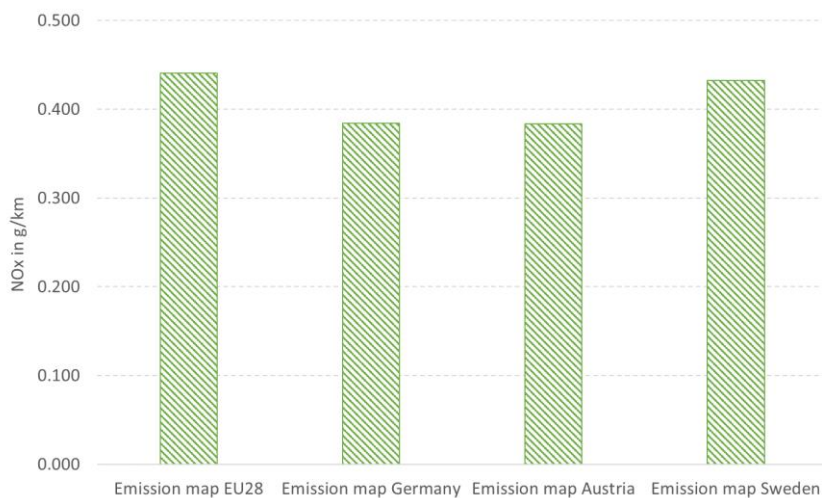


Figure 10: Average hot NO_x EFs for the German mix of traffic situations from average EURO 6ab diesel car using differently weighted engine emission maps

In summary, a country-specific weighting has significant influence on EFs but the overall uncertainties in NO_x-EFs for local situations resulting e.g. from driving cycles, model inaccuracies, etc. are most likely higher. If a higher accuracy is needed for simulation of local emissions, the model PHEM may be applied for locally measured cycles with engine emission maps weighted for the local fleet. However, such a local weighting is only reasonable for vehicle segments where a sufficient number of measurements are available.

The NOx emissions from LCVs decreased constantly from EURO 0 (3254 mg/km) to EURO 5 (1255 mg/km) by around 14% per EURO class. As for diesel cars, also for LCVs a huge drop in NOx emissions is found from EURO 5 to EURO 6. The EURO 6 N1-III results are based on 14 measured vehicles. For EURO 6c, d-Temp and d, no test data is available yet. Thus, the PC emission maps converted to LCV rated power levels were used, leading to a drop in the emissions similar to PCs.

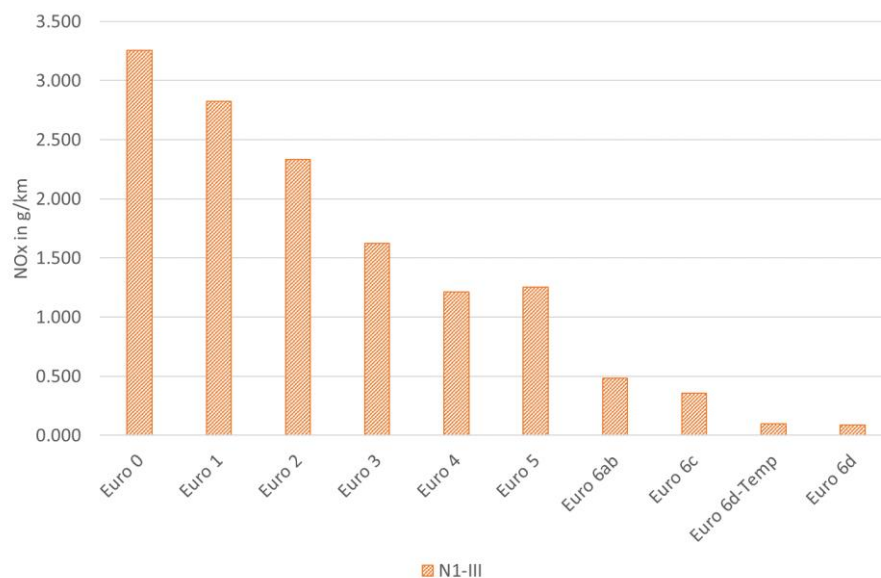


Figure 11: Average hot NOx EFs of the LCV segments for HBEFA (calibrated to German driving and vehicle conditions)

The NOx emissions from motorcycles above 250 ccm also show a significant drop (Figure 12). The 11 measured EURO 4 motorcycles resulted in an average hot NOx emission level of 37 mg/km.

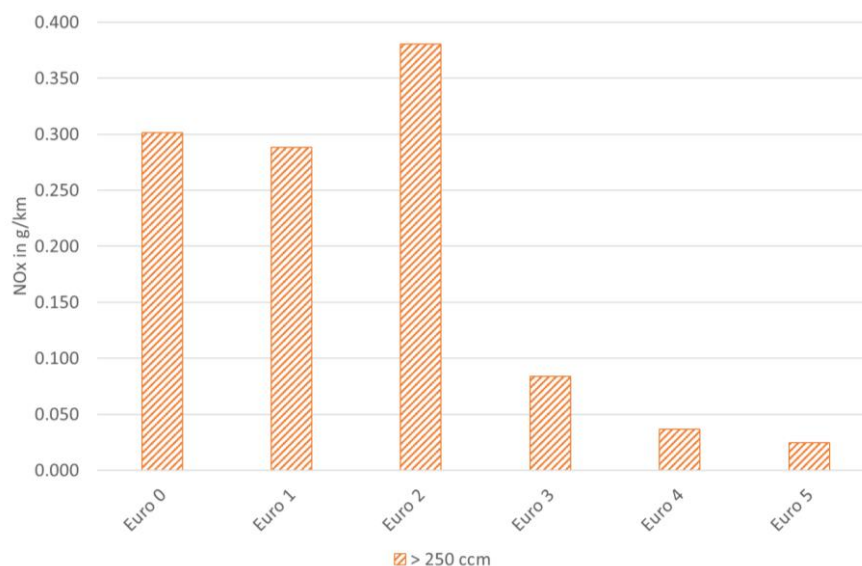


Figure 12: Average hot NOx EFs of the motorcycle vehicle segments >250 ccm for HBEFA (calibrated to German driving and vehicle conditions)

Also for HDVs and busses the introduction of more representative test procedures led to significant NOx reductions. In contrary to PCs and LCVs this was a more continuous process, starting from EURO III with the transient ETC (European Transient Cycle) test up to the introduction of the WHTC (World Harmonized Transient Cycle) which considers cold start effects and the In-Service Conformity (ISC) tests with EURO VI. The ISC is an on-board emission test, which led to further significant NOx reductions compared to EURO V (Figure 13).

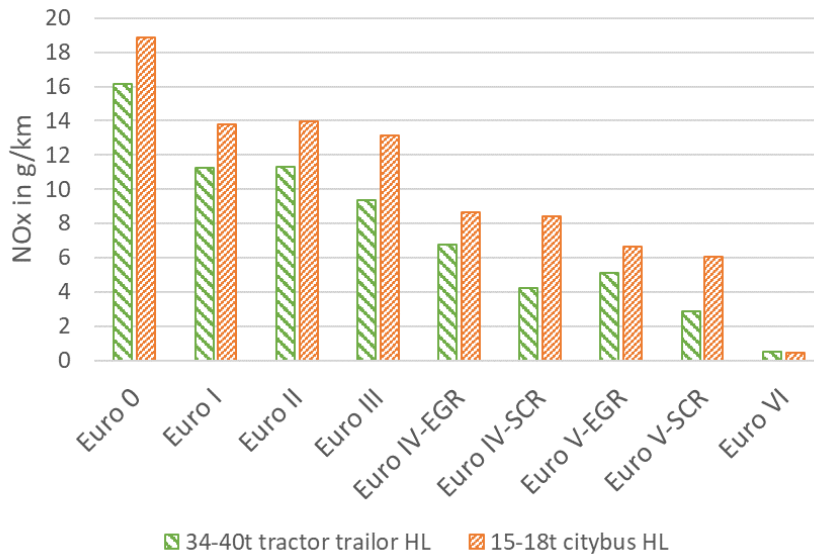


Figure 13: Average hot NOx EFs for tractor trailers (TT) 34–40t and city buses (CB) 15-18t for HBEFA with half loading (HL)

While NOx emissions from the passenger cars fleet seem to meet emission limits the first time also in real world operation from EURO 6d-temp on, particle emissions have been reduced successfully already since introduction of EURO 5 (Figure 14). The introduction of limits for particle numbers for diesel cars led to the installation of wall flow particle filters (PF) with high removal efficiency for particle number emissions (PN). PN emission factors are related to the regulatory PN test procedure and thus cover particles above 23nm. EURO 5 diesel cars have 99.2% less PN, EURO 6d-temp 99.9% less PN compared to EURO 4 without PF. The PN emission factors from PHEM consider also the extra emissions during PF regeneration phases. The low PN emission level from modern diesel cars lead to the effect, that gasoline cars have higher PN emissions than diesel cars from EURO 5 on. To meet the PN limits in RDE tests from EURO 6c on, also gasoline cars are equipped with PFs. The 15 measured EURO 6c and d-temp gasoline cars showed a PN level in the range of $6 \cdot 10^{11}$ PN/km in real driving. This level is higher than EURO 6d-temp from diesel cars ($5 \cdot 10^{10}$ PN/km) but below EURO 5 diesel ($\sim 1 \cdot 10^{12}$). Overall, all test data used for HBEFA 4.1 provides a quite optimistic view on the future development of real world passenger cars pollutant emissions.

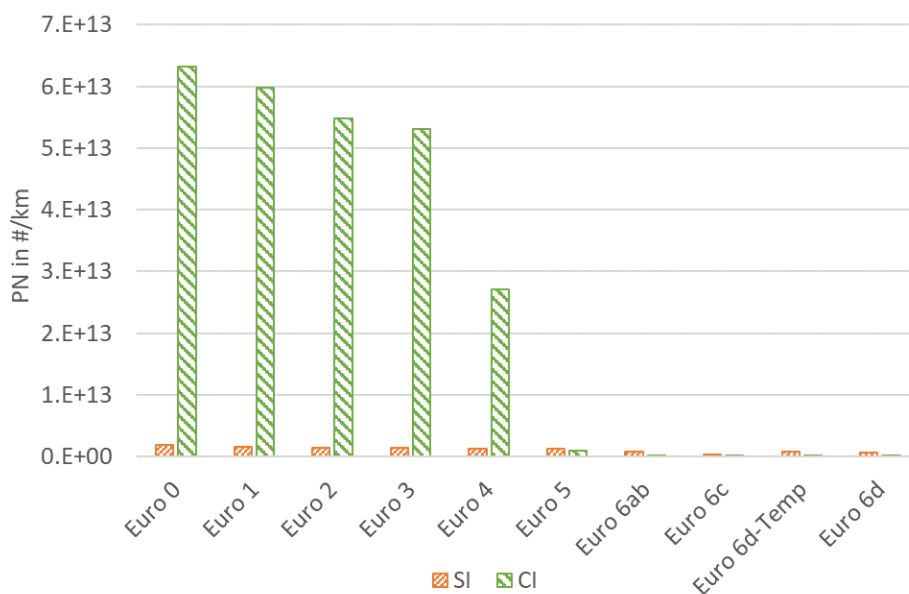


Figure 14: Average hot PN EFs of the PC segments for HBEFA (average for German driving and vehicle conditions)

Figure 15 shows PN emissions from two HDV segments. EURO III had the highest emission level, which is – due to the NOx-PN trade-off - a result of the reduction of NOx emission limits and the introduction of the ETC test procedure which made an engine calibration for low NOx necessary in a wider engine operation range compared to the former 13-mode test. With EURO VI a PN limit value was introduced for HDV, since then the HDV are equipped with particle filters. The average EURO VI city bus emits $9 \cdot 10^{10}$ particles/km, which is similar to the EURO 6 diesel passenger car emission levels. In general, PN emissions from HDVs are per km not much higher than those from passenger cars, which can be explained by higher cylinder volumes and lower engine speeds leading inter alia to better combustion of soot in the cylinder. The more transient operation of city buses compared to tractor-trailers – which drive mainly in long haul operation – lead to slightly higher PN emissions for the city bus.

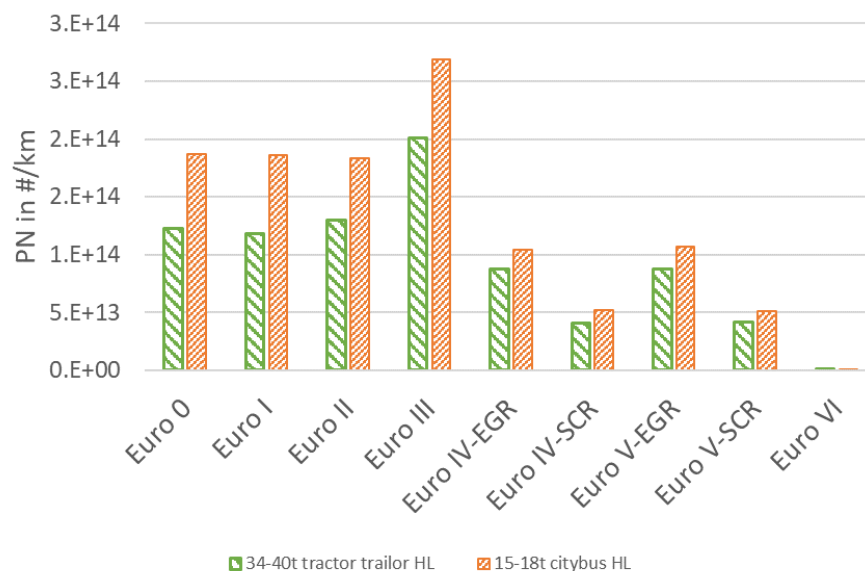


Figure 15: Average hot PN EFs of tractor-trailer combinations (50% loaded) and of city buses for HBEFA (average for German driving and vehicle conditions)

Summary

To provide the emission factors for the HBEFA version 4.1, new emission test data of current vehicle technologies was collected for cars, LCVs, HDVs and 2-wheelers. To handle the huge amount of vehicle tests, the production of engine emission maps was automated to a large extent. For this process a novel method to calculate the engine power from engine speed and CO2 signals was applied successfully. Compared to the former HBEFA versions, the fuel consumption and CO2-EFs were calibrated to fit average real-world data by adjustments of the PHEM model input parameters. This method lead to calibration functions to convert road load, loading, auxiliary power demand etc. from type approval test settings to representative real-world values.

With the calibrated vehicle parameters and the average engine emission maps the updated EFs for hot running conditions were calculated with the model PHEM. The results for average real-world driving with PCs in Germany are:

- CO₂ improvements between Euro 0 und EURO 6 were on average 0.14% per year for diesel cars and 0.9% per year for gasoline cars. The low reduction concerning diesel cars is also caused by increasing vehicle sizes and weights.
- NOx emissions from diesel cars from EURO 0 to EURO 5 are around 800 mg NOx/km, the current EURO 6d-temp diesel cars have an average NOx level of 44 mg/km.
- The introduction of diesel particle filters drastically reduced emitted PN. The comparison of cars with DPF (e.g. Euro 6) to cars without DPF (e.g. EURO 3) shows a reduction of 99.95%. EURO VI HDV have similar low PN emissions per km as the diesel passenger cars
- CO₂ emissions of HDVs show an average annual reduction of 0.78% from EURO 0 to EURO VI.

- NOx emission reduction for HDVs became more and more effective over the last years due to stricter limits and test cycles which cover a broader area of the engine map. The introduction of EURO VI led to even further reductions due to the implementation of on-board tests.
- Electrification of LDVs show a CO₂ saving potential of about 35% for PHEVs compared to conventional propulsion systems. BEVs showed approx. 40% CO₂ reduction compared to comparable diesel cars, provided an average EU power plant mix is used to assign CO₂ emissions to electric energy. Emissions related to fuel supply, vehicle and battery production are not considered in these numbers. However, in the current BEV fleet, high powered vehicles with large electric range and thus heavy batteries do not provide much overall CO₂ reduction when using electricity according to the average EU power plant mix.

Thus, achievement of future CO₂ targets for the transport sector needs the use of higher shares of renewable energies, the permanent monitoring of gaps between type approval and real-world energy consumption, prompter adjustments of test procedures and also an accounting of CO₂ related to electric energy consumption to incentivize fleet penetration of energy efficient PHEV and BEV vehicles.

Acknowledgements

The authors would like to acknowledge the contribution of Umweltbundesamt Germany and Umweltbundesamt Austria to the work and to the funding of projects for updating the HBEFA. We also want to thank Mario Keller and Benedikt Notter (Infras) for the access to the ERMES db and for all the related support. Heinz Steven is thanked for the support and the update of the driving cycles for HBEFA 4.1.

References

- EEA (2018): Monitoring of CO₂ emissions from passenger cars – Regulation (EC) No 443/2009, <https://www.eea.europa.eu/data-and-maps/data/co2-cars-emission-14>
- Hausberger S. (2003): Simulation of Real World Vehicle Exhaust Emissions, *VKM-THD Mitteilungen*, Heft/Volume 82, Verlag der Technischen Universität Graz, ISBN 3-901351-74-4, Graz, Austria
- Hausberger S., Rexeis M., Luz R. (2012): New Emission Factors for EURO 5 & 6 Vehicles, TAP conference 2012, Thessaloniki, Greece
- Lipp S., Hausberger S., Schreiber L. (2017): Measurement and simulation of hybrid and plug in hybrid vehicles for the handbook of emission factors, TAP conference 2017, Zurich, Switzerland
- Matzer C., Hausberger S., Lipp S., Rexeis M. (2016): A new approach for systematic use of PEMS data in emission simulation, TAP conference 2016, Lyon, France
- Matzer C., Hausberger S., et.al. (2017): Update of Emission Factors for EURO 6 Diesel Passenger Cars for the HBEFA, TAP conference 2017, Zurich, Switzerland
- Matzer C., Hausberger S. (2017): Update of Emission Factors for EURO 4, EURO 5 and EURO 6 Diesel Passenger Cars for the HBEFA Version 3.3, Rep.No. I-09/17/ CM EM 16/26/679, IVT of TU Graz, Graz, Austria
- Mock P., Tietge U., et.al. (2014): From laboratory to road, A 2014 update of official and „real-world“ fuel consumption and CO₂ values for passenger cars in Europe, International Council on Clean Transportation Europe, Berlin, Germany
- Rexeis M., Quaritsch M., Hausberger S., Silberholz G., Steven H., Goschütz M., Vermeulen R. (2017): VECTO tool development: Completion of methodology to simulate Heavy Duty Vehicles' fuel consumption and CO₂ emissions, Final Report By order of EUROPEAN COMMISSION DG CLIMA, Rep.No. I 15/17/Rex EM-I 2013/08 1670, IVT of TU Graz, Graz, Austria
- Weller K., Rexeis M., Hausberger S., Zach B. (2016): A comprehensive evaluation method for instantaneous emission measurements. TAP conference 2016, Lyon, France

2.1.2 Euro 3 and Euro 5 Diesel vehicles' particles evolution in ageing chamber

B. Vansevenant¹, Y. Liu^{1}, C. Ferronato², L. Fine², P. Tassel¹, C. Louis³ and M. André³*

¹ Univ Lyon, IFSTTAR, AME, EASE, Bron, 69675, France, yao.liu@ifsttar.fr

² Univ Lyon, Université Claude Bernard Lyon 1, CNRS, IRCELYON, F-69626, Villeurbanne, France

³ Univ Lyon, IFSTTAR, AME, Bron, 69675, France

Introduction

Air quality and atmospheric pollution are more than ever major societal concerns which have impacts on climate (IPCC, 2013), agriculture, visibility and public health. Aerosols in urban areas lead to a great number of hospitalizations and to premature deaths. The International Agency for Research on Cancer (IARC) classified diesel engines exhausts as group 1 carcinogen for humans in 2012. Since 1996, mass concentrations of aerosols below 10 μm in diameter (PM_{10}) and 2.5 μm ($\text{PM}_{2.5}$) are regulated. Annual mean concentrations are limited to 40 $\mu\text{g}\cdot\text{m}^{-3}$ and 25 $\mu\text{g}\cdot\text{m}^{-3}$, respectively. However, particle concentrations are still high in spite of regulations acting on their emissions.

Vehicular emissions are well known when it comes to regulated compounds. However, unregulated pollutants are also emitted by diesel and gasoline engines in the gas or particle phase. Some of those unregulated emissions are Secondary Organic Aerosols (SOA) precursors, such as volatile, intermediate volatility and semi volatile organic compounds (VOCs, IVOCs and SVOCs) (Kleindienst et al., 2004; Caplain et al., 2006; Camredon et al., 2007; Ng et al., 2007; Ravindra et al., 2008; Shakya and Griffin, 2010; Kim et al., 2016; Louis et al., 2016). In spite of the number of articles on this topic, a great uncertainty remains in quantifying the emissions of primary particles and SOA precursors, and in the characterization of their role in SOA formation. The uncertainty is induced in part by quantification difficulties since SOA precursors dynamically partition between the gas and particle phase, with a great dependence on sampling methodology (Kim et al., 2016). Some studies have shown that cooling and dilution conditions greatly influence SOA formation, due to condensation or nucleation of particle precursors (Morawska et al., 2008; Mamakos et al., 2011; Mamakos and Martini, 2011; Kozawa et al., 2012; May et al., 2013). May et al. (2013) tested light-duty gasoline vehicles on the cold start unified cycle, and showed that low dilution levels in a constant volume sampler system would create particle mass concentrations at least 10 times greater than typical ambient levels. Moreover, the motorization with different exhaust after-treatment technologies also influences particle and precursor emissions, and SOA formation, but with contradictory results. Gentner et al. (2012) estimates that diesel vehicles are responsible for 65 to 90% of the SOA formation due to road traffic in California, while other studies indicate that gasoline vehicles should have a bigger impact (Bahreini et al., 2012; Platt et al., 2013; Gordon et al., 2014). Currently, the VOCs, IVOCs and SVOCs are not regularly followed and their emission factors are rarely measured. Their emission factors for several exhaust after-treatment technologies or vehicle categories are missing from inventories. As a consequence, the database is not complete for most vehicles of the fleet. This prevents a good understanding of air quality by different models. With evolution of the fleet composition due to European regulations, the influence of the exhaust after-treatment technologies on the emissions, especially the particle precursor emissions should be investigated. In addition to the lack of knowledge on particle precursor emissions, the processes leading to SOA formation are not completely clear. Several processes play an important role on SOA formation, such as photochemistry, oxidation, condensation/evaporation, nucleation and coagulation (Kleindienst et al., 2004; Camredon et al., 2007; Hallquist et al., 2009; Platt et al., 2013; Gordon et al., 2014; Seinfeld and Pandis, 2016). Determining the role of each of these processes is complex and requires additional studies on the ageing of vehicular aerosols in different conditions. Many of these studies simulate conditions of photochemistry experiments, but the specific role of physical processes has rarely been studied alone. Overall, the complexity of the physical and photochemical processes influencing SOA formation, together with - methodological difficulties on particle and precursor quantification, lack of emission factors for the fleet, and the diversity of atmospheric and technological parameters - leads to a great uncertainty remaining on the contribution that road traffic plays on atmospheric pollution.

This study investigates the physical evolution of particles emitted by Euro 3 and Euro 5 passenger cars, with diesel motorization that represents 67% of the French fleet. The goal is to better

understand the specific role that physical processes play on SOA formation. Emission factors of organic compounds are measured and characterized based on their volatility. Different driving conditions are tested in order to investigate their impact on SOA formation. Finally, impacts of Euro 3 without particle filter and Euro 5 with catalysed particle filter vehicles are discussed with a consideration for the current French passenger car fleet.

Experimental setup

Two diesel passenger cars were tested on a chassis dynamometer. Vehicle #1 was a Euro 5 diesel car, equipped with a catalysed diesel Particle Filter (cat. DPF), and vehicle #2 was a Euro 3 car. Detailed characteristics of the vehicles are given in Table 1.

Table 1: Characteristics of the vehicles.

	Vehicle #1	Vehicle #2
Engine	1.3 VCDI	1.9 JTD
Energy	Diesel	Diesel
European norm	Euro 5	Euro 3
Catalyst	DOC	DOC
Filter	Cat. DPF	

Vehicles were tested in two driving conditions: Artemis Urban Cold Start (UC) cycle, and Artemis Motorway (MW) cycle. During a driving cycle, exhaust gas is injected into two sampling ways simultaneously (Figure 1): a) Constant Volume Sampler (CVS) at $9 \text{ m}^3 \cdot \text{min}^{-1}$, and b) ageing chamber (8 m^3) through a 4-meter-long stainless steel line heated at 120°C . Exhaust gas is injected into the ageing chamber through the heated line by a Dekati DI-1000 diluter and dry clean air heated at 120°C . The dilution ratio is around 8 for the Dekati diluter. Injections into the chamber last 16 and 25 min at $42 \text{ L} \cdot \text{min}^{-1}$ for UC and MW cycles respectively, leading to respective global dilution ratios of 97 and 65.

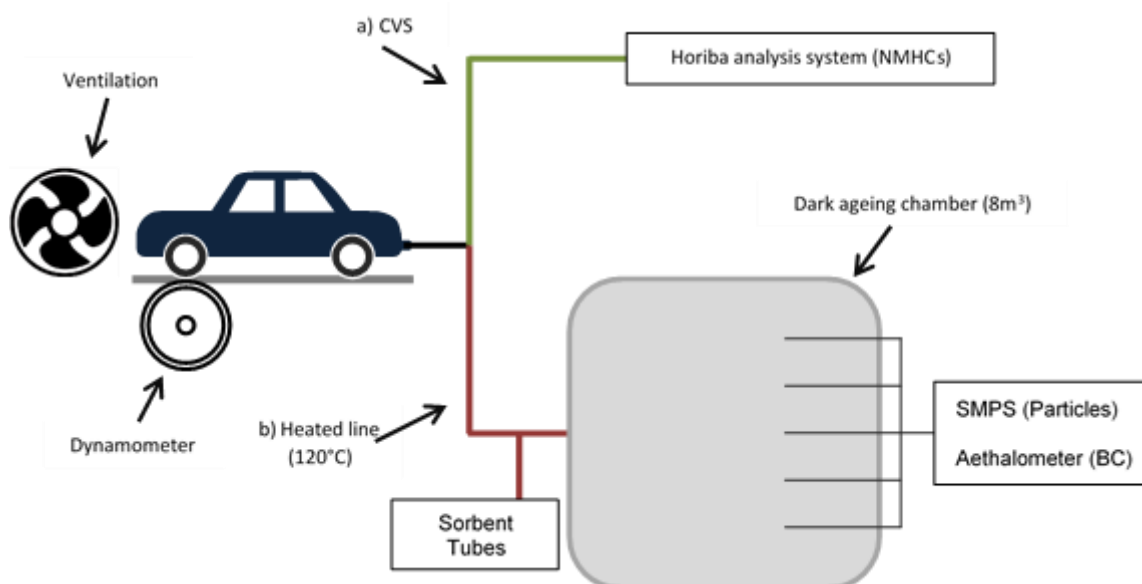


Figure 1: Scheme of the experimental setup.

- Emission measurements

VOCs and IVOCs are collected from the heated line by sampling diluted exhaust through stainless steel tubes filled with Tenax TA at a flow rate of $50 \text{ mL} \cdot \text{min}^{-1}$. The samples are collected during

the entire driving cycle. Two adsorbent tubes are connected in series to control if breakthrough of the sorbent happened. No IVOC was measured on the second tube. Collected samples are further analysed by automatic thermal desorption coupled with gas chromatography-mass spectrometry detector (ATD-GC-MS), using the Markes Unity thermodesorber and a GC6890 gas chromatograph from Agilent fitted with the MS5973 mass spectrometer from Agilent. The thermal desorption system consists in a two stage desorption. During the first desorption step, the compounds are desorbed by heating the Tenax TA under a stream of helium and are condensed on a trap filled with adsorbent and maintained at -5 °C. During the second desorption, the second trap is flash-heated to 300 °C for a rapid introduction of the compounds into the chromatographic column. The chromatographic column used is an Agilent HP1MS 30 m x 0.25 mm, 0.25 µm. The mass spectrometer operates in scanning mode at an electron ionization of 70 eV. Mass spectral data are acquired over a mass range of 33-450 amu. Qualitative identification of compounds is based on the match of the retention time and confirmed by matching their mass spectra with those of standards and from the NIST mass spectral library. Quantification is conducted by the external standard method. Known amount (1 µL) of standards solutions of VOCs and IVOCs are introduced into cleaned Tenax TA tubes, using an automatic heated GC injector. The calibration tubes are analyzed in the same conditions as mentioned before. The chromatogram show an unresolved complex mixture, mainly composed of co-eluted hydrocarbons which cannot be further separated by a single-dimensional GC. The alkanes (linear and branched) are quantified by SIR-based response factor of these compounds using the fragment of $m/z=57$. For the aromatic, the fragment m/z 78 was used for benzene, 91 for alkylbenzenes. The fragments m/z 84 and 83 were used for the quantification of cyclohexane and of the other cyclic compounds respectively.

Non-methane hydrocarbon concentrations are measured after the CVS by flame ionization detector with a Horiba analysis system.

- Ageing chamber measurements

The temperature, relative humidity and pressure in the chamber are monitored for all experiments. For the physical ageing of the particles, all experiments are carried out in a dark chamber, without any exposition to natural or artificial lights. The chamber is operated at a slight over pressure (5 Pa) in order to avoid contamination from the outside. Concentrations of black carbon (BC) and particle number with size distribution are measured during 10 hours.

The BC concentration was measured using an AE33-7 Aethalometer from Magee Scientific. Aerosol sample is collected at 2 L.min⁻¹ on filter tape. Attenuation of transmitted light is continuously measured at different wavelengths from UV to IR (370, 470, 520, 590, 660, 880, 950 nm). Black carbon concentration is given by absorption measurements at 880 nm (Andreae and Gelencser, 2006). Concentrations between 10 and 10⁵ ng.m⁻³ can be measured, with a detection limit at 1 hour of 5 ng.m⁻³. Acquisition data is given with a time-scale of one minute.

Particle concentrations and distributions are measured with a Scanning Mobility Particle Sizer (SMPS) from TSI, composed of a Differential Mobility Analyzer (DMA) column, a Condensation Particle Counter (CPC) and a radioactive sealed source. Air is sampled at 0.3 L.min⁻¹, and goes through an inertial impactor that removes aerosols too large for the DMA column. Then, sampled air passes through a bipolar neutralizer with a β source in order to bring particles in a known charge state. The aerosol flow is then mixed to a dry, laminar sheath flow towards the DMA column. Particles with diameter between 14 and 615 nm are classified depending on their electrical mobility Z_p , which is a function of their diameter D_p and their charge q : $Z_p \propto q/D_p$, and counted by a CPC. Moreover, by applying an arbitrary density to the particles - considered spherical - their mass distribution can be calculated. In this study, a density of 1.2 was applied (Barone et al., 2011; Totton et al., 2010). Data is given with a 5-minute time scale, with a 5% analytic uncertainty.

Each emission and chamber experiment was repeated 2 or 3 times under similar experimental conditions. The pollutant concentrations at emission and during evolutions showed good repeatability. Specific experimental conditions are given in Table 2.

Table 2: Experimental conditions.

Vehicle	Cycle	Emission		Chamber			Repetitions
		Sorbent tubes	Volume (mL)	Injection time (min)	Global dilution ratio	Initial RH (%)	
Diesel Euro5	Urban cold start	Tenax TA	760	16	96.68	1.8	2
Diesel Euro5	Motorway	Tenax TA	1188	25	65.22	3.4	2
Diesel Euro3	Urban cold start	Tenax TA	760	16	96.68	1.6	2
Diesel Euro3	Motorway	Tenax TA	1188	25	65.22	3.1	3

Results and discussion

- Chamber characterization

Within the chamber, concentrations of pollutants are affected by leakage, dilution and wall-loss deposition. For particle mass (PM), the concentrations were corrected with the decay of the BC concentration (BC is considered to be inert). Its decay depends only on leakage, dilution and wall losses. The [BC] evolution in the chamber has an exponential decay during experiments, which can be expressed as $[BC]_t = [BC]_0 \times e^{-kt}$. Overall experiments, the average decay coefficient k was found to be:

$$k = (1.83 \pm 0.15) \times 10^{-3} \text{ min}^{-1} \quad (\text{Equation 1})$$

As BC is in the particle phase, it follows the same evolution as particles, faced with leakage, dilution and wall losses. The coefficient was therefore used to correct both PM and BC concentrations. Moreover, in order to get a good homogenization in the chamber after injection, all measurements start 20 min after the end of the injection. Figure 2 shows an example of the time evolution of the [BC] inside the chamber during injection, homogenization and the 10h evolution (black dots), for UC driving condition with the Euro 5 cat. DPF vehicle. [BC] corrected for dilution, leakage and wall-loss deposition according to Equation 1 is also presented (red triangles). After correction, the [BC] remains stable.

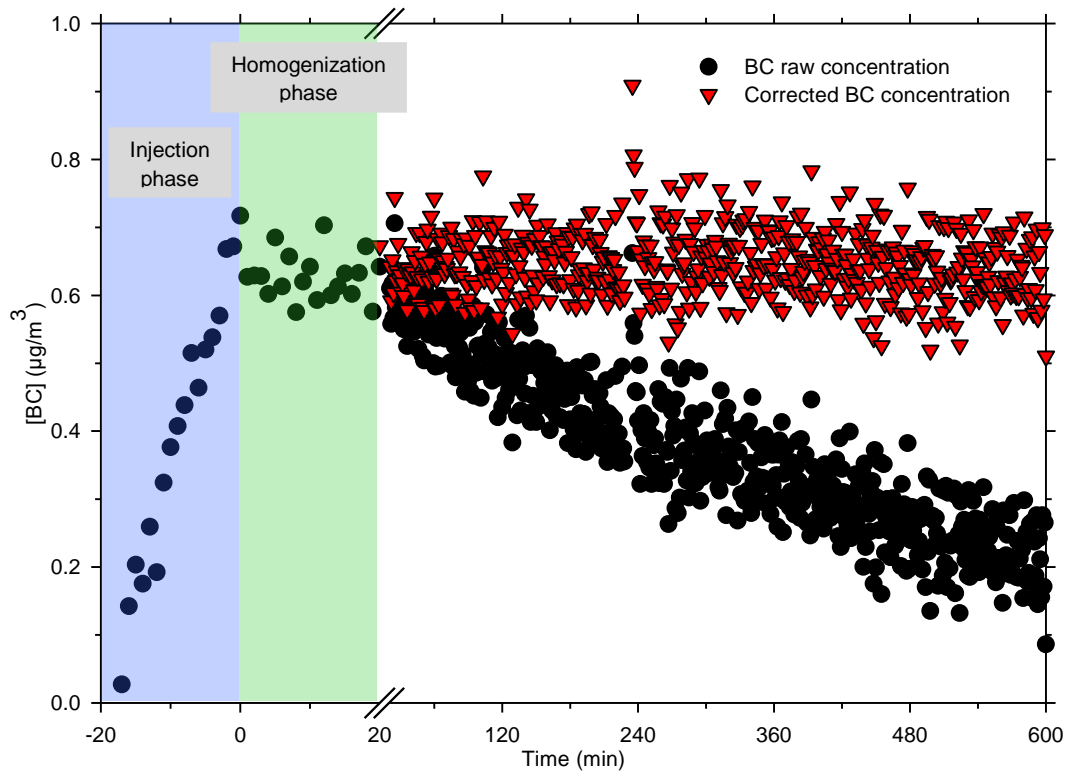


Figure 2: Evolution of the BC concentration, during injection (blue), homogenization (green), and the 10h evolution (white). Black dots: raw [BC] data; red triangles: [BC] corrected for leakage, dilution and wall losses.

- Particle evolution

Figure 3 shows the total [PM] evolution in the chamber after corrections for the Euro 3 diesel vehicle (a) and the Euro 5 diesel vehicle with cat. DPF (b). The corrected total [PM] during 10h are presented for Artemis motorway (red dots) and urban cold start (black triangles) driving conditions.

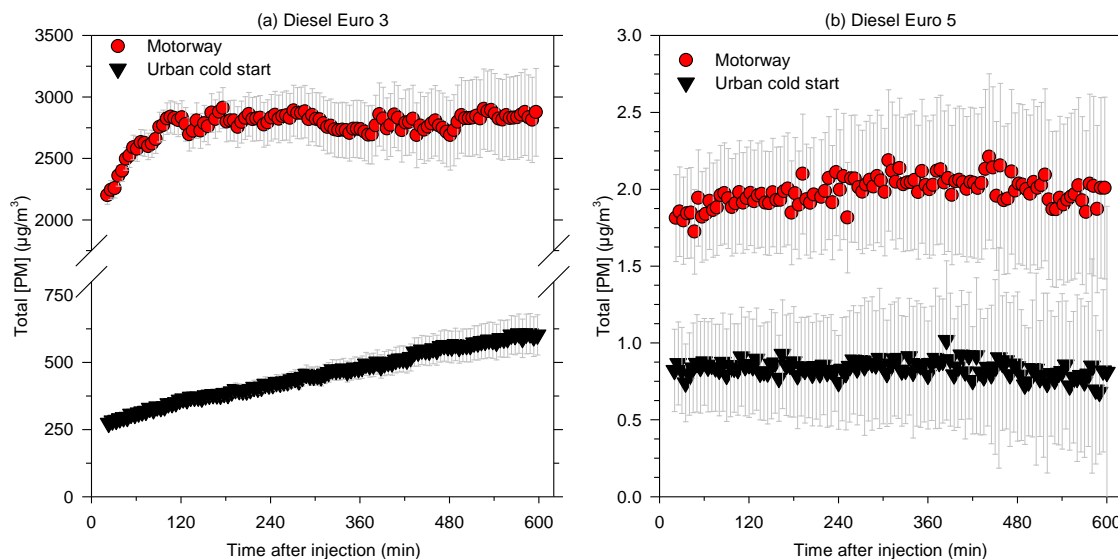


Figure 3: Total PM evolution after correction during 10h under motorway (black) and urban cold start (red) conditions, for the Euro 3 (a) and Euro 5 cat. DPF (b) vehicles.

Figure 3 shows that the Euro 3 vehicle emits between 250 (UC) and 1000 (MW) times more PM than the Euro 5 cat. DPF vehicle. For the Euro 3 in UC condition, initial PM concentration is $270 \mu\text{g}\cdot\text{m}^{-3}$, and increases continuously during 10 hours, up to $607 \mu\text{g}\cdot\text{m}^{-3}$. PM increases of 125% in 10 hours. In MW condition, initial PM concentration is $2200 \mu\text{g}\cdot\text{m}^{-3}$. It increases rapidly of 29% during 90 minutes, up to $2800 \mu\text{g}\cdot\text{m}^{-3}$. Then, it remains stable. For the Euro 5 vehicle, initial PM concentration is around $0.8 \mu\text{g}\cdot\text{m}^{-3}$ in UC condition, and $1.8 \mu\text{g}\cdot\text{m}^{-3}$ in MW condition. It remains steady with uncertainty in UC conditions, and seems to have a very slight increase tendency in MW condition during 200 min, going from 1.8 to $2 \mu\text{g}\cdot\text{m}^{-3}$.

The particle size was also monitored during the experiments, for both vehicles, in MW and UC conditions. The size range most commonly found in the distribution is given by the main mode (a secondary mode is found on a bimodal distribution); their evolution is presented in Figure 4. The PN modes of the Euro 3 vehicle (110 and 170 nm) are higher than those of the Euro 5 (19 and 70 nm). For the Euro 3 vehicle (Figure 4(a)) in UC condition (black triangles), the initial main mode increases continuously with time from 110 nm to 270 nm after 10 hours of evolution. In MW condition (red dots), the initial mode is at 170 nm, and increases during the first 3.5 hours up to 350 nm. Between 3.5h and 10h, larger particles are more concentrated, and the mode remains stable around 450 nm (measurement values are not affected by saturation). For the Euro 5 vehicle (Figure 4(b)), the particle number concentrations in the UC condition (black triangles) are close to the background limits, and do not show a clear mode. As a consequence, the mode evolution is not analysed here. In MW condition (in red), measurements show a bimodal distribution, with a main and secondary modes. Initially, the main mode is at 19 nm (red dots), and is due to the regeneration of the DPF. This regeneration occurred once during 430 sec, and induced emissions of total hydrocarbons 9 times higher than during the same driving phase without regeneration. Similar results have been observed by Louis et al. (2016). They showed that small particles with diameter < 40 nm were emitted during DPF regenerations from Euro 5 diesel vehicles. This main mode increases steadily over the experiment and reaches 27 nm after 10 hours. The second mode is at 71 nm (red crosses). It increases slightly and continuously up to 85 nm.

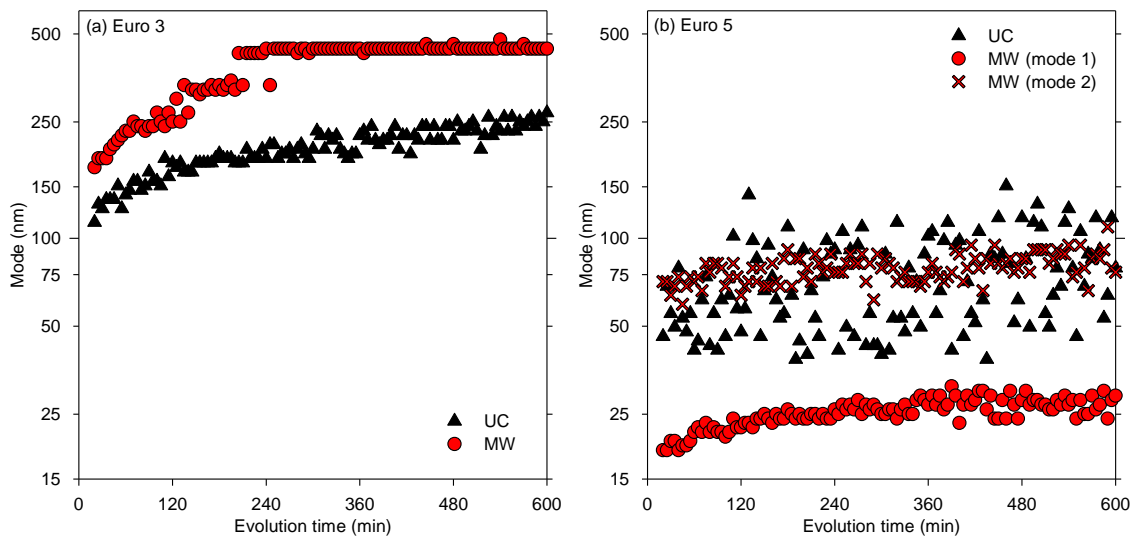


Figure 4: Evolution of the mode during 10 hours for the Euro 3 (a) and the Euro 5 cat. DPF (b) vehicles, in both UC (black) and MW (red) conditions. The MW Euro 5 condition ((b), in red) shows a bimodal distribution, referred to as “mode 1” (dots) and “mode 2” (crosses).

The increase of [PM] and the particle growth can be explained by physical phenomena such as nucleation, coagulation and condensation. Depending on the initial particle and precursor concentrations in the chamber, and particle size, different physical processes can occur and explain the evolutions presented in Figure 3 and Figure 4. To further investigate these phenomena, the particle number (PN) size distribution has been analysed. Figure 5 shows evolutions of PN concentrations (in $dN/d\log D_p$ scale) of small particles with size range between 14.1 and 40 nm, for the Euro 5 cat. DPF vehicle in MW condition. Evolutions of the particles are shown for three groups: 14.1-21.7 nm (a), 22.5-24.1 nm (b), and 25-40 nm (c). Blue dashed lines indicate the time after the end on injection for which the [PN] of the corresponding size is at its maximum.

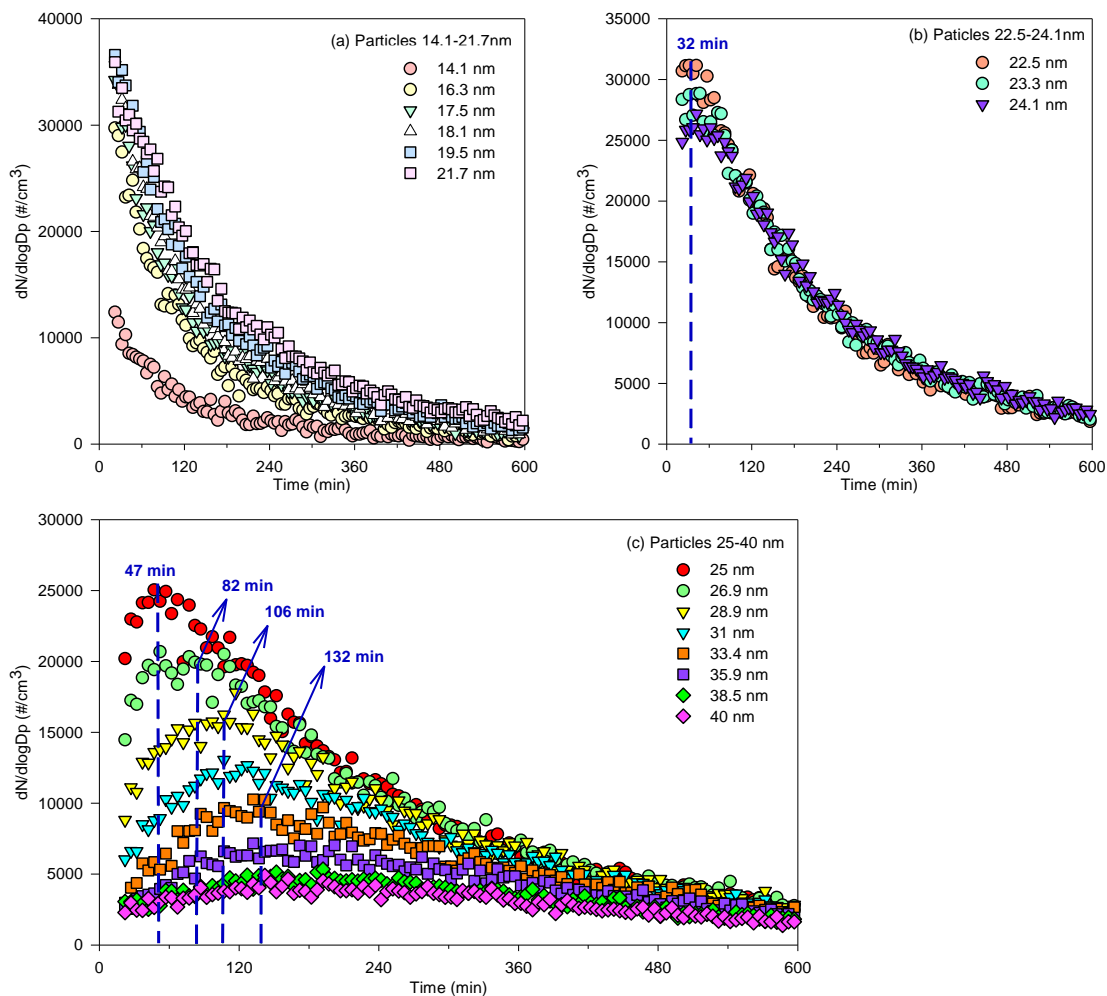


Figure 5: Time evolution of particles for the Euro 5 cat. DPF diesel vehicle in MW condition. Evolutions are given for particles of diameters between 14.1 and 21.7 nm (a), 22.5 and 24.1 nm (b), and 25 and 40 nm (c). Blue dashed-lines indicate the time for which the particle number of a specific size range is at its maximum.

Figure 5 shows that concentrations of particles under 21.7 nm (a) decrease during the experiment. Concentrations of particles between 22.4 and 24.1 nm (b) increase during the first 32 min after injection, and then decrease. Similar behaviours are observed for bigger particles (c). The particle growth time increases from 32 to 132 min with the increase of particle diameters (from 22 to 33 nm). The diminution of the smaller particles with the larger particle formation might be explained in part by the coagulation process in these conditions (initial concentration around 10^4 #.cm^{-3} , main mode around 19 nm). This observation is in agreement with Seinfeld and Pandis (2016), who give characteristic coagulation times varying between 30 and 450 minutes for an initial PN concentration of $5 \cdot 10^4 \text{ #.cm}^{-3}$. Moreover, nucleation and condensation processes might also explain the particle growth observed on Figure 3 and Figure 4, with the slight increase of PM during the first 200 min under MW condition. However, since Euro 5 cat. DPF particles are small, it is natural that their contribution to PM is low.

For the Euro 3 vehicle, initial particle concentrations are of the order of 1.0×10^5 and $2.4 \times 10^5 \text{ #.cm}^{-3}$ in UC and MW conditions respectively, with modes around 110 and 170 nm. The characteristic coagulation time varies between 75 and 220 minutes (Seinfeld and Pandis, 2016). Those conditions are also likely to enhance the condensation process with the increase of total PM (Figure 3). Condensation of organic matter onto pre-existing particles would also induce an increase of the mode, which is observed in Figure 4. For Euro 5 and Euro 3 vehicles, it seems that different physical processes might be predominated during particle ageing. Since nucleation

and condensation phenomena can only occur in the presence of organic matter, concentrations of several VOCs and IVOCs were measured at emission for both vehicles.

- Quantification of organic matter at emission

The organic compounds were sampled on cartridges at emission at 120°C. Table 3 gives the emission factors (EFs) of alkanes, single-ring aromatics, cyclic compounds and NMHCs, for both vehicles in UC and MW conditions. Alkanes are divided into two subcategories based on their volatilities, according to Zhao et al. (2016). Alkanes (linear and branched) from C6-C11 are VOCs, and those from C12-C22 are IVOCs. Table 3 also gives the IVOCs/NMHCs ratio.

Table 3: Emission factors (EFs) of alkanes, single-ring aromatics, cyclic compounds and non-methane hydrocarbons (NMHCs), for the Euro 3 and the Euro 5 cat. DPF vehicle in both UC and MW conditions. EFs are expressed in mg.km⁻¹.

	Euro 5 UC	Euro 5 MW	Euro 3 UC	Euro 3 MW
VOCs	8.6 ± 2.0	0.12 ± 0.03	2.2 ± 0.1	1.52 ± 0.03
IVOCs	0.8 ± 0.1	0.24 ± 0.03	1.3 ± 0.3	1.5 ± 0.1
Single-ring aromatics	0.7 ± 0.1	0.01 ± 0.01	0.60 ± 0.03	0.13 ± 0.01
Cyclic compounds	2.3 ± 0.6	0.02 ± 0.01	0.8 ± 0.1	0.40 ± 0.01
Total	12.4 ± 2.7	0.4 ± 0.1	4.9 ± 0.3	3.6 ± 0.1
NMHCs	57	2	103	23
IVOCs/NMHCs (%)	1.4	12	1.2	6.5

Results show that for the MW cycles, IVOCs EFs are 0.24 and 1.5 mg.km⁻¹ for the Euro 5 and the Euro 3 vehicle, respectively. In UC condition, IVOCs EFs are 0.8 and 1.3 mg.km⁻¹ for the Euro 5 and the Euro 3 vehicles, respectively. In both cases, the Euro 3 diesel vehicle emits more IVOCs than the Euro 5. Table 3 also shows that the Euro 3 vehicle emits more single-ring aromatics (0.13 mg.km⁻¹) than the Euro 5 vehicle (0.01 mg.km⁻¹) in the MW condition. The IVOCs/NMHCs ratio is 1.4% (UC) and 12% (MW) for the Euro 5 vehicle, 1.2% (UC) and 6.5% (MW) for the Euro 3. In UC condition, the mean IVOCs/NMHCs ratio is of the same order as the one found by Zhao et al. (2016) (4% ± 2%) for gasoline vehicles on a cold start unified driving cycle. In MW condition, the IVOCs/NMHCs ratio is 5 (Euro 3) and 9 (Euro 5) times higher than in UC condition. According to Zhao et al. (2016), single-ring aromatics and IVOCs are important precursors of SOA. The higher emissions of those precursors from the Euro 3 vehicle could explain in part, with the condensation process, the formation of SOA observed in Figure 3.

- Discussion

Particle precursor emissions and SOA formation with only physical processes from Euro 3 and Euro 5 diesel vehicles are discussed in this section, in regards to the current French passenger car (PCs) fleet (Figure 6).

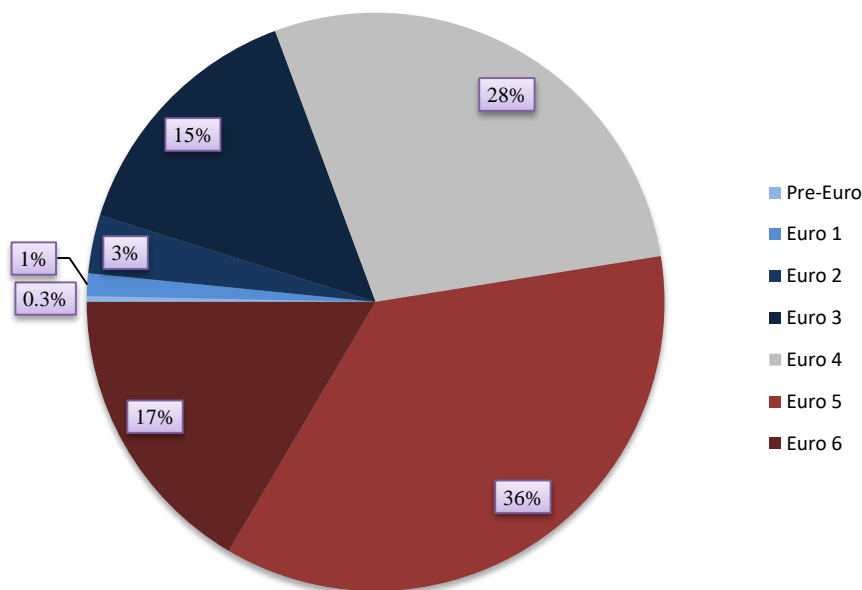


Figure 6: French fleet in 2017 for diesel-engined PCs. Pre-Euro to Euro 3 vehicles are in shades of blue, Euro 4 vehicles in grey, and Euro 5 and Euro 6 vehicles in shades of red.

Figure 6 shows the French passenger car fleet partitioning for diesel vehicles with respect to European norms. The first subcategory (in blue) includes diesel vehicles that do not have a particle filter (pre-Euro to Euro 3). The second subcategory (in red) includes diesel vehicles that have a particle filter (Euro 5 and Euro 6). Euro 4 vehicles are not taken into consideration, as they can either have or not have a particle filter. diesel PCs of the Pre-Euro to Euro 3 category represent only 19% of the diesel PCs fleet, against more than half (53%) for Euro 5&6 Diesel PCs. However, as discussed previously, PM emitted by the Euro 3 vehicle are 250 (UC) and 1000 (MW) times higher than for the Euro 5 cat. DPF vehicle. In addition to that, IVOCs EFs are between 1.6 and 6.2 times higher for the Euro 3 vehicle than for the Euro 5, which leads to 125% (UC) and 29% (MW) of PM increase during the 10 hours of ageing for the Euro 3 vehicle. Pre-Euro to Euro 3 vehicles could therefore have a significant impact on air quality even though they represent only a small fraction of the fleet.

Conclusion

This study investigated the time evolution in a dark ageing chamber of particles emitted by a diesel Euro 3 and a diesel Euro 5 cat. DPF vehicles, in urban cold start and motorway conditions. Results showed that the Euro 3 vehicle emitted more PM than the Euro 5 vehicle. In addition to higher PM emissions, total particle mass for the Euro 3 vehicle increased of 125% in 10 hours in UC conditions, and of 29% in 90 minutes in MW conditions. However, for the Euro 5 cat. DPF vehicle, total particle mass remained stable in UC conditions, and showed a very slight increase tendency in MW conditions. The PN distribution evolution showed the particle growth with an increase of the mode for both vehicles. For the Euro 5 vehicle in MW conditions, a bimodal distribution was observed. The evolution of the small particles seemed to be mainly due to coagulation processes. Nucleation and condensation could also affect particle ageing, but with a low impact on total PM as the particles are small, and have a weak contribution to particle mass. For the Euro 3 vehicle, the high PM increase observed in both conditions indicated that the condensation process could be predominant in the particle evolution. Presence of SOA precursors (VOCs and IVOCs) in the tailpipe exhaust confirms that nucleation and condensation processes could occur and participate in the formation of SOA. Considering high particle and precursor emissions for the Euro 3 vehicle, and SOA formation of 125% (UC) and 29% (MW), the impact of older diesel passenger cars on air quality could be significant, even though they only represent 19% of the fleet.

Acknowledgements

This work was supported by the French Environment and Energy Management Agency (ADEME).

Submission

We would like to consider our work for inclusion in the special issue of *Atmospheric Environment*.

References

- Andreae, M.O., Gelencser, A., 2006. Black carbon or brown carbon? The nature of light-absorbing carbonaceous aerosols, *Atmos. Chem. Phys.*, 18.
- Bahreini, R., Middlebrook, A.M., de Gouw, J.A., Warneke, C., Trainer, M., Brock, C.A., Stark, H., Brown, S.S., Dube, W.P., Gilman, J.B., Hall, K., Holloway, J.S., Kuster, W.C., Perring, A.E., Prevot, A.S.H., Schwarz, J.P., Spackman, J.R., Szidat, S., Wagner, N.L., Weber, R.J., Zotter, P., Parrish, D.D., 2012. Gasoline emissions dominate over diesel in formation of secondary organic aerosol mass: GASOLINE DOMINATES SOA FORMATION, *Geophysical Research Letters*, 39, n/a-n/a. <https://doi.org/10.1029/2011GL050718>
- Barone, T.L., Lall, A.A., Storey, J.M.E., Mulholland, G.W., Prikhodko, V.Y., Frankland, J.H., Parks, J.E., Zachariah, M.R., 2011. Size-Resolved Density Measurements of Particle Emissions from an Advanced Combustion Diesel Engine: Effect of Aggregate Morphology, *Energy & Fuels*, 25, 1978–1988. <https://doi.org/10.1021/ef200084k>
- Camredon, M., Aumont, B., Lee-Taylor, J., Madronich, S., 2007. The SOA/VOC/NO_x system: an explicit model of secondary organic aerosol formation, *Atmos. Chem. Phys.*, 12.
- Caplain, I., Cazier, F., Nouali, H., Mercier, A., Déchaux, J.-C., Nollet, V., Joumard, R., André, J.-M., Vidon, R., 2006. Emissions of unregulated pollutants from European gasoline and diesel passenger cars, *Atmospheric Environment*, 40, 5954–5966. <https://doi.org/10.1016/j.atmosenv.2005.12.049>
- Gentner, D.R., Isaacman, G., Worton, D.R., Chan, A.W.H., Dallmann, T.R., Davis, L., Liu, S., Day, D.A., Russell, L.M., Wilson, K.R., Weber, R., Guha, A., Harley, R.A., Goldstein, A.H., 2012. Elucidating secondary organic aerosol from diesel and gasoline vehicles through detailed characterization of organic carbon emissions, *Proceedings of the National Academy of Sciences*, 109, 18318–18323. <https://doi.org/10.1073/pnas.1212272109>
- Gordon, T.D., Presto, A.A., May, A.A., Nguyen, N.T., Lipsky, E.M., Donahue, N.M., Gutierrez, A., Zhang, M., Maddox, C., Rieger, P., Chattopadhyay, S., Maldonado, H., Maricq, M.M., Robinson, A.L., 2014. Secondary organic aerosol formation exceeds primary particulate matter emissions for light-duty gasoline vehicles, *Atmospheric Chemistry and Physics*, 14, 4661–4678. <https://doi.org/10.5194/acp-14-4661-2014>
- Hallquist, M., Wenger, J.C., Baltensperger, U., Rudich, Y., Simpson, D., Claeys, M., Dommen, J., Donahue, N.M., George, C., Goldstein, A.H., Hamilton, J.F., Herrmann, H., Hoffmann, T., Iinuma, Y., Jang, M., Jenkin, M.E., Jimenez, J.L., Kiendler-Scharr, A., Maenhaut, W., McFiggans, G., Mentel, T.F., Monod, A., Prevot, A.S.H., Seinfeld, J.H., Surratt, J.D., Szmigielski, R., Wildt, J., 2009. The formation, properties and impact of secondary organic aerosol: current and emerging issues, *Atmos. Chem. Phys.*, 82.
- IPCC, 2013. Working Group I Contribution to the Fifth Assessment Report of the Intergovernmental Panel on Climate Change, *Cambridge University Press*, IPCC (International Panel on Climate Change), Cambridge, United Kingdom and New York, NY, USA.
- Kim, Y., Sartelet, K., Seigneur, C., Charron, A., Besombes, J.-L., Jaffrezo, J.-L., Marchand, N., Polo, L., 2016. Effect of measurement protocol on organic aerosol measurements of exhaust emissions from gasoline and diesel vehicles, *Atmospheric Environment*, 140, 176–187. <https://doi.org/10.1016/j.atmosenv.2016.05.045>
- Kleindienst, T.E., Conner, T.S., McIver, C.D., Edney, E.O., 2004. Determination of Secondary Organic Aerosol Products from the Photooxidation of Toluene and their Implications in Ambient PM 2.5, *Journal of Atmospheric Chemistry*, 47, 79–100. <https://doi.org/10.1023/B:JOCH.0000012305.94498.28>
- Kozawa, K.H., Winer, A.M., Fruin, S.A., 2012. Ultrafine particle size distributions near freeways: Effects of differing wind directions on exposure, *Atmospheric Environment*, 63, 250–260. <https://doi.org/10.1016/j.atmosenv.2012.09.045>
- Louis, C., Liu, Y., Tassel, P., Perret, P., Chaumont, A., André, M., 2016. PAH, BTEX, carbonyl compound, black-carbon, NO₂ and ultrafine particle dynamometer bench emissions for Euro 4 and Euro 5 diesel and gasoline passenger cars, *Atmospheric Environment*, 141, 80–95. <https://doi.org/10.1016/j.atmosenv.2016.06.055>
- Mamakos, A., Dardiotis, C., Marotta, A., Martini, G., Manfredi, U., Colombo, R., Sculati, M., Lijour, P.L., Lanappe, G., 2011. Particle Emissions from a Euro 5a Certified Diesel Passenger Car 36.

- Mamakos, A., Martini, G., 2011. Particle Number Emissions During Regeneration of DPF-equipped Light Duty Diesel Vehicles 16.
- May, A.A., Presto, A.A., Hennigan, C.J., Nguyen, N.T., Gordon, T.D., Robinson, A.L., 2013. Gas-particle partitioning of primary organic aerosol emissions: (1) Gasoline vehicle exhaust, *Atmospheric Environment*, 77, 128–139. <https://doi.org/10.1016/j.atmosenv.2013.04.060>
- Morawska, L., Ristovski, Z., Jayaratne, E.R., Keogh, D.U., Ling, X., 2008. Ambient nano and ultrafine particles from motor vehicle emissions: Characteristics, ambient processing and implications on human exposure, *Atmospheric Environment*, 42, 8113–8138. <https://doi.org/10.1016/j.atmosenv.2008.07.050>
- Ng, N.L., Kroll, J.H., Chan, A.W.H., Chhabra, P.S., Flagan, R.C., Seinfeld, J.H., 2007. Secondary organic aerosol formation from m-xylene, toluene, and benzene, *Atmos. Chem. Phys.*, 14.
- Platt, S.M., El Haddad, I., Zardini, A.A., Clairotte, M., Astorga, C., Wolf, R., Slowik, J.G., Temime-Roussel, B., Marchand, N., Ježek, I., Drinovec, L., Močnik, G., Möhler, O., Richter, R., Barmet, P., Bianchi, F., Baltensperger, U., Prévôt, A.S.H., 2013. Secondary organic aerosol formation from gasoline vehicle emissions in a new mobile environmental reaction chamber, *Atmospheric Chemistry and Physics*, 13, 9141–9158. <https://doi.org/10.5194/acp-13-9141-2013>
- Ravindra, K., Sokhi, R., Vangrieken, R., 2008. Atmospheric polycyclic aromatic hydrocarbons: Source attribution, emission factors and regulation, *Atmospheric Environment*, 42, 2895–2921. <https://doi.org/10.1016/j.atmosenv.2007.12.010>
- Seinfeld, J.H., Pandis, S.N., 2016, *Atmospheric chemistry and physics: from air pollution to climate change*.
- Shakya, K.M., Griffin, R.J., 2010. Secondary Organic Aerosol from Photooxidation of Polycyclic Aromatic Hydrocarbons, *Environ. Sci. Technol.*, 44, 8134–8139. <https://doi.org/10.1021/es1019417>
- Totton, T.S., Chakrabarti, D., Misquitta, A.J., Sander, M., Wales, D.J., Kraft, M., 2010. Modelling the internal structure of nascent soot particles, *Combustion and Flame*, 157, 909–914. <https://doi.org/10.1016/j.combustflame.2009.11.013>
- Zhao, Y., Nguyen, N.T., Presto, A.A., Hennigan, C.J., May, A.A., Robinson, A.L., 2016. Intermediate Volatility Organic Compound Emissions from On-Road Gasoline Vehicles and Small Off-Road Gasoline Engines, *Environmental Science & Technology*, 50, 4554–4563. <https://doi.org/10.1021/acs.est.5b06247>

2.1.3 Real world emission factors based on roadside increment concentrations of NO_x and CO₂

C. Johansson^{*1,2}, L. Burman², M. Norman² and M. Elmgren²

¹ Department of Environmental Science and Analytical Chemistry, Stockholm university, Stockholm, 106 91, Sweden

² Environment and Health Administration, SLB analys, Stockholm, 104 20, Sweden

christer.johansson@aces.su.se

Abstract

Knowledge of real world emission factors (EFs) is important when assessing efficiencies of actions to reduce impacts of traffic emissions on concentrations and exposure in urban areas. We have deployed continuous roadside measurements of NO_x, black carbon (BC) and CO₂ along a motorway. The increment in upwind – downwind concentrations between different sides of the motorway is due to the emissions from all vehicles passing the sites. The purpose is to compare the measured overall fleet emission factor with the corresponding emission factor calculated using the Handbook Emission Factors for Road Transport (HBEFA).

Automatic number plate camera recordings were obtained in parallel with the pollutant measurements. All recordings have been aggregated in 15 minute periods with detailed info on vehicle type (passenger car, light duty truck, bus etc) and emission standards (Euro class). Based on this information and specific EFs from HBEFA we can calculate the fleet average emission factors for all pollutants every 15 minutes. The ratio of the EF for each pollutant to CO₂ was compared with the measured pollutant concentration increment ratio. Assuming that the fleet average HBEFA CO₂ EF is correct we can also calculate absolute pollutant emission factors.

NO_x and CO₂ EFs based on HBEFA for the vehicle categories, weighted according to the Euro class distributions. We assumed different degrees of free flow and saturated traffic depending on the time of day. The overall NO_x/CO₂ ratio is 2.19 mg g⁻¹ as compared to the measured ratio of 3.28 mg g⁻¹. Multiplying the measured ratio with the HBEFA EF for CO₂ gives a NO_x emission factor of 0.62 g vkm⁻¹, which is 42% higher compared to the NO_x EF based on HBEFA. This assumes that the HBEFA CO₂ emission factor is correct.

The measured EFs for BC were a factor of 3 higher than the calculated for light duty vehicles and 20% lower than the calculated EF for heavy duty vehicles. The overall measured EF is a factor of 2 higher than the calculated EF.

Introduction

Knowledge of real world emission factors (EFs) is important when assessing efficiencies of actions to reduce impacts of traffic emissions on concentrations and exposure in urban areas. In Stockholm and in many other cities/countries in Europe the emission factors of Handbook Emission Factors for Road Transport (HBEFA, , version 3.3, Hausberger et al., 2009) is used. They are based on simulations using an emission model and validation based on a combination of real-world driving, remote sensing and dynamometer measurements. Several studies have reported comparisons between HBEFA and real-world emissions with varying degrees of agreement/disagreement (Chen and Borken-Kleefeld, 2014; Carslaw et al., 2011; Hueglin et al., 2006; Colberg et al., 2005).

The purpose of the present study was to compare real-world emission factors based on roadside stationary measurements with emission factors estimated for the vehicle fleet based on HBEFA.

Methods

We have deployed continuous roadside measurements of NO_x, black carbon (BC) and CO₂ along a motorway and at urban background and street. The increment in upwind – downwind concentrations between different sides of the motorway or between street and roof-top sites is due to the emissions from all vehicles passing the sites. The purpose is to compare the measured overall fleet emission factor with the corresponding emission factor calculated using the Handbook Emission Factors for Road Transport (HBEFA, version 3.3, Hausberger et al., 2009). For BC we applied the fraction BC of exhaust particles as reported in the TRANSPHORM project (Transphorm, 2017) and HBEFA for exhaust particle emissions.

NO_x and NO₂ was measured based on chemiluminescence using AC32M, Environnement SA., (France) and BC was measured based on light absorption using Aethalometers AE31, Magee Scientific (Berkely, USA). CO₂ was recorded by absorption of infrared light using CO12M, Environnement SA (France).

At both the motorway and street canyon site automatic number plate camera recordings were used to identify vehicles and extract information via the Swedish car registry (technique developed by Facility Labs Analytics, <http://facilitylabs.com/>). All recordings have been aggregated in 15 minute periods with detailed info on vehicle type (passenger car, light duty truck, bus etc) and emission standards (Euro class). Data on total traffic flow and vehicle speeds were also obtained from radar sensors as part of the Motorway Control System (MCS) of the Swedish Transport Administration.

Figure 1 shows the location of the measurements ca 4 m from the road with air intakes at 2 m above the road surface. Traffic flow and number plate recordings were made close to the measurement sites.



Figure 1: Left: Yellow dots indicates positions of the measurements at both sides of the highway (E18) North of Stockholm. Right: Instrument container below the traffic counting and vehicle recording cameras.

Results

Traffic and vehicle composition

Figure 2 shows the diurnal variation of the number of cars, light and heavy duty trucks and busses passing the measurement sites during 2018. In total there was 68 768 vehicles per day (annual mean value including weekdays and holidays) with 80% cars, 14% light duty trucks, 3.5% heavy duty trucks and 3.3% busses.

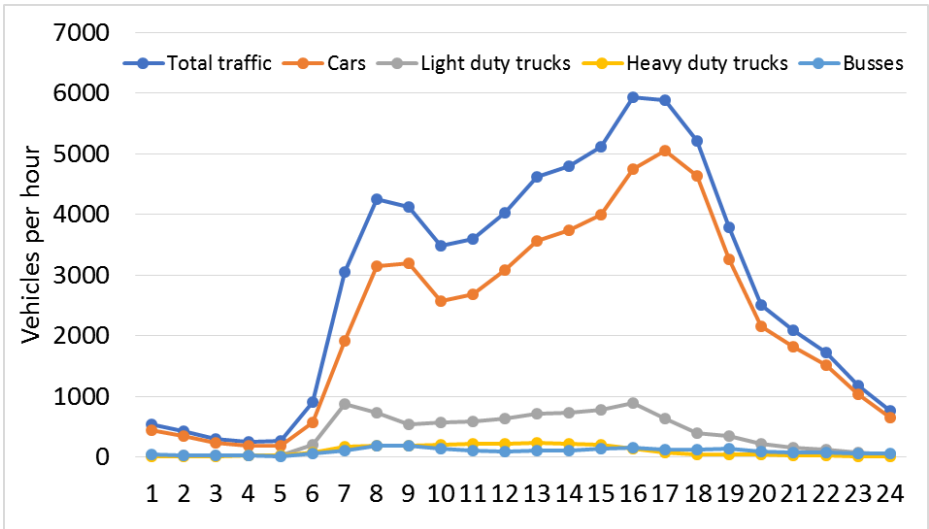


Figure 2: Diurnal variation in total number of vehicles passing the site.

Figure 3 shows the Euro-class shares for gasoline and diesel cars and light and heavy diesel trucks for 2016, 2017 and 2018. The fleet composition is changing quite rapidly being dominated by Euro 5 and 4 in 2016 to Euro 6 and 5 in 2018. In 2018 most of the vehicles are Euro 6 except for light duty trucks, for which most are Euro 5. Diesel cars and trucks are mainly Euro 5 or Euro 6, whereas gasoline cars 40% are Euro 6 and 40% are either Euro 4 or 5.

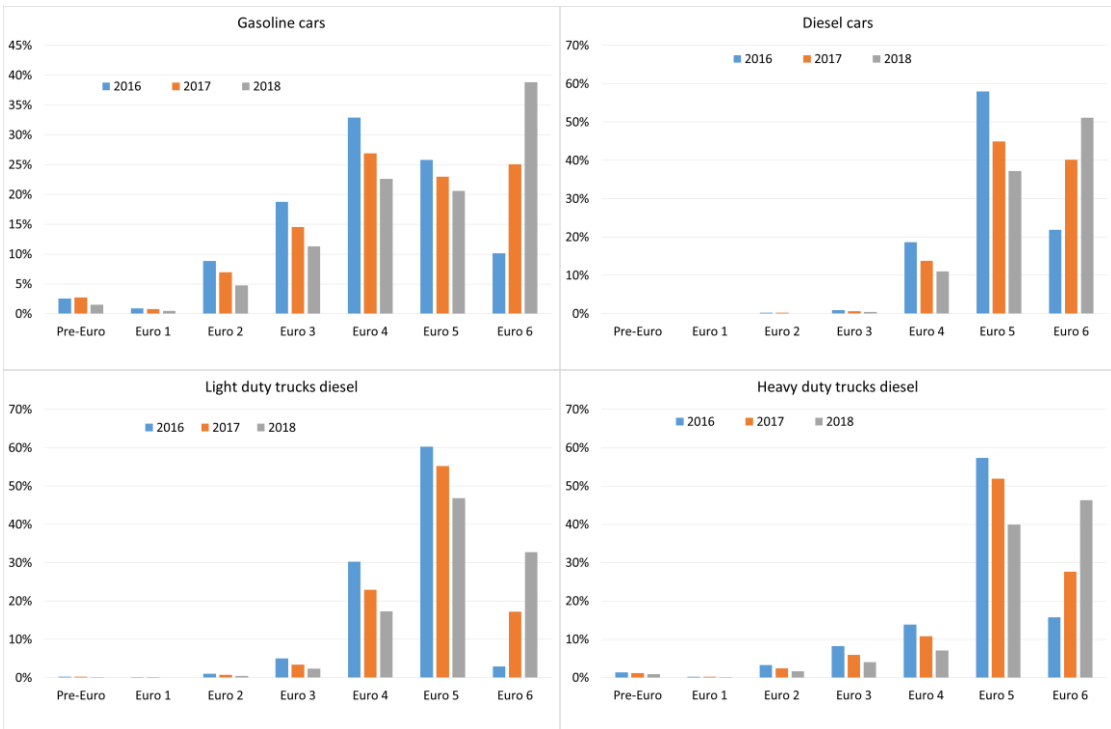


Figure 3: Euro-class shares of the vehicle fleet 2016, 2017 and 2018 at the measurement site along the highway (E18) in Stockholm.

Based on this information and specific EFs from HBEFA we calculated the fleet average emission factors for all pollutants every 15 minutes. The ratio of the EF for each pollutant to CO₂ may then be compared with the measured pollutant concentration increment ratio. Assuming that the fleet average HBEFA CO₂ EF is correct we also calculated absolute pollutant emission factors.

Emission factors NO_x

Table 1 summarises NO_x and CO₂ EFs based on HBEFA for the vehicle categories, weighted according to the Euro class distributions. We assumed different degrees of free flow and saturated traffic depending on the time of day. The overall NO_x/CO₂ ratio is 2.19 mg g⁻¹ as compared to the measured ratio of 3.28 mg g⁻¹. Multiplying the measured ratio with the HBEFA EF for CO₂ gives a NO_x emission factor of 0.62 g vkm⁻¹, which is 42% higher compared to the NO_x EF based on HBEFA. This assumes that the HBEFA CO₂ emission factor is correct.

Table 1. Weighted EFs along the motorway for vehicle categories according to HBEFA 3.3.

	NO _x ^b (g vkm ⁻¹)	CO ₂ (g vkm ⁻¹)	NO _x /CO ₂ (mg g ⁻¹)
Passenger car diesel	0.51 [0.70]	111	4.57
Passenger car gasoline	0.06 [0.15]	134	0.48
Passenger car gas	0.04 [n a]	106	0.38
LCV diesel	0.50 [0.60]	175	2.87
LCV gasoline	0.34 [n a]	156	2.17
HGV diesel	1.9 [2.1]	794	2.34
Urban bus diesel	2.1 [4.0]	679	3.03
Overall weighted whole vehicle fleet	0.44 [0.62]	188	2.31
Measured	0.62^a		3.28
Measured/HBEFA	1.42		

^aCalculated as measured NO_x/CO₂ ratio times the HBEFA EF for CO₂.

^bEFs in brackets were used to obtain the best agreement with measurements as shown in Figure 1. "n a" = not adjusted.

Figure 4 shows mean diurnal variations in NO_x/CO₂ ratios based on the measurements and for adjusted and unadjusted HBEFA EFs. The emission factors for NO_x and CO₂ represented more or less saturated traffic during the day and free flow rest of the time. Adjusted HBEFA EFs was obtained by multiplying the different vehicle categories by a factor. This could be done in many different ways but best fit (minimal sum of squared differences between measured and calculated emission factors) was obtained by increasing EFs as shown in Table 1 (EFs in brackets). The EFs for CO₂ were unchanged.

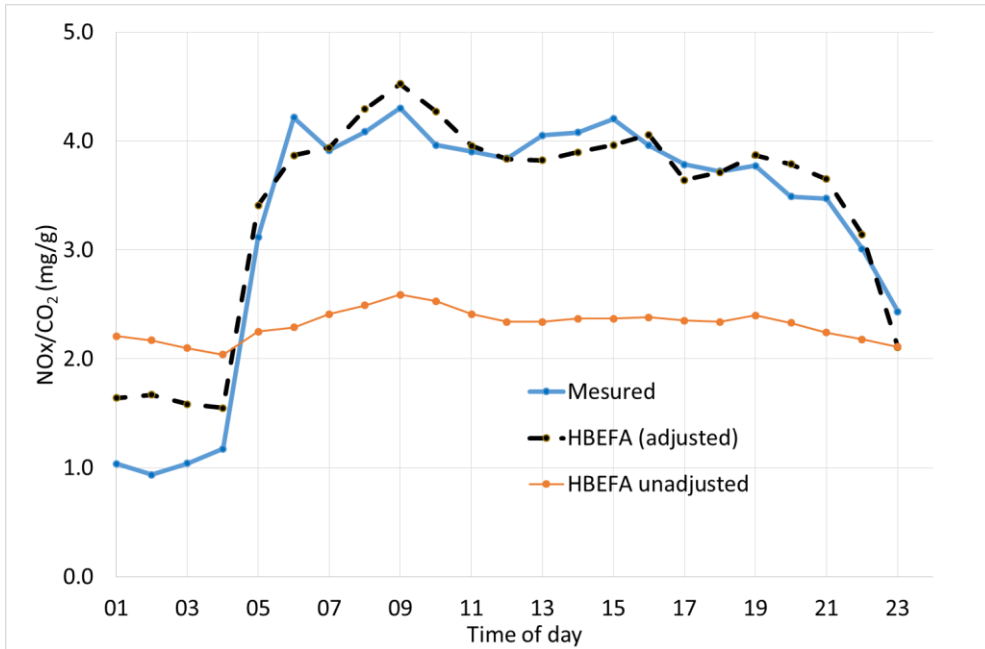


Figure 4: Comparison between measured NO_x/CO₂ increment ratio with an adjusted HEFA ratio (see text) for the motorway site. Mean diurnal variation for all data from Dec 2017 to Aug 2018.

Emission factors BC

The shares of BC in exhaust were obtained from the TRANSPHORM project as shown in Figure 5.

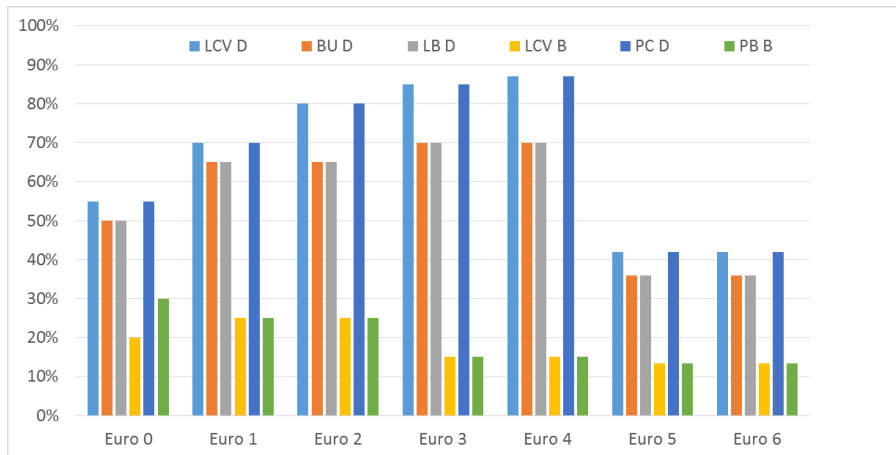


Figure 5: Share of BC in total exhaust PM according to TRANSPHORM. LCV D = Light duty diesel truck, BU D = Diesel bus, LB D = Heavy duty diesel truck, LCV B = Light duty gasoline truck, PC D = diesel passenger car, PC B = gasoline passenger car.

BC EFs were calculated based on the shares of BC in exhaust PM as shown in Figure 5 and HBEFA emission factors for exhaust particles for the different vehicle types and Euro classes. Table 2 shows a comparison between calculated BC emission factors and measured EFs. The measured EFs were based on the ratio of the incremental concentrations of BC and CO₂ and HBEFA EFs for CO₂. As can be seen the measured EF is a factor of 3 higher than the calculated for light duty vehicles and 20% lower than the calculated EF for heavy duty vehicles. The overall measured EF is a factor of 2 higher than the calculated EF.

Table 2. Light duty and heavy duty EFs for BC (mg vehicle-km⁻¹) according to HBEFA (exhaust) and TRANSPHORM (share of BC in exhaust) and EFs based on the measured BC/CO₂ ratio using the HBEFA CO₂ emission factor.

	Light duty vehicles	Heavy Duty vehicles	Total
HBEFA & TRANSPHORM	1.40	18.42	2.05
Measured ratio of BC/CO ₂ and CO ₂ from HBEFA	4.14 ± 0.50	15.28 ± 4.04	4.57
Ratio of measured/calculated	3.0	0.8	2.2

Acknowledgements

This work was supported by the Swedish Transport Administration.

References

- Carlaw, D., Beevers, S. et. al (2011). Trends in NO_x and NO₂ emissions and ambient measurements in the UK, *Report prepared for DEFRA*, https://uk-air.defra.gov.uk/assets/documents/reports/cat05/1108251149_110718_AQ0724_Final_report.pdf (accessed March 2019).
- Chen, Y., and Borken-Kleefeld, J., (2014). *Real-driving emissions from cars and light commercial vehicles - Results from 13 years remote sensing at Zurich/CH*. Atmospheric Environment 88, 157-164.
- Colberg, C.A. et al. (2005). *Comparison of a road traffic emission model (HBEFA) with emissions derived from measurements in the Gubrist road tunnel, Switzerland*. Atmospheric Environment, 39, 4703-4714.
- Hausberger, S.; Rexeis, M.; Zallinger, M.; Luz, R. *Emission Factors from the Model PHEM for the HBEFA Version 3*; Report Nr. I-20/2009 Haus-Em 33/08/679 from 07.12.2009. Graz University of Technology, Institute for Internal Combustion Engines and Thermodynamics, 2009. Available online: www.hbefa.net/e/index.html and http://www.hbefa.net/e/documents/HBEFA3-3_TUG_finalreport_01062016.pdf (accessed March 2019).
- Hueglin, C., Buchmann, B., Weber, R.O., (2006). *Long-term observation of real-world road traffic emission factors on a motorway in Switzerland*. Atmospheric Environment, 40, 3696-3709.
- TRANSPHORM, (2017). *Methodology for the Quantification of Road Transport PM-Emissions, Using Emission Factors or Profiles*. Deliverable D1.1.2, Updated February 2013. Available online: www.transphorm.eu/Portals/51/Documents/Deliverables/NewDeliverables/D1.1.2_updated.pdf (accessed on 21 February 2017).

2.1.4 Cold-Start Emissions and Excess Fuel Consumption at Low Ambient Temperatures - 2019 Update and Historic Review

*J. Laurikko*¹

¹VTT Technical Research Centre, Finland, FI0204 VTT, Espoo, Finland, Juhani.laurikko@vtt.fi

Introduction

Latest development of engines and emission control devices in passenger cars to bring them in compliance with the last amendments of European directives for exhaust emissions (Euro 5 and especially Euro 6) has apparently improved also their performance with regard to cold-start related emissions. This is the case, even if the targeted test procedure to specifically measure and control cold-start emissions at low ambient was included in the type approval requirements of new types already in year 2002, and the limit values associated with it have not tightened.

VTT has measured cold-start emissions of new cars, both petrol and diesel fuelled, regularly since 1993, and since 1998, the procedure has been constantly the same. The test results presented in this paper demonstrate that cold-start performance has been gradually improved, and emission rates measured at low ambient temperature (-7 °C) have declined. However, the negative effect of cold environment with regard to fuel consumption and CO₂ emissions has not much lessened. Furthermore, regarding type approval, diesel-fuelled cars are not subject to cold-start emissions test at all. Yet according to the test results, they emit high levels of oxides of Nitrogen (NO_x) after a cold start at low ambient temperature. This may partly contribute to the apparent air quality problem encountered in many urban areas of the European Union, and applying cold temperature testing also to diesel cars should be carefully considered, when envisioning the future of emissions regulations within EU.

Regulatory Procedures on Cold-start Emissions in EU

Due to the progress in Regulations covering tailpipe emissions from cars, new cars release today less and less harmful emissions. However, ambient air quality around Member States has not been improving at the same pace, and one contributor probably is elevated emissions released at cold-start in low ambient temperature conditions.

This was for the reason that especially since catalytic converters were introduced in early 1990's, emissions at cold-start and during the very first few minutes and kilometres of the driving were relatively high. Hence, their contribution was greatly increased, as they were not adequately subjected to the control, because the test procedure at that time was not addressing them properly. Therefore, directive 98/69/EC was adopted in 1998, and in this amendment by the EU Commission features were included that were targeted to make manufacturers to enhance the performance of the emission control especially in the cold-start phase. One such feature was the modification of the test procedure to omit the 40 seconds idle that has been in the beginning of the test, and start collecting the exhaust sample immediately after the engine has fired-up. Therefore, the exhausts from the most-critical cold-start phase were not anymore by-passed, but included in the sample.

Furthermore, the directive included a separate cold-start test at low operating temperatures, namely at -7 °C. This test (referred as "Type VI" test in the Directive 98/69/EU) consisted of just the UDC phase of the revised European dynamometer driving schedule. As it is slightly over 4 km in length, it can be regarded as a fair representative of a short urban early-morning cold-start trip, as the vehicle subjected to the test needs to be soaked at that cold temperature at least 12 hours. Naturally, this test has its own set of standards. Limit values were given for CO (≤ 15 g/km) and total hydrocarbons, THC (≤ 1.8 g/km). However, there was no limit value for oxides of nitrogen (NO_x), as NO_x was not expected to increase markedly. Also, this type of test was applicable only for petrol-fuelled cars, because diesel engines were then considered to be less affected by the cold start.

Although part of the package, this additional requirement was not, however, introduced at the same time as Euro 3 standards (starting on 1.1.2000 for new type approvals), but two years after in 2002. And even then, it was only for new types. Therefore, the full implementation was rather slow. Even so, testing has shown that the modifications of the emission control system required

due to this revised test procedure in the normal temperature have greatly improved the performance at low ambient temperature, as well.

Since the original adoption of the cold-start test, the limit values have not been revisited, even if the limit values for the normal ambient temperature test have been tightened in two occasions, Euro 5 in 2008/2009 and Euro 6 that is now fully enforced since September 2015. However, as mentioned before, this tightening should also result in improvement in cold start performance at low ambient conditions, too, and our test results corroborate that assumption.

Objective and previous work

The objective of the original work at VTT on cold-start emissions (Laurikko et.al.,1995), (Laurikko, 1998a) was to show the weak points of the technology and underline the necessity to address this shortage. Along with the similar research made concurrently in Sweden and the Netherlands, the evidence was clear enough for the legislators to amend regulations with the inclusion of a separate low ambient temperature test, referred in the Directives as “type VI test”. Subsequently, the effect of ambient temperature on the spread of results of in-laboratory exhaust emissions measurements was studied also in the European project ARTEMIS (Wailenmann et.al., 2005).

As part of the original mission, VTT has evaluated and reported cold-start performance of new cars since 1993, addressing also durability of the technology in Nordic conditions in (Laurikko, 1997) (Laurikko, 1998b), (Laurikko, 2000), (Laurikko, 2001), (Laurikko, 2003).

The work has been continued even after the legislation was passed, and the initial objective was reached. Each year a batch of some 10 to 20 cars representing that particular model year has been tested. The objective of this work has been to make an assessment of the cold-start performance, and evaluate how it has been developing. Furthermore, the aim has been to provide first-hand results for the motoring press of those cars for their annual evaluation tests. Therefore, measuring NOx emissions and fuel consumption (as of CO₂) has been part of our test, even if they are not part of the legislative procedure. In later years we have also added particulate mass (PM), and even particulate number (PN) to the portfolio.

In 2008 we reported the status quo (Laurikko, 2008), including Euro 4 vehicles that are fully in compliance with the cold-start regulation. In 2016 we reviewed the impact of Euro 5 and the latest Euro 6 vehicles in (Laurikko, 2016). This 2019 update brings now more results from the latest Euro 6 vehicles to the test database, and also reviews historical data from tests in 1993 to 1998.

Test fleet composition

Even if the objective has been to portray typical new car performance, the selection of each annual fleet has been rather random and not statistically composed. This was the case, as the work has been made jointly with some motor magazines, and the eventual choice of cars was made by these magazines. However, they usually tried to favour cars of high sales volumes in Finland, but occasionally new, some marginal but interesting vehicles were included.

Although cold-start excess emissions are primarily associated with petrol-fuelled cars, we have also tested diesel-fuelled cars, because emission inventories do need cold-start data also for diesel cars, and cold-start inflicts also fuel consumption, which we wanted to assess. Most of the cars were fairly new, with odometer readings usually below 5,000 km. In only a few cases the driven distance was lower than the suggested minimum (1500 km) for emissions testing, and similarly, in a few odd cases the driven distance was higher than the suggested maximum (15,000 km) for measurements regarding compliance with fuel consumption type approval figures.

Table 1. lists some characteristics for the different sub-fleets that in total comprise 437 vehicles, of which 353 were running on petrol, and 84 on diesel. The Table also contains the division of each sub-fleet to different EU-classes. Unfortunately, for some sub-fleets there was not enough information to make the exact breakdown. These are marked in the table with shading, and we have assumed a 50/50 split between the classes available. In doing so, we come to 83 cars for EU2, 50 for EU3, 116 for EU4, 93 for EU5 and 54 for EU6. In addition, 41 cars were tested in 1993-1998 that complied with regulations implemented in European Trade Area (ETA), consisting of Austria, Finland, Norway, Sweden and Switzerland, equalling with U.S. regulations for MY'83.

Table 1: Main characteristics of annual sub-fleets tested by VTT.

Test Fleet ID	# cars	average displ. dm ³ [dm ³]	average inertia, kg [kg]	Euro-class					
				ETA	EU2	EU3	EU4	EU5	EU6
Tested with FTP-cycle @ 0 °C				41	24	ETA=reg. like U.S.'83			
TM Winter '93	17	1.982	1322	17					
TM Winter '94	10	1.730	1195	10					
TM Winter '95	14	1.650	1133	14					
TM Winter '96	6	1.827	1360		6				
TM Winter '97	8	1.343	1085		8				
TM Winter '98	10	1.743	1283		10				
Tested with ECE15-cycle @ -7 °C									
EcoCar '98	9	1.254	1069		9				
TM Winter '99	16	1.536	1241		16				
EcoCar '99	9	1.413	1136		9				
TM Winter '00	7	1.787	1327		7				
EcoCar '00	9	1.373	1134		9				
EcoCar '01	6	1.580	1247		6				
EcoCar '02	4	1.365	1050			4			
TM Winter '01	15	1.788	1354			8	7		
TM Winter '03	19	1.593	1289			7	12		
TM Winter '04	11	1.775	1400			7	4		
TM Winter '05	20	1.738	1305				20		
TM Winter '06	12	1.629	1275				12		
TM Winter '07	21	1.626	1334				21		
TM Winter '09	17	1.692	1339				16	1	
TM Winter '10	19	1.544	1344				10	9	
TM Winter '11	2	1.648	1360					2	
TM Winter '12	15	1.439	1331					15	
TM Winter '13	20	1.480	1353					20	
TM Winter '14	11	1.521	1305					11	

TM Winter '15	12	1.206	1224					6	6
TM Winter '17	11	1.386	1464						11
TM Winter '18	12	1.205	1418						12
TM Winter '19	11	1.451	1515						11
petrol, in total	353				45	37	102	64	40
EcoCar '98	3	1.930	1247		3				
TM Winter '00	6	2.074	1456		6				
EcoCar '00	3	1.837	1323		3				
EcoCar '01	7	1.776	1249		7				
EcoCar '02	8	1.951	1305			8			
TM Winter '08	15	1.459	1464				14	1	
TM Winter '11	18	1.668	1492					18	
TM Winter '12	3	1.738	1592					3	
TM Winter '13	3	1.706	1590					3	
TM Winter '14	4	1.653	1439					4	
TM Winter '15	6	2.036	1382						6
TM Winter '17	4	2.015	1785						4
TM Winter '19	4	1.742	1755						4
diesel, in total	84				14	13	14	29	14
all fleets, in total	437			41	83	50	116	93	54

NB: Test fleets for MY'93, MY'94 and MY'95 were complying with regulations implemented in European Trade Area (ETA), consisting of Austria, Finland, Norway, Sweden, Switzerland, equalling with U.S. regulations for MY'83. Hence, FTP75 cycle was used.

Because the two motor magazines that were contracting the tests had different views in their work, the fleets were somewhat different in terms of vehicle size and engine capacity. As the name already suggests, the "EcoCar" fleets were tested for the Finnish motor magazine "Tuulilasi" mainly for their annual story "Search for the Most Eco-logical Car". Therefore, most of these sub-fleets were of smaller size and with less engine power, as sometimes, the initial selection was based on CO₂ emissions and the most low-emitting vehicles usually are small and low-powered. With petrol cars this was especially true, as on average all "EcoCar" fleets were some 15% lighter and with smaller displacement engines about the same amount compared to those sub-fleets tested for "Tekniikan Maailma" (TM), whose choices were more favouring cars with high sales volumes or technologically interesting types rather than low consumption or CO₂. However, in diesel-fuelled fleets this tendency was less visible.\

Experimental procedures and equipment

All the testing has been conducted in a climatic test chamber at VTT. Figure 1 shows a picture of the chamber. The main dimensions of this chamber are: length 12.5 m, width 6.5 m and height (gross) 5.5 m. However, the free height of the cell is reduced by the air circulation system and blower. The air is blown from a 1.2 m² nozzle in front of the vehicle, and the wind speed can be synchronised with the speed of the dynamometer rollers up to 100 km/h.

The use of such a blower system should give better results of vehicles real-life low-temperature performance with a positive cooling effect on the engine bay, exhaust manifold and the rest of the system as well as on the converter itself. However, as we know that in the legislative test procedures such system is not in use, all work reported has been done using only fixed blower speed (about 25 to 30 km/h) for better correlation with the results of the legislative procedure.

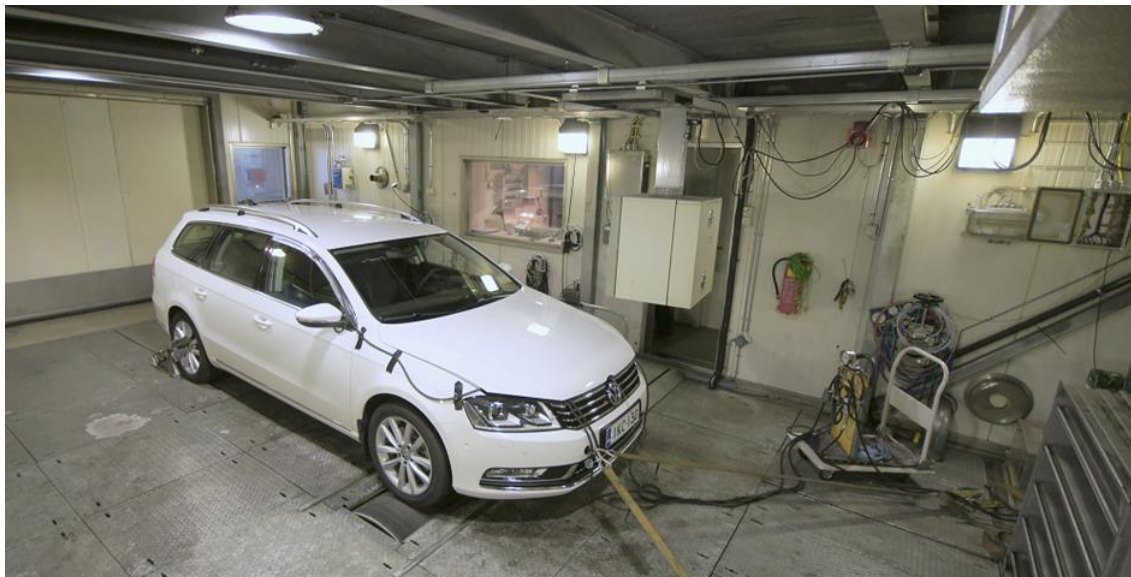


Figure 1: Emissions and fuel consumption test facility with a single-roller (1.0 m) 2WD dynamometer at VTT, Finland. Ambient test temperature between -30 and +30 °C.

In the early years (1993-1997), tests were performed using the U.S.FTP75 urban driving cycle, and test temperature was 0 °C. However, since 1998 tests has been run at -7 °C nominal temperature, and using ECE15 urban driving cycle (UDC). Thus, they conform to the type VI test specifications of the Directive 98/69/EU, and the results can be compared to the official limit values. Even those cars that were originally type approved according to Euro 2 (EU2) specification, were tested with the new procedure to give comparative assessment of their performance.

Furthermore, all cars were tested also over the same driving cycle, but now after a thorough warm-up (EUDC cycle). This second UDC cycle was initiated with a hot engine restart after a one minute pause. Such a procedure gave the opportunity of assessing the difference between the cold-start and hot-start results, and after deducting the hot restart value from the cold-start results, it gives a fair estimate of the cold-start/warm-up excess emissions. However, we are not considering these warm-up engine emissions in this context, as typically they were very low.

Even if in principle, comparability with the legislative procedure was our target, the objective of this work was, however, neither to make an official check of the emissions output, nor to assess the conformity of production (COP). Therefore, for fair reasons of simplicity and cost-effectiveness, all tests were run using commercial fuel of good quality.

Vehicle preparation and preconditioning was also carried out along with to the definitions in the Directive. Accordingly, cars were soaked in the test cell for at least 12 hours, but not more than 24 hours, although the certification procedure allows cold-soak up to 36 hours. However, instead of running the regulatory preconditioning in the test cell, cars were run on road with at least a 20 km trip before garaging them into the test chamber for the cool down and overnight soak. Furthermore, dynamometer settings were based on the vehicles' reference mass and the corresponding factors were taken from the look-up table in the Directive.

For measurements during the period of 1993-2011, a PDP-CVS system was used for all exhaust dilution and sampling, and an AMA2000 exhaust emission analysis system, also from Pierburg AG (FRG) was used for determining the concentrations of the regulated compounds as well as CO₂. Since 2012 these equipment has been renewed. First the CVS was replaced with a multi-venturi unit (AVL CVS i60), and since 2014 the gas analytics was replaced with an AVL i60 set.

Results and Discussion

General Remarks

The database of results allows us to portray the evolution of the emissions performance over the period from year 1993 to date, sub-fleet by sub-fleet, petrol and diesel-fuelled cars separately. Furthermore, it allows comparison of the performances between different Euro classes. Table 1 listed the number of vehicles in each category. However, with some sub-fleets the type approval category was not explicitly known, so in case of the averages for Euro 2 and Euro 3, there is some level of uncertainty, but for Euro 4, Euro 5 and Euro 6 cars, information on the compliance was definitely resolved. The average emissions levels for each sub-fleet are given in Appendix 1.

Emissions of Carbon Monoxide (CO)

Figure 2 illustrates the test results for CO emissions, presented as a cold-start result, comparable to the cold-start type VI test described in Directive 96/69/EU, derived from the ECE15 driving cycle at -7°C ambient. The results are shown as average values for each sub-fleet and grouped separately for petrol and diesel fuelled cars, and sorted by year the sub-fleet has been measured. Error bars are also shown for the purpose of describing the spread of values between individual vehicles in each sub-fleet. We have also noted the number of cars that were exceeding the limit values imposed for new types after 2002.

As Figure 2 clearly shows, CO performance has been almost constantly improved over this period from year 1993 to present day. In the 1990's the levels of CO emitted were extremely high, on average more than 15 g/km, and occasionally reaching 40 g/km, or even higher. This was due to the fact that the majority of the cars at those days had an underfloor TWC that heated and lit-up very slowly. Typically, the driving distance that was needed to light-off was around 2 kilometres. In modern cars, this light-off distance has been cut down to as low as about 50 meters, at best.

Furthermore, those very high emissions levels that were typical for the 1990's started to become more moderate, once the regulation was in place. Concurrently, the number of cars exceeding the limit value (15 g/km) has vanished with the exception of TM Winter'04 sub-fleet, where we encountered two high emitters.

We believe that mostly the progress has probably resulted from the various improvements that the manufacturers have made to the engines and the associated emissions control systems already, when they have sought compliance with Euro 3 level of standards. Because Euro 3 required testing with the revised European Test, without the 40 second idle, the emphasis was clearly in much faster warm-up performance of the catalyst, and using more reasonable cold-start enrichment strategies than in Euro 2, when the first 40 seconds of idling was vented out of the sampling. Therefore, also low-ambient temperature performance was duly enhanced. We can see this happening continuously, as the level of emissions has been gradually lowered, even if the limit value for this cold-start cold ambient test have not been tightened. The improvement are strictly echoing the changes in normal ambient temperature limit values with respective modifications of the emission control systems, like close-coupling of the catalytic converter (or even incorporation of it) with the exhaust manifold, as well as more precise control of fuel injection.

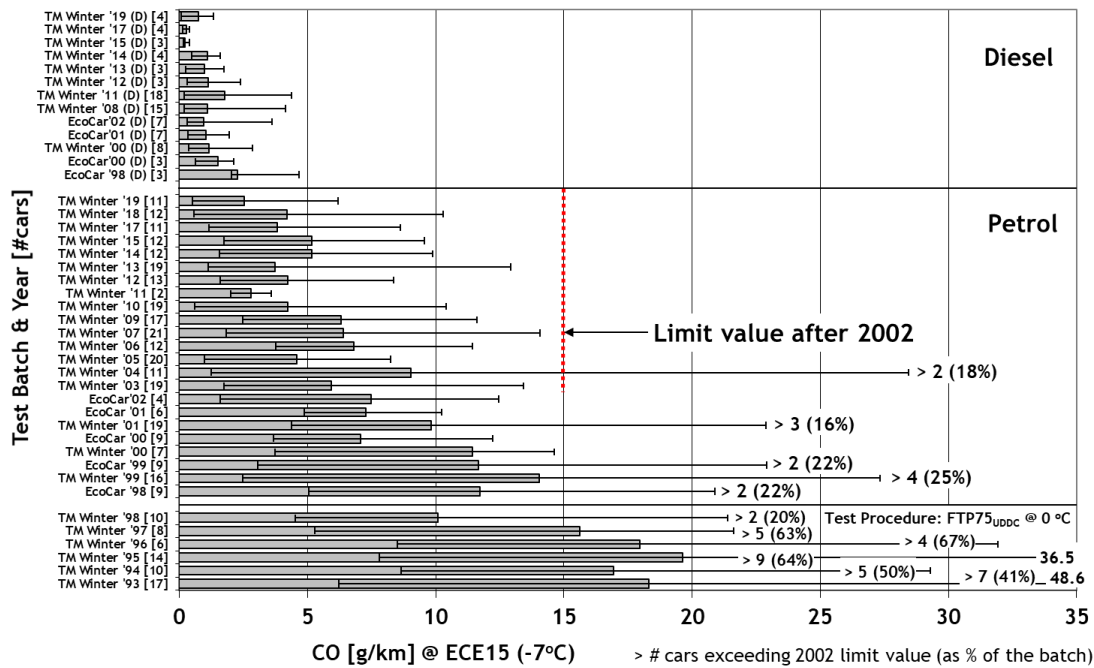


Figure 2: Emissions of Carbon Monoxide (CO) in cold-start/cold-ambient tests for various test fleets.

Overall, the level of emissions from diesel-fuelled cars is only about 20 % of the level typical for petrol-fuelled ones. However, the spread in performance seems to be relatively large, and this leads to a situation, where the best of the petrol-fuelled cars emit less than the worst of the diesels.

Furthermore, when looking at Figure 3, which depicts the CO emissions by type approval level, we see that the average for petrol-fuelled cars has lowered constantly from Euro 2 to Euro 5, but the average level for Euro 6 cars is about the same as for Euro 5.

On the contrary, for diesel cars the average levels are – albeit being very low – almost constant for Euro 2 to Euro 5 (which has the highest average), but Euro 6 shows a clear improvement.

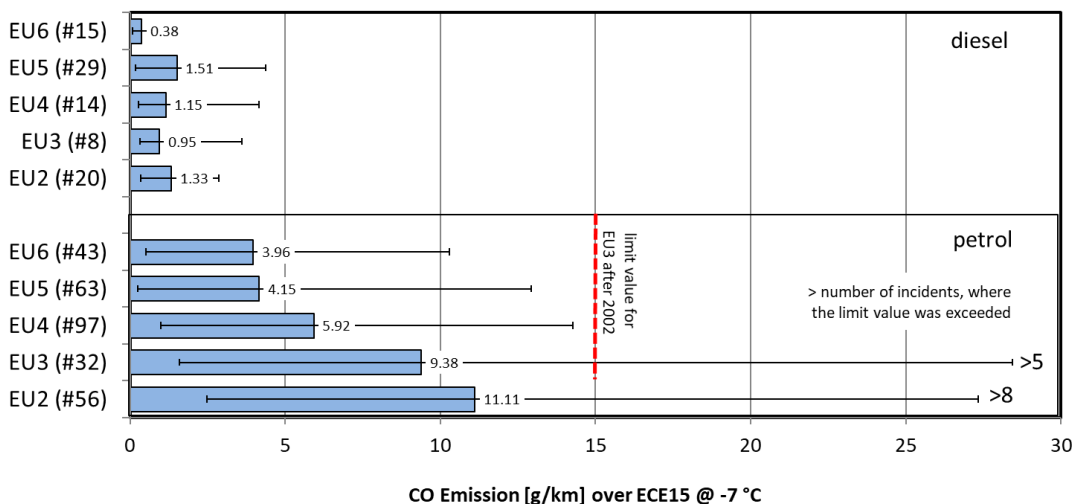


Figure 3: Emissions of Carbon Monoxide (CO) in cold-start/cold-ambient tests according to the type approval level of the tested cars.

Hydrocarbon emissions (HC)

Emissions of hydrocarbon (HC) are basically unburnt fuel escaping from the engine with the other gases. Actually, there are a high number of different species detected, and the content is highly dependent on type of fuel used. Hence, in emissions legislation they are usually referred as total hydrocarbons (THC). Among the species there are compounds that are nearly benign, but also a number of toxic or even carcinogenic species are detected, the most common being benzene. There are limit values for emissions of HC, but due to the complex nature of the group, no gross limit value for ambient concentrations, only for some species. Furthermore, hydrocarbons are known to react with the other substances in ambient air, and in the presence of sun's radiation, they take part in formation of atmospheric pollution called smog.

Figure 4 illustrates the test results for HC emissions, presented as a cold-start result, comparable to the cold-start type VI test, consisting of ECE15 driving cycle at -7°C ambient. The results are shown as average values for each sub-fleet and grouped separately for petrol and diesel fuelled cars, and sorted by year the sub-fleet has been measured. Error bars are also shown for the purpose of describing the spread of values between individual vehicles in each sub-fleet. We have also noted the number of cars that were exceeding the limit values imposed for new types after 2002.

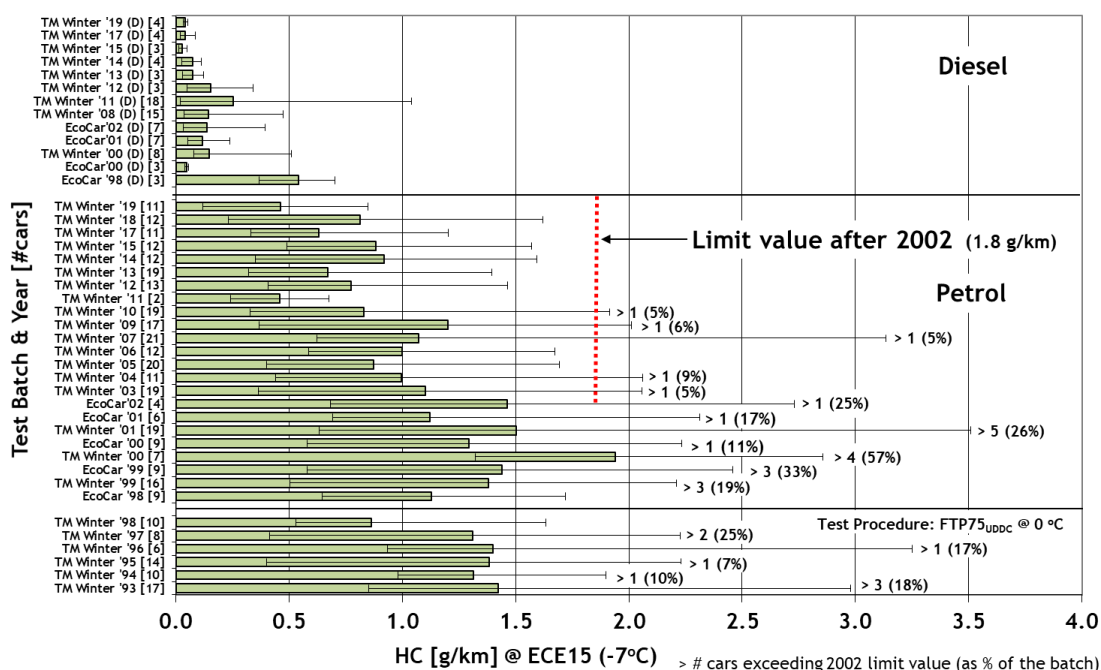


Figure 4: Emissions of Hydrocarbons (HC) in cold-start/cold-ambient tests for various test fleets.

When we view Figure 4, we can see that the story seems to unfold somewhat differently for this type of emission. At first, we notice that levels of HC emissions in the “historic” era (1993-1998) were not any higher than the levels in Euro 2 and first Euro 3 cars. Additionally, the recorded results do not show much improvement over the period until MY2010. The highest average value recorded actually seem to be associated with sub-fleet TM Winter '01, expected to contain mostly Euro 3 compliant cars, but without the obligation for cold testing, as it was implemented in 2002.

Furthermore, we have not been able to come up with any straightforward explanation to this kind of trend. Nevertheless, our experience suggest though, that low HC and low CO do not necessarily come together, as in many cases seeking very low cold-start CO can result in higher values of HC than those with slightly higher CO output. This may be a result of a too lean air-fuel ratio setting during cold-start phase resulting in rough running and non-firing working cycles releasing unburned hydrocarbons in the exhaust. With a reasonable enrichment, CO may be slightly higher, but with more stable combustion and less non-firing cycles, the HC output remains lower.

Figure 5 depicts the averages for the test results for HC emissions, presented as a cold-start result, comparable to the cold-start type VI test described in Directive 96/69/EU. The results are shown as average values for each sub-fleet and grouped separately for petrol and diesel fuelled cars, and sorted by the type approval levels. Error bars are also shown for the purpose of describing the spread of values between individual vehicles in each group. We have also noted the number of cars that were exceeding the limit values imposed for new types after 2002.

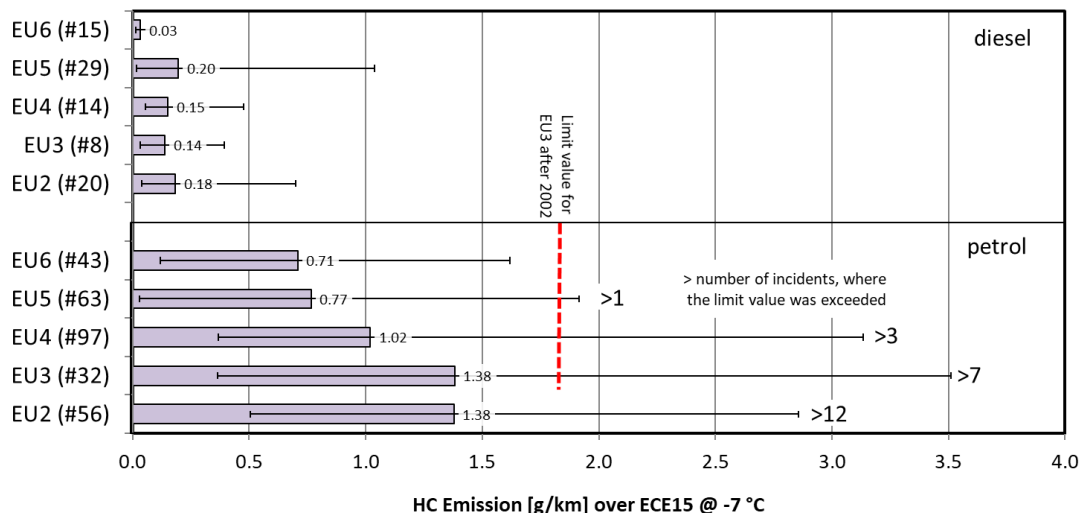


Figure 5: Emissions of Hydrocarbons (HC) in cold-start/cold-ambient tests according to the type approval level of the tested cars.

Emissions of Nitrogen Oxides (NOx)

Even if it has been demonstrated that a cold-start is by far less influencing the emissions of NOx, and no specific limit values are imposed to their emissions in this type VI cold-start, low ambient temperature test, we have also measured NOx, and the results are depicted in Figure 6 exactly the same way as previously with CO and HC results.

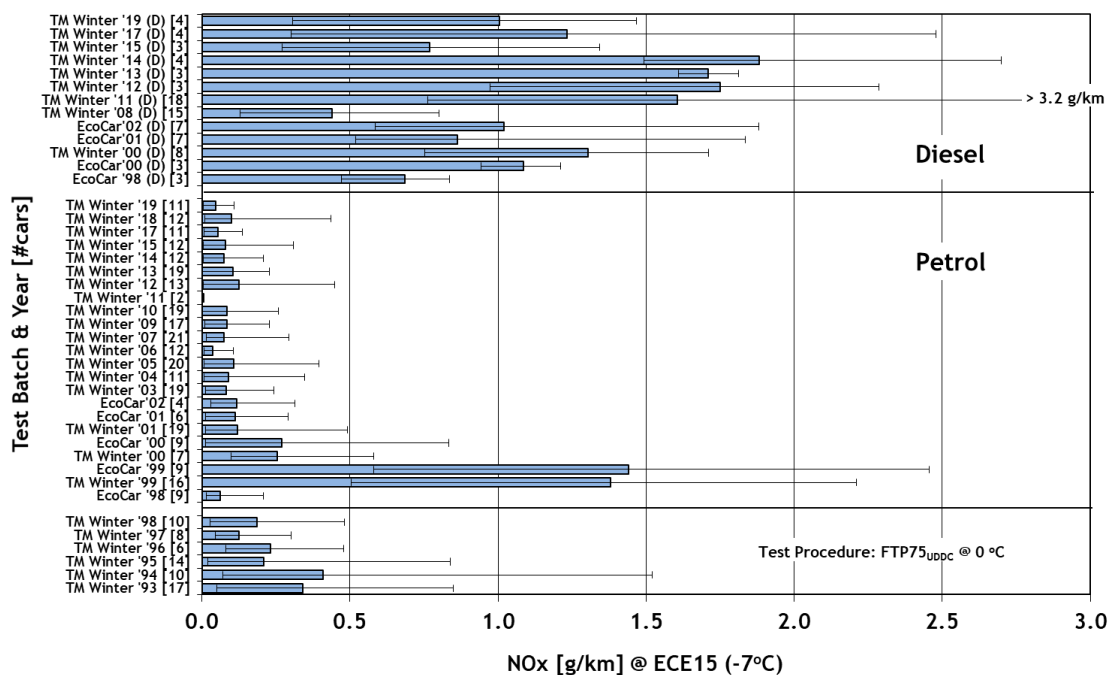


Figure 6: Emissions of Oxides of Nitrogen (NOx) in cold-start/cold-ambient tests for various test fleets.

While looking at the bars in this Figure 6, we immediately notice the clear difference between petrol and diesel-fuelled cars. Excluding the fleets that consisted of Euro 2 petrol cars (1998-1999), the emissions of NOx are clearly much higher for diesels. Regarding petrol cars, the MY2000 fleets emit about 0.25 g/km, but starting from MY2001 (“TM Winter ‘01” fleet) the average levels of NOx levels to a figure about 0.1 g/km. The very latest fleets emit only some 0.05 g/km, which is on par with the respective limit value in normal ambient conditions (0.06 g/km).

Turning into the diesels then, we can see that with the exception of the good performance of MY2008 sub-fleet (consisting of only Euro 4 cars), MY2011 to MY2014 fleets show a rising tendency in emissions level, emitting all on average over 1.5 g/km. However, from MY2015 with more Euro 6 cars coming to market the average levels drop, but the averages are still around 1 g/km, which is about 12 times of the limit value for Euro 6 diesels in normal ambient (0.08 g/km). Relatively, the higher rates for Euro 5 fleets are only about tenfold compared to limit value in normal temperature test (0.180 g/km).

Therefore, we can conclude that high cold-start/cold ambient NOx emissions are predominantly an issue for Euro 5 diesels, which can clearly be seen in Figure 7, where the emissions are depicted for each Euro class. The average levels for Euro 2 and Euro 3 seem to be alike at around 1.0 g/km, whereas Euro 4 has the lowest average level, about 0.6 g/km. Conversely, the Euro 5 average is almost three times higher, at 1.6 g/km, and some cars have showed as high as over 3 g/km emissions. However, as the Figure shows, Euro 6 is again a step forward, with an average of 1.0 g/km,

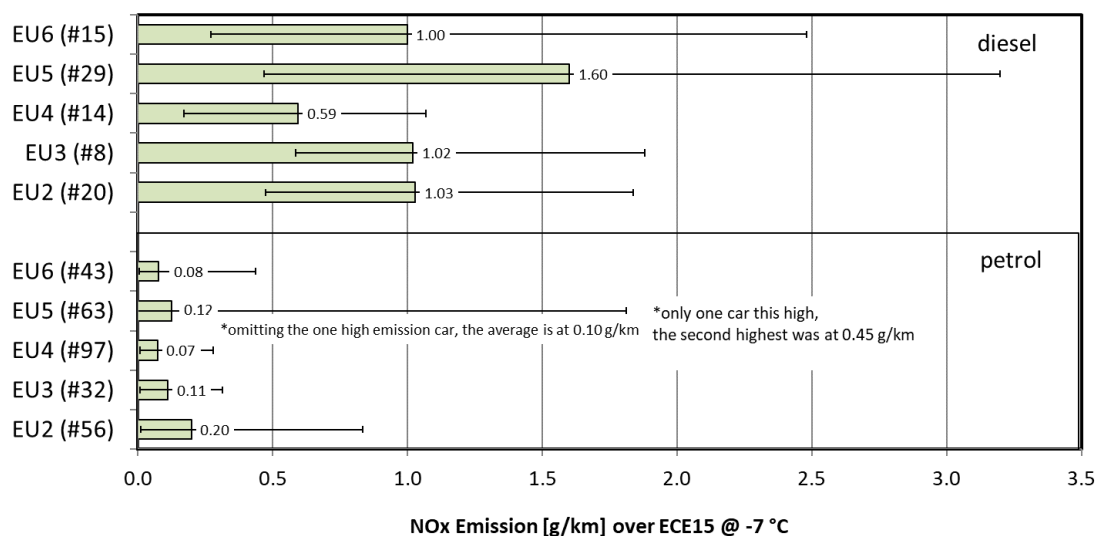


Figure 7: Emissions of Oxides of Nitrogen (NOx) in cold-start/cold-ambient tests according to the type approval level of the tested cars.

Furthermore, as the Figure 7 shows, among the Euro 5 petrol-fuelled cars, there was one that had exceptionally high NOx output, up to the level of 1.8 g/km, which is the same level as average diesels of the same group. However, this was only one car (although measured twice with almost the same results), and omitting just this one car lowers the average NOx level by some 20 % and the next highest level emitted is then 0.45 g/km, not much higher than the highs for Euro 4 or Euro 6.

Emissions of Particulate Mass (PM)

Although the dataset is not complete on emissions of particulate matter (PM) since results for Euro 2 and Euro 3 petrol-fuelled fleets are missing, we have included PM values, as well, into this review. Figure 8 depicts the Euro-class averages separately for diesel and petrol-fuelled models. It is quite interesting to observe the evolution in diesels from Euro 2 to Euro 5/Euro 6, where DPF's are employed. The PM levels drop about an order of magnitude. However, in this context even the petrol-fuelled cars emit particulates in considerable amounts that actually are much higher than the respective levels for diesels (Euro 4). According to our data, Euro 4 petrol cars emit at cold start on average 2.4 times more PM than Euro 4 diesels. Furthermore, for Euro 5 this

ratio is 9, and for Euro 6, nearly 20, as the average levels for petrol-fuelled cars is around 13 to 20 mg/km. However, due to the effective DPF, diesels emit only 1 to 2 mg/km. Mostly this discrepancy is due to the increasing share of direct-injection petrol engine (SI-DI) that are prone to emit carbon particulates at cold-start. Unfortunately, not enough data and resources were available to differentiate the SI-PFI and SI-DI engine types among the tested cars.

However, we could split the Euro 6 fleet between Euro 6b and Euro 6d_temp, because the latest fleet for MY2019 consisted of those cars that have been tested with RDE, but more importantly conform also with the PN standard of 6×10^{11} . In effect, this means that many petrol cars have now also a particulate filter. This had the effect that the average PM level for petrol cars of Euro 6b was about 0.025 g/km, but the PM level for fleet of Euro 6d_temp emitted only about 10% of that. Apparently, the filters and other measures attributed mainly to low for low PN also paid dividend on PM.

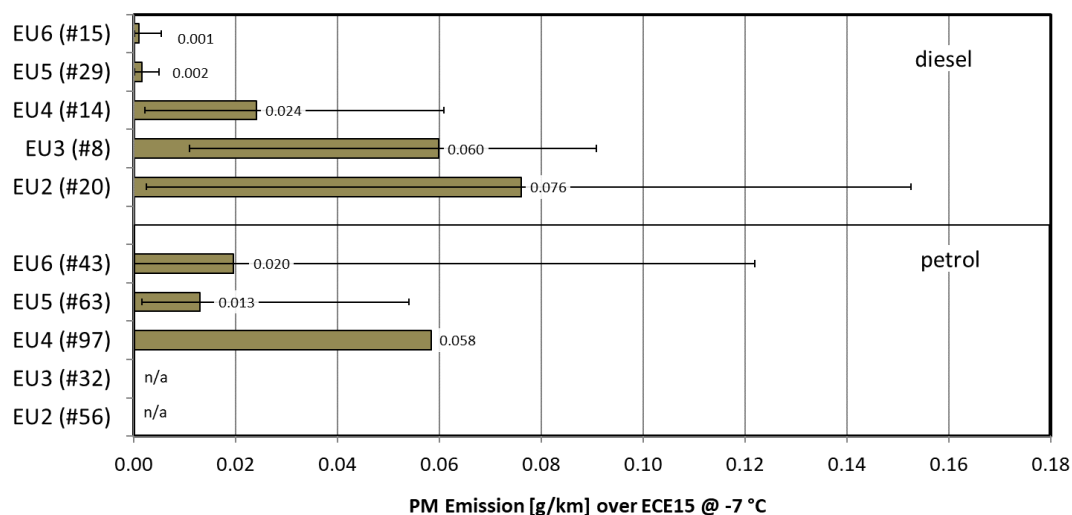


Figure 8: Emissions of Particulate Matter (PM) in cold-start/cold-ambient tests according to the type approval level of the tested cars.

Furthermore, a more thorough and comprehensive analysis on particulates should also include particulate number (PN). However, we have measured PN only from the very latest fleets of Euro 6 cars, and we have not yet enough data to support a good analysis. However, when we continue this work, more and more PN values will become available for further fleets.

CO₂ emissions

As already commented earlier, our aim in assessing the cold-start, low ambient temperature performance was also to address the impact of these conditions to fuel consumption and CO₂ emissions respectively. Their importance has in recent years risen enormously, especially the when effective emission control technology introduced to comply with Euro 5 and Euro 6 standards has drastically reduced the regulated emissions.

Figure 9 depicts average CO₂ emissions measured in type VI cold start test for each sub-fleet tested. Already at a glance, one sees that for petrol-fuelled cars no apparent trend is present until 2010, if not a slight raise reflecting the slight increase in average weights of the later-model cars. On average, the petrol-fuelled Euro 4 sub-fleets had 7 % higher weight than those of Euro 2 level, and Euro 3 fleets were falling in between these two. Furthermore, to compensate that added mass, the later-model fleets also had on average some 10 to 12 % larger engines by displacement, and most probably power output was even more increased, as specific power (kW/dm³) has definitely not decreased. Therefore, higher consumption was expected from newer vehicles.

This increase in mass continues for Euro 5, but due to more efficient engines, the CO₂ figures start to fall somewhat. However, for Euro 6 the fleets are heavier on average, and that is reflected also in CO₂ results that are for the latest fleets somewhat higher than for Euro 5, despite the fact that the latest engines do show better engine efficiency, which we also measure as part of the test routine.

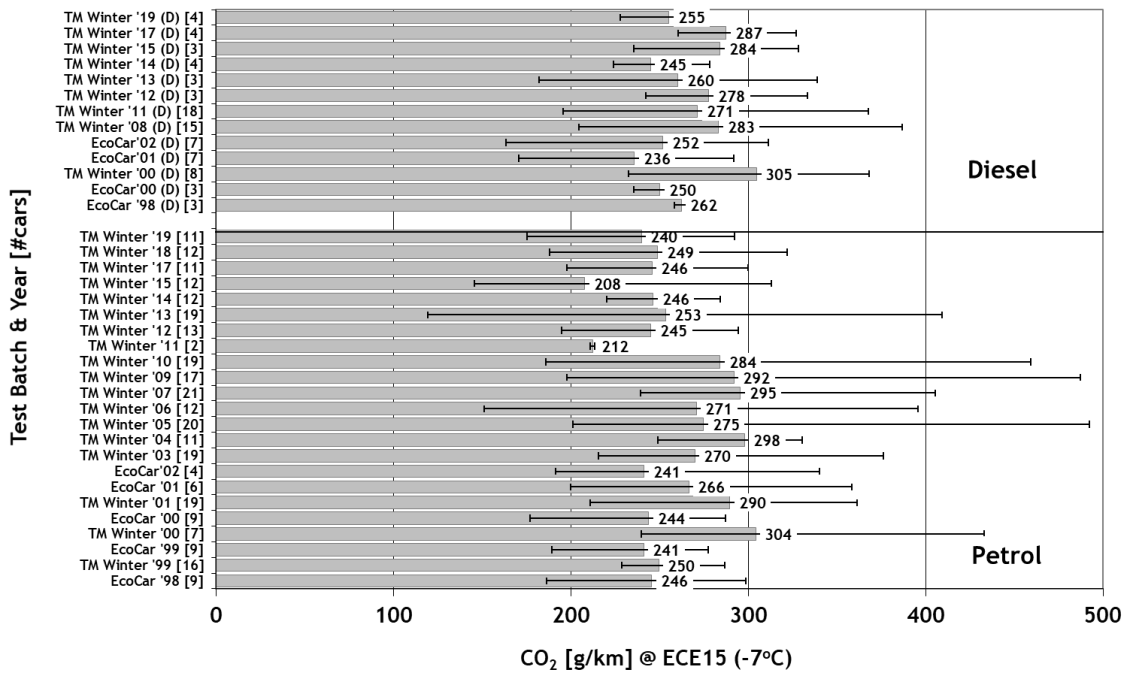


Figure 9: Emissions of Carbon Dioxide (CO₂) in cold-start/cold-ambient tests for various test fleets.

The comparison between Euro-classes is easier with Figure 10, depicting the average CO₂ values for each of the type approval levels.

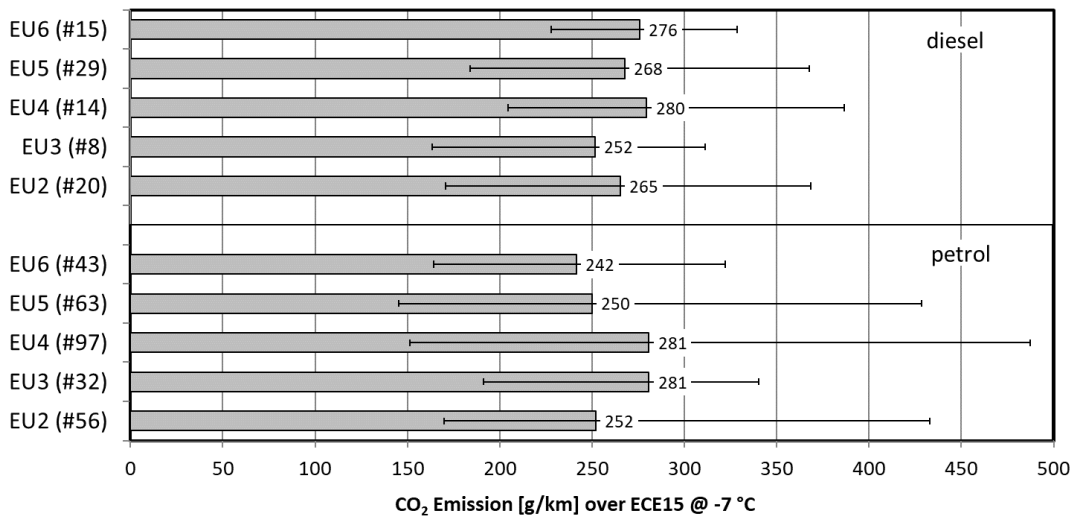


Figure 10: Emissions of Carbon Dioxide (CO₂) in cold-start/cold-ambient tests according to the type approval level of the tested cars.

As the Figure shows, for petrol cars the Euro 6 vehicles have the lowest average CO₂ emissions, quite as expected. However, diesels do not show a similar trend. The latest Euro 6 diesels emit on average more CO₂ than the Euro 2 or Euro 3 class cars in late 1990's and early 2000. More efficient emissions control may have quite strongly attributed to this, but we must also note that the average weight of the diesel fleets has a steady increase from the Euro 2 to the Euro 6 fleet. The Euro 6 fleet for diesels in its present composition is almost 30% heavier than the Euro 2 and Euro 3 fleets, and Euro 4 (+13%), and Euro 5 (+15%) fall in between. Despite better efficiencies, this must make an impact towards higher fuel use and hence more CO₂ emissions, too.

Conclusions

The database used in this review has been collected by the author over a period of 25 years. Since the last 20 years the measurement procedure has also remained the same, the material gives an excellent basis for an overview of the progress that has been made on this subject.

As the test results presented in this paper demonstrate, cold-start performance has been gradually improved, and emission rates measured at low ambient temperatures have declined. The extremely high CO emissions typical for the first generation of TWC-equipped cars in 1993-1998 are now “a thing of the past”, and for petrol-fuelled cars the average cold-start CO emission result has fallen about 50 % between the fleets of Euro 2 and Euro 4 cars. However, Euro 5 and Euro 6 have not anymore contributed that much being almost at the same level, but about 25% lower than for Euro 4. Furthermore, regarding HC emissions the improvement has not had the same magnitude, as only some 25% improvement was observed from Euro 2 to Euro 4, but some further improvement was seen for Euro 5 and Euro 6. Furthermore, those extremely high values have been cut down, though, starting with the introduction of the Euro 4 cars.

According to the results, elevated emission levels for CO and HC at cold-start are indeed mostly associated with petrol-fuelled cars, and much lower levels were measured for those with diesel engines. Overall, the difference is almost of an order of magnitude. However, the worst performing diesel cars are close to the best-performing petrol cars.

In addition, although neither formally measured nor controlled by the Type VI test, emissions of NO_x increase quite extensively at cold-start in diesel engines. The average levels of NO_x emissions from diesels are 5 to 13 times higher than from the petrol-fuelled types of the comparable Euro class. Furthermore, even if the performance in regulated emissions has been improved quite substantially during this 20 years timeframe, excess fuel consumption has not been lowered that much at all, and in practice, and quite high CO₂ figures are still measured.

We have not considered warm-up engine emissions in this analysis, as typically they were very low, albeit NO_x, which in cold-start was typically only 2 to 3 times higher, compared to warm engine. Furthermore, for CO₂ the cold-start phase typically attributed to about 30% to 60% increase over warm engine, regardless of the EURO-level or fuel type.

Acknowledgements

The Author wishes to thank the Finnish motor magazine “Tekniikan Maailma” for their persisting efforts in testing cars at low ambient conditions, which has made possible this more than two-decade long evaluation of the cold-start/cold ambient emissions performance of passenger cars.

References

- Laurikko, J. (1997) Exhaust emissions from motor vehicles in low ambient temperature conditions. *Int. Journal of Vehicle Design*, Vol 18. Vol. 18, Issue 3-4, pp. 280-292. DOI: 10.1504/IJVD.1997.062054
- Laurikko, J. (1998a) On Exhaust Emissions from Petrol Fuelled Passenger Cars at Low Ambient Temperatures. Espoo 1998, Technical Research Centre of Finland. VTT Publications 348. 210 p. + app. 37 p. (Doctoral Thesis)
- Laurikko, J. (1998b) ‘Regulated and unregulated exhaust emissions from in-use catalyst cars at normal and at low ambient temperatures’. *Int. J. of Vehicle Design*, Vol. 20, January 1998, Nos 1-4 (Special Issue), pp 159-171. DOI: 10.1504/IJVD.1998.001828
- Laurikko, J. (2000) Exhaust emissions from in-use TWC cars driven in Nordic conditions: durability, stability and tune-up issues. *Proc. 9th Int. Symposium on Transport and Air Pollution*, Vol 70, INRETS (ed.), Arcueil, France, 2000, pp. 103-110.
- Laurikko, J. (2001), Exhaust emissions from in-use TWC cars driven in Nordic conditions: durability, stability and tune-up issues. *Int. Journal of Vehicle Design*, Vol 27, Issue 1-4, 2001, pp 44-54. DOI: 10.1504/IJVD.2001.001950
- Laurikko, J. (2003) Cold-start emissions performance of late-model EU2 and EU3 passenger cars in low ambient temperature conditions. 12th Int. symposium «Transport and air pollution» Avignon, 16-18 June 2003. *Proceedings*, n° 92, Volume 2, Inrets ed. Arcueil, France. 2003, p. 165-170.
- Laurikko, J. (2008), Cold-Start Emissions and Excess Fuel Consumption in Low Ambient Temperatures – Assessment of EU2, EU3 and EU4 Passenger Car Performances. Paper F2008-09-049, *Proc. of FISITA 2008 World Automotive Congress*, Munich, Germany, September 2008.
- Laurikko, J. (2016), Cold-Start Emissions and Excess Fuel Consumption at Low Ambient Temperatures: Update on the Impact of EU5 and EU6 Technology on Passenger Cars. Paper F2016-ESYD-004, *Proc. FISITA World Automotive Congress*, September 26-30, 2016, Busan, Republic of Korea. 15 p.
- Weilenmann, M. (2005), Soltic, P, Saxer, C, Forss, AM, Regulated and Nonregulated Diesel and Gasoline Cold Start Emissions at different Temperatures, *Athmospheric Environment*, Vol. 39, No 13, pp 2433-2441, April 2005.

Appendix 1. Average emissions for each sub-fleet.

	CO	HC	NOx	CO₂	PM	PN
Test Fleet ID	avg, g/km	avg, g/km	avg, g/km	avg, g/km	avg, g/km	#x10 ¹¹
Petrol-fuelled, tested with FTP-cycle @ 0 °C						
TM Winter '93	18.30	1.42	0.34	n/a	n/a	n/a
TM Winter '94	16.93	1.31	0.41	n/a	n/a	n/a
TM Winter '95	19.62	1.38	0.21	n/a	n/a	n/a
TM Winter '96	17.97	1.40	0.23	n/a	n/a	n/a
TM Winter '97	15.62	1.31	0.12	n/a	n/a	n/a
TM Winter '98	10.08	0.86	0.19	n/a	n/a	n/a
Petrol-fuelled, tested with ECE15-cycle @ -7 °C						
EcoCar '98	11.73	1.13	0.06	246	n/a	n/a
TM Winter '99	14.03	1.38	1.38	250	n/a	n/a
EcoCar '99	11.68	1.44	1.44	241	n/a	n/a
TM Winter '00	11.43	1.94	0.25	304	n/a	n/a
EcoCar '00	7.06	1.29	0.27	244	n/a	n/a
EcoCar '01	9.83	1.50	0.12	290	n/a	n/a
EcoCar '02	7.27	1.12	0.11	266	n/a	n/a
TM Winter '01	7.47	1.46	0.12	241	n/a	n/a
TM Winter '03	5.93	1.10	0.08	270	n/a	n/a
TM Winter '04	9.04	0.99	0.09	298	n/a	n/a
TM Winter '05	4.58	0.87	0.11	275	n/a	n/a
TM Winter '06	6.80	1.00	0.04	271	n/a	n/a
TM Winter '07	6.41	1.07	0.08	295	n/a	n/a
TM Winter '09	6.30	1.20	0.09	292	n/a	n/a
TM Winter '10	4.23	0.83	0.08	284	n/a	n/a
TM Winter '11	2.80	0.46	0.01	212	n/a	n/a
TM Winter '12	4.24	0.77	0.13	245	n/a	n/a
TM Winter '13	3.74	0.67	0.10	253	0.011	n/a
TM Winter '14	5.18	0.92	0.08	246	0.019	n/a
TM Winter '15	5.17	0.88	0.08	208	0.023	n/a
TM Winter '17	3.82	0.63	0.06	246	0.016	14

TM Winter '18	4.21	0.81	0.10	249	0.032	16
TM Winter '19	2.52	0.46	0.05	240	0.003	58
Diesel-fuelled, tested with ECE15-cycle @ -7 °C						
EcoCar '98	2.27	0.54	0.69	262	0.114	n/a
TM Winter '00	1.51	0.05	1.09	250	0.074	n/a
EcoCar '00	1.16	0.15	1.30	305	0.100	n/a
EcoCar '01	1.05	0.12	0.86	236	0.056	n/a
EcoCar '02	0.95	0.14	1.02	252	0.060	n/a
TM Winter '08	1.09	0.14	0.44	283	0.023	n/a
TM Winter '11	1.77	0.25	1.61	271	0.002	n/a
TM Winter '12	1.14	0.15	1.75	278	n/a	n/a
TM Winter '13	0.99	0.08	1.71	260	0.001	n/a
TM Winter '14	1.10	0.07	1.88	245	0.000	n/a
TM Winter '15	0.22	0.03	0.77	284	0.001	n/a
TM Winter '17	0.27	0.04	1.23	287	0.002	0.1
TM Winter '19	0.76	0.04	1.00	255	0.000	14

2.1.5 Review of Legislative Requirements and Methods for the Estimation of PN/PM Emissions for Advanced Light-duty OBD Applications

D. Kontses¹, S. Geivanidis¹ and Z. Samaras^{1}*

¹ Laboratory of Applied Thermodynamics, Department of Mechanical Engineering, Aristotle University of Thessaloniki, 54124, Greece

*Corresponding author. Tel.: +30-2310-99-6014; fax: +30-2310-99-6019, *E-mail address*: zisis@auth.gr

Abstract

Future On-Board Diagnostics (OBD) legislative requirements will include even lower threshold values for Particulate Mass (PM) emissions, and a limit for Particle Number (PN) emissions to provide detection of failures both for Diesel Particulate Filters (DPFs) and Gasoline Particulate Filters (GPFs). Screening vehicles environmental performance, remote fleet monitoring, Smart Emission Measurement Systems (SEMS) or an alternative method to ensure the effectiveness of the pollution control devices, are also included in the list of studies to be performed and are liable to be object of the next legislative proposal by the European Commission in the field of OBD (European Commission, 2018). Thus, these requirements have created a demand for improved PN/PM sensors and methods able to combine the positive aspects both of OBD sensors and PEMS. The selection of the most appropriate and prominent solution requires the investigation of both the objectives of each application and the characteristics of each technology.

This paper reviews the current and future requirements of advanced OBD in Europe and the corresponding technologies and sensors regarding the PN/PM estimation. Resistive PM sensors are thoroughly analysed in the first part as the most commonly used solution for current legislation. Electrical charge-based and optical methods are also included in this analysis as widely used technologies in the automotive field and possible solutions for advanced OBD applications. The review ends up with the discussion of the readiness and maturity of the methods and sensors for OBD applications.

Abbreviations: Al₂O₃, Aluminium Oxide; CPC, Condensation Particle Counter; DPF, Diesel Particulate Filter; ECM, Electronic Control Module; ECU, Electronic Control Unit; US, United States; EU, European Union; GPF, Gasoline Particulate Filter; Johannes Kepler University Linz, JKU; LII, Laser-Induced Incandescence; NEDC, New European Driving Cycle; NH₃, Ammonia; NO_x, Nitric Oxides; NPTI, New Periodic Technical Inspection; OBD, On-board diagnostics; OBM, On-board Monitoring; OSC, Oxygen Storage Catalyst; PASS, Photoacoustic Soot Sensor; PEMS, Portable Emissions Measurement Systems; PM, Particulate Mass; PN, Particle Number; PPS, Pegasor Particle Sensor; RDE, Real Driving Emissions; SEMS, Smart Emissions Measurement Systems; ZrO₂, Zirconium Dioxide; WLTC, Worldwide harmonized Light-duty vehicles Test Cycle

Introduction

Many conducted studies since the middle of the previous century, have noted the adverse effect of particulate matter emissions from internal combustion engines both on the human beings and the atmospheric environment (Kotin P, Falk HL, 1954, Hesterberg et al., 2012, Campbell et al., 2018). Particulate matter mass and number are considered the two most commonly used properties to characterize particulate matter (Hinds, 1999). In this paper, the abbreviation PM will be used for particulate mass and PN for particle number. Particulate matter after combustion can be classified into 3 categories with the following characteristics: the nucleation mode (5-30nm diameter) contains most of the PN, the accumulation mode (30-500nm diameter with average 40-80nm), with the majority of the PM and finally the coarse mode with a few large particles (Kittelson, 1998, Grose et al., 2006). Automotive sector for road transportation contributes to this degradation of health and air quality in the order of magnitude of 10% for particulate mass (Uherek et al., 2010) and significantly higher, reaching the level of 60% for particle number (Giechaskiel et al., 2015).

The attention historically was focused on the reduction of PM owing to the fact that legislation limits were referred only to mass until the European Union (EU) limits included in 2011 (Euro 5b exhaust emission standards) for the first time, the PN limit of 6×10^{11} [# / km] for diesel engines (Delphi, 2018). During the past decades, a significant reduction of particle emissions has been achieved due to improved engine operation and effective after-treatment technologies driven by the exhaust emission standards and On-Board Diagnostics (OBD) requirements (Braisher et al., 2010). In the case of the EU, the current type-approval legislation for passenger cars and light-duty vehicles, forces the automotive manufacturers to install Diesel and Gasoline Particulate Filters (DPF and GPF) respectively, to conform with the PM and PN limits (Demuyne et al., 2018). These aftertreatment devices are continuously monitored by the OBD system to identify malfunctions or deterioration of components (UNECE, 2017). The most common reasons for a reduced filtration efficiency of a particulate filter are cracks in the substrate, melting of the substrate due to extreme temperature during the regeneration and intentional removal of part or all of the plugs for tampering reasons (Haralampous et al., 2015) (Figure 1).

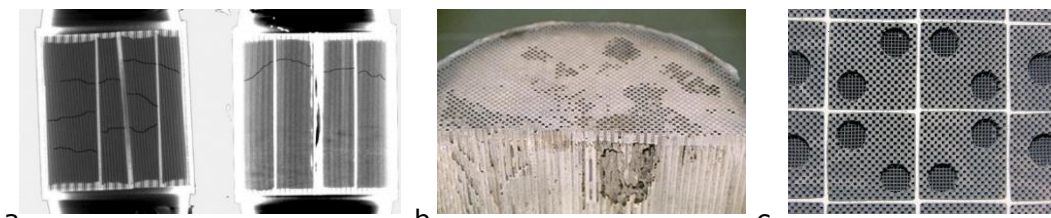


Figure 1: a) Cracks in the substrate, b) melting of the substrate and c) removal of DPF plugs

Primarily resistive PM sensors and secondarily advanced delta-pressure sensors have been already installed by automotive manufacturers in diesel vehicles to conform with the new Euro 6-2 OBD legislation. Also, the market for particulate matter sensors is predicted to be significantly grown until 2020 (Marketsandmarkets, 2015). Nevertheless, their effectiveness for future more stringent limits or new market requirements is in question (Giechaskiel et al., 2014). On the other hand, Portable Emissions Measurement Systems (PEMS) can accurately measure both PM and PN emissions according to the latest Real Driving Emissions (RDE) legislation (European Commission, 2017) but due to their negative aspects such as their high cost, weight and power consumption or the limited maximum continuous operation, are not suitable for current and future OBD applications. Also, the target group of customers for these devices is limited in companies, laboratories and authorities that perform RDE tests in the framework of type approval related projects.

Based on the above, a market gap for improved PN/PM sensors is imminent. These sensors should be able to combine the positive aspects of current OBD sensors with PEMS merits aiming to monitor the emission levels rather than accurately measure them.

In this analysis, the demands and methods for PN/PM estimation as it may be required by future legislation for advanced on-board diagnostics and monitoring are reviewed. To support this

analysis, the key points of the current and upcoming OBD legislation are discussed in the first part. The review continues with the analysis of the resistive PM sensors and its implementation in the current OBD systems. The study continues with the possible solutions for advanced OBD for PN/PM sensor-based methods: optical and electrical charge-based sensors are presented. Finally, the conclusions include the discussion of the readiness and maturity of each technique for OBD applications.

Legislation and market requirements

Focusing on Euro 6 legislation, for better guidance through different levels of PM and PN legislation, three main categories are presented in Table 1. The emission limits with the driving cycle as the core of every regulation for the type-approval of vehicles, the OBD requirements for emission control through vehicle's lifetime and the RDE limits as a representative of the real-world operation of every vehicle. Euro 6-2 OBD legislation for diesel engine passenger cars requires the monitoring of the DPF to ensure the proper performance of the system (UNECE, 2017). The ultimate requirement is to detect a malfunction of the system before the PM emissions exceed the current limit of 12mg/km during the legislative driving cycle and illuminate the Malfunction Indication Light (MIL). Currently, there is no PN limit for OBD, but it is included in the list of studies to be performed for the new EU limits which are now developed (European Commission, 2018). Regarding the two biggest automotive markets in the world, China has adopted the same OBD approach and limits as Euro 6-2, and similarly, the United States regulation controls the PM below 17.5mg/mi with no limit on PN emissions. All other markets use as a template the EU and US limits to define their legislation.

Table 1: EU legislation limits for first registration of vehicles

	9/2014	9/2018	1/2020	>2020
Emission	Euro 6a, b, NEDC		Euro 6a, b, WLTC	
PM	4.5 [mg/km]		4.5 [mg/km]	
PN	6x10 ¹¹ [# /km] *		6x10 ¹¹ [# /km]	
OBD	OBD Euro 6–1		OBD Euro 6–2	
PM	25 [mg/km]		12 [mg/km]	
PN	<i>No limit</i>		<i>No limit</i>	
RDE			E6d Temp. RDE	E6d RDE
PM			<i>No limit</i>	<i>No limit</i>
PN			9x10 ¹¹ [# /km]	9x10 ¹¹ [# /km]

* 6x10¹² [# /km] for GDI

The homologation procedure for approving the compliance of a vehicle with the latest OBD limits consists of three steps. Starting from the simulation of the DPF failure, a defective filter is installed in the exhaust line. This faulty part is usually created by removing some plugs from the DPF outlet, thus creating open channels through which the exhaust gas flows without filtration (Samaras et al., 2014). The second part is the preconditioning period which for the EU can vary starting from minimum of two consecutive driving cycles. Upon request from the manufacturer, alternative or

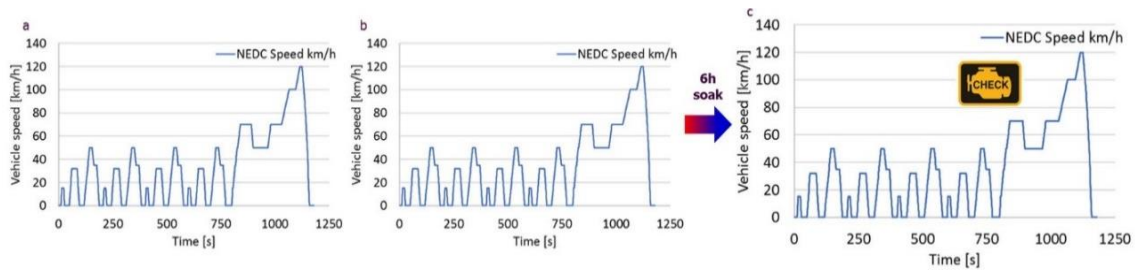


Figure 2: Certification procedure for OBD compliance. Example of NEDC

additional precondition cycles are permitted. The last step to certify that an OBD system successfully ensures the effectiveness of the DPF is the exhaust emission test. Regarding the driving cycle, legislation is currently in a transition period, and both the New European Driving Cycle (NEDC) or the Worldwide harmonized Light-duty vehicles Test Cycle (WLTC) are permitted (Delphi, 2018). Before the end of the emission tests cycle, a vehicle set with the criteria limits for the DPF diagnosis must diagnose the malfunction and illuminate the MIL (Figure 2).

Besides the discussed current legislation, the next step for EU emission legislation which is currently prepared (European Commission, 2018), contains work-packages for assessment of lower limits and additional features of emission legislation. In the following paragraphs, the main topics that the research committee is confronted with, are presented.

Lower OBD threshold values for PM emissions

Euro 6-2 PM standard of 12mg/km was a reasonable limit considering the maturity of the available technology for PM estimation. Delta-pressure and resistive PM sensors are the current solutions for DPF diagnosis. Improved and new sensors can aid in further reducing the limit for a quicker and more effective DPF diagnosis. Nevertheless, this will not improve the expectations for correct GPF failure detection. The range of mass emissions from a gasoline engine before the particulate filter is significantly lower even than the type approval limit of 4.5mg/km. An additional PN limit is discussed in the next paragraph to solve this issue.

OBD limit for PN emissions

Currently, there is not an OBD limit for PN emissions. DPF failures can be sufficiently diagnosed based on the PM OBD limit, but the correct diagnosis of the GPF is not secured due to the low PM emissions of gasoline vehicles which allow a non-GPF equipped vehicle to fulfil the legislative requirements (AVL, 2017). Jessen et al., 2018 presented the four solutions that Bosch examined for GPF diagnosis. Starting from the resistive particle sensor which is used in DPF diagnostics, it appears to be unsuitable for GPF diagnosis. The Oxygen Storage Capacity (OSC) method which uses two lambda sensors, can effectively diagnose only the total removal of a catalysed filter. The temperature sensor-based method can additionally recognize total failures of a non-catalysed filter but again fails to diagnose any partial failure. Finally, the differential pressure sensor seems to be the most promising concept, being able to diagnose a partially failed filter but the achieved accuracy is not considered robust. Therefore, a limit of particles per km is of paramount importance for a flawless diagnosis of GPF removal or functional failure.

Fleet monitoring with on-board sensors and Smart Emission Measurement Systems (SEMS)

The lifetime emission compliance of a vehicle is guaranteed through the OBD system and the periodic inspection (Denis et al., 2005). There are though, clear evidence of OBD tampering especially for DPFs (European Commission, 2018b). Also, periodic inspections have been proved outdated due to low sensitivity, and a New Periodic Technical Inspection (NPTI) is investigated (G. Kadijk et al., 2017). In addition, there are ongoing discussions for new approaches on taxation and traffic regulations such as “polluter pays” schemes. Advanced on-board PN/PM sensors incorporated in smart systems, is a requisite for the adoption of fleet-monitoring.

On-Board Monitoring (OBM) of PN/PM emissions

Emission monitoring can augment the significance and value of new OBD legislation on the target of emission reduction. Being able to measure, record and share data of the performance of vehicle

environmental protection systems is feasible through the advanced sensors, coupled with the necessary software and infrastructure for data sharing and online processing.

In-service conformity:

The questionable effectiveness of current in-service conformity specifications (European Commission, 2018a), forces the legislation authorities, to assess new methods for laboratory tests but also for real-world driving evaluation with PEMS in the light of extended lifetime operation of a vehicle. SEMs and OBM with advanced sensors are considered effective tools in this direction.

Market requirements

Apart from the legislative requirements, there are additional market needs that justify the demand of advanced sensors for OBD applications. The automotive industry could utilise these sensors to improve the new engines and aftertreatment devices or strategies through the plethora of data from the fleet that can be gathered with SEMs. Many research laboratories and organizations, could also be benefited by supplementation of PEMS or laboratory equipment and procedures (such as PMP protocol, SPN method) for creating different layers of particulate matter data in less time and resources consuming manner. The aim is to monitor the emission levels rather than accurately measure them.

These requirements have created a demand for improved PN/PM sensors which are directly installed in the exhaust line and able to combine the positive aspects of current OBD sensors with advantages of PEMS.

Advanced sensors could be incorporated in a sensor-based measurement system which includes an on-board power source, weigh less than 7kg in total, can be quickly set-up and ready for measurement and have accuracy within 10% of current PEMS (Wikipedia, 2019). This system can be easily installed into a vehicle to measure, calculate and deliver real-time data for real-world tailpipe emissions and allows for on-board monitoring in large scale with minimum or no calibration requirements. Example of such system has been already presented as a prototype for gaseous emissions SEMs from TNO and Horiba (Gerrit Kadijk et al., 2016) (TNO, 2018). It records the way the vehicle is operated, enables emission monitoring during the normal operation and provides new insights into real-world nitric oxides (NO_x) and ammonia (NH₃) emissions.

Resistive PM sensors on OBD systems

The resistive sensor along with the correlated OBD model for DPF diagnosis, are presented as a well-established solution for current legislation. A resistive PM sensor consists of a sensor probe and the Electronic Control Module (ECM) (Figure 3) necessary for control and communications with the Electronic Control Unit (ECU) of a vehicle. The probe of a sensor consists of the sensor tip to condition the flow before it reaches the sensing element. This element is a ceramic plate from aluminium oxide (Al₂O₃) or zirconium dioxide (ZrO₂) (2 typical material examples according to the patent (Berger et al., 2009)) and is vertically fitted into the exhaust line. Two or more Platinum electrodes are mounted on the ceramic plate in a specific distance between them. When the sensor is clean from soot, the electrical resistance between these two electrodes is infinite. During the sensing mode, soot deposits and accumulates between the electrodes and gradually decreases the resistance. The measured value could be the voltage in a steady-current circuit or the current in a steady-voltage circuit. Above a specific value of the resistance, the regeneration mode of the sensor is activated to clean the soot deposits, increasing the value of resistance to infinite. During the regeneration process, the temperature is high enough to oxidise soot, but simultaneously under a specific threshold to protect the sensor's material. This process lasts a few minutes depending on the settings of the ECM. The critical measurable quantity of a PM sensor is the duration of the sensor's accumulation event which is called response time. To protect the sensor element from damage and to eliminate measurement discrepancies due to water condensation in the exhaust, the sensor is activated after the temperature in the exhaust reaches a predefined dew point.

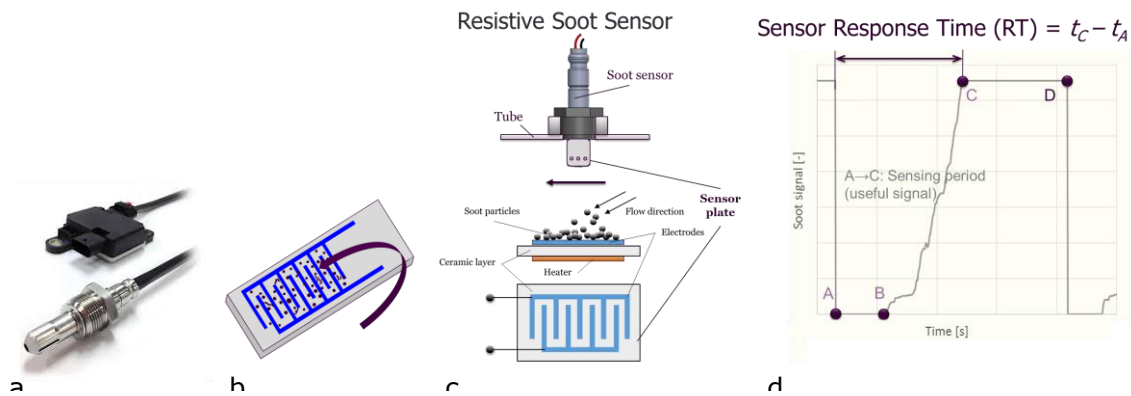


Figure 3: a) ECM with tip, b) element, c) operating principle and d) response time of the Stoneridge resistive PM sensor

Errors associated with resistive sensor accuracy

The sensor itself has a limited accuracy compared to soot measurement laboratory equipment. Khalek, 2015 evaluated six different PM sensors and concluded in $\pm 60\%$ accuracy compared to a reference device. The calculated deviation - even though it is considered encouraging according to that report - is significantly improved in the case of the resistive soot sensor by Stoneridge investigated in this paper. Fragiadoulakis et al., 2018 developed an advanced physical model that evaluates all physical mechanisms and variables governing the operating principle of resistive soot sensors. Although that based on this analysis, the errors associated with the operation of the sensor and the accuracy of the sensor is not possible to be directly calculated, the governing mechanisms that result in this sensor inaccuracy can be clarified, and thus the sensor's inaccuracy can be estimated as presented below.

Physical mechanisms and corresponding variables

The operating principle of the resistive soot sensors as described previously relies on the accumulation of particles on the sensor's element and the resulting decrease of the resistance between the two electrodes. The main deposition mechanisms are thermophoresis, electrophoresis, convective diffusion, inertial impaction and turbulence impaction. Primary inputs for all mechanisms are the exhaust soot concentration, temperature and velocity.

The sensor element has a lower temperature than the exhaust gas due to thermal losses to the environment outside of the exhaust pipe. This temperature difference between the exhaust gas and the sensor element creates a thermophoretic force which attracts particles on the sensor element (Hinds, 1999). The intensity of thermophoretic velocity is primarily defined by the magnitude of the temperature gradient. Sensors electrodes create an electric field near the sensor element which can attract the naturally charged soot particles of the exhaust gas. Electrophoretic velocity depends fundamentally on the intensity of the electric field and the charge of soot particles (Friedlander, 2000). Convective diffusion and consequently deposition on sensor element is possible due to the gradient in particle concentration that exists between the exhaust flow and the sensor element (Bergman et al., 2006). The primary inputs of this mechanism are gas velocity (parallel to the sensor element vector), gas temperature and geometry of the sensor element. The curvilinear motion of the exhaust gas near the element can deviate particles from the streamlines and inertially deposit them on sensor element (Hinds, 1999). Main input variable of this mechanism is the exhaust gas velocity (vertical to the sensor element vector). Except for the inertial impaction, turbulence can also create normal to the sensor element velocity vector and consequently particles deposition (Housiadas et al., 2005). The shear stress developed at the surface of the sensor element is the parameter that defines the significance of this mechanism.

The above mechanisms are described from separate models which output the deposition velocities of soot particles on the sensor element. The main inputs on these models as described above and the corresponding source of errors are summarised in Table 2. According to the specifications of the pre-production source sensor used for this study, the expected maximum inaccuracy is $\pm 25\%$.

Table 2. Input variables for deposition mechanisms and associated errors

Variables	Source of error/inaccuracy
Particle size distribution (d_p, σ_g, μ_g)	Scanning Mobility Particle Sizer Spectrometer (All mechanisms)
Sensor plate geometry ($L, A_{pl}, A_b, V_{pl}, V_b$)	Measurement (All mechanisms)
Sensor plate temperature (T_{plate})	Simulation (Thermophoresis)
Shear stress [N/m ²]	Simulation (Turbulence impaction)
Electric field [V/m]	Simulation (Electrophoresis)
Particle charge distribution	Literature (Electrophoresis)

The sensor signal is fed into an OBD model developed using the commercial software MATLAB/Simulink. This model consists of 3 sub-models (Soot Model, DPF Model and Sensor Model), the signal of the PM sensor and the OBD algorithm which executes the final DPF diagnosis as illustrated in Figure 4. The OBD monitoring is activated when the sensor is in sensing mode, and the DPF regeneration has been already completed. If the DPF efficiency is unacceptable, a flag shall be raised to indicate the Particulate Matter OTL has been reached.

Advanced sensors

As already discussed, future PM/PN sensors need to combine characteristics of current OBD sensors and PEMS and to be integrated into smart systems and advanced OBD models for efficient on-board diagnosis and monitoring. A list of the candidates which are close to the market or in an advanced development phase apart from the previously explained resistive sensor is presented and categorized based on their operating principle (Table 3).

Optical principle

Optical sensors are benefitted from the result of the interaction between the exhaust particles with a laser beam. The incident light can be scattered by a particle, and in parallel, a portion of its energy can be absorbed by the particle. The combination of both effects is extinction. Sensitive detectors are used in all cases to measure and quantify this interaction based on scattering, absorption or extinction. A plethora of laboratory PN/PM instruments are based on the optical method: Condensation Particle Counter (CPC), PhotoAcoustic Soot Sensor (PASS), opacity meters, spotmeters and aethalometers are typical examples (Giechaskiel, 2014). For OBD applications, only a few candidates could cope with the demands for low cost, compact dimensions, no need for calibration during lifecycle and accurate PN/PM measurement. At a

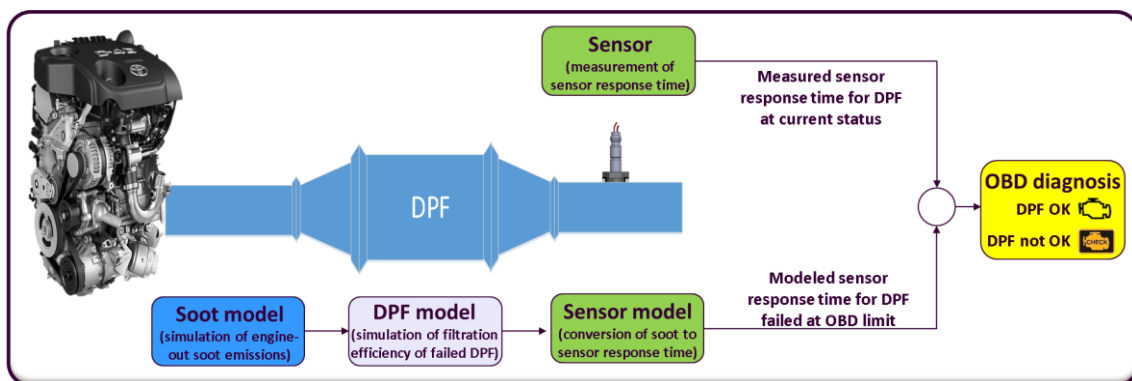


Figure 4: Overview of the OBD model developed in Matlab/Simulink

Table 3: Overview of methods for PN/PM estimation

<i>Operating principle</i>	<i>Particle property</i>	<i>Application</i>
Resistive	PM	OBD
Optical	PN/PM	Advanced OBD
<i>Absorption</i>		
<i>Scattering</i>		
<i>Extinction</i>		
Electrical charge-based	PN/PM	Advanced OBD
<i>Electrostatic</i>		
<i>Diffusion charger</i>		

mature research level, Johannes Kepler University Linz (JKU) has presented a Laser-Induced Incandescence (LII) sensor based on light absorption (Zhang et al., 2017, Zhen Zhang, 2016, Zhen Zhang et al., 2014). Also, 3DATX parSYNC device combines three low-cost environmental sensors based on scattering, extinction and ionization technique (Johnson et al., 2018).

Laser-Induced Incandescence

In the LII technique, the temperature of the particles is increased approximately to 4000K just below the soot sublimation temperature due to particles interaction with the laser beam and the consequent light absorption. Because of the higher temperature, the particles radiate more strongly. This increase in radiation (incandescence) is the LII signal. Its peak is proportional to soot mass and is measured using collection optics and photodetectors. After being heated, the soot particles cool and the incandescence signal will decay with time. This decay time lasts approximately 200–500 ns depending on the size of the primary particles (excitation time=5–20 ns). From the measured LII signal and by application of energy transfer process models, one can obtain the information about the mass fraction (PM) and size distribution of the illuminated particles. Afterwards, the calculation of PN is feasible. The probe is vertically fitted in the exhaust and needs externally cooling (e.g. by pressurized air) which is an issue for OBD applications. Also, concerns are raised about the signal drift due to the clogging of the optical window, but this has been addressed by delivering the laser beam and collecting the incandescent light through the same access. Thus, only one optical window is in contact with the soot in the tail-pipe, and the high power pulsed laser radiation continuously cleans it.

3DATX parSYNC

The unit consists of 3 different sensors sensitive to different size fractions: ionization for fine/ultrafine particles (up to 500nm), scattering for intermediate particulate groups (300nm to 2.5µm) and opacity for coarse particles (approximately 2.5-10+µm). It also provides surrogate outputs for PN and PM. The unit is light-weight (3.7kg) and compact for SEMS applications. Post-processing of the three signals with appropriate transfer function and models can provide good estimations of mass and number for OBD applications. Few studies are available for its performance. Also, there are no data for the performance against instruments compatible with the legislation needs for OBD evaluation.

Electrical charged-based principle

Exhaust particles carry a physical electrical charge. According to Maricq, 2006 and Bilby et al., 2016 the exhaust particles can be considered electrically neutral. 30-45% of particles are positively charged, 30-45% negatively and 10-40% are neutral following a Boltzmann charge

distribution (Maricq, 2008). This charge distribution was found to be the same for engine-out and post DPF measurements of a diesel engine and similar to gasoline engines (Maricq, 2006).

Electrostatic sensors

Electrostatic sensors exploit this natural charge. Continental (Continental Automotive GmbH, 2019), EmiSense (Allmendinger et al., 2013) and Honeywell (Honeywell Laboratories Plymouth, 2010) have developed or evolved sensors based on the electrostatic principle. The EmiSense sensor seems to have the most highly evolved design consisting of two coaxial electrodes protected by an optimized sensor tip and is positioned vertically to exhaust gas flow. The principal of operation is to separate the positive and negative particles onto two electrodes, create dendrites of particles in each electrode which carry an amplified charge and afterwards measure the produced current from the electrically induced mobility created by the bouncing of agglomerates between the two electrodes. Owing to the high amplification gained by charge accumulation on the agglomerates (2-3 order of magnitude higher than the natural charge) the insulators and amplifiers of the sensor are simple and low-cost. The measured current is well correlated to PM (Steppan et al., 2014). Correlation to PN has not been validated yet. Also, cross-sensitivity to exhaust flow was investigated by Maricq et al., 2018. High flow increases the drag force of the dendrites and tilts them away from the opposite electrode without significant fragmentation. This phenomenon creates a quiescent period with artefacts on the sensor signal. Low concentration can deteriorate this phenomenon. Finally, contrary to the accumulation sensors, cross-sensitivity to ash is not a significant issue for the lifetime of the sensor.

Diffusion charger sensors

Particles are also able to acquire additional electrical charge by diffusion, field and flame charging and static electrification. A corona diffusion discharger achieves highly concentrated unipolar ion charging. Dekati investigated this ionizing technique by diffusion as a miniature device or sensor with ETaPS (Electrical Tail Pipe Sensor) (Rostedt et al., 2009) which was further refined and developed by Pegasor with the PPS (Pegasor Particle Sensor). Recently NGK/NTK presented a miniature PPS which is highly portable, cost-effective and integrated into the NGK/NTK compact emissions meter (NCEM) along with NO_x and lambda sensors. Rostedt et al., 2017 presented a miniaturized sensor for OBD applications which is also a compact PPS in terms of operating principle and hardware components. Details of the operation of the PPS and the first results on a diesel engine were presented by Ntziachristos et al., 2009. A series of publications followed in the next years about the operating principle, sensor calibration and various applications for Pegasor-type DC sensors. These are all summarised by Besch, 2016 and are briefly described below.

A high voltage corona discharge produces unipolar ions. Particles are pumped inside the sensor body by an ejector diluter using sheath air and subsequently are charged by ions via diffusion charging. The excess of ions that are not attached to particles is removed from an ion trap. The escaping current of the particles exiting the sensor body, demands an additional current to maintain the electrical balance of the isolated part of the sensor. This current is measured by an electrometer and is proportional to the particle surface area. Proper calibration with diesel exhaust of this signal was performed by (Leonidas Ntziachristos et al., 2013), to report the PM and the PN concentration. Enhanced performance and accuracy on PN/PM estimation can be achieved using two Pegasor sensors in parallel with different ion trap voltages. This set up yields two different signals because of the different fraction of the size distribution collected by the two sensors. The comparison of the two signals provides information for the particle size distribution which ameliorates the performance of PN and PM calculation and significantly reduces the PPS error (Amanatidis et al., 2016). Nevertheless, this complicated set-up is not suitable for OBD applications. A critical drawback of Pegasor-type sensors is the requirement for compressed air. This needs to be addressed for OBD applications (Rostedt, 2017). Finally, durability tests are not currently available, and the drift of the sensor due to internal contamination should be investigated.

Conclusions

This study presented the requirements and the methods for particulate mass and particle number estimation for advanced on-board applications. The review of the current and imminent OBD legislative requirements revealed the different levels and challenges that the sensors will confront. Lower mass limits, additional number limit, on-board and fleet monitoring with smart systems and more sensitive and effective in-service conformity checks, require advanced sensors able to be set-up and be ready for measurement in a short period. Calculation and delivery of real-time data in the framework of on-board monitoring necessitate integrating these sensors in smart systems similarly to already available gaseous emissions SEMS. The level of accuracy desired will be different among each application or requirement, but undoubtedly it will be better compared to the currently available resistive soot sensors. The method developed for current OBD using the resistive technology should be used as the template for advanced on-board applications.

Optical and electrical-charged based principles were presented as candidate sensor solutions. The LII sensor can provide an accurate and direct measurement of both PN and PM, but improvements are needed for OBD application focusing on contamination and cooling issues and the high complexity of high-power laser. 3DATX parSYNC combines low-cost technology with advanced algorithms to calculate the PN and PM levels. The available data though is not sufficient to extract solid conclusions for the accuracy and sensitivity of the system. Electrostatic sensors are for many years in the market but the cross-sensitivities to high flow and their inadequate performance on low emission levels, entail the need for further investigation and improvements. Finally, sensor based on diffusion charge technology, have been proved accurate for OBD applications. Nevertheless, the sophisticated design and the need for clean pressurised air restrain presently a wide adoption for advanced OBD applications.

A natural progression of this work and a proposal for future research is to analyse and to perform measurements with the presented sensors and technologies in order to create solid conclusions for the readiness level and the necessary improvements needed for OBD applications.

Acknowledgements

This work was supported by Greek State Scholarships Foundation under the “Scholarship program for postgraduate studies”.

References

- Allmendinger, Klaus, Brett Henderson, Jim Steppan, Anthoniraj Lourdhusamy, Victor Wang, Joe Fitzpatrick, Matti Maricq, and Dave Kubinski Ford Motor Company,2013,“Comparison of Experimental and First Principles Modeling Results for the PMTrac © Electrostatic Soot Sensor.”
- Amanatidis, Stavros, M. Matti Maricq, Leonidas Ntziachristos, and Zissis Samaras,2016,“Measuring Number, Mass, and Size of Exhaust Particles with Diffusion Chargers: The Dual Pegasor Particle Sensor.” *Journal of Aerosol Science* 92: 1–15. <https://doi.org/10.1016/j.jaerosci.2015.10.005>.
- AVL,2017,“AVL Powertrain Engineering Techday # 4 Gasoline Particle Filter Development and Calibration AVL Experience on GPF System.”
- Berger, J., R. Strohmaier, D. Heimann, N. Breuer, R. Wirth, K.F. F Reinhart, R. Schmidt, et al.,2009,“Modeling Soot Formation in Diesel Engines Using Conditional Moment Closure.” *Fuel* 135 (November): 269–78. <https://doi.org/10.1016/j.fuel.2014.06.046>.
- Bergman, Theodore, Adrienne Lavine, Frank Incropera, and David DeWitt,2006,*Fundamentals of Heat and Mass Transfer*.
- Besch, Marc Cyrill,2016,“In-Line, Real-Time Particulate Matter Sensors for OBD and Exhaust After-Treatment System Control Applications.”
- Bilby, David, David Kubinski, and Matti Maricq,2016,“Investigating the Operating Principle of the Emisense PMTrac Sensor.”
- Braisher, Mike, Richard Stone, and Phil Price,2010,“Particle Number Emissions from a Range of European Vehicles,” no. Ci. <https://doi.org/10.4271/2010-01-0786>.
- Campbell, Patrick, Yang Zhang, Fang Yan, Zifeng Lu, and David Streets,2018,“Impacts of Transportation Sector Emissions on Future U.S. Air Quality in a Changing Climate. Part II: Air Quality Projections and

- the Interplay between Emissions and Climate Change." *Environmental Pollution* 238 (July): 918–30. <https://linkinghub.elsevier.com/retrieve/pii/S0269749117350790>.
- Continental Automotive GmbH,2019,"Continental Automotive - Sensors." Continental. 2019. <https://www.continental-automotive.com/en-gl/Off-Highway/Agriculture/Powertrain/Exhaust-Management-After-treatment/Sensors/Electrostatic-Particulate-Matter-Sensor>.
- Delphi,2018,"Delphi-Emissions for Pass Car and Light Duty 2018-2019." https://d2ou7ivda5raf2.cloudfront.net/sites/default/files/inline-files/booklet_emission_complete_PC18.pdf.
- Demuynck, Joachim, Cecile Favre, Dirk Bosteels, Heather Hamje, and Jon Andersson,2018,"Real-World Emissions Measurements of a Gasoline Direct Injection Vehicle without and with a Gasoline Particulate Filter Experimental Set-Up." <https://doi.org/10.4271/2017-01-0985>.Copyright.
- Denis, Michael St, and Jim Lindner,2005,"Review of Light-Duty Diesel and Heavy-Duty Diesel Gasoline Inspection Programs." *Journal of the Air and Waste Management Association* 55 (12): 1876–84. <https://doi.org/10.1080/10473289.2005.10464773>.
- European comission,2017,"Commission Regulation (EU) 2017/1154."
- European Comission,2018,"Framework Contract for Studies and Technical Assistance in the Field of Emissions-No 688/PP/2018/FC."
- European Commission,2018a,"EU 2018/1832."
- ,2018b,"Horizon 2020 Smart Green and Integrated Transport." https://ec.europa.eu/research/participants/data/ref/h2020/wp/2018-2020/main/h2020-wp1820-transport_en.pdf.
- Fragkiadoulakis, Pavlos, Savas Geivanidis, and Zissis Samaras,2018,"Modeling a Resistive Soot Sensor by Particle Deposition Mechanisms." *Journal of Aerosol Science* 123 (May 2016): 76–90. <https://doi.org/10.1016/j.jaerosci.2018.06.005>.
- Friedlander, Sheldon K.,2000,*Smoke, Dust, and Haze: Fundamentals of Aerosol Dynamics*.
- Giechaskiel, Barouch, Matti Maricq, Leonidas Ntziachristos, Christos Dardiotis, Xiaoliang Wang, Harald Axmann, Alexander Bergmann, and Wolfgang Schindler,2014,"Review of Motor Vehicle Particulate Emissions Sampling and Measurement: From Smoke and Filter Mass to Particle Number." *Journal of Aerosol Science* 67 (January): 48–86. <https://doi.org/10.1016/J.JAEROSCI.2013.09.003>.
- Giechaskiel, Barouch, Francesco Riccobono, Theodoros Vlachos, Pablo Mendoza-Villafuerte, Ricardo Suarez-Bertoa, Georgios Fontaras, Pierre Bonnel, and Martin Weiss,2015,"Vehicle Emission Factors of Solid Nanoparticles in the Laboratory and on the Road Using Portable Emission Measurement Systems (PEMS)." *Frontiers in Environmental Science* 3 (December): 1–17. <https://doi.org/10.3389/fenvs.2015.00082>.
- Grose, Melissa, Hiromu Sakurai, Jake Savstrom, Mark R. Stolzenburg, Winthrop F. Watts, Christopher G. Morgan, Ian P. Murray, Martyn V. Twigg, David B. Kittelson, and Peter H. McMurry,2006,"Chemical and Physical Properties of Ultrafine Diesel Exhaust Particles Sampled Downstream of a Catalytic Trap." *Environmental Science & Technology* 40 (17): 5502–7. <https://doi.org/10.1021/es052267+>.
- Haralampous, Onoufriou A, and Dimitrios Mastellos,2015,"A Multi-Channel Mathematical Model for Partially Failed Diesel Particulate Filters." In *8th GRACM International Congress on Computational Mechanics*.
- Hesterberg, Thomas W., Christopher M. Long, William B. Bunn, Charles A. Lapin, Roger O. McClellan, and Peter A. Valberg,2012,"Health Effects Research and Regulation of Diesel Exhaust: An Historical Overview Focused on Lung Cancer Risk." *Inhalation Toxicology* 24 (sup1): 1–45. <https://doi.org/10.3109/08958378.2012.691913>.
- Hinds, William C.,1999,*Aerosol Technology : Properties, Behavior, and Measurement of Airborne Particles*. Wiley.
- Honeywell Laboratories Plymouth,2010,"Demonstration of Particulate Matter (PM) Sensor in Post-DPF Environment Innovative Clean Air Technologies (ICAT) 2008 Grant Program." <https://www.arb.ca.gov/research/seminars/krafthefer/krafthefer.pdf>.
- Housiadas, C, and Y Drossinos,2005,"Thermophoretic Deposition in Tube Flow." *Aerosol Science and Technology* 39 (4): 304–18. <https://doi.org/10.1080/027868290931069>.
- Jessen, Holger, Markus Willimowski, and Frank Meier,2018,"Bosch Solutions for Gasoline Particulate Filter Monitoring Bosch Solutions for GPF Monitoring Gasoline Particulate Filter OBD Requirements and Configurations Pressure Based Monitoring Hose Line Monitoring." In .
- Johnson, Kent, Kanok Boriboonsomsin, and Matthew Barth,2018,"Dynamic Energy and Emissions Management (DEEM)." In *PEMS Workshop 2018*.

- Kadijk, G., and A. Mayer, 2017, "White Paper NPTE – the New Periodic Technical Inspection Emission Test Procedure for Vehicles with Emission Control Systems .," 12.
- Kadijk, Gerrit, Norbert Ligterink, Pim van Mensch, and Richard Smokers, 2016, "NOx Emissions of Diesel Cars in the Lab and on the Road." <https://doi.org/10.13140/RG.2.2.30386.61126>.
- Khalek, Imad, 2015, "Ormance & Durability for OBD Applications & Beyond."
- Kittelsohn, David B., 1998, "Engines and Nanoparticles: A Review." *J. Aerosol Sci.* 38 (2): 197–204. [https://doi.org/10.1016/S0021-8502\(97\)10037-4](https://doi.org/10.1016/S0021-8502(97)10037-4).
- Kotin P, Falk HL, Thomas M., 1954, "Aromatic Hydrocarbons. II. Presence in the Particulate Phase of Gasoline-Engine Exhausts and the Carcinogenicity of Exhaust Extracts."
- Maricq, M. Matti, 2006, "On the Electrical Charge of Motor Vehicle Exhaust Particles." *Journal of Aerosol Science* 37 (7): 858–74. <https://doi.org/10.1016/j.jaerosci.2005.08.003>.
- , 2008, "Bipolar Diffusion Charging of Soot Aggregates." *Aerosol Science and Technology* 42 (4): 247–54. <https://doi.org/10.1080/02786820801958775>.
- Maricq, M. Matti, and David Bilby, 2018, "The Impact of Voltage and Flow on the Electrostatic Soot Sensor and the Implications for Its Use as a Diesel Particulate Filter Monitor." *Journal of Aerosol Science* 124 (June): 41–53. <https://doi.org/10.1016/j.jaerosci.2018.07.002>.
- Marketsandmarkets, 2015, "Exhaust Sensor Market by Sensor Type, Fuel Type, Region – 2020 | MarketsandMarkets." <https://www.marketsandmarkets.com/Market-Reports/automotive-exhaust-sensor-market-98474123.html>.
- Ntziachristos, L., T. Tzamkiozis, and J. Tikkanen, 2009, "A New Sensor for On-Board Diagnosis of Particle Filter Operation - First Results and Development Potential." In *FAD Conference, Dresden, Germany*.
- Ntziachristos, Leonidas, Stavros Amanatidis, Zissis Samaras, Kauko Janka, and Juha Tikkanen, 2013, "Application of the Pegasor Particle Sensor for the Measurement of Mass and Particle Number Emissions." *SAE International Journal of Fuels and Lubricants* 6 (2): 2013-01-1561. <https://doi.org/10.4271/2013-01-1561>.
- Rostedt, Antti, Marko Marjamäki, Jaakko Yli-Ojanperä, Jorma Keskinen, Kauko Janka, Ville Niemelä, and Ari Ukkonen, 2009, "Non-Collecting Electrical Sensor for Particle Concentration Measurement." *Aerosol and Air Quality Research* 9 (4): 470–77. <https://doi.org/10.4209/aaqr.2009.03.0023>.
- Rostedt, Antti, Leonidas D. Ntziachristos, Pauli Simonen, Topi Rönkkö, Zissis C. Samaras, Risto Hillamo, Kauko Janka, and Jorma Keskinen, 2017, "A New Miniaturized Sensor for Ultra-Fast On-Board Soot Concentration Measurements." *SAE International Journal of Engines* 10 (4): 2017-01-1008. <https://doi.org/10.4271/2017-01-1008>.
- Samaras, Zissis, Geivanidis Savas, Vonk Willar, Andersson Jon, Sindano Hector, Hausberger Stefan, Stadlhofer Werner, and Perujo Adolfo 5Carriero, 2014, "Evaluation of Soot Sensors for DPF Failure Monitoring." In *FISITA 2014 World Automotive Congress, Maastricht, Netherlands*.
- Steppan, Jim, Brett Henderson, Anthoniraj Lourdhusamy, Victor Wang, Joe Fitzpatrick, and Klaus Allmendinger, 2014, "Characterization of an In Situ Electrostatic Soot Sensor with Laboratory Measurement Instruments," 1–13.
- TNO, 2018, "HORIBA and TNO Bundle Forces to Promote Smart Emission Measurement System (SEMS) | TNO." 2018. <https://www.tno.nl/en/about-tno/news/2018/6/horiba-and-tno-bundle-forces-to-promote-smart-emission-measurement-system-sems/>.
- Uherek, Elmar, Tomas Halenka, Jens Borken-Kleefeld, Yves Balkanski, Terje Berntsen, Carlos Borrego, Michael Gauss, et al., 2010, "Transport Impacts on Atmosphere and Climate: Land Transport." *Atmospheric Environment* 44: 4772–4816. <https://doi.org/10.1016/j.atmosenv.2010.01.002>.
- UNECE, 2017, "Addendum 82: Regulation No. 83." *Inland Transport Committee*, no. March 1958.
- Wikipedia, 2019, "Portable Emissions Measurement System." 2019.
- Zhang, Z., L. Del Re, and R. Fuerhapter, 2017, "Fast Hybrid Sensor for Soot of Production CI Engines." *SAE Technical Papers* 2017–Sept. <https://doi.org/10.4271/2017-24-0137>.
- Zhang, Zhen, Richiard Fuehrapter, Harald Waschl, and Luigi Del Re, 2016, "Calibration and Performance of a Novel In-Situ Soot Sensor for Production Engines." *Procedia Engineering* 168: 43–46. <https://doi.org/10.1016/j.proeng.2016.11.135>.
- Zhang, Zhen, Stephan Stadlbauer, Richard Viskup, Luigi Re, Alexander Bergmann, Tristan Reinisch, Stephan Stadlbauer Richard Viskup, and Richard Fuerhapter Luigi del Re, 2014, "Fast Measurement of Soot by In-Situ LII on a Production Engine." *Proceedings of the ASME 2014 Internal Combustion Engine Division Fall Technical Conference*, no. October: 1–8. <https://doi.org/10.1115/ICEF2014-5555>.

2.1.6 Real-world Vehicle Emission Measurements using PEMS in Hong Kong

C.K.L. Wong^{1*}, T.S. Lo¹, K.L. Ng¹, H.L.A. Wong¹, C. Keramydas², G. Papadopoulos²

¹ Mobile Source Group, Hong Kong Environmental Protection Department, Hong Kong SAR Government, China, carolw@epd.gov.hk

² EMISIA S.A., 21 Antoni Trisi str., P.O. Box 8138, GR57001 Thessaloniki, Greece

Introduction

Hong Kong Environmental Protection Department (HKEPD) has been conducting real-world vehicle emission measurements using Portable Emission Measurement System (PEMS) since 2008. The applications include evaluating various emission reduction initiatives (Keramydas et al., 2018), identifying and measuring the emissions of high emitters, and estimating the emission factors of vehicles using the vehicle emission model EMFAC-HK (EMFAC, <https://www.arb.ca.gov/emfac/>).

One of the most interesting findings in our PEMS measurement is about the identification and investigation of the high emitters. In April 2016, the UK Department for Transport published the results of the emission testing programme which was designed to test a wide range of best-selling passenger cars (Department for Transport, 2016). Emissions were measured by dynamometer using New European Driving Cycle (NEDC) and reverse NEDC. They found that the NO_x emissions of the reversed NEDC were approximately 5 times higher than the standard NEDC. Furthermore, conducting emission tests on public roads (Real Driving Emissions testing), they found that the NO_x emissions were 854 mg/km, namely 5 times higher than the Euro 5 standard emission limit (180 mg/km). In May 2016, the German Federal Ministry of Transport and Digital Infrastructure (BMVI, 2016) published the results of the field investigation of the Federal Motor Transport Authority into unlawful defeat devices in diesel vehicles. For some vehicles with unlawful defeat devices, the average NO_x emissions for the cold NEDC were 117 mg/km, ranging from 103 to 136 mg/km, for the warm NEDC were 289 mg/km, ranging from 106 to 375 mg/km, for the on-road NEDC were 499 mg/km ranging from 246 to 797 mg/km and for the on-road NEDC reverse were 676 mg/km, ranging from 412 to 901 mg/km. In (Franco 2014), the NO_x emission is found to be several times higher when compared the results in the road tests to the laboratory tests. The contrasting emission results in standard NEDC tests, modified NEDC tests and road tests indicate that the emission control devices are functioning significantly differently in different situations.

In this study, we shall show our similar study of PEMS and dynamometer tests of some brand of vehicles. We shall also show the emission results for a vehicle fitted with defeat device before and after remediation. In addition, a completely new brand of high emitters is presented. Besides high emitters, we have also devoted much effort to measure the emissions of taxis because they are one of the major contributors to road side emissions (HK Environment Bureau, 2017). In this paper, we shall describe our measurement results. Finally, we shall present our method to derive the second by second altitude of the testing vehicle. The method involves combining data from different sources. They include barometer and GPS measurement, spot-height, and road polygon and road centreline. We shall present the problems identified, and their resolutions.

Measurement Procedure

For all the PEMS measurements we mentioned in this study, the testing procedure of PEMS followed the most stringent testing requirements stipulated in ISO 16183, US CFR 1065 Subpart J and PEMS requirements in Euro 6 regulation with a few exceptions. Zero checking / calibrations were performed every hour, and the span checking / calibrations at the beginning and the end of the day. Audit check was also performed every 3 hours. If the audit check fails, the test will be flagged as invalid and dropped. The PEMS tests were conducted in both real-world driving and on the dynamometer in test cell. The recruited drivers are professional drivers of the same vehicle type. There are two types of PEMS measurements: i) the testing vehicle followed the vehicles of the same vehicle class (e.g., bus, taxi) to simulate their driving; and ii) the testing vehicle was driven on a pre-determined route which comprises both urban and highway driving. The payload was 50-60% of the maximum for heavy duty vehicles, whereas the weight of PEMS and its accessories is >50% of the maximum payload for the light duty vehicles. 2-3 fuel samples from

the fuel tank of each vehicle were analysed to ensure no abnormality in the fuel specification. For the dynamometer testing, only constant volume sampling (CVS) and bag samples were taken using standard NEDC driving cycle (the certification test) whereas measurements for other cycles were taken by both CVS and bag samples and PEMS analysers simultaneously.

SEMTECH-DS or AVL GAS PEMS was used for CO₂, CO, NO, NO₂ and THC real-time measurements. Exhaust flow meter was used to measure the exhaust flow rate and the exhaust flow temperature. A speedometer was attached to the wheel of the vehicle to record the vehicle speed. A weather probe was installed at the top of the vehicle to record the ambient temperature. An engine speed sensor was used to record vehicle engine speed. GPS with dead reckoning was used to record the position of the vehicle. Its result was combined with barometer measurements, and the survey data to estimate the road gradient of the testing vehicle. The data frequency of all these measurement is 1Hz. The example installation of PEMS is shown in figure 1.

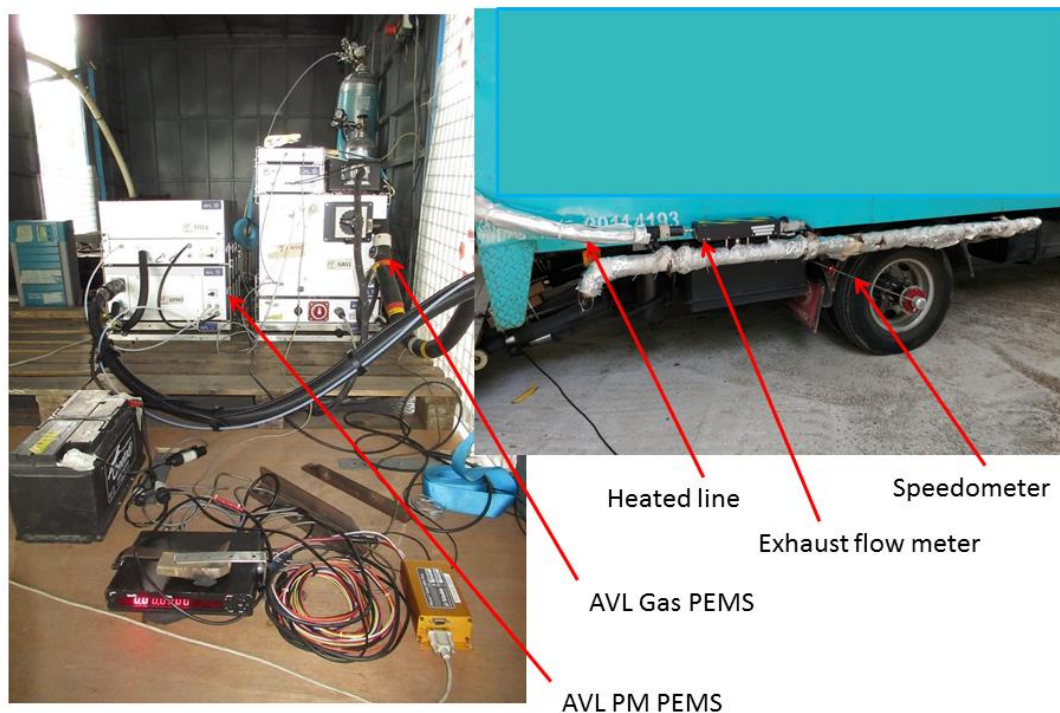


Figure 1: Example PEMS set-up for a double deck bus.

Before being analysed, the collected data were post-processed: i) the measurements from various analysers were synchronized by human eyes, with the help of algorithms which suggest the synchronization time that matches the maximum correlations between signals, and the sudden changes in signals when starting from idling; ii) since the exhaust gas was measured dry (except THC), the dry-to-wet correction was applied to convert the measurements to wet; iii) a drift correction was applied to compensate the drift of the analyser throughout the test and iv) a humidity correction was applied for NO and NO₂.

High Emitters

By 2018, EPD has tested 35 vans. The NO_x emissions for the vehicles are shown in figure 2. The NO_x emissions in the graph were calculated by:

1. dividing the whole test (typically last for 1 hour) into segments of every 8 minutes for each road test;

2. calculating the average speed and NOx emission factor (g/km) for each segment;
3. Extracting the segments with each average speed range of $[x - 4 \text{ kph}, x + 4 \text{ kph}]$, where x were selected to be 12, 36, 60 and 84 kph;
4. Taking the average over the NOx emission factors for the extracted segments.

Therefore, the speed dependence of the emission factors is eliminated through selecting a specific speed range. Emissions estimated in (g/km) are typically increasing toward low speed because the time taken to travel for a certain distance is increasing. As shown in figure 2 below, NOx emissions are mostly the highest at low speed and lowest at high speed.

Real-world Emission Testing using PEMS for Diesel Vans

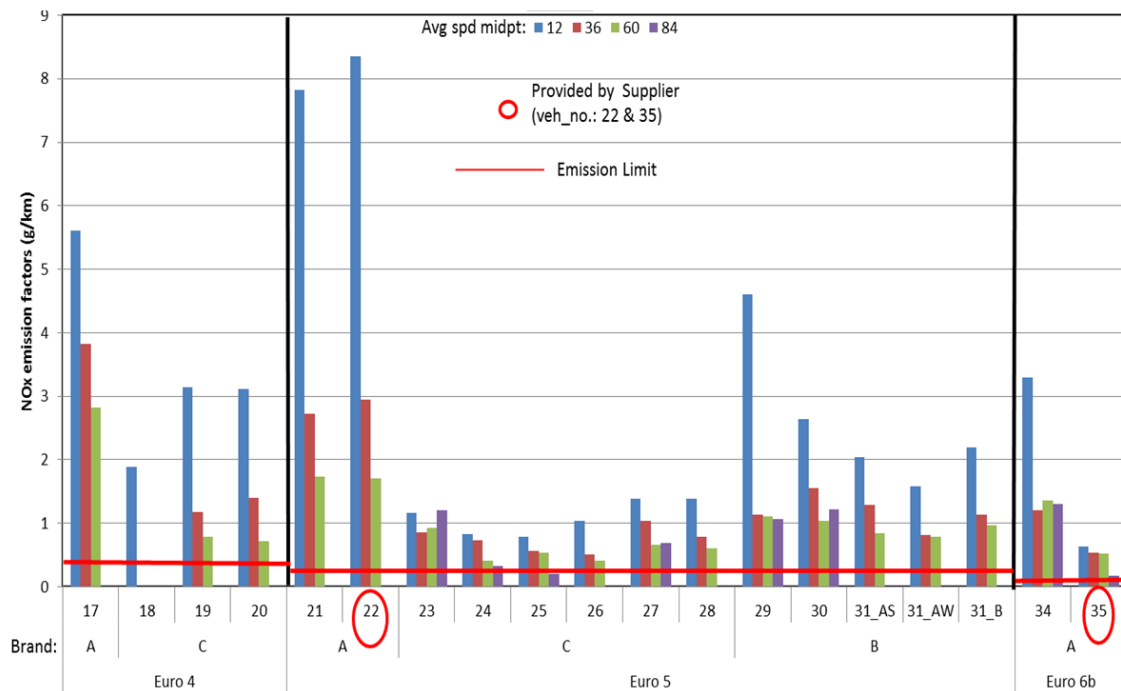


Figure 2: NOx emission of vans

One could observe that for Euro 4 and 5, there are some vehicles having extra-ordinary high emissions, and they are all came from the same brand (Brand A). Next to it, the emissions from the brand marked with (Brand B) are the second highest. Emissions from the Brand C are the lowest, but still considerably higher than the emission limit. According to Kousoulidou et al., 2013; Weiss et al., 2011; and Vlachos et al., 2014, the NOx emissions measured in road tests are significantly higher than that of the laboratory tests.

Brand B

Brand B was the main focus in the study because some of its vehicle models are known to be fitted with defeat device but the LGV34_29 and LGV34_30 are not included. Nevertheless, the emissions of these two vehicles are considerably higher than Brand C. Figure 3 compares the trip based NOx emission factors for these two vehicles (Brand B) with those from the vehicles in the Brand C, with different vehicle speeds. It shows that their NOx emissions are higher than that of the Brand C of the same emission standard (EURO 5), but comparable that of the lower standard (EURO 4).

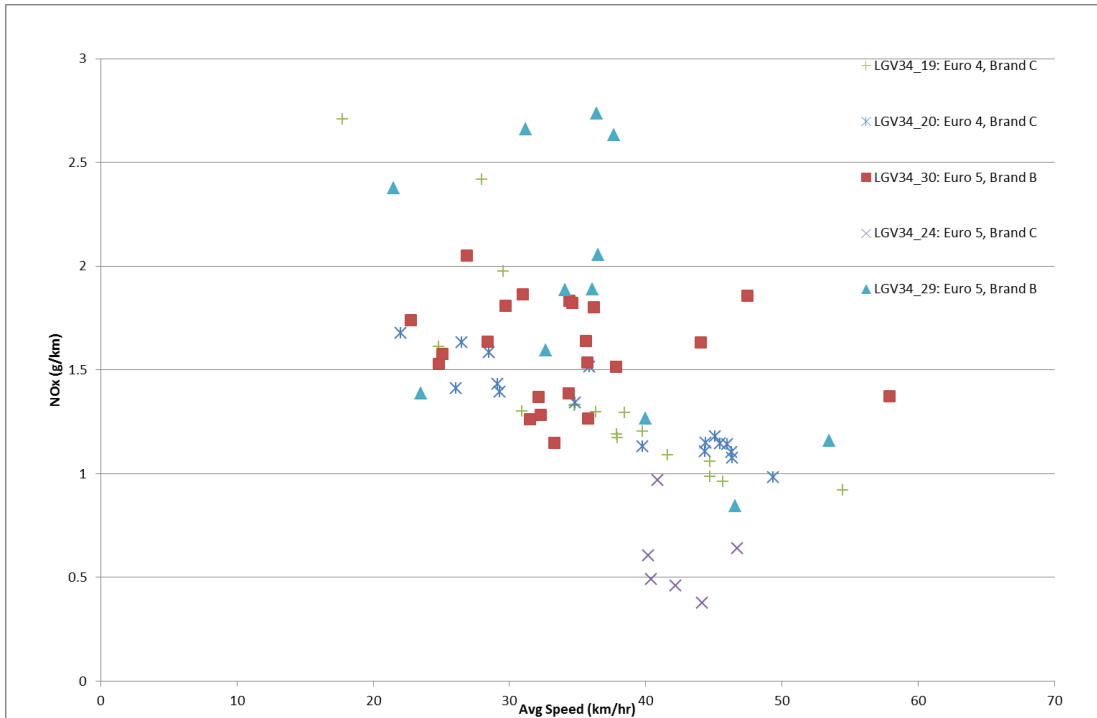


Figure 3: Trip based NOx emission factors for LGV34_30, LGV34_29 of Brand B and the vehicles in the Brand C.

Table 1 shows the information about vehicles of Brand B under testing

Table 1: Vehicle Description

Description	LGV34_29	LGV34_30	LGV34_31
Brand	B		
Reg Year	2015		2013
Fuel	Diesel		
Euro Standard	Euro 5		
Emission control technology	DPF, EGR		
Mileage (km)	864	83	~ 68,000
Transmission	Automatic		
Gross Vehicle Weight (t)	2.82	2.8	2.28
Weight before/after PEMS installation (t)	2.1/2.8	2.0/2.5	1.6/2.0
Number of cylinders	4		
Engine displacement (lt)	2		1.6
Engine rated power (kW@rpm)	132@4000	103@3500	75@4400
Engine peak torque (Nm@rpm)	420@1750	340@1750-2500	250@1500-2500

To further investigate their emissions, we compare the dynamometer test and road test for two vehicles, LGV34_29 and LGV34_30 (figure 4).

Note that the configurations of the dynamometer tests are different for two vehicles. For LGV34_30, the vehicle was loaded with PEMS analyzers during the test. The vehicle was heavier

than that of the normal certification test. This could explain why NOx emissions are higher than the regulatory limit. For LGV34_29, the vehicle weight is the same as that in the certification test. The results show that the NOx emissions in the road tests are about five times higher than that of the dynamometer tests.

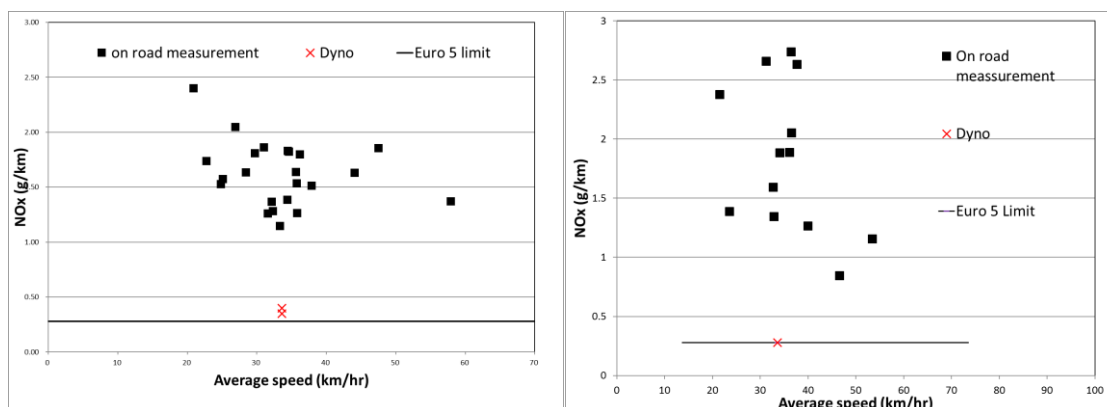


Figure 4: Comparison of NOx emissions from road tests to dynamometer tests. Left panel: LGV34_30, Right panel: LGV34_29.

Comparison tests of a vehicle known to be fitted with defeat device (LGV34_31-33) were conducted. The vehicle was tested for 3 times: i) with defeat device (LGV34_31_B) (avg. ambient temp.: 30°C & Avg. RH:71%); ii) with the defeat device remediated in summer (LGV34_31_AS) (avg. ambient temp.: 31°C & Avg. RH:61%); and iii) with the defeat device remediated in winter (LGV34_31_AW) (avg. ambient temp.: 23°C & Avg. RH:42%).

In i) and ii) tests, both dyno tests and road tests were conducted. Four different dyno testing conditions were carried out:

1) NEDC certification tests (NEDC-C)

Certification conditions were followed. Only bag measurements (CVS measurements) were measured.

2) Hot NEDC driving cycle (NEDC-H)

The vehicle was warmed up before the measurements and emissions were measured using both PEMS and CVS and bag.

3) “reverse” NEDC cycle (NEDC-RH)

By “reverse”, position of the high speed “highway” part and the low speed “urban” of the cycle are switched (figure 5). The vehicle was warmed up before the test. Emissions were measured using both PEMS and CVS and bag.

4) EPD cycle

The driving cycle was synthesized using speed time trace data collected by PEMS. The testing vehicle was warmed up before the test. Emissions were measured using both PEMS and CVS and bag.

Three repetitions were taken for each type of tests above.

As for the road tests, data from three road routes are selected (figure 5). The average speeds of the three routes are about 26-39 kph, which is similar to the average speeds of the cycles (33 kph for NEDC and its NEDC-RH, 40 kph for EPD cycle). The testing information is summarized in table 2 for easy reference. The testing information for LGV34_29 and LGV34_30 are shown as well.

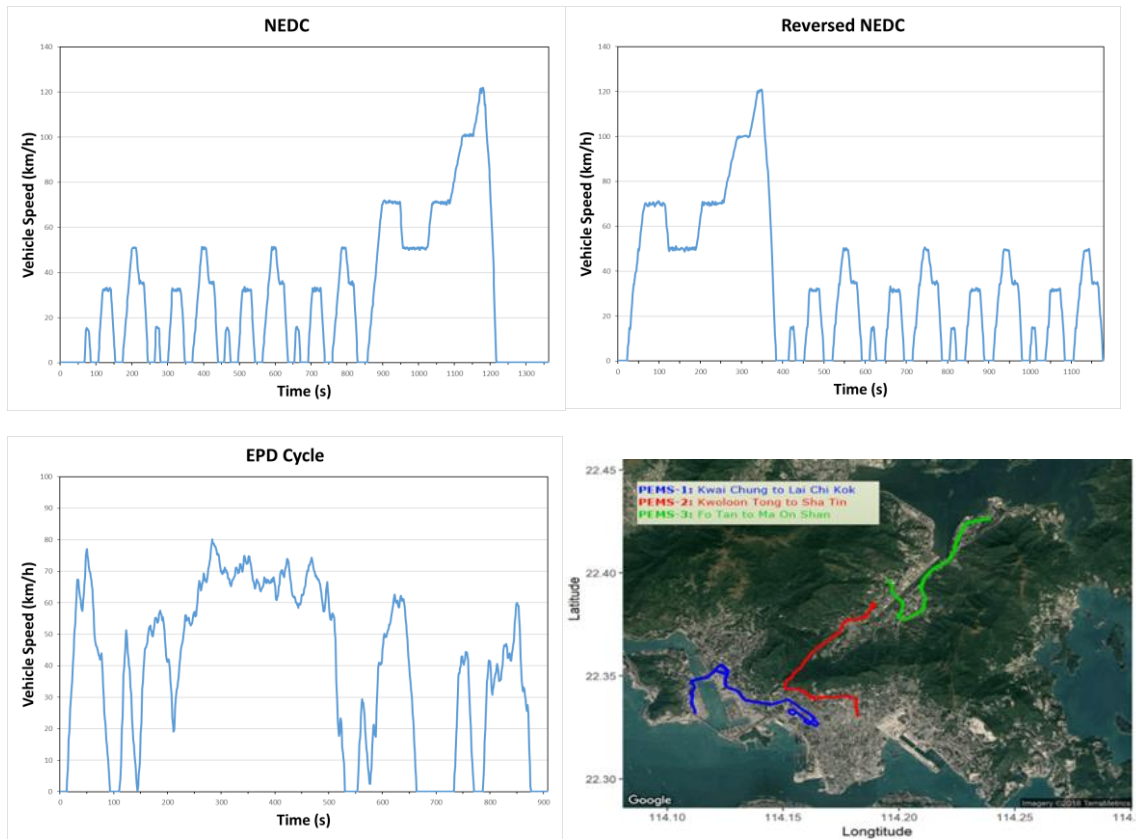


Figure 5: Different driving cycles used in the testing: upper left: NEDC-C and NEDC-H; upper right: NEDC-RH; lower left: the EPD cycle; lower right: three routes in which the PEMS data were analyzed.

Table 2. Testing conditions for LGV34_29-31

No of repetitions		NEDC-C	NEDC-H	NEDC-RH	EPD	PEMS
Setup		CVS/ PEMS	CVS/ PEMS	CVS/ PEMS	CVS/ PEMS	PEMS
LGV34_31	Before remediation	3/-	3/3	3/3	3/3	12 (4/4/4)*
	After remediation, tested in Summer	3/-	3/3	3/3	3/3	10 (4/3/3)*
	After remediation, tested in Winter					8 (3/2/3)*
LGV34_30			2/2			23
LGV34_29		1/-				16

*(x/y/z) number of trips per fixed route, PEMS-1(x)/PEMS-2(y)/PEMS-3(z)

Figures 6-7 show the NO_x emissions before and after remediation of the CVS and PEMS tests, respectively. Before the vehicle was remediated, the NO_x emissions are low for the NEDC-C and NEDC-H tests. However, when the driving cycles are different from the NEDC cycle, the emissions increased dramatically (figure 6). The emissions are even higher for the road tests, in which the emissions could be ten times higher than that of the NEDC-C and NEDC-H tests (figure 7). All these are signatures of the defeat device. After remediation, the emission of NEDC-C is almost the same, and that of the NEDC-H a little bit higher. For the NEDC-RH and EPD tests, however, the emissions drop significantly from 0.51-0.54 g/km to 0.22-0.25 g/km (figure 6). As

for the road tests, the reductions are not that significant and season dependent. Before remediation, the NOx emissions are 1.16 – 1.47 g/km. After remediation, the emissions become 1.05 – 1.29 g/km in summer, and 0.72 – 1.00 g/km in winter. For the NEDC-RH and EPD laboratory tests, the NOx reductions of 54-57% are brought by the remediation. In the road tests conducted in summer, the reductions are -5-22%, whereas 32-38% in winter. Evidently, the removal of the defeat device could reduce the NOx emission considerably. However, this is more effective in the laboratory tests than in road tests. Also, it is more effective in winter than in summer. One should note that the weather is very hot during the summer tests. On the average the temperature is around 33°C and therefore the loading of the air conditioner should be very high. This could account for the increase in NOx emissions during the summer.

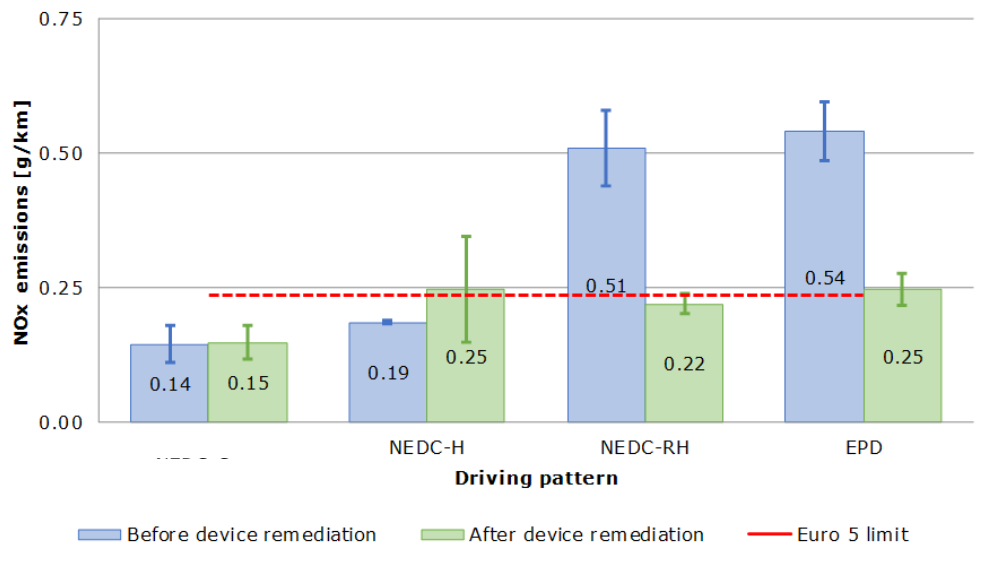


Figure 6: NOx emissions of LGV34_31_X measured by CVS and bag samples: Blue bar: before remediation; green bar: after remediation

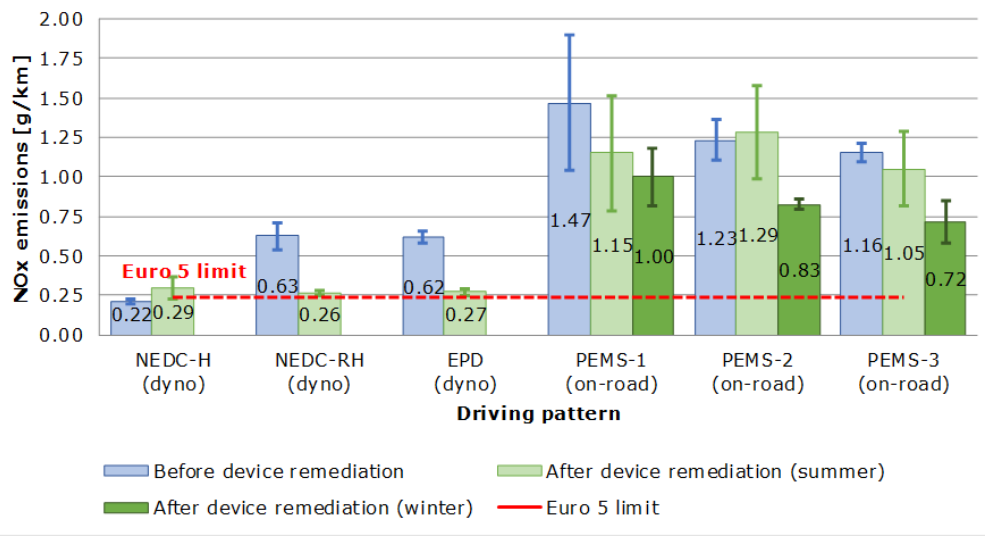


Figure 7: NOx emissions of LGV34_31_X, measured by PEMS analyzers: Blue bar: before remediation (LGV34_31_B); green bar: after remediation (summer) (LGV34_31_AS); Dark green: after remediation (winter) (LGV34_31_AW);

Brand A

Although LGV34_31 of Brand B is known to be fitted with defeat device, all vehicles of the same brand is not the highest emitter in our measurements. As shown in figure 2, NOx emissions from the vehicles of Brand A are almost double those from all the vehicles of Brand B, even before the remediation of the defeat device. NOx emissions from Euro 4 and 5 vehicles of Brand A are

similar, and both are higher than those from Euro 4 vehicles of Brand C. Figure 8 shows real-time NOx concentrations and vehicle speeds for one Euro 4 vehicle of Brand C, one Euro 5 and two Euro 6 vehicles of Brand A. Typical NOx concentrations are 200-400 ppm from Euro 4 vehicles of Brand C. NOx concentrations are typically 200-600ppm from Euro 5 vehicle of Brand A, but could reach 1500ppm at high speed. Two Euro 6 vehicles of Brand A have very different NOx emissions. LGV34_35 has lower emissions. On the other hand, LGV34_34 has a much higher emissions comparable to Euro 5 of other brands.

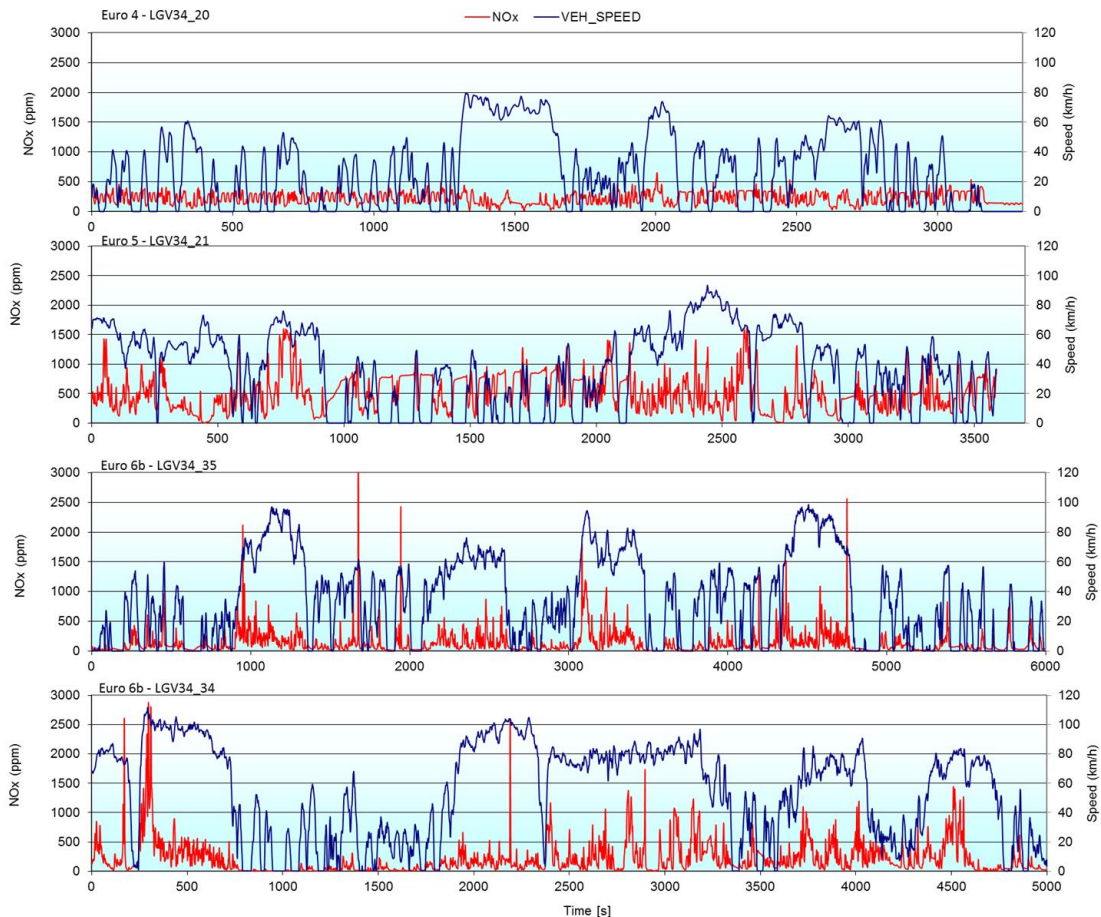


Figure 8: Real-time NOx concentrations: Top: Euro 5 vehicle of Brand A; Middle: Euro 6 vehicle of Brand A; Bottom: Euro 4 vehicle of Brand C. Red line: NOx concentration (Primary axis); Blue line: vehicle speed (secondary axis).

NOx concentrations of the Euro 6 vehicle of Brand A are generally lower (<500ppm) but there are some sharp emission peaks (> 1500ppm). Typical NOx concentrations of Euro 4 vehicles of Brand C are 200-400 ppm, which are lower than those of Euro 5 vehicles of Brand A.

To further investigate NOx emissions from vehicles of Brand A, dynamometer tests were conducted for one Euro 5 (LGV34_22) and one Euro 6b (LGV34_35) vehicles provided by the supplier. For each vehicle, NEDC-C, NEDC-RH and EPD tests were conducted. The results in figure 9 show that for both Euro 5 and 6 vehicles, NOx emissions are lower for the NEDC-C test, but much higher for the NEDC-RH and EPD tests. NOx emissions of Euro 5 vehicles in the non-certification tests are about 4 times higher than Euro 5 standard. The NOx emissions of Euro 6 vehicles in the non-certification tests are around 3 times higher than Euro 6 standard.

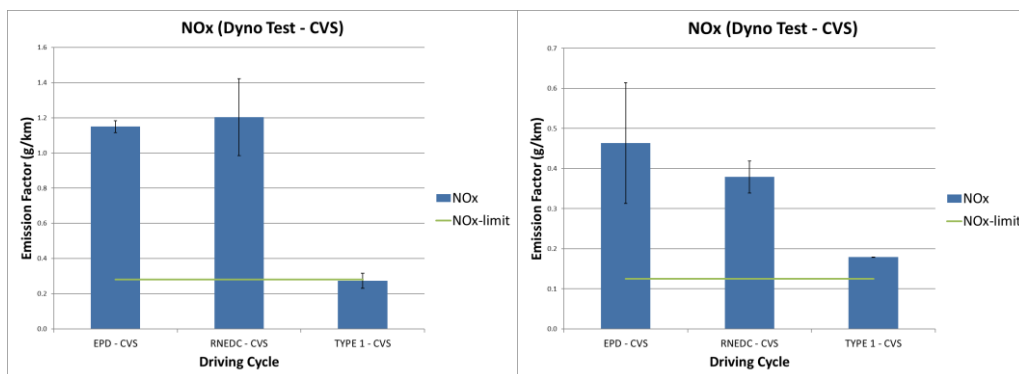


Figure 9: NOx emissions from CVS measurement from a Euro 5 vehicle (left panel) and a Euro 6 vehicle (right panel) of Brand A.

All the results suggest that NOx emissions of the vehicles of Brand A are very high. Their NOx emissions are extraordinarily higher than vehicles from the other brands, even for the vehicle that is known to be fitted with defeat device. In addition, the CVS tests with the modified cycles have higher NOx emissions than the certification results.

Taxi emissions

LPG taxi is one of the major contributors of the road side NOx emissions in Hong Kong and therefore the real-world measurements are focused on them. Since 1999, most of the taxis driven in Hong Kong are Euro 2 and 3 vehicles. They are gradually replaced by Euro 5 taxis from June 2012 to June 2017. The number of Euro 5 taxis rises from 5,924 by end 2015 to 8,603 by end 2018, comprising 33% to 41% of the total taxi population, respectively. Typical taxi in Hong Kong is driven 24 hours (by shifting duty drivers), so its annual mileage of about 150,000 km is about 15 times as much as that for private car in Hong Kong. Therefore, the durability of control devices, especially for Euro 5 taxis, is very important in Hong Kong (Papadopoulos et al., 2018).

HKEPD has tested 41 LPG taxis using PEMS since 2008. One target is to estimate their emissions and deterioration rates over ages. Figure 11 shows NOx emissions of Euro 2 to 5 taxis, with the same method as that of figure 2. The results show a vast reduction in NOx emissions from Euro 2-3 and 4 LPG taxis. Another reduction is brought by Euro 5 taxis of which the emission factors are less than 0.1 g/km. Some of Euro 4 taxis have much higher emissions and the inter-vehicular variability of the emissions is higher.

Real-world Emission Testing using PEMS for LPG Taxi

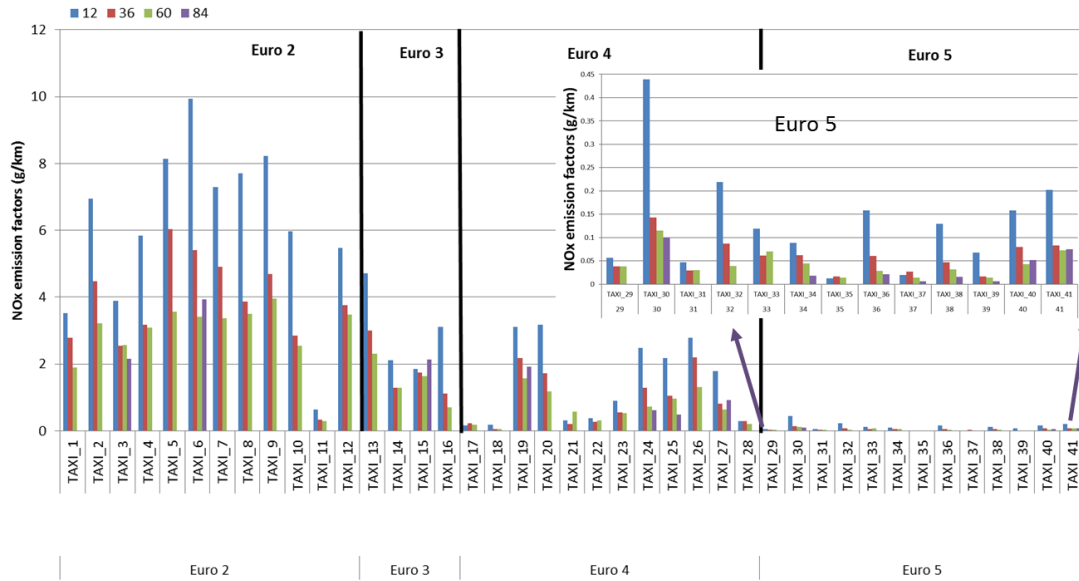


Figure 11: NOx emissions of the taxis of Euro 2 or above. Inset: zoomed NOx emissions of Euro 5 taxis.

The data were further analyzed to understand the age effect on NOx emissions. Figure 12 shows 8-minute average of NOx emission factors (g/km) in the speed range of [25,35) kph from Euro 4 and 5 taxis against the vehicle ages. The results show that NOx emissions are clearly increasing with age for Euro 4 taxis. While NOx emissions could be as low as 0.25g/km when age is lower than 5 years and increase to 2.2 g/km for older vehicles. However, one should note that in 2013, HKEPD has initiated the program for replacement of catalytic converter and oxygen sensor (Cat Replacement Program (2013)). Therefore, some Euro 4 taxis are fitted with different brand of control devices, which may have different aging effect. For Euro 5 taxis, NOx emissions remain low for all ages except for one vehicle at age of 9. So far the results suggest that Euro 5 taxis could maintain low NOx emissions, but we need more data of old vehicles to draw a conclusion.

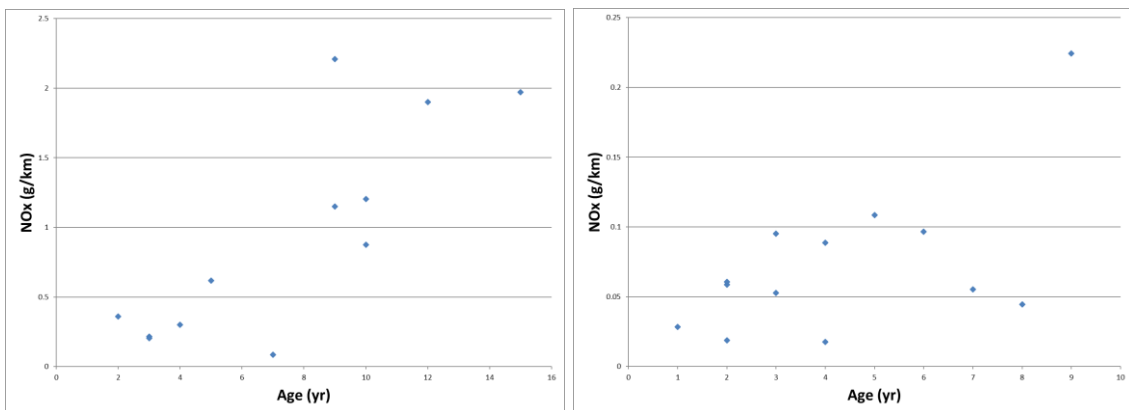


Figure 12: 8-minute average NOx emissions in the speed range of [25,35) kph of taxis against the vehicle ages; Left panel: Euro 4 taxis, Right panel: Euro 5 taxis

Acknowledgements

We thank Leonidas Ntziachristos for the valuable discussions

References

- BMVI. (2016). Bericht der Untersuchungskommission "Volkswagen." Retrieved from https://www.bmvi.de/SharedDocs/DE/Anlage/VerkehrUndMobilitaet/Strasse/bericht-untersuchungskommission-volkswagen.pdf?__blob=publicationFile
- Department for Transport. (2016). Vehicle Emissions Testing Programme: Moving Britain Ahead. London. Retrieved from https://assets.publishing.service.gov.uk/government/uploads/system/uploads/attachment_data/file/548148/vehicle-emissions-testing-programme-web.pdf
- EMFAC, <https://www.arb.ca.gov/emfac/>
- Cat Replacement Program (2013): Replacement of catalytic converters and oxygen sensors on petrol and LPG taxis and light buses*, <https://www.info.gov.hk/gia/general/201310/01/P201309300656.htm>
- Franco V., Posada F., German J., and Mock P (2014). Real-world exhaust emissions from modern diesel cars. A meta-analysis of PEMS emissions data from EU (EURO 6) and US (Tier 2 Bin 5/ULEV II) diesel passenger cars. Part 1: Aggregated results. ICCT White Paper, October 2014. Available at: http://www.theicct.org/sites/default/files/publications/ICCT_PEMS-study_dieselcars_20141013.pdf
- Frey, H.C., A. Unal, J. Chen, S. Li, and C. Xuan (2002), Methodology for Developing Modal Emission Rates for EPA's Multi-Scale Motor Vehicle and Equipment Emission Estimation System, EPA420-R-02-027, Prepared by North Carolina State University for the Office of Transportation and Air Quality, U.S. Environmental Protection Agency, Ann Arbor, MI, October 2002
- Hong Kong Environment Bureau (2017). Clean air plan for Hong Kong: 2013-2017 Progress Report, Available at: http://www.enb.gov.hk/sites/default/files/CleanAirPlanUpdateEng_W3C.pdf
- Keramydas, C., Papadopoulos G., Ntziachristos L., Lo T.S., Ng K.L., Wong H.L.A. and Wong C.K.L. (2018). Real-World Measurement of Hybrid Buses' Fuel Consumption and Pollutant Emissions in a Metropolitan Urban Road Network. *Energies*, 11, 2569.
- Kousoulidou, M.; Fontaras, G.; Ntziachristos, L., et al., 2013. Use of portable emissions measurement system (PEMS) for the development and validation of passenger car emission factors. *Atmos. Environ.* 64, 329-338.
- MOVES, <https://www.epa.gov/moves>
- Papadopoulos G., Keramydas, C., Ntziachristos L., Lo T.S., Ng K.L., Wong H.L.A. and Wong C.K.L. (2018b). Emission Factors for a Taxi Fleet Operating on Liquefied Petroleum Gas (LPG) as a Function of Speed and Road Slope. *Front. Mech. Eng.*, 04, 19.
- Vlachos, T., Bonnel, P., Perujo, A., Weiss, M., Mendoza-Villafuerte, P., and Riccobono, F. (2014). In-use emissions testing with portable emissions measurement systems (PEMS) in the current and future Europe an vehicle emissions legislation: overview, underlying principles and expected benefits. *SAE Int. J. Commer. Veh.* 7, 199-215.
- Weiss, M.; Bonnel, P.; Hummel, R., et al., 2011. On-Road Emissions of Light-Duty Vehicles in Europe. *Environ. Sci. Technol.* 45, 8575-8581.

2.1.7 PEMS accuracies under harsh environmental conditions

L. Landl^{1}, T. Vuckovic¹ and S. Hausberger¹*

¹ Institute for Internal Combustion Engines and Thermodynamics, Graz University of Technology, Graz, 8010, Austria

Introduction

On-board measurements have become more and more important in recent years due to new Real Drive Emissions (RDE) emission regulations. Consequently it is essential that the Portable Emission Measurement Systems (PEMS) provide correct measurements of exhaust emissions under real driving conditions. In particular, the accelerations acting on the PEMS during a car journey can have effects e.g. on all optical sensors due to possible relative movements of light source and detector and due to moving filters, while temperature and pressure changes can affect the accuracy of mass flow controllers. Until now, the PEMS devices only have to be compared with the laboratory devices in a stationary state at narrow temperature and pressure conditions on the test bench. In the validation procedure for PEMS, the measurement results for WLTC tests of the PEMS devices must lie within defined tolerances to the laboratory devices. ((EU) 2017/1151, (EU) 2017/1154)

To identify whether the PEMS measure correctly when they are exposed to accelerations, pressure- and temperature variations occurring when driving on real roads, the Portable Emission Accuracy Test bench (PET) has been designed, built and tested at the Institute for Internal Combustion Engines and Thermodynamics (ICE, TU Graz). The PET enables to expose PEMS to accelerations in two directions during exhaust measurements on the chassis dynamometer. The modal data of the shaking PEMS can be compared with the stationary laboratory analysers. In a first application, PEMS systems were measured on the PET during tests on HDVs on the chassis dynamometer of TU Graz.

As part of the measurements at TU Graz, four PEMS from three different manufacturers have been tested for their robustness and accuracy under harsh environmental conditions.

This paper gives an overview on:

- The development of the PET at ICE and the measurement setup of the first measurements (Chapter 1)
- Measurement results for analysers of gaseous pollutant components (Chapter 2)
- The measurement results of the particle number measurement (Chapter 3)

1. Test bench design and measurement set up

This chapter explains the kinematic conditions acting on the PEMS during real world driving. Furthermore, the design of the PET test bench is described in detail and the measurement setup is explained.

In the validation procedure, PEMS systems today are compared to lab analysers in steady state conditions (no movement of the PEMS, no temperature and pressure changes as occur in real PEMS testing). To compare results from PEMS with lab analysers in realistic conditions, the PET was developed.

The PET test bench allows realistic movements of the PEMS according to acceleration profiles measured on vehicles in RDE tests (see Figure 1). This acceleration profile was measured on a real road drive around Graz, where the PEMS was mounted on the trailer hitch. The PET can be positioned on chassis dynos or any other test stand to compare PEMS with lab analyser results while moving the PEMS. With this acceleration profile and under consideration of other boundary conditions such as maximum size of the test bench, strength of the linear motors, etc., the following demands on the PET design have been made:

- Acceleration: +/- 20 m/s²
- Movement: +/-100 mm
- Maximum dimensions: 1500x1500x1500 mm

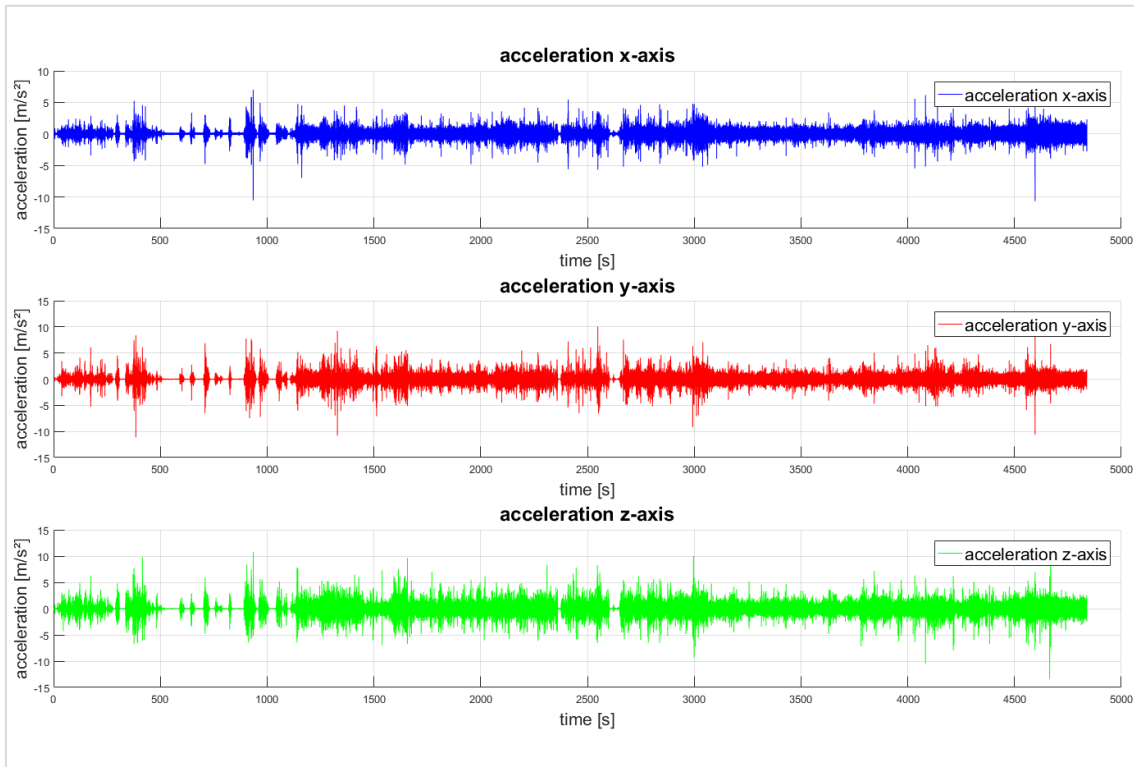


Figure 1: Acceleration profile of a RDE test

The design of the PET test bench is based on a tripod with each leg consisting of a linear motor and a spring. These linear motors are supported at both ends by joint head bearings to ensure maximum freedom of movement. The springs are used to absorb the static weight forces and relieve the linear motors that set the PEMS in motion. The construction allows movements in vertical z-direction, horizontal y-direction and combined movements in the y-z plane. For the first test sequences, which results are shown in chapter 2 and 3, the PEMS where only moved in z-direction. Figure 2 shows the PET construction with the main components. Figure 3 shows the real PET test bench with a mounted PEMS at the chassis dyno. For a more detailed description of the PET design, the motion calculation and the linear motor control, see (Landl, 2018).

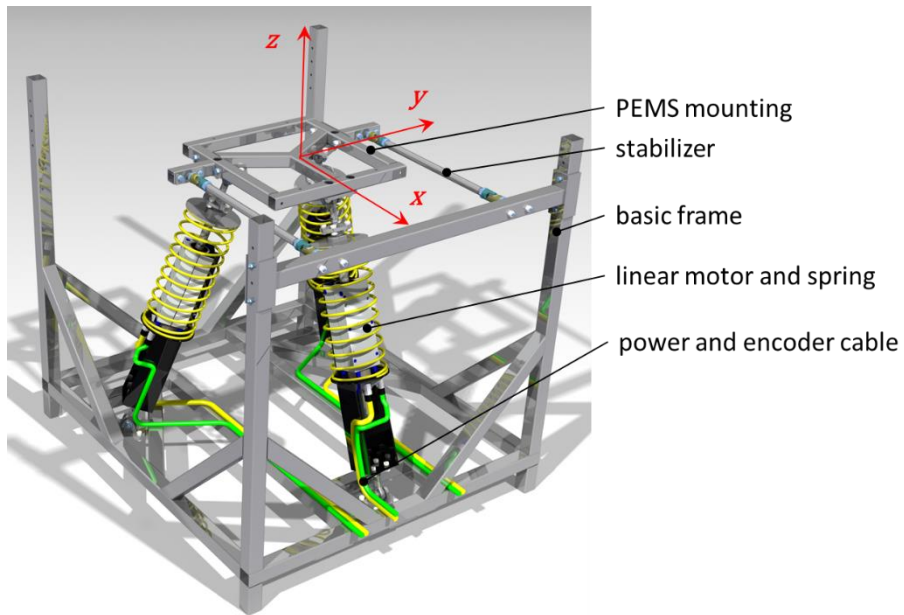


Figure 2: PET construction



Figure 3: Picture of the PET test bench with mounted PEMS at the chassis dynamometer

With the information from Figure 1, a test procedure was set up. The final version of the PET controller will allow to follow measured movements from RDE tests directly. For the first tests just several sinusoidal cycles with different vertical amplitudes and frequencies and a jump (maximum acceleration) with an amplitude of 80mm have been driven (see Table 1 and Figure 4). The total duration of this movement profile is 300 seconds. For the tests, which last 15 or 30 minutes, this profile was repeated 3 or 6 times.

Table 1: Overview of the used sinusoidal cycles

	Sinus equation	duration
1)	$z \text{ [mm]} = 10 \cdot \sin(2 \cdot \pi \cdot t) + 40 \text{ [mm]}$	5-15s
2)	$z \text{ [mm]} = 6 \cdot \sin(3 \cdot 2 \cdot \pi \cdot t) + 40 \text{ [mm]}$	15-100s
3)	$z \text{ [mm]} = 16 \cdot \sin(4 \cdot 2 \cdot \pi \cdot t) + 40 \text{ [mm]}$	105-170s
4)	$z \text{ [mm]} = 8 \cdot \sin(5 \cdot 2 \cdot \pi \cdot t) + 40 \text{ [mm]}$	170-230s
5)	$z \text{ [mm]} = 6 \cdot \sin(6 \cdot 2 \cdot \pi \cdot t) + 40 \text{ [mm]}$	230-290s

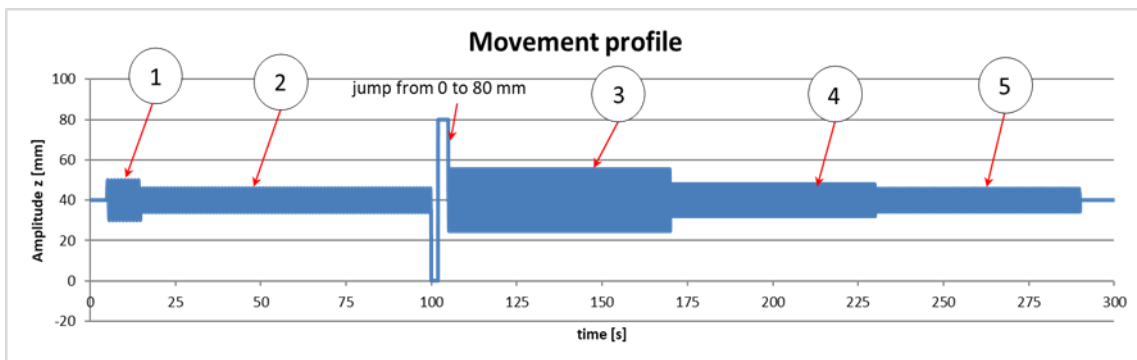


Figure 4: Movement profile of the PET test bench

The PET measurement set up for the first application is shown in Figure 5. Four PEMS systems from three different manufacturers have been tested. Two of these PEMS measured only the number of particles (PN), but with different measuring methods, one PEMS measured only gaseous pollutants, and one PEMS measured gaseous pollutants and PN.

The following laboratory instruments were used for comparison:

- FTIR for gaseous pollutants (CO₂, CO, NO, NO₂) diluted sampling at the CVS
- PMP dilution with CPC3790 (sampling CVS)
- PN PEMS (sampling tailpipe, marked with dashed frames in Figure 5). It was only set up for certain tests (see Figure 11, yellow line).

The measurement setup was almost the same for all 4 tested PEMS to compare all measurement results well. Only the PN PEMS sampling tailpipe, which was only used to compare PN was not mounted by every test. The cycles driven on the truck chassis dynamometer as well as the measured trucks varied from each other. The driven cycles are described in more detail in the following chapters.

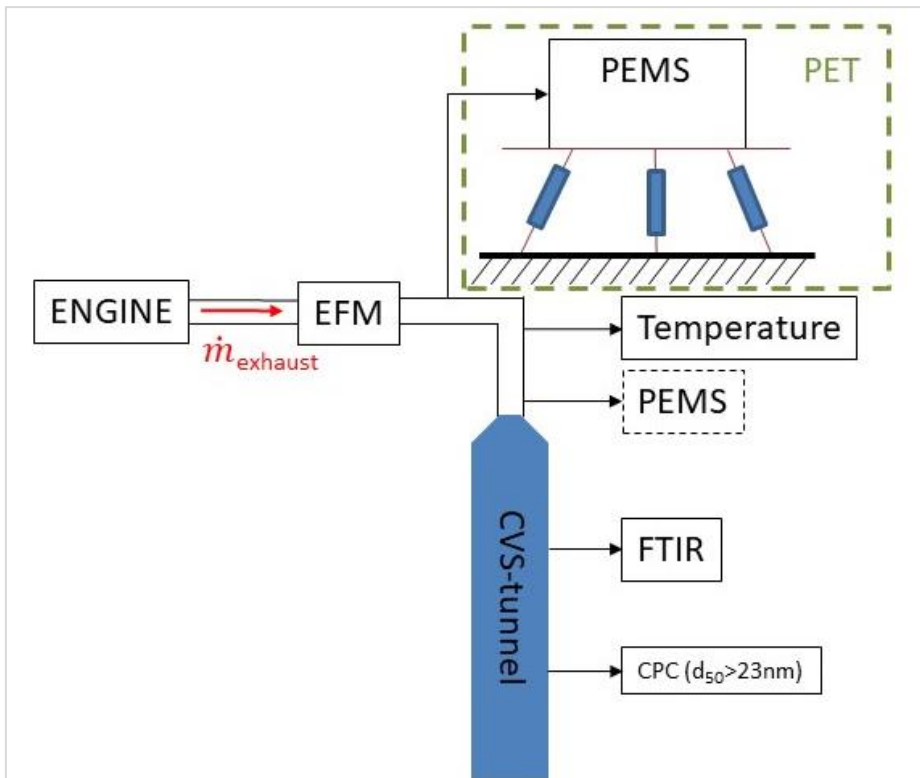


Figure 5: PET measurement set up

2. Measurement results for gaseous pollutants

This chapter shows the measurement results of the two PEMS measuring gaseous pollutants (now called PEMS1 and PEMS2). In the course of this paper, the individual tailpipe mass emissions of PEMS and FTIR were compared with each other, which in this case are equivalent to the concentration of the measuring instruments, since both measuring instrument concentrations were multiplied by the same exhaust gas volume flow (measured by the EFM(exhaust flow meter)) to get the mass emissions.

Figure 6 and Figure 7 show the results for CO_2 and NO_x for PEMS1, Figure 8 illustrates the modal NO_x values for PEMS2 at a constant speed of 50 km/h, 1% gradient and a duration of 30 min on the HD chassis dynamometer. The tested vehicle was a EURO VI tractor with DPF and SCR. In the first 15 min the PEMS was at rest, the second 15 min it was shaken (see Figure 4 for the profile). The green line shows the beginning of shaking, while the red line shows the PEMS results and the blue line the FTIR test bench results. The CO_2 values of PEMS1 show no influence on PET movements. It is the same for PEMS 2 and consequently these results are not shown in this paper. But there is a clear difference in the NO_x measurements when the PET starts shaking (only one of the two tested PEMS showed this effect at the NO_x values). The influence is visible by the differences between PEMS1 (blue line) and FTIR (red line) signal without shaking PET (before second 900) and with shaking (second 901 to end of test). NO values showed the same behaviour as NO_x values for PEMS1 but they are not plotted separately. The reason why the modal NO_x plot in Figure 7 and Figure 8 differs, although the same test was driven with the same truck, is partly due to the driver and partly due to the engine control. For detailed information about the gaseous emission measurement systems installed in the PEMS see (Reif (2015), Wiegleb (2016)).

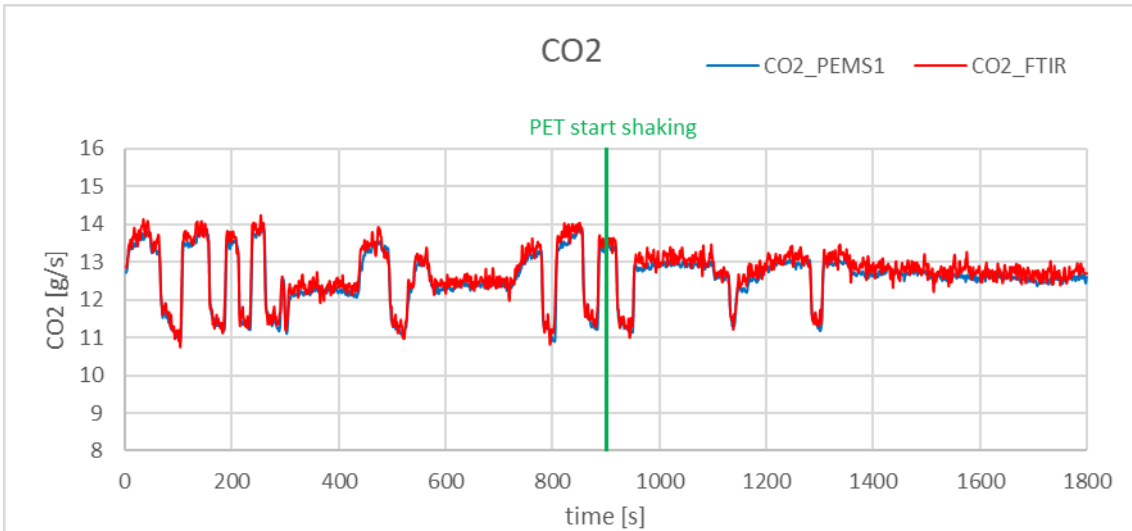


Figure 6: CO₂ PEMS1 and FTIR signals during a HDV EURO VI constant speed test with and without shaking of the PEMS on the PET

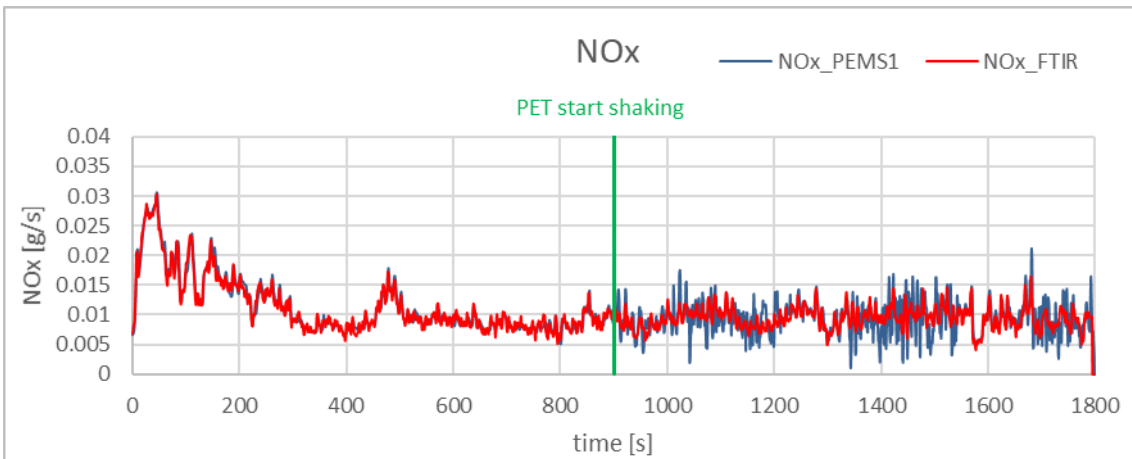


Figure 7: NO_x PEMS1 and FTIR signals during a HDV EURO VI constant speed test with and without shaking of the PEMS on the PET

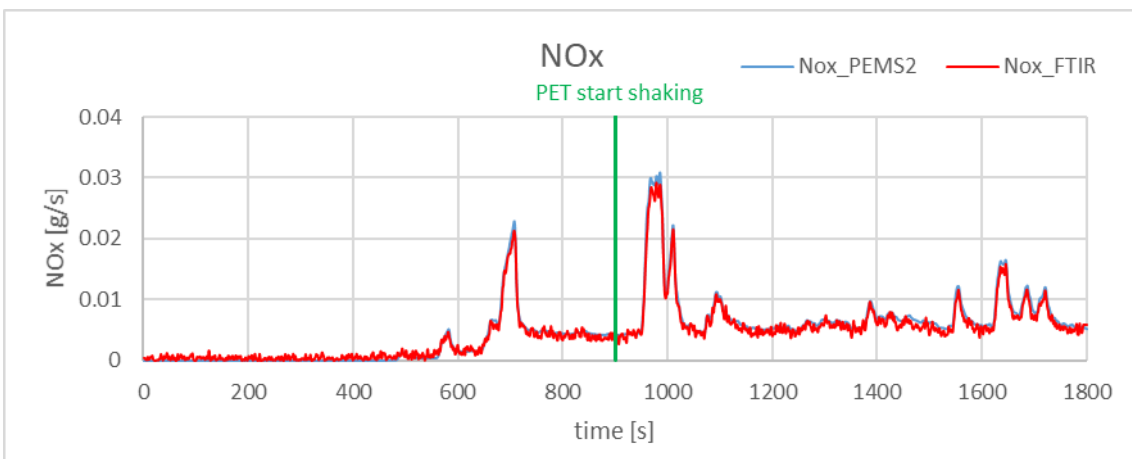


Figure 8: NO_x PEMS2 and FTIR signals during a HDV EURO VI constant speed test with and without shaking of the PEMS on the PET

Table 2 shows the results in [g/km] of two WHVC cycles, first with stationary PEMS1, second with shaken PEMS1. Here the NOx deviations over the entire cycle are at about 17% (worst case deviations). The deviations from PEMS to FTIR are calculated using the following equation:

$$Deviation [\%] = \frac{EM_{FTIR} - EM_{PEMS}}{EM_{PEMS}} * 100$$

EM_{FTIR} ...cycle mean value emission mass FTIR [g/km]

EM_{PEMS} ...cycle mean value emission mass PEMS [g/km]

Table 2: Deviation PEMS1-FTIR for WHVC (stationary and shaken PEMS1)

Deviation: PEMS1-FTIR for a WHVC				
	CO ₂	CO	NO	NOx
Stationary PEMS1	4.9%	- 60.3%	5.4%	4.6%
Shaken PEMS1	7.4%	- 64.2%	14.5%	17%

For the further analysis of the measurement results, the time-resolved FTIR measured values were plotted over the PEMS1 measured values. Figure 9 shows that the NOx measured values scatter significantly more during vibration than during static measurement.

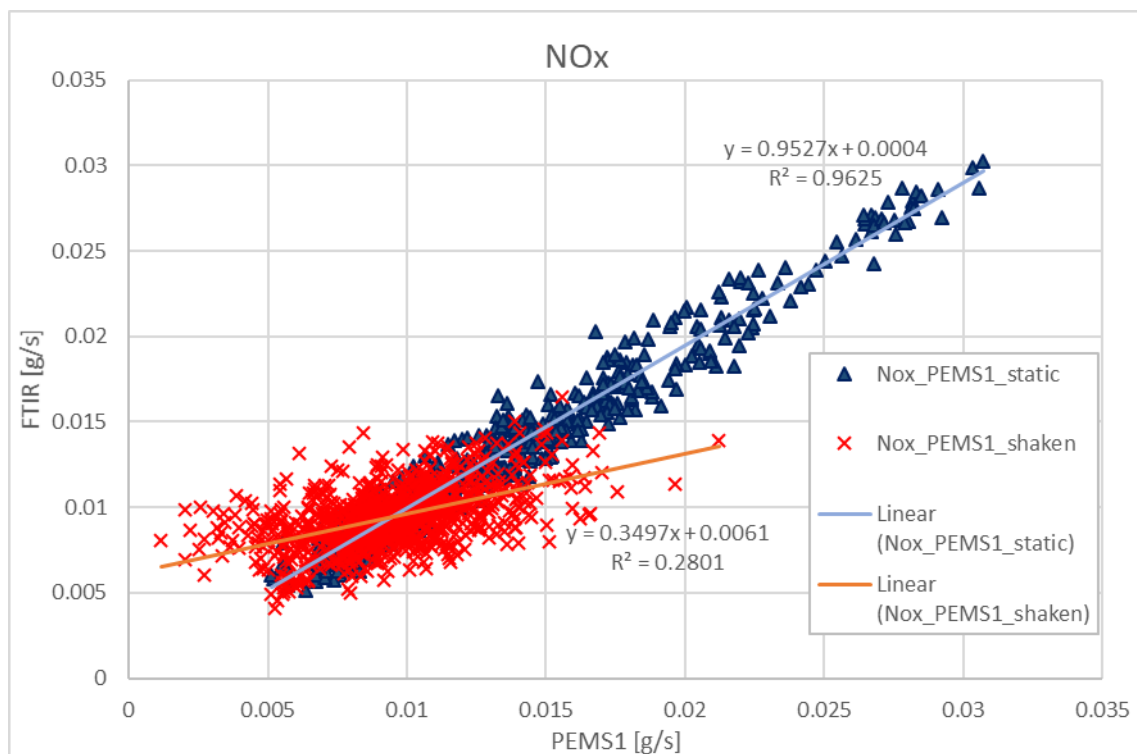


Figure 9: FTIR measured values over PEMS1 measured values

A linear regression analysis was performed with the parameters PET acceleration, PET frequency and PET amplitude as independent variables and the difference between the PEMS signal and the FTIR signal as dependent variable for the conspicuously behaving exhaust components NO and NOx. The aim was to test the possibility of a mathematical function describing the effects of vibration. No significant dependence of the NO or NOx difference of PEMS1 and FTIR on the

acceleration in z-direction, frequency or amplitude could be found. Consequently a possible mathematical correction of the measured values can be rejected. Some modification work regarding the hardware of the PEMS devices could probably minimize the influence of motion on the measurement results.

3. Measurement results for particles

This chapter deals with the measurement results of the PEMS particle measurements. Three PEMS (now called PEMS1, PEMS3 and PEMS4) with PN measuring devices were tested. It is worth mentioning that PEMS4 has a different PN measuring method than PEMS1 and PEMS3.

Figure 10 shows the PN results of PEMS1. The blue line represents the PN measurement data from the PEMS1, the red line shows the measurement data from the reference measuring device, which is a PMP conform dilution with a CPC3790 sampling at the CVS tunnel. The green line indicates the beginning of the PET shaking. The driven cycle was a vehicle test at a constant speed of 50 km/h, 1% gradient and a duration of 30 min on the chassis dynamometer. The average deviation for this test cycle from PEMS1 to PMP is -19% (static PEMS) and +16% (moving PEMS). If this difference in the deviation can be attributed to the shaking is questionable since it is in the repeatability range of PN PEMS systems.

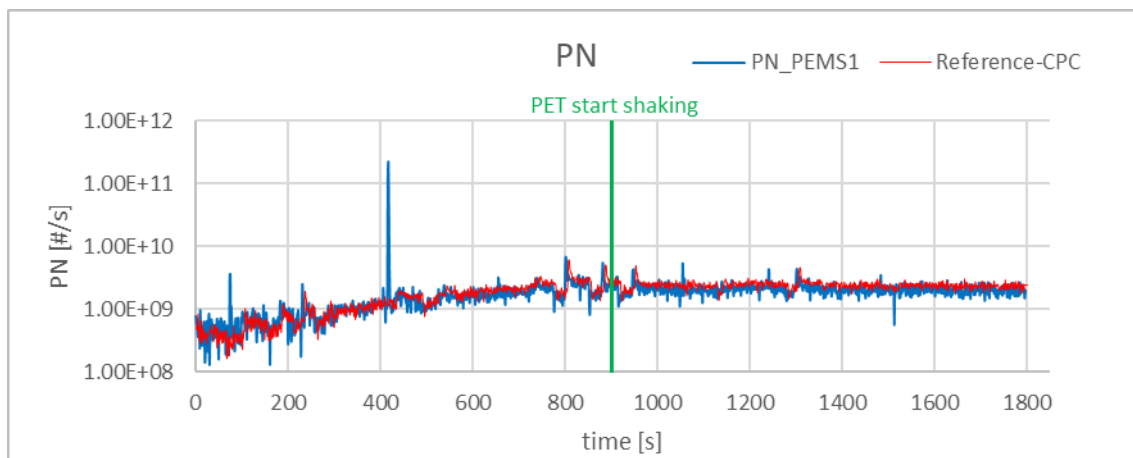


Figure 10: PN signal from PN_PEMS1 and Reference-CPC during a HDV EURO VI constant speed test with and without shaking of the PEMS on the PET

The deviation from PEMS1 to the reference system in WHVC tests (one whole WHVC with static PEMS and the other one with shaking PEMS) are shown in Table 3 (worst case deviations). The modal data are not listed separately in this paper.

$$Deviation [\%] = \frac{PN_{Reference-CPC} - PN_{PEMS}}{PN_{PEMS}} * 100$$

$PN_{Reference-CPC}$...cycle mean value particle number Reference-CPC [#/#km]

PN_{PEMS}cycle mean value particle number PEMS [#/#km]

Table 3: Deviation PEMS1-PMP for WHVC (stationary and shaken PEMS)

Deviation: PEMS1-PMP for a WHVC	
	PN
Stationary PEMS	-19%
Shaken PEMS	-25%

Figure 11 and Figure 12 show the PN measurement results for PEMS3 and PEMS 4. For reasons of clarity, the diagrams below only show a section of the modal data when the PET begins to shake. The driven cycle in the case of PEMS3 was a constant speed test with 50km/h and 50% engine power, for PEMS 4 a constant run with 50km/h and 25% engine power. Furthermore, the two measuring cycles also differ in the injection quantity of the urea in the SCR catalytic converter. The PEMS measurement data (blue lines) can be compared with the reference measurement data (red lines, CPC with dilution system sampling at CVS tunnel). In Figure 11 there is also the modal PN data of the PEMS4 (yellow line) shown. The PEMS4 was also sampling at tailpipe, but it was not shaken (see Figure 5 PEMS with dashed border).

In both figures there is no difference in the deviation of the measured values of the PEMS and the reference measuring instrument without and with shaking, although, as already mentioned, the two PEMS differ in the PN measuring method. The different modal measurement values caused by the different measurement methods are visible in Figure 11 (difference between the blue line and the yellow line). For detailed information about the PN measurement systems installed in the PN-PEMS see (Hinds 2012).

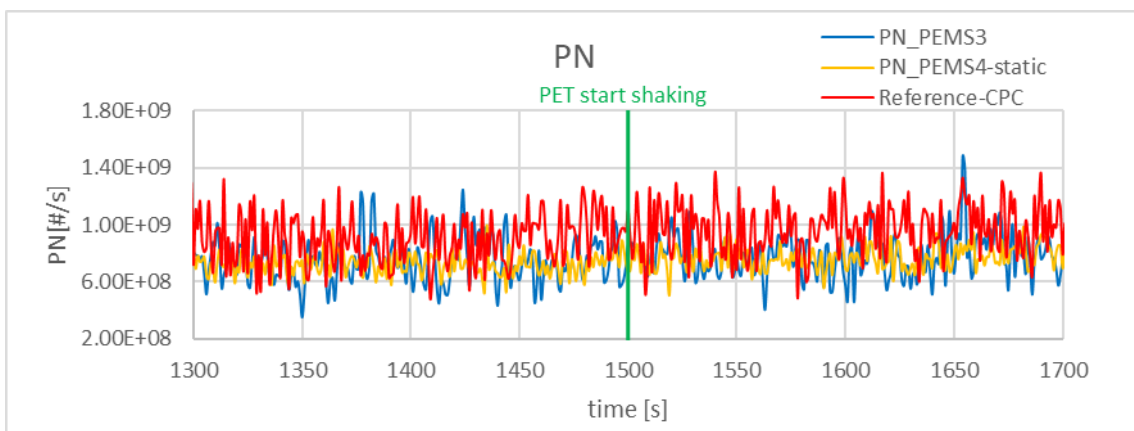


Figure 11: PN signal from PEMS3, Reference-CPC and PEMS4 during a HDV EURO VI constant speed test with and without shaking of the PEMS on the PET

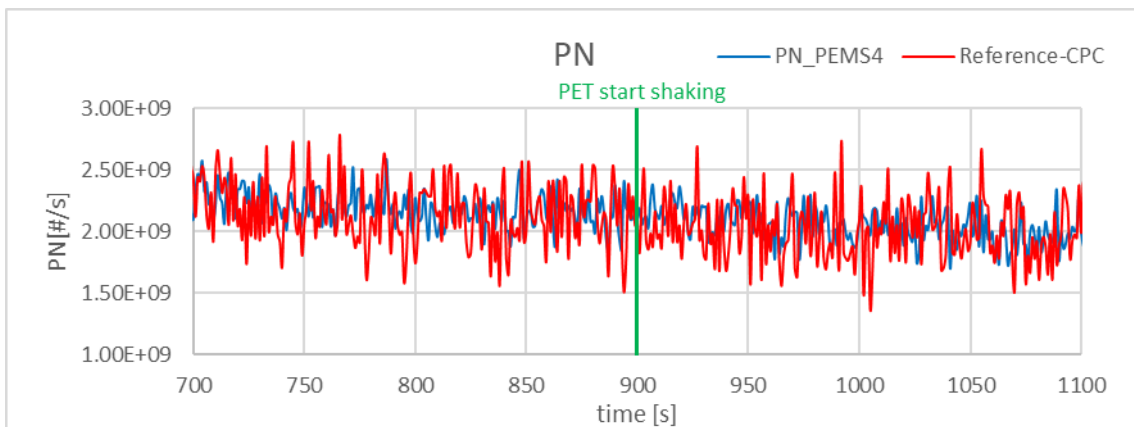


Figure 12: PN signal from PEMS4 and Reference-CPC during a HDV EURO VI constant speed test with and without shaking of the PEMS on the PET

Conclusions

At the institute for Internal Combustion Engines and Thermodynamics a test bench called PET (Portable Emission Accuracy Test bench) was developed, which allows to expose measuring instruments, especially PEMS, to accelerations during measuring cycles in order to verify whether the tested measuring instruments deliver correct measuring results even under these hard conditions.

The results of the PET measurements at the ICE show a clear offset of the measured values for NO and NO_x with moving PEMS1 in comparison with the FTIR analyser. Thus it can be assumed that the NDUV analyser or the mass flow controllers act incorrectly during accelerations. An exact cause investigation is still being carried out. Since NO_x emissions are a very critical emission component, these measurement errors are not acceptable in real operation.

The investigations of the PN measurements also show a difference between PEMS measurements and the reference device measurements. However, since there are differences without and during shaking and also the magnitude of the deviation is within the repetition range of PN PEMS, it is difficult to make a statement yet, whether movements of the measuring instrument affected the measurement results.

Acknowledgements

The development of the PET system was funded by the Austrian FFG. The tests performed are carried out within the Horizon 2020 project Down to Ten. The authors would like to thank all colleagues from TU Graz who participates in this project.

References

- Hinds, William C. (2012), *Aerosol Technology: Properties, Behavior, and Measurement of Airborne Particles*. New York: John Wiley & Sons.
- Landl L. (2018), Konstruktion, Aufbau und Inbetriebnahme eines Prüfstandes zum Test von PEMS-Systemen in realen Fahrsituationen, Master Thesis, TU Graz
- Official Journal of the European Union, COMMISSION REGULATION (EU) 2017/1151 of 1 June 2017
- Official Journal of the European Union, COMMISSION REGULATION (EU) 2017/1154 of 7 June 2017
- Reif, Konrad (2015), *Abgastechnik für Verbrennungsmotoren*. Wiesbaden : Springer.
- Wiegleb, G. (2016), *Gasmesstechnik in Theorie und Praxis*, Springer Fachmedien Wiesbaden

2.1.8 Trends in Light Duty Gasoline Vehicle Emissions Based on Real-World Measurements

H.C. Frey¹, T. Wei¹, T. Khan¹, W. Yuan¹, N. Rastogi¹

¹Department of Civil, Construction, and Environmental Engineering, North Carolina State University, Raleigh, North Carolina, 27695-790, United States. Contact: frey@ncsu.edu

Introduction

Vehicle emissions are highly variable over space and time (e.g., Franco et al., 2013). Furthermore, real-world fuel use and emissions can deviate from measurements made during type approval or certification testing for a variety of situations (Ntziachristos et al., 2014). Portable Emission Measurement Systems (PEMS) enable the measurement of actual tailpipe emissions at any location driven by a vehicle (Frey et al., 2003). Using PEMS, it is possible to quantify factors that affect variability in emissions, such as speed, acceleration, road grade, fuel, engine design, vehicle size, emission controls, and others.

In 1995, the U.S. Environmental Protection Agency developed an on-board measurement system (Scarbro, 2000). Vojtisek-Lom and Cobb developed a low cost, portable, and non-invasive method for measuring vehicle emissions, and demonstrated the use of the equipment in a study of shuttle bus emissions (Vojtisek-Lom and Cobb, 1997). The concepts employed by Vojtisek-Lom and Cobb were commercialized by Clean Air Technologies International, Inc. in 1999, which produced the first commercially available PEMS, the OEM-2100. The OEM-2100 was used for several studies, including evaluation of the effect of traffic signal timing and coordination emissions for an arterial corridor (Frey et al., 2001). Sensors, Inc. followed shortly thereafter with higher precision PEMS, including the SEMTECH-G for gasoline powered vehicles and a prototype SEMTECH-D for diesel vehicles, that was used by EPA and others in several pilot studies to evaluate approaches for using real-world 1 Hz data to model vehicle emission factors (Frey et al., 2002; Barth et al., 2002; Environ, 2002; EPA, 2002b). A common finding of PEMS studies is that emissions are highly variable with speed and acceleration and depend on the driving cycle (Ropkins et al., 2007).

An example of a simplified PEMS is the GlobalMRV Axion R/S system, which is the size of a carry-on suitcase, and weighs 35 lbs. This instrument measures CO₂, CO, and HC using NDIR, uses electrochemical cells for NO and O₂, and an optional laser-light scattering detector for PM. Simplified PEMS typically use OBD data for RPM, manifold absolute pressure (MAP), intake air temperature (IAT), mass air flow (MAF), and mass fuel flow (MFF), as available, to estimate the engine air flow rate either directly (if MAF is available) or indirectly. The air/fuel ratio can be inferred from the carbon species (CO₂, CO, HC) exhaust concentrations. Thus, using MFF and air/fuel ratio, air flow can be inferred. Alternatively, air flow can be estimated from RPM, MAP, and IAT using the speed density method (Sandhu and Frey, 2013). Simplified PEMS are more easily installed and operated, and are useful for many comparative studies, but not for regulatory application.

Light duty gasoline vehicles (LDGVs) have the largest share of all onroad vehicles in the U.S. in terms of vehicle numbers and vehicle-miles travelled (Frey, 2018). The purpose of this work is to illustrate a methodological approach to identify and compare sources of variability in real world emissions, including intra-vehicle variability related to engine load, inter-vehicle variability, inter-route, and inter-run variability. The approach is illustrated with a sample of data for light duty gasoline vehicles.

Methods

A methodology for quantifying intra-vehicle, inter-vehicle, inter-route, and inter-run variability is demonstrated. Since 2008, data have been collected for over 200 light duty gasoline vehicles based on a study design developed by Frey et al. (2008). Here, we focus on a subset of the measured vehicles, which are certified to the California Low Emission Vehicle (LEV) standard.

Each vehicle was measured on four designated routes in the Research Triangle Park, NC region, shown in Figure 1. These routes include alternative paths with one way distances of 10 and 11 miles between NC State University and North Raleigh, designated as Routes A and C, respectively, and alternative paths with one distances of 16 and 18 miles between North Raleigh and Research Triangle Park, designated as Routes 1 and 3, respectively. These routes are comprised of a wide range of road types, including feeder/collector streets, minor arterials, primary arterials, ramps, and limited access freeways. Furthermore, they are comprised of segments with a range of posted speed limits, ranging from 25 mph to 70 mph, and a range of road geometry in terms of factors such as number of lanes, type of traffic control, type of median, and so on. The total driving distance for vehicle measurement is approximately 111 miles for the designated routes, plus a few additional miles for travel to and from a local gas station to top off the fuel tank before and after the measurements. The actual amount of fuel consumed is compared to the estimated fuel consumed based on data logging and measurements during field data collection.

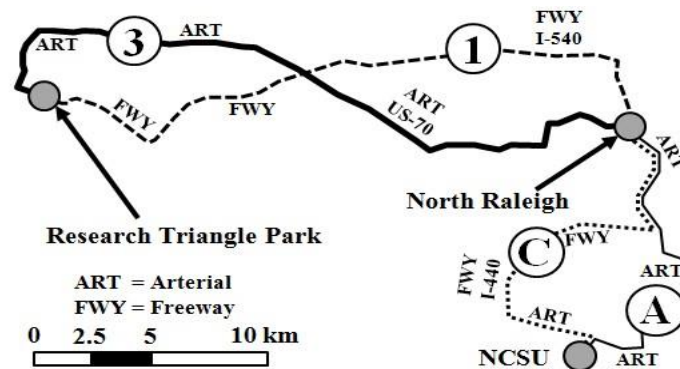


Figure 1. Routes Used for Vehicle Data Collection in the Raleigh and Research Triangle Park, NC (USA) Study Area.

Each vehicle was instrumented with a PEMS, on-board diagnostic (OBD) data link 'scantool' for recording data from the vehicle electronic control unit (ECU), and global positioning system (GPS) receiver with barometric altimeter. The PEMS measures exhaust concentrations of carbon dioxide (CO₂), carbon monoxide (CO), hydrocarbons (HC), and nitric oxide (NO). From the OBD data, second-by-second vehicle speed and engine data are recorded. The engine data typically include mass fuel flow (MFF), mass air flow (MAF), manifold absolute pressure (MAP), engine revolutions per minute (RPM), and engine intake air temperature (IAT). Not all vehicles broadcast all of these parameters. For vehicles that broadcast MFF, the mass per time emission rate of each pollutant for each second is estimated based on MFF and the mass per gallon emission rate. The latter is inferred from the molar ratio of the measured gases and knowledge of the fuel composition. For vehicles that broadcast MAF but not MFF, pollutant emission rate is estimated based on inference of the air-to-fuel ratio (AFR) from the PEMS exhaust concentration, and use of recorded MAF, estimated AFR, and exhaust composition. For vehicles that broadcast neither MFF or MAF, the mass air flow is inferred from MAP, RPM, and IAT using the so-called 'speed-density' method based on engine design characteristics (Sandhu and Frey, 2013).

GPS and barometric altimeter data are used to infer road grade along the path driven by the vehicle (Yazdani and Frey, 2014). Vehicle speed from the OBD data is to estimate acceleration. Vehicle speed and acceleration based on OBD data, and road grade data inferred from the GPS/altimeter data, are used to calculate "Vehicle Specific Power" on a second-by-second basis (Frey et al., 2010):

$$VSP = v \{ a(1 + \varepsilon) + gr + gC_R \} + \frac{1}{2} \rho v^3 \left(\frac{C_D A}{m} \right) \quad (1)$$

Where,

- a = vehicle acceleration (m/s²)
- A = vehicle frontal area (m²)
- C_D = aerodynamic drag coefficient (dimensionless)

- C_R = rolling resistance coefficient (dimensionless, ~ 0.0135)
- g = acceleration of gravity (9.8 m/s²)
- m = vehicle mass (in metric tons)
- r = road grade
- v = vehicle speed (m/s)
- VSP = Vehicle Specific Power (kW/ton)
- ϵ = factor accounting for rotational masses (~ 0.1)
- ρ = ambient air density (1.207 kg/m³ at 20 °C)

VSP depends on speed, acceleration, and grade and takes into account kinetic energy, changes in potential energy associated with hill climbing, rolling resistance, and aerodynamic drag. Each second of vehicle fuel use and emission rate data are divided into VSP bins to develop a VSP “modal model” for each measured vehicle (Frey et al., 2002b), as shown in Table 1.

Table 1. Definition of Vehicle Specific Power (VSP) Modes (Frey et al., 2002b).

VSP Mode	Definition (kW/ton)
1	$VSP < -2$
2	$-2 \leq VSP < 0$
3	$0 \leq VSP < 1$
4	$1 \leq VSP < 4$
5	$4 \leq VSP < 7$
6	$7 \leq VSP < 10$
7	$10 \leq VSP < 13$
8	$13 \leq VSP < 16$
9	$16 \leq VSP < 19$
10	$19 \leq VSP < 23$
11	$23 \leq VSP < 28$
12	$28 \leq VSP < 33$
13	$33 \leq VSP < 39$
14	$39 \leq VSP$

The driving cycle for a vehicle, or a particular route for a vehicle, is inferred based on the number of seconds spent in each VSP mode for that route. The second-by-second data can be aggregated to represent route-based emission rates.

Results

The example data includes eight LEV vehicles whose characteristics are given in Figure 2. The vehicles range from 1999 to 2003 model years, with engine displacement ranging from 1.6 liters to 3.8 liters, engine horsepower ranging from 106 hp to 205 hp, and engine compression ratio ranging from 9.0 to 10.6. All of the vehicles had port fuel injected engines. The vehicle curb weight ranged from 2339 lbs to 3795 lbs. Rated fuel economy ranged from 16 miles per gallon (MPG) to 27 MPG for the city rating, and 20 MPG to 33 MPG for the highway rating. At the time that these vehicles were measured, the accumulated mileage ranged from 84,031 miles to 187,510 miles. Thus, this vehicle sample represents a wide range of vehicle sizes of older model year vehicles with high mileage accumulation.

Each vehicle was measured on Routes A, C, 1, and 3. The vehicles were driven by their respective owners. Data were typically collected during the afternoon peak traffic period on a

weekday. The distribution of average travel time in each VSP mode for each route is shown in Figure 3. Routes A and 3 are arterial routes. However, they differ in that Route A typically has lower average speed than Route 3. Thus, Route 3 has a larger proportion of time spent in high power demand VSP modes 11-14 compared to Route A. Routes C and 1 both include freeway (motorway) driving. However, Route 1 is almost entirely comprised of freeway driving, whereas there is a smaller proportion of travelled miles on a freeway in Route C. Thus, Route 1 has a higher proportion of time in high VSP modes compared to Route C. Routes A, C, and 3 have a high proportion of time at idle, included in VSP Mode 3, than Route 1. The varying distributions of VSP among the four routes, and for each vehicle run on a given route, lead to variability in the distribution of emission rates.

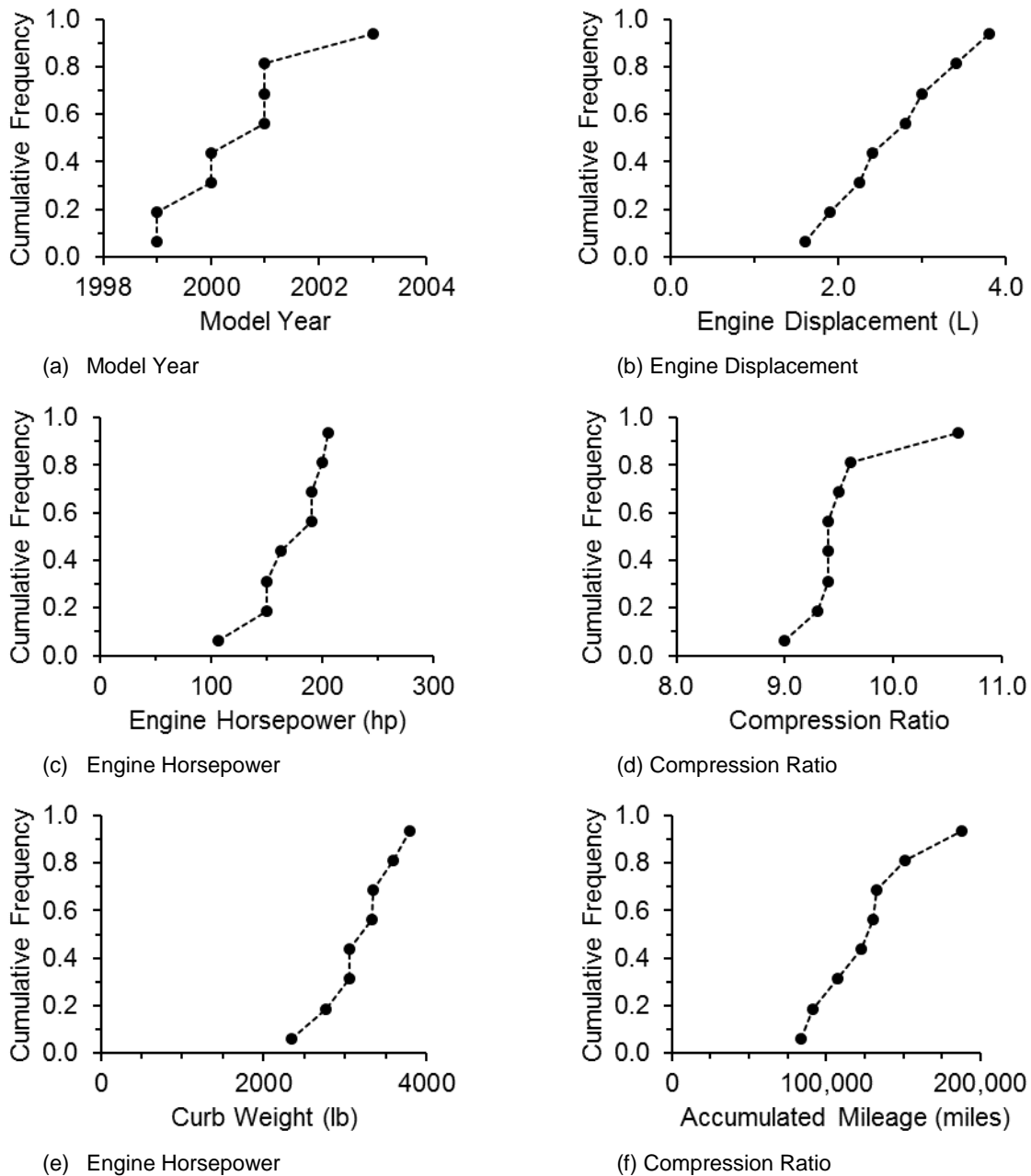


Figure 2: Frequency Distributions of the Characteristics of the Measured Low Emitting Vehicle (LEV) Light Duty Gasoline Vehicles

The typical trends in average emission rates for CO₂, CO, HC, and NO_x for VSP modal rates are shown in Figure 4 based on the average of the eight measured vehicles. For all pollutants, the modal average rate increases with positive VSP, is lowest for Mode 3 which includes idle, and is slightly higher in Modes 1 and 2 for negative values of VSP compared to Mode 3. The emission rates tend to be higher in the negative VSP modes versus idle because during deceleration the

engine is typically running at higher RPM than during idle. Because VSP is based on the physics related to tractive power demand on the vehicle, the fuel use rate is typically a linear function of positive VSP. Since the vast majority of carbon in the fuel is emitted as CO₂, the CO₂ emission rate is also a linear function of positive VSP. Note that the width of VSP modes is not equal and thus the trend in Figure 4(a) may not look perfectly linear, even though the underlying trend is actually linear.

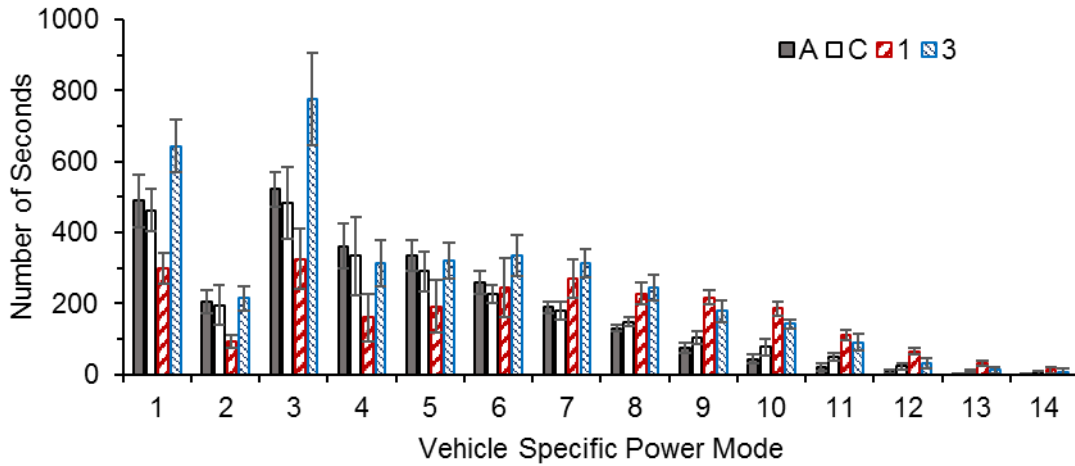
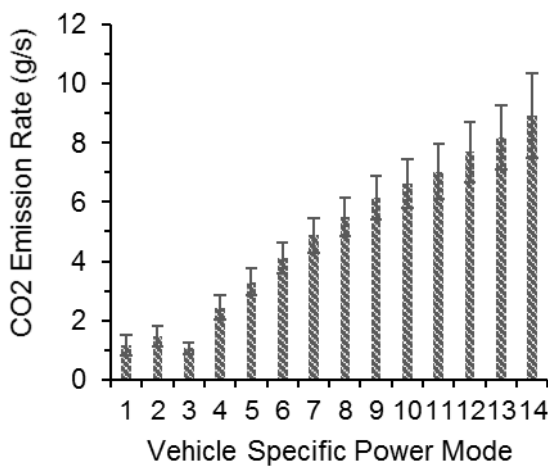
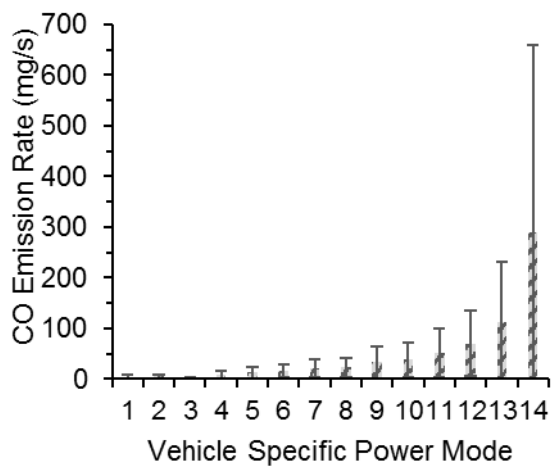


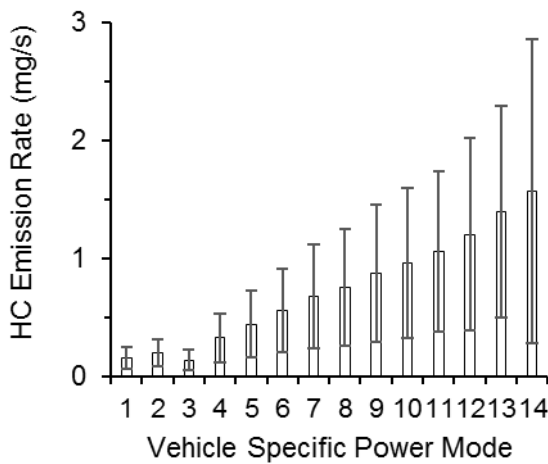
Figure 3: Distribution of Average Time Spent in Each VSP Modes for Routes A, C, 1, and 3 in the Raleigh, NC (USA) Study Area for Eight LEV Light Duty Gasoline Vehicles. Error bars are the 95% confidence interval on the mean.



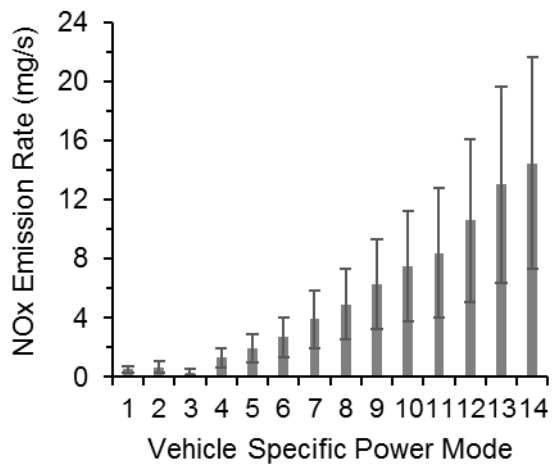
(a) Carbon dioxide (CO₂)



(b) Carbon Monoxide (CO)



(c) Hydrocarbons (HC)



(d) Nitrogen Oxides (NO_x)

Figure 4: Average Vehicle Specific Power (VSP) Modal Emission Rates for CO₂, CO, HC, and NO_x in the Raleigh, NC (USA) Study Area for Eight LEV Light Duty Gasoline Vehicles. Error bars are the 95% confidence interval on the mean.

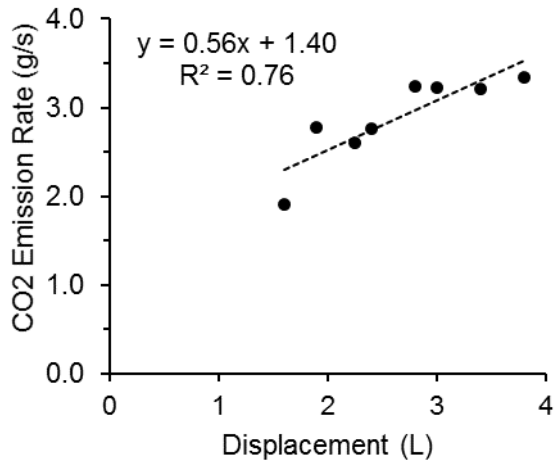
The highly nonlinear trend in VSP modal average emission rates for CO is related to the phenomenon of closed loop operation at low to moderate VSP and open loop operation at high VSP. Gasoline engines with downstream three way catalysts (TWCs) have air/fuel ratios very close to stoichiometric to provide just enough oxygen in the exhaust to oxidize CO and HC while having low enough oxygen to promote reduction of NO_x to N₂. One or more oxygen sensors in the exhaust are used as input to a closed loop control system to control the air/fuel ratio. However, at high power demand, the mass flow of CO is increased. Oxidation of CO in the TWC is exothermic. At high VSP, the heat released from oxidation of CO can potentially overheat and sinter the catalyst. To protect the catalyst, the engine is operated with open loop control in which the air/fuel ratio is commanded to be fuel rich, to starve the exhaust of oxygen and thereby prevent overheating of the catalyst. Open loop operation may occur for only a few seconds at a time, but leads to very high tailpipe exhaust CO emission rates. The frequency of open loop operation is highest in VSP mode 14. The very wide confidence intervals for the CO modal average rates are because of large inter-vehicle variability in emission rates. The HC and NO_x VSP modal average emission rates are slightly nonlinear particularly at high VSP.

The average CO₂ emission rate for each vehicle on the combined set of Routes A, C, 1, and 3 were estimated based on the VSP modal rates for each vehicle and the amount of time spent in each VSP for each vehicle. Trends in the average CO₂ emission rates for each vehicle with respect to vehicle characteristics are shown in Figure 5. Since CO₂ emission rate is proportional to fuel flow rate, the trends in CO₂ emission rate are proportional to the trends in fuel flow rate. As expected, the CO₂ emission rate is proportional to the engine size in terms of displacement and horsepower, and increases with vehicle weight. Given that the compression ratios of the engines of these eight vehicles have some variability, engine horsepower is a better predictor than engine displacement for the CO₂ emission rate for this vehicle sample. The trend in CO₂ emission rate is inversely related to the rated fuel economy, as expected, with a high coefficient of determination. Although this sample is small, it is indicative that the fuel economy ratings are reasonable. Khan and Frey (2016) have done a more extensive comparison, based on a larger vehicle sample, of real-world versus rated fuel economy, with similar findings.

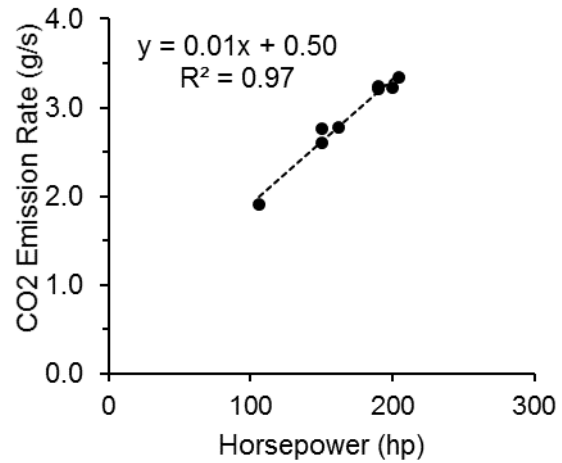
Figure 6 compares the route average emission rates for each vehicle and each route based on each pollutant. The CO₂ emission rates are proportional to engine size and influenced by engine displacement and curb weight, as indicated in Figure 5. The emission rates (g/s) are lowest for the lower speed routes with a high proportion of arterial roads, and are highest for Route 1, which is primarily comprised of driving on I-540, which has a 70 mph speed limit.

For the route average CO emission rates, there is a bi-modal distribution. Four of the vehicles have very high CO emission rates compared to the other four vehicles. Thus, inter-vehicle variability is very high on a relative basis for CO compared to CO₂ emission rates. The vehicles with very high CO emission rates range from 1999 to 2001 model year, whereas the vehicles with low CO emission rates range from 1999 to 2003 model year. The vehicle with the highest accumulated mileage, the 2001 Toyota Tundra, is among those with the lowest CO emission rates. The average accumulated mileage of the vehicles with high CO emission rates is 129,000 miles, versus 123,000 miles for those with the lower rates. Thus, the differences in emission rates are not likely to be related to model year or mileage accumulation, but may be indicative of poorly functioning TWC for some vehicles but not others. The CO emission rates for a given vehicle are typically highest on Route 1, and lowest on Route A.

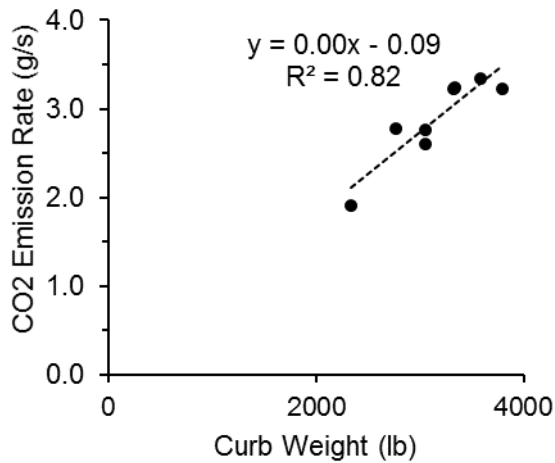
Compared to the inter-vehicle trend in CO emission rates, the inter-vehicle trend in HC emission rates is more evenly distributed. However, on average, the highest emitting of the eight vehicles has emission rates nearly 30 times greater than the lowest emitting vehicle. For a given vehicle, the ratio of the highest versus lowest route average emission rate varies from 1.24 to 1.71, with Route 1 having the highest rates and Route A having the lowest rates. For NO_x, the highest emitting vehicle has emission rates approximately 12 times higher than the lowest emitting vehicle. The ratio of highest to lowest route NO_x emission rates ranges from 1.55 to 2.23 among the eight vehicles.



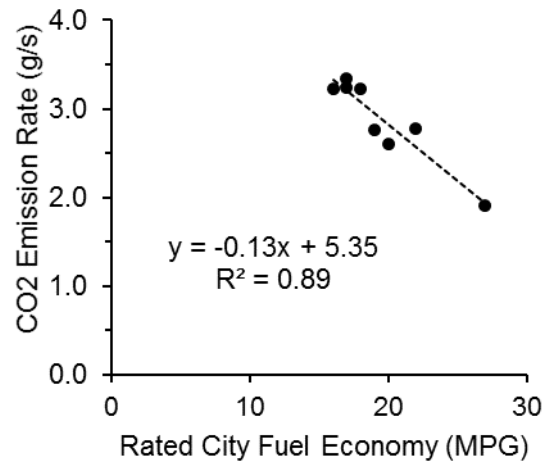
(a) CO₂ Versus Engine Displacement



(b) CO₂ Versus Engine Horsepower



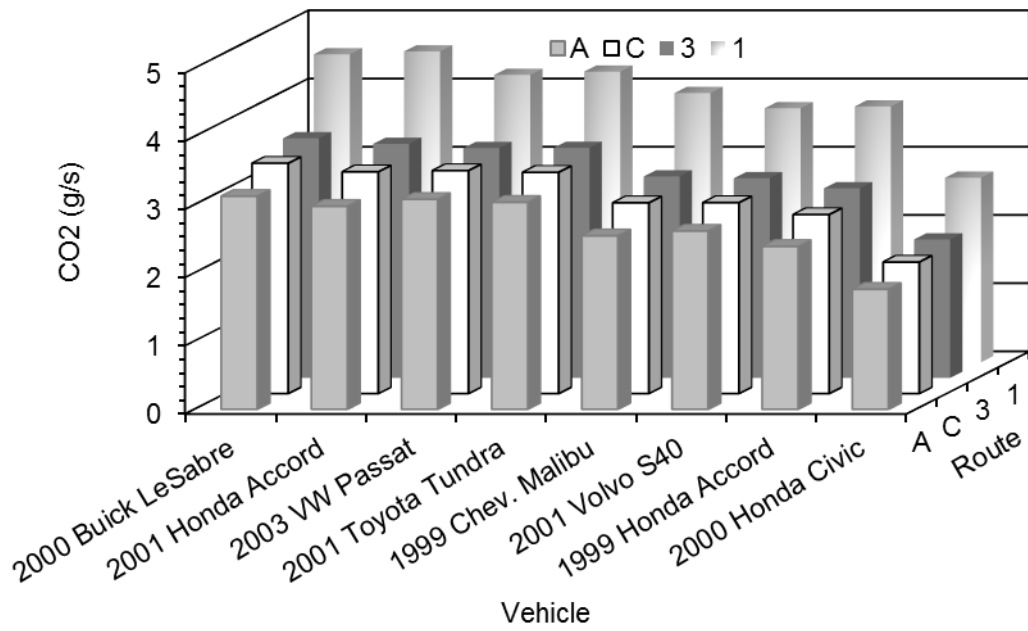
(c) CO₂ Versus Curb Weight



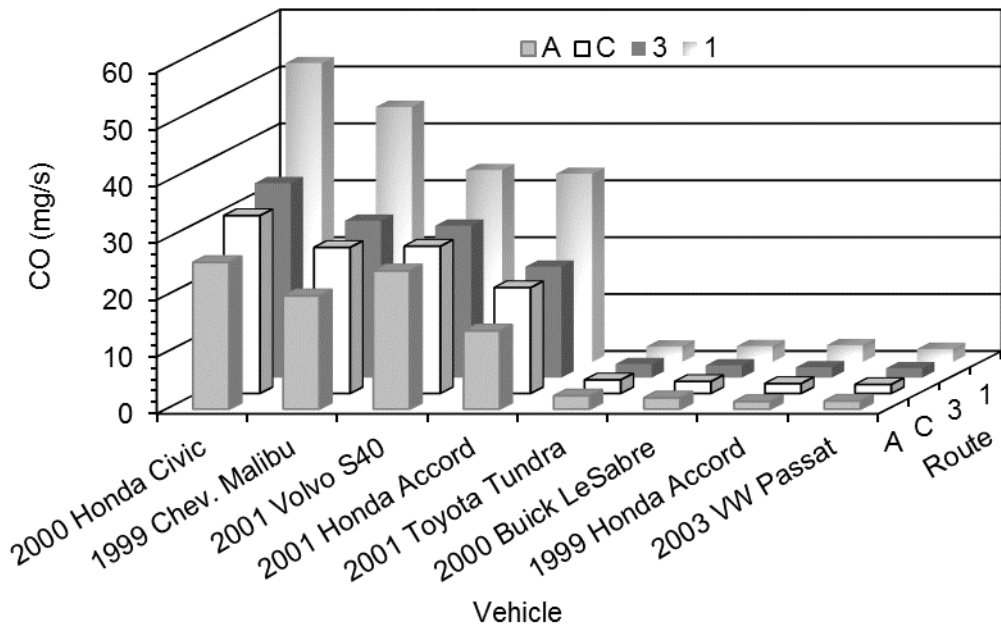
(d) CO₂ Versus Rated City Fuel Economy

Figure 5. Trends in Average CO₂ Emission Rates Versus Vehicle Characteristics for Eight Low Emission Vehicle (LEV) Light Duty Gasoline Vehicles Measured in the Raleigh and Research Triangle Park, NC (USA) Study Area.

The route average emission rates for CO, HC, and NO_x are uncorrelated to the route average emission rates for CO₂, indicating that the emission rates of the regulated pollutants are not determined based on vehicle size. However, there is correlation in route average emission rates among the vehicles between CO, HC, and NO_x. The correlation between CO and HC emission rates for this vehicle sample is 0.54. Given that CO emission rates are more sensitive to very high VSP, and that the trend in VSP modal rates for CO are more nonlinear than HC, it is not surprising that the correlation is not higher. HC and NO route average emission rates have a correlation of 0.65. CO and NO_x route average emission rates have a correlation of 0.78. These correlations are indicative of complex interactions related to the time and temperature history of the fuel and air mixture and combustion processes in the cylinder, the role of wall cooling and crevices particularly for hydrocarbons, and the operation of the TWC.

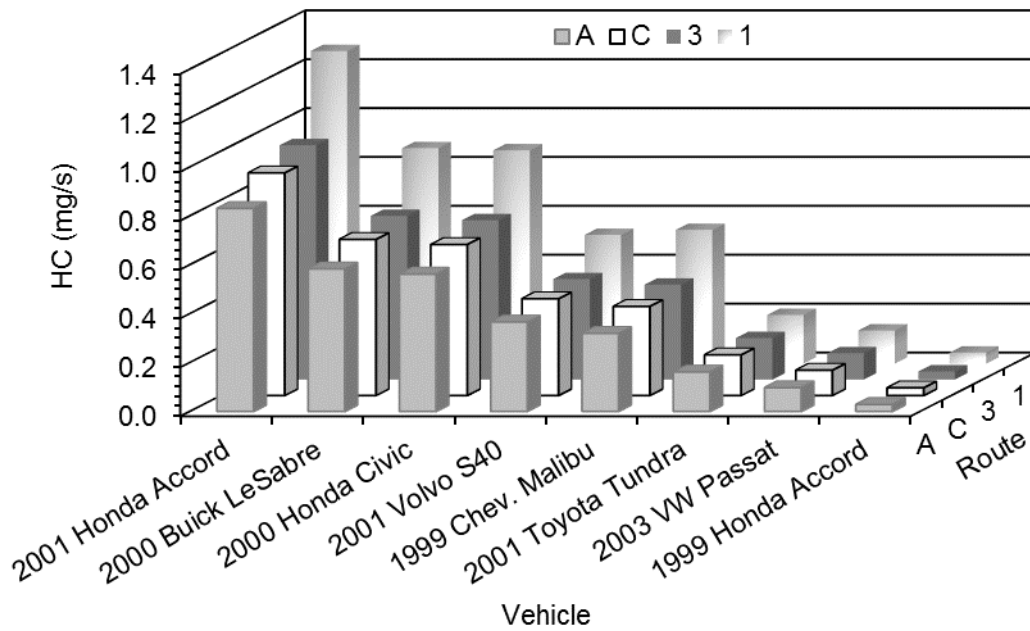


(a) Route Average CO₂ Emission Rates for Each Vehicle and Each Route

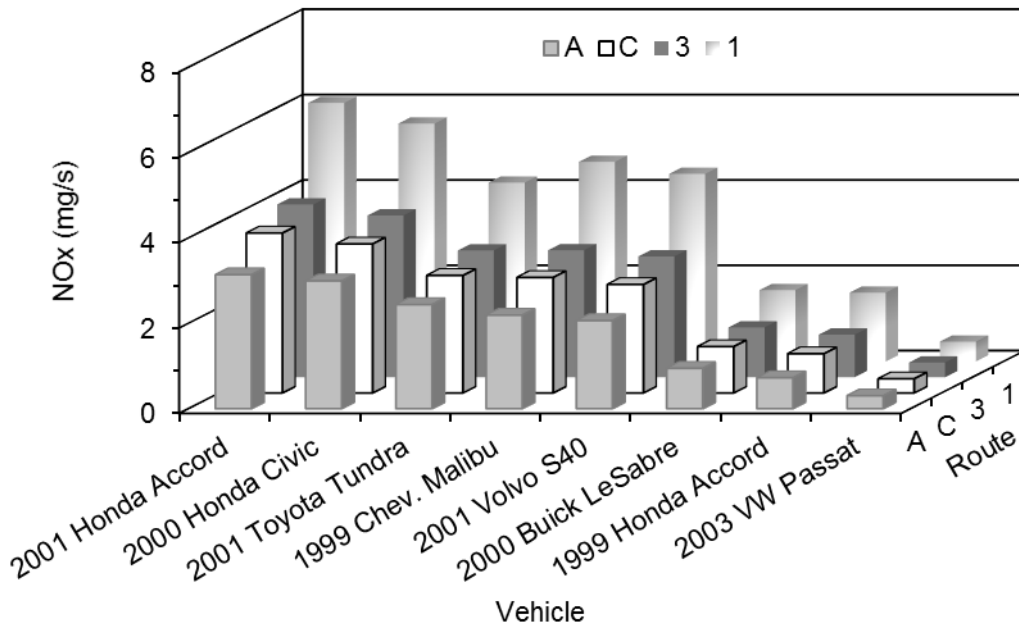


(b) Route Average CO Emission Rates for Each Vehicle and Each Route

Figure 6. Route Average Emission Rates for Each Vehicle and Each Route, by Pollutant, Based on Measurements Made in the Raleigh and Research Triangle Park, NC (USA) Study Area. Continued on Next Page.



(c) Route Average HC Emission Rates for Each Vehicle and Each Route



(d) Route Average NO_x Emission Rates for Each Vehicle and Each Route

Figure 6. Continued from Previous Page. Route Average Emission Rates for Each Vehicle and Each Route, by Pollutant, Based on Measurements Made in the Raleigh and Research Triangle Park, NC (USA) Study Area.

To illustrate the role of inter-route and inter-run variability in real-world driving cycles, route average emission rates were estimated for each of the observed driving cycles for eight vehicles on each of the four routes based on the average VSP modal rates given in Figure 4. The cycle average emission rates for an average vehicle are given in Figure 7. For CO₂, the lowest cycle average rate is 281 g/mile and the highest is 381 g/mile. Thus, the highest rate is 36% greater than the lowest rate. The CO₂ emission rate is clearly related to the cycle average speed, with the larger rates occurring for the lowest observed cycle average speed of 24 mph and the highest rates occurring for the highest observed cycle average speed of 52 mph. These cycles are different than most standard cycles used in dynamometer measurements because they represented longer durations and distances. For example, Route A has a round-trip distance of over 20 miles, and Route 3 has a round trip distance of over 34 miles. There is typically less variability in cycle average rates as the duration and distance of the cycle becomes longer. Nonetheless, this example result for an average of the eight measured LEVs indicates that there is substantial inter-cycle variability related to cycle average speed.

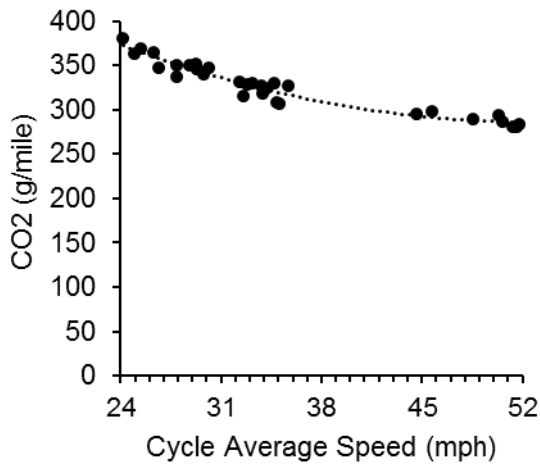
For CO, the lowest cycle average rate is 1.43 g/mile and the highest is 1.79 g/mile, for a difference of 25% from the lowest to the highest cycle average rate. Although there appears to some trend with regard to cycle average speed, the trend is very weak for this sample of cycles. There is a large range of inter-cycle variability at a given average speed, however. For example, for four cycles that range in average speed over a narrow range from 33.8 mph to 34.9 mph, the cycle average rates range from 1.45 g/mile to 1.77 g/mile, for a difference of 22 percent. Thus, the inter-cycle variability at a given average speed is approximately the same as the overall inter-cycle variability for the entire sample shown in Figure 7(b). This is indicative that the distribution of VSP, and not the cycle average speed, is a more relevant consideration in estimating cycle average emission rates. Differences in the VSP time distribution for these four cycles are given in Figure 8. Figure 8 illustrates that there are large differences in the fraction of time in each VSP mode even though these cycles have very similar average speeds. In particular, the cycle with the highest average CO emission rate, which is the 34.9 mph average speed cycle, has a higher proportion of time in the high VSP modes than any of the other three cycles. The cycle with the lowest cycle average emission rate, which has an average speed of 34.1 mph, has relatively little time in the high VSP modes.

The inter-cycle variability in HC emission rate is from 40 mg/mile to 52 mg/mile, which is a difference of 30 percent from the lowest to the highest emission rate. The inter-cycle variability in NO_x emission rate is from 230 mg/mile to 280 mg/mile, which is a difference of approximately 20 percent. For NO_x, the inter-cycle variability related to differences in VSP time distribution is substantial. For example, the difference in average emission rates for two cycles with average speeds of 44.6 mph and 45.7 mph is 13 percent.

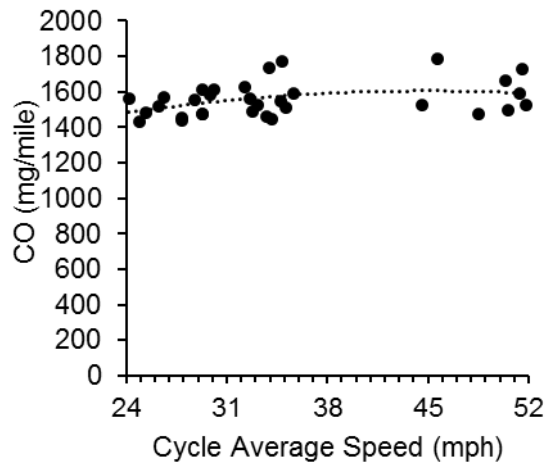
Conclusions

The purpose of this work was to illustrate a methodological approach to identify and compare sources of variability in real world emissions, including intra-vehicle variability related to engine load, inter-vehicle variability, inter-route, and inter-run variability. Field measurements were conducted on eight light duty gasoline vehicles certified to the California Low Emissions Vehicle (LEV) standard. Each vehicle was measured on four round-trip routes over a total travel distance of 111 miles. For each vehicle, modal average emissions rates for CO₂, CO, HC, and NO_x were quantified for 14 Vehicle Specific Power (VSP) modes. The vehicle sample represents 1999 to 2003 model year vehicles with high accumulated mileage, and wide ranges of engine displacement, engine horsepower, and curb weight.

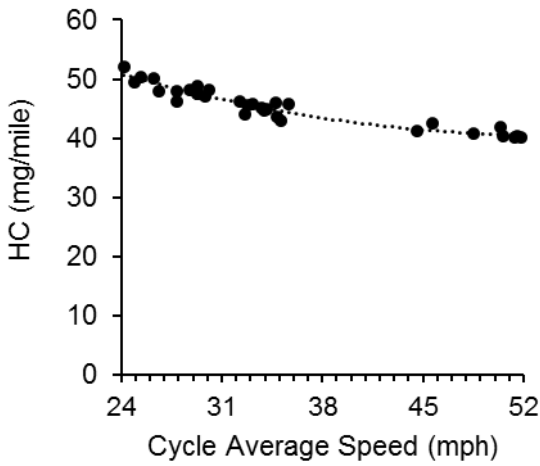
The average trends in VSP modal rates for each pollutant quantify intra-vehicle variability related to engine load. For the average of the 8 vehicles, the ratio of the highest to lowest VSP modal rates (i.e. Mode 14 to Mode 3) was 6.9 for CO₂, 108 for CO, 11 for HC, and 45 for NO_x. Thus, there is substantial variability in the vehicle emission rates related to the power demand required for tractive effort of the vehicle. These results indicate that emission rates for a given driving cycle are expected to be sensitive to the distribution of time spent in each VSP mode.



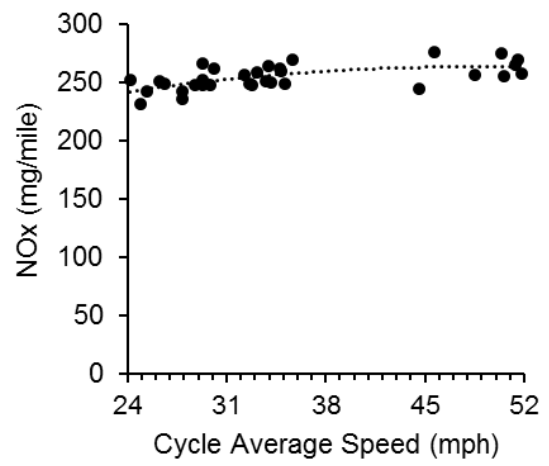
(a) Carbon dioxide (CO₂)



(b) Carbon Monoxide (CO)



(c) Hydrocarbons (HC)



(d) Nitrogen Oxides (NO_x)

Figure 7. Trends in Cycle Average Emission Rates (mass per mile) versus Cycle Average Speed for CO₂, CO, HC, and NO_x Based on an Average Low Emissions Vehicle (LEV) and 32 Real-World Driving Cycles

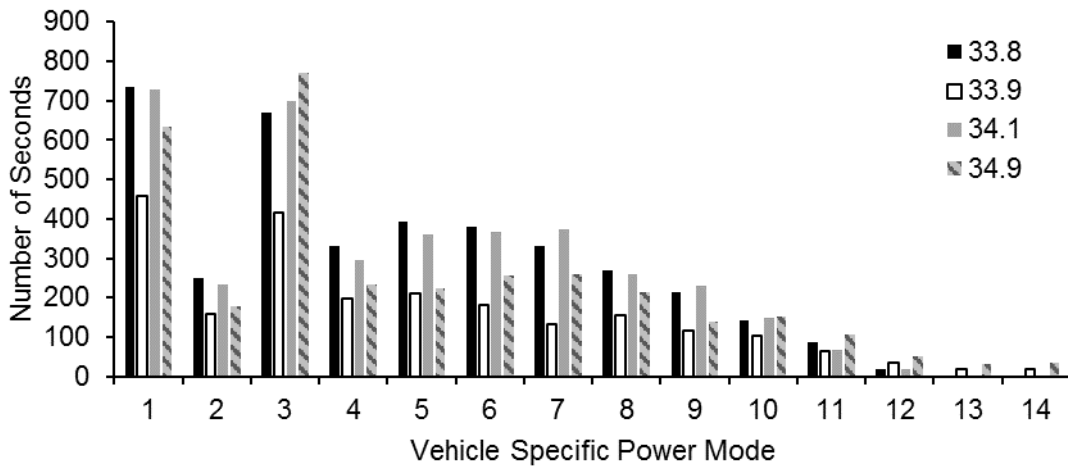


Figure 8. Comparison of the Vehicle Specific Power Time Distribution of Four Measured Real-World Driving Cycles with Similar Average Speeds Ranging from 33.8 mph to 34.9 mph.

The inter-vehicle variability in route average emissions rates was also substantial, even though the routes were long in terms of travel distance (ranging from approximately 20 miles to 34 miles). The ratio of the highest to lowest route average emission rates was 1.7 for CO₂, 21 for CO, 28 for HC, and 12 for NO_x. These results indicate that to obtain a stable estimate of fleet average emission rates requires an adequately large vehicle sample, since the confidence interval in mean emission rate will be sensitive to the sample size and the observed standard deviation in emission rates.

Inter-route variability was substantial among the four measured route. On average over the eight measured vehicles, the CO₂ emission rate (g/s) for Route 1 was 48 percent higher than that for Route A. Compared to Route A, the time-based emission rates for Route 1 were higher by 82 percent for CO, 50 percent for HC, and 92 percent for NO_x.

On a mass per distance basis, the inter-run variability at a given average speed can be comparable to the variability in cycle average emission rate versus cycle average speed. For example, for cycle average CO emission rates for an average vehicle, the inter-run variability for 32 cycles with average speeds ranging from 24 mph to 52 mph was 24 percent. However, the inter-run variability among four cycles with average speeds from only 33.8 mph to 34.9 mph was 22 percent. Thus, variability in cycle average emission rates is, at least in some cases, highly sensitive to the distribution of VSP at a given average speed, rather than directly related to variability in average speed.

The methodology illustrated here can be applied to larger vehicle samples for a particular vehicle group (e.g., LEVs), to compare vehicle groups (e.g., SULEV vs. LEV, Tier 3 vs. Tier 2, EURO 6 vs. EURO 5), to compare vehicle technologies (e.g., gas direct injection vs. port fuel injection), to compare vehicle fuels (e.g., ethanol-gasoline blends), to compare driving cycles for situations other than roundtrip routes (e.g., segments for particular road types), and so on. Although this work is based on a relatively small vehicle sample, the generic findings of large intra-vehicle variability, inter-vehicle variability, inter-route variability, and inter-run variability are consistent with past work. These sources of variability need to be taken into account when designing field data collection studies particularly with regard to the choice of sample size of vehicles and routes.

Acknowledgements

This work has been conducted over a period of time between 2008 and the present, during which portions of the work have been supported by grants from the National Science Foundation and the U.S. Environmental Protection Agency. The authors are solely responsible for the content of this paper.

References

- Barth, M., T. Younglove, C. Malcom, and G. Scora. 2002. Mobile Source Emissions New Generation Model: Using a Hybrid Database Prediction Technique. Ann Arbor, MI: Prepared by University of California at Riverside for U.S. Environmental Protection Agency.
- Environ. 2002. On-Board Emission Data Analysis and Collection for the New Generation Model. Ann Arbor, MI: Prepared by Environ International Corporation for U.S. Environmental Protection Agency.
- EPA. 2002. EPA's On-Board Emission Analysis Shootout: Overview and Result. EPA420-R-2-26. Ann Arbor, MI: U.S. Environmental Protection Agency.
- Franco, V., M. Kousoulidou, M. Muntean, L. Ntziachristos, S. Hausberger, and P. Dilara. 2013. Road Vehicle Emission Factors Development: A Review. *Atmos. Environ.* 70 (Supplement C): 84–97. doi:10.1016/j.atmosenv.2013.01.006.
- Frey, H. C., A. Unal, and J. Chen. 2002. Recommended Strategy for Onboard Data Analysis and Collection for the New Generation Model. Ann Arbor, MI: Prepared by North Carolina State University for the U.S. Environmental Protection Agency.
- Frey, H.C; Unal, A.; Chen, J.; Li, S.; Xuan, C. (2002b), "Methodology for Developing Modal Emission Rates for EPA's Multi-scale Motor Vehicle & Equipment Emission System," EPA420-R-

02-02, Prepared by North Carolina State University for Office of Transportation and Air Quality, U.S. Environmental Protection Agency, Ann Arbor, MI

Frey, H. C., N. M. Roupail, A. Unal, and J. D. Colyar. 2001. Emissions Reduction Through Better Traffic Management: An Empirical Evaluation Based Upon On-Road Measurements. FHWA/NC/2002-001. Raleigh, NC: Prepared by North Carolina State University for North Carolina Department of Transportation. <https://trid.trb.org/view/661327>.

Frey, H.C., "2018 Critical Review: Trends in Onroad Transportation Energy and Emissions," Journal of the Air & Waste Management Association, 68(6):514-563 (2018). DOI: 10.1080/10962247.2018.1454357.

Frey, H.C., A. Unal, N.M. Roupail, and J.D. Colyar, "On-Road Measurement of Vehicle Tailpipe Emissions Using a Portable Instrument," Journal of Air & Waste Manage. Assoc., 53(8):992-1002 (August 2003)

Frey, H.C., K. Zhang, and N.M. Roupail, "Fuel Use and Emissions Comparisons for Alternative Routes, Time of Day, Road Grade, and Vehicles Based on In-Use Measurements," Environmental Science and Technology, 42(7):2483–2489 (April 2008).

Frey, H.C., K. Zhang, and N.M. Roupail, "Vehicle-Specific Emissions Modeling Based Upon On-Road Measurements," Environmental Science and Technology, 44(9):3594-3600 (2010)

Khan, T., and H.C. Frey, "Evaluation of Light Duty Gasoline Vehicle Rated Fuel Economy Based on In-Use Measurements," Transportation Research Record, 2570:21-29 (2016). <http://dx.doi.org/10.3141/2570-03>.

Ntziachristos, L., G. Mellios, D. Tsokolis, M. Keller, S. Hausberger, N. E. Ligterink, and P. Dilara. 2014. In-Use vs. Type-Approval Fuel Consumption of Current Passenger Cars in Europe. Energy Policy 67 (April): 403–411. doi:10.1016/j.enpol.2013.12.013.

Ropkins, K., R. Quinn, J. Beebe, H. Li, B. Daham, J. Tate, M. Bell, and G. Andrews. 2007. Real-World Comparison of Probe Vehicle Emissions and Fuel Consumption Using Diesel and 5% Biodiesel (B5) Blend. Sci. Total Environ. 376 (1): 267–284. doi:10.1016/j.scitotenv.2006.11.021.

Sandhu, G.S., and H.C. Frey, "Effects of Errors on Vehicle Emission Rates from Portable Emissions Measurement Systems," Transportation Research Record, 2340:10-19 (2013). DOI:10.3141/2340-02.

Scarbro, C. 2000. An Investigation of Rover's Capabilities to Accurately Measure the In-Use Activity and Emissions of Late-Model Diesel and Gasoline Trucks presented at the Tenth CRC On-Road Vehicle Emissions Workshop, San Diego.

Vojtisek-Lom, M., and J. T. Cobb. 1997. Vehicle Mass Emissions Measurement Using a Portable 5-Gas Exhaust Analyzer and Engine Computer Data. In , 656–727. Pittsburgh, PA: Air and Waste Management Association.

Yazdani, B., and H.C. Frey, "Road Grade Quantification Based on Global Positioning System Data Obtained from Real-World Vehicle Fuel Use and Emission Measurements," Atmospheric Environment, 85:179-186 (March 2014). <http://dx.doi.org/10.1016/j.atmosenv.2013.12.025>

2.1.9 NO_x Emissions of Heavy-Duty Vehicles with Euro VI Certified Engines

R.J Vermeulen^{1}, R.N. van Gijlswijk¹, S. van Goethem¹*

¹ TNO, the Netherlands Organisation for applied scientific research , The Hague, the Netherlands, robin.vermeulen@tno.nl

Summary

In the Dutch in-service emissions testing programme, the nitrogen oxide (NO_x) emissions of 46 vehicles with Euro VI certified engines were measured during normal daily operation using the Smart Emission Measurement System (SEMS). To screen the in-service conformity, a number of vehicles were tested over the prescribed in-service conformity test routes using SEMS and in some cases the Portable Emission Measurement System (PEMS).

All the screened vehicles showed indicative good results over the in-service conformity routes using the pass-fail evaluation method. In daily operation however, the NO_x emissions vary a lot from case to case and are often not as low as one might expect based on the EU standard. The variation in NO_x emissions is largely caused by the spread in operation profiles between the vehicles. Average speeds vary and especially at low speed, low load the probability that NO_x emissions increase is higher. The cause is the fact that in these conditions the NO_x abatement technology that is present on Euro VI step A to C certified engines is not always fully effective.

In September 2019 the EU implements step D in Euro VI legislation. Later on it will round off Euro VI with the implementation of step E. These steps contain some changes for the road test with PEMS, which are intended to better cover the low load, low speed operation of heavy-duty vehicles as occurring in normal daily operation. It is however still recommended to add provisions in the EU regulation for testing vocational vehicles over routes that represent their normal use.

Continuation of monitoring new heavy-duty vehicle emissions will show the possible impact of the changes of step D and step E on the real world NO_x emissions. For diesel engines in non-road mobile machinery (NRMM) in principle the same issue exists. It is therefore recommended to intensify monitoring of NO_x emissions of NRMM in normal use.

Introduction

In cities and near roads with dense traffic, concentrations of NO₂ in the air still exceed the EU limits. Locally, traffic is the main source but remote sources contribute to background concentrations as well. From traffic, vehicles with a diesel engine emit the most NO_x and NO₂ which means that for areas with a high density of vehicles with a diesel engine, the contribution of traffic is high. Reduction of the tail pipe NO_x emissions from these vehicles is desirable from an air quality point of view. In the last two decades, EU emissions regulations tried to command a reduction of the NO_x emissions from vehicles with a diesel engine, but only managed to establish substantial reductions as of the introduction of Euro VI (Vermeulen et al., 2016). The substantial reduction of the NO_x emissions from diesel engines is mainly achieved by the application of an exhaust gas aftertreatment system that uses Selective Catalytic Reduction (SCR). The SCR system is often complemented by Exhaust Gas Recirculation that reduces the NO_x load entering the SCR.

For vehicles with the first generation of Euro VI engines it was reported (Vermeulen et al., 2016) that NO_x emissions of vehicles with Euro VI certified engines have on average decreased substantially compared to the NO_x emissions of previous generations of engines. This is partly due to a more stringent limit for the NO_x emissions, but also due the introduction of an emission test that has to be conducted on the public road. As of Euro VI (31 December 2013), the test with a Portable Emission Measurement System (PEMS) became a mandatory part of the EU type approval process in the form of an in-service conformity test.

Studies by (Vermeulen et al., 2016) and (Söderena, P., Nylund, N., 2018) showed that for certain heavy-duty vehicle applications despite the more stringent requirements NO_x emissions may be higher than expected, based on the limits for the engine test and the in-service conformity (ISC) test on the public road. In (Vermeulen, Ligterink, 2018) it was demonstrated that substantial parts of normal driving, such as driving at a low engine load and driving in the city, may fall outside of the boundaries of the ISC test on the public road. Together, this leads to the situation that NO_x emissions levels of vehicles with a Euro VI certified engine still depend on actual driving conditions and exceed the Euro VI limit values. Therefore, within the Dutch in-service emissions testing programme, TNO is conducting for the Ministry of Infrastructure and Water management, it was decided to test a number of different representative HDV vehicles of different types of applications in normal daily operation, to determine actual NO_x emissions levels.

The general objectives of the Dutch in-service emissions testing programme are to:

- Determine the emission factors for heavy commercial vehicles
- Determine trends over the different EU standards and steps:
 - Are the vehicles getting sufficiently cleaner each generation/step in the real world?
 - Use the data and insights in Brussels in discussions about the improvement of the test procedures
- Screen the in-service conformity
- Assess new/alternative technologies
- Provide information to stakeholders, to help make purchase decisions for cleaner and more fuel efficient transport

This paper presents NO_x emissions data that was gathered throughout the programme in the period 2015 to 2019 for 46 vehicles with Euro VI certified engines and gives an overview of the data, with a focus on:

- the determination of NO_x emissions of heavy-duty vehicles with Euro VI-step A and a few C (as of Sept. 2016) certified engines, under a range of normal representative driving conditions which are considered normal use in the Netherlands,
- the limited coverage of normal operation in the Netherlands by the EU PEMS test for in-service conformity

Method: Real-world emission monitoring using SEMS and PEMS

The emissions measurement programme aimed at determining the real-world NO_x emission levels of heavy-duty vehicles. The Smart Emissions Measurement System (SEMS), a sensor-based system developed by TNO (Heijne et al. 2016), was used to measure and analyse the tail-pipe NO_x emissions and a range of vehicle/engine parameters to be able to characterize the typical operation of the vehicles. In this way, for the group of vehicles, weeks up to months of data was collected per vehicle.

The SEMS uses an automotive NO_x sensor, GPS and a data-acquisition system to record the sensor data and CAN data from the vehicle and engine at a sample rate of 1Hz. The system can operate autonomously and wakes up at ignition/key-on of the vehicle. The system can be stowed away so that normal operation is not hindered by the measurement. The recorded data is sent hourly to a central data server.

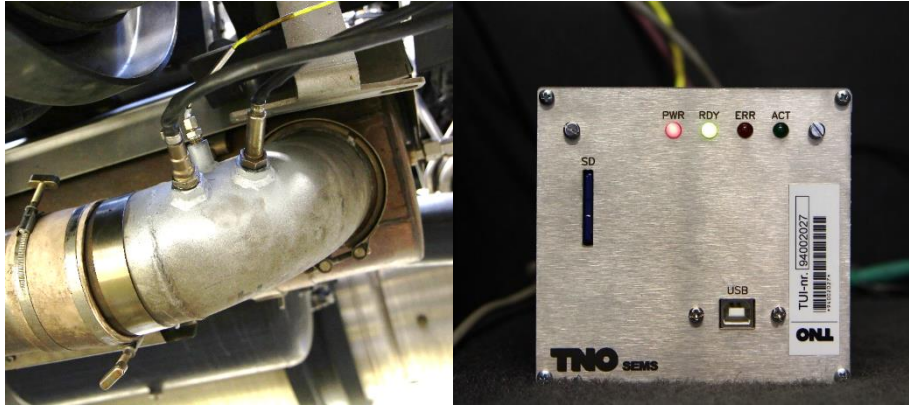


Figure 1: SEMS. Left, calibrated NO_x-O₂ sensor, NH₃ sensor and temperature sensor mounted in the tail-pipe. Right, autonomously running data recording unit with hourly data transmission to a central server via GPRS.

The raw data on the central server is post-processed automatically to filter and check the data. Sensor output is corrected using sensor specific calibration values. Mass-emissions and instantaneous engine power are calculated combining sensor data and CAN data such as manifold-air flow, fuel rate, engine torque, and sensor O₂ concentration where possible. For the vehicles for which no sufficient engine data were available to calculate the work specific emissions, an estimation of the average brake specific fuel consumption and CO₂ emission of the engine was used to estimate the vehicle's emissions in g/kWh.

For more accurate technology assessment and in-service conformity checking in some occasions also a Portable Emissions Measurement System (PEMS) has been used to measure the NO_x emissions on the public road. A limitation is that the tests rebound to well-defined test routes and represent only a few hours of vehicle operation while a merit is the more accurate measurement and the fact that it is the formally prescribed instrument for in-service conformity testing.

In-service conformity screening

The Dutch in-service emissions testing programme aims to screen the in-service conformity. This means that indicative tests are performed to determine whether or not there is an increased probability that an Euro VI certified engine in a vehicle fails the formal in-service conformity test. The process contains a number of steps:

1. *SEMS screening test*: When SEMS is mounted, the vehicle is also checked (MI and display error codes) and the owner is asked to provide information about the history of the vehicle. The SEMS data from the vehicle in daily operation is used to determine the SEMS Factor (Heijne, 2016) applying the pass-fail evaluation rules of a formal PEMS test, using the SEMS data instead. In the case the SEMS Factor is higher than 1.5 proceed to 2, otherwise proceed to 4.
2. *SEMS screening ISC route*: Perform additional checks on the vehicle. Read OBD for error codes, check Malfunction Indicator and display for possible error signs. Run an in-service conformity test route using the SEMS that is already mounted on the vehicle. The SEMS Factor is calculated for this trip applying the pass-fail evaluation rules of a formal PEMS test. In the case the SEMS Factor is higher than 1.5 the result is communicated to the national Type Approval Authority. If the SEMS Factor is lower than 1.5: proceed to 3 or 4.
3. *PEMS ISC test*: Optionally, it can be decided to perform an additional test according to the formal test requirements with PEMS.
4. Archive test data in the database. Report overall results in an annual report. Send a summary of the result of each vehicle to the national TAA.

After each step of the process the OEM is invited to discuss the results.

Vehicle selection: heavy-duty vehicles with Euro VI certified engines

Since the introduction of Euro VI on the market in 2013 the focus of the Dutch programme changed to testing the new generation of engines and emissions abatement in heavy-duty vehicles. Each year a ranking for each vehicle class (city bus, medium truck, heavy truck, RCV) was made, based on the number of registrations of each Euro VI engine type/family. This has led to a test sample containing 46 individual heavy-duty vehicles, most with a diesel engine. The second group were 'specialties'. Vehicles in this group were selected not only by their engine type/family, but also by the purpose of the vehicle. Waste collection trucks and city buses were selected for this purpose. For an assessment of environmental technology, vehicles on alternative fuels have been tested as well. See the table for the categories of vehicles that have been tested and the tests performed with those vehicles. A limitation of the dataset is that the vehicle mileages, as read from the odometers at the start of the tests, are still relatively low. Odometer readings range from 20.000 km to about 400.000 km for one N3 class tractor in a single case while for instance for the latter lifetime mileage expectance would be 1.2 to 1.5 million kilometres. It means that there are no old vehicles in the dataset and possible ageing effects are accounted for given the relatively fresh fleet of test vehicles.

Table 1: overview of the test sample with vehicle categories tested, types of vehicles tests and number of vehicles of each type tested.

		PEMS	SEMS
Tractor (semi) trailer	CI*(Diesel) N3	6	8
	SI** (LNG) N3	2	
	HDDF*** LNG -diesel N3,1A	1	1
Rigid	CI (Diesel) N2	1	4
	CI (Diesel) N3		4
Refuse Vehicle	Collection	CI (Diesel) N3	8
		SI (LNG) N3	1
		SI (CNG) N3	1
Buses	CI (Diesel) 12m	2	2
	CI (Diesel) 18m		3
Tipper	CI (Diesel) N3		1

*CI: Compression Ignition engine. **SI: Spark Ignition engine. ***HDDF: Heavy-Duty Dual Fuel engine.

Results: in-service conformity screening

The majority of vehicles has been put to a screening test with SEMS and/or PEMS. Result of this is for the tested vehicles that in 5 cases the initial SEMS screening test lead to false positives. I.e. when eventually the applicable SEMS ISC route was driven the SEMS screening Factor was lower than 1.5. In the case of one PEMS test, the test proved not fully compliant with the formal ISC requirements. For one vehicle, an N3 class, diesel Refuse Collection Vehicles (RCV) white deposits were found in the tail-pipe rendering the SEMS measurement invalid. The white deposits gave cause for further investigation of the vehicle by the OEMS which is not yet finished. Four vehicles are currently being tested with SEMS.

Table 2: overview of ISC screening test results.

EU vehicle engine	category,	PEMS Test
N3, CI		CF<1.5 (6)
N2, CI		CF>1.5 (1, trip not compliant)
N3, SI (LNG)		CF>1.5 (2)
N3 HDDF (LNG -diesel)		CF<1.5 (1)
M3, CI		CF<1.5 (2)

	SEMS screening test	SEMS screening route	ISC
N3, CI	CF<1.5 (6)		
	CF>1.5 (3)	CF<1.5 (3)	
	CF=? (1) SCR deposits	Investigation running (1)	
	Test running (4)		
N2, CI	CF<1.5 (4)		
	CF>1.5 (2)	CF <1.5 (2)	
M3, CI	CF<1.5 (4)		
	CF>1.5 (1)	CF<1.5 (1)	

Results: Real world NO_x emissions levels for the different vehicle categories

Total average NO_x emissions were determined for all vehicles. There is a large spread in average speed and NO_x emissions between all vehicles.

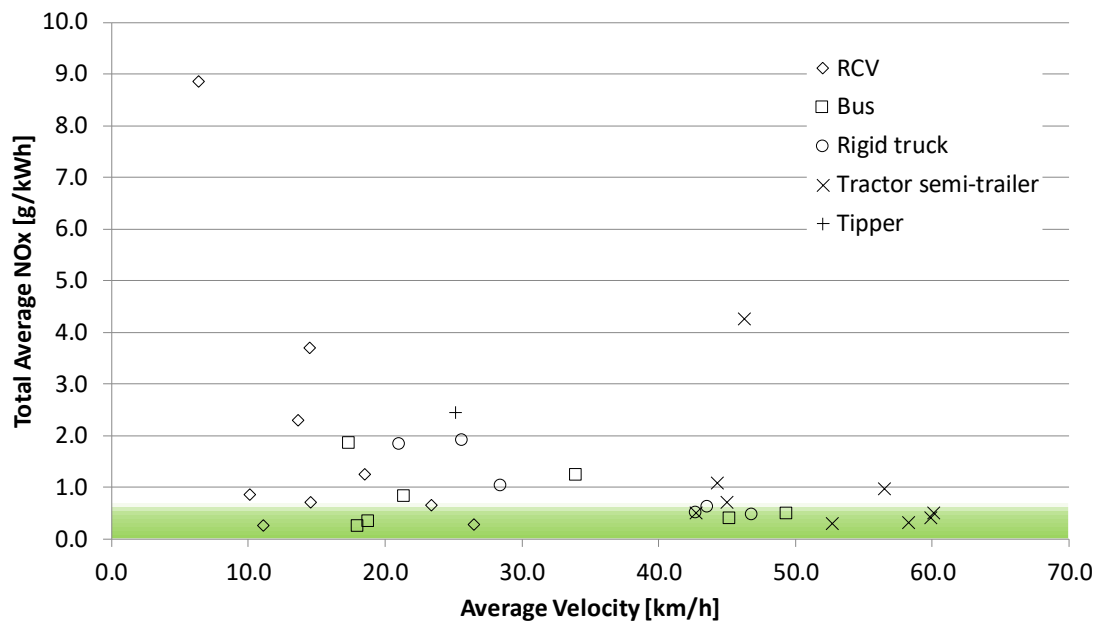


Figure 45: total average NO_x emissions versus average speed for all vehicles tested with SEMS in normal daily operation. The upper side of the green area represent a NO_x emissions level of 0.69 g/kWh, which is the limit of the conformity factor of 1.5 expressed in gNO_x/kWh ($1.5 \times 0.46 = 0.69$ g/kWh) for the formal ISC test.

Refuse collection vehicles have the lowest average speeds, from 6 to about 26 km/h and the largest spread in NO_x emissions and this results in a large spread of average NO_x emissions, from 0.3 to 9 g/kWh. RCV operation is characterized by stops for refuse collection and stop times depend on type of refuse collected (small containers, large containers, garbage bags, coarse refuse) and driving speeds depend on the area that is serviced. In cities speeds are lower as opposed to rural areas and small villages. The highest NO_x emission was measured in a case of coarse refuse collection with long stops for manual loading of the refuse and short driving intervals. Measurements for this vehicle were executed in winter time and the emission abatement concept was 'SCR only', meaning there is no additional Exhaust Gas Recirculation to reduce diesel engine NO_x emissions. For another vehicle, NO_x emissions were low despite a low average speed. This vehicle used a high amount of power from the power take off to lift large under floor containers. Another vehicle has a throttle valve which can control diesel engine lambda (air to fuel ratio) so that exhaust temperatures remain higher at low speeds and NO_x remains low, even at low speeds.

Buses have higher average speeds, from 17 to 49 km/h. However, from the dataset over individual city bus lines average speeds are noted as low as 13 km/h. The higher speeds are for buses that service rural areas and villages from a larger city. Usually, these buses stop at less bus stops in a city and often exit and re-enter the city centre straight away. This means that average driving speeds will be higher in urban areas and on average higher because driving contains rural roads and sometimes a motorway. Average NO_x emissions remain below 2 g/kWh.

Average speeds of *rigid trucks* spread a lot as well but are not as low as for buses and refuse collection vehicles. Rigid trucks include the lighter versions around 10t that are used for city distribution (delivery of goods and parcels) and typically show the lowest average speeds. In those cases NO_x emissions are generally the highest, on average up to 2 g/kWh down to 0.5 g/kWh for

the operations with higher average speeds. Some of the trucks distribute through the country and drive a lot of motorway to enter a city and deliver goods throughout a city which brings average speed downward.

The *long haulage trucks or tractor semi-trailers* have the highest average speeds up to about 60 km/h. Still not all these vehicles run mainly motorways. Three of the vehicles are used to service supermarkets from distribution centres and clothing shops. These vehicles tend to have a lot of starts and semi-warm operation because the vehicle is moved around at distribution centres and near shops. One vehicle distributes flowers to France but despite a lot of motorway time also spends a lot of time (about 30% of total operational time) in northern French cities to distribute flowers to the shops. NO_x emissions for all tested vehicles vary from as low as 0.3 g/kWh to about 1 g/kWh. A high NO_x emission was measured for one vehicle of 4.3 g/kWh. The vehicle hardly uses reagent (AdBlue) the consumable which is needed for an SCR to work.

The 4x8 *tipper* hauls sand to construction sites. It drives from a depot to the site where work consists of a lot of idling, low speed dumping and manoeuvring at the site. Hence, the relatively low average speed. Also the operation has periods of high engine load when the vehicle is fully loaded with sand versus low engine loads for running empty. The prolonged periods at the construction sites and low payload afterwards together lead to average NO_x emissions being somewhat higher and around 2.5 g/kWh on average.

When the data of all vehicles is divided over speed bins for low, medium and high speed it becomes apparent that at low speeds NO_x emissions for most of the vehicles are higher.

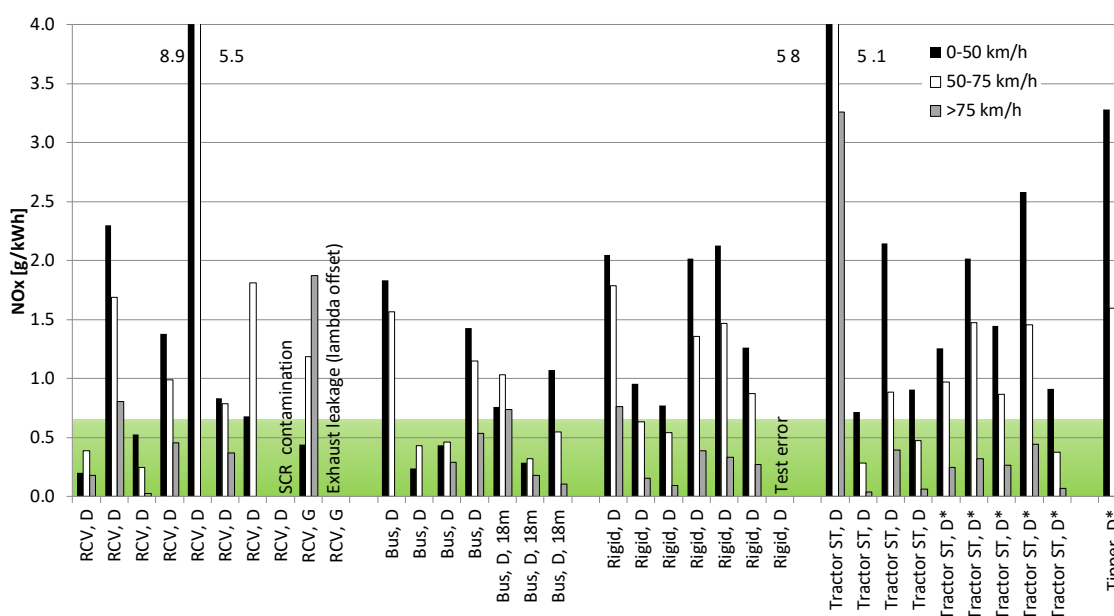


Figure 3: overview of real world NO_x emissions as measured with SEMS during daily operation for a number of different vehicle types, all with Euro VI certified engines. Three speed ranges are distinguished. * represents Euro VI step C, all others Euro VI step A. D=Diesel, G=Gaz (CNG or LNG). The upper side of the green area represent a NO_x emissions level of 0.69 g/kWh, which is the limit of the conformity factor of 1.5 expressed in gNO_x/kWh (1.5x0.46=0.69 g/kWh) for the formal ISC test.

For a certain share of total emissions this is caused by cold engine operation. Warming up of a heavy duty engine is most often done by idling or running at low speeds. Elevated emissions produced during this period, because emission abatement is not yet active, contribute to the higher emissions. Cold engine operation (Coolant temperature is below 70° C) is for most vehicles 3 to 10% of the total time, but individual cases show cold operation up to 32% when vehicles idle a lot. Cold emissions shares in total emissions depend a lot on how much is emitted when the engine is warm. For example emissions after cold starts can contribute 30% to total emissions when the overall emissions are low (0.5 g/kWh). A large share of the higher NO_x emissions at low

speeds is caused during warm engine operation when SCR temperatures drop below working temperatures.

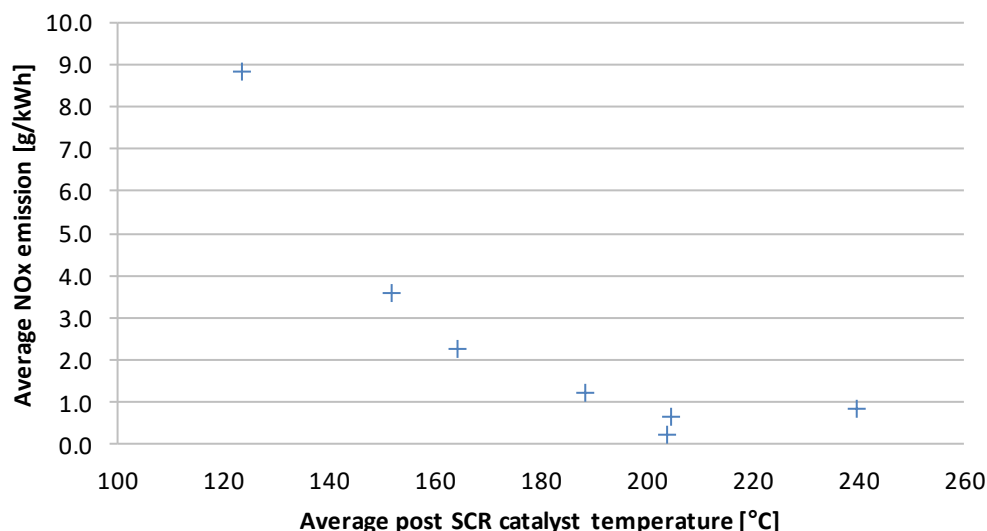


Figure 3: relation between total average NO_x emissions and average post SCR exhaust gas temperature for the refuse collection vehicles.

Euro VI and PEMS test for ISC: limited coverage of normal operation

For the regulation of NO_x emissions of engines of heavy-duty vehicles a number of measures are implemented in the type approval framework. The basis is a type approval emissions test of the engine that demonstrates the emission performance with regard to the regulated gaseous pollutant emissions of the given engine type. This is amongst others complemented by additional requirements to check the conformity of production, on-board diagnostics (functionality of emissions critical components), the NO_x measures (e.g. AdBlue consumption) and in-service conformity. The latter is an important test that as of Euro VI (31 December 2013) needs to be conducted with the engine in a representative vehicle, on the public road. Engines have to comply to a so called maximum conformity factor standard of 1.5 that relates to the emissions limit of the engine test, for NO_x $1.5 \times 0.46 \text{ g/kW} = 0.69 \text{ g/kWh}$. Vehicles need to be in-service, comply over the useful life that depends on the legislative category (e.g. 700.00km for N3, GVW>12t trucks) and have no malfunctions. Malfunctions are to be detected by on-board diagnostics, with a threshold limit for NO_x and the NO_x measures. In certain cases drivers/owners are forced to make necessary repairs because a torque inducement may render normal operation of the vehicle impossible until the repair is done. The whole package of test and requirements should guarantee sustainably low emissions over the useful life of a heavy-duty vehicle. Previous tests on heavy-duty vehicles reported in (Vermeulen et al., 2016) showed higher NO_x emissions than expected based on in-service conformity test limits which indicate a limited coverage of normal operations by the in-service conformity PEMS test. This has led to the decision for the Dutch test programme to extend testing, to vehicle categories that operate in cities (RCV, buses, distribution trucks).

Table 3: Overview of most important NO_x requirements in EC Regulation numbers 595/2009, 582/2011 and subsequent amendments

<hr/>								
NO_x limit WHSC/WHTC engine test		400 / 460 mg/kWh						
PEMS test for OCE/TA and ISC		Yes						
PEMS Conformity Factor limit		1.5 (1.5 x 0.46 g/kWh)						
PEMS data exclusions		10% highest MAW, power threshold, cold start (see below)						
<hr/>								
Euro VI step	NO_x OBD threshold limit [g/kWh]	Addition al OBD monitors	PEMS Power threshold	PEMS Cold start	PEMS PN	PEMS urban MAW	PEMS payload	Implementation date all vehicles
A	1.5	N	20	N	N	n.b.	50-60%	31-12-2013
B	1.5	N	20	N	N	n.b.	50-60%	01-09-2015
C	1.2	Y	20	N	N	n.b.	50-60%	31-12-2016
D	1.2	Y	10	N	N	Y	10-100%	01-09-2019
E	1.2	Y	10	Y	Y	Y	10-100%	t.b.d
<hr/>								

For the first generations of Euro VI engines, step A to C, low load and low speed operations fall outside the boundaries of the PEMS test for in-service conformity¹. Low power operation and high emissions events are excluded from the test evaluation (Vermeulen et al., 2018). Also for the heavy category of vehicles >12t (N3) urban operation is not, or partly in the test evaluation and the mentioned exclusions may delete the remainder of urban operation from the test evaluation. Up to step C, only medium payloads are prescribed for the test, while in normal use payloads from 0 to 100% are common. Vocational vehicles are tested according their GVW category over mostly either an N2 distribution trip (GVW 3.5-12t) or an N3 long haulage trip (GVW>12t). Refuse collection vehicles are often build on an N3 chassis and as such the engine is only tested in a long haul truck with the majority of the test being motorway operation while urban driving and low loads are being excluded. For city buses (M3, class 1) there is already a dedicated bus route, the M3 route which contains 70% of urban driving. Nevertheless, low loads had still to be excluded, according evaluation rules up to a maximum of 50% of the test windows (Moving Averaging Windows). High emissions events (10% of the test windows (MAW)) are also still excluded from the PEMS test.

The observed higher and varying NO_x emissions, especially at low load low speed operation, has been debated in the Brussels EU PEMS expert working group in the recent years. This has led to improved test procedure and new more stringent requirements as of step D (Implementation date 'All vehicles': 1 September 2019):

- Lower power threshold from 20 to 10%.
- Extension of payload range from 50-60% to 10-100%.

¹ EC regulation nr. 582/2011

- Inclusion of mandatory urban moving averaging window, mainly relevant for N3 and possibly also for N2.
- Extension of the urban part of the N3 route from 20 to 30% of the test time. This is excluding the cold period.
- Better definitions for the trip sub parts and longer allowed total test time.

Further improvements are expected for step E (implementation date is not fixed yet) with inclusion of the cold start, a particle number test and additional requirements auxiliary emission strategies (AES).

Monitoring the NO_x emissions by means of real world emissions testing would reveal the impact of these changes on the NO_x emissions levels for normal daily operation of heavy duty vehicles.

Conclusions

In the Netherlands in-service emissions testing programme for heavy-duty vehicles a number of vehicles with Euro VI certified engines of different categories were tested. Tail-pipe emissions levels of vehicles with Euro VI engines were examined using a Smart Emissions Measurement System to determine the level of NO_x emissions when operated on their normal daily routes, i.e. under real-world conditions. A selected group of vehicles was tested with PEMS over specified test routes of a few hours long. When high NO_x emissions were observed, vehicles were also tested over specified in-service conformity routes to get an indication of the NO_x emission conformity of the vehicle in-service. The vehicles were selected based on ranking of registrations of engine type and are a good representation of the Dutch fleet of heavy-duty vehicles with a Euro VI certified engine.

When a formal in-service conformity route was driven, all vehicles had an indicative in-service conformity factor below the limit of 1.5.

For the Euro VI certified diesel engines the overall average NO_x emissions levels in normal daily operation still vary a lot from case to case, from about 0.3 g/kWh to 4 g/kWh and 9 g/kWh in a special case. Largest variations and high NO_x emissions were observed for the cases with higher shares of low speed and low engine load operations for instance at urban driving combined with a lot of idling, where NO_x emissions tend to be clearly higher. Typical examples are city refuse collection, city bus lines, city distribution of goods, also by long haulage trucks and in one case construction services. For those cases, in local driving situations, but also for average operation, the limit value² that is set for the formal EU type in-service conformity test, a specific test to be conducted on the public road, are regularly exceeded.

At motorway speeds NO_x emissions are consistently low, typically around 0.1-0.5 g/kWh.

The increase of NO_x emissions at low average speeds for diesel vehicles is related to the way the emission abatement technology with selective catalytic reduction (SCR) works. The catalyst of this type of emission control system needs to be warm to effectively reduce the NO_x emissions of the diesel engine. At low engine loads (power), the catalyst may cool down due to the cooler exhaust gas of the diesel engines at those conditions. Actual NO_x emission levels thus depend on if and how much during a trip the SCR catalyst cools down due to low load operation.

The observed good results for NO_x emissions over indicative in-service conformity screening tests on the one hand and the large spread of NO_x emissions for the same vehicles in normal daily operation in the Netherlands on the other hand, show that not all representative and normal operations are well-covered by the EU emissions legislation. This accounts for the Euro VI certified engines of step A to C.

For Euro VI step D additional requirements are implemented that should improve the situation and especially the higher NO_x emission at lower speeds and loads. The impact has to be measured once step D certified vehicle enter the market as of September 2019.

² the Conformity Factor of the EU in-service conformity test represents 1.5 times the limit value for the WHTC engine certification test ($1.5 \times 0.46 = 0.69$ g/kWh)

There are no provisions for testing vocational vehicles. Refuse collection vehicles for instance are tested as N3 vehicle over a long haulage test route. It is recommended to adapt the EU regulation so that engines of heavy-duty vehicles that usually operate in urban driving are always tested with sufficient urban driving and with representative driving cycles. For engines that are used in refuse collection vehicles the bus route could be used.

Continuation of monitoring the emissions of heavy-duty vehicles during the life time of the vehicles reveals trends of these emissions and the effectiveness of EU emissions legislation in achieving sustainably low emissions over the useful life of the category of heavy-duty vehicles.

Acknowledgements

Acknowledgments go to all transport companies which provided their vehicles for testing in the Netherlands in-service emission testing programme and The Ministry of Water management which funds the testing programme.

References

- Heijne, V.A.M. et al. (2016) Assessment of road vehicle emissions: methodology of the Dutch in-service testing programmes, TNO 2016 R11178, October 2016
- Vermeulen R.J., et al. (2016) The Netherlands In-Service Emissions Testing Programme for Heavy-Duty Vehicles 2015-2016 Annual Report, TNO report TNO 2016 R11270, 10 October 2016
- Vermeulen, R.J., Ligterink, N.L.I. (2018) Evaluation of the EU real-world PEMS test for heavy-duty vehicles, TNO report TNO 2018 R11328, 15 November 2018.
- Vermeulen, R.J. et al. (2018) Tail-pipe NO_x emissions of refuse collection vehicles with a Euro VI engine in daily operation in the Netherlands, TNO report TNO R 2018 10313v2, 15 June 2018
- Merkisz, Jerzy et al. (2016) Actual emissions from urban buses powered with diesel and gas engines, 6th Transport Research Arena April 18-21, 2016
- Söderena, P., Nylund, N., Pettinen, R., and Mäkinen, R. (2018) Real Driving NO_x Emissions from Euro VI Diesel Buses, SAE Technical Paper 2018-01-1815, 2018, <https://doi.org/10.4271/2018-01-1815>

2.1.10 Measuring real emissions with simplified PEMS

P Öhlund^{1*}, L Eriksson²

¹Swedish Transport Agency, Vehicle Regulations, Borlänge, Sweden ^{*}per.ohlund@transportstyrelsen.se

² Ecotraffic AB, Göteborg, Sweden

Introduction

The stringency of the emissions legislation for type approval of vehicles has increased significantly during the last years. Despite this, the same rate of improvement has not been observed regarding emissions in real world. Together with increased traffic in EU, many cities reports of exceedance of the requirement for air quality. Especially regarding NO₂ and particles.

Introduction of new requirement for type approval like real driving emissions (RDE) for light duty vehicles is an improvement of the legislation. Nevertheless, to assure that a reduction of emissions in real world is followed by the strengthened legislation, new methods to assess and monitor real emissions is needed. With the introduction of the fourth package of RDE in EU the requirement for in service conformity has been strengthened. Giving independent organisations and third parties possibility to perform tests that can be assessed by the granting type approval authority (GTAA) in the in-service conformity procedure. To assess the validity of the type approval with respect to in use performance, the tests defined in the legislation needs to be performed under the responsibility of the GTAA.

For independent tests the regulation opens up for other methods to indicate if there is a problem with the emissions performance of a vehicle type and the in-service requirements. If an indication is identified it is possible to inform the GTAA.

These other methods can be remote sensing and on-board monitoring of emissions. To be able to assess a larger number of vehicle types the Swedish Transport Agency together with TÜV Nord and Ecotraffic AB started a study to investigate the possibility to use a simplified method for on-board measurement of vehicle emissions, in this report named simplified PEMS.

Background

Since many years, the Swedish Transport Agency has been responsible for an In-Service test programme to assess that vehicles comply with the legislation also when in use.

In the last years, we have extended the test programme to include also measurement of emissions in real world, using PEMS according to the RDE legislation. The development of a method for simplified PEMS measurement of light duty vehicles will allow measuring a larger number of vehicle types for screening of the emissions performance of vehicles in the national fleet, compared to the use of legislative method according to RDE.

Even vehicle models that otherwise never are subject to testing can now be evaluated, for example niche vehicles. It is also possible to perform measurement trips that are much longer compared to the legislative RDE method. Testing of vehicles at low ambient temperatures, below zero degrees, can give problems with condensation in the sampling tubes if the vehicle with the installed measurement system is parked and soaked outside. With simplified PEMS this is not a problem and the test trip can start with a vehicle cooled to ambient temperature.

The simplified method could also be used for monitoring of the emissions performance on vehicle fleets. For example vehicles used by communities and other public authorities. In these cases, the simplified PEMS system can be installed in a more permanent way.

The test programme in 2017 included a comparison of a PEMS test route driven in Germany and a route driven in Sweden together with evaluation of the simplified PEMS method. The background to these tests were to find out if there is any differences between using a PEMS route in Sweden or in Germany, and to compare a legislative RDE test with a test with simplified PEMS test. Two vehicles were used, one with compression ignition engine (vehicle 1) and one with positive ignition engine (vehicle 2), both approved to Euro 6. The tests showed that there is not

any significant differences regarding CO₂ (fuel consumption) between the different test route driven. The NO_x emission were higher in the tests performed in Germany and the main explanation can be the higher speeds on the German autobahns compared to the Swedish motorways.

During the last two years (2017 and 2018) several screening tests with a simplified PEMS method using sensors has been performed. Beside the comparative tests described in this report, additional about 45 vehicles have been tested with the simplified PEMS method. The correlation between using legislative RDE system and simplified PEMS were high during these tests regarding NO_x, CO₂ and fuel consumption (within +/- 5 percent).

Development of test method for simplified PEMS

This study indicate that it is possible to use a simplified measurement system for RDE tests with relatively high accuracy. Which will enable a larger number of vehicle models to be included in the surveillance. Making the in-service checks more cost effective.

The simplified PEMS system uses two ceramic sensors, one for CO/CO₂ and one for NO_x (including O₂ and Air to Fuel ratio). In principle, the sensors could be installed on the vehicles original exhaust pipe. In order for a simple installation on different vehicle types the sensors have been installed on a tube that can be mounted on the vehicle with a rubber/silicon tube. The measurement system with data logger, signal processing and power supply is mounted inside the vehicle.

With a legislative RDE system the emissions is measured with heated sample lines and gas analysers normally installed inside the vehicle. The power supply must be from external sources, and is normally provided with power pack or external generator.

Description of the measurement system for simplified PEMS and legislative RDE is described in annex 1.

Figure 1 shows a vehicle with both simplified PEMS and legislative RDE measurement system. Compared to a vehicle with only simplified PEMS system in figure 2.



Figure 1: Vehicle 1 with legislative PEMS and simplified PEMS system installed.



Figure 2: Vehicle with simplified PEMS system installed on tailpipe.



Figure 3: Installation in the vehicle of the simplified PEMS measurement system compared to the legislative RDE measurement system.

As can be seen in figure 3, there is a big difference in the size of the system installed in the vehicle. For the simplified PEMS system the complete system does fit in the black bag. Depending on the required size of the external power pack it can be placed either in the bag or if a larger power pack is needed it can be placed outside of the bag. The legislative PEMS systems fill up the luggage compartment of the vehicle with gas analysers, data logger, signal processing, power supply etc.

Both the gas analyser on the legislative RDE system and the sensors on the simplified PEMS system measure concentrations of the respective exhaust gas components. To calculate the mass emission, it is necessary to also know the exhaust flow.

In a legislative RDE system, the exhaust flow is measured by using an exhaust flow meter installed at the tailpipe of the vehicle.

In the case of simplified PEMS the exhaust flow is determined in a different way compared to legislative RDE. Exhaust flow is the sum of the fuel flow and the inlet air flow to the engine. In this case the air flow is taken from the vehicle's own air mass flow meter (MAF). (In some cases the values are taken from the OBD system and in some cases direct as an analogue signal from the MAF).

During simplified PEMS measurements the exhaust flow were determined by adding the fuel flow to the signal from the vehicles mass air flow meters (MAF). The correlation to the Semtech flow meter was very good, se figure 4.

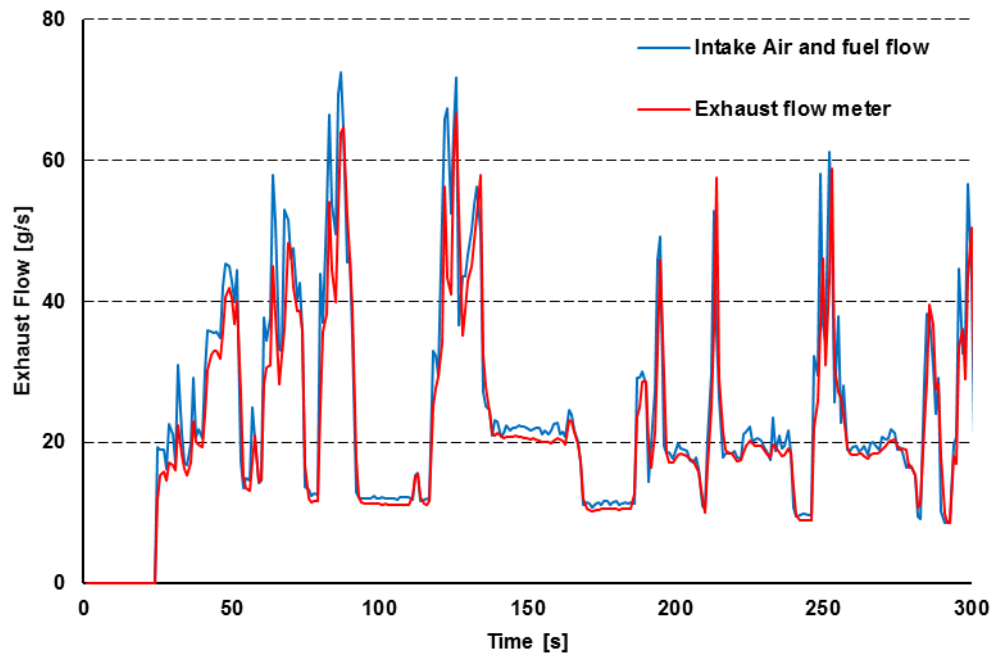


Figure 4: Correlation of exhaust flow determination between legislative RDE exhaust flow meter and simplified PEMS with intake air flow and fuel flow determined from lambda measurement.

If vehicle models with high emissions is detected, a more detailed investigation can be performed including legislative RDE tests. An independent organisation can also inform the GTAA of its findings from the tests with other methods than the tests according to the legislation. The GTAA are then obliged to consider this information in the in-service procedure for the type approval in question.

Table 1: Properties comparing simplified PEMS with legislative RDE.

	Simplified PEMS	Legislative RDE PEMS
Measuring technology	Ceramic sensors Installed in the exhaust pipe	Gas-analysers Placed inside the vehicle and the exhaust gas is pumped from the exhaust pipe in heated lines
Exhaust flow	Air mass flow (to engine) from OBD system or the engines own air mass flow sensor	Exhaust flow measuring tube installed at the end of the exhaust pipe
Power consumption	Relatively low A power supply of 60 Ah is sufficient for 20 hours driving with on-board measurement	Relatively high A power supply of 150 Ah can normally give 2,5 hours driving with on-board measurement
Time for installation	About 1 to 2 hours if possible to use existing pipes from earlier tests ³ .	About 1 to 2 days, normally needs to perform a validation type 1 test on a chassis dynamometer
Accuracy	A deviation from legislative RDE up to +/- 5 percent	

Correlation with legislative RDE and simplified PEMS

The objective was to evaluate if there is any differences between driving a RDE compliant PEMS route in Sweden or in Germany. Two vehicles was used, one with compression ignition and one with positive ignition engine, both approved according to Euro 6 emissions standard.

The study was performed in following order:

- Installation of the RDE compliant PEMS systems and the simplified PEMS system on the two vehicles
- Validation test on chassis dynamometer using WLTP. During these tests the PEMS installation were checked and compared with the result from the chassis dynamometer emissions measurement system.
- Two tests per vehicle driving a RDE compliant route in Germany (Essen).
- The vehicles were transported to Sweden.
- Two tests per vehicle driving a RDE compliant route in Sweden (Göteborg).

During this study, the exhaust flow was calculated from the MAF signal of the vehicle.

Results

The conducted tests show a relatively high correlation between the simplified PEMS system with sensors and the legislative RDE system equipped with heated sample lines and gas analysers, see figure 5 below.

³ On some modern vehicle types, where the exhaust pipe is part of the design, it can be a challenge to fit the measurement tube.

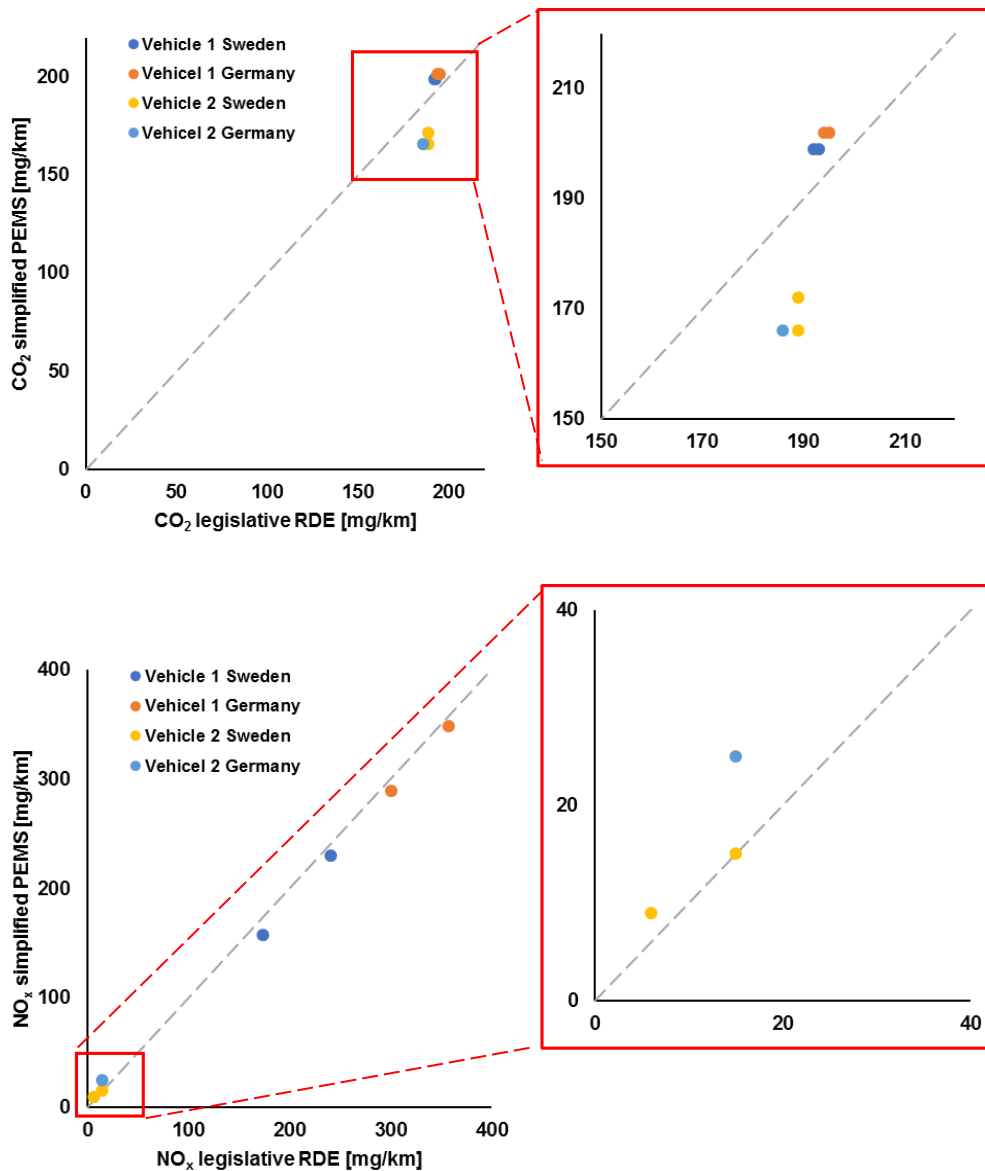


Figure 5: Results from on-board measurement of two vehicles driven in Germany and Sweden with simplified PEMS and legislative RDE.

The NO_x emissions from vehicle 1 with compression ignition engine is significantly higher during the tests driven in Germany compared with tests driven in Sweden. The reason for this can be explained with higher average speed and accelerations on the German motorways (Autobahn) compared with driving on the Swedish motorways, see figure 8, below.

The emission of NO_x was low in all tests with vehicle 2 with positive ignition engine, as expected. Close to the detection limit for the simplified PEMS system. During the first test driven in Germany there was a technical problem with the exhaust flow determination with the simplified PEMS system, therefore some results are missing in figure 5.

There was not any significant differences in CO₂ emissions (fuel consumption) between simplified PEMS and legislative RDE system from the two PEMS test routes driven in Germany and Sweden respectively.

Figure 6 and 7, shows the modal signals from the simplified PEMS system with sensors and the legislative RDE system equipped with heated sample lines and gas analysers. The correlation between the two measurement systems for NO_x and CO₂ emissions is relatively high.

During some cases, the simplified PEMS signal shows a spike of NO_x emissions. This can be caused by a better response time for sensor based measurement compared to the gas analysers in the legislative RDE system.

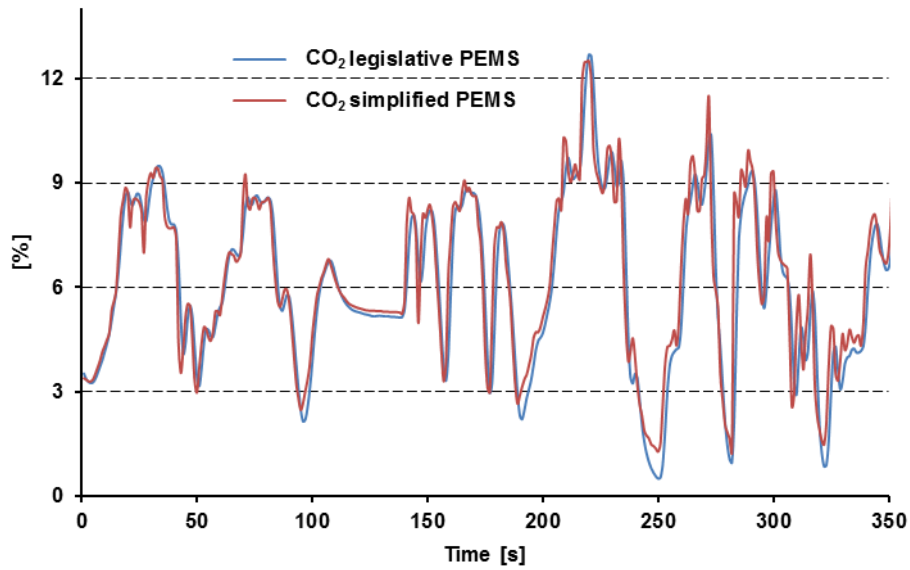


Figure 6: Correlation of CO₂ signal between simplified PEMS and legislative RDE.

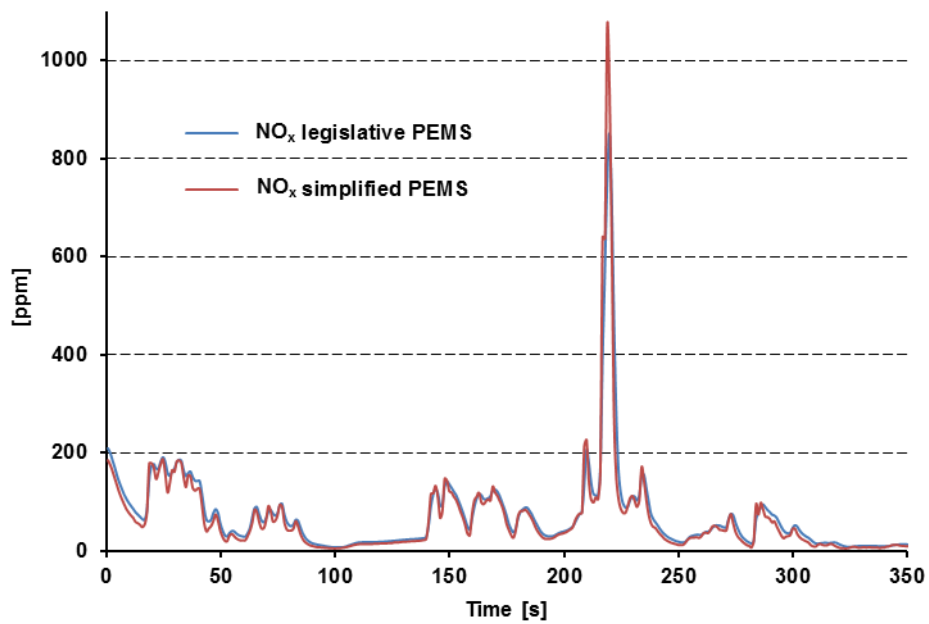


Figure 7: Correlation of NO_x signal between simplified PEMS and legislative RDE.

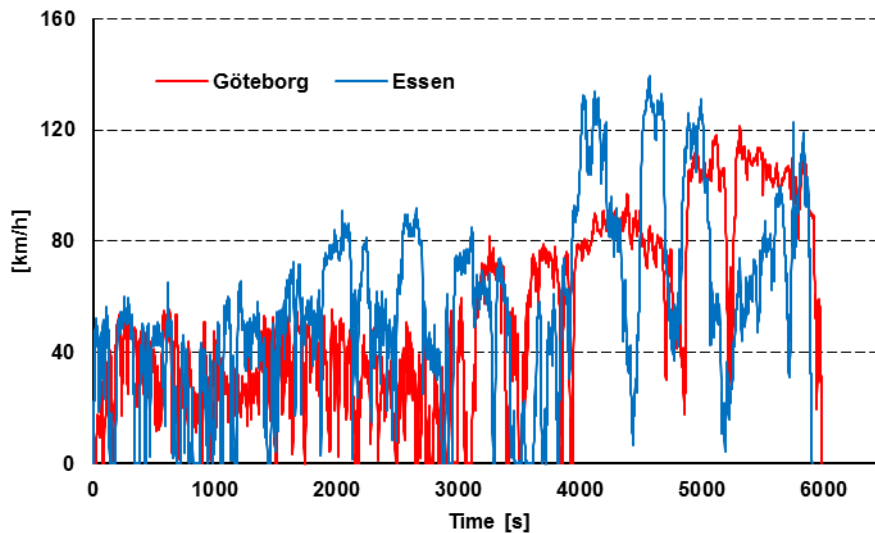


Figure 8: Speed profile from RDE compliant route in Germany and Sweden.

Screening of the national vehicle fleet

A number of screening tests has been performed using different routes. Up to now around 45 vehicles have been tested. For reference one route compliant to the RDE legislation is always driven.

In order to assess the emission performance of vehicles in real driving this study also included a city commuter route, figure 9, and a weekend motorway route, figure 10. A user behaviour that is relatively common is to use the vehicle for commuting to the work on the morning and back home on the evening. During the weekend, it is common to drive longer distances on motorway and rural roads.

The results from the screening is summarised in table 1 in annex 2. For some tests it was not possible to determine exhaust flow, therefore measured results are missing in the table. The city route and motorway route was included for the latest 21 tested vehicles.

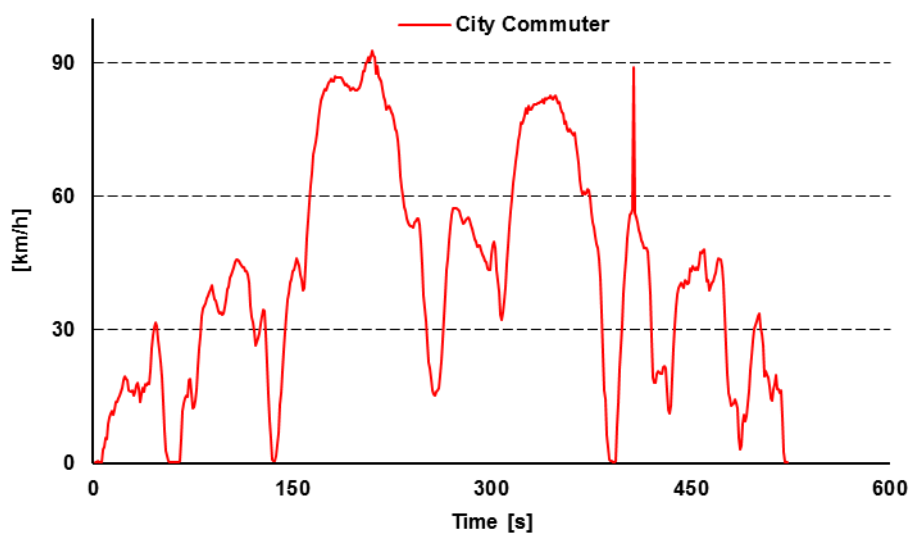


Figure 9: Speed profile from city commuter route.

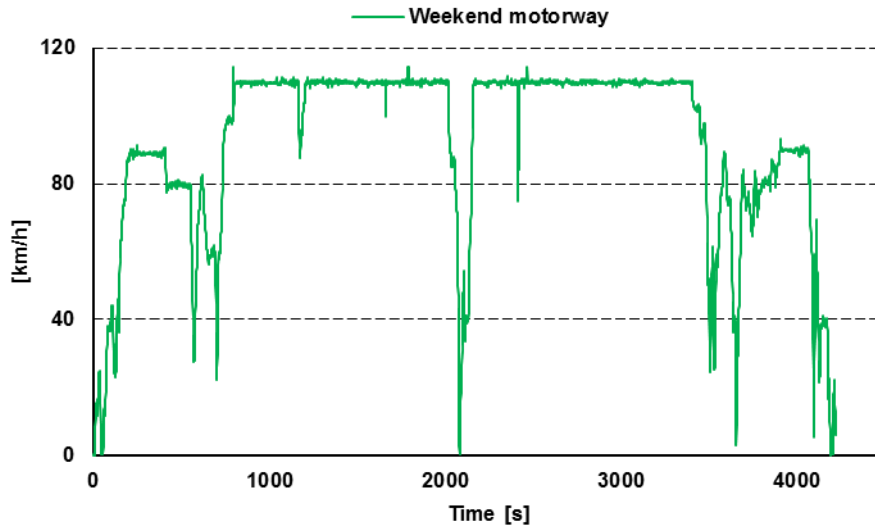


Figure 10: Speed profile from weekend motorway route.

Development of evaluation method

In order to calculate the emissions of NO_x from a vehicle in grams per km a necessity is the exhaust flow from the engine. Measuring the exhaust flow is often relatively complicated. This will require installation of a mass flow meter. This is time consuming and adds complexity to the test procedure.

An alternative approach for a rough estimation of the NO_x emission in mg/km – without measurement of the exhaust flow - is to use an emission index (EI), for example the relation between NO_x and CO_2 emissions.

By measure the concentration of NO_x and CO_2 the Emission index can be calculated with this formulae:

$$\text{EI} = 0,1045 \cdot (w\text{-ppm NO}_x / w\text{-\% CO}_2)$$

- w = wet concentration
- molar weight:
 $\text{NO}_2 = 46,00 \text{ g/mole}$ and
 $\text{CO}_2 = 44,01 \text{ g/mole}$,
- $0,1 \cdot (46/44,01) = 0,1045$ (0,1 unit conversion)

This formula gives the unit $\text{mg NO}_x / \text{gCO}_2$ for the emission index.

To get a representative value of the emission index there is a need to measure over a longer time or distance and use the average value. In a test with a Euro 6 vehicle with compression engine, the importance of this fact is clearly showed. When the vehicle pass by a remote sensing measuring station an emission index value of $2,5 \text{ mg NO}_x$ per g CO_2 was measured, see figure 11.

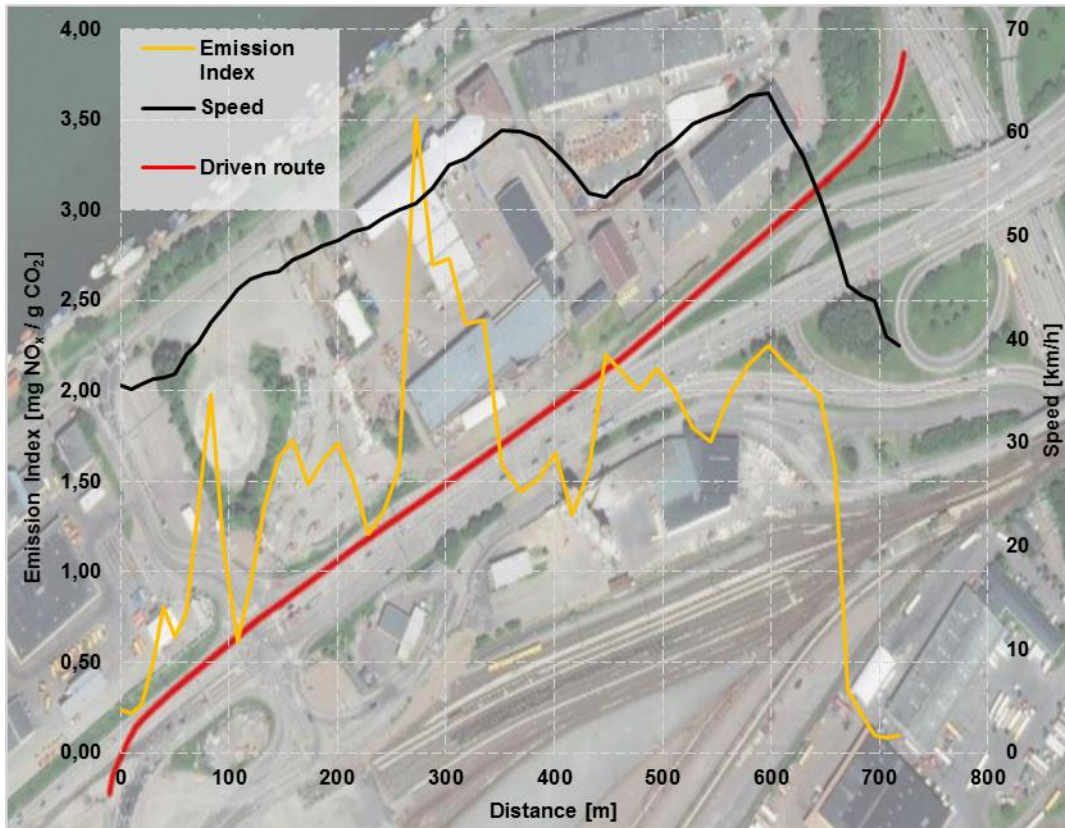


Figure 11: Measuring NO_x and CO₂ when driving through a remote sensing station. The red line is the driven route on the map, and the yellow line is the Emission Index in mg NO_x / g CO₂. The remote sensing station was placed somewhere during the first 250 metres of the route, which was driven from right to left in the picture.

At the same time, when measuring the vehicle with simplified PEMS the emission index varied between 0 and 3,5 mg NO_x / g CO₂ when driving on the road passing the remote sensing station. The average Emission Index was 1,4 mg NO_x / g CO₂.

The same vehicle was also measured on an 87 km long RDE compliant PEMS route. And the emission index was then 1,31 mg NO_x / g CO₂. During this PEMS route the emission index were in the interval between 0-25 mg NO_x / g CO₂. This test show that it is important to measure over a longer time and calculate the average value over the trip. By using the value from the remote sensing station in this example the NO_x emission from the actual vehicle will be overestimated with over 90 percent.

Recently made tests indicate that using emission index during RDE tests and the declared WLTP CO₂ emissions values give representative NO_x values.

One way to use this roughly method is given as an example in figure 12 below. In this example the Emission Index of a fictive vehicle have been measured, and determined to 1 mg NO_x / g CO₂. The declared WLTP CO₂ value for this fictive vehicle is 120 g/km. The combination of this two values give 120 mg NO_x / km. The figure also illustrate that the car seems to be under the 168 mg/km line describing the conformity factor 2,1 for the first stage of euro 6 RDE.

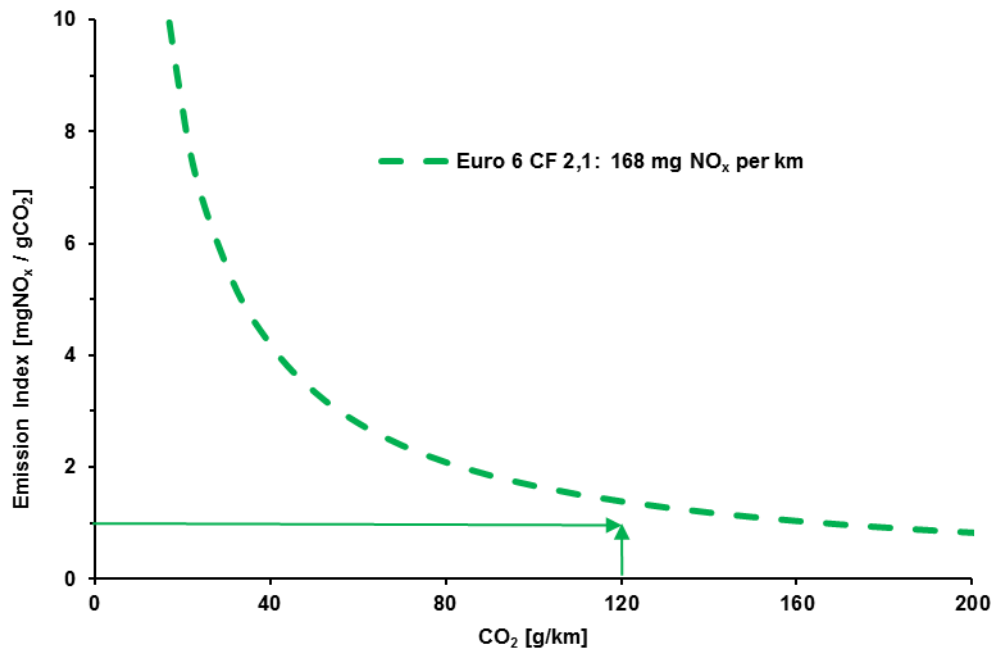


Figure 12: Emission Index as a function of declared WLTP CO₂ emissions.

Another approach to calculate an estimate of the emissions performance is to calculate the NO_x emissions in mg/km from a test trip using the emission index times the declared WLTP CO₂ emissions in g/km. The measured CO₂ emissions can also be used if this is available.

This approach has a good correlation to measured emissions for the tested vehicles as is shown in figure 13. Where the measured CO₂ emissions was used in the calculation.

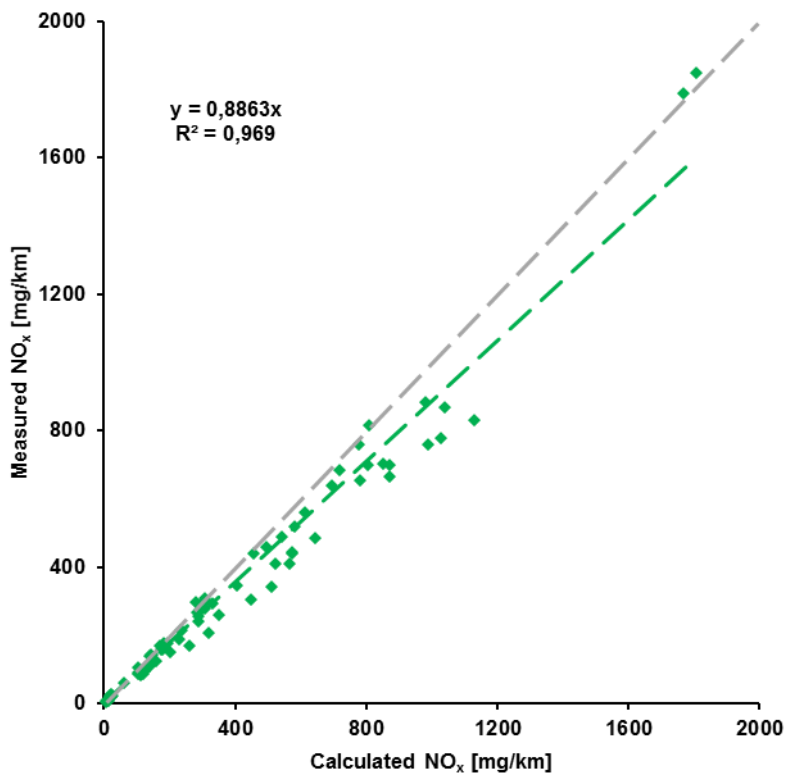


Figure 13: Correlation between measured and calculated NO_x emissions.

Discussion and conclusion

This study shows that the use of simplified PEMS is a method with good correlation to the legislative RDE method.

Simplified PEMS can be used for continuous monitoring of emissions of NO_x and CO₂ (fuel consumption) from vehicles. Driving different routes, pre-defined or just following the normal driving of the vehicle. It will also simplify the possibility to conduct longer test campaigns.

Testing with the legislative PEMS method at lower ambient temperature, below zero degrees, can be limited because of technical problem with the measurement system, for example condensation in the sampling tubes. Simplified PEMS allows for testing with inclusion of the cold start at lower ambient temperature. With the possibility to monitor the emissions performance from the cold start.

The method can be used for cost effective screening of the emissions of NO_x from the vehicle fleet. Covering vehicle types that normally would not be subject for test with legislative RDE checks, like niche vehicles.

The emission index is a powerful evaluation method to calculate a rough estimate of the emissions performance. To compare with emission limits and not to exceed limits. The method only needs the concentration of NO_x and CO₂ emissions to calculate the NO_x emissions from a test. With no need to measure the exhaust flow.

Maybe not to assess legal compliance, but to give an indication on outliers and which vehicle types a more thorough investigation needs to be performed by the granting type approval authority. This evaluation method using emission index can also be developed for other categories of vehicles and engines. For example motorcycles, mopeds, heavy duty vehicles and non road mobile machinery.

Further studies should be done to develop the method for other emission components and also particle emissions. The simplified PEMS test equipment has potential for further development. Making it even smaller to allow for permanent installation to be able to monitor real driving emissions performance over longer times.

Abbreviations

GTAA	Granting Type Approval Authority
PEMS	Portable Emissions Measurement System
RDE	Real Driving Emissions
WLTP	Worldwide harmonised Light vehicle Test Procedure

Annex 1

Description of measurement systems

The simplified PEMS system used in this study included the following parts:

- CAN Module for 10 analogue signals (mA, V, Hz)
- CAN Module for reading OBD-parameters
- CAN Module for GPS (including antenna) – 10 Hz
- CAN Module (ceramic sensor) for CO/CO₂
0-20% CO/CO₂ (+/- 0,15%),
0,4-25 lambda,
0-25% O₂ (+/- 0,1%),
AFR 6,0-364
Response time < 200 ms
- CAN Module (ceramic sensor) for NO_x (also lambda, O₂, AFR),
0-5000 ppm NO_x (+/- 20 ppm 200-1000 ppm, +/- 2,0 % elsewhere),
Lambda (+/- 0,008 at lambda 1, +/- 0,016 at lambda 0,8 to 1,2, +/- 0,018 elsewhere)
Response time < 1 s (NO_x), < 150 ms (Lambda, AFR, O₂)
- Logger (Kaser Memotrator)

The legislative RDE system used in this study included the following parts:

- Gas system: SEMTECH LDV GAS
 - NDUV for NO and NO₂ measurement
 - NDIR for CO and CO₂ measurement
- PN system: SEMTECH LDV CPN
 - condensation particle counter (CPC) using Butanol
- Sample conditioning system: SEMTECH LDV SCS
- Exhaust flow meter: SEMTECH LDV EFM4
- Weather probe system: VAISALA HMP155

The entire system fulfils requirements in regulation (EU) 2017/1151.

Annex 2

Results from screening of vehicles emission performance

Table 2: Screening of emissions performance from a number of vehicle types.

Vehicle type	Emission standard	Engine type ¹	NO _x [mg/km] RDE route	NO _x [mg/km] City route	NO _x [mg/km] Motorway route	Emission Index route	Emission Index RDE route	Emission Index City route	Emission Index Motorway route	CO ₂ combined [g/km] NEDC (WLTP ²)
BMW 318d	EU 6	CI	145	297	154	1,00	1,57	0,89		114
Peugeot 3008	EU 6	CI	119	293	321	0,59	1,57	1,54		108
Peugeot 5008	EU 6	PI				0,41	0,88	1,11		120
Mercedes C200	EU 6d _{temp}	CI				0,03	0,46	0,03		159
Peugeot Partner	EU 6	CI	202	245	351	0,99	0,85	1,84		108
Mercedes C200 – hybrid	EU 6d _{temp}	PI				0,05	0,04	0,02		163
Toyota Yaris	EU 6	PI	15	16	18	0,10	0,23	0,14		109
Volvo V60 D2	EU 6	CI	613	851	297	4,33	3,34	2,20		101
VW Passat	EU 6	CI	23	102	83	0,16	0,57	0,53		96
Mercedes B180	EU 6	PI				0,12	0,02	0,13		137
Volvo V60 D3	EU 6	CI	287	543	206	2,04	3,56	1,52		105
KIA Stonic	EU 6d _{temp}	PI				0,12	0,21	0,09		135
Volvo V60	EU 6	PI	6	10	11	0,03	0,05	0,07		135
Peugeot 308	EU 6	CI	139	223	199	0,86	1,20	1,46		99
Mercedes A180D	EU 6d _{temp}	CI				0,06	0,10	0,04		127
VW Caravelle	EU 6	CI	62	86	57	0,32	0,22	0,27		166

¹ Compression ignition (CI) or positive ignition (PI).

² For Euro 6d_{temp} vehicles the declared values are from WLTP.

Vehicle type	Emission standard	Engine type ¹	NO _x [mg/km] RDE route	NO _x [mg/km] city route	NO _x [mg/km] motorway route	Emission Index RDE route	Emission Index city route	Emission Index motorway route	CO ₂ combined [g/km] NEDC (WLTP ²)
Audi A6 Avant	EU 6	CI	5	43	5	0,04	0,20	0,04	133
Mercedes E220D	EU 6	CI				0,09	0,40	0,05	120
Volvo V40	EU 6	CI	139	185	71	1,16	1,10	0,56	89
Ford Focus	EU 6	CI	178	256	90	1,30	1,18	0,68	98
Volvo V70	EU 5	CI	456	617	348	2,71	2,80	1,99	144
Volvo XC60	EU 6d _{temp}	CI	49			0,24			181
Volvo V70	EU 5	CI	1786			12,49			144
Skoda Octavia	EU 6	CI	119			0,66			106
Audi A6	EU 6	CI	21			0,18			115
Volvo V90	EU 6	CI	246			1,64			119
Renault Traffic	EU 6	CI	273			1,32			145
BMW 118d	EU 6	CI	139			0,96			114
Ford Kuga	EU 6	CI	212			1,55			115
Nissan Qashqai	EU 6	CI	751			4,00			122
KIA Ceed	EU 6	CI	296			2,21			104
Mercedes C220D	EU 6	CI	109			0,70			108
Volvo V40	EU 6	PI	16			0,08			-
Volvo XC60	EU 6	CI	256			1,01			-
Kia Optima	EU 6	CI	783			4,96			120
Ford Mondeo	EU 6	CI	359			1,73			128
Mercedes A180D	EU 6	CI	810			7,04			102
VW Sharan	EU 5	CI	201			1,24			146

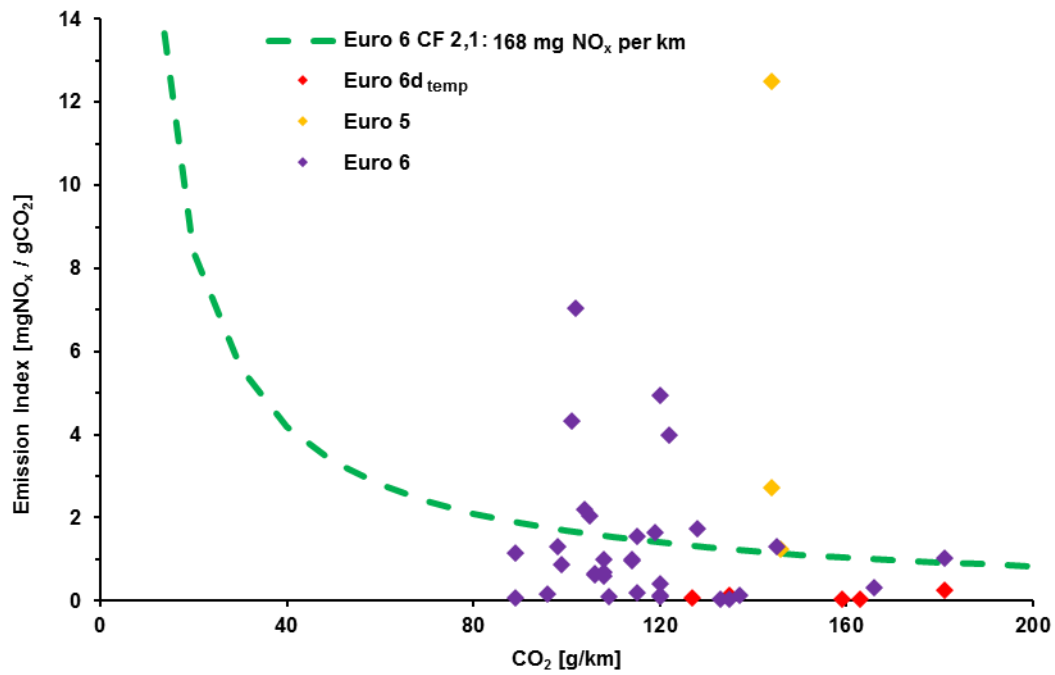


Figure 14. Emission index from RDE route.

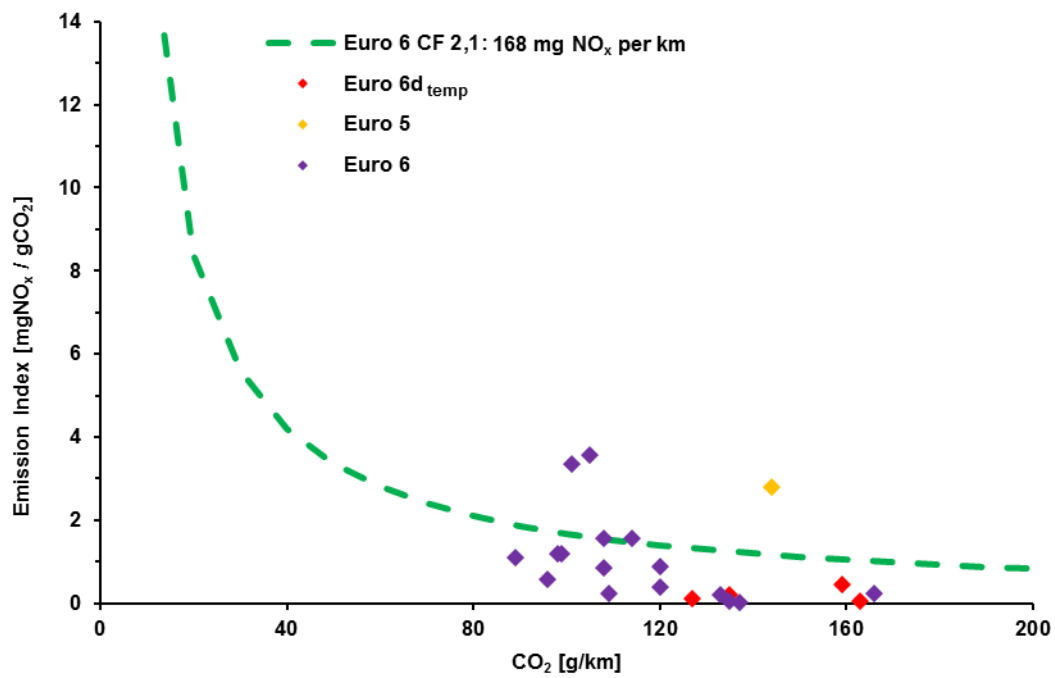


Figure 15. Emission index from city commuter route.

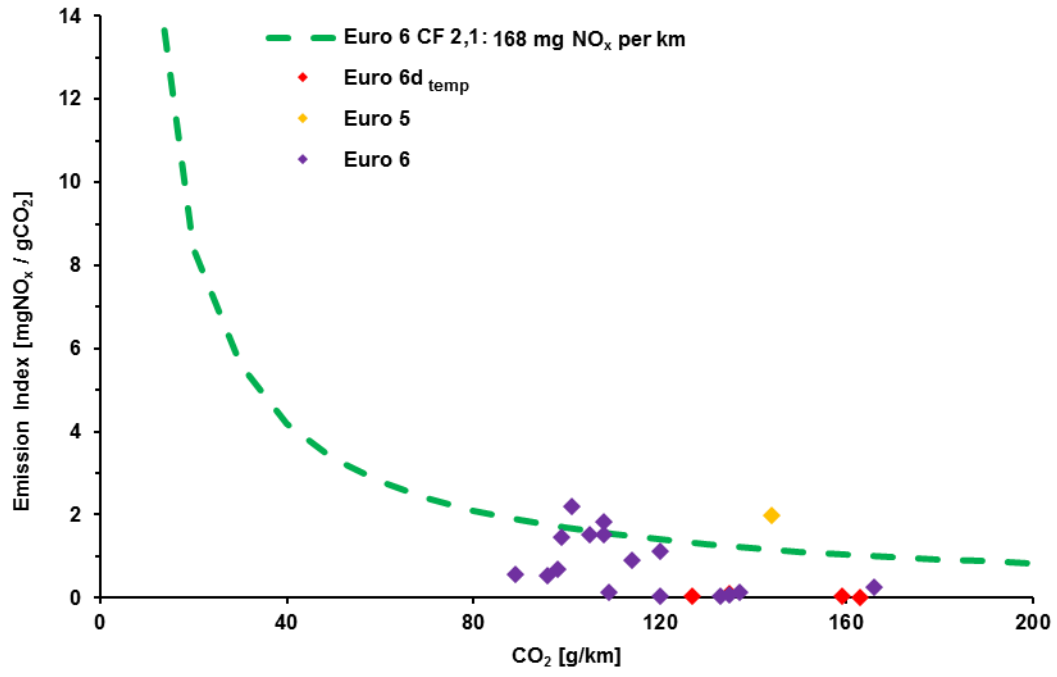


Figure 16. Emission index from weekend motorway route.

2.1.11 Exhaust Gas Temperature and NO_x After-treatment Performance of Euro 6 Passenger Cars

Z. Mera^{1,4}, N. Fonseca^{2*}, J. Casanova³ and J.M. López¹

¹University Institute for Automobile Research (INSIA), Universidad Politécnica de Madrid, 28031, Madrid, Spain

²Department of Energy and Fuels, Universidad Politécnica de Madrid, 28003, Madrid, Spain, natalia.fonseca@upm.es

³Department of Energy Engineering, Universidad Politécnica de Madrid, 28003, Madrid, Spain

⁴Faculty of Applied Sciences, Universidad Técnica del Norte, 100105, Ibarra, Ecuador

Key-words: NO_x, cold start, real driving emissions (RDE) tests, passenger cars

Introduction

Pollution affect air quality of cities around the world. With the objective to constrain this problem, new homologation procedures have been introduced for a long time. In Europe, the real driving emissions (RDE) tests by means of portable emissions measurement systems (PEMS) has the potential to assess emissions in a more realistic driving with a more robust framework (Hooftman et al., 2018). They also could be used to find gaps in emission models and to increase knowledge of transportation pollution phenomena.

Operating temperatures of aftertreatment systems are relevant to their performance, which is crucial for urban air quality. During cold start, which mainly occurs in urban (Weiss et al., 2017), cool combustion conditions of internal combustion engine (ICE) limit exhaust gas temperatures, so thermal heat transfer to aftertreatment systems is reduced (Chan and Hoang, 2000; Roberts et al., 2014). Aftertreatments need an initial stage of warming-up until reach the optimal operating temperatures, and they also could be affected by conditions of cooling down.

Engine gas recirculation (EGR) has been widespread used to control NO_x emissions. Depending on the application, it could be complemented with after-treatment technologies as: three-way catalyst (TWC), lean-NO_x trap (LNT) or selective catalytic reduction (SCR). Although SCR has shown high efficiency reducing NO_x emissions in diesel vehicles, it is affected by low operating temperatures produced by stop periods ($v < 1 \text{ km h}^{-1}$) and low engine loads (Weiss et al., 2011). In the same way, long engine-off periods (engine speed $< 50 \text{ rpm}$) of hybrid vehicles could affect to the performance of their TWC systems (Koltsakis et al., 2011).

In light of these considerations, this study aims to show the association between the exhaust gas temperature at tailpipe and the NO_x reduction performance of aftertreatment systems installed in different Euro 6 passenger cars. For this objective, cold start emissions were analysed from real driving tests during engine warming-up in a unique close loop urban route. In addition, RDE tests were performed to correlate the exhaust gas temperatures with the performance of NO_x aftertreatments. The tested fleet represent the most common fuel / powertrain / aftertreatment architectures in the market.

Methods

Driving routes and tests

Three types of tests were performed: cold start (CS), hot-running (HR) and RDE tests. The CS and HR tests had the same driving conditions in an urban route, which consisted in a close loop around Universidad Politécnica de Madrid (UPM) South Campus, as shown in Fig 1a. CS test complied with (EU) 1151/2017 requirements for cold start testing, and it included the first five minutes ($t \leq 5 \text{ min}$) of driving, with the inclusion of 15 seconds of idling at the start. HR test covered the consecutive five minutes to CS test (i.e., $5 < t \leq 10 \text{ min}$). Then, the vehicles performed several hot-start RDE tests in a unique route, which covers some areas of Madrid city (Spain) and its surroundings. These tests complied with main RDE regulations of (EU) 1151/2017 and the main characteristics can be seen in Table 1. To avoid driving style influence on the tests, they were carried out by one professional driver, and they were done on weekdays. Figure 1 shows the trace of the routes.

In order to observe the vehicle's uninterrupted warm-up behaviour in urban conditions for CS and HR tests, long stop periods were minimized. Therefore, the CS and HR testing route had no traffic lights or

heavy congestion, where vehicles equipped with stop-start system would spend much of the time with the engine off. This public route included several crosswalks with speed reducers instead. The main parameters that describe the tested routes are shown in Table 1, and the number of tests performed per vehicle are shown in Table 2.



Figure 1. Test routes a) route of cold start (CS) and hot-running (HR) tests b) route of RDE tests

Table 1: Tested routes parameters

	Cold start (CS)	Hot-running (HR)	RDE			
			Entire test	Urban	Rural	Motorway
Testing time [min]	5	5	101.2 (4.2)	60.8 (3.5)	26.3 (1.0)	14.2 (1.1)
Distance [km]	2.12 (0.23)	2.57 (0.17)	76.5	23.2	28.8	24.5
Average speed [km h ⁻¹]	25.5 (2.7)	30.8 (2.0)	45.4 (1.8)	23.0 (1.3)	65.9 (2.3)	104.2 (6.5)
RPA [m s ⁻²]	0.22 (0.03)	0.21 (0.04)	0.19 (0.01)	0.25 (0.03)	0.19 (0.01)	0.13 (0.01)

Table shows mean and (standard deviation) of performed tests

Test vehicles

The tested fleet was composed of five modern (2016-2017) Euro 6b sport utility vehicles (SUV) fuelled by gasoline or diesel, with different NO_x aftertreatment systems. Also, one gasoline hybrid electric vehicle (HEV) was tested. Their characteristics are shown in Table 2.

Table 2: Characteristics of tested vehicles

ID	Fuel	Fuel injection type	NO _x control	Stop-start system	CS / HR tests	RDE tests
G-DI	Gasoline	Direct injection (stratified air fuel mixture)	EGR + TWC	√ (off) ^a	1	3
G-HEV	Gasoline	Port-fuel injection (PFI)	EGR + TWC	X ^b	3	5
D-SCR	Diesel	Common rail	EGR + SCR	√	2	5
D-LNT	Diesel	Common rail	EGR + LNT	√	2	5
D-EGR	Diesel	Common rail	EGR	√	2	5

^a Stop-start system was deactivated during the test

^b Hybrid system acts as stop-start system.

Measurement system

The MIVECO-PEMS was developed and validated by the Universidad Politécnica de Madrid in (Fonseca González, 2012). For this measurement campaign, the system was simplified to reduce its weight and size. NO_x concentration was directly measured, and CO₂ was estimated using carbon balance method by means of lambda value measured by the PEMS. This system was also used in the study of high instantaneous NO_x emissions in (Mera et al., 2019), with a sample frequency of 10 Hz. The PEMS consists of exhaust flow meter (EFM), NO_x exhaust gas analyser, exhaust gas temperature sensors, a global positioning system (GPS), and a weather station for recording ambient temperature and humidity. Additionally, PEMS records data from vehicle's on-board diagnosis (OBD) port. The MIVECO-PEMS measures exhaust gas concentration of NO_x by means of a Horiba Mexa 720 ceramic zirconium sensor. The EFM is a differential pressure Pitot tube type, which is detailed in (Fonseca González et al., 2016). The exhaust gas temperature was measured at the exhaust flow meter by means of K-type thermocouples. Approximately 190 kg were added to the mass of the vehicle, including the PEMS system, the driver, the co-driver and the batteries as power source for PEMS. The recorded data was checked and synchronized in the postprocessing stage.

Emission factors

The raw distance-specific emission factors (in mg NO_x km⁻¹) for section *i*, and from vehicle *j*, were computed as:

$$EF_{i,j} = \frac{m_{i,j}}{s_{i,j}} \quad (1)$$

where *m* is the mass NO_x emission (in mg NO_x) produced during distance *s* (in km).

Results and Discussion

Cold start and exhaust gas temperature profile

CS and HR tests were performed under the same urban testing conditions; therefore, they are directly comparable. As shown Table 2, CS and HR tests had average speed and RPA similar to the RDE urban section values. Additionally, these values are in line with RDE regulation, which establishes an average speed between 15 to 40 km h⁻¹, and a maximum of 60 km h⁻¹ speed limit for urban section.

One exhaust gas temperature profile per vehicle is shown in Figure 2. All vehicles evidence a growing temperature pattern during CS and HR driving. As it was said before, stop periods were minimized during CS and HR tests, so a constant warm-up profile is reflected, except for HEV vehicle. Hybrid

vehicle shows a saw profile due to combustion engine-off periods which represented 61 % of CS and HR testing time. It implies less warming-up time of TWC aftertreatment, so aftertreatment light-off temperature could take more time to be reached. Also, long engine-off periods could yield to TWC cooling, with the reduction of performance depending of its thermal energy management.

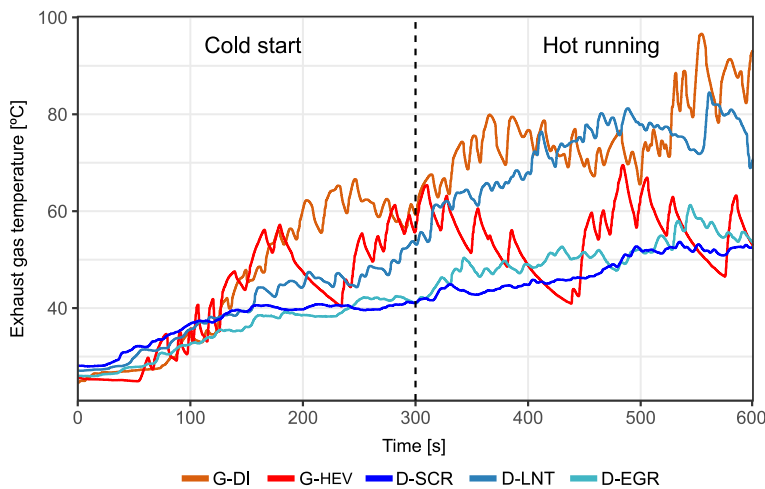


Figure 2. Exhaust gas temperature profiles during cold start (CS) and hot-running (HR) tests.

NO_x Emission factors

As shown in Figure 3, for the cold start test (CS) none of the tested vehicles could meet Euro 6 limits. The performance of G-HEV and D-SCR aftertreatment systems at CS was the most affected, being observed that CS emission factors are higher than HR and RDE emission factors; however, their RDE emissions comply with Euro 6 NO_x limits. The CS emission factors of G-HEV and D-SCR were 5.5- and 2.8-times Euro 6 limits, respectively. Curiously, the emissions from cold start tests of SCR and EGR-only diesel vehicles were the same (223 mg NO_x km⁻¹).

The vehicles G-DI, D-LNT and D-EGR show opposite patterns to G-HEV and D-SCR in the emission factor values. Firstly, they increase their emission factors in the following order: CS-HR-RDE. Secondly, none of their average RDE emissions complied with Euro 6 limits, which reflects the general performance of those vehicles. They surpassed in 6.0, 7.4- and 9.0-times Euro 6 limit, for G-DI, D-LNT and D-EGR vehicles, respectively.

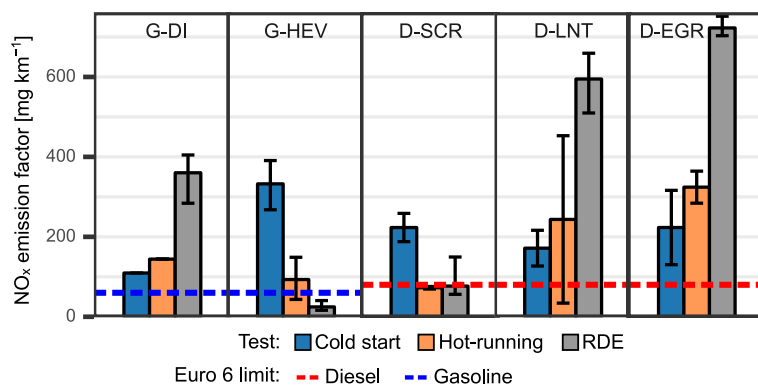


Figure 3. Average emission factors of cold start (CS), hot-running (HR) and RDE tests. Error segments represents maximum and minimum tests values.

Comparing CS and HR tests, it is remarkable the fast reduction of CS emissions of G-HEV and D-SCR. CS emissions were reduced in 72 % and 68% by G-HEV and D-SCR, respectively. Thus, their HR emissions resulted near to Euro 6 limits in the time expected by European regulation, namely 5 minutes. It means that light-off temperature of TWC and SCR was reached within these test periods. On the contrary, the other vehicles showed HR emission factors slightly higher than CS.

Exhaust gas temperature and NO_x emissions

In this study, stop periods were only relevant in urban section of RDE tests, and they were similar for all vehicles, namely 28% (s.d 3%). On the other hand, motorway stop periods were negligible. Due to the action of stop-start, engine-off periods are directly correlated to stop periods. However, it is not always the case of HEV vehicles, where hybrid system controls combustion engine switching-on by its complex strategy for energy storage/demand. Also, stop-start system of G-DI vehicle was intentionally deactivated to measure the exhaust gas temperature without the cooling down effect of TWC produced by that system. In this way, the opposite stop-start behaviours of HEV and G-DI could be contrasted.

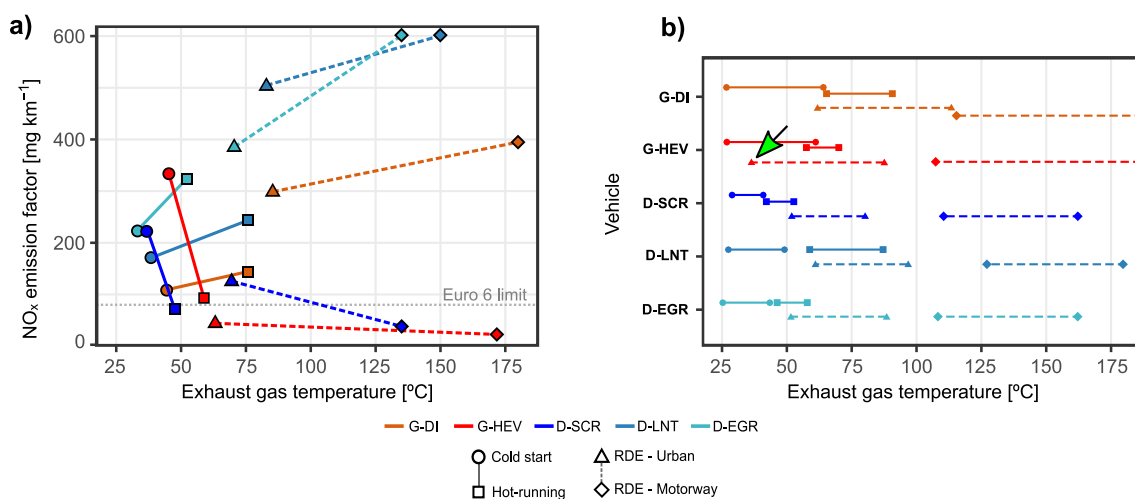


Figure 4. Exhaust gas temperatures for each vehicle and test, engine-off periods were not taken into consideration a) raw distance-specific emission factors and average exhaust gas temperature b) endpoints of horizontal lines represent 5th and 95th percentiles of test.

As function of exhaust gas temperature, measured at the external exhaust flow meter, Figure 4 compares CS with HR emissions and urban with motorway sections of RDE tests. Figure 4a shows that SCR and hybrid vehicles emissions were affected by temperature. Their emission

factors decrease as curves go from “low” to “high” gas temperature conditions (CS → HR, urban → motorway), while the other vehicles show opposite patterns. SCR system is affected by low temperatures, and it need an activation threshold of ~200 °C (Ntziachristos et al., 2016). TWC system also need to reach a light-off operating temperature of 250-350 °C (Dardiotis et al., 2013). It implies that G-HEV and D-SCR vehicles, both with catalyst-type NO_x control systems, are more effective controlling NO_x emissions in motorway than urban. In urban and during cold start, low operating temperatures and low load conditions affect the performance of catalytic converters.

Surprisingly, computing engine-off periods, hybrid vehicle combustion engine works much more time in motorway (99%) than urban (26%), but emissions in urban are higher due to influence of low temperature in TWC. It reflects a better performance of G-HEV’s TWC in motorway compared with urban. As noted (Huang et al., 2019) comparing Hybrid and conventional models in a novel convoy-type RDE tests, frequent stops, restarts and low exhaust gas temperatures of HEV vehicles, reduces the performance of oxidation catalyst. The low exhaust gas temperatures in urban of hybrid vehicle (green arrow in Figure 4b), with a 5th percentile value of 29.8 °C could be mainly attributed to additional time with combustion engine turned off by hybrid system, where convection heat transfer from exhaust gas to TWC is cut out. For G-DI and diesel vehicles (averaged), the 5th percentile of urban was 61.7 °C and 50.6 °C, respectively. These exhaust gas temperature values are for reference, because they were measured at exhaust flow meter of PEMS equipment.

Conclusions

This study shows the association between the exhaust gas temperature and the performance of NO_x aftertreatments installed in different Euro 6 SUV vehicles. The tested fleet contain the common architectures of modern passenger cars in the current market: fuel (diesel, gasoline), powertrain (conventional, HEV), and NO_x control system (TWC, EGR-only, LNT, SCR). The main conclusions of this work are the following:

The diesel vehicle equipped with SCR and the hybrid-electric vehicle equipped with TWC had the best real-world performance reducing NO_x emissions in RDE tests, showing their potential to comply with Euro 6 limits. Conversely, both vehicles had the worst performance during cold start owing to low operating temperatures of aftertreatment systems. SCR and TWC systems, both catalytic converters, require a minimum operating temperature, which is decisive for their optimal performance. It is also important note that both vehicles quickly reduced their emission near to Euro 6 limits after 5 minutes of CS testing time.

The gasoline vehicle with stratified air fuel mixture direct injection and the diesel vehicles with EGR-only and LNT aftertreatment were far to meet Euro 6 limits. Also, they showed a positive correlation between emission factors and the exhaust gas temperature, so their emission factors increased as tested sections went from “low” to “high” exhaust gas temperatures (i.e., CS → HR, urban → motorway). G-HEV and D-SCR vehicles showed the opposite behaviour, reducing efficiently NO_x emission at high exhaust temperature conditions, and therefore, showing a negative correlation between emission factors and average exhaust gas temperature.

For G-HEV and D-SCR vehicles, NO_x reduction efficiency in motorway is higher than urban. Stop-start system and low load in urban constrain heat transfer from exhaust gas to catalytic converters. In the case of HEV, combustion engine-off periods further restrict this heat transfer. For this reason, although its combustion engine works much more time in motorway (99%) compared with urban (26%), motorway emission factors resulted lower.

Incorrect operating temperatures of exhaust gas aftertreatments and cold start are major issues, because it led to increased emissions of NO_x and other pollutants, especially for catalytic converters. Therefore, it is important to model accurately actual emissions from vehicles in those conditions. The findings of this study suggest that emissions of HEV and SCR equipped vehicles could be sub estimated in driving cycles widely represented by urban driving. Finally, these vehicles could improve their aftertreatment thermal management to further exploit their emissions reduction potential.

Acknowledgements

The authors gratefully thank Victor del Pozo, Nuria Flores, and Bernardo Martínez at the University Institute for Automobile Research (INSIA) for their work on the testing campaign. Thanks to Sandra Rodriguez for her time post processing the data.

References

- Chan, S.H., Hoang, D.L., 2000. Chemical Reactions in the Exhaust System of a Cold-start Engine. *Chem. Eng. Technol.* 23, 727–730. [https://doi.org/10.1002/1521-4125\(200008\)23:8<727::AID-CEAT727>3.0.CO;2-D](https://doi.org/10.1002/1521-4125(200008)23:8<727::AID-CEAT727>3.0.CO;2-D)
- Dardiotis, C., Martini, G., Marotta, A., Manfredi, U., 2013. Low-temperature cold-start gaseous emissions of late technology passenger cars. *Appl. Energy* 111, 468–478. <https://doi.org/10.1016/j.apenergy.2013.04.093>
- Fonseca González, N., Casanova Kindelán, J., López Martínez, J.M., 2016. Methodology for instantaneous average exhaust gas mass flow rate measurement. *Flow Meas. Instrum.* 49, 52–62. <https://doi.org/10.1016/j.flowmeasinst.2016.04.007>
- Fonseca González, N.E., 2012. Aspectos de la medición dinámica instantánea de emisiones de motores. Aplicación al desarrollo de un equipo portátil y una metodología para estudios de contaminación de vehículos en tráfico real. Universidad Politécnica de Madrid. <https://doi.org/10.20868/UPM.thesis.14269>
- Hoofman, N., Messagie, M., Van Mierlo, J., Coosemans, T., 2018. A review of the European passenger car regulations – Real driving emissions vs local air quality. *Renew. Sustain. Energy Rev.* 86, 1–21. <https://doi.org/10.1016/j.rser.2018.01.012>
- Huang, Y., Surawski, N.C., Organ, B., Zhou, J.L., Tang, O.H.H., Chan, E.F.C., 2019. Fuel consumption and emissions performance under real driving: Comparison between hybrid and conventional vehicles. *Sci. Total Environ.* 659, 275–282. <https://doi.org/10.1016/j.scitotenv.2018.12.349>
- Koltsakis, G.C., Samaras, Z., Karvountzis-Kontakiotis, A., Zacharopoulou, T., Haralampous, O., 2011. Implications of Engine Start-Stop on After-Treatment Operation. *SAE Int. J. Engines* 4, 1571–1585. <https://doi.org/10.4271/2011-01-1243>
- Mera, Z., Fonseca, N., López, J.-M., Casanova, J., 2019. Analysis of the high instantaneous NO_x emissions from Euro 6 diesel passenger cars under real driving conditions. *Appl. Energy* 242, 1074–1089. <https://doi.org/10.1016/j.apenergy.2019.03.120>

- Ntziachristos, L., Papadimitriou, G., Ligterink, N., Hausberger, S., 2016. Implications of diesel emissions control failures to emission factors and road transport NO_x evolution. *Atmos. Environ.* 141, 542–551. <https://doi.org/10.1016/j.atmosenv.2016.07.036>
- Roberts, A., Brooks, R., Shipway, P., 2014. Internal combustion engine cold-start efficiency: A review of the problem, causes and potential solutions. *Energy Convers. Manag.* 82, 327–350. <https://doi.org/10.1016/j.enconman.2014.03.002>
- Weiss, M., Bonnel, P., Hummel, R., Provenza, A., Manfredi, U., 2011. On-road emissions of light-duty vehicles in Europe. *Environ. Sci. Technol.* 45, 8575–8581. <https://doi.org/10.1021/es2008424>
- Weiss, M., Paffumi, E., Clairotte, M., Drossinos, Y., Vlachos, T., Bonnel, P., Gieschaskiel, B., 2017. Including cold-start emissions in the Real-Driving Emissions (RDE) test procedure. *JRC Sci. policy Rep.* <https://doi.org/10.2760/70237>

2.2 Marine and aviation emissions

This section includes papers presented in the context of the “Marine and aviation emissions” session of the TAP conference. Table 3 provides an overview of these papers, as they are listed in the following sub-sections of the report.

Table 3. Titles and authors of “Marine and aviation emissions” papers

	Paper Title	Authors
2.2.1	Effects of present (2016) versus future (2030) Baltic Sea ship emissions	J.E. Jonson, M. Gauss, J.P. Jalkanen and L. Johansson
2.2.2	Shipping fuel consumption and emissions modelling in fourteen Queensland port areas	R. Smit and F. Khan
2.2.3	Current and future impacts of ship emissions on air quality and human health in the urban area of Gothenburg	M. O. P. Ramacher, L. Tang, V. Matthias and J. Moldanova
2.2.4	The impact of marine traffic on the present and future air quality of the port of Piraeus and surrounding urban areas	G. Tsegas, N. Moussiopoulos, L. Ntziachristos, E. Chourdakis and M. Drakoulas
2.2.5	Impact assessment for a potential emission control area in the Mediterranean Sea	J. Cofala, J. Borken-Kleefeld, C. Heyes, M. Holland, H. Frageli, A. Nyiri, A. Gomez-Sanabria, R. Sander and M. Amann
2.2.6	An Improved Model for Calculation of Emissions Based on Typical Flight Records	V. Sraga, P. Ilinčić, G. Šagi, and Z. Lulić

2.2.1 Effects of present (2016) versus future (2030) Baltic Sea ship emissions

Jan Eiof Jonson¹ *, Michael Gauss¹ , Jukka-Pekka Jalkanen² , and Lasse Johansson²

¹Norwegian Meteorological Institute, Oslo, NO-0313, , Norway

²Finnish Meteorological Institute, P.O. Box 503, 00101 Helsinki, Finland

Keywords: Ship emissions, Baltic region, Effects of SECA/NECA regulations.

Presenting author email: j.e.jonson@met.no

This paper is a shortened version of a recently published acpd paper:

Jonson, J. E., Gauss, M., Jalkanen, J.-P., and Johansson, L.: Effects of strengthening the Baltic Sea ECA regulations, *Atmos. Chem. Phys. Discuss.*, <https://doi.org/10.5194/acp-2019-51>, in review, 2019.

Introduction

Even though emissions of most air pollutants have decreased in the countries surrounding the Baltic Sea (BAS) in past decades (Tista et al., 2018), air pollution and atmospheric depositions affecting ecosystems remain a problem in the region. Significant contributions to the emissions also come from shipping, both inside and outside the region. Obtaining reliable data on emissions from international shipping has always been challenging, but in recent years ship emissions estimated based on AIS (Automatic Identification System) positioning data have become available, continuously tracking the position of the vessels, resulting in substantial improvements in the reliability of ship emissions data. A number of IMO (International Maritime Organisation) and EU regulations have been implemented in the recent past, or will be implemented in the near future, affecting ship emissions in European waters. Most noteworthy are the SECA (Sulphur Emission Control Area) regulations, reducing the maximum sulphur content allowed in marine fuels from 1.0 to 0.1% from 1. January 2015 (IMO, 2008). Fuels with higher sulphur content may be used in combination with emission reduction technology reducing sulphur emission to levels equivalent to the use of compliant low-sulphur fuels. In European waters the North Sea (NOS) and BAS are designated as SECAs by the IMO. These two sea areas are also accepted as NECAs (NO_x Emission Control Areas) from 2021 (IMO, 2017). Reductions of NO_x emissions are expected to occur only gradually in the NECAs as these regulations only apply to new ships or when major modifications are made on existing ships.

Several regional studies focusing on the effects of NOS and BAS ship emissions have been performed. Jonson et al. (2015) studied the effects of reducing the sulphur content in marine fuels from 1.5 to 1% in 2011 on air pollution, including also calculations of health effects as well as effects of future (2030) ship emissions. They found that the introduction of a NECA from 2016 (later postponed to 2021) would reduce the burden on health due to shipping in the BAS region. Reductions in future PM_{2.5} (particulate matter with diameter less than 2.5µm) levels as a result of the 2021 NECA are also predicted by Karl et al. (2018). Brandt et al. (2013) calculated the effects of ship emission on Europe for the years 2000 and 2020. They found that the implementation of the stricter SECA regulations in the BAS and the NOS would result in substantial health improvements in Europe. Karl et al. (2019) compared the effects of BAS shipping calculated by three different chemistry transport models using year 2012 emissions and meteorology. They found that in the entire BAS region the average contribution from ships to PM_{2.5} is in the range of 4.3 - 6.5% for the three CTMs, and deposition of oxidised nitrogen to the Baltic Sea in the 20 - 24ktN per year range. Claremar et al. (2017) calculated the dispersion of air pollutants and depositions from NOS and BAS shipping for the period 2011 to 2050 with the main focus on sea-water acidity in BAS. They found that, also in the future, ship emissions could remain a major source of acidity, in particular when assuming high penetration of open loop scrubbers in combination with the use of high sulphur-content fuels.

In this paper we have calculated the effects of ship emissions in the BAS on air pollution and depositions of oxidised sulphur and nitrogen in adjacent countries. Calculations have been made applying BAS emissions prior to (2014) and after (2016) the implementation of the stricter SECA regulations, which went into force on 1 January 2015. Furthermore, model calculations have been made with future (2030) land-based and ship emissions. The health impacts of air pollutants and the increased depositions of acidifying and eutrophying species from BAS shipping based on these results will be discussed in two companion papers in preparation (Barregård et al., 2019; Repka et al., 2019).

1 Experimental setup

1.1 Emissions

Land-based emissions have been provided by the International Institute for Applied Systems Analysis (IIASA) within the European FP7 project ECLIPSE. In this study we use version 5a (<http://www.iiasa.ac.at/web/home/research/researchPrograms/air/ECLIPSEv5.html>) (hereafter ECLIPSEv5a), a global emission data set on 0.5 x 0.5 degree resolution, which has been widely used in recent years by the scientific community. ECLIPSEv5a is available in 5-year intervals from 2005 onwards, and in this study we have chosen data for 2015 and 2030. In regard to ship emissions in the BAS, we use emission data provided by FMI for the year 2014 (i.e. with 1% maximum sulphur content in fuels in the SECA) and 2016 (maximum sulphur content reduced to 0.1% in the SECA). For the remaining sea areas, ship emissions for year 2015 are used from a previous global data set (Johansson et al., 2017).

The emissions from shipping have been calculated with the Ship Traffic Emission Assessment Model (STEAM) based on ship movements from the automatic identification system (AIS) which provides real time information on ship positions. The STEAM model is described in Jalkanen et al. (2009, 2012, 2016) and Johansson et al. (2013, 2017). Daily emission grids for Baltic Sea ship emissions were produced based on vessel-specific modelling, considering the changes in fuel sulphur content that occurred between 2014 and 2016. Differences between 2014 and 2016 emission data also include changes in ship activity and routing, but on a regional scale these effects are assumed to be small, so that the modelled difference in air pollution and deposition mainly reflects the change in sulphur content in ship fuel. From 2021 onward, NO_x emissions in the North Sea and the Baltic Sea for new ships have to comply with IMO Tier 3 regulations. These regulations were taken into account in the emission modelling. Future emission projections for the year 2030 also include changes in:

- energy efficiency improvements, modelled following the method of Kalli et al. (2013), which goes beyond the Energy Efficiency Defined Index (EEDI) requirements of the IMO;
- vessel size growth, assuming a linear annual growth dependent on ship types;
- fleet size increase.

Annual growth rates in fleet size are implemented as percentage increase per type of ship: For example, if the annual percentage growth is n% for container ships we duplicate n% of the container ships in the current fleet in the following year. As the ship emission data are used for multiple meteorological years, we did not retain the high (hourly) temporal resolution in the original data but rather aggregated them to monthly resolution before use in the chemistry transport model.

1.2 Model calculations of air pollutants and depositions

Concentrations of air pollutants and depositions of sulphur and nitrogen have been calculated with the EMEP MSC-W model (hereafter 'EMEP model'), version rv4.14, on 0.1 x 0.1 degrees resolution for the domain between 30 degrees W and 45 degrees E and between 30 and 75 degrees N. The calculations of dry depositions are made separately for each sub-grid landcover classification. These sub-grid estimates are aggregated to provide output deposition estimates for broader ecosystem categories as deciduous and coniferous forests. The ecosystem specific depositions are not shown here, but will be used in a companion paper when calculating exceedances of critical loads for acidification and eutrophication. A detailed description of the EMEP model can be found in Simpson et al. (2012) with later model updates being described in Simpson et al. (2018) and references therein. The EMEP model is available as Open Source (see <https://github.com/metno/emep-ctm>), and is regularly evaluated against measurements as part of the EMEP status reports. See Gauss et al. (2016, 2017, 2018) for evaluations of the meteorological years 2014, 2015 and 2016, respectively. In addition, the EMEP model has successfully participated in model inter-comparisons and model evaluations presented in a number of peer-reviewed publications (see Jonson et al. (2019) for references).

In the present study the model is driven by meteorological data from the European Centre for Medium-Range Weather Forecasts (ECMWF) based on the CY40R1 version of their IFS (Integrated Forecast System) model. All simulations for this paper have been run for the three meteorological years 2014, 2015 and 2016, and then averaged, in order to cancel out meteorological variability. The simulations are:

- Present_Base: Base case with ship emissions of 2016. Land-based emissions for 2015 (from ECLIPSEv5);
- Present_NoShip: As Present_Base, but without ship emissions in the BAS;
- Present_HiSulphur: As Present_Base, but with ship emissions of 2014 (i.e high sulphur content) in the BAS;
- Future_Base: Ship emissions of 2030 (assuming NECA and business as usual development) and land-based emissions of 2030 (from ECLIPSEv5);
- Future_NoShip: As Future_Base, but without ship emissions in the BAS.

In the future scenarios it is assumed that ships that are in compliance with the NECA regulations will operate the equipment (i.e. be compliant) also when sailing outside the NECA.

2 Model results

In this section model results for parts of Europe centred around the BAS are shown. Concentrations and depositions are shown as averages for three meteorological years for Present_Base and Future_Base and for differences between the two Base runs and the perturbation scenarios as described in Section 1.2. The impact on PM 2.5 levels and on the depositions of oxidised nitrogen and sulphur species derived from the perturbation model runs presented here, forms the basis for coming papers discussing the effects on human health (Barregård et al., 2019) and assessing the environmental impacts, including the exceedances of critical loads from ship emissions in the BAS (Repka et al., 2019).

2.1 Air pollution due to Baltic Sea shipping

Concentrations of NO₂ for Present_Base are shown in Figure 1a. The lifetime of NO₂ is short, and as a result the concentrations largely reflect the locations of the main source areas. Concentrations of NO₂ are high in Central Europe and in and around the English Channel with markedly lower concentrations north and east of the BAS. In the NOS and the BAS the major ship tracks are clearly visible. Figure 1c shows the difference between the Present_Base and the Present_NoShip scenarios. The calculations show that ship emissions account for more than 50% of NO₂ in central parts of the BAS and for a substantial percentage also in coastal zones, in particular in Denmark, southern parts of Sweden and Finland and the Baltic states (Estonia, Latvia and Lithuania). This is also further illustrated in Jonson et al. (2019), where measured NO₂ at sites located in the BAS coastal regions are compared to the Present_Base, Present_NoShip and Present_HiSulphur model calculations. In the Present_NoShip case NO₂ levels are clearly underestimated and correlations and RMS errors deteriorated compared to the Present_Base calculation, demonstrating the impact of ship emissions in many coastal areas. The comparisons with measurements convincingly show that the measurements can only be reproduced when BAS ship emissions are included.

In Jonson et al. (2019) we show that measured SO₂ levels are relatively well reproduced by the model for the Present_Base calculation. The effects of excluding the BAS ship emissions in the Present_NoShip scenario have only minor effects on the SO₂ levels. Replacing 2016 BAS emissions with 2014 (Present_HiSulphur) has much larger effects, resulting in an overestimation of SO₂ levels at most of the sites. This clearly illustrates the effects of the stricter SECA regulations. With the high ship emissions of 2014, the measurements for 2016 can not be reproduced. This is also a strong indication that the ships are largely in compliance with the SECA regulations.

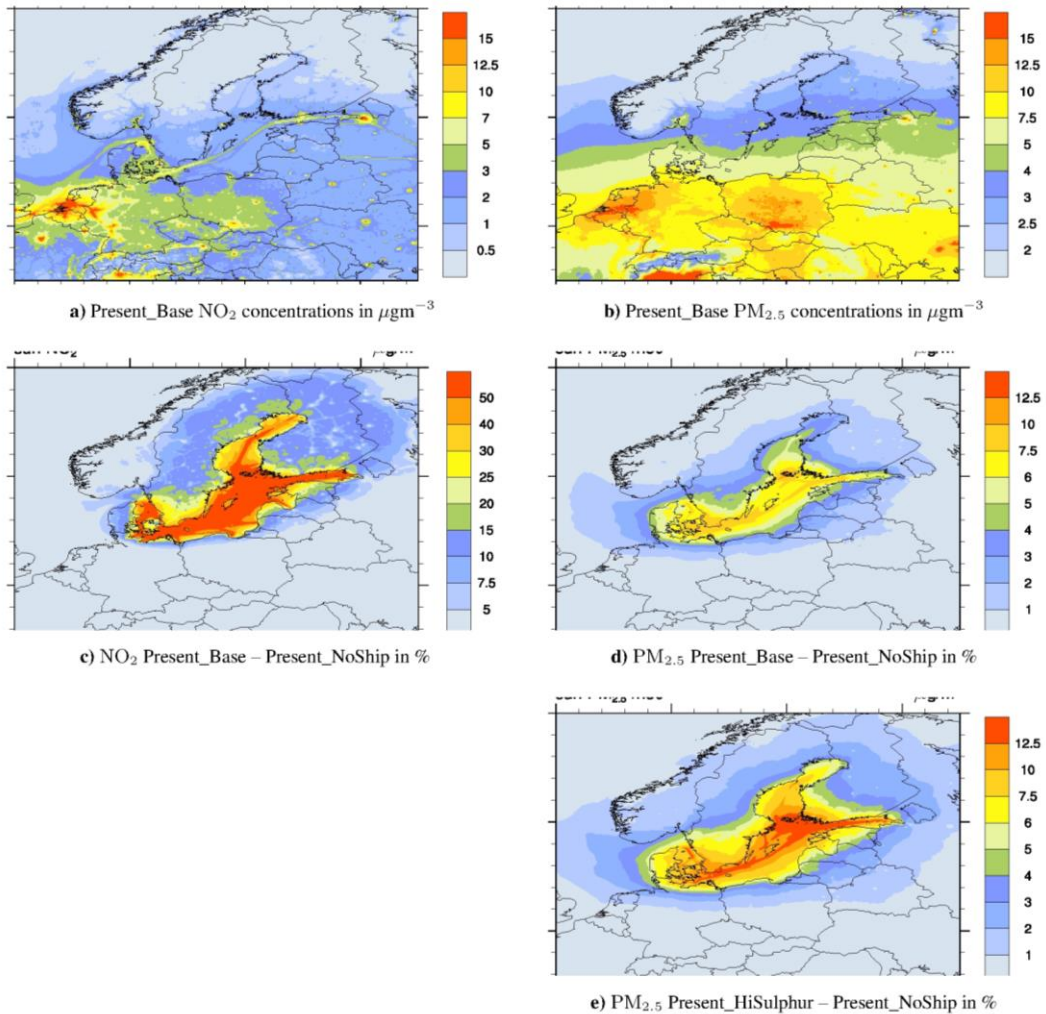


Figure 1: Top panels: concentrations of NO₂ and PM_{2.5} in the Present_Base case. Middle panels: present percentage contribution from BAS ship emissions to NO₂ and PM_{2.5} after the new sulphur regulations. Bottom panel: percentage contribution to PM_{2.5} concentrations before the new sulphur regulations. Figure from Jonson et al. (2019).

PM_{2.5} (Figure 1b) in the atmosphere is a mixture of many chemical species of both natural and anthropogenic origins. It is emitted both as a primary pollutant and formed as a secondary pollutant in the atmosphere. As a result PM_{2.5} concentrations are more spread out compared to NO₂. Concentrations decrease from south to north from a maximum in central Europe. As shown in Figure 1d the percentage contributions from BAS shipping, calculated as Present_Base – Present_NoShip, are much smaller for PM_{2.5} than for NO₂ but with noticeable contributions in coastal zones, in particular in parts of Denmark, Sweden and Finland. Figure 1e shows higher contributions when assuming BAS shipping at 2014 levels (Present_HiSulphur), prior to the implementation of the stricter SECA regulations. For PM_{2.5} differences between the Present_Base and the Present_NoShip cases are much smaller than for NO₂. Likewise, differences are smaller than for SO₂ between Present_Base and Present_HiSulphur. In Jonson et al. (2019) we show that the model results underestimate the measurements at most of the sites listed. Based solely on the comparisons between measurements and the different model scenarios for PM_{2.5} one can not conclude that the Present_Base scenario is more realistic than the other two.

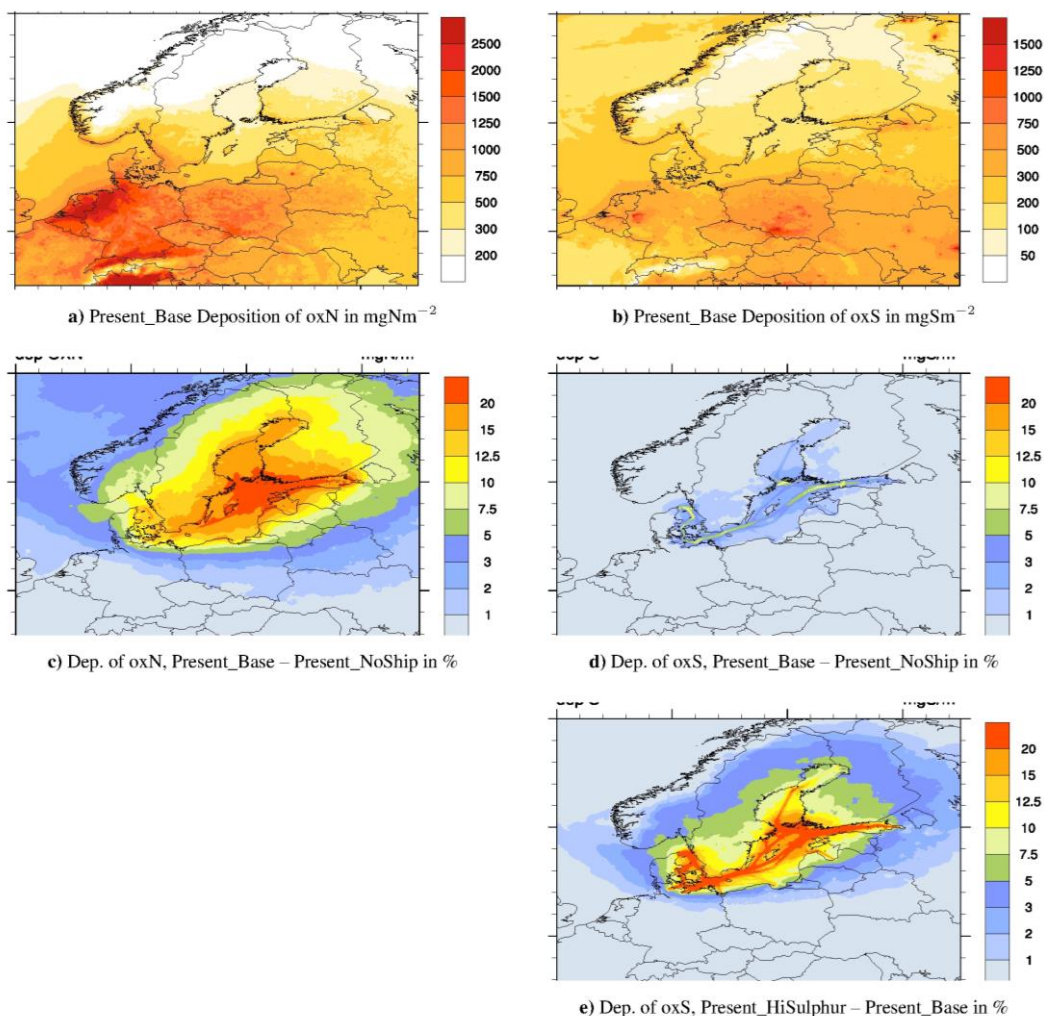


Figure 2: Top panels: calculated depositions of oxidised nitrogen and sulphur. Middle panels: present percentage contributions from BAS ship emissions to depositions of oxidised nitrogen and oxidised sulphur with reference to Base 2016. Bottom panel: percentage contribution to depositions of oxidised sulphur with reference to 2014 BAS emissions. Figure from Jonson et al. (2019).

2.2 Depositions of sulphur and nitrogen from Baltic Sea shipping

Total depositions (wet and dry) of oxidised sulphur and nitrogen for Present_Base are shown in Figure 2a,b. The highest depositions of both sulphur and nitrogen are seen over Central Europe. For nitrogen, high levels of depositions also extend into northern Germany and Denmark. Based on the difference between Present_Base and Present_NoShip a significant amount of the nitrogen depositions can be attributed to BAS shipping (Figure 2c), contributing to more than 15% of the total nitrogen depositions in major parts of the BAS and also in parts of Sweden, Finland and the Baltic states (Estonia, Latvia and Lithuania). Dry deposition is parameterised as a function of sub grid-scale ecosystems and is typically higher than the grid average for forest ecosystems (both coniferous and deciduous). This will affect the calculations of critical loads for acidification and eutrophication as the sub grid-scale ecosystem depositions are used in the critical load calculations. Critical loads will be discussed in a later companion paper (Repka et al., 2019). Figure 2d shows that the calculated contributions from BAS shipping in 2016 to depositions of sulphur are very low (Present_Base – Present_NoShip) and much lower than what has been calculated assuming 2014 emissions (Present_HiSulphur – Present_Base) as shown in Figure 2e, with percentage contributions exceeding 10% in many coastal zones. These findings for the depositions of oxidised nitrogen and sulphur are further discussed in Jonson et al. (2019) where we compare measured concentrations in precipitation at sites located in the BAS coastal regions to the Present_Base, Present_NoShip and Present_HiSulphur model calculations. Compared to Present_Base, averaged concentrations in precipitation are about 14% lower for oxidised nitrogen when BAS ship emissions are excluded (Present_Base – Present_NoShip). The effects of the stricter SECA

regulations is demonstrated by an increase of about 9% in the calculated concentrations of oxidised sulphur in precipitation in the Present_HiSulphur scenario compared to the Present_Base calculation.

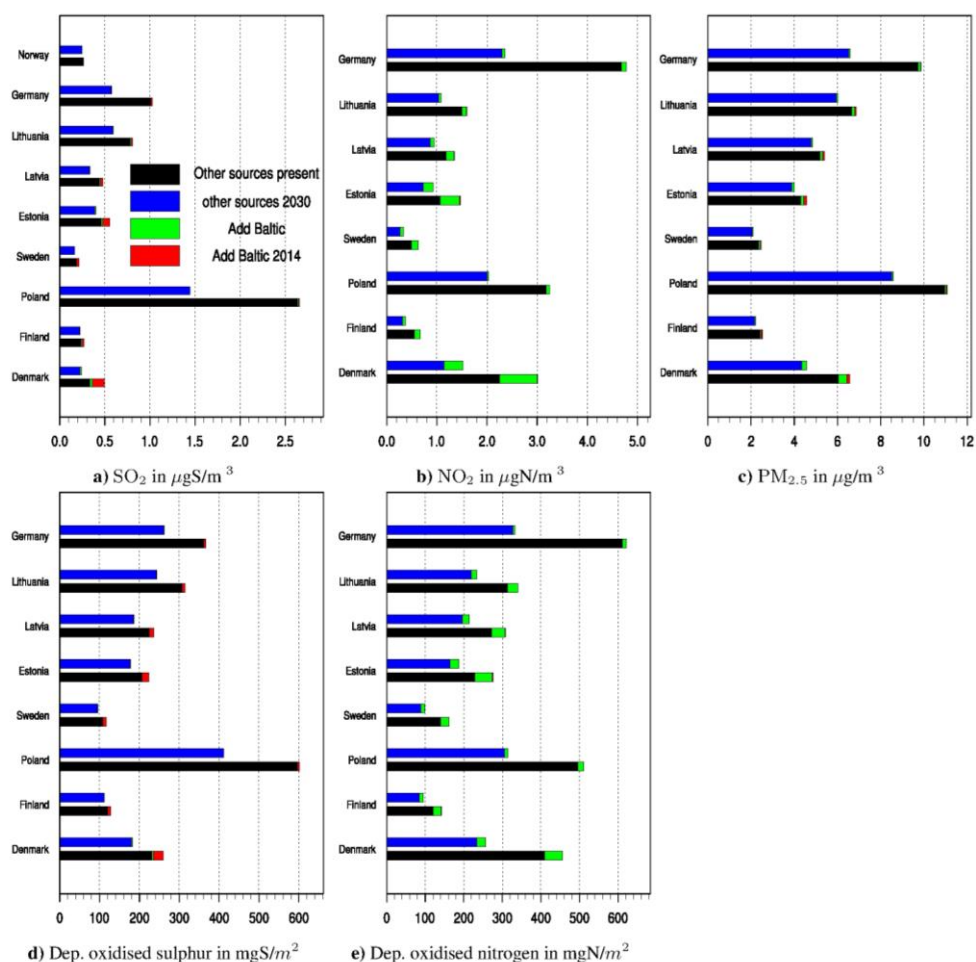


Figure 3: For each country, the upper bar shows the present case and the lower bar the future case country average concentration. a) SO₂, b) NO₂, c) PM_{2.5}, and depositions of oxidised sulphur (d) and oxidised nitrogen (e). The black and blue bars represent the Present_NoShip and Future_NoShip calculations respectively. The additional contributions from BAS are shown in green and the additional effect assuming high sulphur fuel emissions in red. Figure from Jonson et al. (2019).

2.3 Contributions to individual countries from BAS shipping.

Figure 3 shows the concentrations of NO₂, SO₂, PM_{2.5}, and the depositions of oxidised sulphur and oxidised nitrogen averaged over the individual countries bordering the BAS. The black (Present) and blue (Future) bars represent contributions from all other sources (both anthropogenic and natural) than BAS shipping. The green part of the bars represents the (present and future) contributions from BAS shipping calculated as Base – NoShip where Base can be either Present_Base or Future_Base and NoShip can be either Present_NoShip or Future_NoShip. The sum of the black or blue and the green parts of the bars then adds up to the total concentrations and depositions averaged over the individual countries bordering the BAS for the Present_Base and the Future_Base scenarios. The red part is the additional BAS contributions assuming BAS ship emissions at 2014 levels calculated as Present_HiSulphur – Present_Base. The calculations are made assuming linearity. Previous calculations, adding up contributions from different sources, have shown that this assumption is reasonable (Jonson et al., 2017, 2018). Irrespective of species and depositions, the largest contributions are seen for smaller countries with long coastlines exposed to the BAS as Denmark and the Baltic States, and the least for large countries as Germany and Poland with major parts of their areas located far from the shipping routes.

Following the expected reductions between 2016 and 2030 in both land-based and ship emissions, calculated concentrations and depositions are reduced over the 2016 to 2030 time-span. For SO₂ and

depositions of sulphur, BAS shipping is already an insignificant source in 2016 and the differences between 2030 and 2016 are almost entirely caused by changes in land-based emissions. For NO₂ concentrations and depositions of oxidised nitrogen, reductions of land-based and BAS ship emissions both contribute to the improvements in pollution levels. In the BAS region the fractional reductions of future concentrations attributed to (mainly) land-based, and to BAS ship emissions are roughly in the same range. The largest contributions from BAS shipping is seen for NO₂ (Figure 3b), depositions of oxidised nitrogen (Figure 3d), and partially also for SO₂ (Figure 3a) when assuming 2014 emissions (Present_HiSulphur). However, for SO₂ calculated contributions are insignificant following the implementation of the stricter SECA in 2015. The same conclusion also holds for sulphur depositions (Figure 3d). PM_{2.5} contributions from BAS shipping are markedly smaller than for NO₂. Contributions are higher when assuming Present_HiSulphur emissions. After the implementation of stricter SECA regulations in 2015, PM_{2.5} from shipping mainly originates from NO₂ and, in part, primary PM emissions. As shown in Figure 1d,e elevated PM_{2.5} concentrations from BAS shipping are mainly seen in coastal zones close to shipping lanes. Much of these coastal zones are densely populated. When assessing the health effects of PM in a forthcoming companion paper (Barregård et al., 2019), population weighted PM_{2.5} concentrations are used.

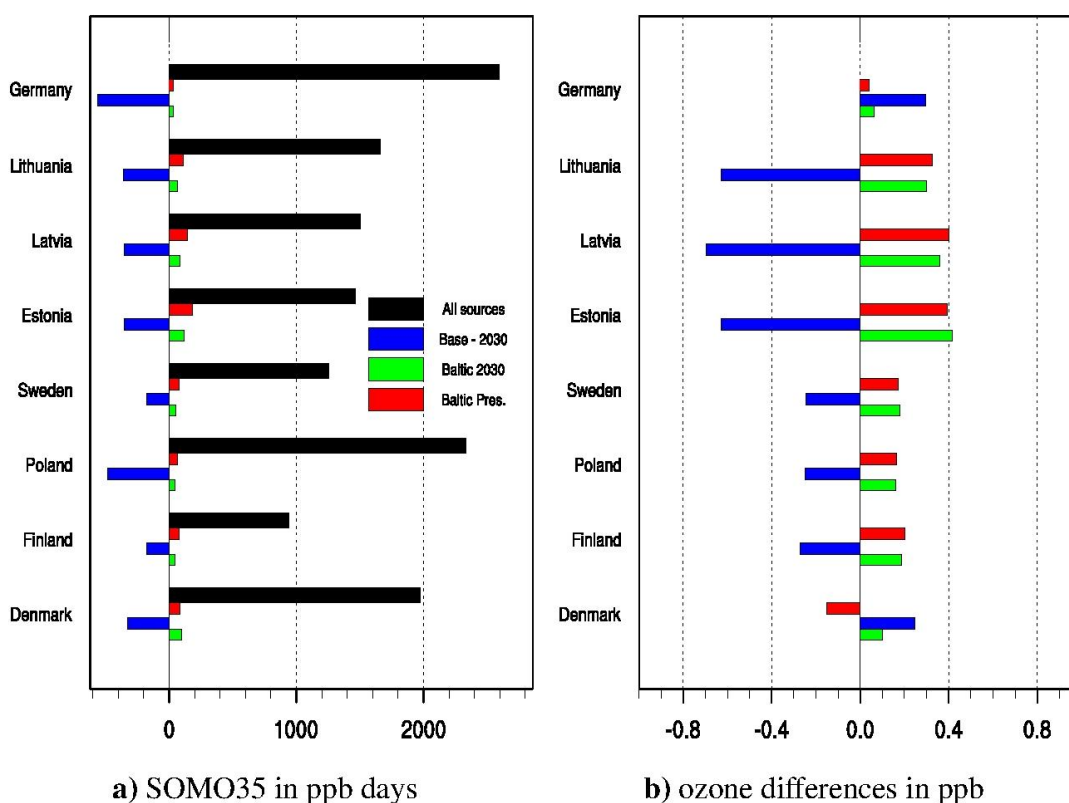


Figure 4: Left, SOMO35 in ppb days where black bars represent Present_Base levels. Right, changes in annual ozone in ppb (annual average ozone is in the 30 - 35 ppb range in all countries). For both SOMO35 and annual ozone blue bars represent changes in levels from 2016 to 2030 (Present_Base – Future_Base), red bars: contributions from BAS (Present_Base – Present_NoShip), green bars: contributions from BAS in 2030 (Future_Base – Future_NoShip). Figure from Jonson et al. (2019).

Figure 4 shows calculated SOMO35⁶ and the effect of BAS shipping on SOMO35 (left) and the effects on annual average ozone (right). For all countries annual averaged ozone is in the 33 - 37 ppb range. Also show are the effects of the expected emission reductions in 2030 and contributions from BAS shipping for the same year. For most countries both SOMO35 and annually averaged ozone increase only slightly as a result of BAS shipping, and more so for SOMO35 than for annually averaged ozone. For most countries the expected emission reductions from year 2016 to 2030 results in reductions in the ozone levels. However, changes in SOMO35 and annually averaged ozone are a combination of net ozone increases, mainly in the summer months, and ozone titration by NO, mainly in winter. In the BAS region net production and titration partially cancel out, and for some regions and countries titration

6 SOMO35 is the indicator for health impacts recommended by WHO calculated as the daily maximum of 8-hour running ozone maximum over 35 ppb

dominates. As a result, the additional emissions from BAS shipping lead to reductions in annual ozone in Denmark. Furthermore, the expected emission reductions from 2016 to 2030 result in increased annual ozone levels in Germany. Even though annual ozone levels decrease, lower emissions will result in SOMO35 reductions in both these two cases as the titration events mainly occur in winter time when ozone levels are mostly below 35 ppb. It has to be noted that in our model calculations the ship emissions are instantly diluted throughout the model grid cell where the emissions occur. Previous studies Vinken et al. (2011); Huszar et al. (2010) have shown that this could lead to an overestimation of ozone formation. However, Vinken et al. (2011) found that the overestimation caused by instant dilution was small in polluted regions, such as the central parts of the BAS.

Conclusions

Our calculations clearly show that, following the stricter SECA regulations from 1 January 2015, sulphur emissions from BAS shipping now contribute little to depositions of oxidised sulphur and PM_{2.5} concentrations in air. This is in contrast to pre-2015 conditions when less stringent sulphur regulations were in place, and even more compared to pre-2011 conditions when up to 1.5% sulphur were allowed in marine fuels in the SECAs. Still, emissions of NO_x and particles from BAS shipping continue to be high, causing health problems and other detrimental impacts on the environment in the BAS region. At present emission levels, particles originating from BAS shipping are mainly formed from NO_x emissions. In addition, emissions of non-sulphur particles from BAS shipping are virtually unaffected by the SECA regulations. Our source-receptor calculations show that, for many countries in the BAS region, they are among the 5 to 6 largest regions/countries contributing to SIA (Secondary Inorganic Aerosols), which is a major constituent of PM_{2.5} (see EMEP reports for the individual countries for year 2016 (Klein et al., 2018)). The largest contributions by far are calculated for the coastal zones. Many of the larger cities in the BAS region are located in the coastal zones. In the companion paper (Barregård et al., 2019) health effects from BAS shipping have been adjusted to the population density resulting in a proportionally higher contribution from shipping than presented here as area averaged concentrations. The implementation of NECA regulations in the BAS (and also NOS) is expected to result in gradual reductions in PM_{2.5} from BAS shipping, as shown in our calculations for future conditions (Future_Base – Future_NoShip). In the future scenario this relative decrease is largely comparable to the decrease from other anthropogenic sources. BAS ship emissions also affect the formation of ground level ozone. In much of the BAS region NO₂ levels are already influenced by large land-based sources, and additional contributions from BAS shipping to ozone and ozone metrics, exemplified by SOMO35, is moderate, and for several regions even negative. In this paper we have shown that for most countries future ozone and ozone metrics are expected to decrease from their present levels. In addition to influencing particle formation and ozone levels, NO_x emissions also contribute to the depositions of oxidised nitrogen, causing exceedances of critical loads for acidification and in particular eutrophication. A significant portion of the depositions of oxidised nitrogen is due to BAS shipping. This is also corroborated by the source-receptor calculations for the individual countries in Europe for 2016, see Klein et al. (2018) where they calculate that BAS shipping is the largest contributor to oxidised nitrogen deposition in Estonia (with 14%), and among the 3 to 5 largest contributors in several other countries in the region. As discussed above, these depositions are projected to be gradually reduced following the implementation of the NECA regulations, with relative reductions largely comparable to the decrease from other anthropogenic sources.

Acknowledgements

This work has been funded by European Union (European Regional Development Fund) project EnviSuM, and partially by EMEP under UNECE. Computer time for EMEP model runs was supported by the Research Council of Norway through the NOTUR project EMEP (NN2890K) for CPU, and NorStore project European Monitoring and Evaluation Programme (NS9005K) for storage of data. Surface measurements have been made available through the EBAS web site: <http://ebas.nilu.no/Default.aspx>

References

Barregård, L. et al.: Impact on population health of emissions of pollutants from Baltic shipping., Manuscript in preparation, 2019.

Brandt, J., Silver, J. D., Christensen, J. H., Andersen, M. S., Bønløkke, J. H., Sigsgaard, T., Geels, C., Gross, A., Hansen, A. B., Hansen, K. M., Hedegaard, G. B., Kaas, E., and Frohn, L. M.: Assessment of past, present and future health-cost externalities of air pollution in Europe and the contribution from international ship traffic using the EVA model system, *Atmospheric Chemistry and Physics*, 13, 7747–7764, <https://doi.org/10.5194/acp-13-7747-2013>, <https://www.atmos-chem-phys.net/13/7747/2013/>, 2013.

Claremar, B., Haglund, K., and Rutgersson, A.: Ship emissions and the use of current air cleaning technology: contributions to air pollution and acidification in the Baltic Sea, *Earth System Dynamics*, 8, 901–919, <https://doi.org/10.5194/esd-8-901-2017>, <https://www.earth-syst-dynam.net/8/901/2017/>, 2017.

Gauss, M., Tsyro, S., Benedictow, A., Fagerli, H., Hjellbrekke, A.-G., Aas, W., and Solberg, S.: EMEP/MS-CW model performance for acidifying and eutrophying components, photo-oxidants and particulate matter in 2014., Supplementary material to EMEP Status Report 1/2016, available online at www.emep.int, Last access: 27 February 2019, The Norwegian Meteorological Institute, Oslo, Norway, 2016.

Gauss, M., Tsyro, S., Fagerli, H., Hjellbrekke, A.-G., Aas, W., and Solberg, S.: EMEP MS-CW model performance for acidifying and eutrophying components, photo-oxidants and particulate matter in 2015., Supplementary material to EMEP Status Report 1/2017, available online at www.emep.int, Last access: 27 February 2019, The Norwegian Meteorological Institute, Oslo, Norway, 2017.

Gauss, M., Tsyro, S., Fagerli, H., Hjellbrekke, A.-G., Aas, W., and Solberg, S.: EMEP MS-CW model performance for acidifying and eutrophying components, photo-oxidants and particulate matter in 2016., Supplementary material to EMEP Status Report 1/2018, available online at www.emep.int, Last access: 27 February 2019, The Norwegian Meteorological Institute, Oslo, Norway, 2018.

Huszar, P., Cario, D., Paoli, R., Halenka, T., Belda, M., Schlager, H., Miksovsky, J., and Pisoft, P.: Modeling the regional impact of ship emissions on NO_x and ozone levels over the Eastern Atlantic and Western Europe using ship plume parameterization, *Atmospheric Chemistry and Physics*, 10, 6645–6660, <https://doi.org/10.5194/acp-10-6645-2010>, <https://www.atmos-chem-phys.net/10/6645/2010/>, 2010.

IMO: Amendments to the annex of the protocol of 1997 to amend the international convention for the prevention of pollution from ships 1973, as modified by the protocol of 1978 relating thereto, Annex vi, IMO (International Maritime Organization), <http://www.imo.org/en/OurWork/Environment/PollutionPrevention/AirPollution/Documents/176%2858%29.pdf>, 2008.

IMO: RESOLUTION MEPC.286(71). Adopted on 7 July 2017. Amendments to the annex of the protocol of 1997 to amend the international convention for the prevention of pollution from ships, 1973, as modified by the protocol of 1978 relating thereto Amendments to MARPOL Annex VI., Available at http://www.imo.org/en/OurWork/Environment/PollutionPrevention/AirPollution/Documents/Res_MEPC_28%2871%29_Tier%20III%20ECA%20and%20BDN.pdf, IMO (International Maritime Organization), 2017.

Jalkanen, J.-P., Brink, A., Kalli, J., Pettersson, H., Kuukkonen, J., and Stipa, T.: A modelling system for the exhaust emissions of marine traffic and its application in the Baltic Sea area, *Atmos. Chem. Phys.*, 9, 9209–9223, <https://doi.org/10.5194/acp-9-9209-2009>, 2009.

Jalkanen, J.-P., Johansson, L., Kuukkonen, J., Brink, A., Kalli, J., and Stipa, T.: Extension of an assessment model of ship traffic exhaust emissions for particulate matter and carbon monoxide, *Atmos. Chem. Phys.*, 12, 2641–2659, <https://doi.org/10.5194/acp-12-2641-2012>, 2012.

Jalkanen, J.-P., Johansson, L., and Kukkonen, J.: A comprehensive inventory of ship traffic exhaust emissions in the European sea areas in 2011, *ACP*, 16, 71–84, <https://doi.org/10.5194/acp-16-71-2016>, <https://www.atmos-chem-phys.net/16/71/2016/>, 2016.

Johansson, L., Jalkanen, J.-P., Kalli, J., and Kukkonen, J.: The evolution of shipping emissions and the costs of regulation changes in the northern EU area, *ACP*, 13, 11 375–11 389, <https://doi.org/10.5194/acp-13-11375-2013>, <https://www.atmos-chem-phys.net/13/11375/2013/>, 2013.

Johansson, L., Jalkanen, J.-P., and Kukkonen, J.: Global assessment of shipping emissions in 2015 on a high spatial and temporal resolution, *Atmospheric Environment*, 167, 403 – 415, <https://doi.org/https://doi.org/10.1016/j.atmosenv.2017.08.042>, <http://www.sciencedirect.com/science/article/pii/S1352231017305563>, 2017.

Jonson, J. E., Jalkanen, J. P., Johansson, L., Gauss, M., and Denier van der Gon, H. A. C.: Model calculations of the effects of present and future emissions of air pollutants from shipping in the Baltic Sea and the North Sea, *ACP*, 15, 783–798, <https://doi.org/10.5194/acp-15-783-2015>, <https://www.atmos-chem-phys.net/15/783/2015/>, 2015.

Jonson, J., Borken-Kleefeld, J., Nyíri, A., Posch, M., and Heyes, C.: Impact of excess NO_x emissions from diesel cars on air quality, public health and eutrophication in Europe, *Env. Res. Lett.*, 12, <https://doi.org/10.1088/1748-9326/aa8850>, 2017.

Jonson, J., Gauss, M., Schulz, M., and Nyíri, A.: Emissions from international shipping, in: Transboundary particulate matter, photo-oxidants, acidifying and eutrophying components. EMEP Status Report 1/2018, pp. 83–

98, The Norwegian Meteorological Institute, Oslo, Norway, http://emep.int/publ/reports/2018/EMEP_Status_Report_1_2018.pdf, 2018.

Jonson, J. E., Gauss, M., Jalkanen, J.-P., and Johansson, L.: Effects of strengthening the Baltic Sea ECA regulations, *Atmos. Chem. Phys. Discuss.*, <https://doi.org/10.5194/acp-2019-51>, in review, 2019.

Karl, M., Bieser, J., Geyer, B., Matthias, V., Jalkanen, J.-P., Johansson, L., and Fridell, E.: Impact of a nitrogen emission control area (NECA) on the future air quality and nitrogen deposition to seawater in the Baltic Sea region, *Atmospheric Chemistry and Physics Discussions*, 2018, 1–58, <https://doi.org/10.5194/acp-2018-1107>, <https://www.atmos-chem-phys-discuss.net/acp-2018-1107/>, 2018.

Karl, M., Jonson, J. E., Uppstu, A., Aulinger, A., Prank, M., Jalkanen, J.-P., Johansson, L., Quante, M., and Matthias, V.: Effects of ship emissions on air quality in the Baltic Sea region simulated with three different chemistry transport models, *Atmospheric Chemistry and Physics Discussions*, 2019, 1–48, <https://doi.org/10.5194/acp-2018-1317>, <https://www.atmos-chem-phys-discuss.net/acp-2018-1317/>, 2019.

Klein, H., Gauss, M., Nyíri, A., and Benedictow, A.: Transboundary air pollution by main pollutants (S, N, O₃) and PM, MSC-W Data Note 1/2018 Individual Country Reports, available online at www.emep.int, The Norwegian Meteorological Institute, Oslo, Norway, last access: 27 February 2019, 2018.

Repka, S. et al.: IMO regulation on ship-originated SO_x and NO_x in the Baltic Sea - assessing the relevance of environmental impacts., Manuscript in preparation, 2019.

Simpson, D., Benedictow, A., Berge, H., Bergström, R., Emberson, L., Fagerli, H., Flechard, C., Hayman, G., Gauss, M., Jonson, J., Jenkin, M., Nyíri, A., Richter, C., Semeena, V., Tsyro, S., Tuovinen, J.-P., Valdebenito, A., and Wind, P.: The EMEP MSC-W chemical transport model – technical description, *Atmos. Chem. Phys.*, 12, 7825–7865, <https://doi.org/10.5194/acp-12-7825-2012>, 2012.

Simpson, D., Wind, P., Bergström, R., Gauss, M., Tsyro, S., and Valdebenito, A.: Updates to the EMEP MSC-W model, 2017 – 2018, EMEP Status Report 1/2018, available online at www.emep.int, The Norwegian Meteorological Institute, Oslo, Norway, http://emep.int/publ/reports/2018/EMEP_Status_Report_1_2018.pdf, last access: 27 February 2019, 2018.

Tista, M., Wankmüller, R., Matthews, B., Mareckova, K., Fagerli, H., and Nyíri, A.: Emissions in 2016, in: Transboundary particulate matter, photo-oxidants, acidifying and eutrophying components. EMEP Status Report 1/2018, pp. 41–64, The Norwegian Meteorological Institute, Oslo, Norway, http://emep.int/publ/reports/2018/EMEP_Status_Report_1_2018.pdf, last access: 27 February 2019, 2018.

Vinken, G. C. M., Boersma, K. F., Jacob, D. J., and Meijer, E. W.: Accounting for non-linear chemistry of ship plumes in the GEOS-Chem global chemistry transport model, *Atmospheric Chemistry and Physics*, 11, 11 707–11 722, <https://doi.org/10.5194/acp-11-11707-2011>, <https://www.atmos-chem-phys.net/11/11707/2011/>, 2011.

2.2.2 Shipping fuel consumption and emissions modelling in fourteen port areas

R. Smit¹, F. Khan²

¹ Emission and Air Modelling, Department of Environment and Science (DES), GPO Box 2454, Brisbane, QLD 4001, Australia, robin.smit@des.qld.gov.au

² Air and Chemical Policy, Department of Environment and Science (DES), GPO Box 2454, Brisbane, QLD 4001, Australia

Abstract

A new empirical shipping (exhaust) emission model has been developed by DES that uses available input data on local shipping movements. The model first estimates fuel consumption by marine fuel type and ship type, and subsequently uses fuel-based emission factors (g/kg fuel) to estimate emissions (NO_x, SO₂, PM₁₀, V, Ni, PAHs, CO₂, etc.). The structure of the model is based on an extensive literature review and model parameters have been calibrated using a ship energy balance approach. The ship fuel (and emissions) model has been set up in a modular fashion, so that default model parameter values can be readily changed to incorporate updated information or to reflect different assumptions, and can be readily used in “what-if” scenario modelling. For example, it can be used to assess the impacts of reduced fuel sulphur content on ship emissions and local air quality. This paper presents the results of emissions modelling (greenhouse gases and air pollutants) for fourteen port areas in Queensland, Australia.

Introduction

Shipping is a significant source of air pollution and greenhouse gas emissions. Ships use large diesel engines that run on heavy bunker fuels, generally without emission controls. Overseas studies have consistently found that ships have significant effects on local air quality in and around port areas (e.g. EEA, 2013). Corbett et al. (2007) estimated that 3-8 per cent of global PM_{2.5} related mortalities are attributable to marine shipping, but the current health impact for Australia is unclear. Until recently, ships have not been subject to local or national emission control measures and policies in Australia. However, shipping impacts have received increasing scrutiny by regulators in Australia as a consequence of nuisance complaints in for instance Sydney harbour.

The local situation will largely determine the impact of shipping emissions on local air quality. This study has conducted a local assessment for the state of Queensland in Australia. The objective of this research project is to accurately and efficiently estimate fuel use and emissions for a broad range of air pollutants for individual ships operating in strategic port areas over a full year (2015).



Figure 1: 40,542 GT Container ship in Port of Brisbane.

Ship activity data

Ship activity data are obtained from processed and verified Automatic Identification System (AIS) data. AIS is a Very High Frequency (VHF) radio broadcasting system, which enables AIS equipped vessels and shore-based ground stations to send and receive identifying information. This is known as terrestrial AIS data. In Australia, the Australian Maritime Safety Authority (AMSA) collects comprehensive AIS data. Specially equipped satellites can also record the same AIS data. AIS is a mandatory collision avoidance system on ships larger than 300 gross tonnes. Each ship transmits a signal giving details regarding the ship's identity, type, position, course, (spot) speed and other safety-related information at frequent intervals. Unique Mobile Maritime Service Identity (MMSI) numbers are sent in the AIS messages.

A data clean-up process was developed to verify data quality, plug data gaps, correct errors (e.g. locational data) and apply statistical data processing techniques. R code was developed to check, correct and impute AIS data using the following steps:

- extract AIS data for each individual ship
- re-order data using date-time stamps
- convert latitude/longitude to UTM X-Y coordinates
- add distance travelled
- add (travel) speed and acceleration
- outlier detection and removal
- impute missing location and speed data

Outliers are associated with locational errors and are flagged as data points with an absolute acceleration larger than 0.15 m/s^2 and a vessel speed larger than 1.15 times the service speed. Service speed is defined as the speed which a ship is stated to be capable of maintaining at sea in normal weather and at normal service draught.

AIS data gaps are addressed in the following fashion. A complete time-series is created for each ship using 1-minute time steps to identify where ship data are missing. For data gaps of less than or equal to 2 hours duration, UTM coordinates are linearly interpolated in space (i.e. time-steps of equal distance) using the last and first available UTM coordinates at either end of the gap. For data gaps larger than 2 hours and ships > 300 GT, a similar spatial interpolation is applied, on the condition that the vessel remains in the same $1 \times 1 \text{ km}$ grid cell and that the last and first recorded speeds at either end of the gap are less than 2.5 km/h . The inclusion of these large data gaps is important because it ensures that time periods with berth/anchorage are captured in the emissions estimation. It is noted that tugs, yachts and dredgers are excluded from this interpolation. Finally, a T4253H filter (Velleman, 1980) is applied to remove noise and unrealistic variations in speed. Ship speeds less than 0.5 km/h are set to zero.

A detailed ship information database was purchased from IHS Markit (previously Lloyds Register). These data provide accurate and detailed information on each ship that operated in Queensland waters in 2015.

The final result is a database with complete time-series information for each individual ship journey, containing ship characteristics and speed (one-minute time steps) in Queensland port areas in 2015. Journeys include all operating modes for ships: berth, anchor, manoeuvring and transit. Visualisation examples of processed AIS data are shown later in the paper (Figure 3 and 4).

Ship fuel use and emission modelling

A new ship (exhaust) emissions model has been built for the research objective. It is based on extensive review of published research, as well as collection of available data. The model first estimates fuel consumption by marine fuel type (three classes) and ship type (ten classes) at a high resolution, and then uses fuel-based emission factors (g/kg fuel) to estimate emissions for a broad range of pollutants.

Ship classification

The main ship types considered in the model are:

- 'bulk carrier'
- 'container'
- 'cruise ship'
- 'general cargo'
- 'reefer'
- 'roro' (roll-on-roll-off)
- 'tanker (oil)'
- 'tanker (other)'
- 'vehicle carrier'
- 'other'

Ship engine type is broadly defined as:

- Main engine ('ME'), auxiliary engine ('AE') and boiler ('BL').
- Slow speed ('SS'), medium speed ('MS') and high speed ('HS') diesel engines, or gas/steam turbines ('GAS'/'STM').
- International Convention for the Prevention of Pollution from Ships (MARPOL) Annex VI NO_x emission certification limits, which relate to year of vessel construction, i.e. 'pre-control' (< 2000), 'Tier I' (2000-2010) and 'Tier II' (2011+).

Regarding fuel type, marine fuel oils can be split into numerous categories based on e.g. their origin and viscosity. For the model they are classified as follows:

- 'RO' – (intermediate) residual fuel oil (50-810 centistokes, 0.5-5.0% sulphur).
- 'MD' – marine distillates, which can be further classified into marine diesel oil ('MDO', 5.5-50 centistokes, typically 1.0% and maximum 2.0% sulphur) and marine gas oil ('MGO', 1-5.5 centistokes, typically 0.1-0.5% and maximum 1.5% sulphur).
- 'ULSD' – ultra-low sulphur diesel (typically 10 ppm S).

The different classes of main ship type, engine type and fuel type lead to a large number of combinations, and therefore create a high level of model complexity. However, certain combinations will dominate ship activity. For instance, large ships are primarily powered by diesel propulsion systems and are usually fuelled by residual oil (RO).

RO is a low-grade fuel that includes high concentrations of impurities such as sulphur, ash, asphaltenes, and metals. Marine distillate oils (MD) are more refined fuels, but due to their higher cost, they are generally only used for small, medium-speed diesel engines, such as auxiliary engines for port activities, and for main engines when manoeuvring in harbour areas.

The main engines that propel moving ships are primarily powered by slow (SS, 2-stroke, typically GT ≥ 2500 and ≤ 150 RPM) and medium speed diesel (MS, four-stroke, typically GT < 2500 and 150-1000 RPM) engines that combust residual oil (RO) or marine distillate (MD). High-speed diesel (HS, 4 typically GT < 2500 and ≥ 1000 RPM) engines are primarily used on smaller vessels. Other engine configurations exist, such as liquefied natural gas (LNG) powered vessels, steam turbines and gas turbines although their numbers are significantly lower.

Fuel use algorithms

Apart from some cases where power cables from land-based sources are connected and used on-board vessels in port, ships are generally self-sufficient regarding energy supply. The majority of large ships shut down their main engines when in port, only relying on their auxiliary engines/boilers for necessary on-board electric power and heat (steam) production. Electric power is typically used for cargo refrigeration, air conditioning, cranes and control systems on-board, while steam is used for heating fuel oil, running cargo pumps, tank cleaning and for heating accommodation units.

Different ship types have different ways of using their engines/boilers, especially during harbour visits. Electricity requirements vary depending on the type of the ship. The energy demand of a large cruise ship with more than a thousand air-conditioned cabins is considerably different from that of a bulk carrier. On the other hand, crude oil tankers typically have large boiler systems for warming their cargo, and all ships using fuel oil have some boiler capacity for heating their fuel to obtain desired viscosity.

Fuel use is dependent on actual power demand on-board a ship. However, real world power requirement on-board a ship can vary substantially and power demand is therefore difficult to quantify

accurately. In essence, there is no generic and simple relationship between the actual on-board power demand delivered by the different combustion systems and other variables (e.g. vessel speed), that would be accurate for individual ships at all times of operation.

However, for ship emission modelling in (several) large areas and over long periods of time (year) a reasonable and feasible approach is required. Following earlier work by other researchers (e.g. Georgakaki et al., 2005; Hulskotte and Denier van der Gon, 2010), generic empirical relationships, were used in this work. The use of generic relationships for shipping fleets in a large (port) areas over a long period of time is warranted as it is expected that prediction errors for individual vessels will tend to offset each other and average out, leading to robust and relatively accurate emission predictions.

As will be discussed later, a ship energy-balance approach was used to calibrate and expand published empirical functions to better reflect the shipping fleet operating in Queensland waters. As an example, the model formulation is shown for two ship types:

Bulk Carrier

$$F_{ME,x} = 0.271 S^{0.524} \Delta d p_x (v/v_{ss})^3$$

$$F_{boiler} = 0.021 S \Delta t / (\tau \eta)$$

$$F_{AE1,x} = 0.012 S^{0.524} \Delta d p_x$$

$$F_{AE2,x} = (\psi 0.004 S \Delta t - F_{boiler}) p_x$$

where $\psi = 3.262 (\tau \eta 0.004 S \Delta t)^{-0.345}$

Cruise ship:

$$F_{ME,x} = 0.257 S^{0.613} \Delta d p_x (v/v_{ss})^3$$

$$F_{boiler} = 0.014 P \Delta t / (\tau \eta)$$

$$F_{AE,x} = 4 P \Delta t p_x / (\tau \eta), \dots \text{for } P \leq 2000$$

$$F_{AE,x} = (22 - 2.3 \text{LN}(P)) P \Delta t p_x / (\tau \eta), \dots \text{for } P > 2000$$

$F_{ME,x}$ = main engine fuel consumption for machinery/fuel type x (kg)

$F_{AE,x}$ = auxiliary engine fuel consumption for machinery/fuel type x (kg)

$F_{AE1,x}$ = auxiliary engine fuel consumption in transit conditions for machinery/fuel type x (kg)

$F_{AE2,x}$ = auxiliary engine fuel consumption (non-transit) for machinery/fuel type x (kg)

F_{boiler} = auxiliary boiler fuel consumption (kg)

S = vessel size or volume, expressed as (unit-less) gross tonnage (GT)

P = passenger capacity (number of passengers)

v = actual (average) vessel speed (km/h)

v_{ss} = vessel service speed (km/h)

Δd = total distance traversed by the ship (km)

Δt = time resolution (h)

η = boiler thermal efficiency (-)

τ = fuel specific lower heating value (MJ/kg)

p_x = proportion of total fuel used by machinery/fuel type x (-)

Full parameterisation of the fuel models for all ship types can be found in DES (2019). These fuel algorithms aim to capture typical fuel consumption rates for different ship classes in four modes of operation, 'transit', 'manoeuvring', 'berth' and 'anchor'. Fuel rates for moving ships in transit are simulated as a function of ship class, ship size, service speed and actual vessel speed. The predicted fuel rates are expected to be average or typical values, but real world variation will occur, as was discussed before. For instance, weather and sea conditions can significantly alter the power demand in the main engine propulsion system.

The fuel consumption for boilers is dependent on the heat demand on these various systems, and whether the main engine is running (waste heat recovery). The fuel consumption by auxiliary engines and boilers is not dependent on ship movement, but rather on the operational status of the ship (i.e. loading/unloading, operation of cranes, etc.). It is assumed that auxiliary boilers are not in use during transit because (main engine) waste heat boilers are used instead.



Figure 2: 70,285 GT cruise ship leaving Brisbane.

Short-term peaks in power demand are often encountered when bow and stern thrusters are operated during departure from or arrival at a port. Engine loads can change rapidly during manoeuvring operations. Fuel use in manoeuvring conditions are therefore modelled separately.

Fuel rates for stationary ships are simulated as function of e.g. ship class and ship size. Once in port, power requirements for ships are usually less, but can still vary depending on the type of ship activity, e.g. hoteling (berth), cargo refrigeration, and in particular, for self-unloaders, which require energy for loading operations (cargo pumps, cranes). Auxiliary engines are usually used for electric power production, while the main engines are shut down, and the boiler generates steam. The main engine is not used when ships are at berth or at anchorage, except for diesel-electric ships, where main engines may be used to generate auxiliary power.

Cruise ships can be diesel-electric and have relatively high electrical loads to supply passenger needs. For simplicity, it is assumed that cruise ship energy demand can be simulated with the generic fuel algorithms used in this study. However, it is acknowledged that the need for more specific algorithms for cruise ships needs to be explored further. The same can be said for smaller ship types such as tugs, ferries, yachts and dredges. Further research, including collection and analysis of real-world fuel consumption data, for these smaller vessels and possible modification of the generic fuel algorithms is recommended.

Ship energy balance - calibration

A ship energy-balance approach was used to calibrate the fuel algorithms, discussed before, to better reflect the shipping fleet operating in Queensland waters. First, plausible ranges in ship energy use were defined. The IHS database reports Maximum Continuous Rating (MCR) for each ship, which is equivalent to maximum installed engine power. It also reports service speed, which is defined as the speed that the ship is capable of maintaining at sea in normal weather conditions, and at normal service draught. Ships travelling at service speed typically use 80-90% of MCR. This is the first verification point in the energy balance.

Second, plausible ranges of auxiliary engine power were developed using literature review and analysis of the IHS database. The ratios of installed auxiliary engine power to MCR were computed for all ships and plausible ranges were defined as the 10 and 90-percentile values for each ship class. Subsequently these minimum and maximum ratio values were multiplied with reported ranges of auxiliary load factors for different modes of operation.

Subsequently, a typical ship speed-time profile (75 hours), including all four modes of operation (cruising, manoeuvring, berth, anchor), was used to calculate minute-by-minute energy use for individual ships (5,510 vessels in total).

Estimated fuel use (kg/min) was then converted to energy use (kW) using information on the fuel type, lower heating value (LHV, MJ/kg fuel) and engine and fuel type dependent thermal efficiency. Figure 3 shows an example of energy plots constructed for a specific container ship built in 2004 with a direct-drive slow-speed diesel engine, about 53,000 GT, a length of 294m and a service speed of 44 km/h.

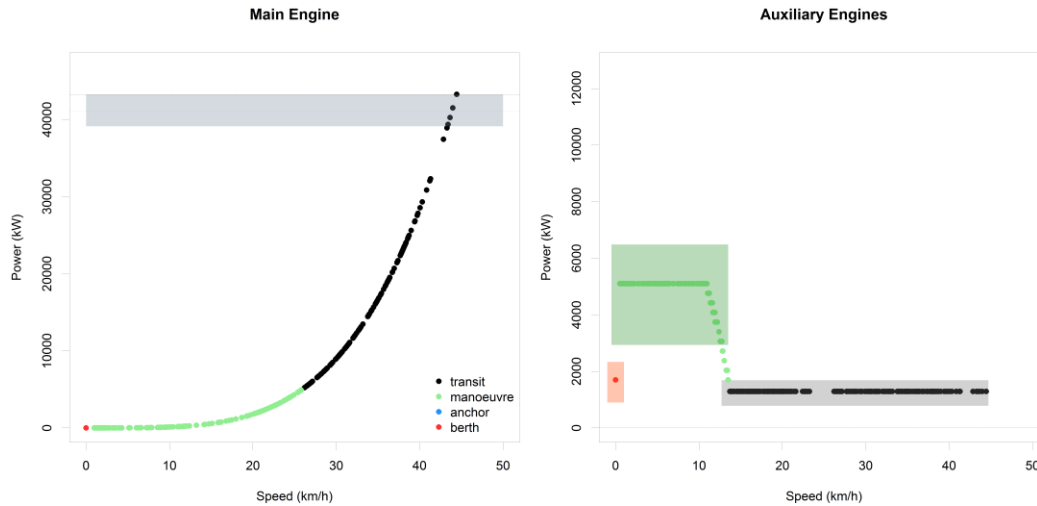


Figure 3: Energy plots for main and auxiliary engines.

The plots show the plausible energy power ranges for specific conditions and for the three engine types. The simulated energy use by the main engine (left plot) at service speed is 5% higher than the average energy use derived from the IHS Markit data. The grey shaded area shows the plausible range of 80-90% of MCR. The simulated energy use falls just outside the plausible range for this vessel. It can be seen that simulated auxiliary engine power (right plot) in transit conditions (grey shaded area), in manoeuvring conditions (green shaded area) and in berth conditions (red shaded area) all fall within the expected and plausible ranges. Note that anchor and berth conditions are assumed to have equivalent auxiliary energy use for this vessel.

Similar plots and associated statistics were computed for all 5,510 vessels for which IHS Markit data are available. An example of the step-wise calibration procedure is shown in Figure 4 for 258 container ships.

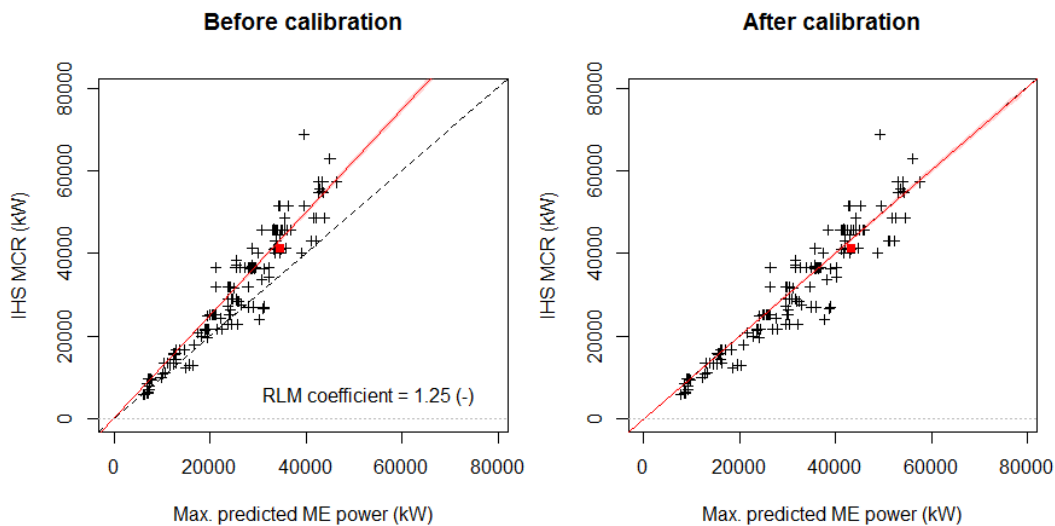


Figure 4: Calibration of main engine fuel algorithm for container ships.

The left plot shows the reported and predicted engine power at service speed. The red square data point reflects the specific container ship that was previously discussed. The initial model parameters appear to generally underestimate main engine power for the fleet of container ships in Queensland waters. A robust linear regression model (RLM) was fitted to estimate a calibration factor for predicted power. In this case, the calibration factor is computed to be 1.25 and used to adjust model parameter values. The result for the calibrated model is shown in the scatter plot on the right. A similar approach was used to adjust the model parameters for other engine types and operating conditions. The calibration procedure is described in detail in DES (2019).

Emission algorithms

An extensive review of published research reports and scientific papers was used to create a set of fuel-based emission factors (g of pollutant per kg of fuel burned) for relevant air pollutants and greenhouse gases. For instance, trace heavy metal content in ship PM emissions is significant. Specific heavy metals such as vanadium, nickel and iron have been reported to be particularly prominent in ship exhaust. Celo et al. (2015) reported a total metal content in PM_{2.5} in the range of 1-4 mass%. Indeed, vanadium concentrations and vanadium-to-nickel ratios have been used to assess and attribute ship emission impacts to local air quality (e.g. Coggon et al., 2012; Zhang et al., 2014). Significant emissions of polycyclic aromatic hydrocarbons (PAHs) from ships, and substantially elevated local concentrations close to ship activity, has attracted research attention (e.g. Moldanova et al., 2010; Pongpiachan et al., 2015). Significant carbonyl emissions have also been reported (Agrawal et al., 2008).

Emission factors, expressed as grams of pollutant per kg of fuel, were generated for a range of pollutants and greenhouse gases, i.e. CO₂, NO_x, SO₂, PM₁₀, PM_{2.5}, VOCs, CH₄, N₂O, Pb, As, Ni, V, Mn, Cd, PAHs (sum), benzo(a)pyrene, 1,3-butadiene, benzene, formaldehyde, toluene, xylenes and ethylbenzene. The emission factor values are a function of engine system (ME, AE, BL), engine type (SS, MS, HS, GAS, STEAM), fuel type (RO, MD, ULSD) and MARPOL Annex VI emission certification limit (NO_x only).

These emission factors are combined with estimates of fuel consumption for each minute of individual ship activity. This is done for all ships that operate in a particular port area in a year and emissions are aggregated to give total emission loads. Total emission loads are aggregated at grid cell level and calculated for each hour of the year.

Results

Figure 5 shows the 14 ports for which fuel consumption and emissions were calculated. The emission estimates are based on detailed ship activity data, i.e. minute-by-minute fuel and emissions estimates for each individual in all port areas over a full year (2015).

In order to analyse the modelling results, minute-by-minute emission predictions for individual ships have been aggregated to 1 × 1 km grid cells within the port areas and allocated to each hour of the year.

Some examples of gridded emission are shown in Figures 6-9. It is noted that DES (2019) provides these maps for all 14 Queensland ports. Major routes followed by vessel entering, leaving or passing by ports clearly visible. In general, some ports have significant passing traffic, with vessels that neither anchor nor berth at port but whose emissions are within the emission modelling area. This is the case for e.g. Port of Brisbane, with substantial shipping traffic east of Moreton and Stradbroke Islands. Likewise, Thursday Island experiences substantial ship activity in the northern part of the modelling area. Anchorage and berth areas are clearly discernible in Figure 6-9. For instance, red/orange cells indicate berth areas or anchorage areas where vessels remain stationary, while waiting for the authorisation to berth.



Figure 5: Queensland Ports selected for emission modelling.

and
ship
are

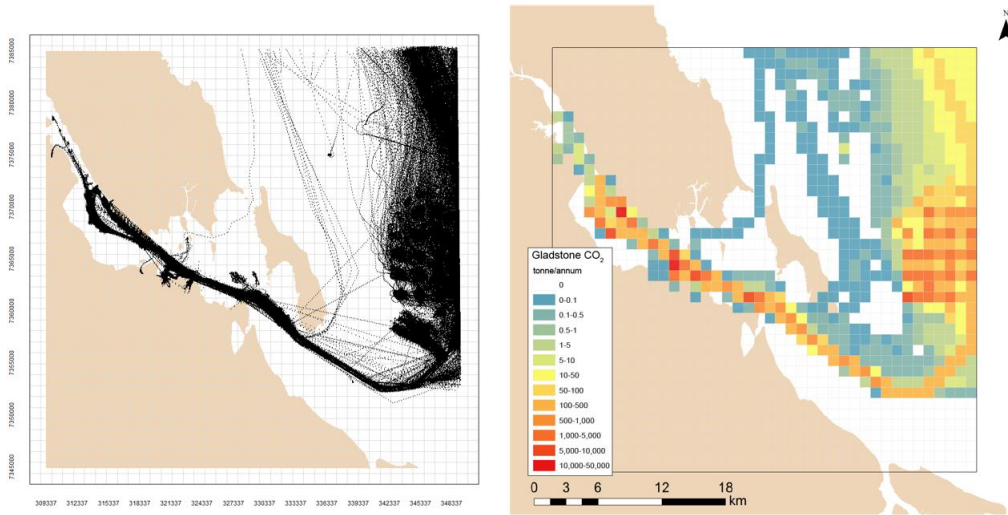


Figure 6: Gladstone – AIS data visualisation (left) and gridded CO₂ emissions (right).

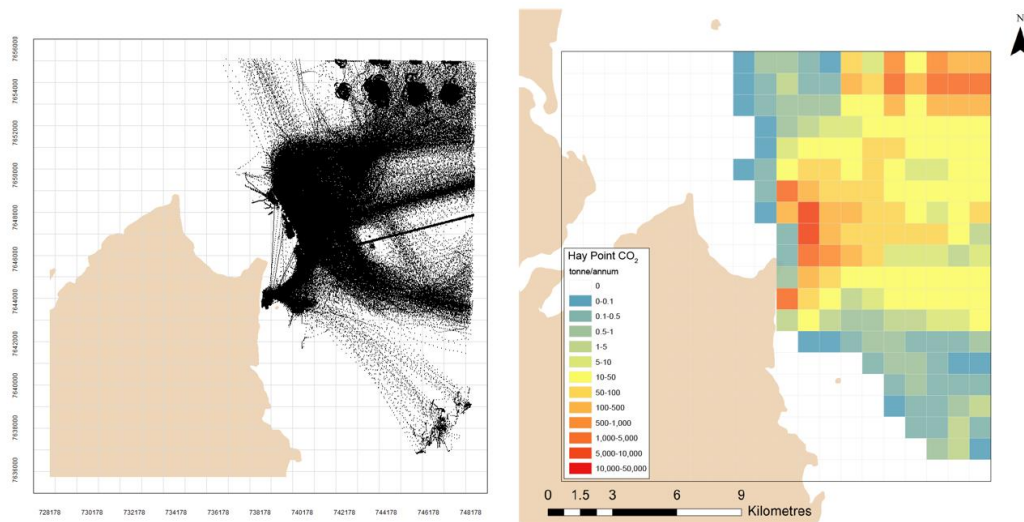


Figure 7: Hay Point – AIS data visualisation (left) and gridded CO₂ emissions (right).

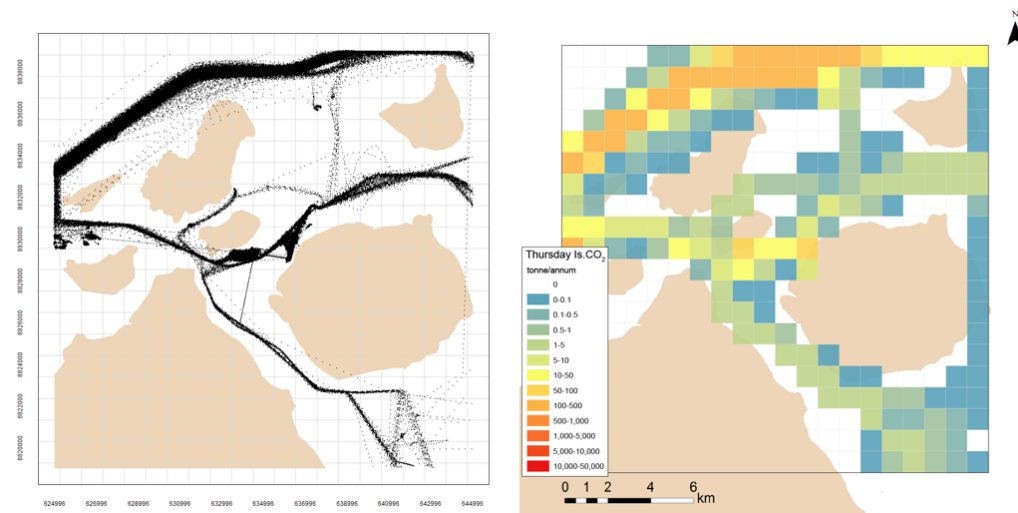


Figure 8: Thursday Island – AIS data visualisation (left) and gridded CO₂ emissions (right).

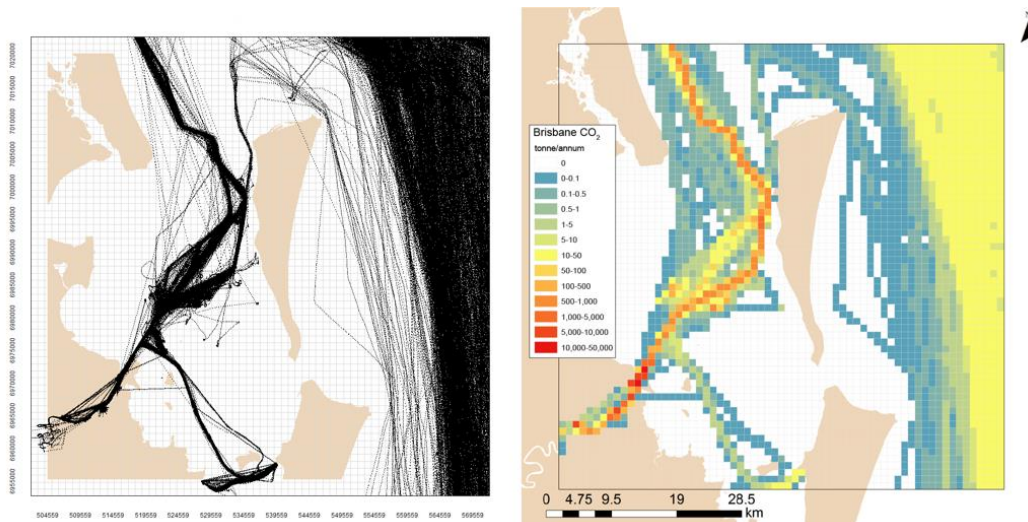


Figure 9: Port of Brisbane – AIS data visualisation (left) and gridded CO₂ emissions (right).

Table 1 presents total emission estimates for a range of selected pollutants and for the fourteen port areas. CO₂ emissions are a good proxy variable for total fuel use. Table 1 shows that Gladstone accounts for approximately 40% of total emissions (with slight variations by pollutant), followed by Port of Brisbane with about 35%, Hay Point with about 10%, and Abbot Point and Townsville both with about 5%.

Table 1: Total emissions by port and by pollutant

Port	CO ₂ (tonne)	NO _x (tonne)	SO ₂ (tonne)	PM ₁₀ (tonne)	PM _{2.5} (tonne)	CO (tonne)	VOCs (tonne)	PAHs (tonne)	B(a)P (kg)	Ni (kg)	V (kg)
APT	23,664	372	247	31	28	30	11	121	8	263	616
BND	577	10	7	1	1	1	0	3	0	7	15
CRN	15,196	310	214	31	29	23	9	138	12	185	422
CFL	8,379	197	131	17	16	9	4	56	5	103	231
GLD	198,421	3,385	2,605	345	317	273	102	1,457	116	2,708	6,357
HPT	42,086	649	505	60	55	51	20	224	16	569	1,344
LUC	451	7	5	1	1	1	0	2	0	5	12
MKY	8,447	144	110	13	12	11	4	45	3	109	252
MRN	544	10	6	1	1	1	0	3	0	6	13
POB	155,270	3,042	2,253	303	279	207	84	1,245	103	2,123	4,932
RKH	786	14	11	1	1	1	0	4	0	11	25
THI	7,439	173	115	16	15	9	4	58	5	91	204
TWN	29,426	503	372	45	41	38	15	163	13	368	855
WEI	12,027	194	121	15	14	15	6	63	4	126	293
TOTAL	502,716	9,011	6,702	880	809	668	260	3,585	285	6,672	15,571

APT = Abbot Point, BND = Bundaberg, CRN = Cairns, CFL = Cape Flattery, GLD = Gladstone, HPT = Hay Point, LUC = Lucinda, MKY = Mackay, MRN = Mourilyan, POB = Port of Brisbane, RKH = Rockhampton (Port Alma), THI = Thursday Island, TWN = Townsville, WEI = Weipa.

However, these proportions do not reflect the different sea surface areas within the modelled port areas, which vary from about 200 km² (Mourilyan) to 3,300 km² (Port of Brisbane). Normalising for sea surface area shows a different picture, and produces the following ranking in terms of the average 'emission intensity', which is expressed as tonne CO₂ per km² per year.

- Gladstone: 226 tonne CO₂/km².annum
- Hay Point: 152 tonne CO₂/km².annum
- Port of Brisbane: 47 tonne CO₂/km².annum
- Weipa: 42 tonne CO₂/km².annum
- Cairns: 35 tonne CO₂/km².annum
- Mackay: 34 tonne CO₂/km².annum

- Thursday Island: 32 tonne CO₂/km².annum
- Townsville: 32 tonne CO₂/km².annum
- Cape Flattery: 27 tonne CO₂/km².annum
- Abbot Point: 24 tonne CO₂/km².annum
- Other ports : < 3 tonne CO₂/km².annum

Further analysis of the shipping activity and emissions data shows that most of the vessels operating in and around Queensland ports are classified as bulk carriers (63%), tankers (13%) and container ships (6%).

The contribution to total emissions roughly follows the proportions of different ship classes in the Queensland shipping fleet, but variations do occur due to differences in the distributions of vessel size, year of manufacture, fuel mix, and actual operating conditions. The contribution of bulk carriers to total emissions is therefore lower than the proportion in the fleet (63%) and varies between approximately 30-45%. In contrast, the contributions of container ships and tankers is higher than would be expected based on the fleet proportions: approximately 10-15% (fleet percentage of 6%) and 20-30% (fleet percentage of 8%), respectively.

Air quality impact assessment

A preliminary assessment of local air quality impacts by ships was conducted for the Australian port areas. Modelled pollutant concentrations (µg/m³) were compared with Australian air quality objectives. Contributions to local air concentrations up to 10% of the objective were found for 11 pollutants. Several of these pollutants are (possibly) carcinogenic and there is no safe threshold concentration level. Contributions to local air concentrations up to 50% of the objectives were found for SO₂, NO₂, vanadium, nickel, PM_{2.5}, PM₁₀, whereas a higher contribution was found for benzo(a)pyrene. For a more detailed discussion of methods and analysis, the reader is referred to DES (2019).

Conclusion and next steps

This paper presents the results of ship emission modelling, both greenhouse gas emissions and air pollutant emissions, for 14 ports in Queensland. The information is useful to identify ports with a relatively high emission intensity and prioritise possible emission mitigation/reduction actions. The data are available at a very high spatial and temporal (minute-by-minute) resolution, and can be used for e.g. detailed air quality impact (scenario) modelling (e.g. impacts of reduced maximum sulfur content in 2020, impacts of shore power, impacts of emission control technology such as scrubbers and SCR), or for detailed analysis of fleet impacts (e.g. type or age of ships vs. emissions).

The next step and focus of the work is validation of the ship fuel/emission algorithms. This will be achieved through different research programs and partnerships with Australian universities. First, the fuel and emission predictions will be compared with on-board emission measurements for two vessels on different port-to-port trips in Queensland. Second, a measurement program is being rolled out that specifically measures local air quality impacts of ships in the Brisbane port area using a dedicated air monitoring station, and will likely combine this with brief measurement campaigns using UAV (drone) emission measurements and on-board fuel surveys.

References

- Agrawal, H., Welch, W.A., Miller, J.W., Cocker, D.R. (2008). Emission measurements from a crude oil tanker at sea, *Environ. Sci. Technol.*, 42, 7098-7103.
- Celo, V., Dabek-Zlotorzynska, E., McCurdy, M. (2015). Chemical characterization of exhaust emissions from selected Canadian marine vessels: The case of trace metals and lanthanoids, *Environ. Sci. Technol.*, 49 (8), 5220-5226.
- Coggon, M.M., Sorooshian, A., Wang, Z., Metcalf, A.R., Frossard, A.A., Lin, J.J., Craven, J.S., Nenes, A., Jonsson, H.H., Russell, L.M., Flagan, R.C., Seinfeld, J.H. (2012). Ship impacts on the marine atmosphere: Insights into the contribution of shipping emissions to the properties of marine aerosol and clouds, *Atmospheric Chemistry and Physics*, 12 (18), 8439-8458.

Corbett, J.J., Winebrake, J.J., Green, E.H., Kasibhatla, P., Eyring, V., Lauer, A. (2007). Mortality from ship emissions: a global assessment, *Environ. Sci. Technol.*, 41, 8512–8518.

DES (2019). *Simulation and Assessment of Shipping Fuel Consumption and Emissions and their Local Air Quality Impacts – 15 Queensland Strategic Ports*, Queensland Government, Department of Science and Environment, Brisbane.

EEA (2013). *The Impact of International Shipping on European Air Quality and Climate Forcing*, European Environment Agency, Technical report No. 4/2013.

Georgakaki, A., Coffey, R.A., Lock, G., Sorenson, S.C. (2005). Transport and Environment Database System (TRENDS): maritime air pollutant emission modelling, *Atmospheric Environment*, 39, 2357-2365.

Hulskotte, J.H.J., Denier van der Gon, H.A.C. (2010). Fuel consumption and associated emissions from seagoing ships at berth derived from an on-board survey, *Atmospheric Environment*, 44, 1229-1236.

Moldanová, J., Fridell, E., Popovicheva, O., Demirdjian, B., Tishkova, V., Faccineto, A., Focsa, C. (2010). Characterisation of particulate matter and gaseous emissions from a large ship diesel engine, *Atmospheric Environment*, 43, 2632-2641.

Velleman, P.F. (1980). Definition and Comparison of Robust Nonlinear Data Smoothing Algorithms, *Journal of the American Statistical Association*, 75 (371), 609-615.

Zhang, F., Chen, Y., Tian, C., Wang, X., Huang, G., Fang, Y., Zong, Z. (2014). Identification and quantification of shipping emissions in Bohai Rim, China, *Science of the Total Environment*, 497, 570-577.

2.2.3 Current and future impacts of ship emissions on air quality and human health in the urban area of Gothenburg

Martin Otto Paul Ramacher^{1*}, Lin Tang², Volker Matthias¹, Jana Moldanova²

¹ Chemistry Transport Modelling, Helmholtz-Zentrum Geesthacht, 21502, Geesthacht, Germany, martin.ramacher@hzg.de

² IVL, Swedish Environmental Research Institute, P.O. Box 530 21, 40014 Gothenburg, Sweden

Shipping & Urban Air Quality

Shipping is an important source of air pollutants, from the global to the local scale. Nearly 70% of ship emissions occur within 400 km of coastlines (Endresen, 2003), causing air quality problems through emissions of SO_x, NO_x and particulate matter (PM). An increase in ship activity in the North Sea and the Baltic Sea has resulted in higher emissions of air pollutants, and subsequently air concentrations, in particular of NO_x, especially in and around several major ports (Matthias et al. 2016, Jonson et al. 2015). To face rising NO_x emissions, the International Maritime Organization (IMO) has designated the North Sea and Baltic Sea as NO_x Emission Control Area (NECA) starting from January 1, 2021 onwards. The NECA regulation applies to all vessels built after 2021 and requires 80% NO_x emission reductions. Due to the long lifetime of ships, it will take at least 30 years after the NECA entry until the entire ship fleet will be renewed (Kalli et al., 2013).

In the framework of the BONUS SHEBA project, the impact of current and scenario emissions from ships on air quality has been investigated on a range of scales with several chemistry-transport models (CTM): from a European domain to city-scale simulations of several harbor cities. Here, we present the contribution of regional and local shipping to concentrations of NO₂ and PM_{2.5} as well as the connected human exposure and the associated health impacts for 2012 and 2040 under several emission scenarios in the Gothenburg urban area.

Urban Air Quality Simulations

To investigate the current and future states of shipping-related urban air pollution, air quality simulations with The Air Pollution Model (TAPM, Hurley et al. 2005) under different future emission scenarios for the Gothenburg urban area were run. Both, current and future simulations used meteorological fields for the year 2012 with regional and local emission data for the years 2012 and 2040. For shipping emissions, data from the STEAM model (Jalkanen et al, 2009) was used to represent emissions to air for 2012 and for future scenarios in 2040. For non-shipping emissions in 2040 scaling factors, derived from GAINS/ECLIPSE have been applied. Thus, the boundary conditions in the local model runs were taken from corresponding regional-scale simulations to integrate background concentrations.

We developed four future scenarios for local shipping, which take into account different technological developments and pollutant regulations. The first scenario is the business as usual (BAU2040) scenario. It is based on current trends of economic growth and shipping and takes into account all of the already decided emission and efficiency regulations (e.g. NECA established in 2021). The second scenario is the EEDI2040 scenario. In the EEDI2040 scenario, improvements of fuel efficiency follow strictly the requirements of the EEDI (Energy Efficiency Design Index) regulation of the International Maritime Organization. Annual efficiency increases of 0.65 % to 1.04 %, depending on ship type, are assumed in the EEDI scenario while the corresponding values in the BAU scenario are 1.3 % to 2.25 %. From the difference between BAU and EEDI the effect of the higher fuel efficiency increase than required by the EEDI regulation, needed to meet the EU White Paper on Transport goal for 2040, can be deduced. Scenarios three and four are based on BAU2040 and EEDI2040 but additionally take into account land-powered electricity for ships in the port of Gothenburg (BAU2040LP & EEDI2040LP).

All future scenarios 2040 were simulated and compared to modelled concentrations of NO₂ and PM_{2.5} in 2012. Based on the simulations, exposure to PM_{2.5} and NO₂ was calculated using population counts on 1 km resolution and health impacts were calculated using the Alpha Risk Poll (ARP) model (Holland et al., 2013).

Shipping Contributions in 2040

Spatial maps of concentrations and population exposure related to shipping for NO_2 and $\text{PM}_{2.5}$ were created and show significant contributions of shipping related concentrations to the total air quality in all 2040 scenarios (Figure 1). Higher concentrations and contributions are detected in and around the port area, while there are some minor impacts in the Northern urban area of Gothenburg due to predominant winds from Southwest. The maximum value for NO_2 in summer 2040 merely reaches 0.8 ppb in the port area and is compared to a maximum of 4.1 ppb in 2012 about 80% lower. The relative contribution of shipping as an average for summer in the research domain changed from 18% to less than 1%. Nevertheless, in the port area of Gothenburg there are still contributions of up to 20%. The particulate pollutant $\text{PM}_{2.5}$ show similar reduction patterns for the change in concentrations in the 2040BAU scenario. The huge reductions in $\text{PM}_{2.5}$ (-85%) emissions are consequently leading to a reduced impact of shipping in 2040. While the contribution of $\text{PM}_{2.5}$ from local ship emissions is relatively low in 2012 summer conditions (maximum of $0.9 \mu\text{g}/\text{m}^3$ in the western port area), the contribution in the BAU2040 scenario is even lower (maximum of $0.15 \mu\text{g}/\text{m}^3$ in the western port area). Nevertheless, the regional impact of shipping for $\text{PM}_{2.5}$ is not shown here, but has to be proven of higher importance for $\text{PM}_{2.5}$ in the Gothenburg area. In sum, the particulate pollution levels due to shipping in the BAU2040 scenario reflect the emission reductions with very low concentrations.

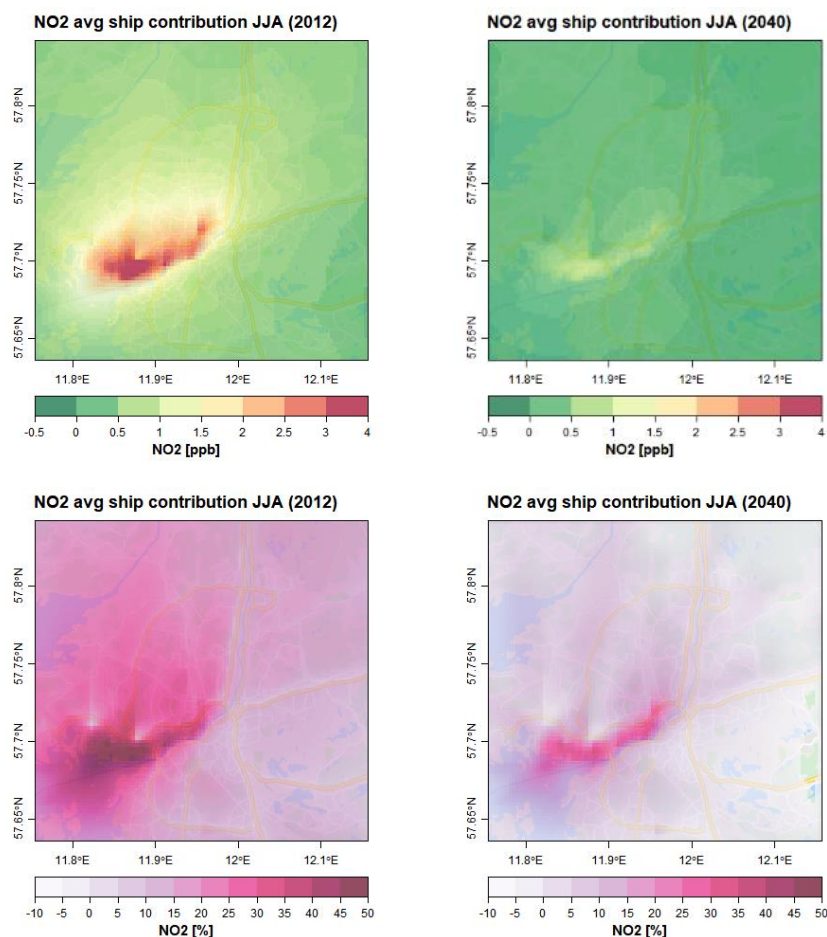


Figure 1: Absolute ship contributions in 2012 and the BAU2040 scenario, as well as relative contributions to NO_2 concentrations.

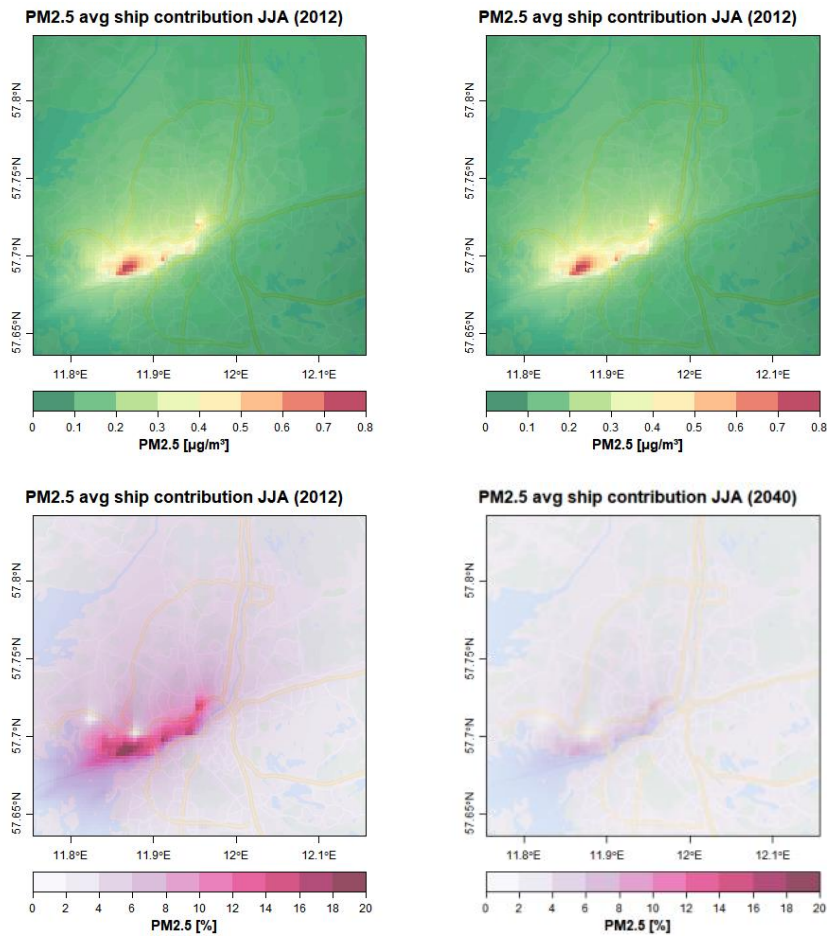


Figure 2: Absolute ship contributions in 2012 and the BAU2040 scenario, as well as relative contributions to PM_{2.5} concentrations.

It has been shown that the contribution of shipping in the BAU2040 scenario is generally focussing on the port area of Gothenburg and shows high reduction potentials for all pollutants in comparison with the present day situation in 2012. Nevertheless, the BAU2040 scenario is only one possible pathway to a future air quality situation and contains all preferable and available developments. Therefore, we present the differences in NO₂ and PM_{2.5} concentrations to the scenarios BAU2040LP, EEDI2040 and EEDI2040LP to demonstrate a pathway for less strict implementations of regional regulations and local port measures in form of onshore electricity in the port of Gothenburg. All changes in concentrations due to the scenarios are compared with the future reference scenario BAU2040 and displayed as relative change in Table 1.

The EEDI2040 scenario results, shows up to 40% higher NO₂ emissions in the port area of Gothenburg but also beyond the city boundaries, while in the city centre and close to major roads the changes compared to BAU2040 are relatively lower but still higher than in the BAU2040 scenario. This is due to the effect of regional boundary conditions, which are taking into account the regional effects of the EEDI2040 scenario. The same trend is visible for PM_{2.5} but with much lower relative changes of up to 4% in the port area, following the shipping routes.

In the results for both land-power scenarios, BAU2040LP and EEDI2040LP, the introduction of onshore electricity to avoid emissions in the port area is clearly visible for both scenarios. For NO₂, local concentration reductions in the port area with up to 30% and in the close and far surroundings areas of Gothenburg between 5% and 20% are identified, in comparison to BAU2040. For the EEDI2040LP there is a similar pattern, but due to the higher regional influence, a decrease in NO₂ concentrations happens only in the port area, while the nearby areas have more or less no change compared to BAU2040 and the outskirts and rural regions are clearly influenced by higher EEDI2040 regional concentrations. An introduction of onshore electricity with lower regional emission regulations can

reduce the emissions in the port and the nearby surroundings to concentration levels similar to BAU2040 reductions in the same region, but cannot reduce the concentration beyond the city core's boundaries.

The results for PM_{2.5} are coming with lower changes for all scenarios but with similar characteristics. In the EEDI scenario the local concentrations due to shipping rise about 4% in maximum in the port area about 1% near the harbour, about 2-3% in the region and not at all close to high industrial emission sources. In the onshore scenarios, the local reduction potential of PM_{2.5} is closely connected to port area, even more than for NO₂. The BAU2040LP shows additional to the regional BAU2040 influences, local reduction potentials of up to 6% in the port area but almost no difference anywhere outside the harbour. The same holds true for the EEDI2040LP scenario but with maximum additional reductions of up to 4% in the port.

Table1: Annually averaged grid mean concentrations and relative changes of NO₂ and PM_{2.5} for the future scenarios BAU2040LP, EEDI2040 and EEDI2040LP, compared the ship contributions in the 2040BAU scenario.

Pollutant	BAU2040		EEDI2040		BAU2040LP		EEDI2040LP	
	abs. avg.	rel. change	abs. avg.	rel. change	abs. avg.	rel. change	abs. avg.	rel. change
NO ₂ [ppb]	0.87	100%	1.12	+27.9%	0.78	-11.1%	0.97	+11.1%
PM _{2.5} [µg/m ³]	1.33	100%	1.36	+2.3%	1.32	-0.5%	1.35	+1.6%

Exposure and Health Effects due to Shipping in 2040

Based on the TAPM scenario simulations, exposure to PM_{2.5} and NO₂ was calculated using population counts on 1 km resolution obtained from Statistics Sweden (SCB) for 2015 (population 572,779 in the city of Gothenburg). The population data for 2015 were used since there are no dramatic changes in population density between 2012 and 2015. The gridded population (250 m × 250 m) was conducted by QGIS (2.18.19, 2017) software. Population weighted average concentrations (PWC) for the model domain were calculated by using share of the total population in each grid square as a weighing factor.

Table 1 shows population exposures to NO₂ and PM_{2.5} due to the shipping taking place in the area of Gothenburg in 2040 in the EEDI2040 scenario and changes in exposure due to large-scale introduction of shore-electricity. Exposures to emissions from local shipping in 2012 are shown for comparison. For the EEDI2040 scenario, the exposures shown in Table 1 represent less than 1% of the total exposure of population to PM_{2.5} and c.a. 20% to NO₂. The difference between these two exposure contributions comes both from the fact that contribution of local shipping to the total PM emission in the city is smaller than that of NO₂ (5.4% and 40%, respectively) and that contribution of background concentrations of PM_{2.5} to the exposure is higher comparing to that of NO₂. It is worth to note that the background contribution also includes pollution from regional scale shipping and that study conveyed for year 2012 have shown that for PM_{2.5} it exceeds the local shipping.

Table 2: Population weighted exposure in Gothenburg area in the different shipping scenarios for 2012 and 2040.

Population weighted exposure	NO ₂ (ppb × capita)	PM _{2.5} (µg/m ³ × capita)
Local shipping 2012	0.68	0.09
Local shipping 2040 EEDI	0.28	0.01
Shore-electricity BAU	-0.11	-0.01

In total, a very low impact of PM_{2.5} due to local shipping activities was simulated for the scenarios with and without land-powered shipping. For NO₂ the contribution of shipping related concentrations to the total air quality is significant within both scenarios (with and without OPS) in 2040, but shows a high reduction potential in the OPS scenario and benefits for the air quality in densely located areas.

Acknowledgements

This work is part of the BONUS SHEBA (Sustainable Shipping and Environment of the Baltic Sea region) research project under Call 2014-41. BONUS (Art 185) is funded jointly by the EU, Innovation Fund Denmark, Estonian Research Council, Academy of Finland, and by the German Federal Ministry of Education and Research under Grant Number 03F0720A, National Centre of Research and Development (Poland) and Swedish Environmental Protection Agency.

Copernicus Services is thanked for the public distribution of Urban Atlas, Corine Land Cover and population density products. We acknowledge ECMWF for ERA 5 synoptic reanalyses. The air quality model CMAQ is developed and maintained by the U.S. Environmental Protection Agency (US EPA). COSMO-CLM is the community model of the German climate research. The simulations with COSMO-CLM, CMAQ, EPISODE-CityChem and the exposure calculations were performed at the German Climate Computing Centre (DKRZ) within the project "Regional Atmospheric Modelling" (Project Id 0302).

References

- Endresen, Ø. (2003) *J. Geophys. Res.* 108(D17).
- Holland, M.R. et al. (2013). European Consortium for Modelling of Air Pollution and Climate Strategies, EC4MACS report.
- Hurley, P., Physick, W., and Luhar, A. (2005) *Environ. Modell. Softw.* 20, 737-752.
- Jalkanen, J.-P., Brink, A., Kalli, J., Petterson, H., Kukkonen, J., and Stipa, T. (2009) *Atmos. Chem. Phys.* 9, 9209-9223.
- Jonson, J., Jalkanen, J., Johansson, L., Gauss, M., and Denier van der Gon, (2015) *Atmos. Chem. Phys.* 15, 783-798.
- Kalli, J.; Jalkanen, J.-P.; Johansson, L. & Repka, S. (2013) *WMU Journal of Maritime Affairs* 12, 129-145
- Matthias, V., Aulinger, A., Backes, A., Bieser, J., Geyer, B., Quante, M., and Zeretzke, M. (2030) *Atmos. Chem. Phys.* 16, 759–776

2.2.4 The impact of port operations on air quality in Piraeus and the surrounding urban areas

G. Tsegas¹, N. Moussiopoulos^{1*}, L. Ntziachristos¹, E. Chourdakis¹ and M. Drakoulas²

¹ Laboratory of Heat Transfer and Environmental Engineering, Aristotle University of Thessaloniki, Thessaloniki, 54124, Greece, moussio@eng.auth.gr

² Department of Maritime and Transport Technology, Delft University of Technology, Delft, 2628CD, The Netherlands

Introduction

The dominant influence of shipping emissions on air quality of port cities and their surrounding urban areas has been demonstrated in a number of case studies, based on both assessment of monitoring data and the application of modelling tools. In the present work, the impact of marine traffic on air quality of Piraeus, Greece, and the neighbouring areas of the Athens urban agglomeration is assessed using chemical dispersion calculations. A comprehensive marine emissions inventory is compiled using a bottom-up methodology on the basis of AIS traffic data, as well as activity and source parameter data obtained from other national databases, covering both merchant and passenger traffic in the area. A set of dispersion calculations are performed using the MEMO/MARS-aero chemical dispersion model for the Attica region, revealing the dominating contribution of the port area on the pollutant levels over the southern part of the city of Piraeus. Assessment of a hypothetical scenario, involving the implementation of cold ironing for ships at berth, indicates that emissions in the hoteling phase are significantly reduced, resulting to a notable reduction of concentrations in the port and the surrounding areas.

Methodology and case setup

In the present work, chemical dispersion calculations are used for assessing the impact of plumes related to marine traffic under various emission and meteorological situations on the air quality of Piraeus, Greece and the neighbouring areas of the Athens megacity.

In the first part of the study, emissions from marine traffic are calculated for two distinct areas, corresponding to the main port area of Piraeus and the designated anchorage area in the Saronic gulf (Figure 1b). Exhaust emissions from passenger and cargo marine traffic are calculated for each individual vessel travelling or stationing inside these areas during the reference year 2015. For the calculation of emissions and emission factors, a bottom-up approach is used, following the guidelines of the EMEP/EEA 2016 guidebook (EEA, 2016). Exhaust emissions are aggregated separately for the cruise, manoeuvring, hoteling and loading/unloading phases, for both passenger and cargo traffic entering the two areas. Activity data are obtained by collecting traffic information in the two designated areas through the Automatic Identification System (AIS) database for the entire year 2015.

Following the Tier-3 approach as specified in the guidebook, separate emission factors can be calculated for the exhaust emissions of the main and auxiliary engines of each vessel according to the engine and fuel type and the operating phase (cruising, maneuvering, hoteling, loading/unloading).

For example, for the maneuvering phase:

$$E_{maneuvering}^i = T_{maneuvering} \cdot \sum_{j=M,A} (P_j \cdot LF_j \cdot EF_j^i \cdot \Pi_j)$$

where i is the pollutant index, j sums over the main and auxiliary engines, T is the maneuvering time, P is the nominal engine power, EF are the emission factors, LF is the charge factor and Π is the total engine duty cycle during the maneuvering phase. The total emissions aggregated for each of the two polygon areas are calculated as the sum of the partial emissions for each operating phase:

$$E_{trip} = E_{cruising} + E_{maneuvering} + E_{hotelling}$$

For the purposes of this calculation, detailed information about engine type and fuel are not usually available for each individual vessel, therefore this information is apportioned to the individual traffic categories (see first column in Table 1) on the basis of statistical data contained in the European Maritime Safety Agency (EMSA) Central Ship Database (URL1). In order to estimate the time spent by each vessel in every operating phase of the route, the total travelling time inside the two designated area polygons is apportioned according to the typical cruising speed, maneuvering time and time at berth for each of the above 9 vessel categories.

For quantifying the air quality impact of the marine traffic, dispersion calculations were performed in a nested grid configuration, covering the entire area of the Attica Peninsula (120 km coarse grid) in a resolution of 2 km, and the Greater Areas of Athens and Piraeus, including the port and anchorage polygon areas (50 km fine grid) in a resolution of 500 m. The non-hydrostatic meteorological model MEMO (Moussiopoulos *et al.*, 2012) and the Eulerian chemical dispersion model MARS-aero (Moussiopoulos *et al.*, 2010) were used to calculate concentrations of O₃, NO₂, PM₁₀ and PM_{2.5}, following a meteorological classification scheme that uses eight representative days to compose the annual average concentration fields.

Table 1: Calculated exhaust emission factors and specific fuel consumption of the main engine, aggregated per vessel category.

Ship Type	Cruise				Maneuvering / Hoteling			
	Emission Factors (g/kWh)			Specific fuel consumption (g fuel/kWh)	Emission Factors (g/kWh)			Specific fuel consumption (g fuel/kWh)
	NO _x	NM VOC	PM ₁₀		NO _x	NMVO C	PM ₁₀	
liquid bulk	15.86	0.57	1.44	199.18	12.68	1.71	2.33	219.40
dry bulk carrier	16.58	0.59	1.62	196.33	13.24	1.78	2.38	216.40
container	16.66	0.59	1.63	195.91	13.31	1.78	2.38	215.95
general cargo	14.60	0.53	1.13	203.67	11.67	1.59	2.20	224.09
ro ro cargo	13.42	0.49	0.88	209.56	10.70	1.47	2.12	230.39
passenger	12.41	0.46	0.73	218.13	9.80	1.38	2.14	239.72
fishing	12.20	0.46	0.32	203.38	9.80	1.39	0.96	223.42
Tugs	11.74	0.34	0.33	203.92	9.38	1.01	1.00	224.01
others	13.60	0.47	0.83	203.30	10.88	1.41	1.69	223.57

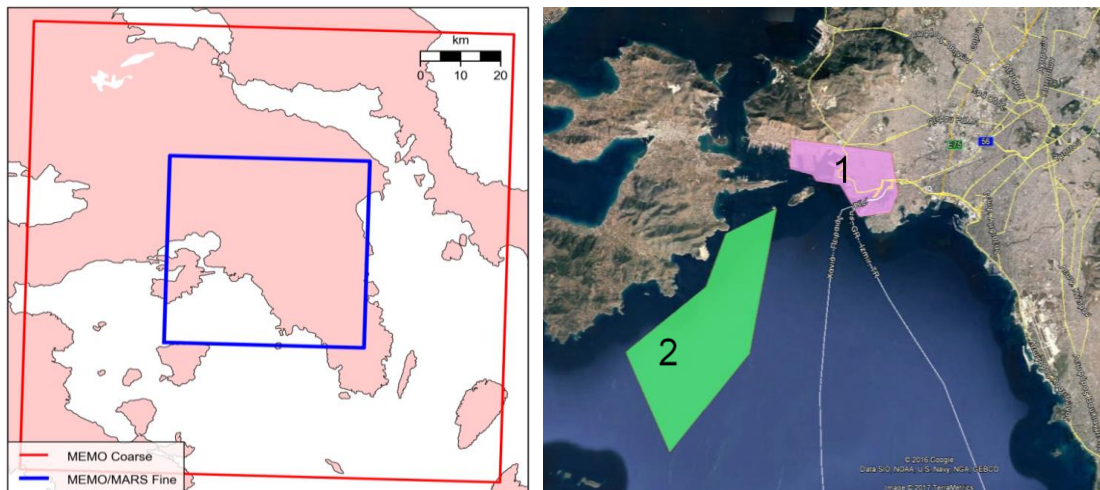


Figure 1: Coarse and fine computational grid used in the dispersion simulations (left) and locations of the designated port (1) and anchorage (2) areas (right) for the Piraeus study

In order to quantify the impact of marine emissions, a zero-out scheme is implemented, whereby dispersion calculations are repeated for an additional baseline scenario that excludes marine traffic. Baseline emissions for the rest of the activities in the Attica region were based on a localized emissions inventory for 2008, previously compiled in the framework of the TRANSPHORM project (Kuenen *et al.*, 2011) and updated for 2015 using appropriate scaling factors.

The monthly variation of total emissions from marine traffic, for the reference year 2015, is shown in Figure 2 (a). The primary trend of increased emissions during the summer period is to be expected in correlation to increased passenger traffic during the vacation season. Nevertheless, an unusual secondary emissions peak appears in the fall of 2015. By examining the contribution of different traffic sectors, it appears that the main contribution to this peak comes from increased cruise ship traffic that has been rerouted to the port of Piraeus due to the terrorist attacks in Istanbul on 10/10/2015. In Figure 2 (b), the distribution of total NO_x emissions over different ship categories is shown. The major contribution comes from passenger traffic (including cruise ships) followed by container ships, the two sectors accounting for over 90% of the emissions.

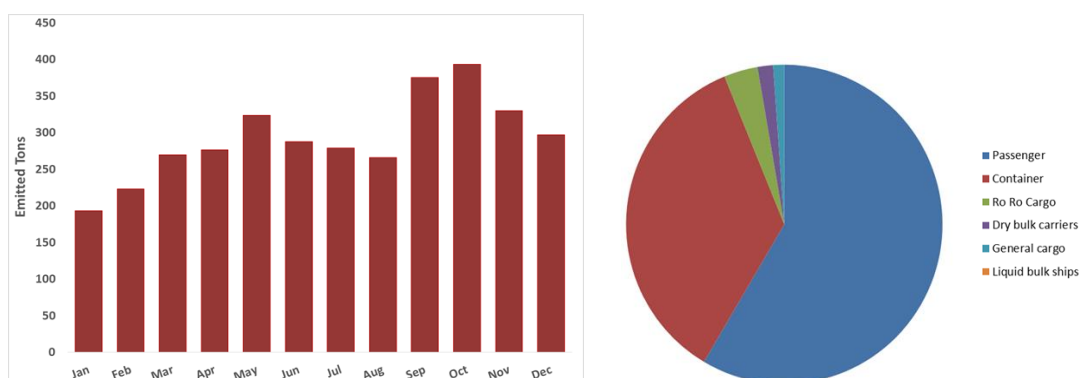


Figure 2: Monthly emissions from passenger ships (left) and emissions share per ship category (right) for the Piraeus Port.

An additional emissions scenario is examined, corresponding to a future implementation of “cold ironing” for all passenger and cargo ships in the port of Piraeus. Under this scenario, every ship spending more than two hours in the hoteling, loading and unloading phases can be assumed to deactivate its auxiliary engines for the entire duration of this phase, minus a period of one hour needed for connecting and disconnecting to the power grid ashore. The implementation of this scenario results in a reduction of about 60% on the total NO_2 and PM_{10} emissions during the time spent in the port area, i.e. excluding emissions in the anchorage area.

Results

In Figure 3, average surface-level concentrations of NO₂ and PM₁₀, as calculated using the full emissions set are shown (a, d). It is evident that the Piraeus area has a dominating contribution in the pollutant levels exceeding the average contribution of the primary road traffic network. The combined effect of marine and road traffic on the surrounding coastal areas, is leading to concentrations of NO₂ and PM₁₀ that exceed the corresponding annual limit values of 40 µg/m³. The secondary dominant source visible in the eastern part of the Attica peninsula is the Athens International Airport with its associated road traffic emissions.

A more precise quantification of the contribution of the port and anchorage areas can be obtained by assuming zero marine emissions and subtracting the resulting concentration fields from the “baseline” field. The result of this calculation is shown in Figure 3 (b, e). It is again noteworthy that in the downtown area of Piraeus the port area has a contribution to ambient concentrations in excess of 18 µg/m³ for NO₂ and of 22 µg/m³ for PM₁₀. For both pollutants, the spatial extent of the port’s impact includes at least part of the densely-populated coastal area, which is already burdened by local traffic sources.

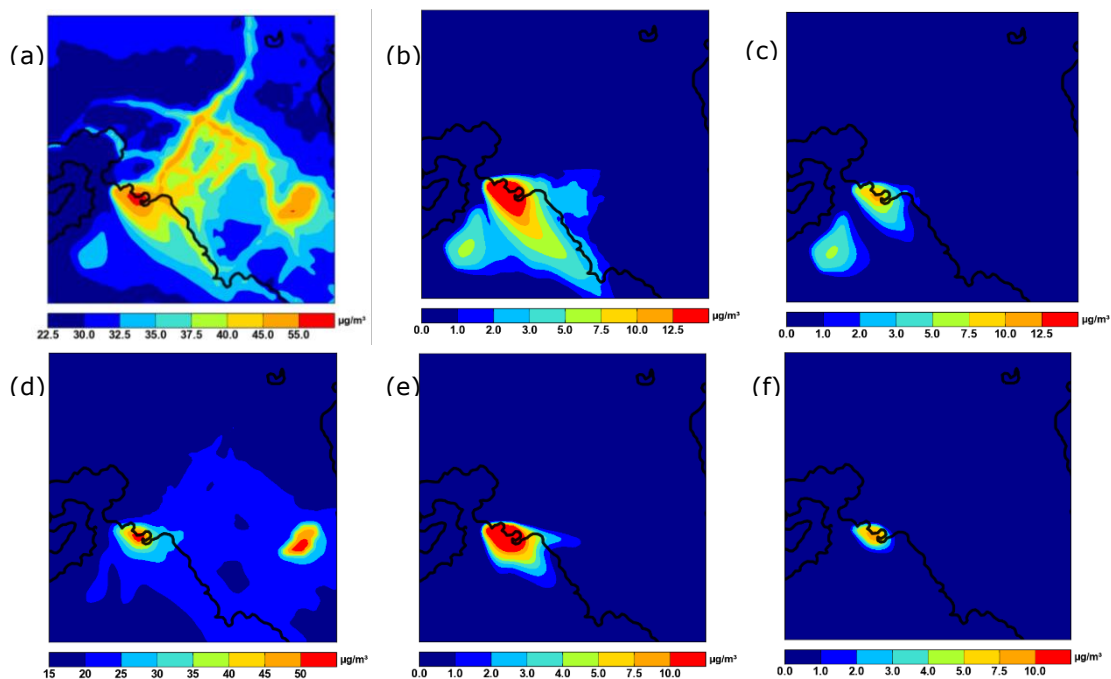


Figure 3: Annual average NO₂ (a, b, c) and PM₁₀ (d, e, f) concentrations calculated for the year 2015: absolute baseline concentrations (a, d), shipping contribution under the baseline scenario (b, e), and shipping contribution under the cold ironing scenario (c, f).

On the other hand, the annual average port plumes seem to have minor effect on the air quality status near the center of Athens, while the impact of traffic in the anchorage area appears to be contained within the boundaries of this offshore area.

The implementation of the “cold ironing” scenario is found to have a significant effect in the port and surrounding areas, reducing NO₂ concentrations by 11 µg/m³ (Figure 2c), which corresponds to a 61% reduction of the shipping contribution in the port area. In the case of PM₁₀ the calculated reduction amounts to 16 µg/m³ (Figure 2f), corresponding to a 73% reduction of the contribution of shipping traffic in the port area. Figure 4 shows the results of the two scenarios compared to observational data.

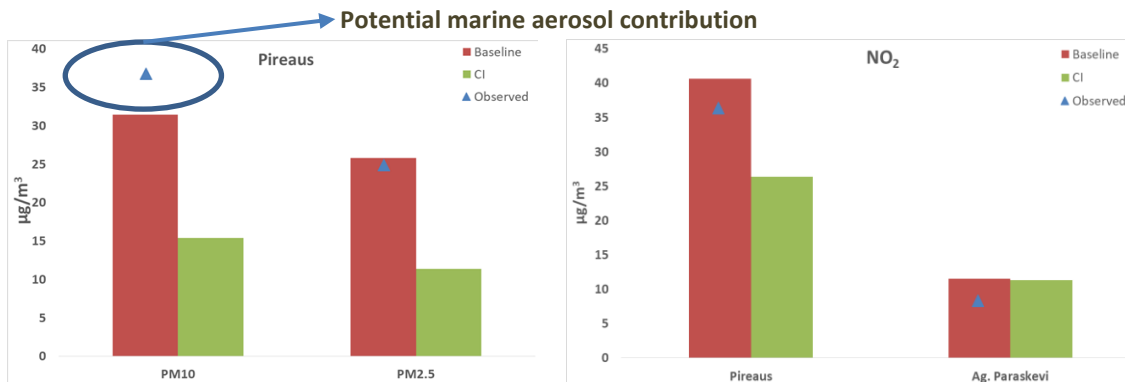


Figure 4: Comparison between theoretical predictions and experimental measurements.

For all three pollutants, the calculated averages show a good agreement with local observations. In the case of the coastal station in Piraeus, an underestimation of PM₁₀ is evident. A potential explanation of higher observed concentrations is the average contribution of marine aerosol which is not accounted for in the calculations.

As deduced from Figure 4, calculations under the cold ironing scenario indicate an impressive potential reduction by 50% of the shipping contributions to the observed concentrations. These results point to the need to prioritize emissions mitigation and other control measures related to the port activities of Piraeus.

Conclusions

The impact of exhaust emissions from marine traffic on the air quality of Piraeus and the surrounding areas was investigated. A bottom-up scheme was used to establish shipping emissions based on emission factors calculated for different classes of vessels and spatial activity data obtained from the Automatic Identification System (AIS), while maps of pollutants concentrations were obtained by applying the MEMO/MARS-aero chemical dispersion system. The calculated concentrations indicate that the port has a dominant contribution to the air pollution in the nearby areas, while the corresponding PM₁₀ and NO₂ concentrations have extended local maxima higher than the legislative limit values. Calculations under a scenario of cold ironing for ships in berth indicated a potential reduction by more than 60% of the shipping sector contributions to the observed concentrations. These results illustrate the significant potential of emissions-mitigation and other control measures in the marine sector towards improving the air quality in the Piraeus port and the surrounding areas.

Acknowledgements

The authors would like to acknowledge the contribution of Dr. Dimitrios Lekkas in facilitating access to AIS information through the Marine Traffic online platform.

References

- EEA (2016), EMEP/EEA Air Pollutant Emission Inventory Guidebook, *European Environmental Agency*.
- Kuenen J., Denier van der Gon H., Visschedijk A., van der Brugh H. (2011). High resolution European emission inventory for the years 2003-2007, *TNO report TNO-060-UT-2011-00588*, Utrecht, 2011.
- Moussiopoulos N., Douros I., Tsegas G., Kleanthous S. and Chourdakis E. (2010). An air quality management system for Cyprus. *Global Nest Journal*, Vol. 12, pp. 92-98.
- Moussiopoulos N., Douros I., Tsegas G., Kleanthous S. and Chourdakis E. (2012). An air quality management system for policy support in Cyprus, *Hindawi Publishing Corporation, Advances in Meteorology 2012*, doi:10.1155/2012/959280.
- URL1. <http://www.emsa.europa.eu/related-projects/central-ship-database.html>

2.2.5 Impact assessment for a potential emission control area in the Mediterranean Sea

*J. Cofala, J. Borken-Kleefeld^{*1}, C. Heyes¹, M. Holland², H. Frageli³, A. Nyiri³, A. Gomez-Sanabria¹, R. Sander¹ and M. Amann¹*

¹International Institute for Applied Systems Analysis, Laxenburg, 2361, Austria

²Ecometrics Research and Consulting, Reading, Berkshire, 0118, UK

³The Norwegian Meteorological Institute, Blindern, Oslo, 0313, Norway

Presenting author's email: borken@iiasa.ac.at

Introduction

Pollutant emissions from ocean-going vessels have remained largely unregulated, causing concern for air pollution. These concerns have led to a gradual reduction of the maximum permissible fuel sulphur content and to a slight tightening of the permissible NO_x emissions from new vessels. In specially designated emission control areas (ECA) much stricter sulphur and nitrogen standards can be required, as for instance in the Baltic and the North Sea. Currently, there is discussion about requesting an ECA also for the Mediterranean Sea.

Here we investigate the health benefits and extra costs of possible new ECAs. We analyse several cases either for a sulphur ECA alone or a combined sulphur & nitrogen ECA. This would require low-sulphur fuels or on-board scrubbers across the fleet and extra technologies to reduce nitrogen oxides emissions. Extra control equipment would potentially increase investment and operating costs. The effectiveness and costs of the controls depend critically on the extent of the control area. We analyse options ranging from an implementation in EU territorial waters only to a coverage of all seas, for implementations starting between 2021 and 2025. We consider impacts up to the year 2050 to capture the effect of full penetration of new technologies in the fleet.

Methods

For the health and cost impact assessment we follow a standard approach from activities over emissions, ambient pollutant concentrations, static exposure to health endpoints. These steps are coded in GAINS, an established integrated assessment model (Amann 2009). It has been often used for cost-effectiveness assessments of land-based emission sources in Europe and is here extended to include international shipping in some detail. Its modules map the standard impact-pathway: Economic and shipping activities drive the emission of air pollutants. These are modulated by a host of different emission control technologies, that typically follow from legislation. Activities are projected into the future, here assuming a higher or lower shipping activity; emission controls are likewise projected assuming a gradual uptake as new technologies, compliant with new emission regulations replace older, higher emitting technologies. The reference case is established assuming no new emission controls beyond what is currently decided. About thirty emission scenarios are created assuming the introduction of a S-ECA and/or a N-ECA in the Mediterranean Sea, either only in territorial waters, only in the Exclusive Economic Zones (EEZ), only in waters of the EU28 MS, the same for all states with coastline and eventually in the whole Mediterranean Sea. Emissions from all other sources (land-based, natural, and long-range trans-boundary) are left unchanged for this analysis at the level of the official EU Reference scenario (Amann et al. 2017). The GAINS model then computes ambient concentrations of particulate matter (PM), NO₂, and ozone and their subsequent health impacts across Europe and Northern Africa (Amann et al. 2017). Costs and benefits of extra emission controls are monetised for the different scenarios and compared. Further details are given a publicly available report (Cofala et al. 2018).

The pollutant emission scenario for shipping are developed as follows: The basis is the gridded CO₂ emission inventory calculated bottom-up with the STEAM model for all European seas for the year 2015 (Johansson, Jalkanen, and Kukkonen 2017). We back-calculate the implied fuel consumption obtaining thus a gridded activity inventory for shipping. This is then linked to our fuel- and technology specific emission factors producing a pollutant emission inventory, gridded in the same way as the original input data.

We explore a broad range of possible developments from the interplay of growth in shipping activities, trends in energy efficiency and climate policies. A 'baseline' scenario extrapolates current trends in economic growth, trade relations and fuel efficiencies. A scenario 'with climate measures' illustrates the

potential consequences of dedicated greenhouse gas reduction policies for maritime activities, and their knock-on effects on fuel burnt and air pollutant emissions. For these scenarios, future fuel consumption trends up to 2030 are derived from the 'business as usual' and 'climate policy' scenarios as in (EC 2015), and follow thereafter the corresponding growth rates assumed in the 3rd IMO GHG Study (Smith et al. 2015). With these assumptions, total fuel consumption for international shipping on European Seas increases in the baseline case from 1.8 EJ in 2015 to about 4.1 EJ in 2050. In contrast, fuel consumption volumes 'with climate measures' would stabilize at a level below 2.0 EJ after 2030. This would still fall short of the aims of the IMO for a global reduction of at least 50 percent by 2050 (IMO 2018).

Trends vary across different vessel types, based on the projections developed by (Smith et al. 2015; Winnes 2015; Åström et al. 2018). These suggest a rapid expansion of container and dry cargo traffic, while much lower increases or even declines are projected for oil tankers, passenger vessels and other vessel types. This leads to a shift in the relative shares notably towards container vessels. By 2050 they are projected to consume 48 percent and 38 percent respectively in the baseline and the 'climate policy' scenario, compared to 31 percent in 2015.

It is expected that liquefied natural gas (LNG) will play a greater role as a marine fuel. We adopt the global LNG trend of the 'New Policy scenario' of the IEA World Energy Outlook 2017 (IEA 2017), assuming that Europe will maintain its 11% share in total global LNG use (CE Delft 2016). Thereby, the share of LNG in the total fuel demand at European Seas would increase from less than 2 percent in 2020 to about 5 percent in 2030 and nearly 12 percent in 2050.

The possible developments of shipping activity are combined with three emission control scenarios: The Current Legislation (CLE) scenario illustrates the impacts of current policies and regulations for maritime emissions. In particular, it assumes full compliance with the IMO MARPOL Annex VI standards for fuel quality and for NOx emissions. This means in particular that from 2020 onwards, the sulphur content of marine fuels will be limited to 0.5 percent outside the SECAs. In addition, vessels built after mid-2011 need to meet Tier II standards for NOx emissions. These assumptions result in two reference emission scenarios (with high and low shipping activity) that form the backdrop of all analysis. Any further emission controls are to be interpreted relative to these reference values.

One set of possible further emission controls focuses on SO₂, the other on NOx emissions: Extended SO₂ Emission Control Areas (SECA) as of 2025, imposing a limit of 0.1 percent on the sulphur content of fuel (or equivalent emissions through scrubbers) for all vessels. The temporal introduction of scrubbers follows the assumptions of (MECL 2017; IHS Markit 2018). Variants explore different target areas (12 mile zones only/all Sea regions/excluding the Atlantic Ocean outside the 12 nm zone). Extended Tier III NOx emission standards as of 2025, for new vessels only or including retrofits of existing vessels. Variants are computed for different Sea regions and earlier introduction (2021).

The emission control costs depend on the choice of technologies by ship owners, which in turn depend on the cost differences between low-sulphur fuels and on-board scrubbers in case of SO_x controls. With the fuel price premiums that have been presented in (MECL 2017; IHS Markit 2018), sulphur scrubbing appears as an economically competitive option for meeting the SO₂ emission standards (cf. Table 1). We assume therefore a gradual increase of scrubber use in the vessel fleet from 2% in 2020 to 80% in 2050.

Table 1: Emission rates and costs for sulphur control options.

*Fuel costs assumed for ~2025, i.e. once prices for low-sulphur fuels have settled.

Fuel type	M% S	SO ₂ kg/GJ	PM _{2.5} kg/GJ	Fuel costs* €/GJ	Scrubber (open - closed) €/GJ
RFO	2.5	1.2	0.143	6.7	
RFO	0.5	0.23	0.054		RFO to 0.5M%: 0.56-1.4
MD	0.4	0.18	0.051	8.5	
MGO	0.1	0.05	0.037	9.4	RFO to 0.1M%: 0.56-1.6 MD to 0.1M%: 0.59-0.84
LNG	0.0	0.0	0.004		

The forthcoming IMO standard requires newly built vessels (or retrofitted engines) to comply with Tier II emissions standards for NO_x. Advanced internal engine modifications (AIEM) allow to reach Tier II emission standards. Reaching Tier III limits, i.e. for vessels operating in a N-ECA, is possible through exhaust gas recirculation in combination with water in fuel injection (EGR+WIF) or through selective catalytic reduction (SCR). Since the EGR+WIF is more expensive per unit of NO_x reduction (Åström et al. 2018), we include only SCR as a way to reduce emissions to the Tier III level. The capital investment for a SCR equipment is substantial. Therefore, annualised costs are lower per unit of fuel consumed the longer the SCR is operated. This is so far only necessary in the North and Baltic Seas. Cargo, container and tanker vessels are assumed to operate only between 750 and 1200 hrs annually in these seas, and hence any SCR installation is annualised only for this fraction of the total operating life. On the contrary, vessels operating mostly on routes in these seas, e.g. scheduled passenger and ferry services, will see their capital investments annualised over much larger times and hence have much lower abatement costs. The relevant emissions and costs are presented in Table 2.

Table 2: Emission rates and costs for NO_x control options. Tier III applies only NECA, and hence the average annualised costs depend on the fraction of time spent in the NECA sea.

Fuel type	NO _x – Cargo kg/GJ	NO _x – Container kg/GJ	NO _x - Tanker kg/GJ	NO _x - others kg/GJ
Tier I	1.66	1.84	1.65	~1.35/1.87
Tier II: EF NO _x [kg/GJ]	1.45	1.64	1.45	~1.15/1.66
AIEM costs [€/GJ]	0.029	0.024	0.022	~0.030
Tier III: EF NO _x [kg/GJ]	0.33	0.37	0.34	~0.28/0.38
Operating hrs if NECA in NORS & BALS/all seas	750/1500	1200/2400	1050/2100	1500-5500/ 3000-5500
SCR costs [€/GJ] NECA in NORS & BALS/all seas	1.067 / 0.64	0.733 / 0.461	0.802 / 0.494	0.6-0.3 / 0.4-0.3

Results

SO₂ emissions from ships will decrease substantially from 2020 onwards, with the mandatory reduction of the fuels' sulphur contents to no more than 0.5%M. In the absence of additional controls, the resulting emissions will from then on scale simply with shipping activity (Figure 1, left: 'Current legislation'). Further emission controls like a complete SECA could reduce the remaining emissions by another 80% in the Mediterranean Sea. Shipping emissions of NO_x develop entirely differently, as there is no step-change of emissions ahead (Figure 1, right: 'Current legislation'). Any scheduled emission reduction therefore comes with fleet renewal, and far from the stringency of SO₂ controls. Even if there was an emission control area declared e.g. by 2025 in the Mediterranean Sea, it would only take effect with the pace of fleet turnover. Therefore, shipping emissions of NO_x would hardly be affected in 2030, and controls would only become relevant with a large fleet renewal expected around the year 2050.

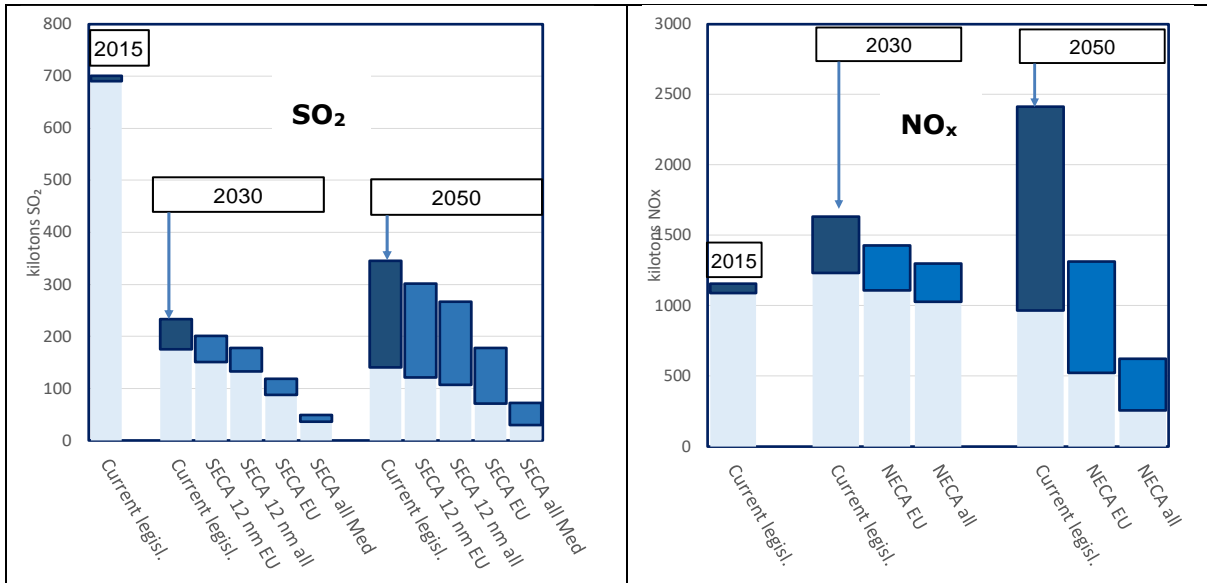


Figure 1: Emissions from international shipping in the Mediterranean Sea under different control scenarios. Left: SO₂ emissions; right: NO_x emissions. The upper/lower end of the boxes reflects emissions under a high/low activity scenario.

Ships currently contribute about 4% to the ambient (population-weighted) PM_{2.5} concentrations averaged across Europe, according to our calculations. Their share reaches 10% and more in Portugal, Spain and for the islands of Cyprus and Malta. With further emission controls the ambient concentrations could be come down as well. In general, the emission reduction scenarios show largest effects along the coast of Mediterranean countries, and in particular along the North African coast where the ship traffic is densest. Here the concentrations of PM_{2.5} decrease by up to 1.2 µg/m³ in 2030 and up to 1.5 µg/m³ in 2050 (Figure 2).

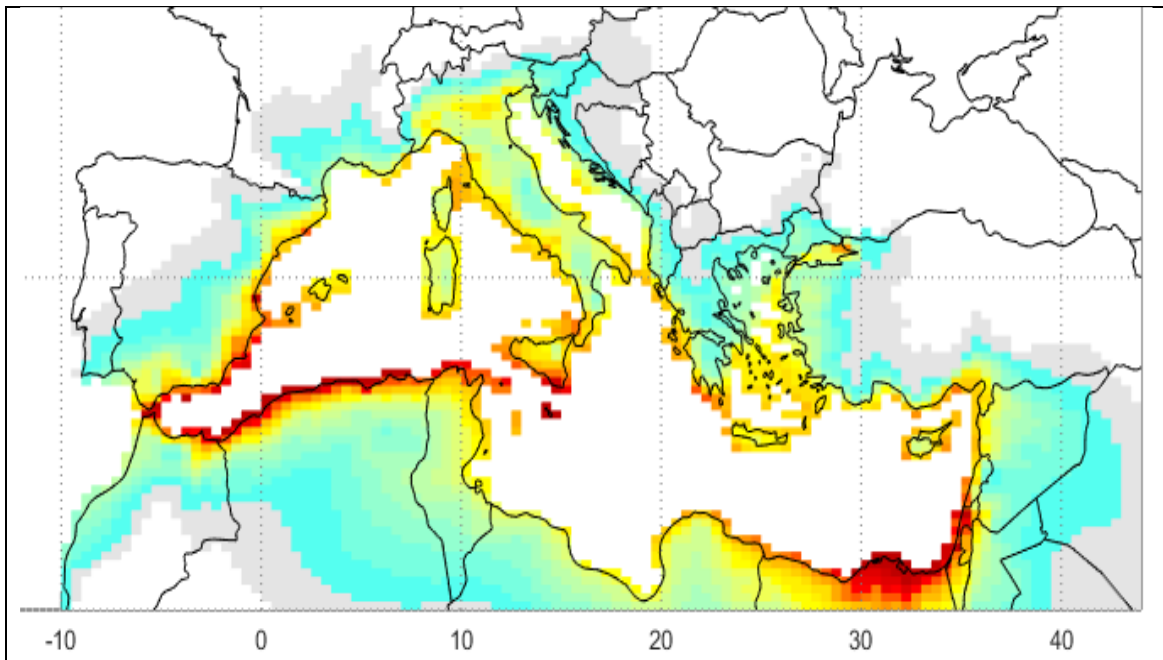


Figure 2: Reduction of ambient PM_{2.5} concentrations in case of a combined Sulphur- and Nitrogen emission control area in the Mediterranean Sea: Maximum feasible reduction in 2050.

Biggest improvements emerge for extended SECAs; NECAs deliver lower reductions, especially in the short run and when the introduction of Tier III standards is limited to new vessels only, i.e. without a retrofit of the existing fleet. Almost one quarter of the population in the model domain lives within a 30 km distance to the coast (27 percent in the EU-28, 16 percent in other European countries, and 24

percent in Africa and Middle East). Especially large impacts of shipping emissions, and subsequently of emission controls, occur in port cities, for which the contributions from shipping to ambient PM2.5 levels estimated is typically between 5 and 15 percent in 2015. Our align well with other assessments (Viana et al. 2014).

In total, about 12,000 premature deaths annually across the EU28 can be attributed to emissions from international shipping. About half of the premature deaths occur in coastal areas, but long-range transport of particles and precursor gases leads to substantial impacts further inland. This impact is expected to drop by about 30% with the reduction in sulphur content of fuels imposed in 2020. In the absence of further controls, the emissions, the subsequent particle concentrations and their consequent health impacts will increase as traffic volumes are expected to increase until 2050.

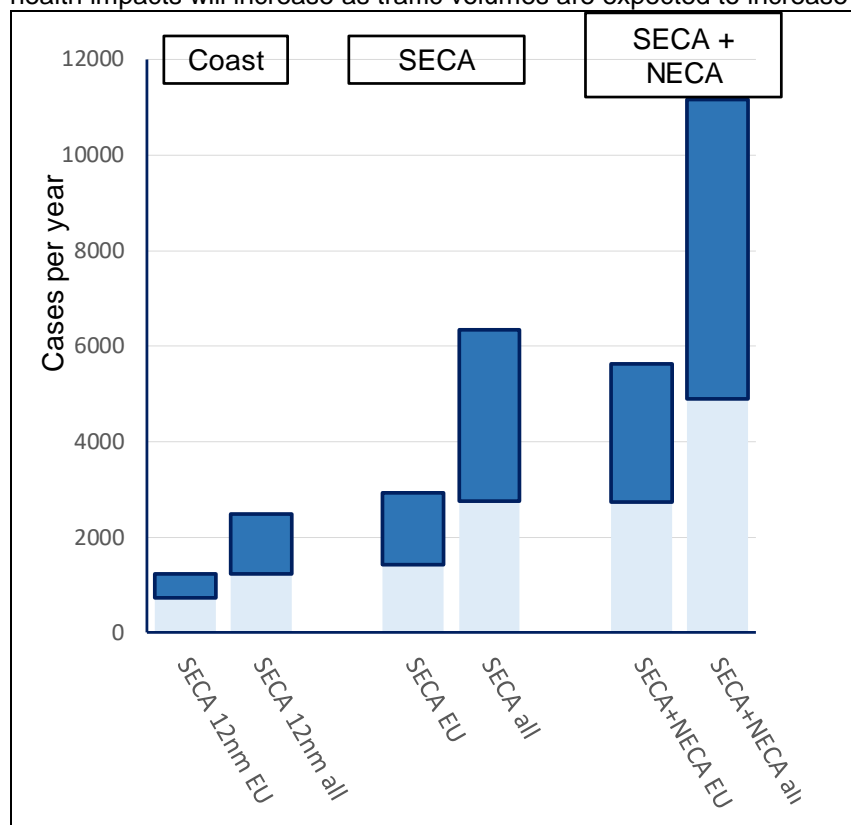


Figure 3: Reduction of premature mortality thanks to the introduction of emission control area in the Mediterranean Sea by 2050: 'Coast': If imposed in the respective 12 nm zone only. 'SECA': If only sulphur controls. 'SECA+NECA': Sulphur and nitrogen emission control area. The upper / lower end of the boxes reflects emissions under a high/low activity scenario.

The health impacts could be reduced by about one quarter in the EU with the imposition of a sulphur emission control area in the Mediterranean Sea (Figure 3). Italy, Spain and Greece would benefit most, with reductions up to 40%. An additional nitrogen emission control area would further reduce shipping emissions-related health impacts. This measure takes time to penetrate the fleet; therefore, the reduction potential of the combined SOx and NOx ECA increases from 40% in 2030 to 65% in 2050 less impact than in the base case. In the named Mediterranean countries, the impact could be 50% in 2030 and by almost 75% in 2050. These substantial health benefits also translate into gains in life expectancy.

For the emission controls in the Mediterranean, the estimates of monetized benefits reach up to 10 billion €/year in 2030 and increase to almost 30 billion €/year in 2050. Benefits outweigh the extra costs for new emission control installations and/or fuels by roughly up to factor of 10 (Figure 4).

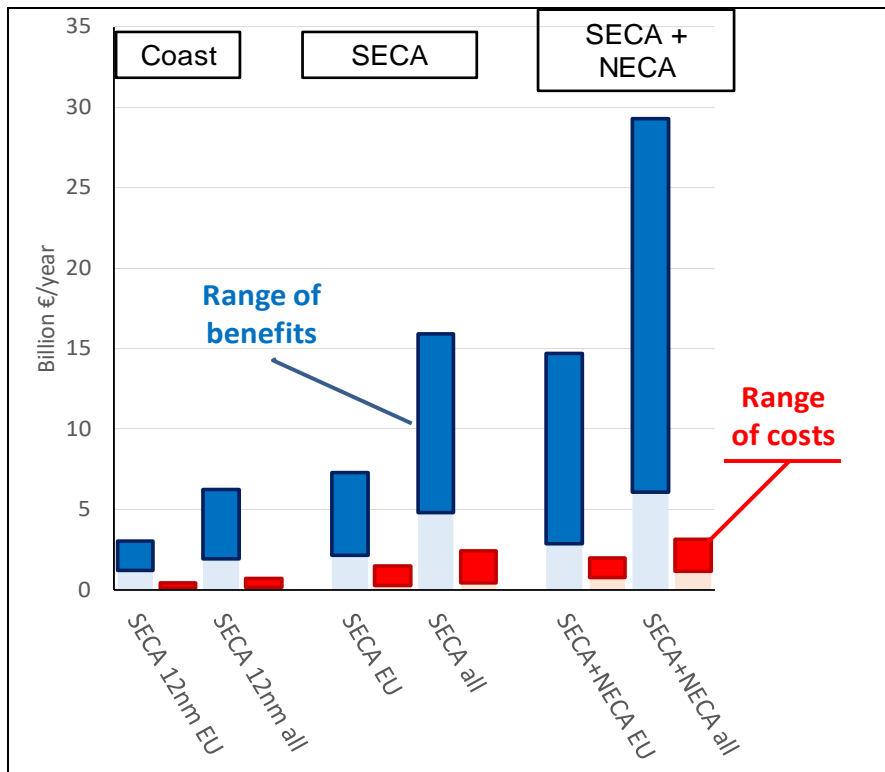


Figure 4: Monetized benefits from higher life expectancy versus extra emission control costs due to possible further emission control measures in the Mediterranean Sea by 2050: 'Coast': If imposed in the respective 12 nm zone only. 'SECA': If only sulphur controls. 'SECA+NECA': Sulphur and nitrogen emission control area. The upper / lower end of the boxes reflects costs/benefits under a high/low ship activity scenario.

The benefits are further enhanced by substantial reductions of the ozone burden. The benefits would decrease, however, with any partial implementation of the emission control area, e.g. if applied only in EU territorial waters or only in the EU Exclusive Economic Zone. NO_x emission controls (so-called Tier III standards) would unfold their full benefits only in the longer term; they could roughly double the health benefits by 2050.

While all coastal countries would benefit from extra emission controls, the North African countries would enjoy the biggest health (and hence monetary) benefits: The PM concentrations would decrease strongest there, affecting a large share of the population in proximity to the dense shipping lanes.

Acknowledgements

Funding for this work was provided within the Framework Contract ENV.C.3/FRA/2013/00131 by the European Commission, DG ENV.

References

- Amann, Markus. 2009. "Integrated Assessment Tools. The Greenhouse Gas - Air Pollution Interactions and Synergies (GAINS) Model." *Pollution Atmosphérique Special Issue*: 73–77.
- Amann, Markus, M. Anderl, J. Borken-Kleefeld, Janusz Cofala, Chris Heyes, L. Hoglund-Isaksson, Gregor Kiesewetter, et al. 2017. "Progress towards the Achievement of the EU's Air Quality and Emission Objectives." Laxenburg, Austria: International Institute for Applied Systems Analysis. http://ec.europa.eu/environment/air/clean_air/outlook.htm.
- Åström, Stefan, Katarina Yaramenka, Hulda Winnes, Erik Fridell, and Michael Holland. 2018. "The Costs and Benefits of a Nitrogen Emission Control Area in the Baltic and North Seas." *Transportation Research Part D: Transport and Environment* 59 (March): 223–36. <https://doi.org/10.1016/j.trd.2017.12.014>.
- CE Delft. 2016. "Assessment of Fuel Oil Availability. Final Report." Delft, NL: CE Delft.
- Cofala, J., M. Amann, J. Borken-Kleefeld, A. Gomez Sanabria, C. Heyes, G. Kiesewetter, R. Sander, et al. 2018. "The Potential for Cost-Effective Air Emission Reductions from International Shipping through Designation of Further Emission Control Areas in EU Waters with Focus on the Mediterranean Sea."

- Final Report. Laxenburg, Austria: International Institute for Applied Systems Analysis (IIASA).
<http://pure.iiasa.ac.at/id/eprint/15729/>.
- EC. 2015. "Analysis of Recent Trends in EU Shipping and Policy Support to Improve the Competitiveness of Short Sea Shipping In the EU. Final Report by COWI, CENIT and VITO." Brussels, Belgium: European Commission, DG Mobility and Transport.
- IEA. 2017. "World Energy Outlook 2017." Paris, France: International Energy Agency.
http://www.iea.org/bookshop/750-World_Energy_Outlook_2017.
- IHS Markit. 2018. "IMO 2020: The Biggest Ever 'Planned Disruption' to Oil Markets?" Webinar August 2018. HIS Markit TM.
- IMO. 2018. "Initial IMO Strategy on the Reduction of GHG Emissions from Ships. Resolution MEPC.304(72) (Adopted on 13 April 2018) at the 72nd Session of the IMO Marine Environment Protection Committee." International Maritime Organization (IMO).
- Johansson, Lasse, Jukka-Pekka Jalkanen, and Jaakko Kukkonen. 2017. "Global Assessment of Shipping Emissions in 2015 on a High Spatial and Temporal Resolution." *Atmospheric Environment* 167 (October): 403–15. <https://doi.org/10.1016/j.atmosenv.2017.08.042>.
- MECL. 2017. "How Much Will 2020 Cost? Study for IBIA, Marine and Energy Consulting Limited (<https://Ibia.Net/How-Much-Will-2020-Cost/>)." Marine and Energy Consulting Limited.
- Smith, T. W., J. P. Jalkanen, B.A. Anderson, J. J. Corbett, J. Faber, S. Hanayama, E. O'Keeffe, et al. 2015. "Third IMO GHG Study 2014." London, UK: International Maritime Organization (IMO).
<http://www.imo.org/en/OurWork/Environment/PollutionPrevention/AirPollution/Pages/IMO-Publications.aspx>.
- Viana, Mar, Pieter Hammingh, Augustin Colette, Xavier Querol, Bart Degraeuwe, Ina de Vlieger, and John van Aardenne. 2014. "Impact of Maritime Transport Emissions on Coastal Air Quality in Europe." *Atmospheric Environment* 90 (June): 96–105. <https://doi.org/10.1016/j.atmosenv.2014.03.046>.
- Winnes, Hulda. 2015. "NOx Controls for Shipping in EU Seas. Study Commissioned by Transport & Environment, Report No. U 5552. I." Gothenburg, Sweden.: IVL Swedish Environmental Research Institute,.

2.2.6 An Improved Model for Calculation of Emissions Based on Typical Flight Records

V. Sraga¹, P. Ilinčić¹, G. Šagi¹, and Z. Lulić¹

¹ University of Zagreb, Faculty of Mechanical Engineering and Naval Architecture, Department of IC Engines and Transportation Systems, Ivana Lučića 5, 10002 Zagreb, vjekoslav.sraga@fsb.hr

Introduction

Negative effects of exhaust gas and particle emissions from fuel combustion are well known (Portier et al., 2010). While cars and other road transport vehicles have advanced systems of treatment and mitigation of emission levels, there are parts of transport which are undeveloped regarding exhaust emission control and mitigation. One typical example of obsolete technology is General Aviation aircraft. Additionally, this type of aircraft as a fuel use AVGAS 100 LL aviation Gasoline with Octane number 100 where LL denotes Low Lead. Despite the LL label, this is a fuel with very high lead content. Leaded fuels are abandoned in 2000 in road transport vehicles in the EU (Directive 98/70/EC). Except for lead, other pollutants like sulphur are also present in aviation gasoline in concentrations fifty (50) times bigger than in EURO 5 diesel fuel (ExxonMobil Avgas; EN 590:2004). That means that this type of aircraft can potentially be a bigger problem than road transport emissions. On the other side, thanks to the number of GA aircraft compared to road vehicles, emissions from the complete GA sector are still much lower (Sraga and Lulić, 2017). To mitigate the problems with emissions, it is mandatory to establish a relevant model of emission measurement and data analysis. With determined levels and known types of exploitation, it is faster and more efficient to determine methods for decreasing emission levels.

Emissions from General Aviation are generally estimated by Tier 1 method. In other words, emissions are calculated by complete sales data of Avgas in a defined period of time. There is no information about the final type of usage of this fuel. A lot of information is missing, like the type of aircraft or engine, type of flights, domestic or international flights, etc. So, many assumptions are made, and Tier 1 gives averaged results for a population which are globally defined and does not include country- or region-specific data important for more precise estimation of emissions. It is assumed that the number of aircraft which uses regular fuel for road vehicles (MOGAS) is increasing because of the benefits for engine maintenance and price per litre. That means that those aircraft are not included in the making of National emission inventories, because emission from general aviation aircraft is estimated by above described Tier 1 method, while road traffic is generally calculated by Tier 3 method with included activity data based on country statistics and research.

To diminish the influence of those problems, an advanced model for emission calculation from General Aviation aircraft is developed. The model includes emission calculation on Tier 3 method from already available data which is obligatorily collected and archived by national or international law (like Croatian Civil Aviation Agency or similar organisations). The new model includes improved data collection, analysis, and processing with a positive effect on emissions results completeness, comparability and precision.

Actual models in general aviation emission calculation

General Aviation (GA) is defined by ICAO as “all civil aviation operations other than scheduled air services and non-scheduled air transport operations for remuneration or hire” (ICAO, 2013). GA aircraft are used in pilot training, recreation, agriculture and many other similar activities. This research is limited to the piston engine powered GA aircraft because of the quantity of other data needed for calculations. The aircraft piston engines do not differ as much as jet aircraft engines in terms of pollutant emissions due to similar and well-known design. A typical example of observed aircraft are piston engine powered, 2-, 4-, or more seaters, shown in Figure 1.

In emission calculation it is not feasible to exact measure emissions from every single pollutant source, so methods with different level of detail are developed to estimate emissions from available or especially collected data. Tier 1 method is the basic level approach of emissions estimation which is made by multiplication of consumed fuel with the corresponding emission factors. Emission factors in Tier 1 are sample-averaged and pollutant-based while fuel consumption data are gathered from sales data.



Figure 1: Typical examples and uses of general aviation aircraft

Advanced methods are grouped in Tier 2. The main advantage is aircraft type related fuel consumption and emission factors. In Tier 2 method, the emissions are divided between landing and take-off (LTO) and climb, cruise and descent (CCD) parts of the flight. Tier 1 and Tier 2 methods are a top-down approach where activity data mean fuel consumption in the observed period.

On the other hand, Tier 3A and Tier 3B methods use a bottom-up approach which includes flight segmentation into typical phases and types and phase dependent emission factors. As opposed to group or type based analysis in Tier 1 and Tier 2, Tier 3 method is based on individual aircraft analysis. Tier 3A differs LTO part of the flight (taxiing, take-off, initial climb, approach and landing) and CCD part, as in Tier 2, but in Tier 3A phases are determined by flight activity (origin and destination airport). Tier 3B method is the most comprehensive because the activity data is real flight path divided into phases. It is the most complex calculation, but it is the most precise method for emission estimation (European Environment Agency, 2017). Methods are graphically presented in Figure 2.

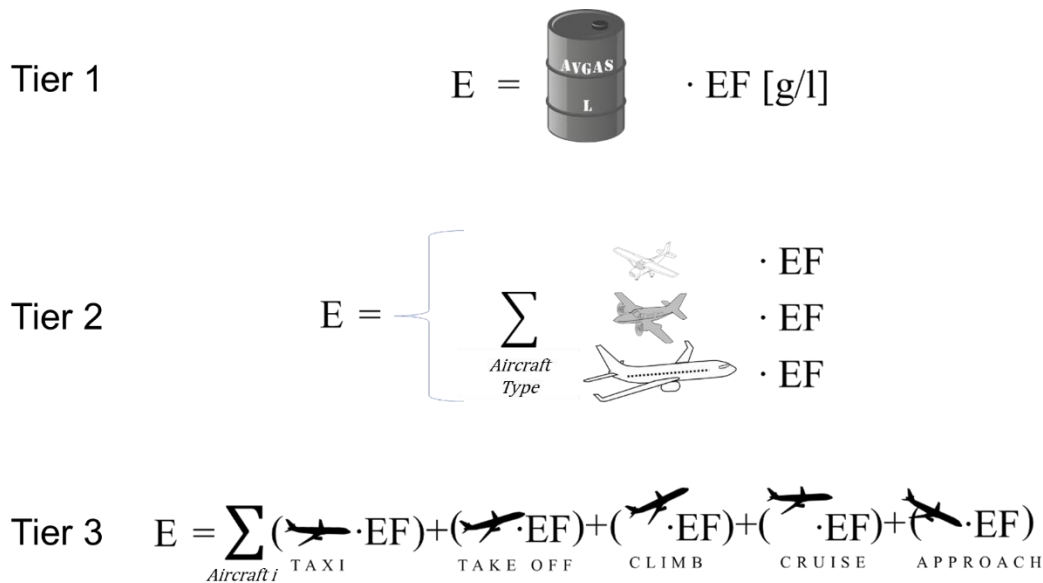


Figure 2: Graphical representation of three different methods for emission estimation

Improved model based on Tier 3 method

For Improved Tier 3A model, input data are typical aircraft owner's flight records, while activity i.e. computation data are emission factors and flight distance.

Every aircraft operator or owner is obligated to record data on flights of aircraft. Data are organised in the form of digital or paper flight logbook. Typical flight record consists of aircraft registration, flight date, take-off time, landing time, flight duration and number of cycles.

The most comprehensive emission factors database for aircraft piston engines is the Database for aircraft piston engines (Ger. *Flugzeug kolbenmotoren Datenbank*) from Swiss Federal Office of Civil Aviation (Federal Office of Civil Aviation, 2007). That organisation had conducted research between 2000 and 2007 in which were emissions from 16 aircraft piston engines measured in ground tests. Emission factors are stated for 5 different flight phases (take-off, climb out, cruise, approach and taxi). For other engines, averaged emission factors according to engine power are stated in the database, so it is possible to get the right emission factors for the observed engine.

Emission factors used are engine mode dependent and engine mode is defined by power setting. Available engine power depends significantly on the ambient conditions i.e. power decreases with ambient air temperature increase and ambient air pressure decrease. Emission factors used are gathered by ground tests so real flight conditions could affect emissions.

It is possible that, for example significant head wind would increase a demand for power to maintain desired air speed. In that case, wind speed change would indirectly affect emission through engine power change. Also, the pressure decreases with altitude increase which significantly affects engine performance and consequently emissions.

FOCA analysis showed that emission factors depend linearly on ambient temperature. Ambient pressure is in direct correlation and depends on ambient temperature, so analysis of temperature influence also covers the influence of the air pressure. Aircraft flight manuals includes a few diagrams with different combination of temperature and altitudes (i.e. pressure) which are combined into so-called density pressure.

It should be noted that to keep the airworthiness of the aircraft, aircraft owners or operators must comply with strict rules on aircraft maintenance. Regular maintenance prescribed by aircraft and engine manufacturers includes periodic checks in every 50, 100 and 250 working hours and Time between overhauls for engine is usually around 2000 working hours. It is expected that emission values will not be affected by the aircraft age as long as the aircraft and engine are maintained in original and airworthy state.

That all support the thesis about the need for in-flight tests in different ambient conditions. Comprehensive comparison between the results of such measurements would lead to appropriate conclusions about ambient conditions and if is needed to limit the temperature and pressure range in tests which could enable results comparability.

The distance between departing and landing airport is important because diversity in flight distance and duration strongly influence the total flight emissions. To determine flight distance, appropriate airport matrix was made with all Croatian airports included. The research is limited to one country because general aviation aircraft usually fly locally. In further research, other European or world airports can be included to extend coverage and possibilities. To automate airport distance calculation, GPS coordinates of the airport were collected. Using the haversinus function, the distance between two airports is calculated. The result represents the distance over the sphere, i.e. Earth.

For Improved Tier 3B model, input data are the flight path records, while other computation data are emissions factors and phase determination by the vertical speed of aircraft.

The main idea of this study was the development of a new model based on the usage of existing data. Great source of publicly available flight path data is web service *flightradar24.com*, the independent webpage for flight tracking. The flight path is recorded in CSV format in which one row represents one recorded point. Data recorded includes the timestamp, UTC date and time, aircraft call sign, GPS position in decimal degrees, altitude in feet, speed in knots and compass bearing.

The first step in data processing is the calculation of time, distance, average aircraft horizontal speed and average aircraft vertical speed between two consecutive records. Since emission factors significantly depend on the phase of flight, i.e. engine load, flight phase is determined by vertical speed. It is usual that aircraft steeply climbs during take-off, moderately climbs during climb-out, while descends during the approach phase of flight. In the cruise phase of flight, aircraft usually maintains the constant altitude which means that vertical speed is equal to or about zero.

With the given typical *modus operandi* of the general aviation aircraft, classification of the flight phases by vertical speed between two consecutive points is made and shown by Table 1. Engine modes defined by FOCA for the research and determining emission factors are made by experimental flight tests. Power percentage is equalized with fuel flow percentage of observed phase to maximum possible fuel flow. In this paper engine load is calculated parameter and is determined from aircraft vertical speed which is one of the most certain flight phase indicator.

Logical operations are done by the order in Table 1, using *Excel's IFS* function. The *IFS* function checks whether one or more conditions are met, and returns a value that corresponds to the first true condition. Ranges of vertical speed are defined by the typical performance of general aviation aircraft. The distinction between cruising with the lean and rich mixture is necessary because of large differences in fuel consumption, engine and exhaust gas temperatures and consequently different chemical reactions which leads to quite different values of emission factors. Furthermore, lean mixture in cruise flight is usually set in true, longer cruise, while the rich mixture is usually set in minor altitude changes or during the manoeuvres. In this flight phase classification, ideal engine mode during taxi is neglected because of the technical limitations of *FlightRadar24* system which loses signal reception below a certain altitude.

Table 1: Flight phases classification by vertical speed

V_{vertical,AB}, ft/min	V_{vertical,AB}, m/s	Flight phase	Engine mode
$v < (-300)$	$v < (-1.524)$	Approach (APP)	45% power
$ v < 6100$	$ v < 60.508$	Lean mixture cruise (CR LEAN)	65% power
$100 < v < 300$	$0.508 < v < 1.524$	Rich mixture cruise (CR RICH)	65% power
$300 < v < 500$	$1.524 < v < 2.54$	Climb (CLIMB)	85% power
$v \geq 500$	$v \geq 2.54$	Take-off (TO)	100% power

Available emission factors are expressed in mass of pollutant per mass of fuel burnt. Fuel flow is expressed in mass of fuel per second of engine operation. So next crucial data which needs to be extracted from records is the duration of each flight phase, i.e. engine mode. The time between records is calculated according to the difference between timestamp values of the two consecutive records and it is typically 6 seconds. Due to technical limitations, time between records is not equidistant and can be larger in case of low signal strength and bad reception. Time between records, i.e. resolution of the records is shown in Figure 3. Average time between records for the given flight example is 10 seconds, while the biggest time difference between records is 86 seconds.

On the shown example, there are 5 distinct peaks in the time resolution. When compared to the flight altitude on Figure 3, from this example can be concluded that peaks usually occur at low altitude, shortly after take-off and before landing.

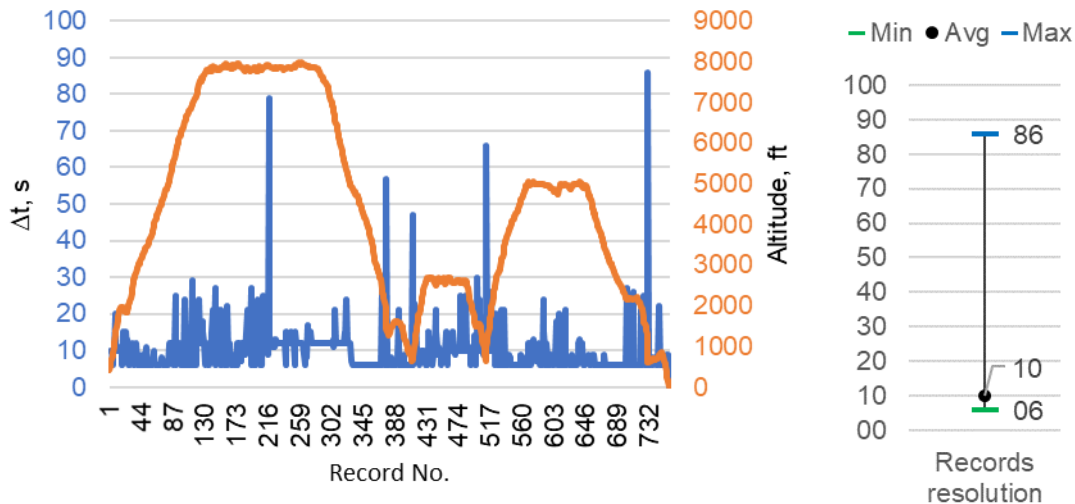


Figure 3: Example of *FlightRadar24* record resolution with altitude change (left), dissipation of time between records (right)

Because of technical limitations, with the usage of *FlightRadar24* data, it is not possible to further improve time resolution which is limited to 6 seconds. That leads to the first assumption in this work – horizontal and vertical speed, engine mode and flight phase are constant between two points of records. Because of that assumption, mentioned peaks can be treated as errors in dynamic part of flight e.g. take-off or landing. Development of set of rules which will reliably and accurately exclude these peaks from calculation needs to be considered and investigated in further research.

After the main input data explanation, it is important to note that the flight of typical general aviation aircraft is very dynamic and varies among aircraft types, pilots and missions. On the other hand, commercial aircraft serving on passenger and freight transport flies in common and well-known flight profiles, so logical operations in determining flight phase would be much simpler. Additionally, commercial aircraft fly on bigger, international airports which are better covered with *FlightRadar24* receivers so entire flight path from engine start-up till engine shutdown could be recorded. Commercial aircraft usually fly with the autopilot engaged, so variations during flight are minimal. As opposed to aircraft piston engines, jet engines emissions are measured during the certification process and are publicly available. All of that allows simple extension of this model to commercial aircraft in future research.

Emission calculation process

For every pair of consecutive points, emissions are calculated from given time-in-mode data from the previous step. From additional Aircraft data table and observed aircraft registration, aircraft type, engine type, number of engines and type of fuel used is loaded. With that information known, corresponding emission factors for the specific engine are used to calculate fuel consumption and emissions on observed part of the flight. Additionally, Carbon dioxide equivalent (CO₂-eq) is calculated for the observed flights. CO₂-eq is a term or measure used to compare different greenhouse gases in a common unit. For any quantity and type of greenhouse gas, CO₂-eq signifies the amount of CO₂ which would have the equivalent global warming impact which is based on their contribution to radiative forcing. Ratio of the radiative forcing of one kilogramme GHG emitted to the atmosphere to that from one kilogramme CO₂ over a period of time is called Global warming potential (GWP). For NO_x GWP value is 265 (Intergovernmental Panel on Climate Change, 2006).

CO₂-eq is useful measure as it allows results comparison of many greenhouse gases expressed as a single number. It is mandatory that compared CO₂ equivalents consist of the same greenhouse gases. In the paper, CO₂-eq is calculated for Carbon dioxide and Nitrous oxide as two main contributors. Described calculation process is made automatically for the entire flight and summarized after that.

Calculation process will be shown by one example of total flight record. Information available on *FlightRadar24* web page stated that aircraft with registration 9ADMG departed from Zagreb Lučko

airport, (LDZL), and landed at Pula Airport (LDPL). With displaying flight path, shown in Figure 4, it is clear that aircraft departed from Zagreb Lučko and landed at Pula Airport, but between that, aircraft completed few landings and take-offs, known as *touch and go* in Portorož Airport.

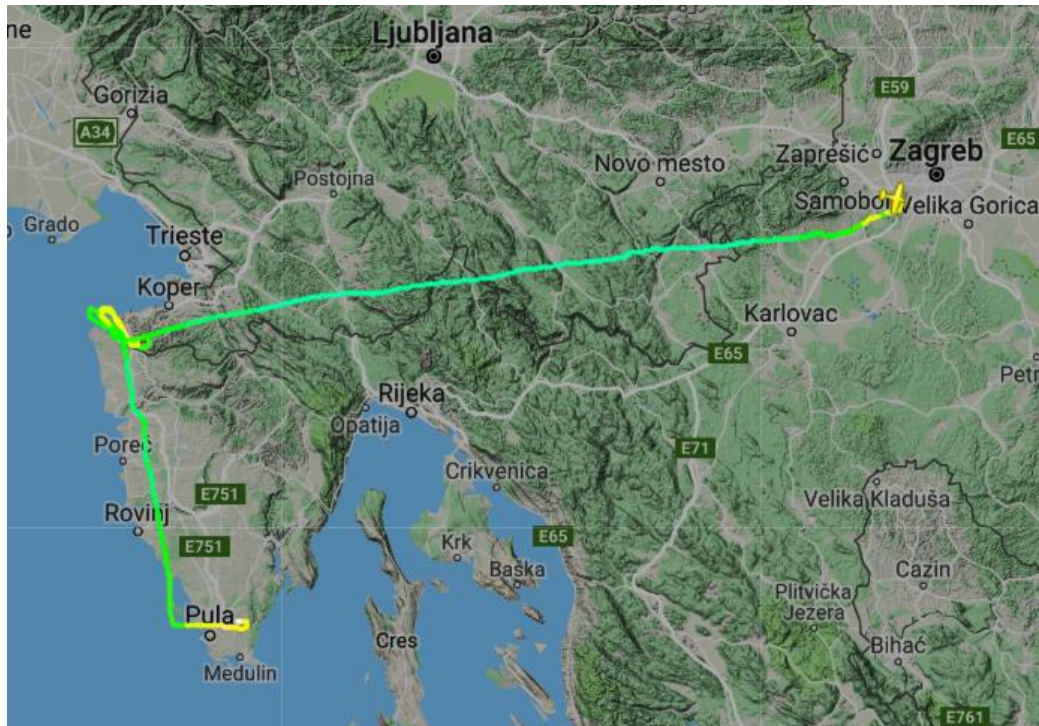


Figure 4: Example of *FlightRadar24* flight path display

FlightRadar24 offers download of flight path file in Comma-separated values (.csv) format. Part of the downloaded file is shown in Table 2. The file is loaded to prepared Excel file.

Table 2: Flight records in .csv format

Timestamp,UTC,Callsign,Position,Altitude,Speed,Direction
1509700707,2017-11-03T09:18:27Z,9ADMG,"45.765015,15.857827",425,61,106
1509700717,2017-11-03T09:18:37Z,9ADMG,"45.764099,15.861712",525,63,108
1509700727,2017-11-03T09:18:47Z,9ADMG,"45.763046,15.865799",625,67,110
1509700737,2017-11-03T09:18:57Z,9ADMG,"45.761875,15.870438",700,72,110
1509700743,2017-11-03T09:19:03Z,9ADMG,"45.761307,15.872564",750,74,110
1509700753,2017-11-03T09:19:13Z,9ADMG,"45.759594,15.876892",875,70,131
1509700763,2017-11-03T09:19:23Z,9ADMG,"45.756912,15.879397",1000,74,157
1509700773,2017-11-03T09:19:33Z,9ADMG,"45.753159,15.880201",1125,80,177

After loading, data are divided into Excel columns, what enables manipulation and calculation. Excel model interprets data in the 2D graph showing altitude and horizontal speed profiles (Figure 5).

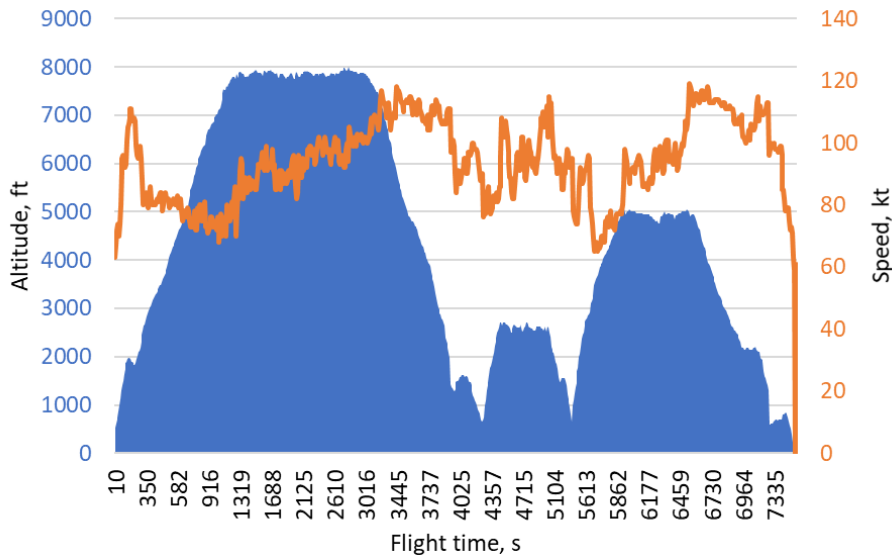


Figure 5: Vertical flight profile and speed of aircraft in Flight 1

After the basic flight analysis, emission calculation is done. Emission results and corresponding fuel used are shown in Table 3. The number of observed gases is limited to availability of emission factors. This improved model enables calculation of a large number of pollutants, as long as emission factors are known. The extraordinary power of the improved model is in various types of result presentation, as in the example shown on Figure 6.

Table 3: Emission results for example flights calculated by Tier 3B improved model

Flight	Fuel, kg	CO ₂ , kg	NO _x , g	VOC, g	CO, kg	CO ₂ -eq, kg
Flight 1	39	119	647	427	29	291
Flight 2	41	125	32	568	468	275
Flight 3	16	51	398	26	0	157

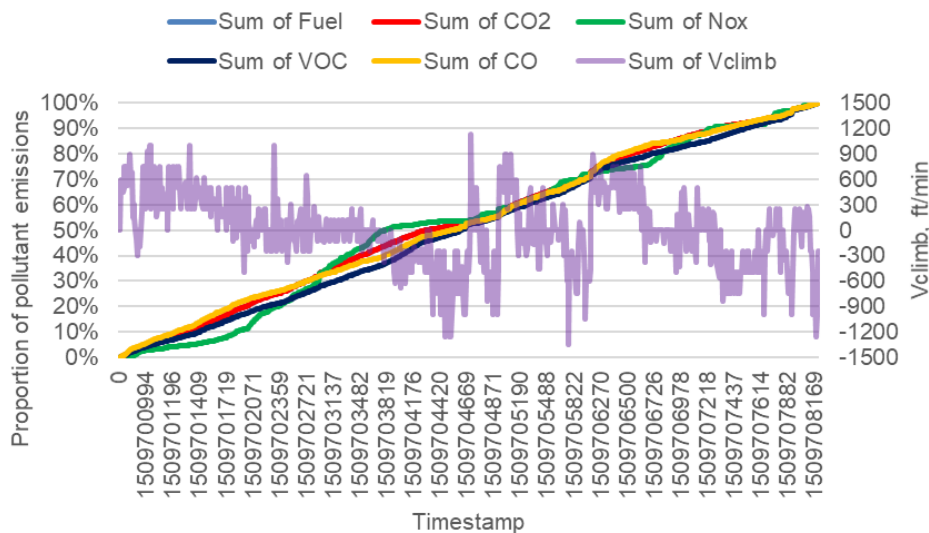


Figure 6: Emissions through flight phases for Flight 1

Results and sensitivity analysis

For the Improved Model, it is necessary to validate results by comparing it with other, well-known models. Sensitivity analysis was done on available recorded data of three different flights. Flight 1, also

shown in Figure 4, is a typical mixed type of flight where aircraft fly on route and practice manoeuvres and take-offs and landing and is common in pilot schools. Flight 2 is mostly the flight for practising and it does not have much time on the route, just minimal necessary to get the aircraft to the practising zone. The aircraft takes-off and lands on the same airfield. Flight 3 is typical route flight. Aircraft fly on a mostly straight route without any unnecessary derouting or manoeuvres. Results of model comparison for Flight 1 is shown in Figure 7, for Flight 2 is shown on Figure 8 and for Flight 3 is shown on Figure 9. For analysis is important to note that Tier 3A model is calculated from collected operator data, Tier 3B model is calculated only from downloaded *FlightRadar24* data and Tier 1 method is used as validation from consumed fuel value of Tier 3B model.

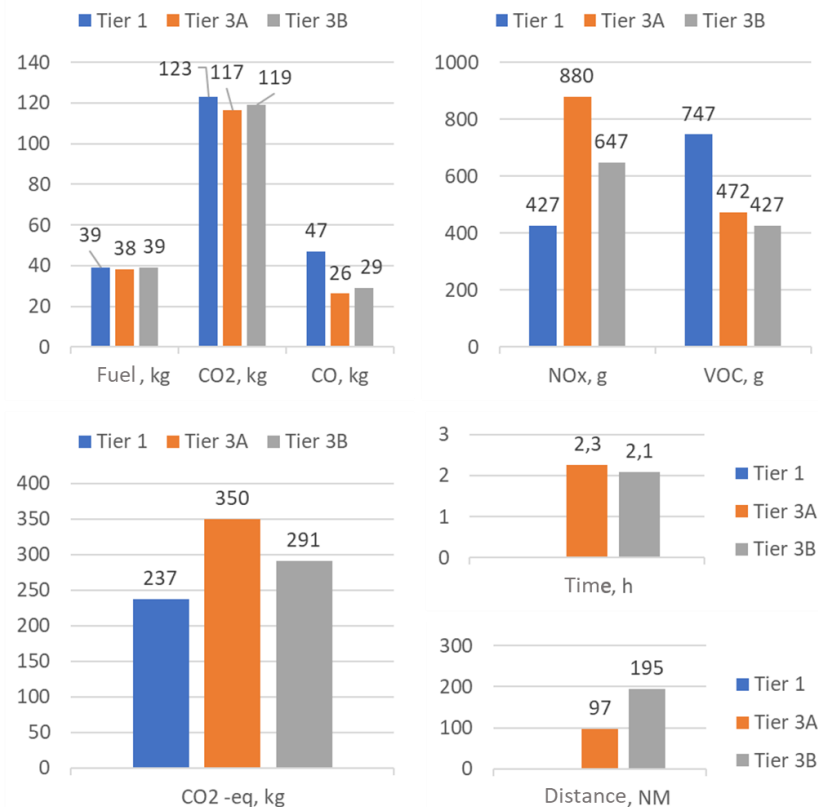


Figure 7: Emission results of different models for Flight 1

For Flight 1, fuel consumed values are very similar among models. CO₂ emissions are also very similar, but CO emission calculated by Tier 1 method is significantly higher. VOC emissions are also higher, while NO_x are much lower. From that is clearly shown the problem of Tier 1 method which does not include real activity data in a calculation. Because of a large part of the flight in route flying, NO_x emissions are higher because of lean mixture usage which causes higher temperatures in a cylinder with consequences of higher NO_x emissions. On the other hand, lean mixture causes a more complete burn of fuel, so CO and VOC emissions are significantly lower. CO₂ equivalent corresponds with other mentioned results.

Flight time is a bit shorter in Tier 3B model because of mentioned reception problems, while Tier 3A Time is from a pilot logbook record which should be considered as an exact data. Distance flown is twice longer because Tier 3B model calculates the distance from the real flight path, while Tier 3A model calculates the shorter distance between airports.

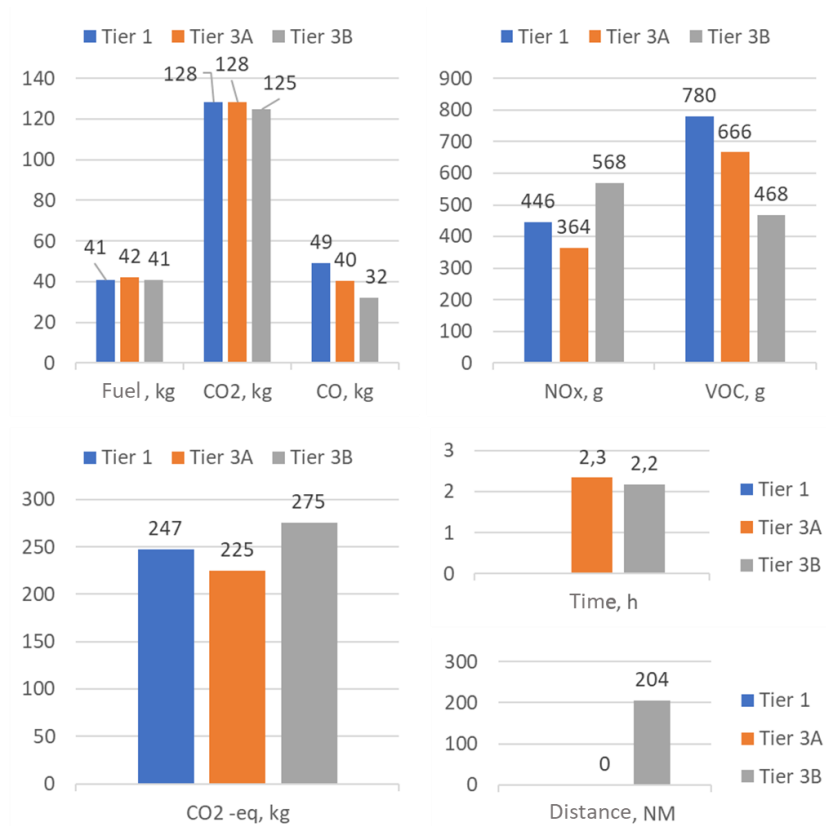


Figure 8: Emission results of different models for Flight 2

Flight 2 is a training school flight. Its take-off and landing airport is the same which deeply affects the results. Fuel consumption is again very similar for all of the models. Similar fuel consumed result is a very good basis for this sensitivity analysis because emissions results are not compromised and show only the influence of flight activity and how is activity recorded and processed. The same airport of start and end of the flight means Tier 3A model does not recognise any distance flown, so emissions are calculated only by flight duration. Because of similar fuel consumed between Flight 1 and 2, emissions calculated by Tier 1 model are very similar between flights. As opposed to Tier 1, Tier 3B emissions results between Flights are much more different, because the type of activity, i.e. flight is different. Tier 3A result of NO_x is very low due to no distance in the calculation and should probably be incorrect.

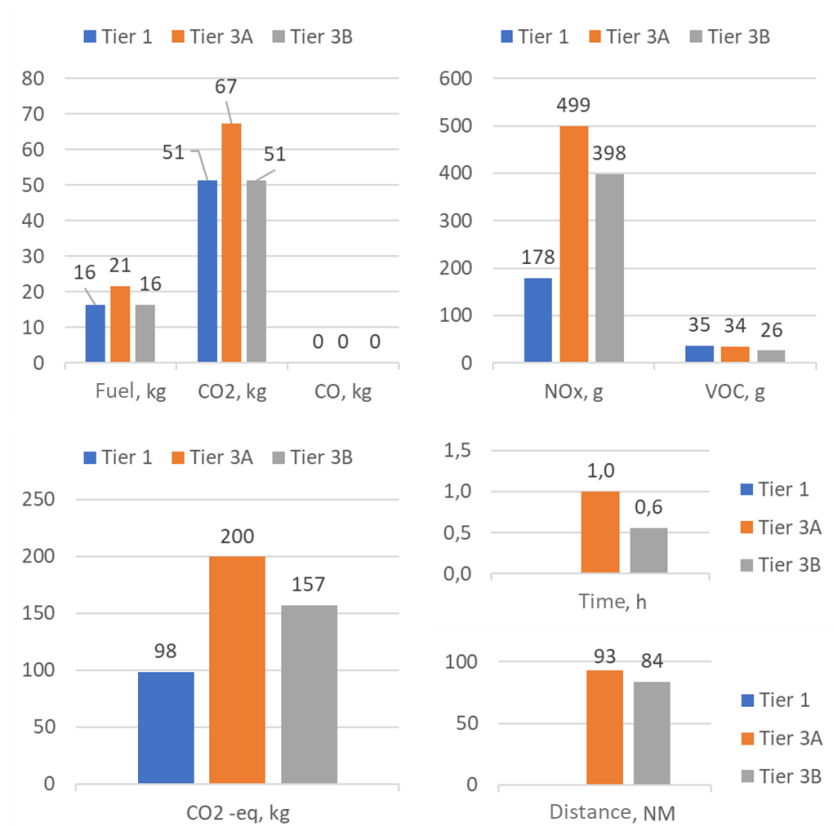


Figure 9: Emission results of different models for Flight 3

Flight 3 is the typical route flight. It is interesting that aircraft in Flight 3 is powered by two Diesel engines. CO and VOC emissions are negligible because Diesel engines do not have manual mixture control, so they operate with constant stoichiometric fuel to air ratio. NO_x emission still exists, and analysis shows that Tier 3A and Tier 3B NO_x emissions are 2 to 3 times higher compared to Tier 1 model. In Flight 3 there is again a disproportion of distance and time between models due to mentioned reception problems in Tier 3B model. In this example flight, incomplete flight record caused approximately 24% lower value of the fuel consumed, so better flight records are necessary for more accurate results.

Conclusion

Improved model for emission calculation were presented and analysed. Based on comparison of the results, it is clear that the basic Tier 1 method needs to be replaced by activity-depended models to get more accurate results of real emissions from aircraft. Although limitation to the GA aircraft, it was showed that extending to all air traffic including commercial flights is not only very simple but also expected.

Sensitivity analysis demonstrated great differences in emission results between different models. For the better comparison and more comprehensive analysis, the best would be to compare the calculated emissions to real in-flight emissions by measuring with Portable Emission Measurement Equipment. With results of that analysis, it could be easier to fine-tune the model, i.e. detection of flight phases, emission factors used, etc.

Further improvement is possible by using updated emission factors determined on more examples of aircraft and flights. Tier 3B flight records should be extended to entire flight including taxiing on the ground, flight phase determination could be improved with aircraft depended on data and automatically .csv data loading. Another improvement would be reprogramming of model in an advanced programming language with a more user-friendly interface.

Acknowledgements

Special thanks to prof. Anita Domitrović, PhD and David Gerhardinger, MEng. AE. from Faculty of Transport and Traffic Sciences, to Croatian Aviation Training Centre and Mr Theo Rindlisbacher from Swiss Federal Office of Civil Aviation.

References

Council Directive 98/70/EC. Official Journal L 350, 28/12/1998, pp. 0058 - 0068

ExxonMobil. Avgas 100LL – Safety Data Sheet, available at: <https://www.exxonmobil.com/english-US/Commercial-Fuel/pds/GLXXAvgas-Series>

EN 590:2004, EU: Fuels: Automotive Diesel Fuel, DieselNet https://www.dieselnet.com/standards/eu/fuel_automotive.php

European Environment Agency (2017). EMEP/EEA air pollutant emission inventory guidebook 2016 – Update July 2017 (1.A.3.a Aviation)

Federal Office of Civil Aviation (2007). Aircraft piston engine emissions – Summary Report, available at: https://www.bafu.admin.ch/dam/bafu/en/dokumente/klima/klima-climatereporting-referenzen-cp1/foca_2007a.pdf.download.pdf/foca_2007a.pdf

International Civil Aviation Organisation (2018). Emissions Databank (05/2018), available at: <https://www.easa.europa.eu/easa-and-you/environment/icao-aircraft-engine-emissions-databank> [online]

Intergovernmental Panel on Climate Change (2006). 2006 IPCC Guidelines for National Greenhouse Gas Inventories, Vol 1, pp. G.3-G.6, available at: <https://www.ipcc-nggip.iges.or.jp/public/2006gl/>

International Civil Aviation Organisation (2017). Glossary v 1.2, Montreal, available at: <https://www.icao.int/cybersecurity/Lists/Glossary/>

Portier, C. et al. (2010). A Human Health Perspective On Climate Change: A Report Outlining the Research Needs on the Human Health Effects of Climate Change, Research Triangle Park, NC:Environmental Health Perspectives/National Institute of Environmental Health Sciences

Sraga, V., Lulić, Z. (2017). Emissions from General Aviation in the Republic of Croatia, Digital proceedings of the 8th European Combustion Meeting, pp. 2372-2377

2.3 Air quality measurement, monitoring and modelling

This section includes papers presented in the context of the “Air quality measurement, monitoring and modelling” sessions of the TAP conference. Table 4 provides an overview of these papers, as they are listed in the following sub-sections.

Table 4. Titles and authors of “Air quality measurement, monitoring and modelling” papers

	Paper Title	Authors
2.3.1	Modelling human exposure to urban air quality: Application to in Paris megacity	A. Elessa Etuman, I. Coll, I. Makni and T. Bennoussaid
2.3.2	Analysis of long term roadside air pollution trends in European cities using ambient data from sparse monitoring networks	P.E. Lang, D.C. Carslaw and S.J. Moller
2.3.3	Mobile air quality measurements using bicycle to obtain spatial distribution and high temporal resolution in and around the city center of Stuttgart	A. Samad and U. Vogt
2.3.4	NO ₂ measurements in the city centre of Wuppertal	R. Kurtenbach, J. Kleffmann, A. Klosterkötter and P. Wiesen
2.3.5	NO ₂ Air Quality in German Cities: Trend Forecast and Scenarios	N. Toenges-Schuller, C. Schneider, R. Vogt and S. Hausberger
2.3.6	Source apportionment of the oxidative potential of ambient fine Particulate Matters: A case study of Athens, Greece	S. Taghvaei, M. H. Sowlat, E. Diapouli, M. I. Manousakas, V. Vasilatou, K. Eleftheriadis and C. Sioutas
2.3.7	Emission compliance over the lifespan of a vehicle	N.E. Ligterink, G. Kadijk, M. Elstgeest and P. van Mensch
2.3.8	Air Quality Impacts of New Public Transport Provision: A Causal Analysis of the Jubilee Line Extension in London	L. Ma, D. J. Graham and M. E. J. Stettler
2.3.9	Investigating the technological impact of European transport research and innovation towards a decarbonised urban landscape	A. Tsakalidis, K. Gkoumas, M. van Balen and F. Pekar
2.3.10	On-road heavy-duty trucks emission factors for black carbon and nitrogen oxides in China	H. Wang, S. Zhang and Y. Wu

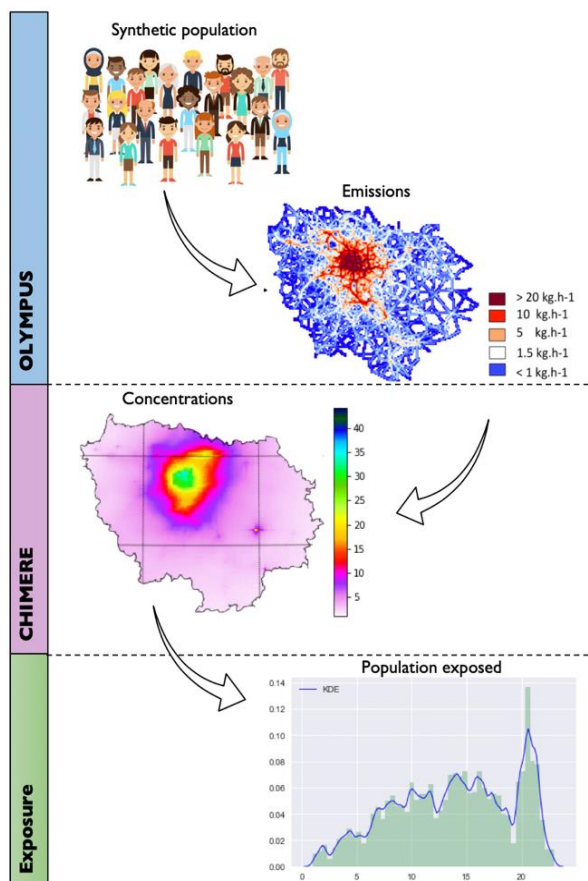
2.3.1 Modelling human exposure to urban air quality: Application to Paris megacity

A. Elessa Etuman¹, I. Coll¹, I. Makni¹, T. Benoussaid¹

¹ Laboratoire Interuniversitaire des Systèmes Atmosphériques (LISA), UMR CNRS 7583, Université Paris Est Créteil et Université Paris Diderot, Institut Pierre Simon Laplace (IPSL), Créteil, France

Abstract

Our work aims to characterize the exposure of urban populations to atmospheric pollutants through a modeling approach. For this, we have developed an integrated modeling chain based mainly on the coupled implementation of the OLYMPUS and CHIMERE models. OLYMPUS is an emission modelling system that provides the mobility of individuals in a city, through an activity-based travel demand approach. CHIMERE is a chemistry-transport model that uses anthropogenic and biogenic emissions, meteorological fields and large-scale chemical fields to produce hourly pollutant concentration fields on a given region. In post-processing, we currently develop a multi-step methodology to estimate the patterns of urban residents' exposure to pollutants. This modelling chain was implemented on the Paris megacity, a large and monocentric urban structure with a high central density of housing and very large peripheral urban areas.



Introduction

Air quality monitoring has been very strongly structured around observations. As measurement methods, measurement quality and uncertainty estimation are based on standard methods, measurements are now considered to reconstitute the actual exposure with a high representativity. Unfortunately, the variability of concentrations near the sources is quite high and the number of measuring stations that can be set up in such urban environments is necessarily very limited. In addition, measurements can hardly help predict the effects of a change in emissions. This is why, since the end of the 1990s, much progress has been made in the development of Eulerian models dedicated to the simulation of air quality. With the opportunity to use models for air quality management in the early 2000s, and the development of numerous prospective emissions scenarios studies in the research community, digital modeling has become an essential tool for the evaluation of air quality and for prospective studies about emission control. Today, most of the numerical modeling is dedicated to the prediction of pollutant concentrations, whether in prospective or hypothetical situations, which are obtained by varying forcing parameters such as meteorological parameters. These studies are conducted in the frame of environmental research, in order to support decision making and provide a comprehensive view of air quality levers in the context of urban planning and environmental policies. Thus, when elaborating new air quality plans, a detailed analysis of the impact of the measures envisaged on the emitting sectors is systematically carried out using modeling approaches. However, the evaluation of public policies should not be limited to the assessment of the effects they have on pollutant concentrations, and further analysis should provide information about the effect of reducing

the exposure of the populations to air pollutants. The health benefits made available through the implementation of policies must indeed be the main indicator of their relevance. However, today, few modeling approaches consider the exposure of individuals as an output. That is why we are developing a modeling chain which purpose is to take into account the entire public policy evaluation chain, from their impact on emission technologies and on the modification of polluting practices, up to the estimation of their effect on the exposure of individuals in the city. The modeling chain that is being set up is presented in this work. It is based on the coupling between an individual-based emission model (OLYMPUS) and a classic air quality model (CHIMERE). The works in progress concern statistical work about the subgrid refinement of concentration fields and its combination with individual trip information.

The purpose of this work, unlike studies on exposure to outdoor air quality based on cohorts such as APHEKOM (Pascal et al., 2013), is to characterize the mobility of an urban population, its emissions, the quality of air and quantify population exposure only through a numerical modeling approach. Jerrett et al., 2005 reviews the different types of exposure models. In particular, he concludes that much work remains in understanding the role of individual mobility in conditioning exposures. Moreover, the studies that come closest to our work are Gulliver and Briggs, 2011; Park and Kwan, 2017.

One of the aims of this project is ultimately to model the social inequality of exposure to air pollution.

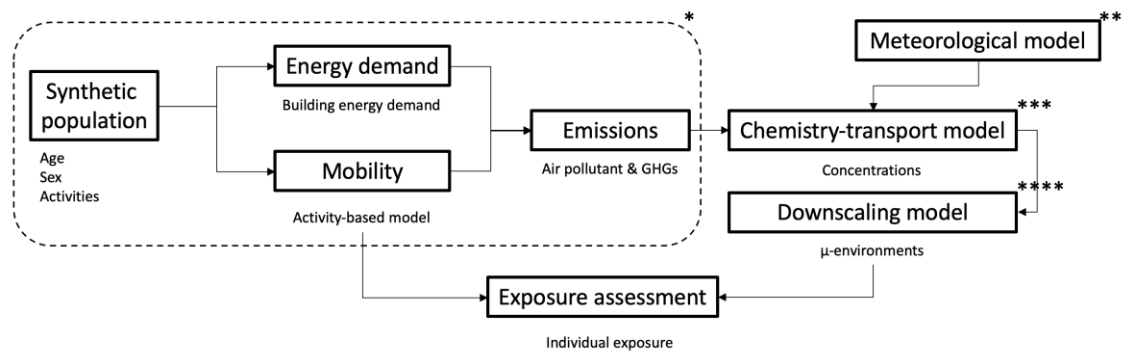


Figure 1. Representation of the modeling platform for the dynamic exposure of urban populations. * air pollutant and GHGs emissions model centered on the individual. ** WRF Meteorological Model, *** CHIMERE Chemistry-Transport Model, **** Downscaling approach of air pollutant concentrations.

Methodology and Results

The objective of the project is to model the exposure of an urban population by considering the mobility of individuals in the city; for this we have developed a modeling chain that is mainly coupling an emissions model integrating an activity-based sub-model (OLYMPUS) and a transport chemistry model (CHIMERE). The ultimate goal is to characterize local concentrations to better quantify population exposure.

The OLYMPUS platform is composed of different modules working in parallel or in series to provide pollutant emissions from individual designed activities. The GAIA module first generates a synthetic population of agents based on conditional probabilities, from sociodemographic surveys and land use information. Then, the combination of the THEMIS, MOIRAI and HERMES modules allows the definition of the mobility of each individual in the city through 1) an activity-based model for the generation of the mobility demand, 2) a gravity approach for the spatial attribution of activities and 3) the allocation of the transport demand on the road traffic, through a shortest path approach considering the congestion of the network. In parallel, the HESTIA module builds the energy demand of the territory from the unit energy consumption of households and employees, based on statistical properties of the buildings and household practices. Finally, the emissions associated with all the modeled activities are calculated in the VULCAN module.

CHIMERE is a chemistry-transport model (CTM) whose application scales cover a wide range of values, from urban air modeling with a resolution of 1-2 km to hemispheric air modeling with a resolution of 100-200 km. Indeed, in order to produce pollutant concentration fields, Eulerian CTMs use a mesh that covers the domain both on a horizontal and vertical scales relevant to the study of the target processes. It is considered that all variables describing the atmosphere and processes are uniform in each cell of

the domain. Then, in each cell, the calculation of the concentration levels of atmospheric pollutants is based on the principle of mass conservation and integrated chemistry, advection, diffusion, emissions and deposition. Like all CTMs, CHIMERE needs to be fed with forcing data such as meteorological fields, primary air pollutant emissions and chemical conditions at the boundaries of the defined Eulerian domain. The OLYMPUS outputs are combined with complementary inventories for industrial activities notably, and transferred to the CHIMERE model as emission inputs. The main operating principles of CHIMERE are described in [Mailler et al., 2016](#); [Menut et al., 2013](#). In our work, CHIMERE was first run at the continental and national scales to provide boundary conditions to the Île-de-France target area of study. Then, it was run at the highest reasonable resolution (1km) over a domain covering the whole region and named hereafter IDF1.

The scale descent model then determines the proximity concentrations.

The main goal is to be able to get fine scale concentration maps. However, the best resolution of CTM CHIMERE is 1km. A correction of CHIMERE outputs is hence needed. It thus had been established that the concentration value at street level was the sum of an urban background concentration value with a more local concentration.

$$C_{prox} = C_{ubg} + C_{local}$$

Cprox represent the proximity concentrations are defined as the cumulative concentration of local concentrations that depend on emissions and background concentrations.

Emissions treatment

The anthropogenic emissions used on the IDF1 domain come from the combination of OLYMPUS, EMEP and AIRPARIF emissions. The emissions modeled by OLYMPUS in its current version only include the "road transport" and "combustion in the residential and commercial sectors" sectors of activity of the SNAP nomenclature. It was initially necessary to complete these emissions with those of the other SNAP sectors (mainly industrial processes). To this end, we have collected from AIRPARIF the inventory data used for the regulatory modeling of air quality, which have the advantage of being obtained by a bottom-up method and to be validated via its daily use for regulatory air quality monitoring. Still, since AIRPARIF and OLYMPUS emissions only cover the administrative territory of Ile-de-France, and the CHIMERE model requires projected emissions on a regular mesh of simple form, it was necessary to develop a module allowing the junction of OLYMPUS / AIRPARIF emissions and another inventory covering the outside of the regional domain. This join was performed using spatialized data from the EMEP European Inventory.

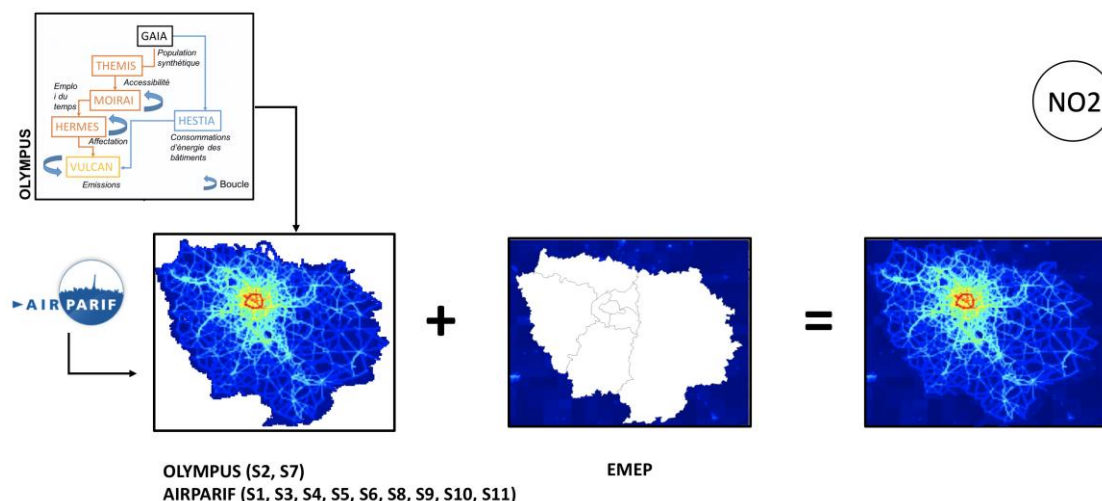


Figure 2. Illustration of the Combination of Nitrogen Oxides Emissions on the IDF1 domain

Configuration of OLYMPUS-CHIMERE simulations

In order to evaluate our toolchain over a significant period of time, we performed the simulation over a full year. The choice of this duration was also based on the need to compare pollutant levels with WHO

regulations and recommendations. The year 2009 was marked by major episodes of pollution. The first took place at the beginning of the year (January 9th to 12th) and the second in the spring (April 3rd to 6th). The pollution events observed in 2009 mainly affect particle concentrations, but three photochemical episodes (NO_2 , O_3) were also observed during this year.

The configuration used in the Olympus model is described in [Elessa Etuman and Coll, 2018](#), with the population characteristics and practices simulated by OLYMPUS being forced by regional surveys and census data. As mentioned earlier, the influence of plumes coming from outside our simulation domain was taken into account through nested simulations. At the boundaries of the continental domain we use climatological concentrations produced by a global modeling chain (LMDZ-INCA). The continental domain simulation is run at a resolution of $0.68^\circ \times 0.46^\circ$ and will in turn provide forcing data to the national simulation domain which is run at a higher resolution of $0.205^\circ \times 0.135^\circ$. The first simulation conducted at the European level intends to better represent the various European contributions from large urbanized areas, as well as emissions from the maritime corridor of the North Sea, which impact air composition on the French territory during the period of study. The 15km-resolution domain was made to finely represent potential transport of air masses from the German Ruhr region to Île-de-France during the anticyclonic situations of January 2009. Finally, these outputs will provide concentrations at the limits of the target Paris area (IDF1). Figure 3 shows a visualization of these simulation domains. The main simulation domain IDF1 is shown in blue.

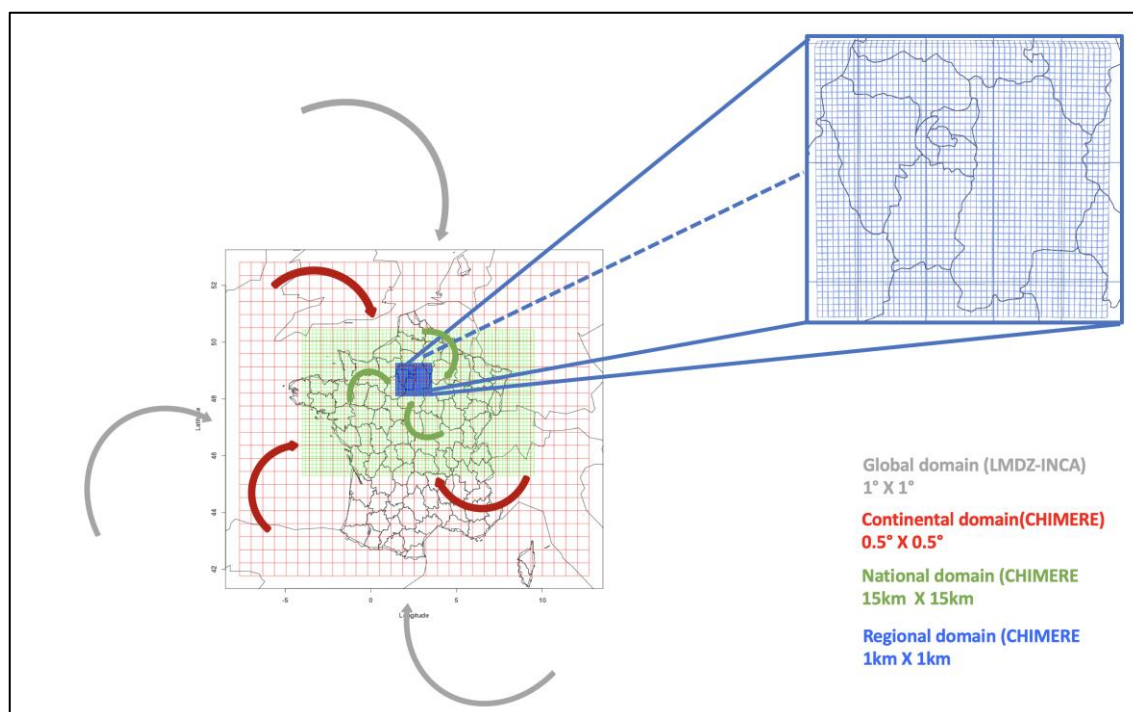


Figure 3. Presentation of the nested simulation domains

Analysis of the results

The simulations were conducted using the resources of the Research and Technology Computing Center (CCRT). The simulation results show a good representation of pollutant concentrations. This is illustrated by the simulated concentration fields and the time series of NO_2 in figure 4. It is observed here that OLYMPUS makes it possible to reproduce the expected concentration gradient for a pollutant such as nitrogen dioxide, with a factor of 4 to 5 times from the suburbs to the heart of the agglomeration - where levels reach $30 \mu\text{g}\cdot\text{m}^{-3}$ in average annual value per square kilometer. This ratio is approximately identical to the one simulated between the central and the peripheral zone for PM_{10} (not shown here), with a gradient of concentrations ranging from 4 to $20 \mu\text{g}\cdot\text{m}^{-3}$ and a relatively high homogeneity of the concentrations in the external and internal zones. For the finer particles ($\text{PM}_{2.5}$) shown in figure 5, the overconcentration factor is lower, with a maximum of 3 from the outermost suburbs to the center of Paris. The mean annual concentrations range from 5 to $13 \mu\text{g}\cdot\text{m}^{-3}$. In all the graphs, the strongest gradient is observed between the small and large suburban rings, and it presents a concentric circle structure that reflects the strongly monocentric vision of the modeled agglomeration.

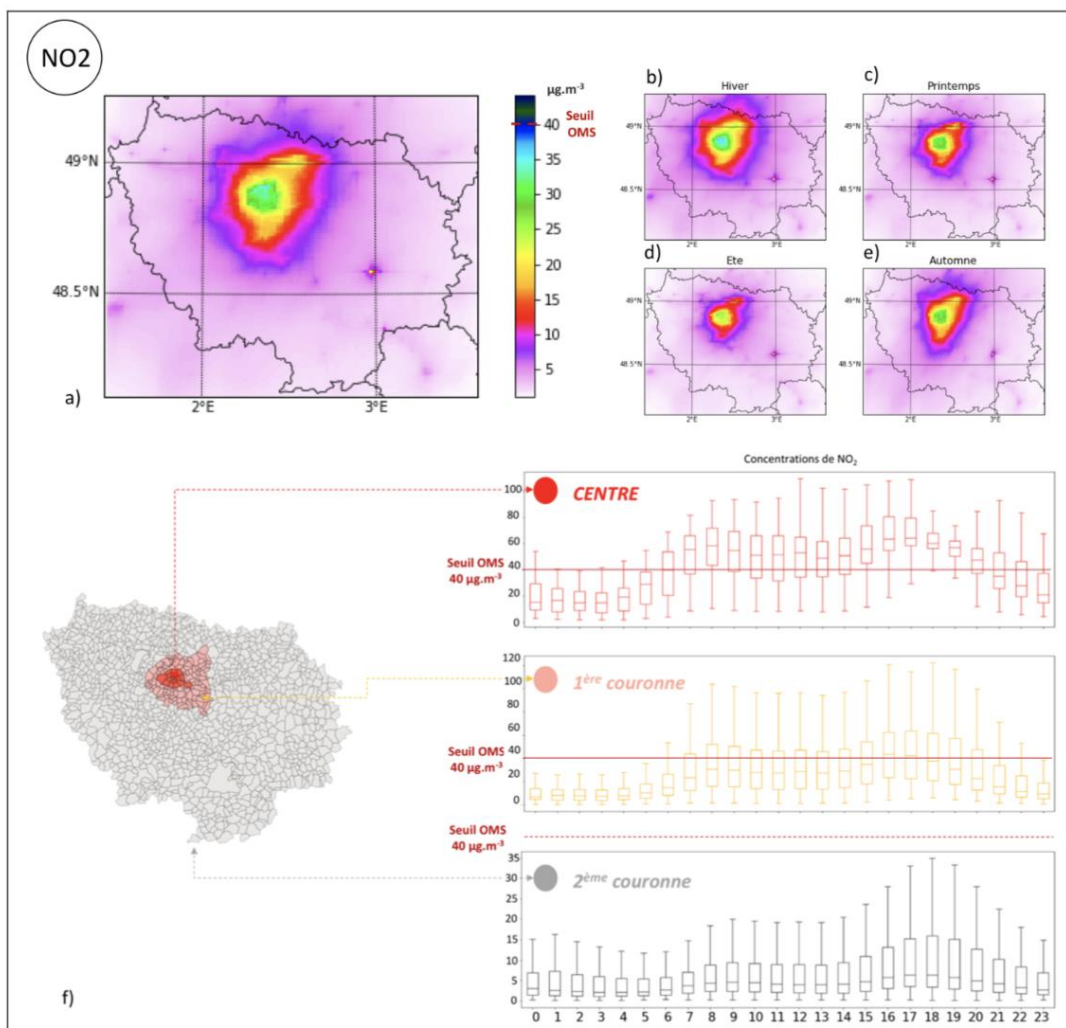


Figure 4. Spatial and temporal distribution of NO₂ concentrations modeled for the year 2009 with the OLYMPUS - CHIMERE platform. All concentrations are in µg.m⁻³. Top left, annual average value. Top right, seasonal averages. Average diurnal evolutions (hourly boxplots) are also shown by zone.

We also conducted the simulation by forcing CHIMERE by the AIRPARIF / EMEP inventory alone ("APF-CHIMERE" version), in order to make a comparison with the data of our platform ("OLP-CHIMERE" version). The objective of this comparison is to evaluate the capacity of our platform to reconstitute the major characteristics of spatiotemporal evolution of concentrations compared to the state of the art. Figure 5 shows box plots of mean hourly concentrations of PM_{2.5} for both simulations, as well as a map of the difference in concentrations. Here we observe that OLP-CHIMERE represents quite well the spatial structure and the intensity of the pollutant concentrations. Its concentration values are higher in the city center than the APF-CHIMERE outputs, which goes in the direction of an improvement of the simulation, but the effect is only of a few micrograms per cubic meter. Conversely, there is a tendency of OLP-CHIMERE to simulate lower concentrations in the remote suburbs compared with APF-CHIMERE, which is most likely the effect of the lack of representation of inter-regional traffic and freight, but probably also of the fact that we don't represent the secondary road network in OLYMPUS.

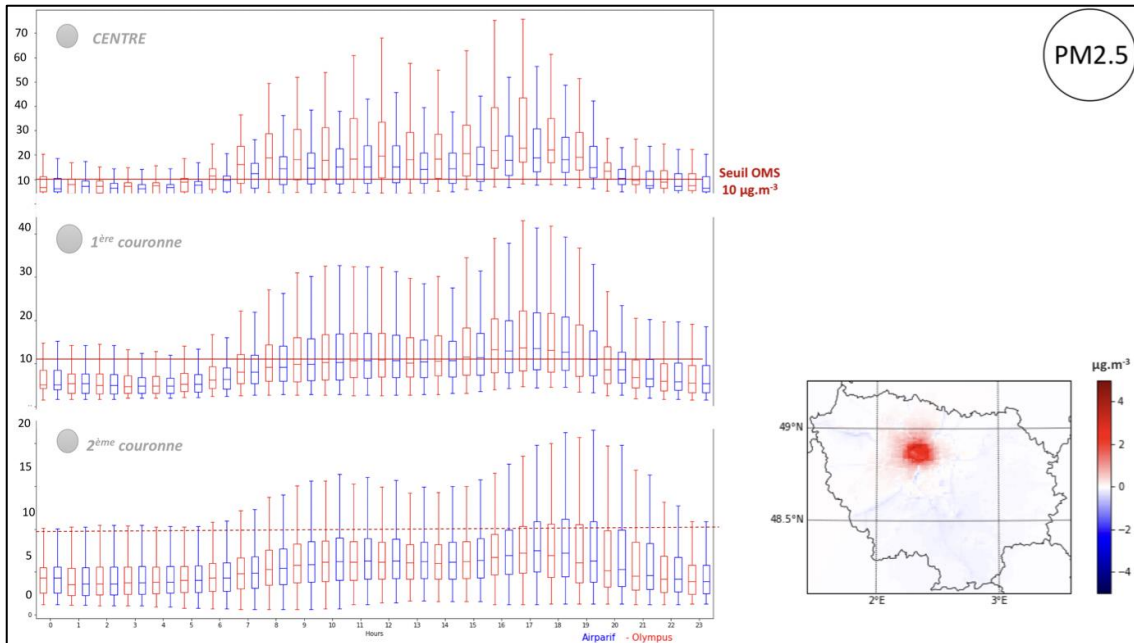


Figure 5. Temporal series of mean hourly PM_{2.5} values modeled by zone by OLYMPUS-CHIMERE (red) and AIRPARIF-CHIMERE (blue). Bottom, difference map of mean annual concentrations ($\mu\text{g}\cdot\text{m}^{-3}$) in the [OLYMPUS - AIRPARIF] direction. Red tones represent stronger concentrations in the simulation based on OLYMPUS calculations, and vice versa.

Analysis of the results

Finally, we used the outputs of the OLYMPUS-CHIMERE modeling chain to quantify the exposure of the population to PM₁₀ and NO₂. We first cross-tabulated the annual concentration maps at a kilometric resolution with population density data simulated by OLYMPUS. This first way of calculating the exposure allowed us to produce diagrams of the percentage of the population exposed per range of NO₂ concentration, on average over the year. We also produced a temporal focus on the different pollution episodes as well as a spatial focus by place of life (Paris, inner and outer suburbs).

But the information produced by OLYMPUS allows us to expect deeper analyses of exposure, through the production of diagrams discriminated according to socio-demographic characteristics and to practices. This can be obtained by crossing the CHIMERE outputs with the daily trip of agents provided by OLYMPUS. The analysis of these graphs makes it possible to go further in the interpretation of exposure gradients, but it also constitutes a reference for the assessment of the impacts of public policies on people's health.

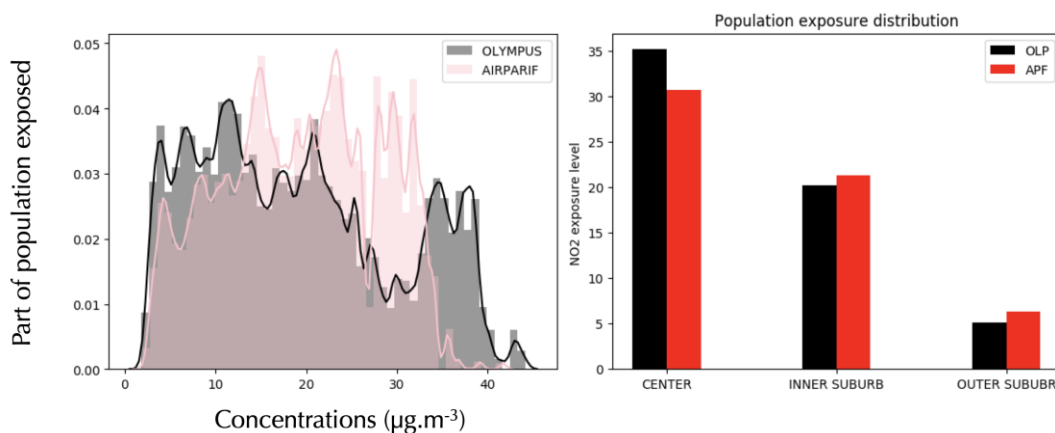


Figure 6. Diagram of the average annual population exposure to nitrogen dioxide in the Paris megacity in 2009.

Finally, we consider that the use of simulated data at a kilometric resolution is not fully satisfactory for the assessment of exposure in cities, especially near roadways. This is clearly visible in the model-measurement in the city-center, and it is a well-known limit of CTMs in the literature. This is why a work of refinement of the concentration fields, based on a statistical treatment of the CHIMERE output data is currently in progress, to better represent the effect of the proximity to the sources on the exposure (Makni et al., 2019). Ultimately, these data will be used to replace the CHIMERE outputs in our exposure graphics so as to produce more accurate assessment of the risk of exposure, especially for the high values affecting daily people downtown.

Conclusion

Our work validated the air quality modeling process based on the production of emissions by the OLP-CHIMERE platform, given the spatial and temporal distribution of concentrations in the Parisian megacity, and with respect to the same data obtained with the AIRPARIF emission inventory. In dense urban areas, differences with APF-CHIMERE favor our approach, which shows a slightly improved recovery of observed concentrations. But even in the Parisian areas where APF-CHIMERE behaves better, the difference between the two simulations is much lower than the average measurement-model gap. Despite the small magnitude of this difference, the variability in the distribution of nitrogen oxide emissions in the suburbs has an impact on ozone production and on exposure to NO₂. Changes made to the OLYMPUS configuration for interregional transport, freight and secondary network assignment should help reducing this gap.

This approach being validated, we have shown that the combination of data from the platform makes it possible to consider a more in-depth analysis of exposure, including the issue of territorial and socio-demographic inequalities. Finally, ongoing work about the refinement of simulated concentration fields will strongly improve the precise character of simulated exposure within dense cities.

Acknowledgements

This work was performed using HPC resources from GENCI-CCRT (grant 2017-t2015017232). This work also received support from the French National Agency for Research (ANR-14-CE22-0013) and the Île-de-France region (DIM R2DS). We also acknowledge AIRPARIF and the LABEX Urban Futures.

References

Elessa Etuman, A., Coll, I., 2018. OLYMPUS v1 . 0 : development of an integrated air pollutant and

GHG urban emissions model – methodology and calibration over greater Paris 5085–5111.

- Gulliver, J., Briggs, D., 2011. Science of the Total Environment STEMS-Air: A simple GIS-based air pollution dispersion model for city-wide exposure assessment. *Sci. Total Environ.* 409, 2419–2429. <https://doi.org/10.1016/j.scitotenv.2011.03.004>
- Jerrett, M., Arain, A., Kanaroglou, P., Beckerman, B., 2005. A review and evaluation of intraurban air pollution exposure models 185–204. <https://doi.org/10.1038/sj.jea.7500388>
- Mailler, S., Menut, L., Khvorostyanov, D., Valari, M., Couvidat, F., Siour, G., Turquety, S., Briant, R., Tuccella, P., Bessagnet, B., Colette, A., Létinois, L., Meleux, F., 2016. CHIMERE-2016: From urban to hemispheric chemistry-transport modeling. *Geosci. Model Dev. Discuss.* 0, 1–41. <https://doi.org/10.5194/gmd-2016-196>
- Makni, I., Coll, I., Elessa-Etuman, A., Benoussaid, T., 2019. Characterization of atmospheric pollution at local scales: implementation of a downscaling method, in: TAP Conference Poster.
- Menut, L., Bessagnet, B., Khvorostyanov, D., Beekmann, M., Blond, N., Colette, A., Coll, I., Curci, G., Foret, G., Hodzic, A., Mailler, S., Meleux, F., Monge, J.-L., Pison, I., Siour, G., Turquety, S., Valari, M., Vautard, R., Vivanco, M.G., 2013. CHIMERE 2013: a model for regional atmospheric composition modelling. *Geosci. Model Dev.* 6, 981–1028. <https://doi.org/10.5194/gmd-6-981-2013>
- Park, Y.M., Kwan, M.P., 2017. Individual exposure estimates may be erroneous when spatiotemporal variability of air pollution and human mobility are ignored. *Heal. Place* 43, 85–94. <https://doi.org/10.1016/j.healthplace.2016.10.002>
- Pascal, M., Corso, M., Chanel, O., Declercq, C., Badaloni, C., Cesaroni, G., Henschel, S., Meister, K., Haluza, D., Martin-Olmedo, P., Medina, S., 2013. Assessing the public health impacts of urban air pollution in 25 European cities: Results of the Aphekom project ☆ Abbreviations: Aphekom, Improving Knowledge and Communication for ... *Science of the Total Environment Assessing the public health impact.* *Sci. Total Environ.* 449. <https://doi.org/10.1016/j.scitotenv.2013.01.077>

2.3.2 Analysis of long term roadside air pollution trends in European cities using ambient data from sparse monitoring networks

P.E. Lang^{1}, D.C. Carslaw^{1,2} and S.J. Moller³*

¹ Wolfson Atmospheric Chemistry Laboratories, University of York, York, YO10 5DD, United Kingdom

² Ricardo Energy & Environment, Harwell, Oxfordshire, OX11 0QR, United Kingdom

³ National Centre for Atmospheric Science, Wolfson Atmospheric Chemistry Laboratories, University of York, York, YO10 5DD, United Kingdom

* Corresponding author email: pl746@york.ac.uk

Introduction

Air pollution is one of the most important problems facing Europe, responsible for an estimated 400,000 premature deaths a year (EEA, 2018). Of particular concern are the concentrations of nitrogen oxides (NO_x), composed of NO and NO₂, and particulate matter (PM).

Frequent and widespread exceedances of the European Union limits on NO₂ and PM concentration have motivated policies aimed at reducing the concentration of these air pollutants. These policies have included the reduction of vehicle emissions through European Directives (Euro Standards) that have set increasingly stringent limits on the emissions from road vehicles. To meet these emission limits, vehicle manufacturers have adopted exhaust technologies such as three-way catalysts on petrol vehicles, diesel particulate filters (DPF) and diesel oxidation catalysts (DOC) (EEA, 2016). The impact of these changes on ambient air quality in Europe is difficult to establish but can potentially be evaluated through analysis of the long term trends in ambient roadside concentrations of air pollutants using data from the extensive European monitoring network. Such an evaluation also has the potential to provide information on the effectiveness of different policies to reduce air pollution.

The vast amount of ambient monitoring data measured at thousands of monitoring stations across Europe provides the ability to directly analyse the large-scale changes in roadside air quality in Europe over time. While the data from a single monitoring station provides information about the local variation in air quality at a specific location, aggregation of data from multiple monitoring stations enables the effects of local variability to be 'averaged out', leaving a better indication of the large-scale trend.

However, there are several limitations inherent in the established methods for calculating aggregate trends using data from air quality monitoring networks. One approach is to compare individual time series from different monitoring stations (e.g. Masiol et al., 2017; Mavroidis and Chaloulakou, 2011), however this becomes impractical in very large monitoring networks, such as the European network.

Another method involves evaluating the trend in the average concentration across all the available monitoring sites. This trend can be biased due to the leveraging effects of site flux (i.e. sites opening and closing during the period of interest) on the average concentration, as demonstrated by Lang et al. in a trend analysis using data from the London monitoring network (Lang et al., 2019). For example, in a given year, the opening or closing of monitoring stations cause new data to be included in the average concentration, potentially resulting in abrupt changes in the average concentration that are driven, not by changes in source emissions strength, but by the sudden inclusion or exclusion of data. Many monitoring networks, particularly those composed of roadside stations, experience considerable site flux, which can have a substantial effect on the calculated trend in average concentration.

To mitigate this issue, data filtering can be applied to ensure that only data from monitoring stations with a complete time series (i.e. measuring constantly over the period of the trend analysis) are included in the analysis (e.g. Font and Fuller, 2016). This approach inevitably results in the exclusion of much of the available data and therefore a considerable loss of information.

The rolling change method is a technique designed to address the above issues, and enable the calculation of aggregate trends in ambient air quality using data from monitoring networks that evolve over time. The method is robust to the biasing effects of site flux, while preserving more data in the trend analysis than data filtering methods (Lang et al., 2019). This approach enables better investigation of the large scale air pollution trends across an area of interest providing the ability to produce trends that are more representative, due to the inclusion of more sites, and driven by genuine concentration changes.

This study uses the rolling change method to calculate large-scale trends in roadside concentrations of NO_x , NO_2 , PM_{10} and $\text{PM}_{2.5}$ in Europe between 2000 and 2017. The trends in roadside air quality are also calculated in 44 individual European functional urban areas (FUAs), and compared with the European-wide trends. The reasons for the observed changes in air pollutant concentrations are discussed in the context of changes in vehicle emissions, and possible explanations for the deviations from the overall trend pattern observed in some FUAs are proposed.

Methods and Data

The long term trends for Europe and for each European FUA were calculated using the rolling change method (Lang et al., 2019). The method involves splitting the period of interest into short moving windows, each offset from the adjacent window by a time step, in this case one year. The data within each window is filtered to exclude data from monitoring sites with an incomplete time series over the period of the moving window (i.e. sites which open or close during the window), to ensure that all time series within the moving window are the same length. The change in concentration over the window is calculated by fitting a linear regression to this filtered data. By shifting the moving window along the period of analysis, and calculating the concentration change at each step, a trend can be estimated. This aggregate trend represents the average change in concentration over all monitoring sites, unaffected by the leveraging effects of changes in the average concentration caused by site flux during the period of analysis. In effect, the method relaxes the data capture requirement to short time periods rather than the whole time series, which increases the amount of data that can be used in trend analysis.

The rolling change method was applied using annual median data, resulting in median trends for each FUA. The advantage of an annual trend, as opposed to a trend with more granular resolution, is to 'average out' the effects of confounders which vary on a shorter time scale, for example, seasonal variation.

All ambient concentration data were obtained from the *smonitor* Europe database (Grange, 2016), which stores data collected from the European Environment Agency AirBase and air quality e-Reporting data repositories (EEA, 2018, EEA, 2019). Only data from roadside monitoring sites were considered. The distribution of monitoring sites contributing to the aggregate trends over the whole of Europe is displayed in Figures 1-2. In each case, the 'number of sites' corresponds to the total number of unique sites that contributed to the trend over the entire period of analysis (2000-2017).

Figures 1 and 2 indicate that the distribution of monitoring sites in the European network is highly heterogeneous, with several countries (Italy, Germany, Spain, France and the UK) dominating the network. Consequently, these countries will dominate the shape of the overall European trends. This provides an additional motivation for examining the trends at a city-scale in complement to the European-scale, as it allows closer analysis of regions which are underrepresented in the European-wide trend.

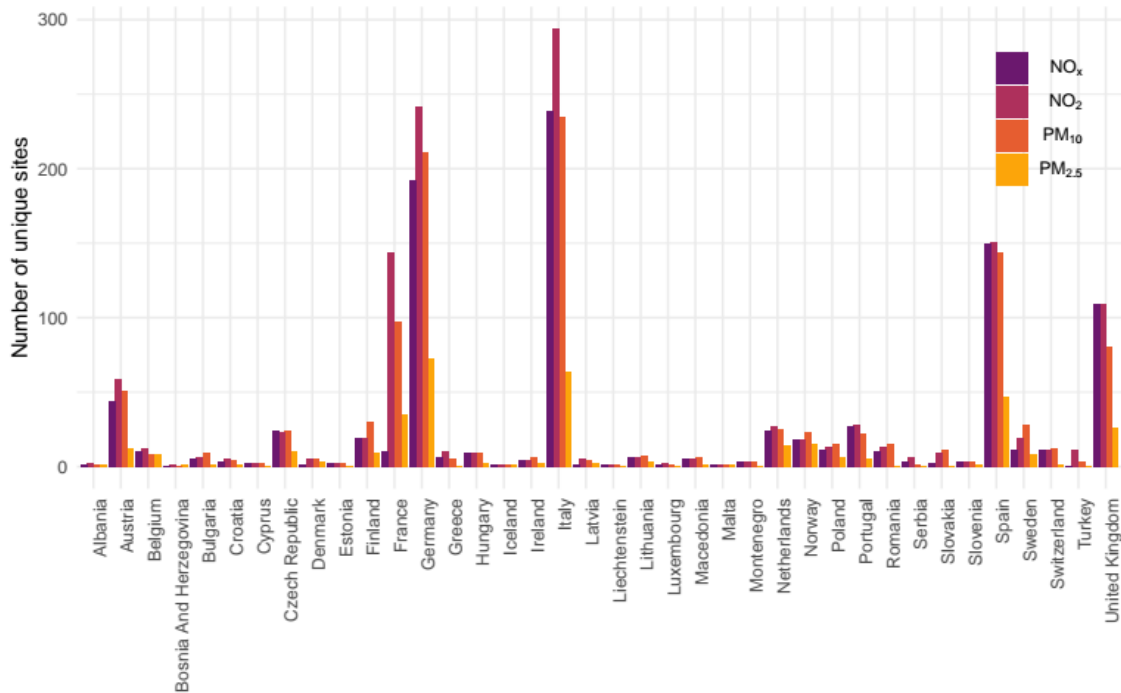


Figure 1: The total number of unique roadside monitoring sites contributing to the rolling change trends in NO_x, NO₂, PM₁₀ and PM_{2.5} concentration over the period 2000-2017, by country and pollutant.

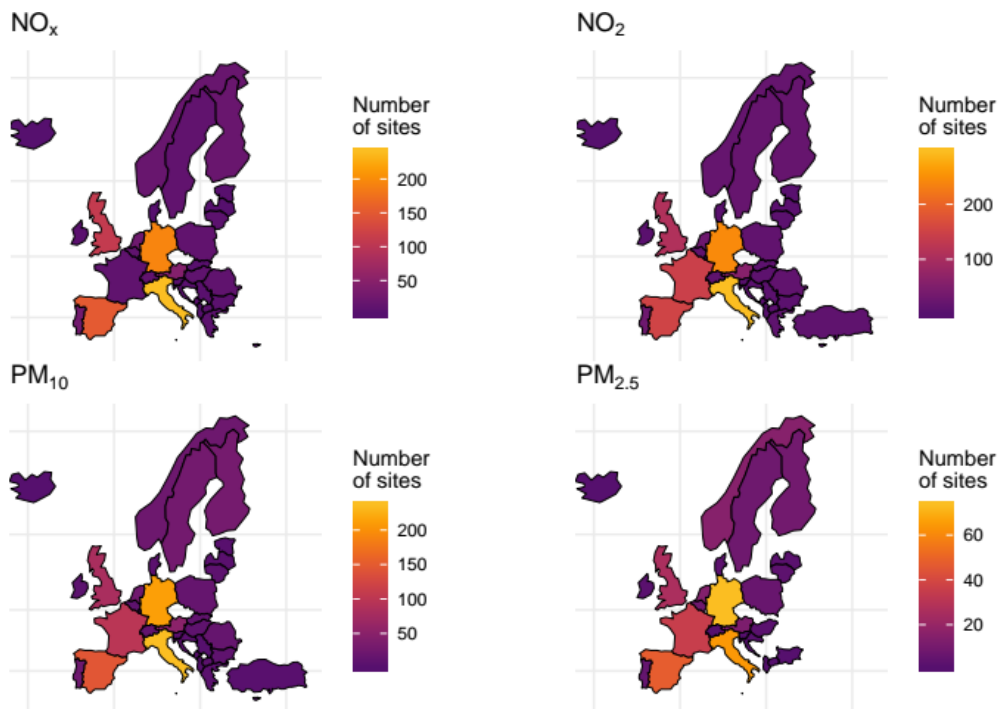


Figure 2: Distribution of roadside monitoring sites contributing to the rolling change trends in NO_x, NO₂, PM₁₀ and PM_{2.5} concentration across Europe. The colours represent the total number of unique roadside monitoring sites contributing to the rolling change trend in each country between 2000 and 2017.

The European city in which each monitoring sites was located was determined using spatial data on the European functional urban areas (FUA). The FUA spatial data were obtained from the European Commission Joint Research Centre (JRC) (Lavalle et al., 2015).

The criteria for an FUA to be included in the analysis was that the FUA must (i) contain at least one monitoring site measuring the pollutant of interest, and (ii) not have a period equal to or greater than the width of the moving window (three years) during which there are no measurements of the pollutant of interest available. The FUAs for which trend analysis was conducted, according to these criteria, are shown in Table 1, along with the total number of distinct roadside monitoring sites that contributed to the trend in each FUA (over the entire time period of the analysis).

The analysis was carried out in R, using the aqtrends R package for the calculation of the rolling change trend (Lang, 2018).

Table 1: Total number of unique roadside monitoring sites measuring NO_x, NO₂, PM₁₀ and PM_{2.5} concentration in each European functional urban area analysed.

FUA	NO _x	NO ₂	PM ₁₀	PM _{2.5}
Amsterdam	7	8	0	0
Athina	0	6	0	0
Barcelona	18	18	23	0
Berlin	16	16	0	6
Bilbao	6	6	0	0
Bologna	0	8	0	0
Braunschweig-Salzgitter-Wolfsburg	0	4	0	0
Bruxelles / Brussel	0	7	0	0
Düsseldorf	0	2	0	0
Frankfurt am Main	0	7	4	0
Gijón	4	4	4	0
Glasgow	0	3	0	0
Hamburg	0	8	5	0
Helsinki	7	7	7	0
Innsbruck	0	5	5	0
Karlsruhe	0	5	6	0
La Spezia	0	5	0	0
Lille	0	5	0	0
Linz	0	7	5	0
Lisboa	8	8	5	0
London	70	70	58	9
Lyon	0	9	7	0
Madrid	24	24	21	7
Mainz	4	4	0	0
Mannheim-Ludwigshafen	5	8	6	5
Marseille	0	6	0	0
Milano	0	14	0	0
München	7	8	6	0
Nürnberg	6	6	5	0
Paris	0	13	9	0
Pescara	0	4	0	0
Pisa	0	4	0	0
Praha	10	10	10	6
Roma	14	14	0	0
Rotterdam	0	6	0	5
Ruhrgebiet	16	21	0	0
Salzburg	0	4	4	0
Stockholm	5	5	8	0
Stuttgart	0	14	12	0

Torino	0	7	0	0
Toulouse	0	6	0	0
Utrecht	4	4	0	0
Valladolid	0	4	6	0
Wien	0	16	0	0

Results and Discussion

Figure 3 shows the long term trends in roadside NO_x , NO_2 , PM_{10} and $\text{PM}_{2.5}$ concentrations, as well as the NO_2/NO_x , $\text{PM}_{10}/\text{NO}_x$ and $\text{PM}_{2.5}/\text{NO}_x$ ratios between 2000 and 2017 across the entirety of Europe. It can be seen that, on average, in Europe the concentrations of NO_x and $\text{PM}_{2.5}$ have been decreasing monotonically since 2000. NO_2 and PM_{10} concentrations increased slightly to 2003, and decreased monotonically subsequently.

The observed decrease in NO_x and NO_2 concentrations in Europe since 2000 and 2002 respectively can be attributed to the introduction of vehicle exhaust technologies aimed at reducing emissions of these species, such as three-way catalysts used on petrol vehicles and the more recent use of Lean NO_x Traps (LNT) and Selective Catalytic Reduction (SCR) on diesel vehicles over this period. Indeed, the rolling trend analysis of roadside NO_x and NO_2 concentrations provide compelling evidence that emissions of NO_x have strongly decreased across Europe as a whole. These conclusions are robust in the sense the rolling trend analysis maximises the use of the large amounts of measurement data available across Europe while largely eliminating any bias introduced due to differing numbers of sites available in each year.

The increase in NO_2 concentration prior to 2002 was most likely due to the increase in the number of diesel passenger vehicles over this period. As shown in Figure 4, the proportion of the new vehicle registrations in Europe composed of diesel vehicles increased from 36% in 2001 to 48% in 2005, then increased more slowly to a peak in 2011/12 of 55%, before starting to decrease (ICCT, 2018). This period also coincided with the introduction of DOCs to new vehicles in compliance with the Euro 3 and Euro 4 emission standards, leading to the emission of more NO_2 from vehicle exhaust (Carslaw et al., 2019).

A study by Grange et al. (2017) considered the trends in average NO_x and NO_2 concentrations in Europe, and found that NO_x concentrations decreased between 1998 and 2015, in corroboration with the findings of this study. The principal finding of Grange et al. (2017) was that the *emissions* ratio of NO_2/NO_x from road vehicles increased from 2000 to about 2009 and then started to decrease. A consideration of the *ambient* roadside concentration NO_2/NO_x ratios also shows a clear increase from 2000 to about 2009 and then a decreasing trend. This behaviour is entirely consistent with Grange et al. (2017) and is related to increased ratio of NO_2/NO_x in vehicle exhaust due to DOC and DPF. In DOC and DPF, the deliberate production of NO_2 through oxidation of NO is used to help oxidise other pollutants such as CO , hydrocarbons and particulate matter.

The more recent decrease in the ambient NO_2/NO_x ratio likely has several origins. Recent vehicle emission remote sensing measurements show that as the vehicle mileage increases for diesel passenger cars, the NO_2/NO_x ratio decreases (Carslaw et al., 2019). This deterioration effect is unlikely to be the only factor affecting the recent decreasing NO_2/NO_x ratio. It is also likely that vehicle emission after-treatment systems have been better optimised so as not over-produce NO_2 . These other factors require further emission measurements and analysis to confirm their contribution. However, given the timing of the change shown in Figure 3, there is consistency with the introduction of Euro 5/V Standards around 2009. It should also be noted that as NO_x and NO_2 concentrations continue to decrease, the ambient concentration ratio of NO_2/NO_x will eventually increase due to the increased availability of O_3 to convert NO to NO_2 , which can be readily confirmed by plotting the NO_2/NO_x ratio against NO_x . For example, at urban background sites, the ratio of NO_2/NO_x is typically around 0.6 to 0.7, which is considerably higher than the peak ratio seen in Figure 3. There might be some indication of this increase shown in Figure 3, although more data are required to confirm whether an increasing trend continues. Such an increase will also be dominated by the increased role of O_3 rather than primary NO_2 emissions from vehicles.

The trend plots for PM_{10} and $PM_{2.5}$ both show substantial reductions in concentration since 2000. While the data shown in Figure 3 are for roadside sites, the concentrations of both species will be strongly influenced by non road sources including secondary particulate matter (principally sulphate and nitrate). A more informative analysis is to consider the ratio of PM to NO_x , where NO_x acts as a local combustion tracer. For PM_{10} and $PM_{2.5}$, the ratio to NO_x has decreased in recent years, which likely reflects the increased use of DPF on heavy and light duty vehicles. The trends in the ratios shown in Figure 3 show that there has been a greater reduction in the ratio of $PM_{2.5}/NO_x$ than PM_{10}/NO_x . This behaviour is consistent with the more effective reduction in $PM_{2.5}$ exhaust emissions than total PM_{10} , the latter of which will also include a stronger influence of coarse fraction ($PM_{2.5}$ to PM_{10}) tyre, brake and road abrasion sources, which have not been mitigated.

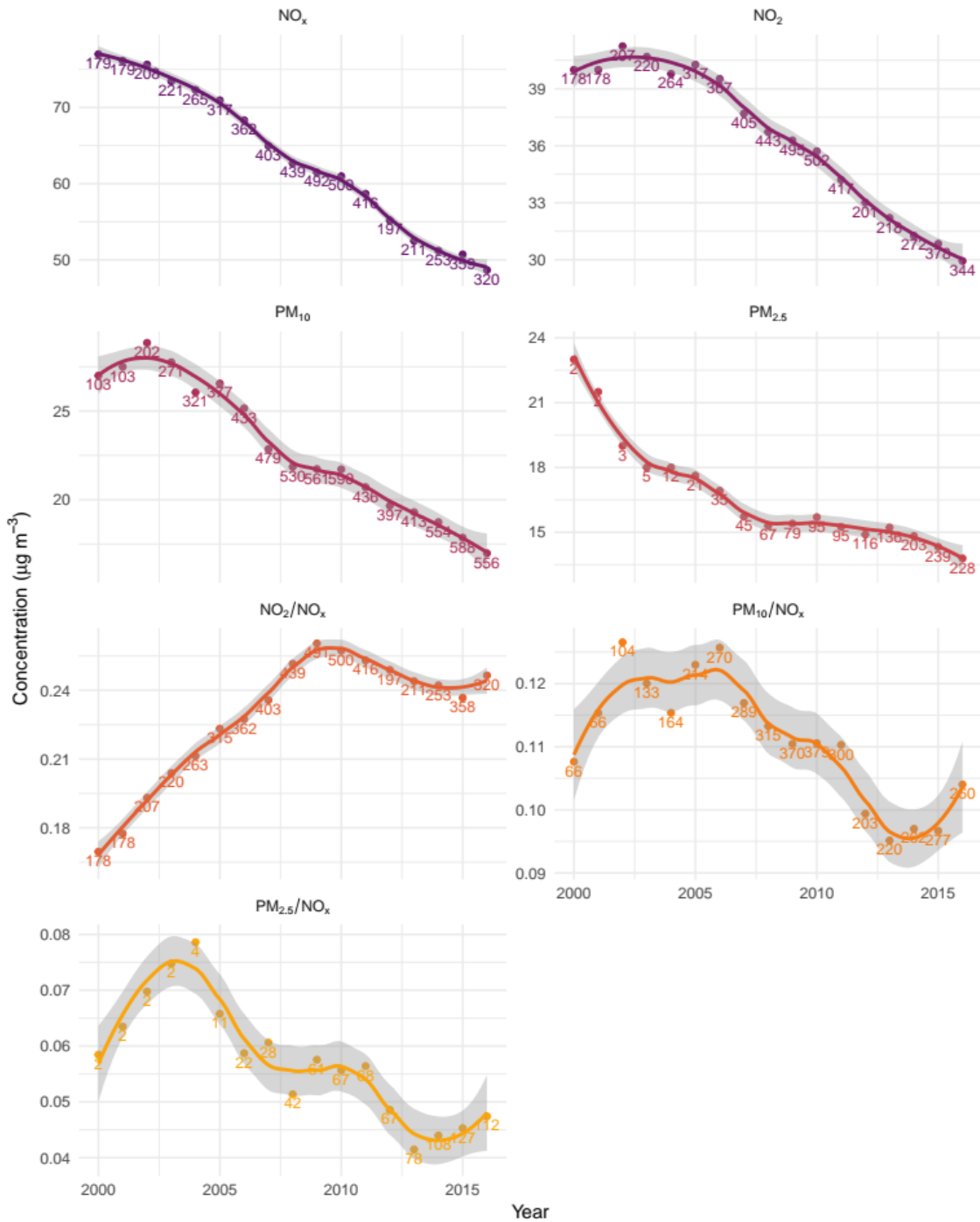


Figure 3: Rolling change trends in NO_x, NO₂, PM₁₀ and PM_{2.5} roadside concentration, and the NO₂/NO_x, PM₁₀/NO_x, and PM_{2.5}/NO_x ratios across Europe between 2000-2017. The smoothed lines are loess (local regression) fits, with the 95% confidence interval represented by the shaded band. The numbers signify the number of monitoring sites contributing to each annual data point. Annual pollutant ratios were calculated as the slope of a regression of the hourly concentration of one pollutant against the other (for each year of data).

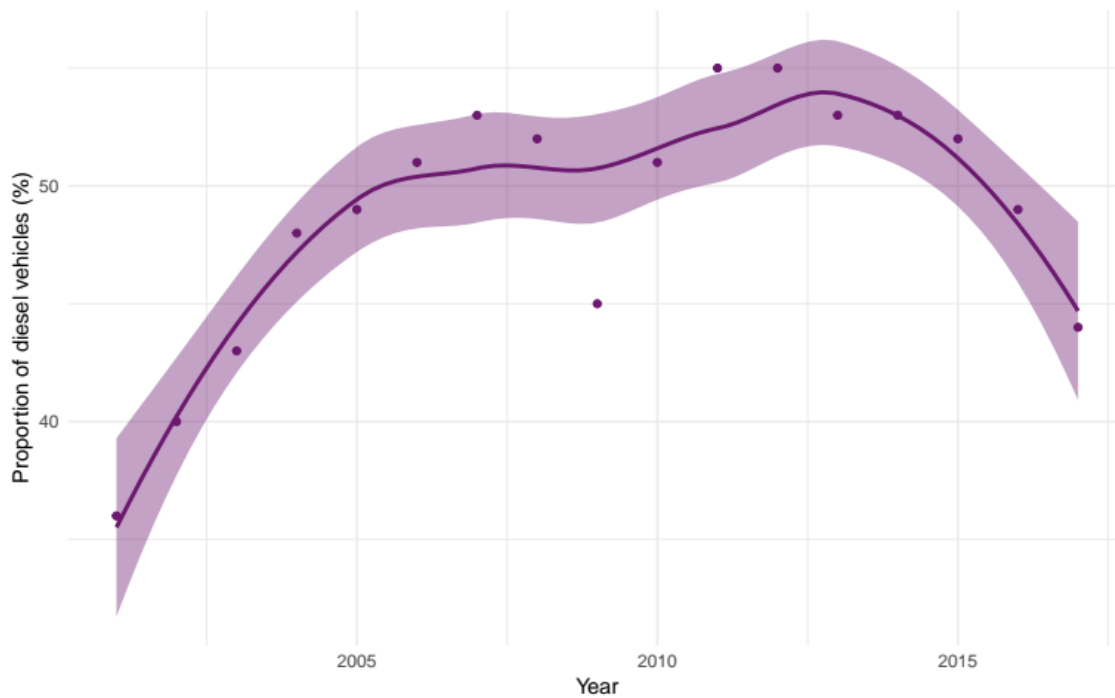


Figure 4: Proportion of new registrations composed of diesel vehicles in Europe by year between 2001 and 2017 (ICCT, 2018). The smoothed line is a loess (local regression) fit, with the 95% confidence interval represented by the shaded band.

The long term trends in the ambient roadside concentrations of NO_x , NO_2 , PM_{10} and $\text{PM}_{2.5}$ in individual functional urban areas (FUAs) are shown in Figure 5. The trends in the majority of FUAs closely resemble the whole-European trends (Figure 3), however a visual inspection of the individual trends revealed that some FUAs exhibit trends that differ considerably from the consensus pattern. These outliers are highlighted in bold in Figure 5, and shown individually in Figure 6.

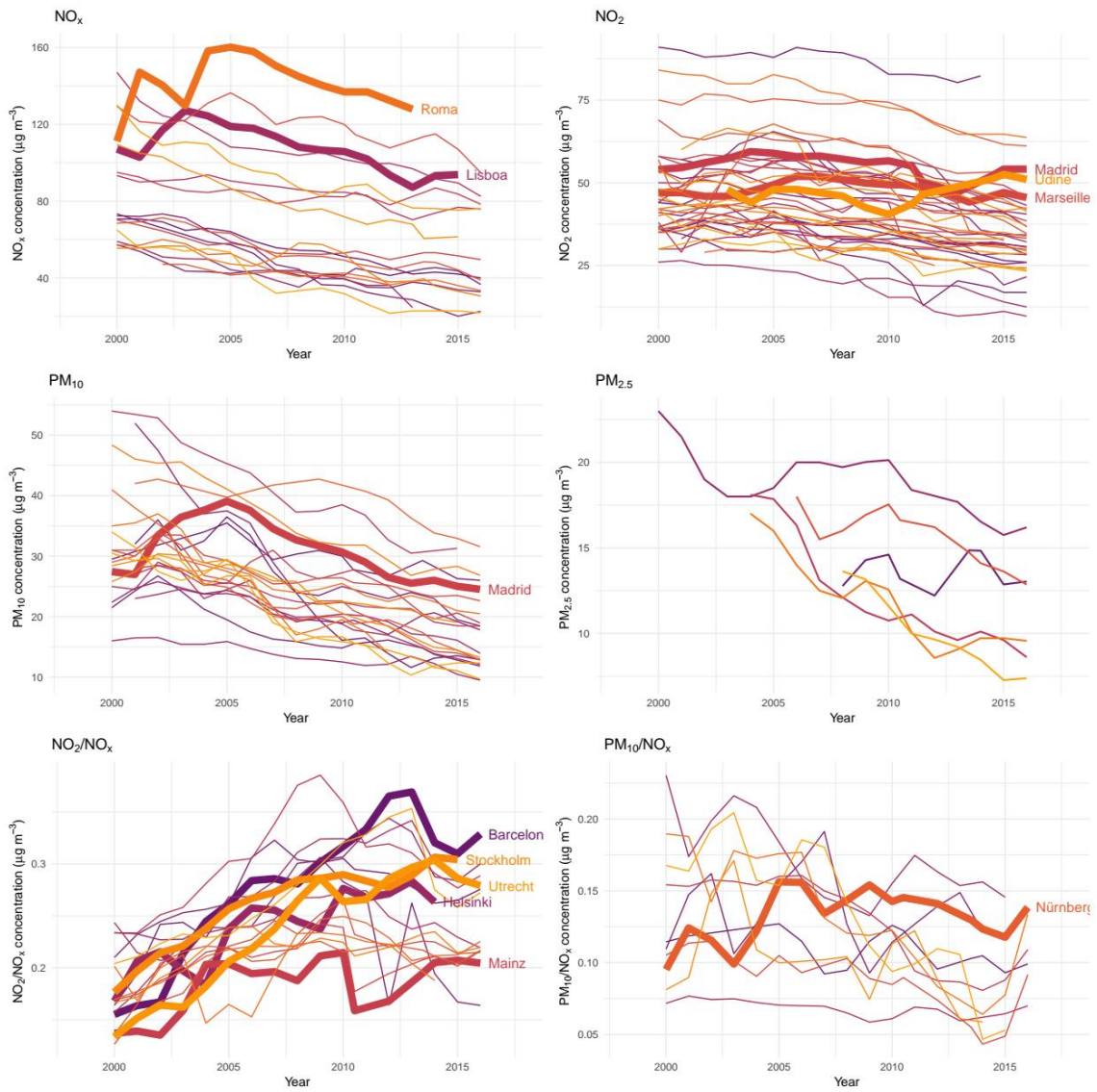


Figure 5: Rolling change trends in NO_x, NO₂, PM₁₀ and PM_{2.5} roadside concentration in individual European FUAs between 2000-2017. The FUAs with trends differing considerably from the overall European trend are shown in bold and labelled.

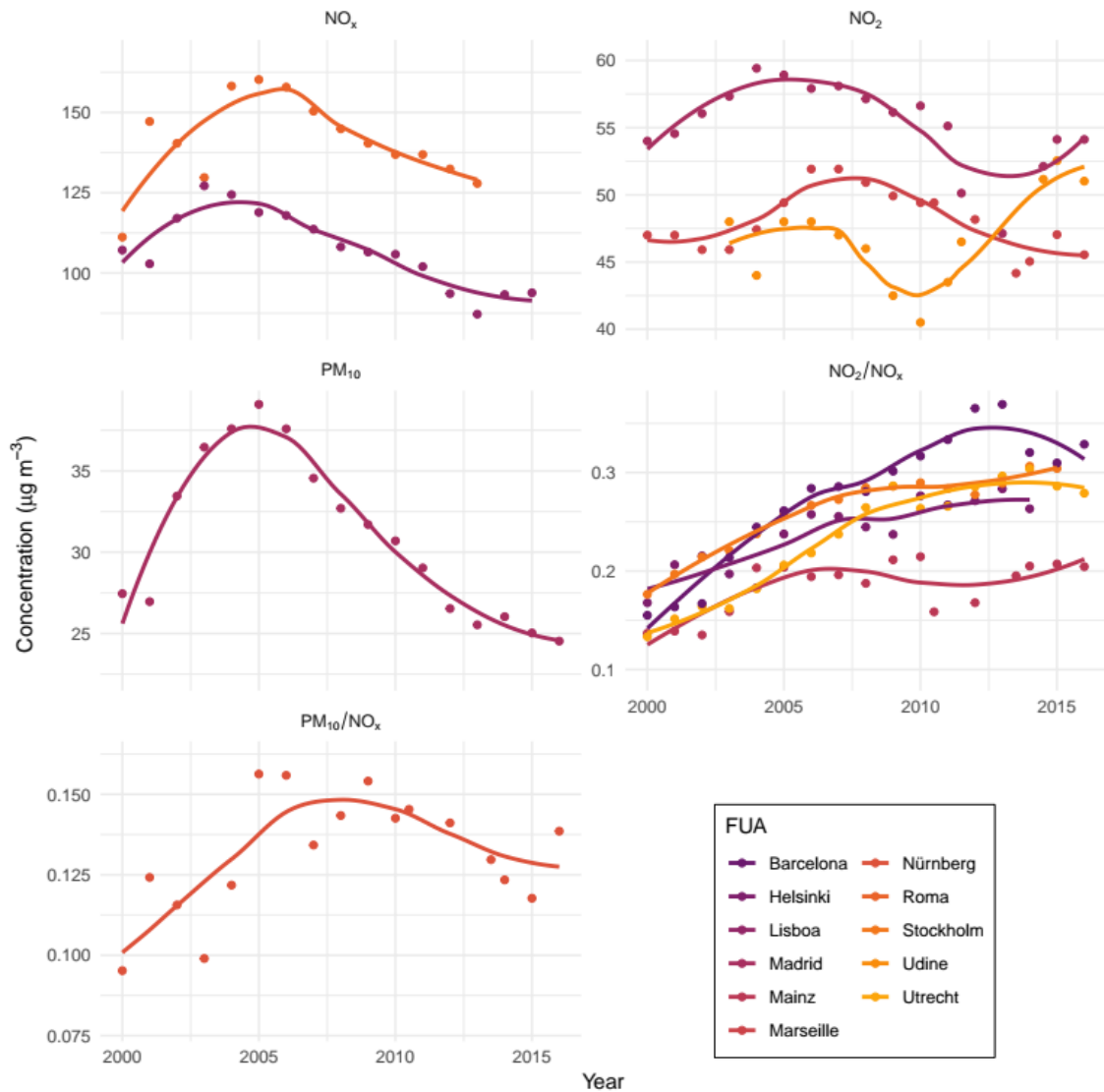


Figure 6: Rolling change trends in NO_x, NO₂, PM₁₀ and PM_{2.5} roadside concentration between 2000 and 2017 in the FUAs in which the trends differ considerably from the overall European trends. The smoothed lines are loess (local regression) fits.

At the city resolution, while the majority of FUAs display a similar pattern in the NO₂ and NO_x concentration trends, the precise nature and location of the turning point in the NO₂ concentration trend varies, with the concentration in some FUAs increasing to a peak, before starting to decrease. It is possible that these differences in the shape of the trends are due to differences in the position of the NO₂ concentration peak resulting from variations in the composition and age of the vehicle fleet between cities.

The exceptions to the pattern of monotonic decrease in NO_x concentration are Roma and Lisboa, where the NO_x concentration initially increases until around 2004-2005, then decreases. One possible explanation for this is a slower than average rate of vehicle turnover and an older vehicle fleet in Italy and Portugal compared with the rest of Europe (as shown in Table 2), resulting in a delay in the widespread presence of vehicles fitted with NO_x reducing emission technologies in these cities.

Table 2: The age of the vehicle fleet in Italy and Portugal, compared with the entire European Union vehicle fleet (ACEA, 2017).

Country	Passenger vehicles		Light commercial vehicles		Medium and heavy commercial vehicles	
	Average age (years)	Proportion of vehicles older than ten years	Average age (years)	Proportion of vehicles older than ten years	Average age (years)	Proportion of vehicles older than ten years
European Union	10.7	0.49	10.7	0.49	11.7	0.53
Italy	10.7	0.52	11.9	0.59	13.2	0.69
Portugal	12.6	0.62	14	0.79	13.7	0.77

Three FUAs possess trends in NO₂ concentration that differ considerably from the European-wide trend. As shown in Figure 6, in Madrid and Marseille NO₂ concentration increased to a peak in 2005-2006, then decreased before beginning to increase again around 2013. As with the FUAs exhibiting outlying NO_x trends, these trends can be interpreted as lagged versions of the common European trends due to variations in the composition of the vehicle fleet in these FUAs. However, the NO₂ concentration trend in Udine is distinct from that in any other FUA, with constant NO₂ concentration until 2007, decreasing to 2010, then increasing to a plateau in 2014. The reason for this is unclear.

As can be seen in Figure 5, the trends in PM₁₀ concentration in all 24 individual FUAs resemble the European-wide trend of monotonic decrease, with the single exception of Madrid, where PM₁₀ concentrations increased to a maximum in 2005, before declining, as shown in Figure 6.

The initial increases in both NO₂ and PM₁₀ concentration in Madrid could result from rapid growth in the number of diesel vehicles outstripping improvements in emission technologies. Between 1999 and 2008, the vehicle fleet in Madrid increased by 34%, with the proportion of the fleet composed of diesel vehicles growing from 28% to 53% (Salvador et al., 2012). Compared with the increase in the total number of vehicles in Europe of 14% between 2000 and 2008 (EEA, 2018), this represents a large increase in vehicles, and a large increase in the number of diesel vehicles specifically. It is likely to have led to an increase in vehicular NO_x and PM₁₀ emissions which overwhelmed the concurrent decreases in per-vehicle emissions.

Only six FUAs contained more than one monitoring site measuring PM_{2.5} concentration that met the data capture requirements for the trend analysis. In all six FUAs, PM_{2.5} concentrations decreased over the period analysed.

Conclusions

A new trend evaluation approach has been applied to European roadside ambient air pollution data that maximises data usage while minimising potentially important biasing effects. Long term trends in roadside concentrations of NO_x, NO₂, PM₁₀ and PM_{2.5} in Europe and in 44 European functional urban areas between 2000 and 2017 were evaluated using the rolling change method. The city-scale trends for the most part displayed a strong consistency with the overall European trends, namely monotonic decreases in NO_x and PM_{2.5} concentrations since 2000, and initial increases in NO₂ and PM₁₀ concentrations until 2002, followed by monotonic decreases. Reductions in vehicle emissions resulting from improvements in vehicle exhaust technologies, such as three-way catalysts, diesel particulate filters and diesel oxidation catalysts are likely responsible for the observed declines in concentration. In almost all cases where the city-scale trends differed considerably from these patterns, the anomalous trends seemed to be lagged versions of the same trend, possibly caused by variations in the traffic fleet composition. For example, an older vehicle fleet, slower rate of vehicle turnover, or increases in the number of vehicles (particularly diesel vehicles) may contribute to a delay in the turning point of the trends in NO_x, NO₂ and PM₁₀ roadside concentration.

Acknowledgements

Polly E. Lang was funded by the Department of Chemistry at the University of York. The authors would like to acknowledge Defra, King's College London and Ricardo Energy & Environment for providing the data used in this study.

References

- ACEA (2017). Vehicles in use in Europe 2017. Retrieved from: https://www.acea.be/uploads/statistic_documents/ACEA_Report_Vehicles_in_use-Europe_2017.pdf
- Carslaw, D.C., Farren, N.J., Vaughan, A.R., Drysdale, W. S., Young, S. and J. D. Lee (2019). The diminishing importance of nitrogen dioxide emissions from road vehicle exhaust, *Atmospheric Environment: X*, Vol. 1, 100002.
- EEA, European Environment Agency (2019). Eionet Central Data Repository. Retrieved from <http://cdr.eionet.europa.eu/>
- EEA, European Environment Agency (2018). Air Quality e-Reporting (AQ e-Reporting). Retrieved from <https://www.eea.europa.eu/data-and-maps/data/aqereporting-8>
- EEA, European Environment Agency (2018). Air Quality in Europe. Retrieved from <https://www.eea.europa.eu/publications/air-quality-in-europe-2018>
- EEA, European Environment Agency (2018). Size of the vehicle fleet. Retrieved from <https://www.eea.europa.eu/data-and-maps/indicators/size-of-the-vehicle-fleet/size-of-the-vehicle-fleet-9>
- EEA, European Environment Agency (2016). Explaining Road Transport Emissions: A Non-Technical Guide. Retrieved from <https://www.eea.europa.eu/publications/explaining-road-transport-emissions>
- Font, A., & Fuller, G. W. (2016). Did policies to abate atmospheric emissions from traffic have a positive effect in London?, *Environmental Pollution*, 218, pp 463–474.
- Grange, S. K. (2016). smonitor: A Framework and a Collection of Functions to Allow for Maintenance of Air Quality Monitoring Data. Retrieved from <https://github.com/skgrange/smonitor>
- Grange, S. K., Lewis, A. C., Moller, S. J., & Carslaw, D. C. (2017). Lower vehicular primary emissions of NO₂ in Europe than assumed in policy projections, *Nature Geoscience*, 10(12), pp 914–918.
- ICCT, International Council on Clean Transportation (2018). European vehicle market statistics 2018/2019. Retrieved from <http://eupocketbook.theicct.org>
- Lang, P. (2018). 'aqtrends'. Available at: <https://github.com/pollylang/aqtrends>.
- Lang, P. E., Carslaw, D. C., & Moller, S. J. (2019). A trend analysis approach for air quality network data, *Atmospheric Environment*.
- Lavalle, C., Kompil, M., & Aurbout, J.-P. (2015). UI - Boundaries for the functional urban areas (LUISA Platform REF2014). Retrieved from <http://data.europa.eu/89h/jrc-luisa-ui-boundaries-fua>
- Masiol, M., Squizzato, S., Formenton, G., Harrison, R. M., & Agostinelli, C. (2017). Air quality across a European hotspot: Spatial gradients, seasonality, diurnal cycles and trends in the Veneto region, NE Italy, *Science of The Total Environment*, 576, pp 210–224.
- Mavroidis, I., & Chaloulakou, A. (2011). Long-term trends of primary and secondary NO₂ production in the Athens area. Variation of the NO₂/NO_x ratio, *Atmospheric Environment*, 45(38), pp 6872–6879.
- Salvador, P., Artíñano, B., Viana, M., Alastuey, A., & Querol, X. (2012). Evaluation of the changes in the Madrid metropolitan area influencing air quality: Analysis of 1999–2008 temporal trend of particulate matter, *Atmospheric Environment*, 57, pp 175–185.

2.3.3 Mobile air quality measurements using bicycle to obtain spatial distribution and high temporal resolution in and around the city center of Stuttgart

A. Samad*, U. Vogt

Institute of Combustion and Power plant Technology (IFK), Department of Air Quality Control, University of Stuttgart, Germany

Corresponding author: Abdul Samad, Email: abdul.samad@ifk.uni-stuttgart.de

Postal address: Pfaffenwaldring 23, 70569 Stuttgart, Germany.

Abstract

Cities often have a problem regarding the air quality because a lot of emissions are produced within these cities and local emission sources among others relate directly to the air quality. In order to investigate this problem, stationary monitoring stations are not sufficient as the information regarding spatial distribution is lacking. Mobile measurements can provide this necessary information. In this research, a case study is presented to illustrate the design and implementation of mobile measurement platform with a bicycle. Different compact measuring devices were selected and installed on the bicycle for mobile measurements along a designated measurement route in a Germany city namely Stuttgart. The measured pollutants included Particulate Matter (PM), Ultrafine Particles (UFP), Black Carbon (BC), nitrogen oxides (NO, NO₂ and NO_x) and ozone (O₃). Meteorological parameters such as air temperature, relative humidity, wind speed, wind direction, solar radiation and air pressure were also measured. The measured parameters were allocated to the measured location using a GPS device. The measurements were carried out during winter period of 2018 in the month of February. A total of 43 rounds were performed on a 12 km long measurement route covering part of the city center with high traffic roads as well as side roads and a park. The results showed a very high spatial variability and the pollutant concentrations depended on different factors such as location, traffic volumes, weather conditions, etc. For NO, NO₂ and UFP, the concentrations in the park (which can be considered as urban background level) were only around 30 % to 50 % of the measured concentrations directly on the roadside. Comparison of PM₁₀ and PM_{2.5} concentrations on the road with urban background concentrations showed a less striking difference however was still very clearly measurable. The mobile measurement platform with the bicycle was reliable and proved to be a highly adaptive method for future air quality monitoring.

Introduction

Mobile measurements are an ever-growing trend for the evaluation of urban emissions, local air quality and air pollutant exposure. Unlike the stationary air quality monitoring methods, mobile measurements with portable and precise measurement devices provides the opportunity to study the behaviour of air pollutants and to investigate the spatial distribution with high temporal and spatial resolution in corresponding study areas. It is undoubtedly a contribution in future urban planning. The city of Stuttgart in Germany is very famous because of its air pollution problems. The main reasons of pollution in Stuttgart are heavy traffic and high population density in combination with a topography which favours the accumulation of air pollutants. Stuttgart is a valley surrounded by mountains from three sides which causes poor ventilation and hinders the dispersion and dilution of pollutants (Regierungspräsidium Stuttgart, 2018). The traffic density in Stuttgart is very high. At some locations on the highway like B14 which passes through Stuttgart, around 100,000 vehicles on average every day (LUBW, 2018). The high traffic load leads to high emissions of nitrogen oxides from the vehicle exhaust and PM from the abrasion of brakes and tires as well as PM and UFP from the exhausts (Baumbach, 1996). Apart from this, the city of Stuttgart does not have any ring road which causes all the traffic to pass unnecessarily through the city center. A ring road could have diverged most of the city traffic outside the city center helping to reduce pollution to some extent, despite the fact that new roads induce more traffic and cannot be the only solution of such a complex problem. Human settlement in most part of Stuttgart is very dense and high buildings form narrow canyons. This causes poor ventilation which leads to poor dispersion and dilution.

Mobile measurement technique has been applied previously as well using different platforms. The University of Applied Sciences in Düsseldorf performed mobile measurements and measured PM and UFP. Two measurement routes were investigated, one through an outer limit of the low emission zone

and the other through the city center. From the investigations carried out in the year 2010, it could be found that the PM concentrations were only 12 % higher on the main road as compared to the secondary road. The UFP on the other hand were found to be about 45 % higher on the main road than on the secondary road (Vogel et al., 2011). Mobile measurements performed in Leipzig in 2011 investigated a measurement route with parking areas, traffic intersections, walkways along a street and a pedestrian zone. The results showed that traffic was the major source of PM pollution in the area. Rapid concentration reductions were observed from a distance of 20 to 30 meters off the main road and relatively low concentrations were monitored in pedestrian zones and parks (Birmili et al., 2013). The Institute for Meteorology and Climate Research in Karlsruhe developed a mobile measuring platform called 'AERO-TRAM', a measuring system setup on the roof of a tram. In this study two routes were chosen, both not only through the city but also in the neighbouring area. The results showed that the concentration of NO_x reduced to 70 % when the distance from the city center increased. PM on the other hand reduced up to 50 % (Hagemann et al., 2014). A similar study was done in the year 2013 by Computer Engineering and Networks Laboratory in Switzerland where UFP were measured using public transport vehicles for more than a year (Hasenfratz et al., 2014).

The "Government Authority for the Environment, Baden-Württemberg" (LUBW) is responsible for the operation and maintenance of the ambient air monitoring network. In 2018, the relevant air pollutants were measured at five monitoring stations in Stuttgart which include rural, urban background and traffic monitoring stations (Stadtklima Stuttgart, 2018). In addition to the permanently existing monitoring stations, so-called spot monitoring stations are installed at selected locations which are considered to be the hot spots. The purpose of the spot monitoring station is the detection of traffic-related air pollution at urban stress centers. In Stuttgart, there are currently two spot monitoring stations namely Stuttgart Hohenheimer Strasse and Stuttgart Am Neckartor. (Stadtklima Stuttgart, 2018). This monitoring station Stuttgart am Neckartor which is close to the city center on the busy federal highway B14 is already in frequent focus of both professional world and public as at this monitoring station the highest NO₂ and PM₁₀ pollution levels in the whole Germany were measured in the recent years (LUBW, 2017).

The German environmental pollution regulation (39th BImSchV) sets the following limit values for NO₂: The hourly average NO₂ concentration must not exceed the limit value of 200 µg/m³ for more than 18 times in a year. The annual mean concentration of NO₂ must not be higher than 40 µg/m³ (Directive 2008/50/EC). Figure 1 shows the NO₂ annual average concentration at the LUBW monitoring station Stuttgart Am Neckartor and Hohenheimer Strasse in the period from 2004 to 2018 (Stadtklima Stuttgart, 2018). It can be seen that the NO₂ annual average concentration at the monitoring station Am Neckartor was regularly between 71 and 121 µg/m³, i.e. by a factor of around 2 to 3 above the permitted limit. The permitted limit was also clearly exceeded at the other spot monitoring station Hohenheimer Strasse.

The ambient air limit values for PM₁₀ and PM_{2.5} are also defined in above mentioned regulation. The long term ambient air limit value averaged over one calendar year for PM₁₀ is 40 µg/m³ and for PM_{2.5} is 20 µg/m³ which is valid since 2015. The short term ambient air limit value is the daily average value for PM₁₀ which is 50 µg/m³. It may not be exceeded 35 times in one calendar year (Directive 2008/50/EC). The count of days with exceeding daily mean PM₁₀ concentration at two Stuttgart spot monitoring stations for the years 2004 to 2018 is shown in Figure 2. As late as 2005, the daily limit value of PM₁₀, which is 50 µg/m³, was exceeded on every other day of the year (187) at the monitoring station Am Neckartor when a maximum of 35 days of exceedances were allowed per year. However, a decreasing trend of exceedances can also be clearly observed. Only in the last year (2018) the number of exceedances at the monitoring station Am Neckartor was under the allowed limit of 35 exceeding days per year.

Investigations done by the LUBW on the source of emissions have shown that 52% of the NO₂ emission at the location of Stuttgart Am Neckartor is attributable to the local road traffic. The contribution to air pollution from the local sources (local road traffic, small and medium combustion plants, others, etc.) is very high with 56% as compared to the air pollution from other sources from regional and urban background (LUBW, 2017). For PM₁₀, at the location Am Neckartor, 47% of the emission is caused by local road traffic (exhaust fumes, attrition and re-turbulence) and approx. 2% by small and medium combustion plants and less than 1% by industry. The remaining 50% are to be assigned to the overall background level which is the combination of urban and large-scale background sources (LUBW, 2017).

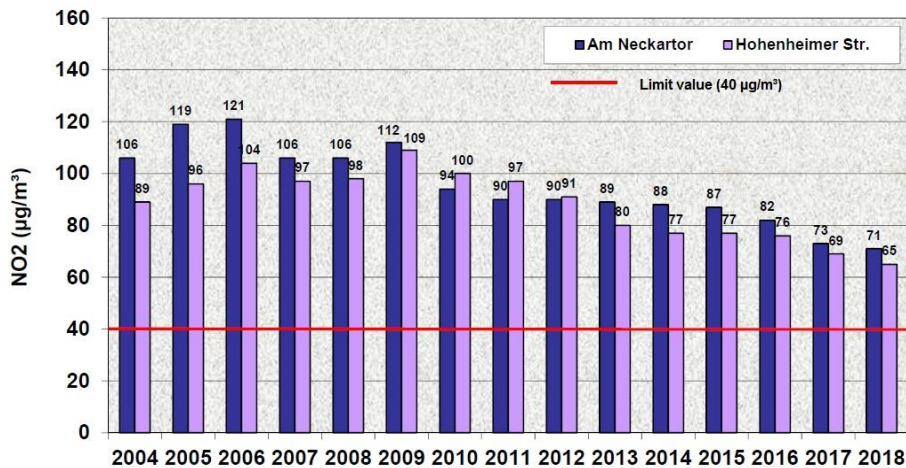


Figure 1: Annual mean NO₂ concentration at the LUBW monitoring stations Am Neckartor and Hohenheimer Strasse in Stuttgart from 2004 to 2018 (Stadtklima Stuttgart, 2019)

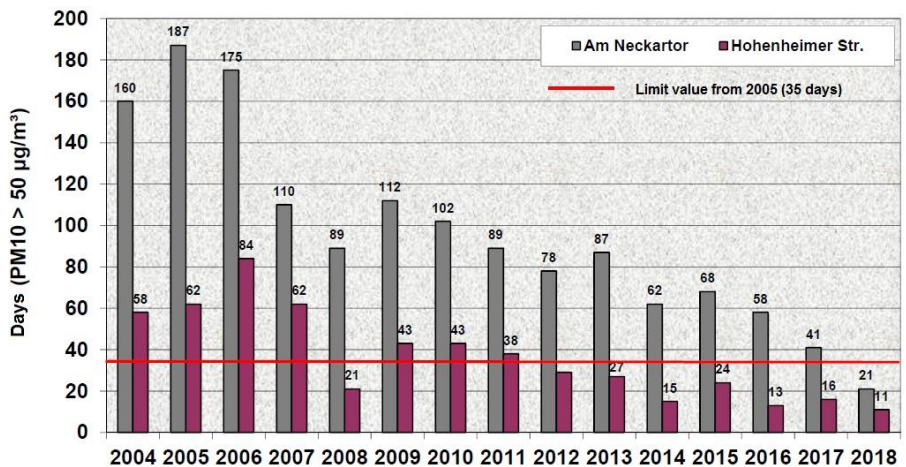


Figure 2: Count of days exceeding the PM₁₀ daily average value of 50 µg/m³ at the LUBW monitoring stations Am Neckartor and Hohenheimer Strasse in Stuttgart from 2004 to 2018 (Stadtklima Stuttgart, 2019)

The federal highway B14, which passes directly by the spot monitoring station Am Neckartor, is an important traffic pathway in the area of Stuttgart. It consists of two directions of travel and has three lanes in each direction. On some sections later, the road has up to five lanes in each direction. According to a traffic survey conducted by the LUBW in 2018, around 70,000 vehicles on average pass by the monitoring station Am Neckartor each day. The proportion of heavy commercial vehicles is around 3.0%. On a Sunday, the average daily traffic decreases by up to 31% and the share of heavy commercial vehicles even decrease by 87% (LUBW, 2018).

This situation clearly indicates the air quality problem in the city of Stuttgart and hence the necessity of air quality measurements which provide good spatial distribution and high temporal resolution is evident. For this problem, mobile measurements using a bicycle equipped with relevant air pollutants and meteorological measurement devices provided the optimum solution. The task of this study was to use mobile measurements in order to investigate some part of the city center of Stuttgart and its surroundings for two main reasons: Firstly, to confirm that stationary monitoring station is representative for the area under study. Secondly, to find if there are other hot spots that might not be covered by the stationary measurements. The route for mobile measurements was selected so that along with the main federal highways, the side roads and parks were also covered in order to observe the variation in the pollutant concentrations.

Measurement technique and methodology

In this investigation different compact measurement devices were selected in order to realize the mobile measurements with a bicycle. These devices were installed on the bicycle. The measurement devices included an aerosol spectrometer working on the principle of light scattering for measuring PM, Condensate Particle Counter (CPC) for measuring UFP, aethalometer working on the principle of light absorption for measuring BC, nitrogen oxide monitor for measuring NO₂ and NO by direct radiation absorbance and ozone monitor for measuring O₃ by light absorption. Meteorological parameters such as air temperature, relative humidity, wind speed, wind direction, solar radiation and air pressure were measured with the aid of a compact weather station. A GPS device was used in order to relate the measured parameters to the location and a video camera was also part of this system to relate the measured data to special events.

The devices used during these measurements were designed especially for mobile use, which is why they have a relatively low weight compared to stationary measuring devices and can be operated with rechargeable batteries. In addition, they are very insensitive to external influences such as shocks and larger temperature changes. The total weight of the measurement system excluding the bicycle was around 20 kg. Keeping the route and the weight of the whole system in mind an electric bicycle was chosen for these measurements. The devices used for these mobile measurements are listed in Table 1. The measuring principle on which these devices operate is also mentioned in this table.

Table 1: List of devices used for the mobile measurements with bicycle

Instrument	Measurement principle	Measured parameters
Aerosol spectrometer	Light scattering	Particulate Matter (PM) with size range 0.3 – 20 µm
Condensate Particle Counter (CPC)	Particle condensation	Ultrafine Particles (UFP) with size range 0.01 to >1 µm
Aethalometer	Light attenuation	Black Carbon (BC)
NO ₂ / NO / NO _x monitor	NO ₂ absorption at 405 nm	NO ₂ , NO, NO _x
Ozone monitor	UV absorption at 254 nm	O ₃
Weather station	Ultrasonic sensors, NTC resistor, Capacitive sensor, MEMS sensor, Pyranometer	Wind speed, Wind direction, Air temperature, Relative humidity, Air pressure and Solar radiation

Figure 3 shows the bicycle along with equipment used to perform the mobile measurements. The GPS and the camera were installed on the front of the bicycle. The aerosol spectrometer and the aethalometer were put in the front basket in order to avoid any influence from the driver on the PM measurements. The gas measurement devices for measuring NO₂, NO, NO_x and O₃, the Condensate Particle Counter (CPC) for measuring UFP and the data logging system were placed inside the box on the back of the bicycle. All of the measurement devices were operated with batteries. The weather station was installed on the rod at the back of the bicycle.

The measurements were carried out intentionally with a bicycle as a measuring vehicle and not with a car, since the measurements should be carried out at the same distance from the road as people are exposed to the pollutants. The spot monitoring station Am Neckartor that is located on the route is also at a distance of about 3 m away from the roadside. Therefore, it is better to perform the measurements away from the source rather than measuring directly on the roads. The closer you get to the source of pollution, the stronger is the gradient to which the concentrations are subjected. Figure 4 shows the entire measuring section in and around the city center of Stuttgart. The blue line shows the bicycle route, the yellow stars are the passive samplers installed on the bicycle route. The route started from the park where the ground station was built for the measurement activity. Then the route went through the park on the other side of train lines, on a side road parallel to the federal highway B27 travelling from north to south and then turning to the federal highway B27. Moving from west to south while covering the city center, the route turned towards the federal highway B14. After going for a short distance on the side road parallel to the federal highway B14, the route came back again to B14 near the monitoring station Am Neckartor and returned to the side road which led the route back to the starting point in the park. The total route length was approximately 12 km. The bicycle was driven with a speed not more than 10 km per hour because of the reason that PM measurement becomes critical

at relatively high speeds above 10 km per hour. It took between 1.2 to 1.5 hours to complete one round. During the rounds, stops were made in order to check the devices, to calibrate them and to take the data from these devices. The measurements were performed continuously during the whole day and night.

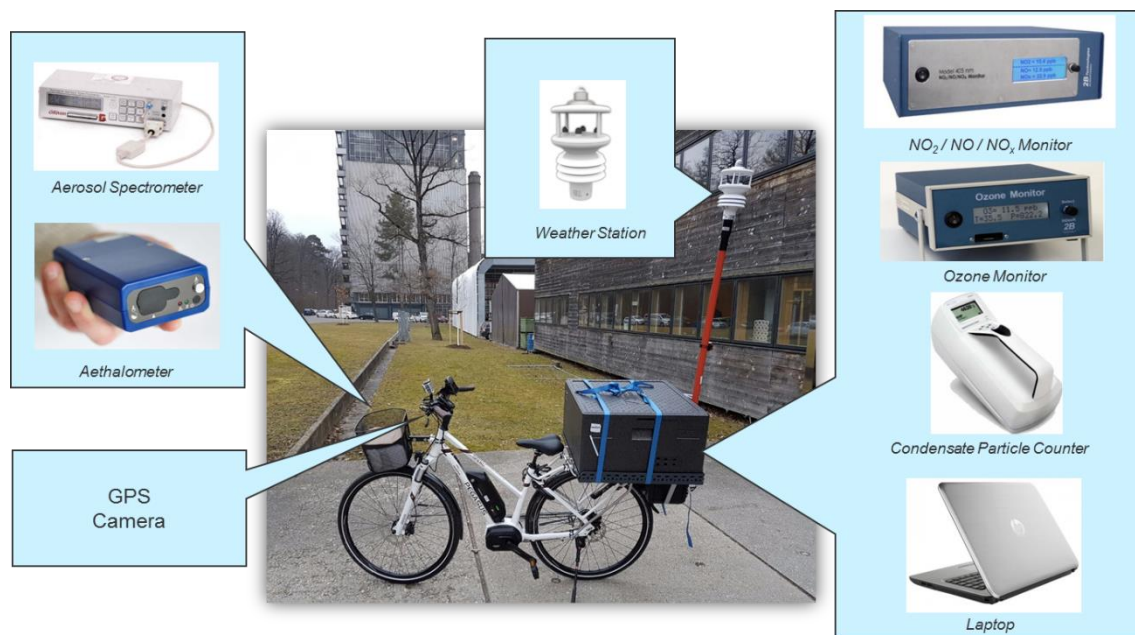


Figure 3: Complete setup installed on the bicycle for mobile measurements

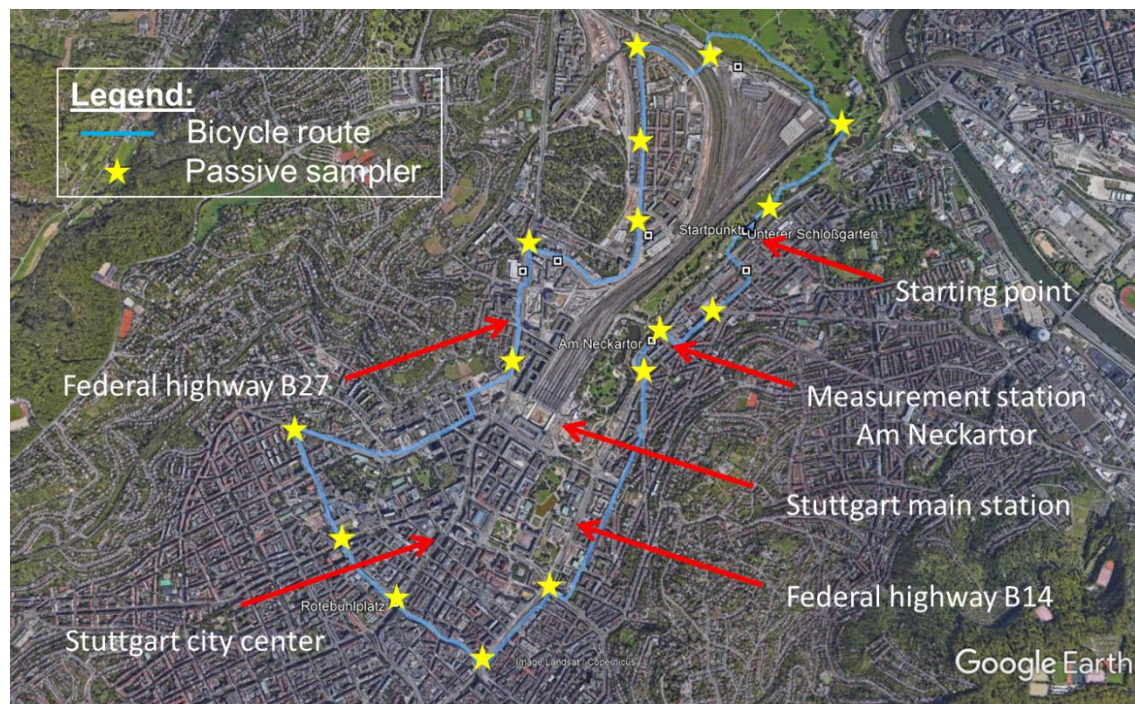


Figure 4: Bicycle route for mobile measurements and location of the passive samplers

The measurements were performed in worst case scenario when high pollutant concentrations were expected. The measurement days were selected by keeping specific weather conditions in mind such as high pressure situations with clear sky and no rain. In these situations surface inversion can build up which trap the pollutants and restrict their transport. The measurement period of the mobile ambient air measurements lasted for around one week from 18th February to 24th February, 2018. This included 8 days of bicycle measurements with a total of 43 rounds on the complete route of around 12 km. The

bicycle measurements lasted for a short time period and the situation varied from one ride to another. So in order to validate the results, the average of the measurement results was then compared to a long term observation method, e.g. in this case the NO₂ passive samplers were installed on the bicycle route for a longer period of time from 18th February until 4th March 2018. For the passive samplers, an average value was obtained for the whole measurement period of two weeks. As part of the quality assurance of the measured data, the gas devices were calibrated regularly using a gas phase titration system. For the PM, UFP and BC measurements, the measurement devices were compared in advance with calibrated devices and also with the stationary monitoring stations.

Results and discussion

These measurements provided high temporal resolution and spatial distribution of the measured parameters. The time resolution of the measured parameters was one second. The results of these measurements are evaluated and plotted with the software ArcGIS. Legend is shown at the bottom right of the result figures. Information about the measurement is provided on the top left corner i.e. measured parameter, starting date and time of the campaign, ending date and time of the campaign, the number or rounds averaged for the which the result is plotted and the distance between averaging two measured points e.g. in these results it is 50 m. This means that the whole route is divided in 50 m sections and the values in this section are averaged and shown by one circle on the route. In order to explain the results on the figures, different segments of the route are given a number for better understanding. These segments are described in Table 2.

Table 2: Description of the segments on the measurement route

Segment	Description
1	Park
2	Area between park and main street (Construction area)
3	Area between main street and federal highway B27 (Construction area)
4	Main road away from the federal highway B27
5	The road from west to south while covering the city center until it reaches the federal highway B14
6	Federal highway B14
7	The road parallel to the federal highway B14
8	Am Neckartor on the federal highway B14 where the LUBW monitoring station is located

The results of average NO₂ concentration measured in 43 rounds during the campaign from 18.02.18 – 24.02.18 is shown in Figure 5. It can be very well observed from the result that the concentration course is subjected to a very strong spatial variation. In some cases very high peak concentrations of approximately 100 µg/m³ NO₂ were measured. However, the values also fell back to a low level of approximately 25 µg/m³ NO₂. These results show that the share of local traffic in the immediate vicinity of busy federal highway B14 accounts for a large proportion of the total NO₂ pollution.

In Figure 5, it can be seen that the NO₂ concentration is relatively high on the federal highways as compared to the NO₂ concentration in the park or on the side roads. This clearly shows the impact of traffic on the current air quality situation of the city. The segment 1 in the park had relatively lower NO₂ concentration, at some points as low as 25 µg/m³. On some spots in the segments 2 and 3, high NO₂ concentrations e.g. from 60 µg/m³ to 100 µg/m³ was observed which was not expected. By further investigation, it was found out that these spots are influenced from the construction work going on for the project “Stuttgart21” in the area near the main station. The NO₂ concentrations on the federal highway B27 were higher than the side roads but still lower than the NO₂ concentrations at the federal highway B14 near the monitoring station Am Neckartor. This section is designated as segment 8 and the NO₂ concentrations here reached 80 µg/m³ until 100 µg/m³. The segment 5 covered the main city center where the NO₂ concentrations were lower as compared to on the federal highways but still some points with higher NO₂ concentrations of 60 µg/m³ to 80 µg/m³ were to be seen. The segment 6 covered a part of federal highway B14 where the concentrations were relatively higher as compared to the

segment 7 which was parallel to this road. A difference NO₂ concentration of around 40 µg/m³ was to be observed between the highway and the side road.

The results shown here are averages of the whole measurement campaign. The NO₂ concentration for the individual rounds varied as high as above 150 µg/m³ at hot spots in some days during the rush hours.

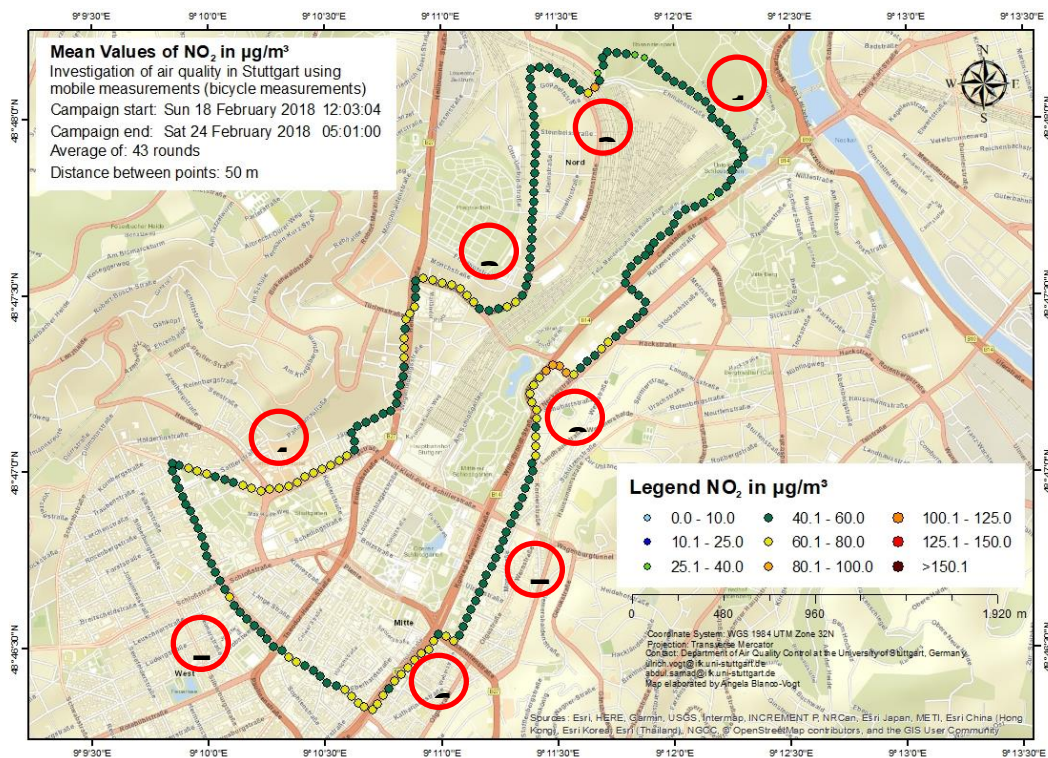


Figure 5: Average NO₂ concentration measured in 43 rounds during the campaign from 18.02.18 – 24.02.18

As mentioned before, results of mobile bicycle measurements are representative only for a short time period and the measurements at each position is at one specific moment, therefore an average of more rounds is considered to present such results in order to validate these measurements. This is why the results discussed here are the averages of the whole measurement campaign. Additionally another tool can be used for the validation of mobile measurements i.e. passive samplers. With this technique an average NO₂ concentration for a certain time period can be measured (Hangartner and Pfeffer, 2009). NO₂ tubes from Passam AG were used which were exposed for a period of two weeks during the mobile measurement campaign and subsequently analysed and evaluated in the laboratory.

The result of these measurements for the period of two weeks from 18.02.18 – 04.03.18 is shown in Figure 6. From this result also it can be seen that during the measurement period of two weeks the highest NO₂ concentration was measured at the federal highway B14 at the monitoring station Am Neckartor and the lowest NO₂ concentration was measured in the park. The average NO₂ concentration for the same measurement period at the hot spot monitoring station Am Neckartor measured by the LUBW was 75.4 µg/m³ which is in a good agreement with the NO₂ concentration measured with passive samplers i.e. 70 µg/m³. Lower NO₂ concentrations were measured on the side roads and near the city center. In summary, it can be stated that the passive sampler measurements were in a good agreement with the mobile measurements.

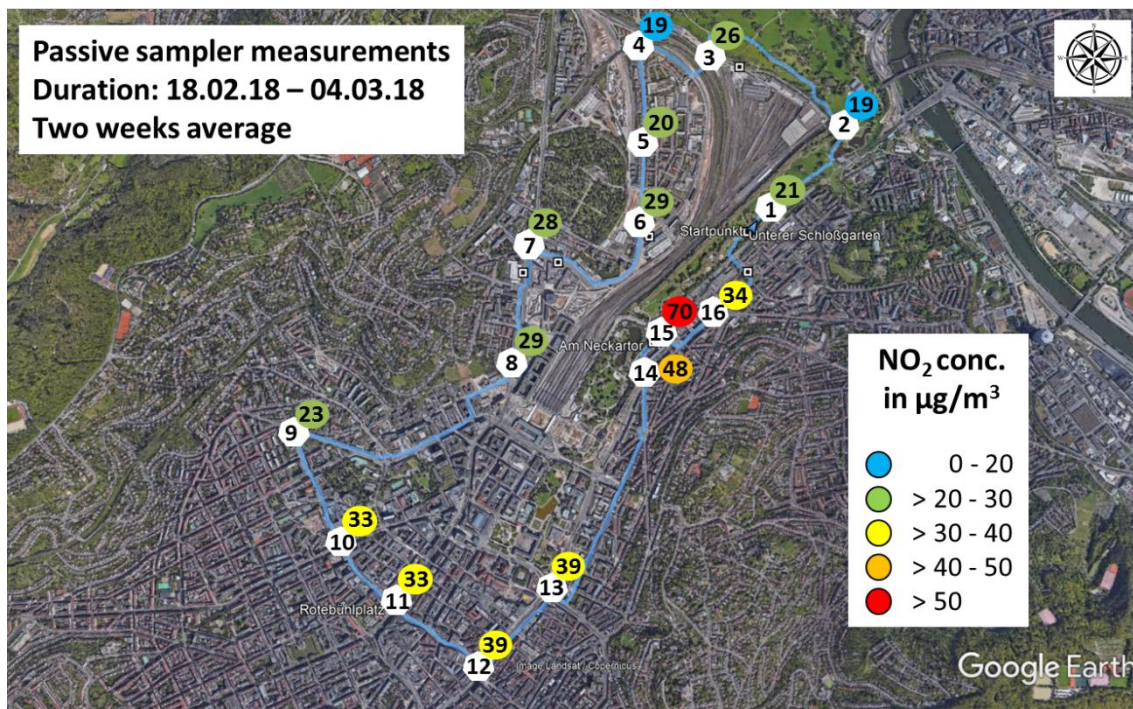


Figure 6: Results from the NO₂ passive sampler measurements for the period of two weeks from 18.02.18 – 04.03.18

The vehicles emit nitrogen oxide directly which can give an indication of the vehicular emissions (Baumbach, 1996). Therefore, the NO concentrations for the same measurements were also monitored and the result is shown in Figure 7. In the park area (segment 1), predominantly low NO concentrations were observed. It is easy to see that the NO concentration measured throughout the park were below 30 µg/m³ and sometimes even below 20 µg/m³. The two hot spots were also identified (segments 2 and 3) where the concentrations were in the range from around 30 µg/m³ until 60 µg/m³. The increase in NO concentration in these segments was not predominantly from traffic but the construction activities in that area. The NO concentration increased on the federal highway B27 and then a drop in concentration on the side road was to be seen but then again an increase in the NO concentration on the main road was observed (segment 4). A drop in the NO concentration was noticed in the segment 5 where the concentration was measured as low as 20 µg/m³. The traffic in that area is usually very low as it is the main area of the city center and some of the area is only accessible to the pedestrians. This clearly explains the low NO concentration in this segment. On the federal highway B14 (segment 6), increasingly high NO concentrations from 60 µg/m³ until more than 75 µg/m³ were measured. There was an immediate drop in the concentration off-road and the measured NO concentration was in the range of 20 to 40 µg/m³. It is noticeable that the NO concentrations measured in the segment 8 were one of the highest with more than 75 µg/m³. Around the same NO concentration was measured on the federal highway B14 at segment 6. The exclusivity that the highest values occurred in the section of the measuring station Am Neckartor was consistently visible in all measurements and for all measured pollutants.

The result of average PM₁₀ concentration measured during the whole campaign is shown in Figure 8. It can be seen that the PM₁₀ concentration was relatively high during the measurement campaign and a variation in the concentration from 30 µg/m³ to 75 µg/m³ can be seen. At some points near the construction sites the PM₁₀ concentration was even above 75 µg/m³. The particulate matters are usually more homogeneously distributed in the study area than the pollutants such as NO and NO₂. This is because the contribution of the urban and regional background sources is higher for PM than for NO₂. Therefore, the gradient between the concentration measured directly at the road and a few meters away from the road is not that strong as it was for NO and NO₂ (Vogt et al., 2017). In Figure 8, it can be seen that the segments 1 and 5 have relatively lower PM₁₀ concentrations (30 µg/m³ to 50 µg/m³) as compared to the PM₁₀ concentrations measured at segments 4, 6, 7 and 8 (40 µg/m³ to 75 µg/m³). The average PM₁₀ concentration measured by LUBW at the monitoring station Am Neckartor for the same time period as the measurement campaign took place was 51 µg/m³ which is almost the same concentration measured during the mobile measurements at this point. The highest

concentrations were measured at some points near the construction site (segments 2 and 3) which is obvious as there are usually a lot of particle emission on the construction sites.

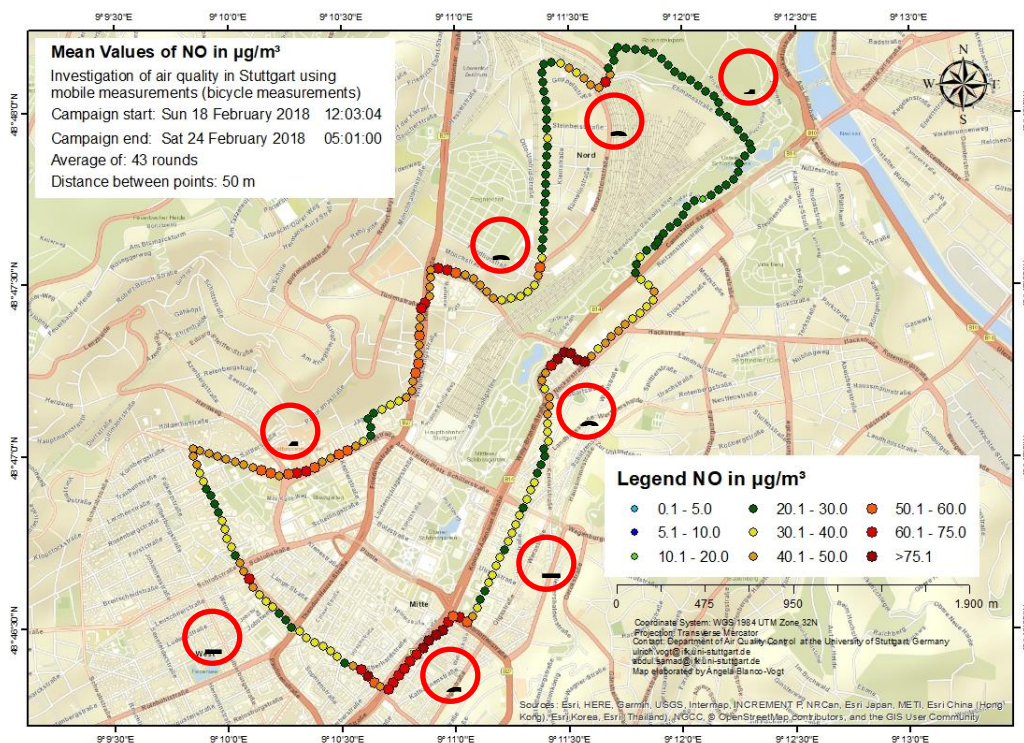


Figure 7: Average of NO concentration measured in 43 rounds during the campaign from 18.02.18 – 24.02.18

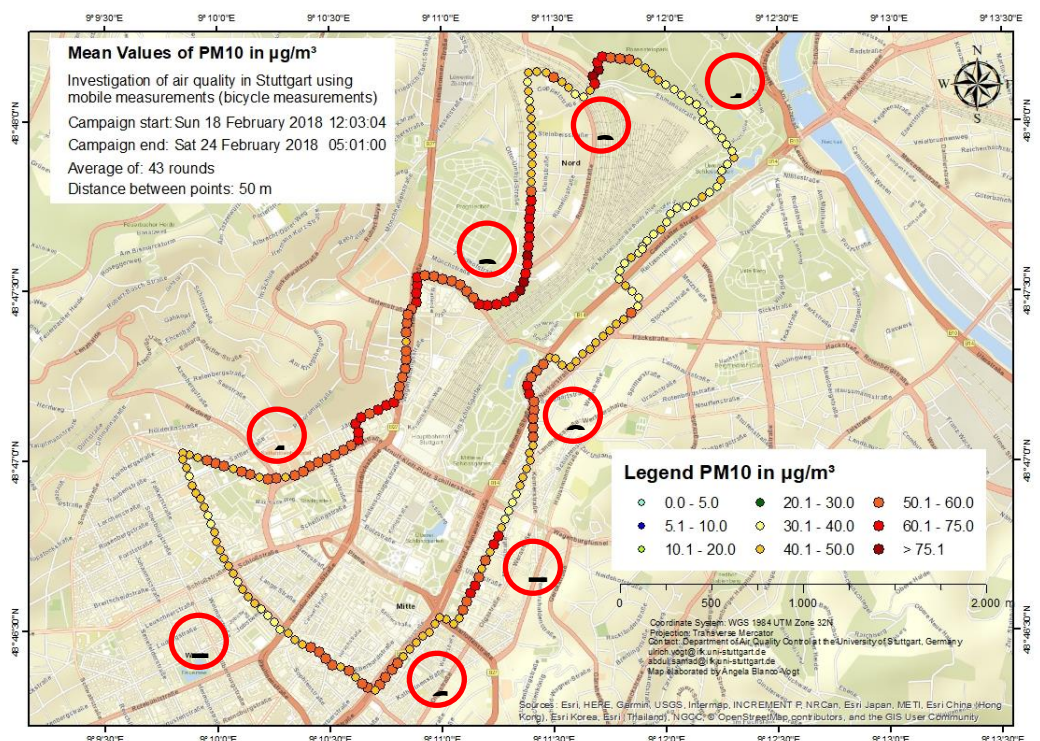


Figure 8: Average of PM10 concentration measured in 43 rounds during the campaign from 18.02.18 – 24.02.18

UFP are assumed to be more dangerous to human health as compared to PM since they are adequately small to penetrate deep into the human body (Oberdörster et al., 2005). The average UFP concentration

during the measurement campaign is shown in Figure 9. The results of UFP concentrations behave more or less similar to NO concentrations which show that the UFP in the study area also have the same source as NO and are emitted mainly from the vehicles. Until now there is not much data available on UFP measurements in Germany and mainly in Stuttgart. The main reason is that there are no limit values set for this pollutant and therefore, it is not measured by the responsible authorities as extensively as the other pollutants for which there are limit values defined.

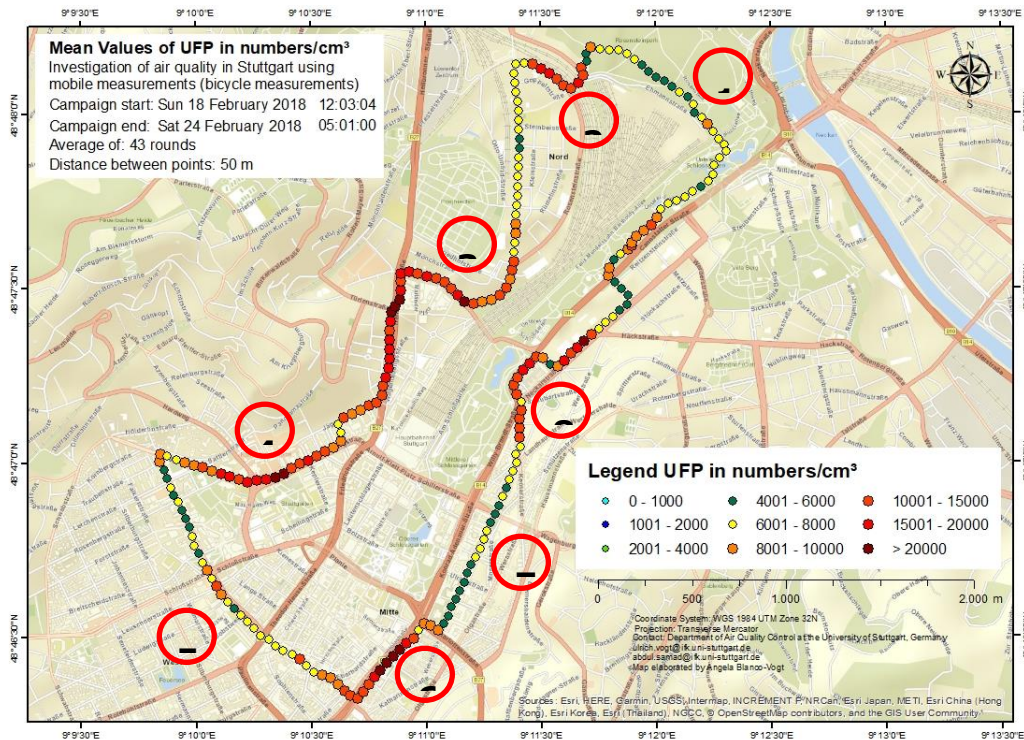


Figure 9: Average of UFP concentration measured in 43 rounds during the campaign from 18.02.18 – 24.02.18

Conclusions

In this investigation, we were able to show that mobile measurement platform using bicycle is reliable and user-friendly, but especially, is a highly adaptive and flexible method for future air quality monitoring. It is very well suited to describe a larger study area for its air quality situation and to detect the urban hotspots of different air pollutants.

The concentrations of ambient pollutants vary by different factors such as location, traffic volumes, weather conditions, etc. Depending on the local dispersion situation at the measuring point, the pollutant concentrations varied. For example, the areas which were located at a street intersection that was better ventilated, the concentrations were lower and the areas which were located in a street canyon where the tall buildings were located very close to each other and the location was poorly ventilated, the concentrations were higher. Also, the distance to the main source of local air pollution, the busy federal highways, played a major role in evaluating the results. The comparison of the mean values of the individual sections show that on average the pollutant concentration along the federal highway B14 on which the LUBW measuring station Am Neckartor is located were highest almost in all measurements. Some of the other sections also had high pollutant concentrations, but the concentration level of the section where the monitoring station Am Neckartor is located was consistently higher.

It was concluded that the stationary monitoring station cannot capture the variability and therefore it is challenging to represent the whole city with a few measurement stations. The mobile measurements are a very useful tool to achieve the spatial distribution, to capture the variability of pollutants and to discover hot spots. During the measurements other hot spots were found in the area under investigation which was not expected before the start of the measurement campaign. It was also concluded that the local sources in the study area play a major role on the air quality situation.

The evaluation of the results has shown that the air pollution near the source is subject to very strong temporal and spatial fluctuations. For NO₂, the concentrations in the park (which can be considered as urban background level) were only around 30% to 50% of the measured concentrations directly on the roadside. Comparison of PM₁₀ concentrations on the road with urban background concentrations showed a less striking difference however was still clearly measurable. The results from the individual rounds for the mobile measurements along the road showed in addition a very large variation, depending on the aeration of the corresponding road sections. At road crossings or larger gaps between buildings where the aeration was better, the concentrations decreased immediately. The rush hours were compared to the times with less traffic in order to quantify the effect of traffic on the measured pollutants and the results verified the fact that the local traffic contributes more than 50% to the measured concentrations of most of the pollutants measured.

Acknowledgements

This work was performed under the project Urban Climate Under Change [UC]² funded by the Federal Ministry of Education and Research (BMBF) Germany.

References

- Baumbach G. (1996), *Air Quality Control*, Berlin – Heidelberg: Springer, 68-70.
- Birmili W., Rehn J., Vogel A., Boehlke C., Weber K., Rasch F. (2013), Micro-scale variability of urban particle number and mass concentration in Leipzig, Germany, *Meteorologische Zeitschrift*, Vol. 22, No. 2, 155-165.
- Directive 2008/50/EC of the European Parliament and of the Council of 21 May 2008 on ambient air quality and cleaner air for Europe, Official Journal of the European Union L 152/1, 2008.
- Hagemann R., Corsmeier U., Kottmeier C., Rinke R., Wieser A., Vogel B. (2014), Spatial variability of particle number concentration and NO_x in the Karlsruhe (Germany) area obtained with the mobile laboratory 'AERO-TRAM'. *Atmospheric Environment* 94, 341-352.
- Hangartner M., Pfeffer U. (2009), Review of the application of diffusive samplers for the measurement of nitrogen dioxide in ambient air in the European Union, 27-41.
- Hasenfratz D., Saukh O., Walser C., Heuglin C., Fierz M., Thiele L. (2014), Pushing the Spatio-Temporal Resolution Limit of Urban Air Pollution Maps.
- LUBW Landesanstalt für Umwelt Baden-Württemberg (2017), Stuttgart Am Neckartor 2004 bis 2016 – Messergebnisse an und im Umfeld der Messstelle, 35.
- LUBW Landesanstalt für Umwelt Baden-Württemberg (2017), Luftreinhaltepläne für Baden-Württemberg, 79-80.
- LUBW Landesanstalt für Umwelt Baden-Württemberg (2018), Verkehrsstärken an ausgewählten Verkehrs- und Spotmessstellen.
- Oberdörster G., Oberdörster E., Oberdörster J. (2005), Nanotoxicology: An emerging discipline evolving from studies of ultrafine particles, *Environmental Health Perspectives* 113, 823-839.
- Regierungspräsidium Stuttgart (2018), Luftreinhalteplan für den Regierungsbezirk Stuttgart, Teilplan Landeshauptstadt Stuttgart, 3. Fortschreibung des Luftreinhalteplanes zur Minderung der PM₁₀- und NO₂-Belastungen, 12-13.
- Seigneur C. (2009), Current understanding of Ultrafine Particulate matter emitted from mobile sources, *Journal of the Air & Waste Management Association*, Vol. 59 no. 1.
- Stadtklima Stuttgart, Luftmessstationen in Stuttgart, Available: https://www.stadtklima-stuttgart.de/index.php?luft_messdaten_stationeninstuttgart (February, 2019).
- Stadtklima Stuttgart, NO₂- und PM₁₀- Überschreitungsstunden bzw. -Tage und Jahresmittelwerte an den LUBW-Spotstationen Am Neckartor und Hohenheimer Straße in den Jahren 2004 – 2018, Available: https://www.stadtklima-stuttgart.de/index.php?luft_messdaten_ueberschreitungen_weitere_grafiken (February, 2019).
- Vogel A., Boehlke C., Weber K., Pohl T., Fischer C., Birmili W., Rehn J., Sonntag A., Weinhold K., Rasch F. (2011), Untersuchung der räumlichen Variation von feinen- und ultrafeinen Partikeln in den Städten Düsseldorf und Leipzig.
- Vogt U. et al. (2017), Räumliche und zeitliche Variabilität von NO₂ und Partikeln entlang einer verkehrsreichen Bundesstraße in Stuttgart – Ergebnisse von Fahrradmessungen und Passivsammler-Messungen, *Tagungsband: Kolloquium Luftqualität an Straßen 2017*, 104-128.

2.3.4 NO₂ measurements in the city centre of Wuppertal

R. Kurtenbach, J. Kleffmann, A. Klosterk other and P. Wiesen*

Institute for Atmospheric and Environmental Research, University of Wuppertal, D-42097 Wuppertal, Germany, kurtenba@uni-wuppertal.de

Introduction

Fine particles and nitrogen dioxide (NO₂) are the key species for increasing air quality in Europe. Whereas particulate matter and the exceedance of PM limiting values have drawn considerable public attention since the year 2005, the NO₂ problem attracted public interest in Germany only after so-called "Diesel Gate" in September 2015 although EU limiting values entered into force already in January 2010.

The reduction of nitrogen oxide emissions has been historically one of the key objectives for improving air quality in Europe. Nitrogen oxide (NO_x=NO+NO₂) emissions have started to decrease considerably since the mid eighties of the last century in many European areas. However, emissions from mobile sources are still important contributors to air pollution, in particular for NO_x. Together with NO_x, non-methane volatile organic compounds (NMVOCs) undergo photochemical reactions producing secondary pollutants such as ozone (O₃), peroxyacetyl nitrate (PAN) and others (Chameides et al., 1997, Atkinson, 2000).

The NO_x and, in particular, the NO₂ emission have been studied in several European cities over the last decade to better understand current NO₂ trends (Carslaw, 2005, Keuken et al., 2009, Anttila et al., 2011, Mavroidis and Chaloulakou, 2011, Kurtenbach et al., 2012, Escudero et al., 2014, Henschel et al., 2015, Carslaw et al., 2016, Degraeuwe et al., 2016 and 2017, and Casquero-Vera et al., 2019).

In particular nitrogen dioxide is still a serious problem in many German cities. In the year 2018 39 % (UBA, 2019) of the roadside monitoring stations reported an exceedance of the annual limit of 40 µg/m³ (EU, 2018). In Wuppertal, Germany an annual value of 45 µg/m³ was measured at the monitoring station "Gathe" of the national monitoring network in 2018.

Since road traffic and particularly Diesel vehicles are still the major source of nitrogen oxides in Germany, it is currently discussed to ban Diesel vehicles from city centres to force NO₂ concentrations below the limit value. It is also known that in a city centre buses can have a significant contribution to the NO_x emission, in particular at bus stations close to monitoring stations (Carslaw et al., 2013, ADAC 2018).

However, there is also a debate in the public whether roadside monitoring stations were positioned in Germany in agreement with the corresponding EU guidelines.

In the present study, NO_x and CO₂ emissions were investigated in the city centre of Wuppertal at the monitoring stations "Gathe" of the national monitoring network, at "Loher Kreuz" and at a central bus terminal during 2018 to estimate the contribution of buses to the NO_x emission.

DESCRIPTION OF THE EXPERIMENTAL PROCEDURES

Measurement sites

The measurement campaign was carried out in the city centre of Wuppertal, Germany at the monitoring stations "Gathe" and "Loher Kreuz" and at the central bus terminal in Wuppertal-Elberfeld, see figures 1 and 2.

During the campaign emissions from the entire vehicle fleet (Gathe and Loher Kreuz) and in particular from the bus fleet (central bus terminal) were studied. The sampling points at the Gathe, Loher Kreuz and the bus terminal were located approx. 5 m away from the traffic lanes. In the city centre of Wuppertal predominant driving conditions were "30 km/h, Stop and Go" and it is reasonable to assume that the engines of the vehicles passing the sampling sites, were under warm operating conditions.

On weekdays 30 - 32 thousand vehicles pass the monitoring station Gathe and 12 bus routes with about 480 buses stop at the bus stop "Karlsplatz", which is close to the monitoring station. For comparison, on weekdays 31 - 33 thousand vehicles pass the monitoring station Loher Kreuz, but only two bus routes with about 230 buses stop at the bus stop "Loher Stra e", which is close to the monitoring station. The central bus station is used by more than 2,000 buses per day.



monitoring station Gathe
(51.260699; 7.147434)

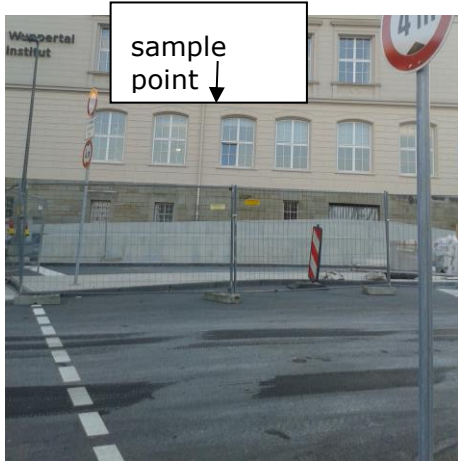


monitoring station Loher
Kreuz (51.265018;

Figure 1: Monitoring stations close to main roads in Wuppertal: Gathe and Loher Kreuz



central bus terminal



monitoring station (sample
point) at the central bus

Figure 2: Monitoring station at the central bus terminal

Analytical Equipment

The analytical equipment used was installed in the roadside monitoring stations and in an office room of the Wuppertal Institute close to the central bus terminal.

Nitrogen monoxide (NO) and NO₂ were measured on-line with a commercial NO_x chemiluminescence analyzer (Environnemental, AC 31M with molybdenum converter). The time resolution was 10 s and the detection limit, which was calculated from the variation of the zero signal was 2 ppbV for NO and 3 ppbV for NO₂. The NO channel of instrument was directly calibrated by undiluted standard NO calibration mixtures (Messer, stated accuracy 5 %). The NO₂ channel was calibrated by using a NO titration unit (Environnemental, GPT). NO₂ was produced by the reaction of NO with O₃ in a flow reactor leading to the quantitative conversion of the calibrated NO ($\Delta\text{NO} = \Delta\text{NO}_2$).

Ozone (O₃) was measured on-line with a commercial O₃ monitor (Environnemental, O3 41M with UV absorption). The time resolution was 10 s and the detection limit, which was calculated from the variation of zero measurements, was 1 ppbV. O₃ was calibrated by using an O₃ calibration unit

(Environnemental, K-O₃, accuracy 10 %). O₃ was produced by the photolysis of synthetic air in a flow reactor leading to the formation of O₃.

Carbon dioxide (CO₂) was measured on-line with a commercial CO₂ monitor (Carbondio-1000 with IR absorption). The time resolution was 1 s and the detection limit, which was calculated from the variation of zero measurements, was 2 ppmV. CO₂ was directly calibrated by undiluted standard CO₂ calibration mixtures (Messer, stated accuracy 2 %).

RESULT AND DISCUSSION

Traffic emissions

NO, NO₂, O₃ and CO₂ mixing ratios were measured at the different monitoring sites.

Figure 3 show as an example the diurnal variation of NO_x and CO₂ mixing ratios on March 20 (strike) and March 21 (no strike), 2018 at the monitoring station Gathe. On the day without strike of public services much higher NO_x and CO₂ mixing ratios up to 480 ppbV and 670 ppmV, respectively, were observed. During strike no buses of the public transport were in operation. At another strike day on April 10, 2018 the same was observed.

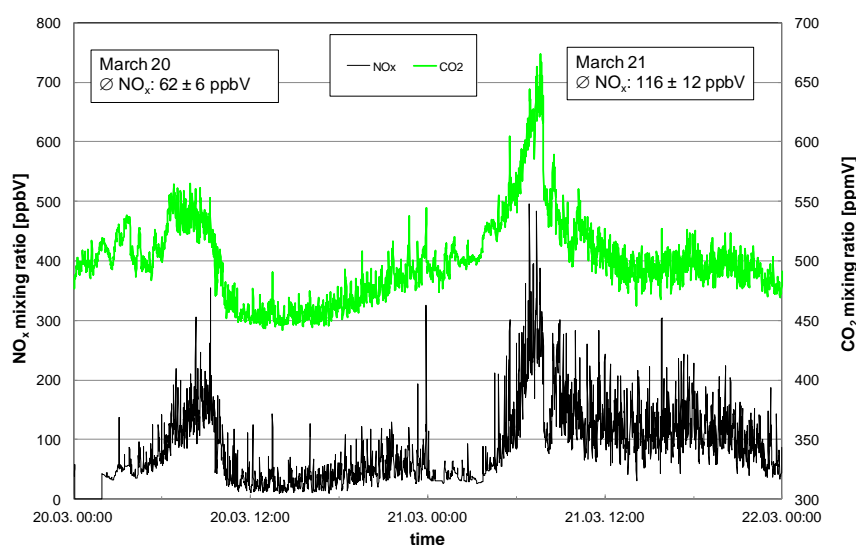


Figure 3: Diurnal variation of the NO_x and CO₂ mixing ratios at the monitoring station Gathe on March 20 and March 21, 2018. On March 20 public services were on strike.

From the measured data daily averaged values $\bar{\text{NO}}_x$ were calculated (see figure 3) showing that on March 21 (no strike) $\bar{\text{NO}}_x$ was about 87 % higher than on the strike day. A similar behaviour has been observed at the monitoring station Loher Kreuz, which is shown in figure 4. However, at this monitoring station the difference between daily average values $\bar{\text{NO}}_x$ was less pronounced, i.e. 46 %. The reason for this difference will be discussed later.

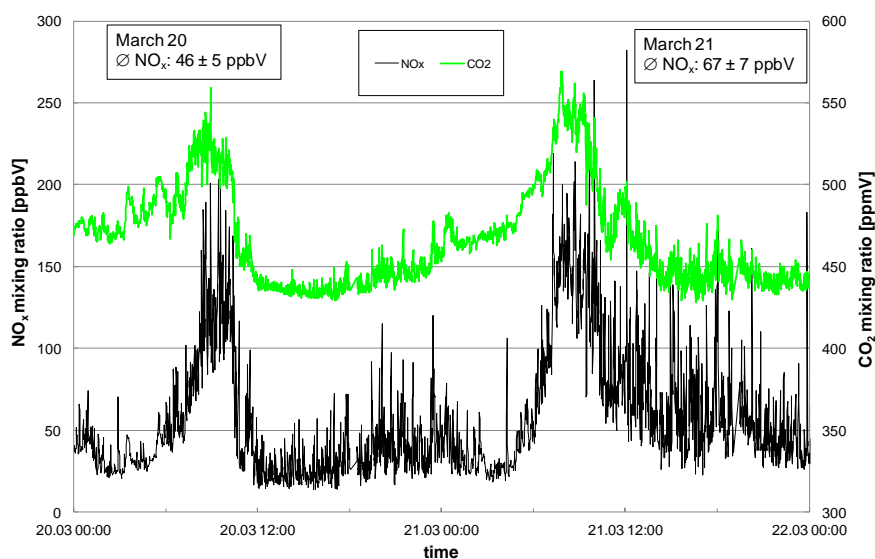


Figure 4: Diurnal variation of the NO_x and CO₂ mixing ratios at the monitoring station Loher Kreuz on March 20 and March 21, 2018. On March 20 public services were on strike.

NO₂/NO_x emission ratio

The contribution of the primarily emitted NO₂ to the measured NO₂ (total) at the monitoring station can be derived by measuring the NO₂/NO_x emission ratio. In order to obtain the correct NO₂/NO_x emission ratio it is important to distinguish between primarily emitted NO₂ and NO₂ (secondary), which is being formed by the reaction of NO with ozone in the exhaust plume. The correct NO₂/NO_x ratio is obtained by plotting O_x, which is the sum of NO₂ and O₃ versus the measured NO_x mixing ratio. (Clapp and Jenkin, 2001). The NO₂/NO_x emission ratio and the local O₃ background mixing ratio are obtained from the slope and intercept of the regression line, respectively.

The primarily emitted NO₂ is obtained by multiplying the NO₂/NO_x emission ratio with the measured NO_x concentration. The difference between the measured NO₂ (total) and the resulting primarily emitted NO₂ is then equivalent to the NO₂ (indirect), which is formed through the titration reaction of NO with ozone. In traffic-related measurements of NO, NO₂ and O₃ in the morning during the so-called "rush hour" usually the O₃ background concentration is almost constant, the RO₂ chemistry in the atmosphere is negligible and the variation in the measured NO_x is greatest. Accordingly, data from this time interval provide the best linear correlation expected between O_x and NO_x. In table 1 the measured daily averaged values at the monitoring station Gathe for $\bar{\text{NO}}_x$, $\bar{\text{NO}}_2$ (total) and $\bar{\text{NO}}_2$ (primary) are listed for March 20 and March 21, 2018.

Table 1: Daily averaged values of $\bar{\text{NO}}_x$, $\bar{\text{NO}}_2$ (total), $\bar{\text{NO}}_2$ (primary) and the % contribution of primary NO₂ to the total NO₂.

date	Daily averaged value			% contribution of NO ₂ (primary) to the NO ₂ (total)
	NO _x [ppbV]	NO ₂ total [ppbV]	NO ₂ (primary) [ppbV]	
March 20 (strike)	62 ± 6	27 ± 3	8 ± 1	30 ± 5
March 21 (no strike)	116 ± 12	37 ± 4	18 ± 2	47 ± 4

From the data on March 20 (strike) daily average values $\bar{\text{NO}}_2$ (total) of (27 ± 3) ppbV and of (8 ± 1) ppbV NO₂ (primary) were obtained, which corresponds to a NO₂ (primary) contribution of (30 ± 5) % to NO₂ (total). However, on March 21 (no strike) significantly higher daily average values $\bar{\text{NO}}_2$ (total) of (37 ± 4) ppbV and $\bar{\text{NO}}_2$ (primary) of (18 ± 2) were found, which corresponds to a NO₂ (primary)

contribution of $(47 \pm 4) \%$ to NO_2 (total). The observed higher NO_2 primary contribution to the total NO_x concentration of about 50 % on March 21 can be attributed to the fact that diesel engines from buses with exhaust after-treatment systems such as oxidation catalysts with PM filter systems (DPF) show high primary NO_2 emissions with a NO_2/NO_x ratio of about 25 to 40 % (Carslaw et al., 2013 and 2015, ADAC 2018).

Emission indices

From the handbook of emission factors (HBEFA) it is well known, that buses emit large quantities of NO_x , i.e. the NO_x emission index (EI_{NO_x}) (mass emitted NO_x per kg burnt fuel) is high. HBEFA reports for the operating condition “30 km/h, Stop and Go” EI_{NO_x} values in the range of 50 g/kg (EURO 0 class), 39 g/kg (EURO I class), 45 g/kg (EURO II class), 44 g/kg (EURO III class), 27 - 45 g/kg (EURO IV class), 25 - 38 g/kg (EURO V class) and 3 g/kg (EURO VI class). For comparison, passenger cars have a much lower EI_{NO_x} of about 14 g/kg (diesel engine) and 1 g/kg (gasoline engine) (HBEFA, 2017). In order to determine the contribution of the public bus fleet to the total NO_x emission at the monitoring station Gathe, the emission indices EI_{NO_x} of the traffic fleet on March 20 (strike) were compared with the EI_{NO_x} on March 21, 2018 (no strike).

In Figure 5 the integrated emission peaks (peak area) for NO_x and CO_2 as ΔNO_x and ΔCO_2 are shown as an example for March 21, 2018 (no strike) at the monitoring station Gathe. If one assumes that the increase of NO_x and CO_2 in the plume is proportional to the emission strength of the vehicle engines, an emission ratio to CO_2 , i.e. $\Delta\text{NO}_x/\Delta\text{CO}_2$, can be easily calculated (Petzold et al., 2008; Carslaw et al., 2013).

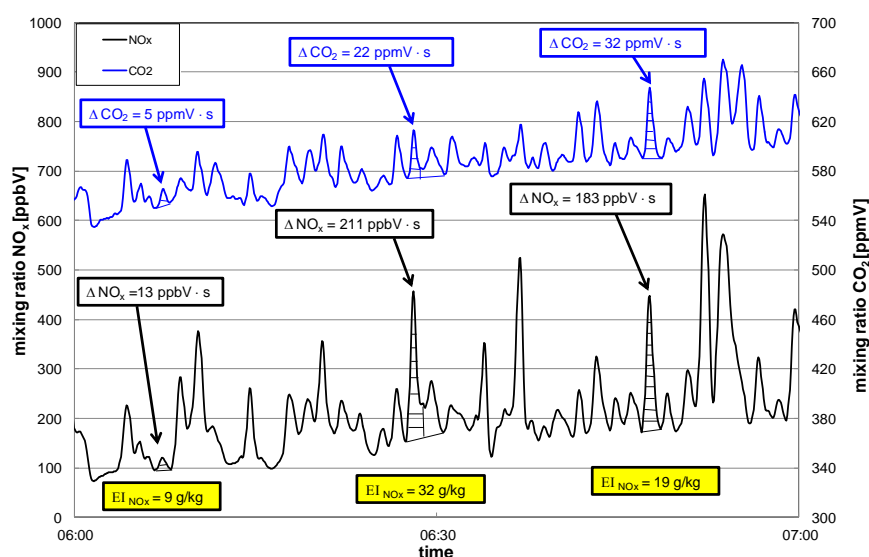


Figure 5: Temporal variation of the NO_x and CO_2 mixing ratios and integrated emission peaks as ΔNO_x and ΔCO_2 peak area for three examples at the monitoring station Gathe on March 21, 2018 (06:00 to 07:00 h).

From the wt% carbon and under the assumption that all fuel is burnt into the final end product CO_2 an emission index EI_{CO_2} of 3,200 g CO_2 per kg burnt fuel was assumed and further used to calculate the corresponding emission index (EI) for the different vehicle. The emission index (EI) is calculated by the following equation (Petzold et al., 2008)

$$\text{EI}(X) = \text{EI}(\text{CO}_2) \times \frac{M(X)}{M(\text{CO}_2)} \times \frac{\Delta(X)}{\Delta(\text{CO}_2)},$$

where M denotes the molecular weight and Δ the peak area of the different species. $M(\text{CO}_2) = 44 \text{ g/mol}$, $M(\text{NO}_x) = 46 \text{ g/mol}$ and NO_x counted as NO_2 were used for the subsequent calculations.

Figure 5 shows a large number of NO_x and CO₂ emission peaks. For the three examples in figure 5 EI_{NO_x} of 9 g/kg, 19 g/kg and 32 g/kg were calculated from the integrated emission peaks. On average per day more than 400 emission peaks from different vehicles were observed and analyzed accordingly. Figures 6 and 7 show as an example the percentage distribution of the EI_{NO_x} obtained at the monitoring station Gathe on March 20 (strike day) and March 21 (no strike day) and at the central bus terminal on November 26 for comparison.

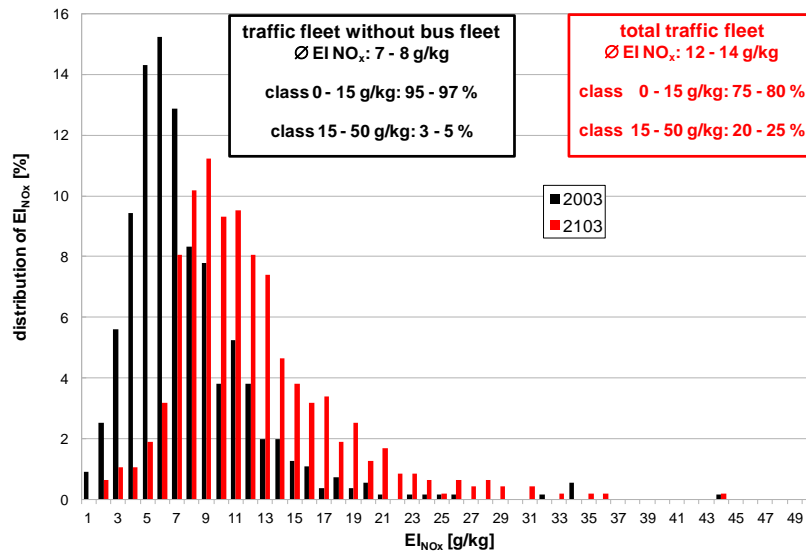


Figure 6: Percentage distribution of EI_{NO_x} at the monitoring site Gathe on March 20 (strike; traffic fleet without any buses from the public transport sector) and March 21 (no strike, normal traffic fleet).

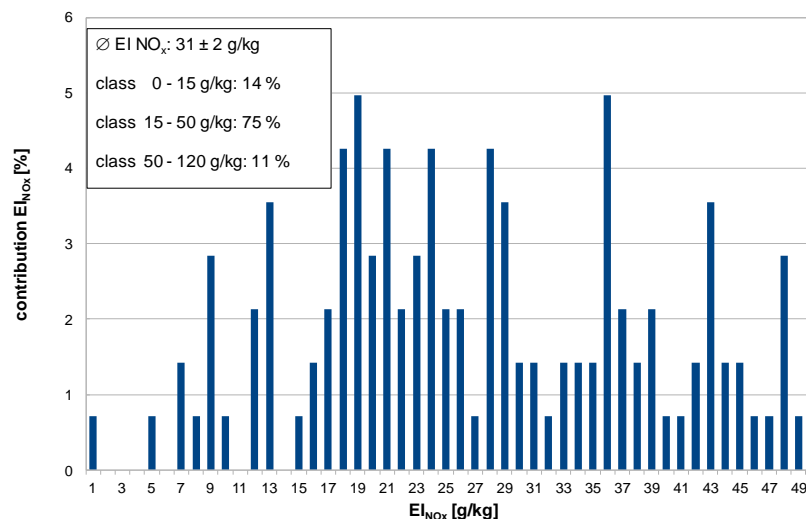


Figure 7: Percentage distribution of EI_{NO_x} at the monitoring site central bus station on November 26 (no strike).

Figure 6 shows two significantly different percentage distributions of EI_{NO_x}. On both strike days (March 20 and April 10 – not shown in the figure) only 3 - 5 % of the EI_{NO_x} distribution were found in the class of 15 - 50 g/kg and a high contribution of 95 - 97 % in the class up to 15 g/kg. Contrary, on a normal day without strike a much higher contribution of 20 - 25 % in the class of 15 - 50 g/kg was observed. This is a strong indication that on a normal day without strike EI_{NO_x} in the class of 15 - 50 g/kg are caused by the bus fleet.

This is supported by the fact, that the EI_{NO_x} derived from the measurements at the central bus terminal (see figure 7), exhibited, that 86 % of the EI_{NO_x} are in the class 15 - 120 g/kg and only 14 % in the class up to 15 g/kg. It is worth mentioning that 11 % of the EI_{NO_x} were found in the class 50 - 120 g/kg. For

the driving condition “30 km/h, Stop and Go”, which refers to the situation at the central bus terminal HBEFA only provides values in the range 3 - 50 g/kg (EURO 0 - EURO VI) (HBEFA, 2017). Previous on road studies (ADAC, 2018) of bus emissions under real driving conditions (RDC) have conclusively demonstrated a strong negative speed dependent NO_x emission. At lower speed of 25, 10 and 5 km/h EI_{NO_x} values of 14, 40 and 90 g/kg were observed, respectively. The results from this study, in particular the high EI_{NO_x} reported at a speed of 5 km/h support the findings from the present study. Furthermore, the authors (ADAC, 2018) reported that about 18 and 60 % of the total NO_x emission are observed for the driving conditions idle and acceleration, respectively. Finally also daily average values \bar{EI}_{NO_x} were calculated (see figure 6) showing that low values of 7 - 8 g/kg on the days when public services were on strike (March 20 and April 10, 2018) compared to normal working days for which 12 - 14 g/kg were obtained. Taking into account the measured EI_{NO_x} distribution for normal working days the contribution of the public bus fleet to the total NO_x emission at the monitoring station Gathe was calculated. Figure 8 shows the average daily percentage contribution of the NO_x emission as a function of the measured EI_{NO_x}.

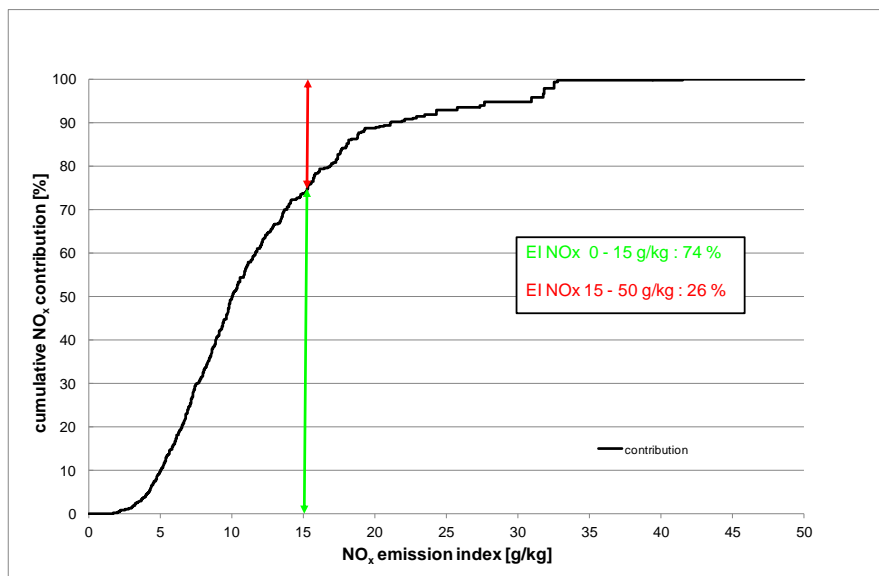


Figure 8: Average cumulative percentage NO_x contribution as a function of the measured EI_{NO_x} at the monitoring station Gathe for a regular working day.

From the measured data an average daily contribution of 24 - 26 % to the total NO_x emission by the public transport bus fleet at monitoring station Gathe was calculated. With respect to the official EU guidelines, a significant impact of a single emission source/category, e.g. buses, on the measured concentrations at an official monitoring station of a national monitoring network must be avoided (EU, 2018). Accordingly, the result of the present study put the position of the monitoring station Gathe into question. Most probably the significant impact of the bus fleet on the NO_x concentration at the monitoring station Gathe is caused to a large extent by the close neighbourhood of the bus stop Karlsplatz. Figures 9 and 10 show in more detail the location of the monitoring station Gathe and Loher Kreuz for comparison.

It can be seen that at the monitoring station Gathe, because of the bus stop, in particular during rush hours with a high bus frequency, buses are forced to stop directly in front of the monitoring station so that the undiluted exhaust can reach the sampling inlet. At the monitoring station Loher Kreuz the situation is somewhat different. Firstly, the number of buses passing the station in total is only ca. half of the station Gathe and secondly the distance between the station and the bus stops on both sides of the road is larger. Accordingly, the impact of the bus fleet passing the monitoring station Loher Kreuz is less pronounced.

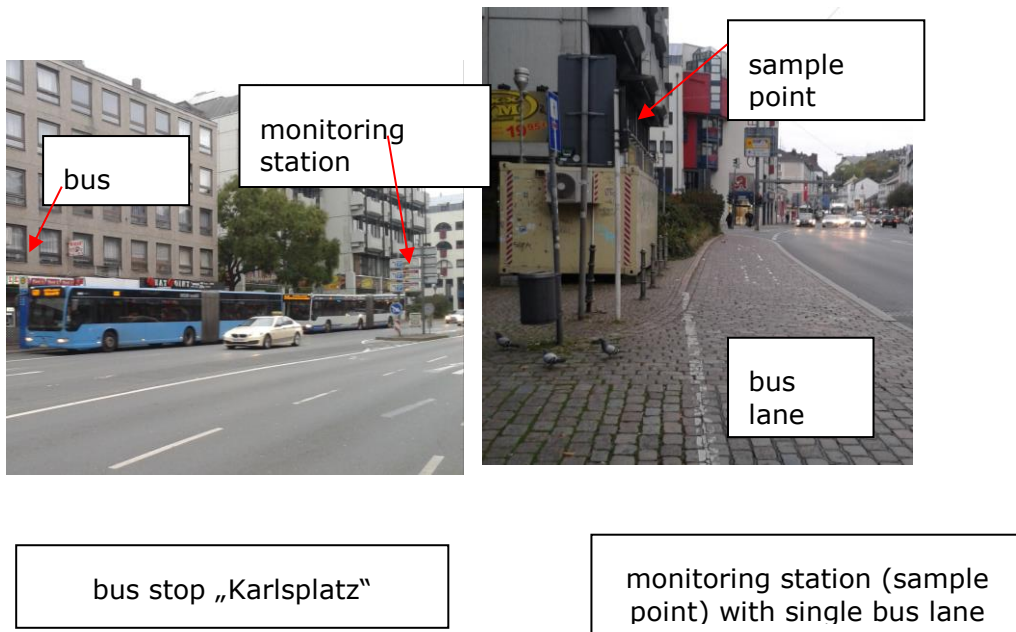


Figure 9: Monitoring station Gathe and the bus stop “Karlsplatz”.

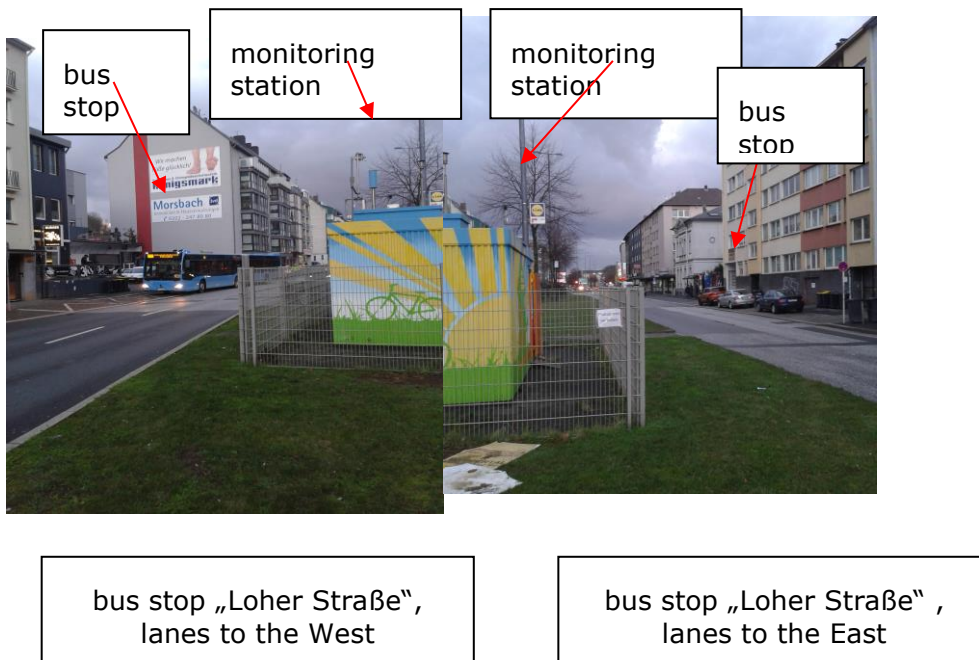


Figure 10: Monitoring station Loher Kreuz with two bus stops “Loher Straße” at the left and right traffic lane.

In conclusion the results of the present study show, that at locations with a high traffic density of buses, the contribution of buses to the total NO_x and, in particular, to the NO_2 emission can be very high. In urban areas buses may contribute significantly to NO_x emissions and primary NO_2 . In 2010 for example, buses contributed on average 33 % to the road transport NO_2 emissions in central London (GLA, 2013). Accordingly, measures to reduce NO_x emissions from buses could significantly improve air quality in urban areas. Previous studies in Berlin (Berlin, 2017) and Stuttgart (Stuttgart, 2018) have shown, that the modernization of the existing bus fleet by introducing a NO_x reduction system (e.g. selective catalytic reduction system, SCR) and/or the simultaneous replacement of old buses significantly reduced the NO_2 . In Berlin at the monitoring station “Hardenbergplatz” close to the bus terminal “Busbahnhof Zoo”

the annual NO₂ concentration went down in the years 2014 and 2015 from 62 to 53 µg/m³. In Stuttgart at the monitoring station “Arnulff-Klett-Platz”, which is also close to a bus stop the annual NO₂ concentration went down from 58 (2016) to 56 (2017) and to 46 (2018) µg/m³.

In the City of Wuppertal currently a modernization of the bus fleet with SCR systems and a simultaneous replacement of the EURO III and IV buses, in particular, buses with DPF (EURO III) is on-going. It is known, that refitting buses with a SCR system reduces the NO_x emission by > 98% and the NO₂/NO_x ratio of about 10 % (Carslaw et al., 2015, ADAC, 2018).

As a result of the present study currently only buses with low NO_x emission (EURO V, EEV and EURO VI) are allowed to pass the monitoring station or to stop at the bus stop “Karlsplatz”. By these measures the city authority hopes to further reduce the NO₂ concentrations to meet the limit of 40 µg/m³ by the end of 2019 at the latest and hereby to avoid driving bans for Diesel passenger cars in the City of Wuppertal.

Acknowledgements

Cooperation with and support by the State Agency for Nature, Environment and Consumer Protection North Rhine-Westphalia (LANUV-NRW) is gratefully acknowledged.

References

- ADAC (2018), NO_x-Reduzierung an einem EURO V/EEV Stadtlinienbus durch Hardwarenachrüstung, https://www.adac.de/mmm/pdf/Schlussbericht_%20ADAC_Nachr%C3%BCstung_Stadtbus_08022018_315129.pdf
- Anttila, P., Tuovinen, J.-P. and Niemi, J. V. (2011). Primary NO₂ emissions and their role in the development of NO₂ concentrations in a traffic environment. *Atmospheric Environment*, 45, 986-992.
- Atkinson, R. (2000). Atmospheric chemistry of VOCs and NO_x. *Atmospheric Environment*, 34, 2063-2101.
- Berlin (2017). Berliner Senatsverwaltung für Umwelt, Verkehr und Klimaschutz, Berliner Luftreinhalteplan: Maßnahmen bei Linienbussen, <http://www.berlin.de/sen/uvk>
- Carslaw, D. C. (2005). Evidence of an increasing NO₂/NO_x emissions ratio from traffic emissions. *Atmospheric Environment*, 39, 4793-4802.
- Carslaw, D. C. and Rhys-Tyler, G. (2013). New insights from comprehensive on-road measurements of NO_x, NO₂ and NH₃ from vehicle emissions remote sensing in London, UK. *Atmospheric Environment*, 81, 339-347.
- Carslaw, D. C., Priestman, M., Williams, M. L., Stewart, G. B., and Beevers, S. D. (2015). Performance of optimised SCR retrofit buses under urban driving and controlled conditions. *Atmospheric Environment*, 105, 70-77.
- Carslaw, D.C., Murrells, T. P., Andersson, J., and Keenan, M. (2016). Have vehicle emissions of primary NO₂ peaked? *Faraday Discussions*, 189, 439-454.
- Casquero-Vera, J. A., Lyamani, H., Titos, G., Borrás, E., Olmo, F. J., and Alados-Arboledas, L. (2019). Impact of primary NO₂ emissions at different urban sites exceeding the European NO₂ standard limit. *Science of the Total Environment*, 646, 1117-1125.
- Chameides, W. L., Fehsenfeld, F., Rodgers, M. O., Cardelino, C., Martinez, J., Parrish, D., Lonneman, W., Lawson, D. R., Rasmussen, R. A., Zimmerman, P., Greenberg, J., Middleton P., and Wang T. (1992). Ozone Precursor Relationships in the Ambient Atmosphere. *Journal Geophysical Research*, 97, 6037-6055
- Clapp, L. J. and Jenkin, M. E. (2001). Analysis of the relationship between ambient levels of O₃, NO₂ and NO as a function of NO_x in UK. *Atmospheric Environment*, 35, 6391-6405.
- Degraeuwe, B., Thunis, P., Clappier, A., Weiss, M., Lefebvre, W., Janssen, S., and Vranckx, S. (2016). Impact of passenger car NO_x emissions and NO₂ fractions on urban NO₂ pollution – scenario analysis for the city of Antwerp, Belgium. *Atmospheric Environment*, 126, 218-224.
- Degraeuwe, B., Thunis, P., Clappier, A., Weiss, M., Lefebvre, W., Janssen, S., and Vranckx, S. (2017). Impact of passenger car NO_x emissions on urban NO₂ pollution – scenario analysis for 8 European cities. *Atmospheric Environment*, 171, 330-337.
- EU (2018) *European guideline 2008/50/EG 21 March 2008*: <https://eur-lex.europa.eu/legal-content/EN/TXT/PDF/?uri=CELEX:32008L0050&from=DE>
- Escudero, M., Lozano, A., Hierro, J., del Valle, J., and Mantilla, E. (2014). Urban influence on increasing ozone concentrations in a characteristic Mediterranean agglomeration. *Atmospheric Environment*, 99, 322-332.

GLA (2013). London Atmospheric Emissions Inventory 2010. <https://data.london.gov.uk/dataset/london-atmospheric-emissions-inventory-2010>

HBEFA (2017), HBEFA 3.3, Handbuch Emissionsfaktoren des Straßenverkehrs, <http://www.hbefa.net>.

Henschel, S., Le Tertre, A., Atkinson, R. W., Querol, X., Pandolfi, M., Zeka, A., Haluza, D., Analitis, A., Katsouyanni, K., Bouland, C., Pascal, M., Medina, S., and Goodman, P. G. (2015). Trends of nitrogen oxides in ambient air in nine European cities between 1999 and 2010. *Atmospheric Environment*, 117, 234-241.

Keuken, M., Roemer, M., and van den Elshout, S. (2009). Trend analysis of urban NO₂ concentrations and the importance of direct NO₂ emissions versus ozone/NO_x equilibrium. *Atmospheric Environment*, 43, 4780-4783.

Kurtenbach, R., Kleffmann, J., Niedojadlo, A., and Wiesen, P. (2012). Primary NO₂ Emissions and their Impact on Air Quality in Traffic Environments in Europe, *Environmental Sciences Europe*, 24:21, 1-8.

Mavroidis, I. and Chaloulakou, A. (2011). Long-term trends of primary and secondary NO₂ production in the Athens area. Variation of the NO₂/NO_x ratio. *Atmospheric Environment*, 45, 6872-6879.

Petzold, A., Hasselbach, J., Lauer, P., Baumann, R., Franke, K., Gurk, C., Schlager, H., and Weingartner, E. (2008). Experimental studies on particle emissions from cruising ships, their characteristic properties, transformation and atmospheric lifetime in the marine boundary layer. *Atmospheric Chemistry and Physics*, 8, 2387-2403.

Stuttgart (2018), 3. Tagung „Motorische Stickoxidbildung“, Luftreinhaltung, Stuttgarter Straßenbahn AG, Wiedemann, Rust 5.-6.Februar 2019.

UBA (2019) Umweltbundesamt, Daten/Luft/Stickoxid-Belastung: <https://www.umweltbundesamt.de/presse/pressemitteilungen/stickstoffdioxidbelastung-geht-2018-insgesamt>.

2.3.5 NO₂ Air Quality in German Cities: Trends Forecasts and Scenarios

N. Toenges-Schuller^{1}, Chr. Schneider¹, R. Vogt² and S. Hausberger³*

¹ AVISO GmbH, Am Hasselholz 15, 52074 Aachen, Germany, nicola.toenges-schuller@avisogmbh.de

² Ford-Werke GmbH, Research & Innovation Center Aachen, Süsterfeldstrasse 200, 52072 Aachen, Germany

³ Institut für Verbrennungskraftmaschinen und Thermodynamik, TU Graz, Inffeldgasse 19/I, 8010 Graz, Austria

Introduction

In 2016, nearly 60% of all traffic-influenced air quality measurement stations were not compliant with the limit of 40 µg/m³ for the annual mean value of NO₂. To estimate the development in future, in this paper, three scenarios are examined, a trend forecast and two scenarios assuming additional actions.

Four German inner-city street canyons were selected, where annual average NO₂ concentrations in 2016 ranged from 43 µg/m³ (“Turiner Straße” in Cologne, only just exceeding the limit) to 82 µg/m³ (“Am Neckartor” in Stuttgart, highest annual average NO₂ concentration measured in Germany in that year). For these stations, air quality model calculations were done, followed by an extrapolation of the results to all traffic influenced air quality stations in Germany.

As a base run, for each station, a trend forecast was done for the years 2020, 2025 and 2030. The expected fleet renewal leads to substantial reductions of NO₂ exceedances with 95% compliance in 2025 and >99% compliance in 2030 (only one exceedance left at “Am Neckartor”, where an annual mean NO₂ concentration of 41 µg/m³ is expected).

In addition to the base run, two further scenarios were examined. In scenario CF (conformity factors), the conformity factors for Diesel Euro 6-d temp and final PC were reduced, assuming the CF NO_x was lowered by the deletion of the error margins. This has only a small impact on air quality. As a third scenario (EZ), the effects of a “Blue Environmental Zone” were examined. Here, significant NO₂ reductions are expected, compliance for all traffic influenced air quality stations in Germany is expected between 2020 and 2025.

Methods

Four German inner-city street canyons with traffic influenced air quality stations were selected:

- “Am Neckartor” (NT) in Stuttgart, annual average NO₂ 2016: 82 µg/m³
- “Clevischer Ring” (CL) in Cologne, annual average NO₂ 2016: 65 µg/m³
- “Corneliusstraße” (CO) in Düsseldorf, annual average NO₂ 2016: 58 µg/m³
- “Turiner Straße” (TU) in Cologne, annual average NO₂ 2016: 43 µg/m³

Air quality measurements for these stations were obtained from UBA (2018). For these stations, emissions and air quality were modelled for the years 2016, 2020, 2025 and 2030 and for three scenarios. Finally, the results were extrapolated to all traffic influenced air quality stations in Germany.

Road traffic emissions

Specific traffic emissions (pollutant per distance and time unit) for the four urban main roads were calculated as the product of emission factors (pollutant per vehicle and distance, depending on vehicle type, motor concept, and traffic situation) and the traffic volume (vehicles per time unit), weighted by fleet composition.

Emission factors were taken from HBEFA3.3 (Keller et al., 2017), except for gasoline Euro 6 and Euro 6c, which were updated by TU Graz for this project. In scenario 2, emission factors of Diesel PC Euro 6 d temp and final were modified.

The traffic volumes and the fractions of the vehicle types (PC: passenger cars, LGV: light goods vehicles of maximum permissible laden weight ≤ 3.5 t, HGV: heavy goods vehicles of maximum permissible laden weight > 3.5 t) for the four streets are shown in Table 1. The data come from actual works in the context of the clean air plans of the three cities (Stuttgart, 2018; Cologne, 2018, 2019; Düsseldorf, 2018), traffic volumes “Am Neckartor” are based on permanent automatic counts, in Cologne and Düsseldorf on projections of temporal counts in combination with traffic models.

Table 1: Traffic volumes (in vehicles/24h) and fractions of vehicle types at the considered streets (data sources: Cologne (2018, 2019), Düsseldorf (2018), Stuttgart (2018))

station	PC	LGV	HGV	total
NT	63,350	2,050	1,900	67,300
	94%	3%	3%	100%
CO	42,850	2,400	750	46,000
	93%	5%	2%	100%
CL	40,950	2,050	2,900	45,900
	89%	5%	6%	100%
TU	24,350	1,450	500	26,300
	93%	5%	2%	100%

The traffic volumes range from around 26,000 vehicles/24h at “Turiner Straße” to around 67,000 vehicles/24h at “Am Neckartor”. The fractions of HGV range from 2% at “Corneliusstraße” (no transit allowed for HGV, only local deliveries) to 6% at “Clevischer Ring”, a value comparably high for inner city main roads in Germany.

The traffic situation was derived from street type, speed limit, and hourly values of traffic volume. The four inner city main roads here were characterised as “distributor, speed limit 50 km/h” according to HBEFA.

As for the traffic volume, the fleet compositions, differentiated by fuel type and Euronorm concept per vehicle type, were taken from actual papers in the context of the clean air plans of the three cities (Cologne, 2018, 2019; Düsseldorf, 2018; Stuttgart, 2018). PC fleet composition is based on local car registration data, using a mileage correction for vehicle age and fuel type. For Cologne, additionally, results of a campaign of automatic licence plate recognition were used. For HGV, the average German fleet composition according to HBEFA3.3 was used. Existing low emission zones were considered. The projection until 2030 was done according to HBEFA3.3, electric vehicles were added. The resulting PC fleet compositions for the three cities are shown in Figure 1.

For Diesel PC Euro 3, 4, 5, and 6, local temperature dependence was explicitly modelled, for each hour of the year based on local ambient temperature. This temperature dependence leads to about 40% higher road traffic emissions of NO_x in winter than in summer in 2016. The effect on the total of annual emissions is much lower: For NT, the difference between annual road traffic NO_x emissions calculated for 10°C and for the local temperatures is less than 1%, for CO less than 4%.

Cold start additions also were calculated based on these temperature series.

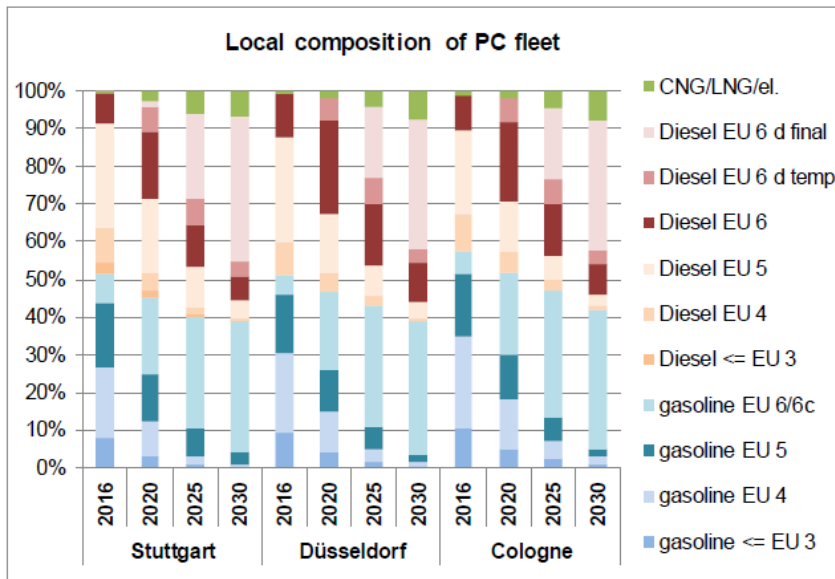


Figure 1: Local composition of the PC fleet in Stuttgart, Düsseldorf, and Cologne (data sources: 2016: Cologne (2018, 2019), Düsseldorf (2018), Stuttgart (2018), projection according to HBEFA3.3, used for base run)

Air quality modelling

The inner-city main roads examined in this paper are all street canyons with high building density on both sides of the road. Thus, air quality modelling can be done with a box model: Gas-phase concentrations of pollutants are calculated for the street canyon, which is modelled as a box of infinite length, the width of the street, and the height of roadside buildings, and assumed to be homogeneously mixed. Concentrations in the box correspond to the concentrations typically measured by an air quality station at the kerbside. This box model was used in the past to simulate NO_2 (Vogt et al., 2010; Kessler et al., 2010; Toenges-Schuller et al., 2016) and particle number (Toenges-Schuller et al., 2015) in street canyons.

The chemistry box model comprises gas-phase chemistry and one-dimensional transport (perpendicular to street). The RADM2 gas-phase chemistry mechanism with 56 species, 140 thermochemical reactions, and 21 photochemical reactions (Stockwell et al., 1990) in combination with the solver of the EURAD-model (Memmesheimer et al., 2007) is used. Not considered are turbulent diffusion, deposition, a variable mixing height, and heterogeneous reactions. As input parameters, urban background concentrations of NO_2 , NO and ozone, roadside concentrations of NO and NO_2 (for calibration), wind speed and direction and global radiation, and traffic emissions in the street are needed in an hourly resolution. Background concentrations and meteorological parameters were taken from air quality measurement stations of the urban background nearby (LANUV, 2018; LUBW, 2018):

1. "Am Neckartor": For annual average NO_2 , the station in Schubartstraße was used. In Schubartstraße, an urban background air quality station in Stuttgart very close to "Am Neckartor", a passive collector for NO_2 is placed, giving an annual average NO_2 value but no time dependence and no NO value. Time variation and NO_2/NO_x ratio were taken from Arnulf-Klett-Platz, the closest air quality station in Stuttgart where hourly values of NO and NO_2 by active measurements are available. Hourly values for O_3 were taken from Arnulf-Klett-Platz.
2. "Clevischer Ring" and "Turiner Straße": Hourly values of NO_2 , NO , and O_3 were taken from the urban background air quality station in Cologne Rodenkirchen. For "Turiner Straße", there were hours in 2016, when measured NO_2 and NO concentrations in the background at Rodenkirchen are higher than at "Turiner Straße". In these cases, the model input background concentrations were reduced accordingly. So, for "Turiner

Straße”, the effective background concentrations of NO₂ and NO are slightly lower than for “Clevischer Ring”.

3. “Corneliusstraße”: The time series of hourly values of NO₂, NO, and O₃ were taken from the regional background air quality station in Düsseldorf Lörick. To account for the difference between regional and urban background, the values were scaled to the annual mean values of Rodenkirchen (There is no urban background station in Düsseldorf, so NO₂ levels in Rodenkirchen were taken as representative also for urban background in Düsseldorf).

Source apportionments and trends for the background concentrations were based on IVU (2014) for NT and on the clean air plan for Cologne (Cologne, 2018, 2019) for the other roads in combination with UBA (2014). It was distinguished between the contributions of non-local road traffic and of other sources. To the trends of the non-local road traffic contributions to background concentrations of NO and NO₂, corrections were applied, since UBA (2014) was based on HBEFA3.1. The resulting projections of annual average NO₂ for NT and CL are shown in Figure 2. For CO, the annual average values are identical to CL (see point 3 above), for TU slightly lower (see point 2 above).

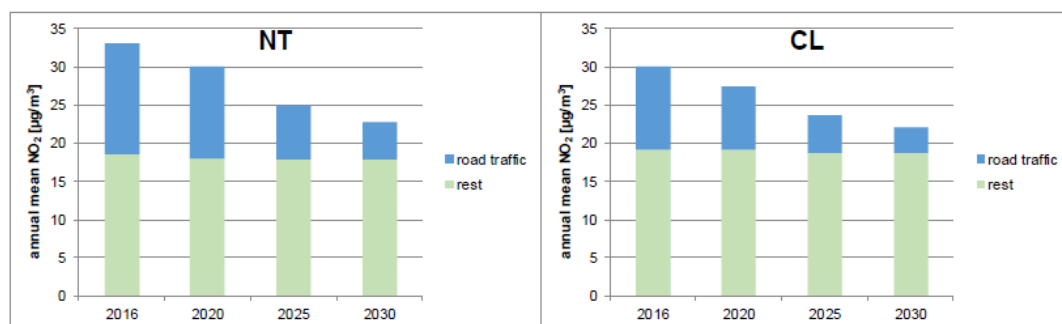


Figure 2: Projections of background annual average NO₂ used as model input until 2030, based on local clean air plans, UBA (2014), and corrections to account for the differences between HBEFA3.1 and HBEFA3.3

The model was calibrated for the base year 2016.

Scenarios

For each street, the following scenarios are calculated for the years 2020, 2025 and 2030:

- **BR** (base run): A trend forecast was done, assuming no further air quality actions. Traffic volume and vehicle types are assumed constant until 2030. A natural fleet renewal according to HBEFA until 2030 is assumed, a share of electric vehicles is added. The projection is shown in Figure 1. This base run can be considered a conservative scenario, since in Stuttgart, Cologne and Düsseldorf, further actions are heavily debated and about to be implemented.
- **CF** (conformity factors): The conformity factors for Diesel Euro 6-d temp and final PC were reduced by deletion of the NO_x error margins. This results in conformity factors of CF=1.6 (instead of 2.1) for Euro 6-d temp and CF=1.0 (instead of 1.5) for Euro 6-d final. The emission factors of HBEFA3.3 were modified accordingly: Euro 6-d temp: reduction factor: 1.6/2.1=76%, Euro 6-d final: reduction factor: 1.0/1.5=67%. Traffic volume, vehicle types and vehicle fleet are taken from the base run.
- **EZ** (blue environmental zone): Definition as proposed by the federal state of Baden-Württemberg: Exclusion of Diesel Euro 2, 3, 4, 5 and gasoline < Euro 3, 20% exceptions in 2020, no exceptions 2025 and 2030, including HGV and busses, traffic volume is constant, non-excluded vehicle fleet is normalised to 100%.

Results

Emission factors

As described above, road traffic emission factors used in this paper come from HBEFA3.3, but the factors for PC gasoline Euro 6 and 6c were updated by TU Graz. In Figure 3, for the traffic situation “Urban distributor, speed limit 50 km/h, heavy” at 10°C, the updated emission factors are shown in comparison to the values from HBEFA3.3. Adjusted emission factors used in scenario CF for Euro 6 d temp and final Diesel PC for that traffic situation are also shown in Figure 3¹.

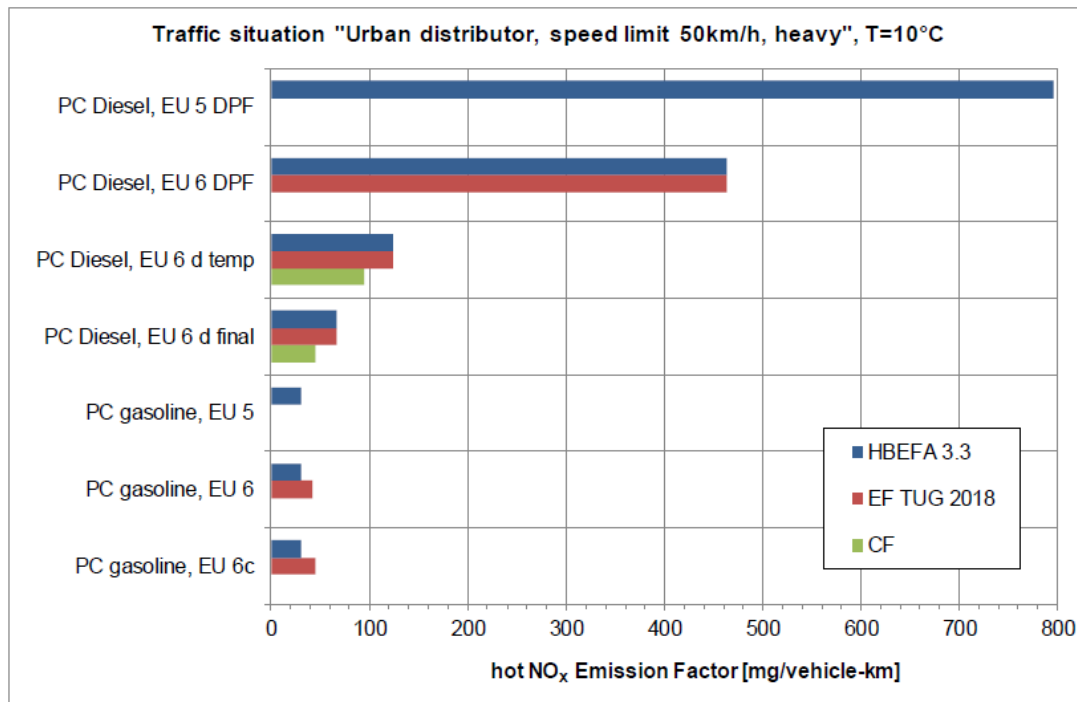


Figure 3: Hot NO_x Emission factors for Euro 5 and 6 PC for the traffic situation “Urban distributor, speed limit 50 km/h, heavy” at 10°C

Emissions

In Figure 4, for the base run 2016, 2020, 2025, and 2030, annual road traffic NO_x emission densities calculated for the for the four sites by vehicle type and, for PC, by motor concept are shown. In 2016, the total ranges from 4,2 t/(km*a) at TU to 11,5 t/(km*a) at NT. The expected natural fleet renewal leads to reductions of the local road traffic NO_x emissions between 65% and 70% 2030 compared to 2016 in the base run.

In Figure 5, the relative contributions of vehicle types and, for PC, motor concepts, to local annual road traffic NO_x emissions for the four sites are shown. At CL, where the fraction of HGV is highest, in 2016, HGV contribute nearly 40% to annual NO_x emissions. This fraction is expected to decrease to about 23% in 2030. At the other sites, local road traffic NO_x emissions are dominated by Diesel PC.

In Figure 6 and Figure 7, these numbers are shown for annual local road traffic NO₂ emissions.

¹ At the time this paper was prepared, HBEFA4.1 was not out yet. However, there are indications that NO_x EF of PC Diesel Euro 6 d temp and final according to HBEFA4.1 might be lower than according to HBEFA3.3. So, scenario “CF” might be closer to reality than the base run.

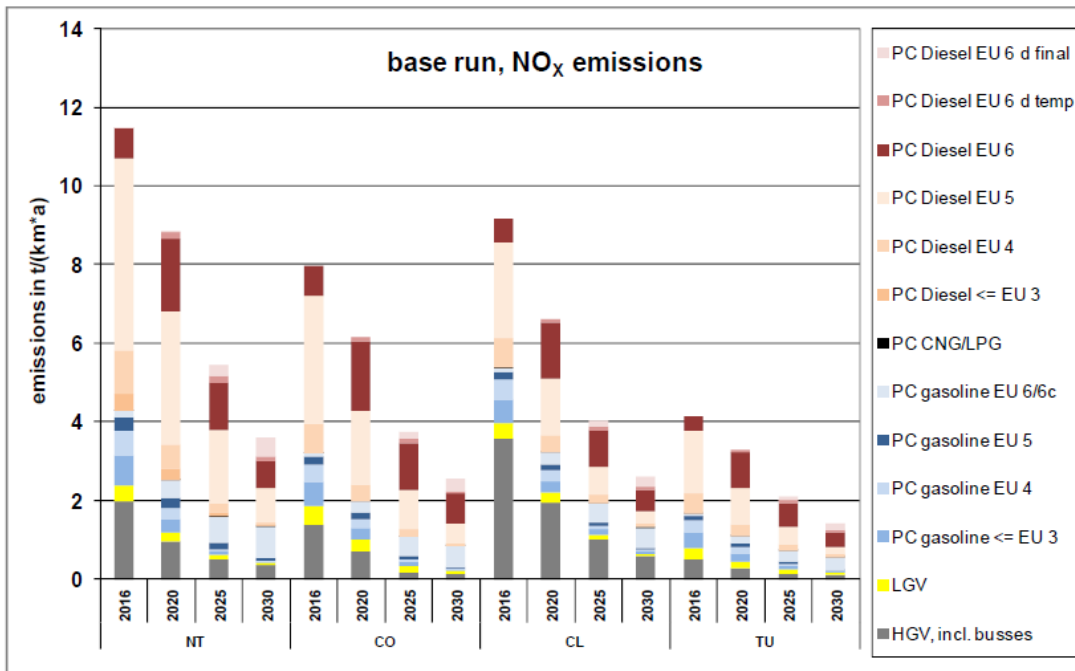


Figure 4: Base run 2016, 2020, 2025, and 2030: Annual road traffic NO_x emission densities calculated for the for the four sites by vehicle type and, for PC, by motor concept

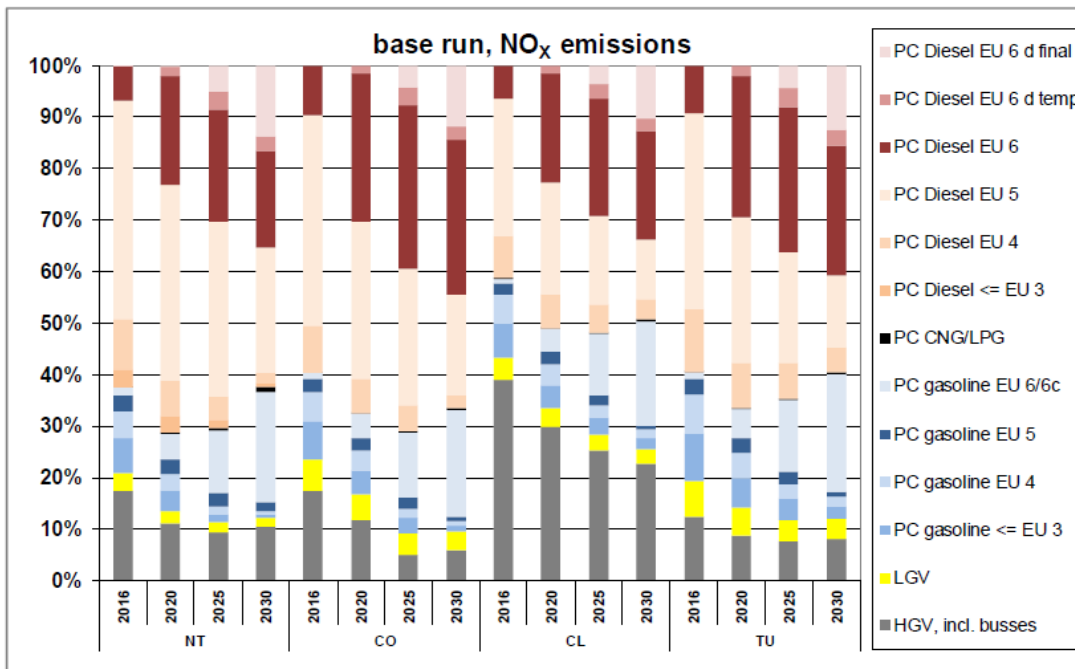


Figure 5: Base run 2016, 2020, 2025, and 2030: Contributions of vehicle types and, for PC, motor concepts, to annual road traffic NO_x emissions for the four sites

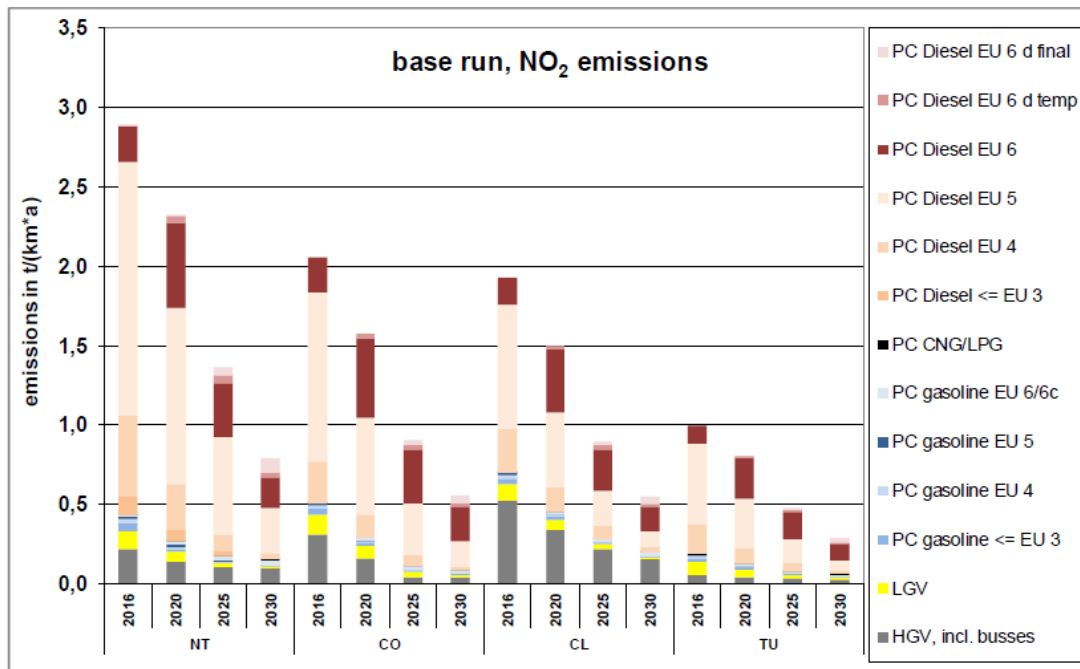


Figure 6: Base run 2016, 2020, 2025, and 2030: Annual road traffic NO₂ emission densities calculated for the for the four sites by vehicle type and, for PC, by motor concept

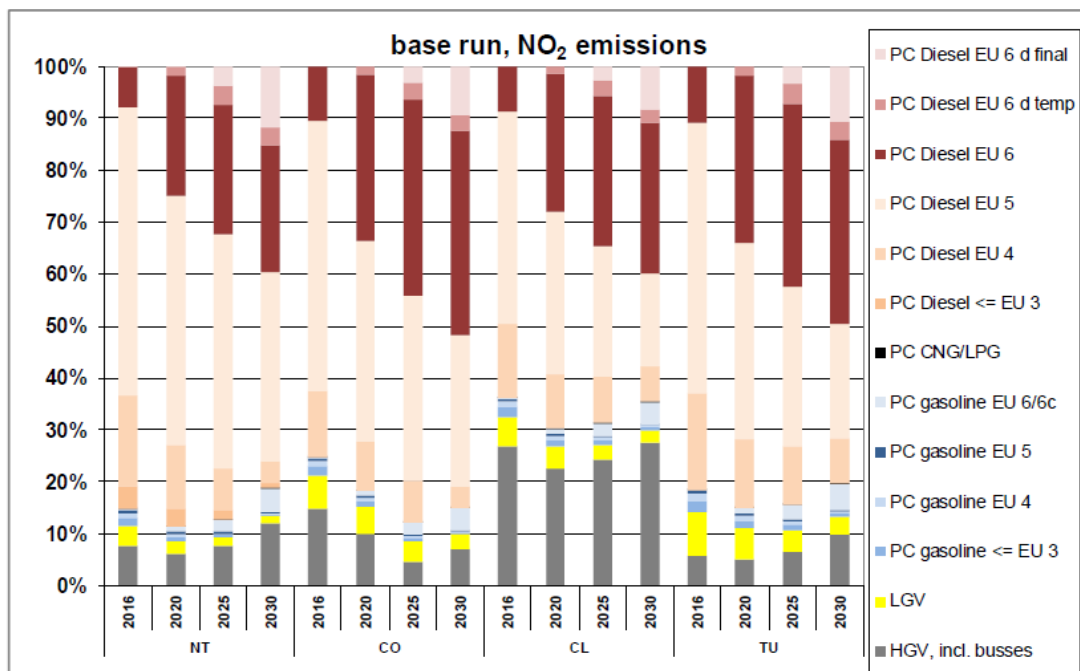


Figure 7: Base run 2016, 2020, 2025, and 2030: Contributions of vehicle types and, for PC, motor concepts, to annual road traffic NO₂ emissions for the four sites

Analog to the base run, emissions were calculated for scenario CF and EZ and the years 2020, 2025, and 2030 for the for the four sites. The reduction of total local road traffic NO_x emissions in scenario CF compared to the base run in 2020 is less than 1% for all sites. Until 2030, this reduction increases to between 6% and 7%, however, on a much lower absolute level.

Expected reductions for scenario EZ are much higher: Depending on site, in 2020, reductions between 30% and 40% compared to the base run are expected, in 2030, these reductions are lower but still range from 18% to 25%.

Air quality calculations

Using the model and the input data described above, air quality calculations were done for the four sites and the three scenarios. The total NO₂ concentrations at the hotspots result from contributions of the background (given as model input), and from local road traffic emissions. The latter contribute by primary NO₂ (directly emitted by the vehicles) and by photochemically produced NO₂ (generated from NO emissions mainly by reaction with O₃). Primary NO₂ is modelled by switching off the chemistry mechanism of the model as the difference between calculated NO₂ without chemistry and background NO₂. Photochemical NO₂ is modelled as the difference between calculated NO₂ with chemistry and without chemistry. In Figure 8, these contributions are shown for the base run for all years and sites.

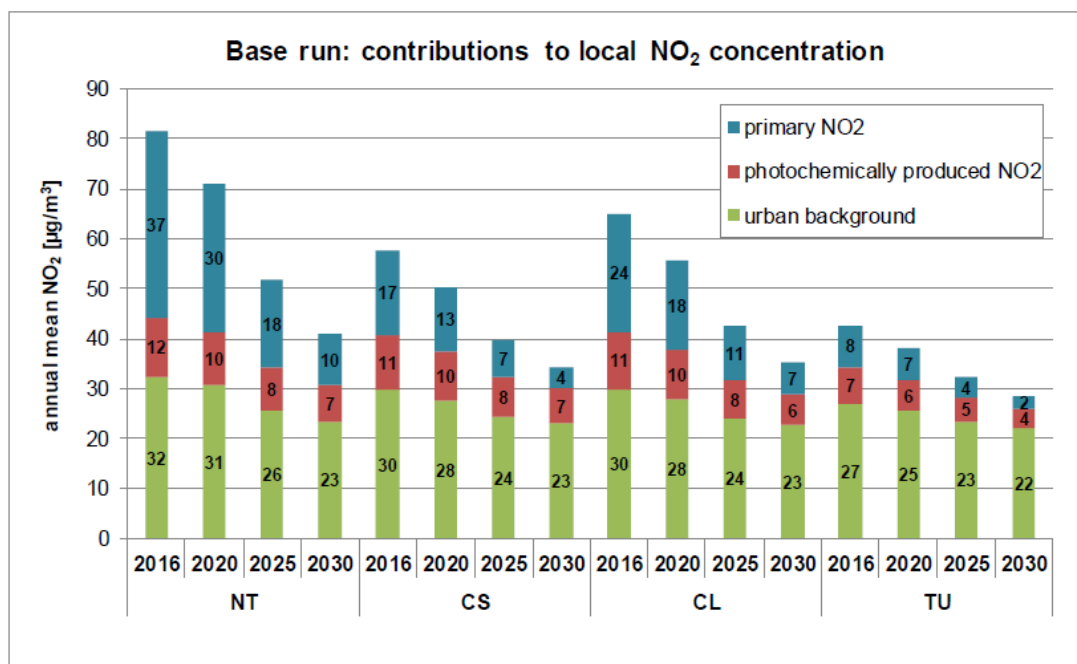


Figure 8: Base run 2016, 2020, 2025, and 2030: Contributions of primary NO₂, photochemically produced NO₂, and urban background to NO₂ concentrations at the four sites

At all sites, air quality is expected to improve, in the base run, expected reductions of annual average NO₂ concentrations between 2016 and 2030 range from 33% (TU) to 50% (NT). This is lower than the corresponding reductions of local road traffic emissions. The reasons for this are the contributions of the urban background, where reductions are slower, and photochemistry, which as a net effect shifts NO to NO₂ for decreasing NO_x concentrations.

From primary and photochemically produced NO₂, the contributions of the vehicle types and motor concepts can be derived: To primary NO₂, they contribute proportionally to their NO₂ emissions, to photochemically produced NO₂, they contribute proportionally to their NO emissions. In Figure 9 to Figure 12 for each site, these contributions are shown for all scenarios and years.

Since the NO₂/NO_x emission ratios of different vehicle types and motor concepts differ, and chemistry behaves non-linearly, the contributions per motor concept derived this way differ from what you get when you switch off the emissions of these motor concepts. The position of the chemical equilibrium between NO and NO₂ is different for the case with and without emissions of a certain motor concept.

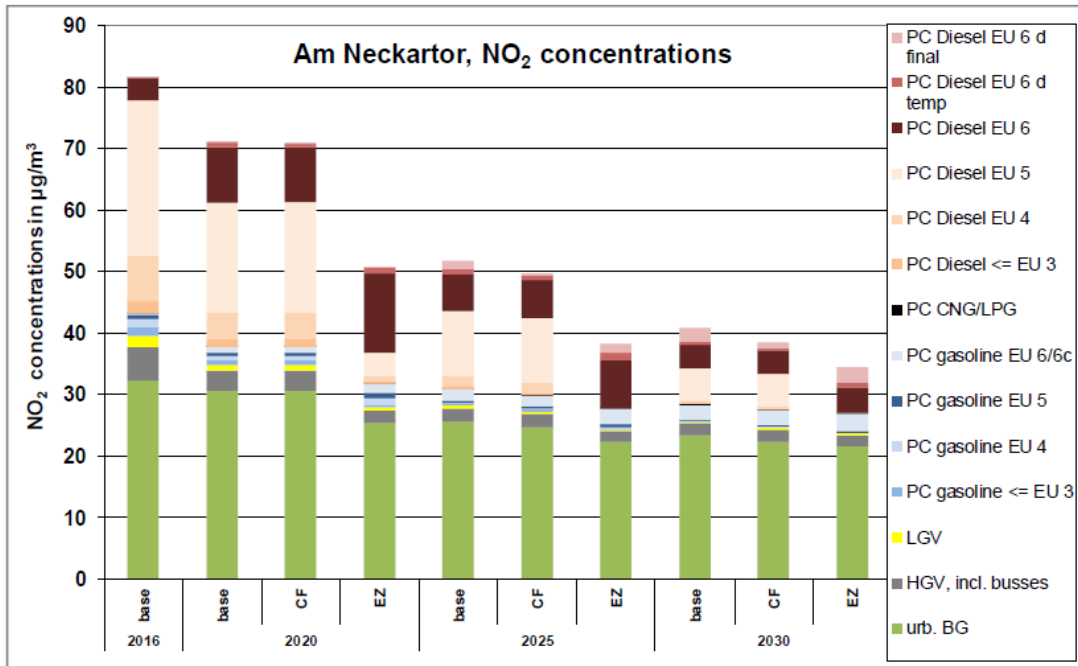


Figure 9: NT, all scenarios, 2016, 2020, 2025, and 2030: Annual average NO₂ concentrations, contributions of vehicle types and, for PC, motor concepts

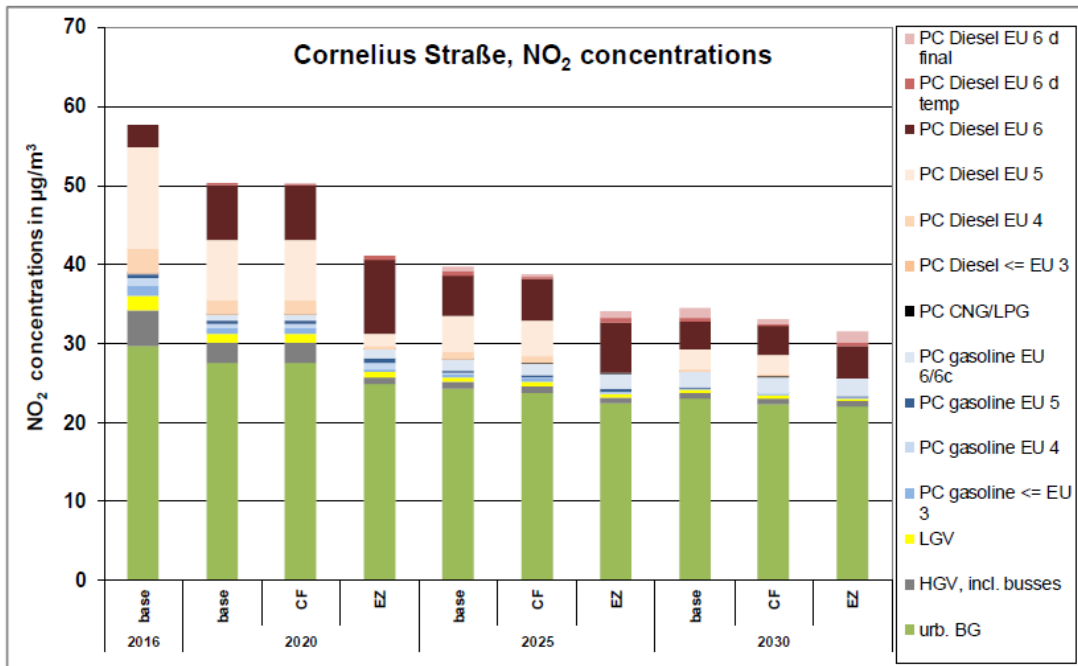


Figure 10: CO, all scenarios, 2016, 2020, 2025, and 2030: Annual average NO₂ concentrations, contributions of vehicle types and, for PC, motor concepts

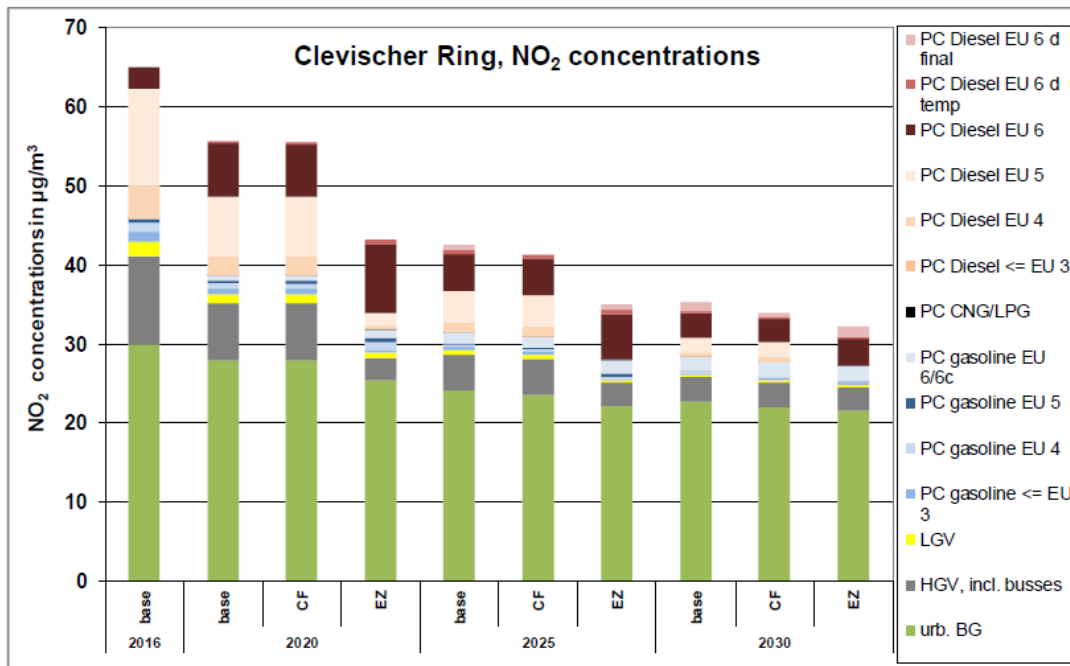


Figure 11: CL, all scenarios, 2016, 2020, 2025, and 2030: Annual average NO₂ concentrations, contributions of vehicle types and, for PC, motor concepts

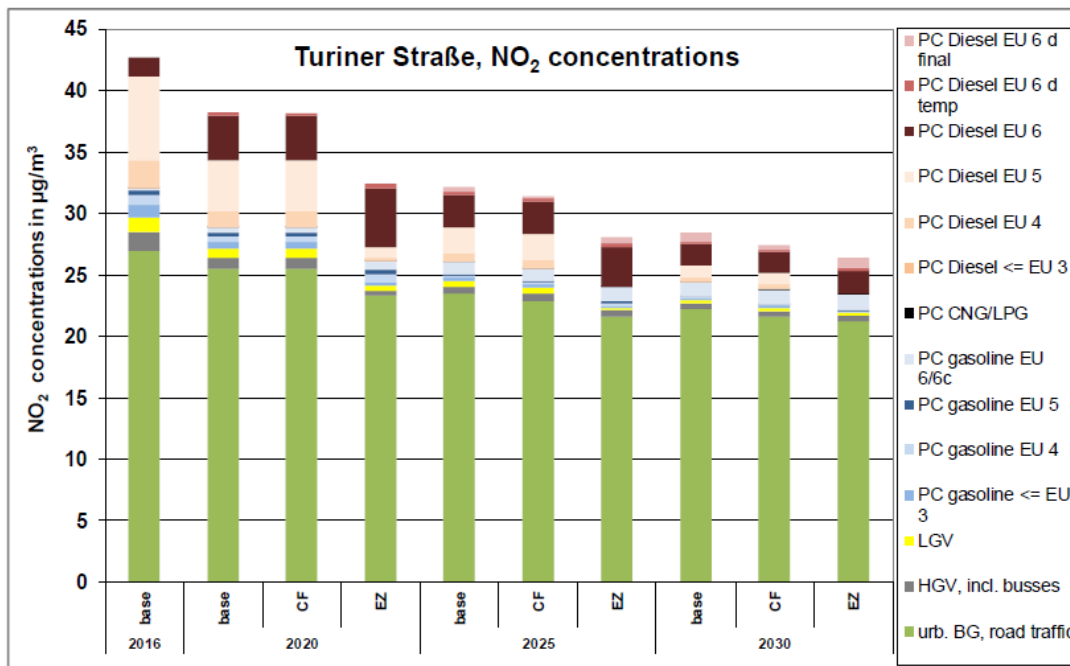


Figure 12: TU, all scenarios, 2016, 2020, 2025, and 2030: Annual average NO₂ concentrations, contributions of vehicle types and, for PC, motor concepts

The expected reductions of annual average NO₂ in scenario CF compared to the base run are negligible in 2020 and increase to between under 4% (TU) and under 6% (NT) in 2030. For scenario EZ, expected reductions in 2020 are highest (between 15% (TU) and 29% (NT)) and decrease until 2030 to between 7% (TU) and 16% (NT).

Extrapolation

The results for the four sites were extrapolated to all traffic-influenced air quality measurement stations in Germany as follows. In Figure 13 the annual average NO₂ values of traffic-influenced air quality measurement stations in Germany 2016 (UBA, 2018) are shown as blue diamonds, sorted by annual average NO₂ (plot cut off after 160 stations). The model results for the four sites for the calibration year 2016 are shown as blue circles. To extrapolate the model results, a logarithmic curve was fitted through the four model values, shown as blue line. As shown in Figure 13, this line can be used as an approximation for the positions of the other measurement stations. Such logarithmic extrapolation curves were fitted to the modelled annual average NO₂ values of all scenarios and years (in Figure 13 shown for the base run only). Also shown in Figure 13 is the air quality limit for the annual mean NO₂ value (black dotted line). The intersections of the extrapolation curves with the limit line give the number of air quality measurement stations with limit exceedances for all years and scenarios.

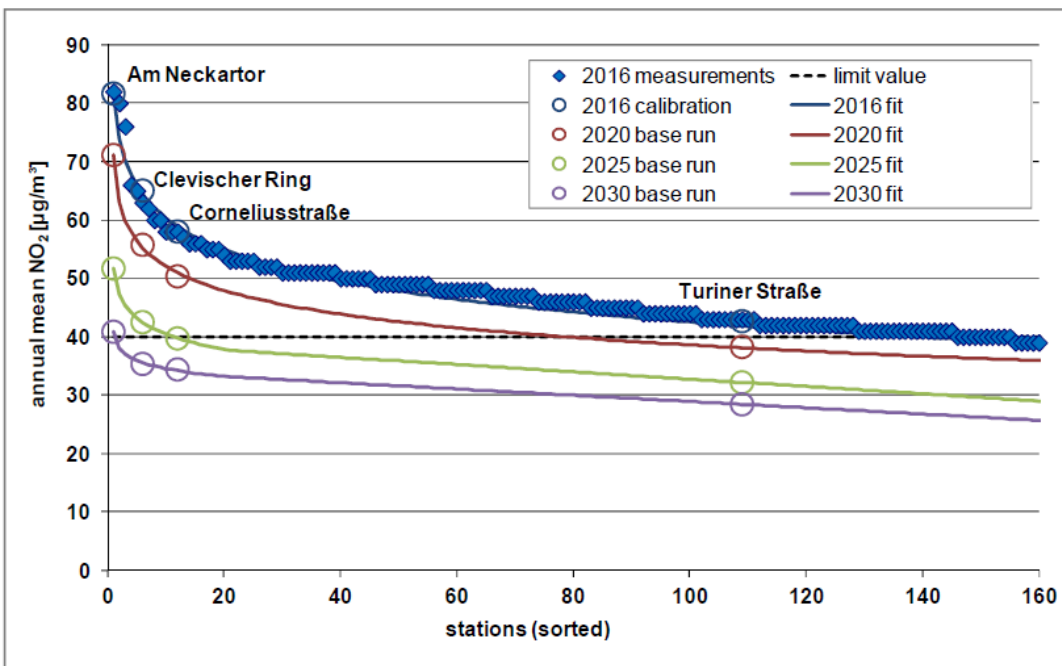


Figure 13: Base run: Extrapolation of the results to all traffic-influenced air quality stations in Germany; data source measurements: UBA (2018)

In Table 2, the total numbers and relative fractions of traffic-influenced air quality stations in Germany expected to exceed the NO₂ air quality limit estimated by this extrapolation are shown for the considered years and scenarios.

While in 2016 nearly 60% of all German traffic-influenced air quality stations exceeded the limit, in the base run, this number is expected to be reduced until 2020 to 33%, and until 2025 to below 5%. In the base run 2030, only one station (NT) is expected to exceed the limit.

For scenario CF, the number of stations expected to exceed the limit is moderately lower than in the base run (2020: nearly no difference, 2025: 8 exceedances instead of 11, 2030: NT also compliant).

For scenario EZ, significant improvements are expected compared to the base run (2020: 15 exceedances instead of 82, 2025: compliance expected for all stations).

Table 2: Estimated number and fraction of traffic-influenced air quality stations in Germany which are expected to exceed the NO₂ air quality limit in the considered years and scenarios, and expected reductions versus the year 2016 and, for scenario CF and EZ, versus the corresponding year of the base run (BR)

	2016	2020			2025			2030		
	BR	BR	CF	EZ	BR	CF	EZ	BR	CF	EZ
stations exceeding the limit										
number	145	82	81	15	11	8	0	1	0	0
fraction	59%	33%	33%	6%	4,5%	3,3%	0,0%	0,4%	0,0%	0,0%
reductions, absolute										
vs. 2016		-64	-65	-130	-134	-137	-145	-144	-145	-145
vs. base 2020			-1	-66	-70	-73	-81	-80	-81	-81
vs. base 2025						-3	-11	-10	-11	-11
reductions, relative										
vs. 2016		-44%	-45%	-90%	-92%	-94%	-100%	-99%	-100%	-100%
vs. base 2020			0%	-81%	-86%	-90%	-100%	-99%	-100%	-100%
vs. base 2025						-27%	-100%	-91%	-100%	-100%

As done by IIASA (2012), an uncertainty range was defined by setting an interval of 5 µg/m³ around the NO₂ air quality limit: When the extrapolation of the model results shows an annual mean NO₂ value

- below 35 µg/m³: stations are expected to comply with the limit,
- above 45 µg/m³: stations are expected to exceed the limit,
- between 35 and 45 µg/m³: stations lie within the uncertainty range.

In Figure 14, the estimated fractions of traffic-influenced air quality stations in Germany which are expected to exceed the NO₂ air quality limit in the considered years and scenarios are shown, also shown are the derived uncertainty ranges.

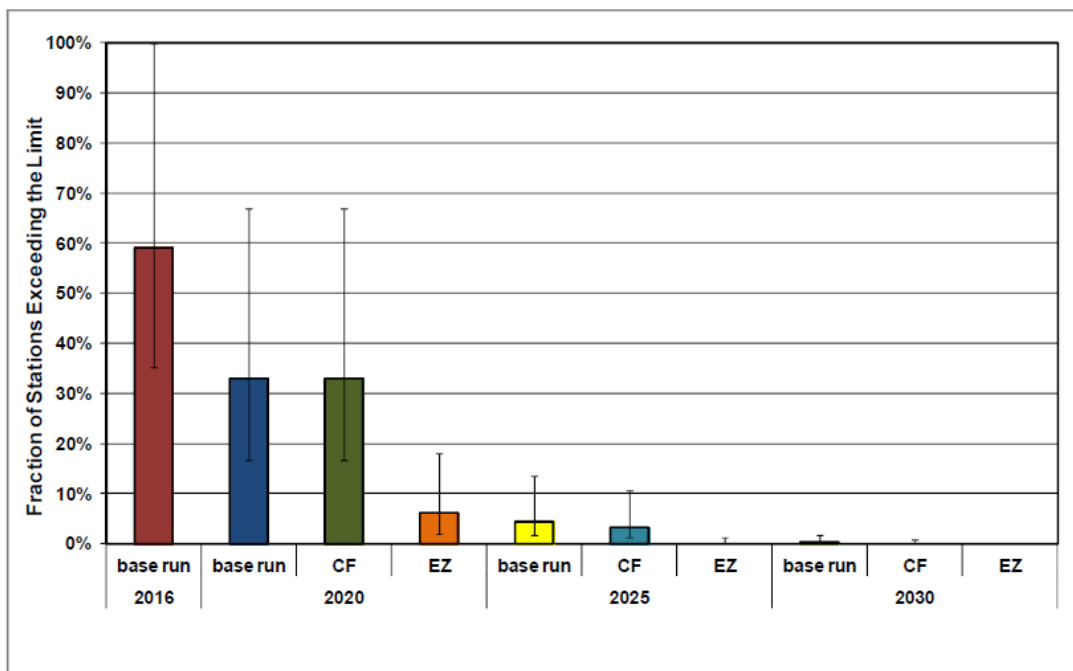


Figure 14: Estimated fraction of traffic-influenced air quality stations in Germany which are expected to exceed the NO₂ air quality limit in the considered years and scenarios

Summary and conclusions

Air quality simulations were done for four German inner-city street canyons, where annual average NO₂ concentrations range from 43 µg/m³ (only just exceeding the limit of 40 µg/m³) to 82 µg/m³ (very high exceedance) in 2016, followed by an extrapolation to all traffic influenced air quality stations in Germany.

A base run (trend forecast without further air quality actions) and two additional scenarios were calculated for the years 2016, 2020, 2025, and 2030. In the first additional scenario, NO_x emission factors of Diesel PC Euro 6 d temp and final were reduced, assuming deletion of NO_x error margins (CF = 1.6 instead of 2.1 for Euro 6 d temp and CF = 1.0 instead of 1.5 for Euro 6 d final). In the second additional scenario, the effects of a “blue environmental zone” as proposed by the federal state of Baden-Württemberg were examined.

The trend forecast for the fleet renewal leads to a substantial reduction of traffic-influenced air quality stations exceeding the limit for annual average NO₂. In 2025, 95% of all traffic-influenced stations are expected to be compliant, in 2030, >99%.

The reduction of the conformity factors for Diesel PC Euro 6 d temp and final by 0.5 has only a small impact on air quality.

“Blue environmental zones” can lead to significant NO₂ reductions which in combination with fleet renewal will lead to an earlier compliance of all traffic-influenced air quality stations expected between 2020 and 2025.

Acknowledgements

We want to say thanks to Christoph Kessler, who originally developed the box model, first working at the Rhenish Institute for Environmental Research at the University of Cologne and later at Ford Research & Innovation Centre Aachen. He was always available for discussions and problem

solving and contributed valuable ideas both scientifically and technically. The project was funded by Ford Research & Innovation Centre Aachen.

References

- Cologne (2018), <https://ratsinformation.stadt-koeln.de/getfile.asp?id=647676&type=do&>
- Cologne (2019), https://www.bezreg-koeln.nrw.de/brk_internet/leistungen/abteilung05/53/luftreinhalteplaene/luftreinhalteplan_koeln_02_fortschreibung_2019.pdf
- Düsseldorf (2018), <https://www.duesseldorf.de/umweltamt/umweltthemen-von-a-z/luft/luftreinhalteplan.html>
- IIASA (2012), TSAP-2012 Baseline: Health and Environmental Impacts, TSAP Report #6, Version 1.0, http://ec.uropa.eu/environment/air/pdf/tsap_impacts.pdf
- IVU (2014), Flächendeckende Ermittlung der Immissions-Vorbelastung für Baden-Württemberg 2010, im Auftrag der LUBW
- Keller M., Hausberger S., Matzer C., Wüthrich P., Notter B. (2017), HBEFA Version 3.3, http://www.hbefa.net/d/documents/HBEFA33_Hintergrundbericht.pdf
- Kessler C., Schneider C., Vogt R. (2010), Städtische NO₂-Luftqualität: Quellenanalyse und zukünftige Entwicklung, *Immissionsschutz* **04.10**
- LANUV (2018), Environmental agency of North Rhine Westphalia, measurement data air quality and meteorology, <https://www.lanuv.nrw.de/umwelt/luft/immissionen/>
- LUBW (2018), Environmental agency of Baden Württemberg, measurement data air quality and meteorology, <https://udo.lubw.baden-wuerttemberg.de/public/>
- Memmesheimer M., Wurzler S., Friese E., Jakobs H.J., Feldmann H., Ebel A., Kessler C., Geiger J., Hartmann U., Brandt A., Pfeffer U., Dorn H.P., Borrego C., Eberhard R. (2007), Long-term simulations of photo-oxidants and particulate matter over Europe with emphasis on North Rhine-Westphalia, *Developments in Environmental Science* **6**
- Stockwell W.R., Middleton P., Chang J.S., Tang X. (1990), The second generation regional acid deposition model chemical mechanism for regional air quality modeling, *J. Geophys. Res.* **95**
- Stuttgart (2018), <https://vm.baden-wuerttemberg.de/de/mensch-umwelt/luftreinhaltung/luftreinhalteplanung-stuttgart/faq-wirkungsgutachten/>
- UBA (2014), Luftqualität 2020/2030: Weiterentwicklung von Prognosen für Luftschadstoffe unter Berücksichtigung von Klimastrategien, *TEXTE 35/2014*, Umweltforschungsplan des Bundesministeriums für Umwelt, Naturschutz, Bau und Reaktorsicherheit, Forschungskennzahl 3710 43 219, UBA-FB 001945
- UBA (2018), German Environment Agency, web interface for air quality data, <https://www.umweltbundesamt.de/daten/luft>
- Toenges-Schuller N., Schneider C., Niederau A., Vogt R., Birmili W. (2015), Modelling particle number concentrations in a typical street canyon in Germany and analysis of future trends, *Atmospheric Environment* **111**
- Toenges-Schuller N., Schneider C., Niederau A., Vogt R., Hausberger S. (2016), Modelling the effect on air quality of Euro 6 emission factor scenarios, *Journal of Earth Sciences and Geotechnical Engineering*, vol.6, no. 4
- Vogt R., Kessler C., Schneider C. (2010), Urban NO₂ Air Quality: Analysis of sources and future projection. *VDA Technical Congress*, Ludwigsburg

2.3.6 Source apportionment of the oxidative potential of ambient fine Particulate Matters: A case study of Athens, Greece

Sina Taghvaei¹, Mohammad H. Sowlat¹, Evangelia Diapoul², Manousos Ioannis Manousakas², Vasiliki Vasilatou², Kostas Eleftheriadis², Constantinos Sioutas¹

¹ Department of Civil and Environmental Engineering, University of Southern California, , Los Angeles, California, USA

²Institute of Nuclear and Radiological Sciences & Technology, Energy & Safety, N.C.S.R. Demokritos, 15341 Ag. Paraskevi, Attiki, Greece

Presenting author email: Sioutas@usc.edu

This work has been published as journal paper: Science of Total Environment, 653: 1407-1416, 2019

Abstract

The main aim of this study was to chemically characterize the ambient fine particulate matters (PM_{2.5}) and quantify the contribution of different sources to its associated oxidative potential at an urban background site in Athens, Greece. Weekly time integrated PM_{2.5} samples were collected during the warm (i.e., June-September of 2017), and cold (i.e., February-March of 2018) periods. The PM_{2.5} samples were then chemically analysed for water-soluble organic carbon (WSOC), metals and trace elements, elemental and organic carbon (EC/OC), and levoglucosan as well-known tracer of biomass burning. The Oxidative potential of PM_{2.5} samples were also quantified using the in vitro alveolar macrophage assays. Then a series of statistical analysis including the Spearman rank-order correlation analysis, principal component analysis (PCA), and multiple linear regression (MLR) was performed to identify and quantify the relative contribution of different sources to PM induced toxicity. Our finding revealed the remarkably higher levels of both intrinsic (per mass) and extrinsic (per volume) ambient PM_{2.5} oxidative potential in urban background of Athens in comparison to many metropolitan locations around the globe. Moreover based on the results of the ambient PM oxidative potential source apportionment analysis, vehicular emissions (identified by EC), secondary organic aerosols (identified by WSOC), and biomass burning (characterized on the basis of levoglucosan) were contributing to 44%, 16%, and 9% of PM induced toxicity. In addition, the oxidative potential of ambient PM_{2.5} was higher in the warm phase compared to cold phase as a result of higher EC, and WSOC concentration during summer. It should be noted that results of this study are of great importance since the remarkably high oxidative potential levels are for an urban background site which is not affected by intense vehicular activities. Our final results also indicated the most toxic sources of PM_{2.5} in Athens and can be used as a guideline for policy makers to make proper policies for mitigation of adverse health effect of exposure to PM_{2.5}.

Introduction

- Fine Particulate matter (PM_{2.5}) is one of the most critical pollutants in the atmosphere, particularly in metropolitan areas.
- Exposure to PM_{2.5} is associated with several adverse health impacts, including increased:
 - Daily mortality
 - Cardiovascular effects
 - Neurodevelopmental and neurodegenerative disorders
 - Respiratory diseases (Dockery and Stone, 2007; Gauderman et al., 2015; Krewski et al., 2009; Li et al., 2008; Ling and Eeden, 2009; Rich et al., 2013)

Comparison of air pollution mortality with other major risk factors (Wang et. al, 2016)

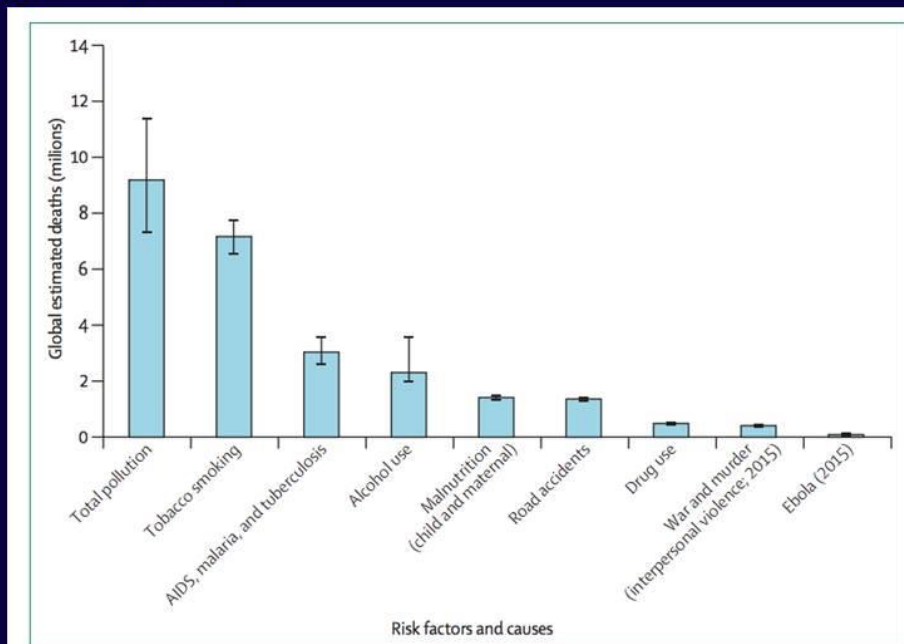


Figure 5: Global estimated deaths by major risk factor and cause, 2015
Using data from the GBD Study, 2016.⁴¹

- One of the main biological mechanisms contributing to PM detrimental health effects is the generation of reactive oxygen species (ROS) in cells.
 - ROS generation triggers an oxidative stress response involving several proinflammatory cascades that ultimately result in pathology (Ayres et al., 2008; Xia et al., 2007).
 - When the intracellular ROS concentration exceeds an equilibrium threshold determined by available antioxidants within the cell, cellular oxidative stress and, in turn, adverse health outcomes ensue.
 - Various biological and chemical assays are used to quantify the oxidative potential of particulate matter as indexed by this cellular oxidative stress response (Kubatova et al., 2006; Verma et al., 2015).
-
- Athens, the capital of Greece, is one of Europe's largest metropolitan areas, with approximately 5 million residents (Economopoulou and Economopoulos, 2002; Karakatsani et al., 2003; Mantas et al., 2014).
 - The economic crisis in Greece, starting in 2010, caused a great increase in the price of residential heating fuel oil, which in turn led to extensive and widespread burning of biomass, particularly wood, as an alternative fuel (Argyropoulos et al., 2016; Diapouli et al., 2017).
 - Consequently, the cold phase concentration of $PM_{2.5}$ and black carbon (BC) have been increased significantly over the past few years across the Athens metropolitan area (Athanasopoulou et al., 2017; Paraskevopoulou et al., 2014; Kalogridis et al., 2018).
 -

- Previous studies have indicated that **PM formation mechanisms and sources, including vehicular activities, secondary aerosols, and biomass burning, are the major contributors to PM_{2.5} in Athens** (Amato et al., 2016; Diapouli et al., 2017; Pateraki et al., 2019).
- Moreover, **secondary organic and inorganic compounds are the major constituents of ambient PM_{2.5} in Athens** (Amato et al., 2016).
- **However, none of the studies have so far** linked the chemical components and sources of ambient PM_{2.5} to its oxidative potential in this city.

Methodology

✓ Sampling site:

- **PM_{2.5} samples** were collected at the **Global AtmosphereWatch (GAW) Demokritos station (DEM_Athens)** in Athens, Greece.
- The **DEM_Athens station** is located inside the National Center for Scientific Research "**Demokritos**" campus (37° 59' 25" N, 23° 48' 34" E, 270 meters above sea level (m.a.s.l.)).
- ✓ The campus is situated in a **suburban region**, approximately **7 km northeast of the metropolitan center of the city**, and covers an area of **600 acres** in a **forest of pine trees**, at the foot of **Mount Hymettus**.
- ✓ Therefore, the site is **not directly impacted** by **fresh urban PM** emissions and is considered as **representative of the urban background** air quality in Athens (Eleftheriadis et al., 2014; Triantafyllou et al., 2016).

Sampling period and instrumentation

- ✓ **Sampling period:**
 - June -September, 2017.
 - February – March, 2018.



Sampling site location

- ✓ **Sampling instruments:**
 - Sioutas™ Personal Cascade Impactor Samplers
 - Sequential low volume reference sampler
(**PM_{10/2.5} SEQ 47/50-CD with Peltier cooler, Sven Leckel GmbH**)

Chemical and toxicological analysis

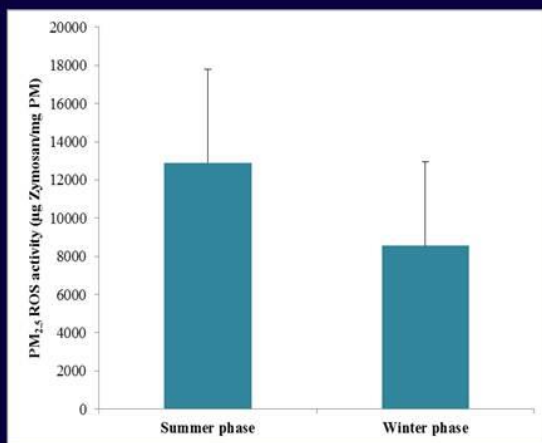
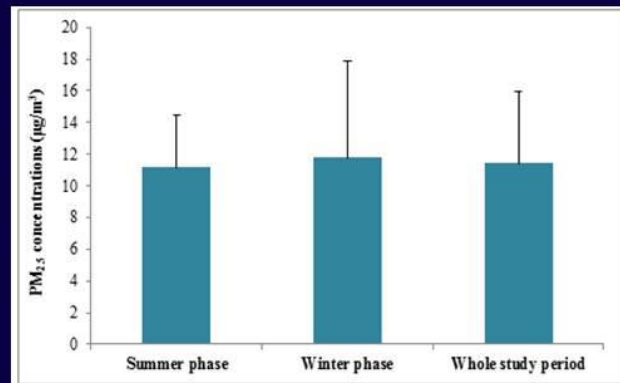
- PM_{2.5} Samples were analyzed for :
 - ❖ Elemental/ Organic Carbon (EC/OC)
 - ❖ Water soluble organic carbon (WSOC)
 - ❖ Metals and redox active trace elements
 - ❖ Levoglucosan (an organic tracer of wood smoke)
 - ❖ PM oxidative potential
- PM_{2.5} oxidative potential source apportionment:
- Spearman rank order correlation analysis & Multiple Regression (**MLR**) analysis between PM oxidative potential and its chemical components (i.e., WSOC, OC, EC, levoglucosan, trace and metal elements).

What is DCFH *in vitro* assay?

- The fluorogenic DCFH *in vitro* assay is used to determine the oxidative potential of PM samples.
- ❖ Cultures of the NR8383 rat alveolar cell line (American Type Culture Collection) are exposed to aqueous PM suspensions 1-20 $\mu\text{g}/\text{mL}$ derived from filter extractions along with 15 μM concentrations of 2',7'-dichlorodihydrofluorescein diacetate (DCFH-DA) in 96-well cell culture plates.
- ❖ The non-fluorescent DCFH is converted to the highly fluorescent dichlorofluorescein (DCF) due to oxidation by reactive species produced in the cytoplasm of the cells.
- ❖ DCF production is monitored spectrophotometrically, which provides a reliable index of PM oxidative potential in fluorescence units per mass of PM ($\text{FU}/\mu\text{g}$ PM).
- ❖ Fluorescence units are converted to units of Zymosan per μg PM- Zymosan is a positive control, i.e., a chemical used to induce experimental sterile inflammation in macrophage cells (Landreman et al., 2008; Rosenkranz et al., 1992; Shafer et al., 2010).

Results

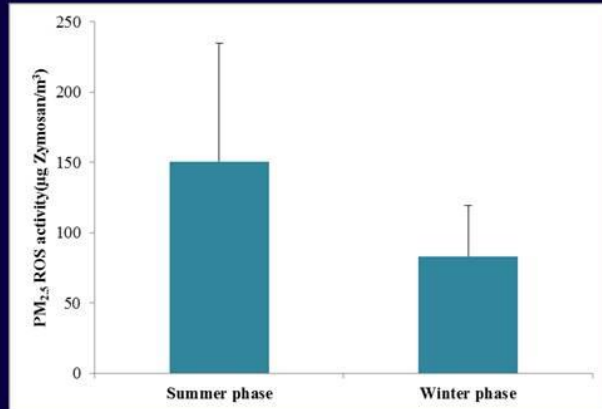
- ✓ The significant contribution of SOA to $\text{PM}_{2.5}$ mass concentrations during warm period counterbalances the impact of meteorological conditions that increase $\text{PM}_{2.5}$ concentrations during cold period, leading to comparable $\text{PM}_{2.5}$ levels in both phases of the sampling.



- ✓ The mass-normalized oxidative potential (in units of μg Zymosan/mg PM) is indicative of the intrinsic PM-induced toxicity and used in conventional toxicology.
- ✓ Higher intrinsic oxidative potential were observed in summer (12910.7 ± 4898.6 μg Zymosan/mg PM) as compared to winter (8549.3 ± 4388.1 μg Zymosan/mg PM).

□ The volumetric oxidative potential (in units of μg Zymosan/ m^3 of air) is a more suitable measure for PM population exposure and inhalation assessment studies.

□ Higher per-volume oxidative potential in the summer ($150.6 \pm 84.4 \mu\text{g}$ Zymosan/ m^3) than in the winter ($83.3 \pm 35.8 \mu\text{g}$ Zymosan/ m^3).



❖ Significantly higher average intrinsic (and extrinsic) oxidative potential levels were measured in this study in comparison to different metropolitan areas around the world (Saffari et al., 2014, 2013; Verma et al., 2007).

- Current study: 11,041.6 μg Zymosan/mg PM
- Denver: 2006.6 μg Zymosan/mg PM
- Thessaloniki: 738.0 μg Zymosan/mg PM
- Los Angeles: 748.5 μg Zymosan/mg PM
- Los Angeles I-710 freeway: 3439 μg Zymosan/mg PM

Spearman rank order correlation analysis between PM oxidative potential and different chemical species

Species	R	Species	R
WSOC	0.66*	Ti	-0.01
OC	0.78*	Mn	-0.24
EC	0.66*	Na	-0.25
Levogluconan	0.03	K	0.20
S	0.48	Zn	0.06
Al	-0.03	Cu	-0.17
Si	0.03	Pb	-0.11
Ca	-0.14	Ni	0.47
Fe	-0.07	Br	0.31

- Organic Carbon (OC) was strongly correlated with PM oxidative potential (with $R > 0.7$).
- Moderate-to-strong associations were also observed between oxidative potential and EC, as well as with WSOC.
- WSOC, EC, and OC associations were statistically significant ($p < 0.05$)

Multi-Linear Regression (MLR) analysis results

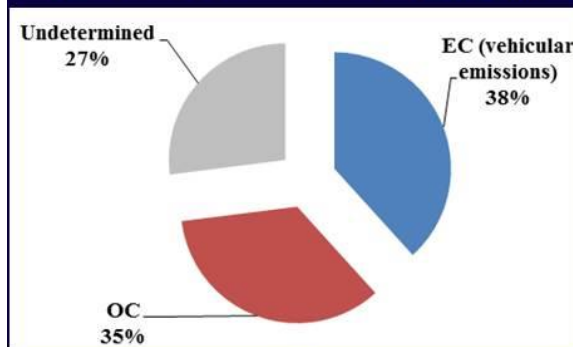
Volumetric PM-induced oxidative potential ($N_{\text{cold}}=6, N_{\text{warm}}=9$)							
Species	Source	Unstandardized coefficient (\pm std. error)	Standardized coefficient (\pm std. error)	P- value	Partial R	VIF	R ²
Constant		-188.74		0.017			0.73
EC	Vehicular emissions	325.63 \pm 125.32	0.50 \pm 0.19	0.023	0.60	1.60	
OC	Multiple sources	101.33 \pm 42.95	0.45 \pm 0.19	0.036	0.56	1.60	

- **EC** (tracer of vehicular emissions) and **Organic Carbon (OC)** were the most important species contributing to PM oxidative potential
- Since OC can be originated from a wide variety of sources (i.e., vehicular, biomass, and secondary sources) (Arhami et al., 2018; Paraskevopoulou et al., 2014), we did another MLR analysis, using OC as the dependent variable and individual marker species used as pollution source tracers as independent variables.

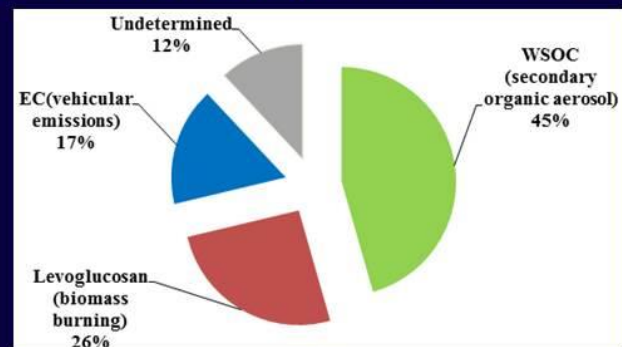
Organic Carbon ($N_{\text{cold}}=6, N_{\text{warm}}=9$)							
Species	Source/Formation Mechanism	Unstandardized coefficient (\pm std. error)	Standardized coefficient (\pm std. error)	P- value	Partial R	VIF	R ²
Constant		1.05		0.000			0.88
WSOC	Secondary organic aerosol (SOA)	0.54 \pm 0.09	0.75 \pm 0.13	0.000	0.87	1.44	
Levogluconan	Biomass burning	0.01 \pm 0.00	0.42 \pm 0.11	0.003	0.76	1.04	
EC	Vehicular emissions	0.57 \pm 0.26	0.27 \pm 0.13	0.055	0.54	1.43	

- **Water Soluble Organic Carbon (WSOC)** (tracer of organic aerosols formed by photochemical reactions, secondary organic aerosols (SOA)), **Levogluconan** (tracer of biomass burning), and **EC** (tracer of vehicular emissions) were the contributors to OC.

Relative contribution of: a) EC and OC to PM_{2.5} oxidative potential b) different sources to OC mass concentrations; and c) different sources to PM_{2.5} oxidative potential.

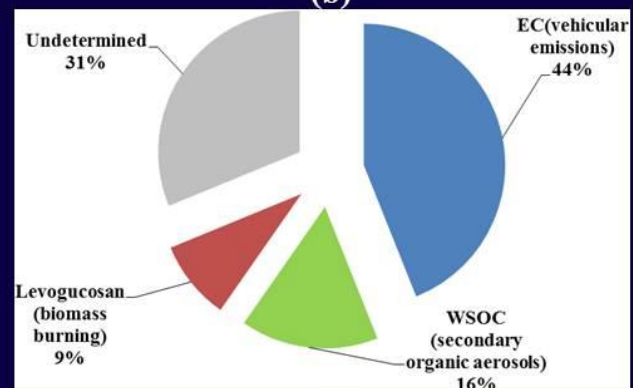


(a)



(b)

- Combining the results of Figure (a), and (b), traffic activities were responsible for approximately 44% of PM-induced toxicity, followed by secondary organic aerosol (SOA) (16%), and biomass burning (9%).



(c)

Summary and Conclusions

- This study sought to identify pollution sources that contribute to the oxidative potential of ambient PM_{2.5} in the urban background of Athens, Greece.
- Significantly higher oxidative potential of the ambient PM_{2.5} collected in the study area as compared to those in many urban areas around the world.
- The significantly higher PM toxicity in our sampling site is one of the most notable observations of this study, since the measured oxidative potential pertains to a site which is not directly impacted by fresh urban PM emissions.
- Our attempt to apportion sources of PM_{2.5} indicated that vehicular emissions were responsible for approximately 44% of PM-induced oxidative potential of the samples, followed by secondary organic aerosol (SOA) (16%) and biomass burning (9%) as the next major contributors.
- Our findings highlight the importance of traffic emissions and photochemical reactions in deriving PM-induced toxicity in Athens, Greece

Acknowledgment

The authors would like to thank National Institute of Health (grant numbers: 2R01AI065617-17A1 and 5R01ES024936-04), and Department of Defense (US-Army Medical Research Acquisition Activity, grant number W81XWH-17-1-0535) for their financial supports. We are also grateful to Wisconsin State Lab of Hygiene (WSLH) for performing chemical analysis. Finally, we acknowledge the support from the Viterbi School of Engineering, USC Ph.D. fellowship award.

Reference

- Amato, F., Alastuey, A., Karanasiou, A., Lucarelli, F., Nava, S., Calzolari, G., Severi, M., Becagli, S., Gianelle, V.L., Colombi, C., Alves, C., Custódio, D., Nunes, T., Cerqueira, M., Pio, C., Eleftheriadis, K., Diapouli, E., Reche, C., Minguillón, M.C., Manousakas, M., Maggos, T., Vratolis, S., Harrison, R.M., Querol, X., 2016. AIRUSE-LIFE + : a harmonized PM speciation and source apportionment in five southern European cities. *Atmos. Chem. Phys.* 16, 3289–3309. doi:10.5194/acp-16-3289-2016
- Argyropoulos, G., Basis, A., Voutsas, D., Samara, C., Sowlat, M.H., Hasheminassab, S., Sioutas, C., 2016. Source apportionment of the redox activity of urban quasi-ultra fine particles (PM 0.49) in Thessaloniki following the increased biomass burning due to the economic crisis in Greece. *Sci. Total Environ.* 568, 124–136. doi:10.1016/j.scitotenv.2016.05.217
- Athanasopoulou, E., Speyer, O., Brunner, D., Vogel, H., Vogel, B., Mihalopoulos, N., Gerasopoulos, E., 2017. Changes in domestic heating fuel use in Greece : effects on atmospheric chemistry and radiation. *Atmos. Chem. Phys.* 17, 10597–10618.
- Ayres, J.G., Borm, P., Cassee, F.R., Castranova, V., Donaldson, K., Ghio, A., Harrison, R.M., Hider, R., Kelly, F., Kooter, I.M., Marano, F., Maynard, R.L., Mudway, I., Nel, A., Sioutas, C., Smith, S., Baeza-squiban, A., Cho, A., Duggan, S., Froines, J., 2008. Evaluating the Toxicity of Airborne Particulate Matter and Nanoparticles by Measuring Oxidative Stress Potential — A Workshop Report and Consensus Statement. *Inhal. Toxicol.* 20, 75–99. doi:10.1080/08958370701665517
- Diapouli, E., Manousakas, M., Vratolis, S., Vasilatou, V., Maggos, T., Saraga, D., Grigoratos, T., Argyropoulos, G., Voutsas, D., Samara, C., Eleftheriadis, K., 2017. Evolution of air pollution source contributions over one decade, derived by PM10 and PM2.5 source apportionment in two metropolitan urban areas in Greece. *Atmos. Environ.* 164, 416–430. doi:10.1016/j.atmosenv.2017.06.016
- Dockery, D.W., Stone, P.H., 2007. Cardiovascular Risks from Fine Particulate Air Pollution. *N. Engl. J. Med.* 356, 511–513.
- Economopoulou, A.A., Economopoulos, A.P., 2002. Air Pollution in Athens Basin and Health Risk Assessment. *Environ. Monit. Assess.* 80, 277–299.
- Eleftheriadis, K., Ochsenkuhn, K.M., Lympetropoulou, T., Karanasiou, A., Razos, P., Ochsenkuhn-petropoulou, M., 2014. Influence of local and regional sources on the observed spatial and temporal variability of size resolved atmospheric aerosol mass concentrations and water-soluble species in the Athens metropolitan area. *Atmos. Environ.* 97, 252–261. doi:10.1016/j.atmosenv.2014.08.013
- Fourtziou, L., Liakakou, E., Stavroulas, I., Theodosi, C., Zampas, P., Psiloglou, B., Sciare, J., Maggos, T., Bairachtari, K., Bougiatioti, A., Gerasopoulos, E., Sarda-Estevé, R., Bonnaire, N., Mihalopoulos, N., 2017. Multi-tracer approach to characterize domestic wood burning in Athens (Greece) during wintertime. *Atmos. Environ.* 148, 89–101. doi:10.1016/j.atmosenv.2016.10.011
- Gauderman, W.J., Urman, R., Avol, E., Berhane, K., McConnell, R., Rappaport, E., Chang, R., Lurmann, F., Gilliland, F., 2015. Association of Improved Air Quality with Lung Development in Children. *N. Engl. J. Med.* 372, 905–913. doi:10.1056/NEJMoa1414123

- Kalogridis, A., Vratolis, S., Liakakou, E., Gerasopoulos, E., Mihalopoulos, N., Eleftheriadis, K., 2018. Assessment of wood burning versus fossil fuel contribution to wintertime black carbon and carbon monoxide concentrations in Athens, Greece. *Atmos. Chem. Phys.* 18, 10219–10236.
- Karakatsani, A., Andreadaki, S., Katsouyanni, K., Dimitroulis, I., Trichopoulos, D., Benetou, V., Trichopoulou, A., 2003. Air pollution in relation to manifestations of chronic pulmonary disease: A nested case – control study in Athens, Greece. *Eur. J. Epidemiol.* 18, 45–53.
- Krewski, D., Jerrett, M., Burnett, R.T., Ma, R., Hughes, E., Shi, Y., Turner, M.C., Pope III, C. a, Thurston, G., Calle, E.E., Thun, M.J., Beckerman, B., DeLuca, P., Finkelstein, N., Ito, K., Moore, D.K., Newbold, K.B., Ramsay, T., Ross, Z., Shin, H., Tempalski, B., 2009. Extended follow-up and spatial analysis of the American Cancer Society study linking particulate air pollution and mortality. Boston.
- Kubatova, A., Dronen, L.C., Picklo, M.J., Hawthorne, S.B., 2006. Midpolarity and Nonpolar Wood Smoke Particulate Matter Fractions Deplete Glutathione in RAW 264.7 Macrophages. *Chem. Res. Toxicol.* 19, 255–261. doi:10.1021/tx050172f
- Landreman, A.P., Shafer, M.M., Hemming, J.C., Hannigan, M.P., Schauer, J.J., 2008. A Macrophage-Based Method for the Assessment of the Reactive Oxygen Species (ROS) Activity of Atmospheric Particulate Matter (PM) and Application to Routine (Daily-24 h) Aerosol Monitoring Studies. *Aerosol Sci. Technol.* 42, 946–957. doi:10.1080/02786820802363819
- Li, N., Xia, T., Nel, A.E., 2008. The role of oxidative stress in ambient particulate matter-induced lung diseases and its implications in the toxicity of engineered nanoparticles. *Free Radic. Biol. Med.* 44, 1689–1699. doi:10.1016/j.freeradbiomed.2008.01.028
- Ling, S.H., Eeden, S.F. van, 2009. Particulate matter air pollution exposure: role in the development and exacerbation of chronic obstructive pulmonary disease. *Int. J. COPD* 4, 233–243.
- Mantas, E., Remoundaki, E., Halari, I., Kassomenos, P., Theodosi, C., Hatzikioseyan, A., Mihalopoulos, N., 2014. Mass closure and source apportionment of PM_{2.5} by Positive Matrix Factorization analysis in urban Mediterranean environment. *Atmos. Environ.* 94, 154–163. doi:10.1016/j.atmosenv.2014.05.002
- Paraskevopoulou, D., Liakakou, E., Gerasopoulos, E., Theodosi, C., Mihalopoulos, N., 2014. Long-term characterization of organic and elemental carbon in the PM_{2.5} fraction: the case of Athens, Greece. *Atmos. Chem. Phys.* 14, 13313–13325. doi:10.5194/acp-14-13313-2014
- Pateraki, S., Manousakas, M., Bairachtari, K., Kantarelou, V., Eleftheriadis, K., Vasilakos, C., Assimakopoulos, V.D., Maggos, T., 2019. The traffic signature on the vertical PM profile: Environmental and health risks within an urban roadside environment. *Sci. Total Environ.* 646, 448–459. doi:10.1016/j.scitotenv.2018.07.289
- Rich, D.Q., Halu, O., Crooks, J., Baxter, L., Burke, J., Ohman-strickland, P., Thevenet-morrison, K., Kipen, H.M., Zhang, J., Kostis, J.B., Lunden, M., Hodas, N., Turpin, B.J., 2013. The Triggering of Myocardial Infarction by Fine Particles Is Enhanced When Particles Are Enriched in Secondary Species. *Environ. Sci. Technol.* 47, 9414–9423. doi:10.1021/es4027248
- Rosenkranz, A.R., Schmaldienst, S., Stuhlmeier, K.M., Chen, W., Knapp, W., Zlabinger, G.J., 1992. A microplate assay for the detection of oxidative products using 2', 7' -dichlorofluorescein-diacetate. *J. Immunol. Methods* 156, 39–45.
- Saffari, A., Daher, N., Samara, C., Voutsas, D., Kouras, A., Manoli, E., Karagkiozidou, O., Vlachokostas, C., Moussiopoulos, N., Shafer, M.M., Schauer, J.J., Sioutas, C., 2013. Increased Biomass Burning Due to the Economic Crisis in Greece and Its Adverse Impact on Wintertime Air Quality in Thessaloniki. *Environ. Sci. Technol.* 47, 13313–13320. doi:10.1021/es403847h
- Saffari, A., Daher, N., Shafer, M.M., Schauer, J.J., Sioutas, C., 2014. Global Perspective on the Oxidative Potential of Airborne Particulate Matter: A Synthesis of Research Findings. *Environ. Sci. Technol.* 48, 7576–7583. doi:10.1021/es500937x

- Shafer, M.M., Perkins, D.A., Antkiewicz, D.S., Stone, E.A., Quraishi, T.A., Schauer, J.J., 2010. Reactive oxygen species activity and chemical speciation of size-fractionated atmospheric particulate matter from Lahore, Pakistan: an important role for transition metals. *J. Environmetsa Monit.* 12, 704–715. doi:10.1039/b915008k
- Triantafyllou, E., Diapouli, E., Tsilibari, E.M., Adamopoulos, A.D., Biskos, G., 2016. Assessment of factors influencing PM mass concentration measured by gravimetric & beta attenuation techniques at a suburban site. *Atmos. Environ.* 131, 409–417. doi:10.1016/j.atmosenv.2016.02.010
- Verma, V., Fang, T., Xu, L., Peltier, R.E., Russell, A.G., Ng, N.L., Weber, R.J., 2015. Organic Aerosols Associated with the Generation of Reactive Oxygen. *Environ. Sci. Technol.* 49, 4646–4656. doi:10.1021/es505577w
- Verma, V., Polidori, A., Schauer, J.J., Shafer, M., Cassee, F.R., Sioutas, C., 2007. Physicochemical and Toxicological Profiles of Particulate Matter in Los Angeles during the October 2007 Southern California Wildfires Physicochemical and Toxicological Profiles of Particulate Matter in Los Angeles during the October 2007 Southern Californ. *Environ. Sci. Technol.* 43, 954–960. doi:10.1021/es8021667
- Wang, H., Naghavi, M., Allen, C., Barber, R., Carter, A., Casey, D., Charlson, F., Chen, A., Coates, M., Coggeshall, M., 2016. Global, regional, and national life expectancy, all-cause mortality, and cause-specific mortality for 249 causes of death, 1980–2015: a systematic analysis for the Global Burden of Disease Study 2015. *Lancet* 388, 1459–1544. doi:10.1016/S0140-6736(16)31012-1
- Xia, T., Kovochich, M., Nel, A.E., 2015. Impairment of mitochondrial function by particulate matter (PM) and their toxic components: implications for PM-induced cardiovascular and lung disease. *Front. Biosci.* 12, 1238–1246. doi:10.2741/2142

2.3.7 Emission compliance over the lifespan of a vehicle

N.E. Ligterink, G. Kadijk, M. Elstgeest, P. van Mensch

Research Group Sustainable Transport and Logistics, TNO, PO Box 96800, 2509 JE Den Haag, the Netherlands, email: norbert.ligterink@tno.nl

Abstract

With a lifetime of 15 years and more, many vehicles on the European roads no longer have to satisfy durability and in-service conformity requirements. If new cars satisfy stringent on-road emission standard, the risk of significant increase in emissions due to aging, malfunctions, poor maintenance and tampering will be substantial. Even a few percent failure average emissions could increase by a factor two or more. In the Netherlands this issue is investigated and a number of problems have been identified. Currently, the impact for air-quality is investigated, as are the options to stem the increase in emissions with age. Specifically, the failure and removal of diesel particulate filters and unnoticed malfunctions of the three-way catalyst system are investigated. Furthermore, options to address such problems are studied.

Keys-words: *particulate emissions, NO_x emission, durability, Light Duty Vehicles, ISC, PTI, RDE.*

Introduction

Once new vehicles have entered the road the responsibility for the proper emission performance is not solely for the manufacturer. The owner, the garage, the type-approval authority, and the inspection authority should all together ensure that the vehicle retains a low environmental impact. Unlike safety, emissions have not been at the forefront in road worthiness of vehicles.

Table shows the (laboratory) pollutant emissions of light-duty vehicles as observed in new, type-approval tests have been reduced significantly over the past decade. However, under real driving conditions some emissions substantially deviate from their type approval equivalents. The real driving nitrogen oxides, or NO_x, emissions of diesel vehicles are currently the largest issue with regard to pollutant emissions and PM emissions are of great concern because DPFs are removed or fail due to, e.g., cracks in the ceramics.

Table 1: The different emission limits for PM and PN associated with the different Euro-classes for passenger cars with diesel and GDI engines (Gasoline Direct Injection).

	introduction dates		PM [mg/km]		PN [# /km]	
	new models	all models	diesel	GDI	diesel	GDI
Euro-4	1-Jan-2005	1-Jan-2006	25	-	-	-
Euro-5a	1-Sep-2009	1-Sep-2010	5	5	-	-
Euro-5b	1-Sep-2011	1-Sep-2012	4.5	4.5	6.0E+11	-
Euro-6	1-Sep-2014	1-Sep-2015	4.5	4.5	6.0E+11	6.0E+12
Euro-6c	1-Sep-2017	1-Sep-2018	4.5	4.5	6.0E+11	6.0E+11

Road traffic is one of the main contributors to air pollution. Since vehicle drive mainly where people dwell, their contribution to human exposure is even larger. For example, modern diesel and gasoline vehicles should have low PM emissions (see Table 1) but during their life time these PM emissions may increase for several reasons. Especially the introduction of specific technologies such as particulate filters (DPF or GPF) or direct fuel injection (GDI) substantially influence the real world PM emissions. Furthermore their technical status may deteriorate and this could increase the PM emissions of these vehicles

Commissioned by the Dutch Ministry of Infrastructure and the Environment, since 1987 TNO regularly performs test programs to determine real-world emission performance of vehicles in the Netherlands. From 2012 onwards, special attention was paid to PM and PN emissions (Kadijk 2013, 2015, 2016a,b, 2017, Ligterink 2016). The main goal of the programs is to gain insight into trends in real-world emissions of light-duty vehicles under conditions relevant for the Dutch and European situations. These test data are the basis for the emission factors of Dutch road traffic.

On different moments in a lifetime of vehicles, emission tests must be performed and the actual emission levels are measured. These moments are:

1. Type approval (TA) of a new vehicle type carried by type approval authorities. The type-approval includes:
 - i. Chassis dynamometer emission tests and from 2018 Real Driving Emission tests on a pre-model or prototype,
 - ii. Durability tests of emission control devices, prior to type-approval, e.g., on an aging bench.
 - iii. Conformity of production (CoP) tests of new vehicles, sampling the factory output.
 - iv. Smoke emission test on a single engine
 - v. In Service Conformity (ISC) by the manufacturer of a limited number of in-use vehicles with a maximum mileage of 100,000 km. Chassis dynamometer tests as well as Real Driving Emission (RDE) tests on the road are to be carried out for new vehicle models from September 2017.
2. Dutch national Periodic Technical Inspections (PTI) for all vehicles, mostly every two years starting at the vehicle age of 4 years carried out by PTI service stations or workshops. This is part of the national implementation of the road worthiness requirements.
3. Road Side Inspections (RSI) at random times carried out by national authorities. This focusses on illegal activities such as DPF removal and SCR tampering, on top of tax evasion, tachograph tampering, weight exceedances, road worthiness, etc..
4. Investigations by the Type Approval authority for prosecution on defeat devices. This had not led to a legal challenge so far.
5. Market Surveillance by the inspection authority (ILentT) from 2020 onwards. For L-cat (light) vehicles such requirement already existed, but no L-cat vehicle was ever tested by the Dutch inspection authority.
6. Granting Type Approval Authority, in the Netherlands: the RDW, has to perform independent ISC emission tests from 2020 onward.

Regarding Diesel PM, PN and smoke emissions in TA, ISC and PTI tests, there are a number of interlinking aspects. In type approval and ISC tests the PM and PN emission of each vehicle type is measured on a chassis dynamometer. The smoke emissions of an engine are determined in full load and free acceleration type approval tests. This free acceleration smoke test is also applied in PTIs. Unfortunately, the operating conditions of a free acceleration test are not representative for real-world operation and the smoke emission limit values for vehicles with a DPF are relatively high (Kadijk 2017), which could result in false positives.

In Figure 1 a picture of the ISC and PTI test regime is shown. Although the ISC PN limit values are quite strict, they are only applicable up to 100,000 km. Mostly at a vehicle age of 4 years the PTI test regime starts. The PTI smoke emission limit values are not strict ($< 0.7 \text{ m}^{-1}$) and not well related to real world PM emissions; Consequently the real-world emissions of older vehicles can be substantial. (Ligterink, 2016)

In the future monitoring programs (Mensch 2017) and periodic technical inspections (PTI) may not have the same function as the current legislation. If high emissions are observed for a vehicle, or vehicle model, in monitoring programs it might not be a priori clear if it is a road-worthiness issue, tampering, or has to be taken up in the in-service conformity.

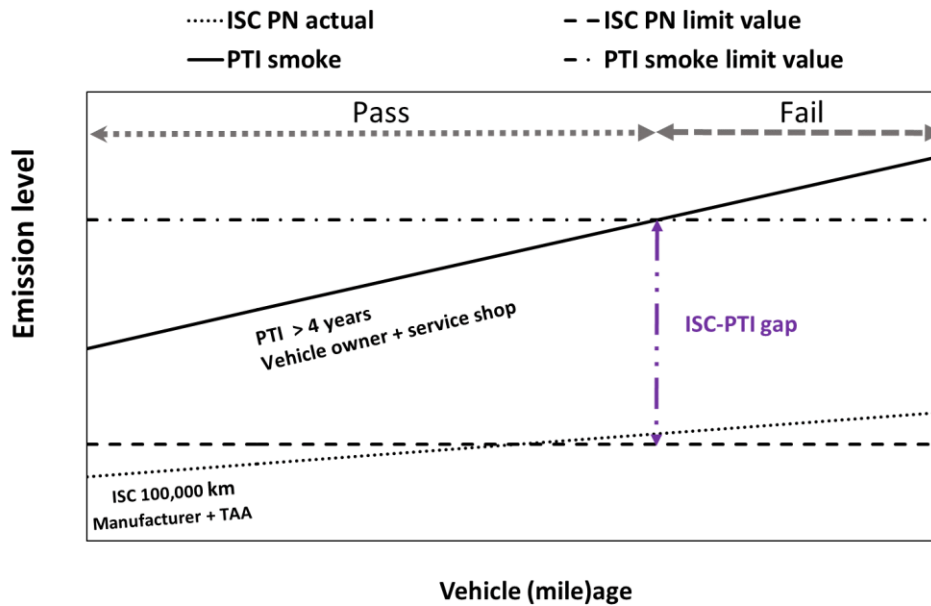


Figure 1: Example of the life time emission behavior of a diesel vehicle and different legislative instruments. The ISC-PTI gap may result in relative high average real world PM emissions of older vehicles.

Relevance of emissions of vehicles with high mileages

Modern Dutch passenger vehicles are on average more than 15 years on the road and often run more than 250,000 km. Many of the older vehicles have more urban usage than the average vehicle. Therefore, as to total annual mileage decreases, the urban mileage does not increase significantly. See Figure 2. (Ligterink 2017)

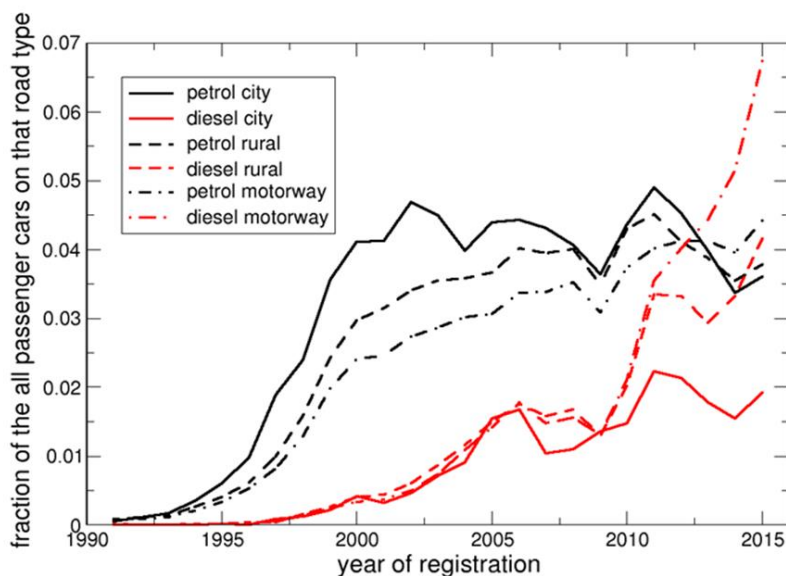


Figure 2: A measurement program collecting data from multiple locations in the Netherlands autumn 2015 show that gasoline vehicles with ages up to 18 years all have similar urban presence.

However, In Service Conformity (ISC) requirements of even the most modern vehicles only control the emission performance up to 100,000 km and durability is defined up to 160,000 km. Vehicles with high mileages contribute significantly to the total emission of Dutch road vehicles. In first test programmes of diesel vehicles with high mileages removed or bad functioning DPFs were detected. Moreover, for gasoline vehicles high NO_x emissions were detected. Maintenance and detecting malfunctions seem critical in retaining low emissions throughout the vehicle life. A typical modern vehicle covers in its lifetime at least double the distance specified in the type-approval requirements. The second half of the vehicle's lifetime is a shared responsibility among owner, manufacturer, road authority, inspection authority and the garage services.

Likewise, the group of older diesel vehicles, typically before 2007, which are not equipped with the DPF, are a major contributor to the Elemental Carbon (EC) emissions in the Netherlands. The rapid decrease of the number of older vehicles is cited as one of the main causes of the rapid reduction of traffic-related EC concentrations in the Netherlands since 2013.

Chassis dynamometer and on-road tests older gasoline vehicles

Older gasoline vehicles are assumed to be a major part in the exhaust particulate matter in the next decade, with the phasing out of diesel vehicles without DPF. It was unclear whether the high mileage of these vehicles, and, for example, higher oil consumption, would lead to higher particulate matter emissions, than below 100,000 km. In order to investigate this aspect and other possible issues, the gasoline vehicles were tested mainly on the chassis dynamometer, since this is still the only accurate method to determine the mass of the particulate matter emissions on a filter, in the range of 0-10 mg/km. From the first initial investigation of 3 vehicles, problems with NO_x emissions were observed, while particulate matter emissions were low. Another 3 vehicles did not lead to a conclusion. At the current level of 12 older gasoline vehicles tested (Kadijk 2018) it can only be concluded that a few vehicles with malfunctions have a major impact on the average NO_x emissions. If a gasoline vehicle operates slightly lean, the emissions are quickly tenfold higher, above 1 g/km NO_x.

In 2017 and 2018 in total twelve Euro 2, 3, 4 and 5 gasoline vehicles with mileages between 155,000 and 254,000 km were tested on a chassis dynamometer in a laboratory (Kadijk 2018). These tests consisted of CADC tests at an ambient temperature of 15 °C, with a real-world road load and test mass. The NO_x emissions varied from 17 to 1234 mg/km, see Figure 1, while all high emitters passed the OBD and four-gas test in the Periodic Technical Inspection (PTI). CO, PM and THC emissions were mostly at regular ISC levels. The Kia Picanto had a new exhaust line fitted, which may have caused additional PM emissions above the norm.

Table 2: Measurement results of 12 older gasoline vehicles on the CADC test.

	Euro Class	CO		THC		NO _x		PM	
		[mg/km]	CF	[mg/km]	CF	[mg/km]	CF	[mg/km]	CF
Citroën Xsara	3	719	0.3	8	0.0	39	0.3	0.1	0.0
Toyota Aygo	5	4135	4.1	25	0.3	17	0.3	1.1	0.2
Ford Focus	3	2476	1.1	97	0.5	254	1.7	2.3	0.5
VW Polo	4	2500	2.5	53	0.5	96	1.2	1.5	0.3
Opel Corsa1	4	724	0.7	23	0.2	375	4.7	3.9	0.8
Fiat Punto 1	4	5133	5.1	138	1.4	1234	15.4	3.7	0.7
Fiat Punto 2*	4	2317	2.3	25	0.3	30	0.4	3.5	0.7
Opel Corsa 2*	4	6187	6.2	86	0.9	275	3.4	3.6	0.7
Renault Megane Scenic*	4	1028	1.0	16	0.2	17	0.2	2.8	0.6
BMW 325i*	4	2021	2.0	130	1.3	1059	13.2	4.4	0.9
Kia Picanto*	3	6545	2.8	29	0.1	18	0.1	9.1	1.8
Volkswagen Golf*	2	1098	0.5	88	-	172	-	3.5	0.7

The high emissions are not correlated with a particular brand or model, nor with the emission class, Euro-2 to Euro-5, age, and specific high mileages. Since the problems could also occur in a Euro-5 vehicle, with the same technology, it is expected that this problem may affect the air-quality until 2030, since Euro-5 vehicles are likely to be present on Dutch road until then. Pending further investigation it is assumed that the average NO_x emissions increase to around 300 mg/km, based on 1-in-6 vehicles developing undetected malfunctions of the aftertreatment system (three-way catalysts and lambda controller). The Dutch government has requested further investigation of this problem, and the possible measures to reduce its severity. A dedicated emission test as part of the period inspection is one of the options.

Periodic Technical Inspection (PTI) tests for detecting high emitting vehicles

From 2015 to 2017 TNO tested 355 Euro 5 and 6 in-use diesel passenger cars and light commercial vehicles with a Diesel Particulate Filter (DPF) in a new PTI Particulate Number (PTI-PN) test at low idle speed (Kadijk 2015, 2016a, 2016b, 2017). High PTI-PN emissions occurred in 21 of the 355 vehicles. A draft PTI-PN test procedure with a dedicated specification of a PTI-PN-tester (related to PMP protocol for the PN standard), an emission test at low idle speed and PTI-PN limit values were developed.

In 2016 investigations of diesel vehicles with stationary tests found 5% to 7% of vehicles with increased particle number emissions, in a large range of values, compared to the very low baseline of properly functioning DPF technologies. In part this could be the result of filter removal, but in the cases it was investigated further, the increased particulate matter emissions were linked mainly to deterioration, i.e., cracked filters. This problem was not detected in maintenance and inspection. The current OBD, maintenance schedule, and road worthiness test do address this problem. A new test method is therefore required to detect elevated particulate matter emissions in vehicle inspection.

In 2018 the prevalence of filter removal leading to a largest increase in particulate matter emissions was investigated with garage workshop visits (Staps 2018). In total 89 car workshops are visited in the Netherlands, 83 workshops (93.3%) were cooperative with the research. However, six workshops (6.7%) were not willing to cooperate. According to the researcher these companies acted strange and they seemed threatened by the research. In the interview, 32 workshops (38.6%) indicated that they know customers who have removed the DPF. Together they know 212 customers with a removed DPF, an average of 2.5 customers per workshop. Within the research 86 workshops are approached, which represent the maintenance of 27.650 diesel vehicles yearly. This represents 1.05% of the total Dutch market of diesel vehicles. Within this diesel passenger and light commercial vehicles in 1.2% the DPF filter is removed. Given the uncertainties in the study, a lower estimate on 1.5% filter removal is assumed. This share represents a total 20,284 vehicles with a removed DPF in the full market. High costs on the filter replacement (an average of € 1200) or filter cleaning motivates most costumers to remove the DPF. The fraction of vehicles with removed filters may increase as the age of DPF equipped vehicles increases. On the other hand, DPF technology may mature after the initial technology from 2000-2008, reducing the malfunctions and maintenance issues.

In 2018 first attempts for a PTI-NO_x emission test method for gasoline vehicles were explored but need to be elaborated in more detail (Kadijk 2018).

PM emissions of vehicles are strongly dependent on the applied technology. In Figure 3 the exhaust particulate emissions (EC and non-EC) from Dutch diesel and gasoline passenger cars in urban traffic with standard traffic flow are shown. Gasoline vehicles with direct fuel injection have little PM emissions, but these emissions are somewhat higher than the typical PM emission of diesel vehicles with a particulate filter. Wall flow diesel particulate filters (DPFs) are a very effective way to reduce emissions of soot particles in the exhaust gases. DPFs reduce the real-world PM emissions of light-duty vehicles with diesel engines strongly to an average of 1-2 mg/km, including the emissions associated with regeneration events. It is however known that DPFs are quite frequently removed if there are problems with DPF regeneration. Removal and tampering or manipulation of the engine software is more economical than a DPF replacement. The actual PM emission of such vehicles increase with a factor 25 to 100. Currently, there are no reasonable accurate tests to assess the presence or functionality of DPFs during periodic technical inspections. The current test that is used for periodic inspection of vehicles with diesel engines, the free acceleration smoke emission test, has a lack of sensitivity and it does not correlate with real world PM or PN emissions (Kadijk 2016b, 2017). Furthermore, the current limit values used for diesel smoke, can even be met without a particulate filter. Table 3 shows an overview of PM and PN emissions and risk of increased PM and PN emissions of gasoline and diesel vehicles.

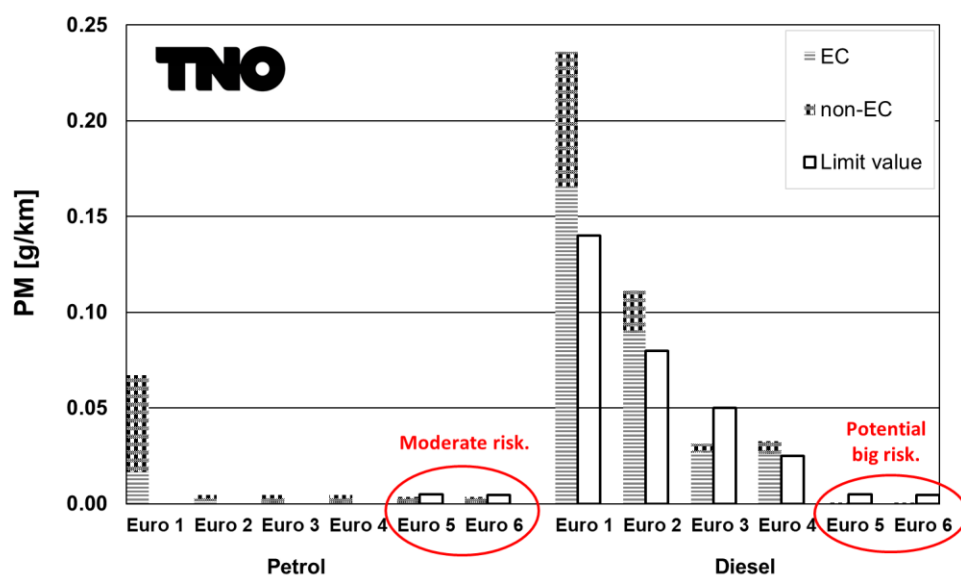


Figure 3: Exhaust particulate emissions (EC and non-EC) from diesel and gasoline passenger cars in urban traffic with standard traffic flow (no congestion). Due to technical failures or manipulation the PM emission of Euro 5&6 vehicles may be higher.

Table 3: PM/PN emissions and risk of increased PM/PN emissions

Field	Emission level	Risk	Emission level	Risk
	Gasoline	Gasoline	Diesel	Diesel
Type approval	++	++	++	++
In Service Conformity	++	++	++	++
Real world emissions (RDE)	+	-	+	-
Durability	+/-	-	-	--
Periodic Technical Inspection	n.a.	n.a.	-	--
Road side inspections	n.a.	n.a.	-	-
Manipulation	-	+/-	--	--

++ very low risk, + low risk, +/- some risk, - reasonable risk, -- high risk

To be able to determine the trends of real world particulate emissions and to assess for possible risks on elevated emissions during the useful life of a vehicle, data was collected of several studies that were performed between 2013 and 2017 (Kadijk 2013, 2015, 2016a,b, 2017, Ligterink 2016) for which the particulate emissions of more than 500 diesel and gasoline passenger cars and light-duty vehicles were tested. The data comes from several types of PM and PN emission tests.

The following tests were performed:

- Chassis dynamometer emission tests according to UNECE R83.
- The EC fractions of the PM of the GDI vehicles were chemically analyzed.
- Smoke emission test for diesel engines according to UNECE R24 of 1958 & 72/306/EEC.
- Free acceleration and PN emission tests at idle speeds for Periodic Technical Inspection (PTI). PN test were done (also with cracked DPFs) with different (handheld) PN-testers which were correlated with the PMP-PN test protocol.

On the basis of the test program a simplified PN measurement standard, compared to the PMP-like protocol, is developed to be the basis of PTI and inspection authority test. It must be noted that a PN-based method is designed to establish the functioning of DPF technology, the connection with PM and air-quality remains tenuous, as particle numbers evolve over time subject to ambient conditions.

Emission compliance over the lifespan of a vehicle

Although Euro 6d real driving emission (RDE) legislation improve real world emissions these vehicles still have limited ISC (up to 100,000 km) and durability requirements (up to 160,000 km) (Mensch 2017). The current OBD and PTI tests are very limited or not suitable for detection of high emitters. Manufacturers, governments, service providers and vehicle owners have shared responsibility for robust vehicle emission performance over the lifetime of a vehicle. Therefore, a more integrated approach of ISC, OBD and PTI in post Euro 6 legislation is needed to improve emissions over the full lifespan.

If the 100,000 km (based on ISC criteria) or 160,000 km (based on durability) criteria, seems to be the proper guarantee date of emission control technology, such as DPFs, three-way catalyst, or lambda sensors that control the operation, it would be proper to insist on replacement of such parts. In a number of cases it is now found that the mileage over 160,000 km is no longer anybody's responsibility. The same as spark plugs, drivebelts, brake pads, and tyres, emission control technology may have wearable parts, which need to be replaced. Such replacements are part of proper maintenance. A PTI test should only be needed to ensure proper maintenance.

Potential ways to improve emission compliance

Current measures for improvement of the emission performance of vehicles are mainly addressed to governments and manufacturers. It is well known that users can have a major impact on vehicle emissions. TNO explores new projects with direct communication to groups of vehicle owners with the aim to improve the fuel consumption, emissions, use and maintenance of vehicles by sharing dedicated knowledge of vehicle emissions and showing best practices to vehicle owners. The H2020 uCARE project, starting May 2019, is dedicated to informing and helping car owners.

Eventually, after 2025, post-Euro-6/VI legislation should cover these aspects. It cannot be expected that manufacturers are alone responsible for the environmental performance. Currently, if there is unauthorised repair, replacement, an unattended MIL warning, etc. the manufacturer no longer takes responsibility for the ISC of the vehicle. This means many vehicles are only at the level of road worthiness, and the consequences of failing any of the requirements for the ISC program are not known. Very likely independent parties will have trouble finding vehicles fit for ISC testing.

Eventually, anybody should be able to check the maintenance state of the vehicle, so authorities can follow-up on different issues, such as illegal adaptations or substandard service. Before this ideal situation is reached, there will be many years of vehicles on the road with a unknown emission performance.

Effectiveness of PTI procedures

Effectiveness of the current In Service Conformity protocol:

The current ISC protocol is not very effective in solving a problem with a substantial rate of faulty vehicles. The procedure is designed to fail a vehicle model if 40% or more develop problems. The malfunctioning should appear within 100,000 km and despite good maintenance and moderate use. If, for example only a 25% of the vehicles develop problems, there is virtually no need for improvement of maintenance procedure, or the replacement of a defective part from the perspective of the ISC protocol. Such problems have been observed with inferior technology DPFs.

Improved PTI test procedure for diesel vehicles with DPF:

A draft PTI test procedure was developed for the detection of removed or broken DPF in a rather simple test procedure which constitutes of an idle test at which particle number concentrations are measured (Kadijk 2017). The procedure is meant to check for problems that concern (highly) elevated PM/PN emissions.

The current PTI smoke emission test procedure for diesel vehicles is outdated because the sensitivity of the opacimeter is too low; small and normal DPF failures and even a removed DPF cannot be detected. An improved PTI test procedure with relatively simple PN-test test equipment was

investigated in cooperation with equipment manufacturers. A simple test performed at low idle speed with an appropriate PN limit value (i.e., 250.000 #/cm³) seems to be a good candidate to detect removed or broken DPFs. The PN emission at low idle speed has a good correlation with the regulated PN emissions in NEDC tests, although more tests are recommended to support this.

Current mobile PN-testers are accurate but too expensive for PTI workshops. A new draft specification for a simplified low cost PTI-PN-tester for diesel vehicles is proposed (Kadijk, 2017) and has been developed by the Netherlands Metrological Institute (NMI). After standardization of this new PTI-PN-tester a final PTI test procedure may be built and implemented as a Type II emission test in UNECE R83 or WLTP regulations. However, the PTI-PN procedure does not cover the performance of the NO_x aftertreatment systems (LNT or SCR). Due to the very specific NO_x reduction technologies a dedicated PTI test procedure would be needed which can preferably also be performed at low idle speed.

The potential increase of PM emissions of older gasoline vehicles with GDI engines is expected to be moderate and can be well monitored in improved ISC test programmes. In case of GDI vehicles with a particulate filter (GPF) a dedicated PTI-PN test might be an option. For this specific PTI test of gasoline vehicles the development of a dedicated PTI-PN tester which can handle exhaust gas with higher water concentrations seems to be needed.

Conclusions

Now the real-world, on-road emissions of new vehicles seem to be controlled by effective RDE legislation. The next step is to ensure these emissions remain at a low level over the lifetime of the vehicle. Investigations by TNO so far have uncovered serious concerns with emission control technologies which were expected to be robust. Both the DPF as the three-way catalyst on older vehicles do not perform as well as may have been hoped.

The procedures to ensure proper performance of emission control in normal use, such as ISC and PTI, have serious flaws. It seems that the responsibility of the emission performance of vehicles in the second half of the vehicle's life is not implemented. Consequently, a small fraction of vehicles with malfunctions or tampered with, cause the average emissions of these groups to double or more.

Better monitoring of PM, PN and NO_x emissions of diesel and also gasoline vehicles seems necessary. This would need to include the following elements:

- Increase of the In Service Conformity (ISC) requirements above the current 100,000 km. A life time of 250,000 km or more seems more appropriate, especially for diesel engines.
- Introduction of a sufficiently accurate but simple PN test for the Period Technical Inspection (PTI), especially for diesel cars.
- Development and introduction of a sufficiently accurate but simple NO_x test for the Period Technical Inspection (PTI), especially for gasoline cars.
- A common definition of a vehicle in a proper environmental state, that connects all elements from type-approval to periodic inspection. This should place any emission test in a general context.

The combination of these elements is essential in addressing the different responsibilities in securing reasonable emissions during the life time of vehicles.

Acknowledgments

This work is part of the in-use compliance program of light-duty vehicles, which is financed since 1987 by the Dutch Ministry of Infrastructure and Water Management (I&W).

References

- Kadijk G. (2013), Roadworthiness Test Investigations of Diesel Particulate Filters, *TNO report 2013 R10160 v3 (30p)*.
- Kadijk G., Spreen J.S. (2015), Roadworthiness Test Investigations of Diesel Particulate Filters on vehicles, *TNO report 2015 R10307 v2 (23p)*.
- Kadijk G., Spreen J.S., van der Mark P.J. (2016a), Investigation into a Periodic Technical Inspection test method to check for presence and proper functioning of Diesel Particulate Filters in light-duty diesel vehicles, *TNO report*

2016 R10735v2 (60 p).

Kadijk G., Spreen J.S., van der Mark P.J. (2016b), Diesel Particulate Filters for light-duty diesel vehicles: Operation, Maintenance, Repair and Inspection, *TNO report 2016 R10958* (19 p).

Kadijk G., Elstgeest M., Ligterink N.E., van der Mark P.J. (2017), Investigation into a Periodic Technical Inspection test method to check for presence and proper functioning of Diesel Particulate Filters in light-duty diesel vehicles-part 2, *TNO report TNO 2017 R10530* (85 p).

Kadijk, G. Elstgeest, M. Ligterink, N.E. van der Mark, P.J. (2018), Emissions of twelve gasoline vehicles with high mileages. *TNO report 2018 R11114* (41p).

Ligterink N.E. (2016), Emissions of three common GDI vehicles, *TNO report 2016 R11247* (17 p).

Ligterink, N.E. (2017), The fleet composition on the Dutch roads relevant for vehicle emissions, *TNO report 2017 R10517* (25 p).

Mensch, P. van. Cuelenaere, R.F.A. Ligterink, N.E. Kadijk, G. (2017) Update assessment of risks for elevated emissions of vehicles outside the boundaries of RDE. Identifying relevant driving and vehicle conditions and possible abatement measures. TNO 2017 R10862_xx (to be published)

Spreen J.S., Kadijk G., Vermeulen R.J., Heijne V.A.M., Ligterink N.E., Stelwagen U., Smokers R.T.M., van der Mark P.J., Geilenkirchen G. (PBL) (2016), Assessment of road vehicle emissions: methodology of the Dutch in-service testing programme, *TNO report 2016 R11178* (86 p).

Staps, J., Ligterink, N.E. (2018), Diesel Particle Filters, *TNO report 2018 R11468* (24p).

Zyl van P.S., Ligterink, N.E., Kadijk G., Borken-Kleefeld J., Chen Y. (2015), In-use compliance and deterioration of vehicle emissions, *TNO report 2015 R11043* (37p).

2.3.8 Air Quality Impacts of New Public Transport Provision: A Causal Analysis of the Jubilee Line Extension in London

Liang Ma, Daniel J. Graham and Marc E. J. Stettler*

¹Centre for Transport Studies, Department of Civil and Environmental Engineering, Imperial College London, London, SW7 2AZ, United Kingdom, m.stettler@imperial.ac.uk

Abstract

Public transport is commonly considered to be associated with benefits such as reducing road traffic congestion and improving air quality. This paper focuses on evaluating the causal impact of a new public transport provision in London, the Jubilee Line Extension (JLE) in 1999, on air quality. Using the regression discontinuity design for a time series analysis, we show that an increase in public transport supply may not necessarily lead to an improvement in air quality. Heterogeneity of impacts is evident in spatial and air quality monitoring location, i.e. roadside versus urban background stations. While the roadside concentration represents the condition near major roads, the urban background concentration is broadly representative of the town/city-wide background condition. The results indicate that JLE increased concentrations of NO₂ and NO_x by 4-12% and that of CO outside 2.5 km by 8-9% at urban background monitoring stations within one year after the second-phase JLE opening. In contrast, the JLE appears to have caused an 8% decrease in roadside concentrations of CO within 2.5 km. The effects of JLE on the trend of pollutant concentrations are also analysed. We have considered changes to residential population and traffic volume for supplementary analyses. Results imply that the provision of public transport needs to be combined with policies to limit potential detrimental effects from induced economic activity and land use redistribution.

Keywords: air quality, public transport, causal analysis, regression discontinuity design.

Introduction

In 2013, more than 3.5 billion people lived in countries with unsafe air quality according to the World Health Organization standards, and poor air quality was estimated to be the main cause of death for about 5.52 million people, accounting for nearly 10% of all global deaths (Angel Hsu et al., 2016). As one of the main sources of air pollutant emissions, the transport sector has implemented various interventions aimed at mitigating air pollution, such as stricter vehicle emissions standards. Public transport is generally considered to be more sustainable than private road transport, with potential benefits including improving air quality. For ex-post assessment and to inform future investments, our aim is to understand whether and to what extent public transport provision has improved air quality in the past.

Our evaluation relies on identifying the *causal* impact of public transport interventions on air quality, instead of quantifying the *association* between them. While *association* describes a non-directed path between two variables and focuses more on the prediction, *causation* indicates a single-directed relationship from the intervention (public transport) to the outcome (air quality), which focuses more on the underlying data generating process. The identification of a causal relationship can be biased by confounding and selection bias. A confounder is defined to be a common cause of both the putative cause and its outcome (Wunsch, 2007). Selection bias arises when the treatment assignment is non-randomised. As a public transport intervention is generally a non-randomised and mostly non-experimental process, our main challenge is to identify and quantify the *causal* relationship between a public transport intervention and air quality in the presence of confounding and selection bias with non-experimental data.

Causal inference methods have been used to quantify the causal relationship between public transport intervention and air quality in previous studies, with mixed results. Chen & Whalley (2012) analysed the effect of a new urban rail transit system in Taipei on air quality with a sharp regression discontinuity method. Controlled on meteorological factors, time trend, and seasonality, they found that the new urban rail transit reduced CO concentration by 5%-15%, but no significant effects were recognised on NO_x and ground-level ozone concentrations. Goel & Gupta (2015) and Gendron-Carrier et al. (2018) also applied the regression discontinuity design in relevant studies. Goel & Gupta (2015) analysed the impact of the Delhi metro system on the ambient concentration of NO₂, CO, and PM_{2.5}. Gendron-Carrier et al. (2018) focused on the impact of the subway opening in 39 cities around the world on aerosol optical depth. Rivers, Saberian & Schaufele (2017) considered the supply variation in public transit in 18 Canadian cities caused by strikes during 1974-2011. The model was based on the differences-in-differences method with two-way fixed effects and with meteorological factors controlled. The findings indicated a 3.5 ppb increase in NO_x and no significant effect on CO or PM_{2.5}. A similar method could be seen in Bel & Holst (2015), which discussed the relationship between bus rapid transit and air pollution

(CO, NO_x, PM_{2.5}, PM₁₀, and SO₂) in Mexico City. It showed a decrease in CO, NO_x, PM_{2.5}, and PM₁₀ concentration caused by the new bus rapid transit system. Beaudoin & Lawell (2016) considered the causal impact of public transit capacity on air quality (CO, Pb, NO₂, O₃, PM, and SO₂) with panel data covering 96 urban areas across the United States during 1991-2001. Instrumental variable regression was used to account for the potential endogeneity of public transit investment. Elasticity estimation suggested that a 10% increase in transit supply resulted in a 2.29% increase in NO₂ concentration and a 2.87% increase in PM₁₀ concentration.

In the previous studies, the results were inconsistent in magnitude and direction (positive/ negative) of the air quality impacts of public transport interventions. We present an empirical study of the Jubilee Line Extension (JLE) in London in 1999 with a regression discontinuity design (RDD), considering the autocorrelation of time series and spatial heterogeneity of impacts. As part of the JLE, six new Underground stations were built and five were enlarged or rebuilt at a cost of approximately £3.5 billion. The extension was opened in two phases: the first phase on 14th May 1999 and the second phase on 22nd December 1999. After the extension, the Jubilee Line included 27 stations. It starts from Stanmore Station in a suburban area in the west, through business centres and tourist attractions (such as Docklands, South Bank, and the West End), and ends at Stratford in the east, which is a locally primary retail, cultural and leisure centre.

In the following sections, Section 2 introduces causal inference and regression discontinuity design in general, and describes the main model used in this paper. Results for background and roadside pollutant concentrations are discussed respectively in Section 3. It also provides the results of robustness tests and supplementary analyses. Conclusions are given in Section 4.

Methods and Data

The causal impacts of the JLE on the background and roadside concentrations of three main transport-related air pollutants (NO₂, NO_x, and CO) within three buffer areas (radius: ≤2.5 km, 2.5 km-5 km, and >5 km) are separately evaluated with an RDD model. Hourly air pollutant concentrations and London general meteorological information are extracted from open-source data from the London Air Quality Network (King's College London, 2018). Mid-year population estimation from the Office for National Statistics of United Kingdom (Office for National Statistics, 2017) and traffic flow statistics from the Department of Transport of United Kingdom (Department for Transport, 2018) are used for supplementary analyses, both of which are at Borough level.

2.1 Regression discontinuity design and causal inference

The Rubin Causal Model is a primary research framework for causal inference. It defines the average treatment effect (ATE) as $\tau = E[Y_i(1) - Y_i(0)]$ where $(Y_i(0), Y_i(1))$ represents a pair of potential outcomes of unit i , assuming a binary treatment experiment where treatment indicator $W_i = \begin{cases} 1, & i \in \text{treatment group} \\ 0, & \text{otherwise} \end{cases}$.

$Y_i(0)$ indicates the outcome of interest that would be realised if the unit i is not exposed to the treatment while $Y_i(1)$ indicates the outcome of interest that would be realised if it is exposed to the treatment (Rubin, 1974). The fundamental problem of causal inference is that we can at most observe one outcome from each pair of $(Y_i(0), Y_i(1))$, because the unit can be exposed to only one level of treatment (Holland, 1986). As a new provision of public transport is generally a non-randomised process, a more complex approach is necessary: a simple comparison of the observed outcome of the treatment group before and after the intervention or a comparison of the observed outcome between the treatment group and the control group can encounter a selection bias, because $E[Y_i(1) - Y_i(0)] \neq E[Y_i(1) | W_i = 1] - E[Y_i(0) | W_i = 0]$ when $W_i \not\perp (Y_i(0), Y_i(1))$.

Sharp regression discontinuity design is a method when the treatment assignment is non-randomised. It assumes the treatment assignment is determined by the value of a forcing variable X_i being on either side of a threshold of the treatment assignment, c . That is $W_i = \begin{cases} 1 & X_i \geq c \\ 0 & X_i < c \end{cases}$. The ATE under a sharp RDD can be represented by $\tau = \lim_{x \downarrow c} E[Y_i | X_i = x] - \lim_{x \uparrow c} E[Y_i | X_i = x]$ (Imbens & Wooldridge, 2009). In a time series analysis for an interruption/intervention/treatment assessment, a general sharp RDD model with t being the forcing variable can be represented by

$$Y_i = \delta_0 + \delta_1 * W_i + \theta_1 * t + \theta_2 * t_2 + \varepsilon_i, \quad (1)$$

where t is the continuous integer index of time; Y_t is the outcome of interest at time t ; $W_t = \begin{cases} 1, & t \geq T \\ 0, & t < T \end{cases}$ is the treatment assignment indicator and T is the start time of the intervention; t_2 is the continuous integer post-intervention index of time t where all the pre-intervention period time equals 0 and the post-intervention period time is coded from 1 (Lagarde, 2011). The main estimand of interest is δ_1 . It represents the difference in intercept at the intervention point, that is $\delta_1 = \lim_{t \downarrow T} E[Y_t | t = T] - \lim_{t \uparrow T} E[Y_t | t = T]$ and $W_t = \begin{cases} 1, & t \geq T \\ 0, & t < T \end{cases}$, and consequently can be interpreted as the average treatment effect (ATE) under the sharp regression discontinuity design (RDD) settings. In addition, while θ_1 controls the long-term trend (secular trend) of Y_t , θ_2 estimates the change in the trend after the intervention.

2.2 Model specification

Based on the general form of a sharp RDD with time being the forcing variable, the main model to evaluate the air quality impact of the JLE is specified. Assume $\{Y_t : t = 1, 2, \dots, T-1, T, T+1, \dots\}$ is the time series of the average hourly air pollutant concentrations (background/roadside) at air quality monitoring sites within a particular area, where T indicates the start of the post-intervention period. The model is specified by:

$$y_t = \delta_0 + \delta_1 W_t + \delta_3 w s_t + \delta_4 t p_t + \theta_1 T_0(t) + \theta_2 T_1(t) + \sum_{l=1}^L \alpha_l y_{t-l} + \sum_{d=1}^D \beta_d S_{dt} + \varepsilon_t \quad (2)$$

where y_t is the natural logarithm transformation of Y_t , that is $y_t = \ln Y_t$; $W_t = \begin{cases} 1, & t \geq T \\ 0, & t < T \end{cases}$ is the intervention indicator; $w s_t$ is the natural logarithm of wind speed; $t p_t$ is the natural logarithm of temperature difference compared with the minimum temperature in research period, that is $t p_t = \ln(TP_t - \min_t TP_t)$ and TP_t is the measured temperature; $T_0(t)$ is the secular trend, assuming $T_0(t) = t$, and $T_1(t)$ is the post-intervention trend, assuming $T_1(t) = \begin{cases} 0, & t < T \\ t - T + 1, & t \geq T \end{cases}$; y_{t-l} is the lagged dependent variable where l is the order of lag and L is the maximum lag order to be considered; S_{dt} is the seasonal dummy variable and D is the size of the seasonal dummy variable set.

As shown in Section 2.1, the main coefficient of interest is δ_1 , which gives the impact multiplier of JLE. Due to the autocorrelation in pollutant concentration, the total effect of the JLE, τ , is the sum of the impact from the current period, δ_1 , and the stacked impacts from the lag periods⁷ (Henderson, 1996). By using the natural logarithm of Y_t , the estimation of τ can be interpreted as the percentage change in air pollutant concentration caused by the JLE (Benoit, 2011).

The candidate number of maximum lag periods, L , is determined by the partial autocorrelation function (PACF) figure of y_t . The partial autocorrelation coefficient at lag l represents the correlation between observations separated by a lag of l , with all the smaller lags controlled (White, 1985).

Seasonality and trend factors are adjusted for confounding control to avoid 'spurious regression'. Meteorological factors are controlled as they play a role in determining emissions dispersion and air pollutant concentrations. As a result of data quality and missing values in our meteorological dataset, only wind speed and temperature are included in the model. However, air quality can also be strongly affected by the rainfall level. Therefore, the hourly data with an available rainfall measurement exceeding a maximum rainfall level (0.1 mm) is excluded in the model estimation. The selection of

⁷ For an AR(L) model with an intervention indicator: $y_t = \delta_0 + \delta_1 W_t + \alpha_1 y_{t-1} + \alpha_2 y_{t-2} + \dots + \alpha_L y_{t-L}$, the corresponding stacking equations are : $y_{t-1} = \delta_0 + \delta_1 W_t + \alpha_1 y_{t-2} + \alpha_2 y_{t-3} + \dots + \alpha_{L-1} y_{t-L} + \dots$, $y_{t-2} = \delta_0 + \delta_1 W_t + \alpha_1 y_{t-3} + \alpha_2 y_{t-4} + \dots + \alpha_{L-2} y_{t-L} + \dots$ etc. By substituting the stacking equations into the main AR(L) model, it can be proved that: the effect from 1st time lag is $\alpha_1 \delta_1$; from 2nd time lag: $(\alpha_2 + \alpha_1^2) \delta_1$; from 3rd time lag: $[\alpha_3 + (2\alpha_1 \alpha_2 + \alpha_1^3)] \delta_1 \dots$. Therefore, suppose in Eq.(2) $L = 3$, the total effect of intervention is then $\tau = \delta_1 + \alpha_1 \delta_1 + (\alpha_2 + \alpha_1^2) \delta_1 + [\alpha_3 + (2\alpha_1 \alpha_2 + \alpha_1^3)] \delta_1$.

seasonal dummy variable set is based on a pattern inspection of the monthly average hourly concentration figure and the 'Day of Week-Hour' relationship figure for the time series of y_t . Both of the trend functions, $T_0(t)$ and $T_1(t)$, are assumed to be linear. Specifying a more complex time trend can give a better approximation of the dependent variable, but it is unlikely to contribute to the causal inference results (Wooldridge, 2015). The robustness of the model specification in terms of trend function form is tested in Section 3.4.

The main model is estimated by Ordinary Least Square (OLS) with Newey-West standard errors. Assumptions to validate the consistency of an OLS estimator are satisfied in our model (Wooldridge, 2015). Newey-west standard error is conducted, as being heteroscedasticity and autocorrelation consistent (HAC). The preliminary form of Eq.(2) with the candidate L , determined from the PACF figure, is estimated first. Any lagged dependent variables or trend variables with statistically insignificant coefficients are then removed. The model with the remaining variables is estimated again. The total effect of JLE, τ , is estimated accordingly based on the final estimation of the impact multiplier δ_1 and the remaining lagged dependent variable coefficients α .

2.3 Case study specification

Three buffer areas are specified according to the distance from Jubilee Line stations (buffer 1: ≤ 2.5 km, buffer 2: 2.5 km - 5 km, and buffer 3: > 5 km), shown in Figure 1.

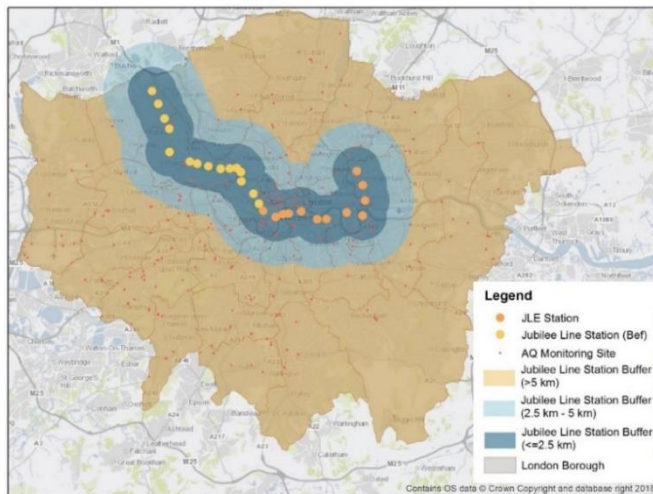


Figure 1: Case study area, including a 2.5 km buffer area (buffer 1: dark blue), a 2.5-5 km buffer area (buffer 2: light blue), and an >5 km buffer area (buffer 3: orange) around the 27 Jubilee Line stations (yellow: original stations; orange: JLE stations); red: air quality (AQ) monitoring sites.

The research period is set to end at 1 year after the second-phase JLE opening. To approximately balance the data in the pre-intervention period and post-intervention period, the research period is determined to be 1997/10/03-2000/12/22. The first post-intervention time is 1999/05/14 05:00:00, considering the operation hour of the London Underground service. This makes two periods of 585 days, and 28,245 hourly time intervals in total. This is reduced to 26,733 (94.6%) after removing data where the time interval has missing values in wind speed or temperature, or a rainfall exceeding the maximum rainfall level. The average hourly background concentrations and roadside concentrations of NO_2 , NO_x , and CO in these 26,733 time intervals in each buffer area then form the main sample of time series.

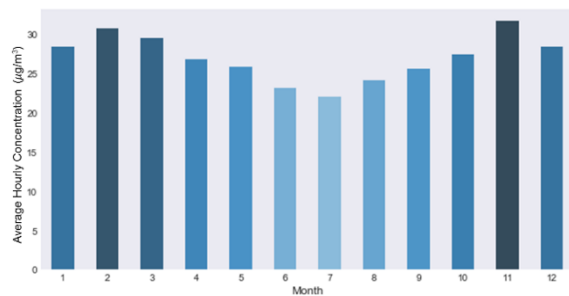
Results and Discussion

Results for impacts on background concentrations

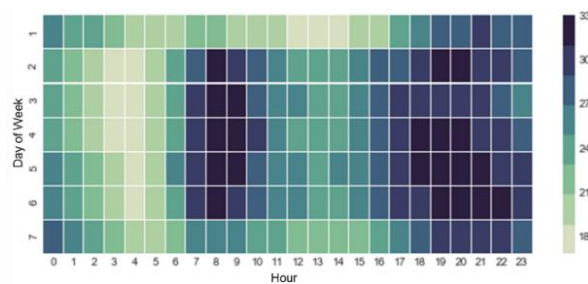
To illustrate the model specification process, we take the estimation of JLE impact on NO_2 background concentration in buffer 1 as an example. Figure 2 indicates the seasonality and autocorrelation features of NO_2 background concentration in that area.

Based on inspection of Figure 2, the preliminary seasonal dummy variables and lagged dependent variables are shown in Table 1. Two dummy variables are created to reflect the classification of the *Month* attribute. The *Hour* attribute is separated to weekday hours and weekend hours and represented by 47 dummy variables. Preliminary model specifications for background concentrations of NO₂, NO_x, and CO in the buffer areas are determined using the same process. The final estimation results are shown in Table 2.

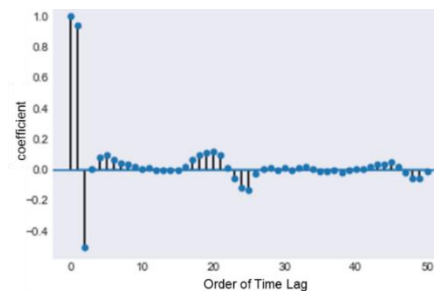
As shown in Table 2, NO₂, NO_x, and CO background concentrations in all buffer areas were significantly increased by the JLE by 4.30% to 12.48% in one year, except the CO background concentration in buffer 1, on which there was an insignificant negative impact. Among the three pollutants, background NO_x concentrations experienced the highest total treatment effect in general. NO_x and NO₂ were more affected in buffer 2 (2.5-5 km) than in the other buffer areas. For CO, the total treatment effect increases as the distance away from the JLE increases. Estimated total effects in different buffer areas are shown graphically in Figure 3.



Monthly average hourly concentration



Day of Week-Hour heat map (µg/m³)



PACF figure

Figure 2: Seasonality and autocorrelation features of the NO₂ background concentration time series in buffer 1, including (a) monthly average hourly concentration; (b) Day of week-Hour heat map where each cell shows the average concentration in the corresponding combination of *day-of-week* and *hour*; and (c) the partial autocorrelation coefficient of each order of time lag.

Table 1: Preliminary model specification for background NO₂ concentration in buffer 1.

Outcome	Autocorrelation	Seasonality	
		Month	Hour
log(NO ₂)	Candidate L=3	Category 1: Month 6 and 7;	Weekday: 24 hours Weekend: 24 hours
		Category 2: Month 5, 8, and 9;	
		Category 3: Month 1, 2, 3, 4, 10, 11, and 12;	

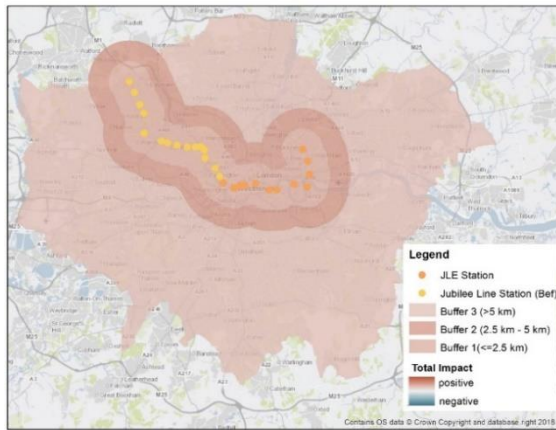
Table 2: Summary of OLS estimation for JLE impacts on NO₂, NO_x, and CO background concentrations.

	NO ₂			NO _x			CO		
	≤2.5 km	2.5-5 km	>5 km	≤2.5 km	2.5-5 km	>5 km	≤2.5 km	2.5-5 km	>5 km
<i>w</i>	0.015***	0.020***	0.009***	0.017***	0.034***	0.015***	-0.009	0.027***	0.037***
<i>w.s</i>	-0.068***	-0.073***	-0.068***	-0.112***	-0.145***	-0.126***	-0.116***	-0.186***	-0.114***
<i>ϕ</i>	-0.034***	-0.037***	-0.035***	-0.086***	-0.096***	-0.078***	-0.073***	-0.086***	-0.090***
<i>T</i> ₀	-1.47×10 ⁻⁶ ***	-1.47×10 ⁻⁶ ***	-1.15×10 ⁻⁶ ***	-2.79×10 ⁻⁶ ***	-3.60×10 ⁻⁶ ***	-2.66×10 ⁻⁶ ***	-2.08×10 ⁻⁶ ***	-7.58×10 ⁻⁶ ***	-3.67×10 ⁻⁶ ***
<i>T</i> ₁	-9.69×10 ⁻⁷ **	-1.31×10 ⁻⁶ ***					2.31×10 ⁻⁶ ***	7.82×10 ⁻⁶ ***	-2.76×10 ⁻⁶ ***
<i>y</i> _{<i>t</i>-1}	1.158***	1.115***	1.342***	1.138***	1.018***	1.245***	0.881***	0.782***	0.829***
<i>y</i> _{<i>t</i>-2}	-0.273***	-0.221***	-0.501***	-0.254***	-0.141***	-0.391***	-0.024**	0.031***	-0.029***
<i>y</i> _{<i>t</i>-3}	-0.035***	-0.043***	0.034***	-0.038***	-0.050***		-0.054***	-0.034***	
Month	2 dummies								
Hour	47 dummies								
Total Effect	6.00%***	7.78%***	4.30%***	6.90%***	12.48%***	4.93%***	-2.73%	7.87%***	9.23%***
Adj. R ²	0.938	0.934	0.958	0.958	0.945	0.967	0.907	0.880	0.910

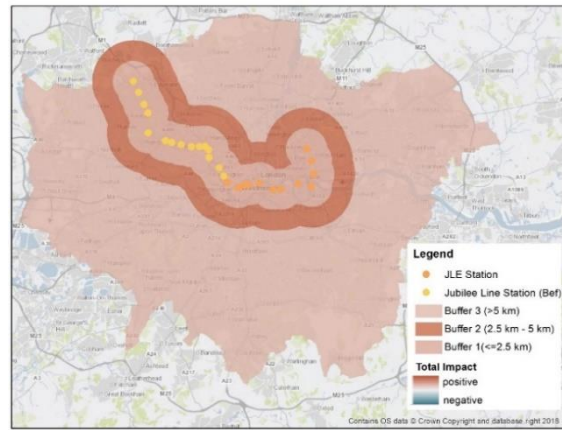
Standard Errors are HAC using 24 lags and without small sample correction;

Significance: *** Significant at the 1% level; ** Significant at the 5% level; * Significant at the 10% level;

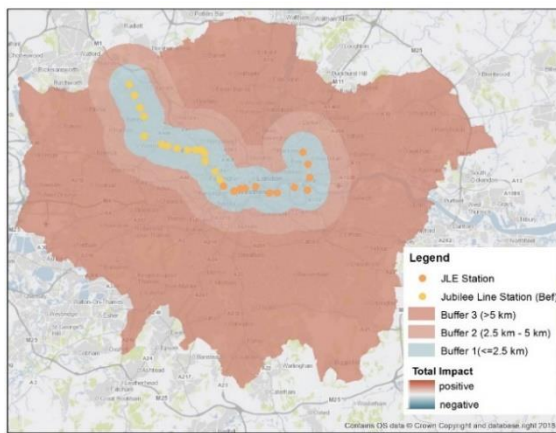
Total effect includes the impact from the current period and the stacked impacts from the lag periods. The significance of the total effect is determined by the significance of relevant coefficients.



NO₂ background concentration



NO_x background concentration



CO background concentration

Figure 3: Total effect of JLE on NO₂, NO_x, and CO background concentrations. For each buffer area, red indicates an increase and blue indicates a decrease caused by JLE. Darker colour indicates a greater absolute total effect.

It is worth noting that all pollutant concentration time series have a significant downward secular trend (T_0). Even though the JLE caused an increase in NO₂ concentrations within 5 km, and an increase in CO concentrations outside 5 km, the decreasing trend in pollutant concentrations was enhanced by a significant negative post-intervention trend (T_1). In contrast, the secular trends for CO concentrations within 5 km are reversed, as there is a positive post-intervention trend which is larger in magnitude than the corresponding secular trend for both buffer 1 and 2. This may indicate a structural change in the transport sector or other industrial sectors in the surrounding area. No significant impacts are found on the trend of NO_x in all buffer areas and NO₂ outside 5 km. The estimated total effect, the secular trend and the post-intervention trend for NO₂ in buffer 2 are plotted in Figure 4, as an example of an enhanced trend with a positive total effect.

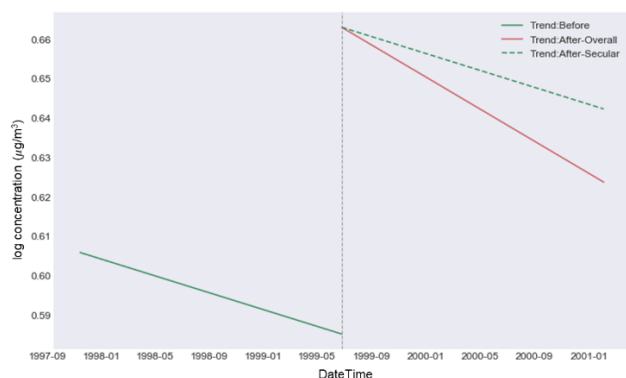


Figure 4: The estimated total effect and trends for background NO₂ concentrations in buffer 2. There is a positive total effect with an enhanced trend. Grey dashed line is the start of the JLE; the discontinuity at the dashed line represents the total intervention effect; the green lines show the secular trends; and the red line shows the overall trend after the intervention.

3.2 Results for impacts on roadside concentrations

Compared with the background monitoring site, the roadside monitoring site locates within 1-5 m of a busy road at breathing height, which generally represents public exposure near major roads. Table 3 shows the final estimation results for JLE impacts on NO₂, NO_x, and CO roadside concentrations. Heterogeneity of impacts is evident in spatial and air pollutant. It shows that JLE had small or insignificant impacts on NO₂ and NO_x roadside concentrations within 5 km (buffer 1 and 2) in one year after the second-phase JLE opening, but significantly decreased the CO roadside concentration within 2.5 km by 7.60%. Compared with buffer 1 and 2, there is a higher treatment effect for all three pollutants in buffer 3, ranging from 4.88% to 9.93%. The total effect of the JLE on NO₂ and NO_x roadside concentrations increases with distance away from the JLE. For CO, the total effect changes from negative to positive between buffer 1 and 2. Estimated total effects on roadside concentrations in each buffering area are illustrated in Figure 5.

The effects of JLE on the trend of roadside pollutant concentrations are also analysed. Although the total effects of the JLE were not significant for NO₂ roadside concentrations within 5 km in one year after the second-phase JLE opening, results show that JLE reversed its increasing trend to a decreasing trend. Similarly, the NO_x concentration in buffer 1 also has an insignificant total effect with a reversed trend. All other combinations of pollutants and buffer areas have a decreasing trend in the long term, except the CO roadside concentration in buffer 1, which had no significant trend. The decreasing trend was enhanced for CO in buffer 2 (2.5 km-5 km) due to the JLE, but it was weakened for CO and NO_x in buffer 3 (>5 km), where the JLE caused a relatively large increase in the magnitude of these roadside concentrations. The estimated total effect, the secular trend, and the post-intervention trend for NO_x roadside concentration in buffer 3 (>5 km) and in buffer 1 (≤2.5 km) are plotted in Figure 6, as examples of (a) a weakened trend with a positive total effect and (b) a reversed trend with a negative total effect.

Table 3: Summary of OLS estimation of JLE impacts on NO₂, NO_x, and CO roadside concentrations.

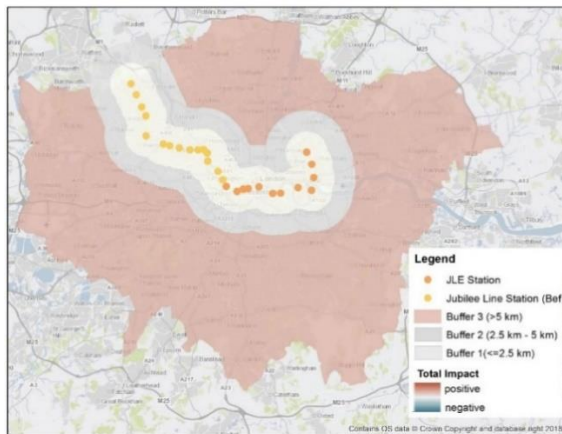
	NO ₂			NO _x			CO		
	≤2.5 km	2.5-5 km	>5 km	≤2.5 km	2.5-5 km	>5 km	≤2.5 km	2.5-5 km	>5 km
<i>w</i>	-0.0003	0.001	0.016***	-0.002	0.009*	0.024***	-0.042***	0.010*	0.015***
<i>w_s</i>	-0.045***	-0.046***	-0.049***	-0.088***	-0.086***	-0.103***	-0.110***	-0.082***	-0.105***
<i>tp</i>	-0.024***	-0.026***	-0.021***	-0.063***	-0.069***	-0.058***	-0.057***	-0.059***	-0.065***
<i>T₀</i>	1.28×10 ^{-6**}	2.23×10 ^{-6***}	-1.34×10 ^{-6***}	-4.75×10 ^{-6**}	-1.65×10 ^{-6***}	-4.65×10 ^{-6***}	-2.06×10 ^{-6***}	-6.19×10 ^{-6***}	
<i>T₁</i>	-1.66×10 ^{-6**}	-4.09×10 ^{-6***}		5.09×10 ^{-6***}		2.28×10 ^{-6***}	-1.78×10 ^{-6**}	4.82×10 ^{-6***}	

y_{t-1}	0.982***	0.907***	1.271***	0.945***	0.903***	1.150***	0.829***	0.825***	0.932***
y_{t-2}	-0.095***	-0.049***	-0.392***	-0.077***	-0.021**	-0.263***			-0.095***
y_{t-3}						-0.024***	-0.039***		-0.032***
Month	1 dummy	1 dummy	2 dummies						
Hour	47 dummies								
Total Effect	-0.09%	0.17%	5.41%***	-0.64%	2.96%*	9.93%***	-7.60%***	1.78%*	4.88%***
Adj. R ²	0.904	0.894	0.959	0.918	0.920	0.969	0.875	0.903	0.952

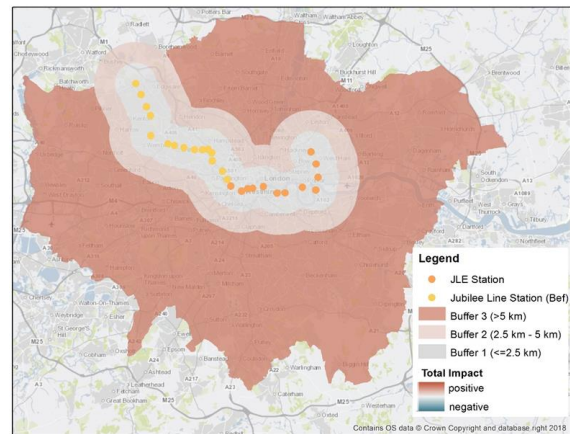
Standard Errors are HAC using 24 lags and without small sample correction;

Significance: *** Significant at the 1% level; ** Significant at the 5% level; * Significant at the 10% level;

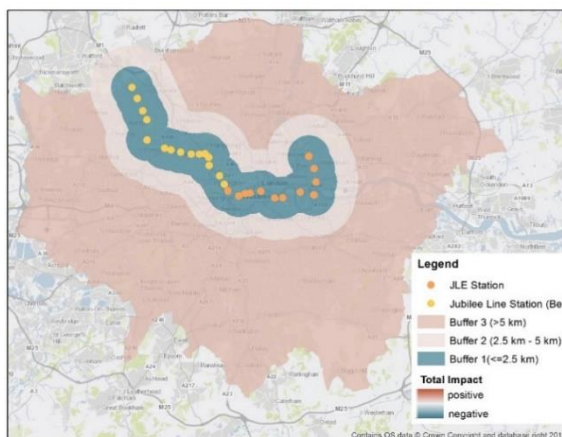
Total effect includes the impact from the current period and the stacked impacts from the lag periods. The significance of the total effect is determined by the significance of relevant coefficients.



NO₂ roadside concentration

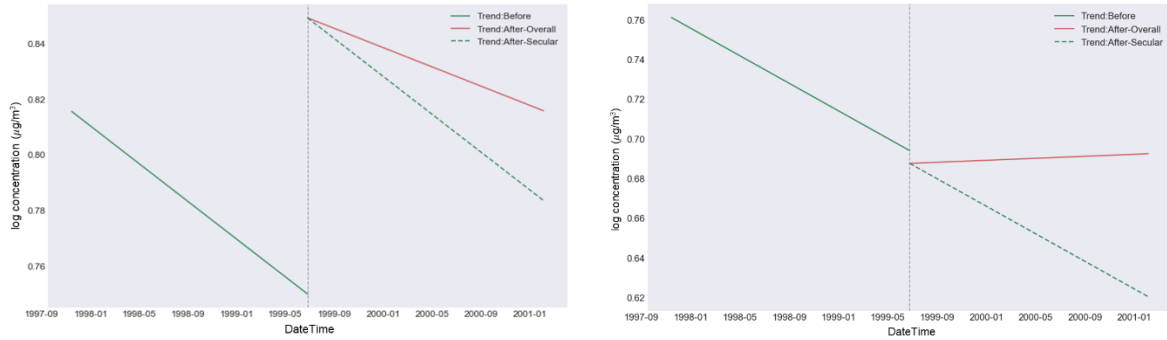


NO_x roadside concentration



CO roadside concentration

Figure 5: Total effect of JLE on NO₂, NO_x, and CO roadside concentrations. For each buffer area, red indicates an increase and blue indicates a decrease caused by JLE. Darker colour indicates a greater absolute total effect.



Positive total effect with a weakened trend
(roadside NO_x in buffer 3)

Negative total effect with a weakened trend
(roadside NO_x in buffer 1)

Figure 6: The estimated total effect and trends for roadside NO_x concentrations in buffer 3 and buffer 1. Grey dashed line is the start of the JLE; the discontinuity at the dashed line represents the total intervention effect; the green lines show the secular trends; and the red line shows the overall trend after the intervention.

3.3 Comparison of impacts on background and roadside concentrations

A summary of the JLE's total effects in magnitude and effects on the trend of background and roadside concentrations is shown in Table 4.

Table 4: Comparison of effects of JLE on background and roadside concentrations.

Pollutant	Buffer	Background			Roadside		
		Total Effect	T_0	T_1	Total Effect	T_0	T_1
NO ₂	2.5 km	6.00%***	decreasing	enhanced	-0.09%	increasing	reversed
	2.5-5 km	7.78%***	decreasing	enhanced	0.17%	increasing	reversed
	>5 km	4.30%***	decreasing		5.41%***	decreasing	
NO _x	2.5 km	6.90%***	decreasing		-0.64%	decreasing	reversed
	2.5-5 km	12.48%***	decreasing		2.96%*	decreasing	
	>5 km	4.93%***	decreasing		9.93%***	decreasing	weakened
CO	2.5 km	-2.73%	decreasing	reversed	-7.60%***		
	2.5-5 km	7.87%***	decreasing	reversed	1.78%*	decreasing	enhanced
	>5 km	9.23%***	decreasing	enhanced	4.88%***	decreasing	weakened

Standard Errors are HAC using 24 lags and without small sample correction;

Significance: *** Significant at the 1% level; ** Significant at the 5% level; * Significant at the 10% level;

Total effect includes the impact from the current period and the stacked impacts from the lag periods. The significance of the total effect is determined by the significance of relevant coefficients.

In summary, the results for the different pollutants indicate that:

NO₂ and NO_x: the JLE significantly increased both roadside and background concentrations in general. Within 5 km, background concentrations of NO₂ and NO_x were more affected than their corresponding roadside concentrations, while the area outside 5 km experienced the opposite situation. Except for

NO_x roadside concentrations within 2.5 km, the overall trend of NO₂ and NO_x concentrations in all buffer areas was decreasing after the JLE.

CO: there was a significant decrease in roadside concentrations caused by JLE within 2.5 km, but no significant impacts were found on background concentrations in the same buffer area. Outside 2.5 km, both roadside and background concentrations were increased, and the total effect was highest for the >5 km buffer. In buffer 2 and 3 (>= 2.5 km), background concentrations of CO were more affected than roadside concentrations.

The results for the different buffer areas indicate that:

Buffer 1 (<=2.5 km): the background concentrations were more affected for NO₂ and NO_x; roadside concentrations of CO were more affected than the background concentrations.

Buffer 2 (2.5 km-5 km): the roadside concentrations of the three air pollutants were not significantly affected by JLE in general. Background sites were more affected for NO_x concentrations, and the effects on CO and NO₂ concentrations are similar. Additionally, among all buffering areas, buffer 2 has the highest total effects for NO₂ and NO_x background concentrations. The CO background concentrations in buffer 2 are the only case that has a positive total effect and a reversed increasing overall trend after the JLE.

Buffer 3 (>5 km): for each pollutant, the roadside concentrations in buffer 3 had the highest increase caused by JLE, compared with other buffer areas. The roadside sites were more affected for NO_x concentrations while the background sites were more affected in terms of CO concentration.

3.4 Robustness tests

We test the robustness of the results by re-running the analysis with: (1) a different trend function, and (2) on pollutants that are less influenced by traffic emissions. Firstly, the robustness of model specification is tested by replacing the linear trend assumption in Eq.(2) with quadratic trends:

$$T_0(t) = \lambda_1 t + \lambda_2 t^2 \text{ and } T_1(t) = \begin{cases} 0 & t < T \\ \lambda_1'(t-T+1) + \lambda_2'(t-T+1)^2 & t \geq T \end{cases}$$

Other variables and estimation methods remain the same as before. Final estimation results are compared and shown in Table 5.

Table 5: Result comparison of robustness test models (quadratic) and baseline models (linear).

Pollutant	Buffer	Background		Roadside					
		Total Effect (Quadratic)	Adj.R ² (Quadratic)	Total Effect (Linear)	Adj.R ² (Linear)	Total Effect (Quadratic)	Adj.R ² (Quadratic)	Total Effect (Linear)	Adj.R ² (Linear)
NO ₂	2.5 km	12.65%***	0.938	6.00%***	0.938	-3.58%	0.904	-0.09%	0.904
	2.5-5 km	7.43%***	0.934	7.78%***	0.934	6.66%***	0.894	0.17%	0.894
	>5 km	3.21%**	0.958	4.30%***	0.958	5.28%***	0.959	5.41%***	0.959
NO _x	2.5 km	6.59%***	0.958	6.90%***	0.958	-0.56%	0.918	-0.64%	0.918
	2.5-5 km	11.90%***	0.945	12.48%***	0.945	14.48%***	0.920	2.96%*	0.920
	>5 km	8.24%***	0.967	4.93%***	0.967	9.79%***	0.969	9.93%***	0.969
CO	2.5 km	3.53%	0.907	-2.73%	0.907	-10.20%***	0.875	-7.60%***	0.875
	2.5-5 km	-3.15%	0.881	7.87%***	0.880	1.59%	0.903	1.78%*	0.903
	>5 km	7.31%***	0.910	9.23%***	0.910	4.42%***	0.952	4.88%***	0.952

Standard Errors are HAC using 24 lags and without small sample correction;

Significance: *** Significant at the 1% level; ** Significant at the 5% level; * Significant at the 10% level;

Total effect includes the impact from the current period and the stacked impacts from the lag periods. The significance of the total effect is determined by the significance of relevant coefficients; Estimations which are relatively sensitive to the trend function specification are highlighted in light blue.

As indicated in Table 5, estimations in baseline models are generally robust in trend function specification. Five cases have a relatively large difference between the baseline model and the robustness test model, among which examples are plotted in Figure 7. These results suggest cases with both statistically significant λ_1 and λ_2 tend to be more sensitive to trend function specification, in which case the JLE changed the convexity/concavity of the trend. The difference in total effect estimation generally becomes larger when the pre-intervention trend or the post-intervention trend has a relatively high convexity/concavity, or has a turning point that is close to the intervention point. As the impact multiplier δ_1 is the difference in intercept at the intervention point, the discrepancy in total effect estimation between the baseline model and robustness test model is typically higher when the difference between the linear trend and the quadratic trend is higher near the intervention point. A turning point close to the intervention point could be indicative of a leading response triggered by the announcement of JLE or a lagged response of any changes that could affect pollutant concentrations following the JLE. These may also be the reason why the quadratic trend models in these five cases tend to show a larger response to the JLE, compared with the corresponding linear trend model.

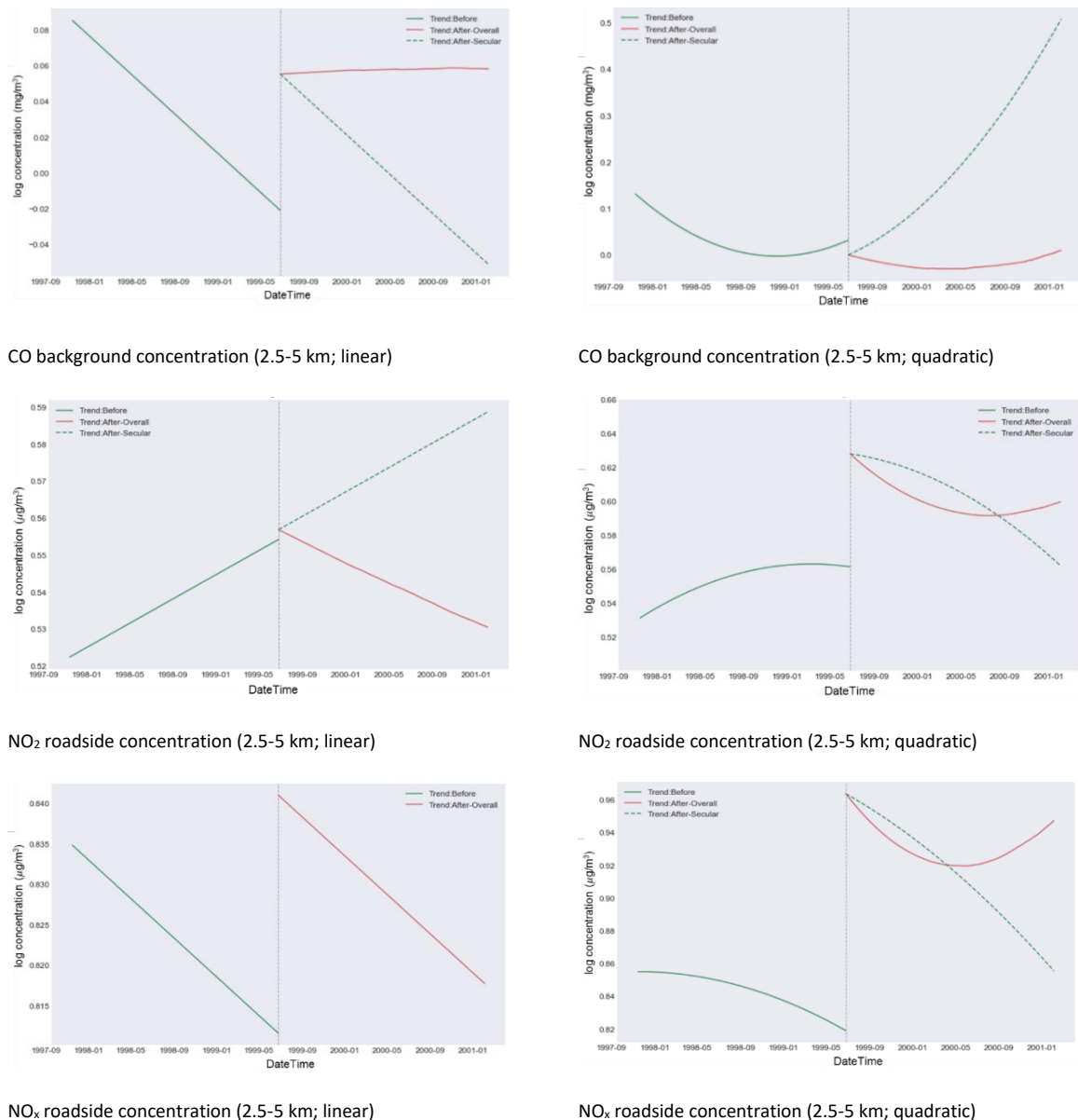


Figure 7: Examples of comparison between the baseline time trend model (linear, left) and robustness test model (quadratic, right). Grey dashed line denotes start of the JLE; the discontinuity at the dashed line is the total intervention effect; green lines are secular trends; red line is the overall trend after the intervention.

Table 6: Summary of JLE impacts on O₃, SO₂, and PM₁₀ background and roadside concentrations

		≤2.5 km		2.5-5 km		>5 km	
		Total Effect	Adj. R ²	Total Effect	Adj. R ²	Total Effect	Adj. R ²
O ₃	Background	-3.56%	0.936	6.60%	0.892	-0.49%	0.994
	Roadside	-0.54%	0.977			-24.21%***	0.952
SO ₂	Background	0.86%	0.880	-1.71%	0.803	2.42%*	0.926
	Roadside	3.03%	0.824	0.93%	0.824	1.42%	0.882
PM ₁₀	Background	0.54%	0.870	6.15%***	0.846	1.83%	0.872
	Roadside	4.64%***	0.802	0.70%	0.858	6.02%***	0.919

Standard Errors are HAC using 24 lags and without small sample correction;

Significance: *** Significant at the 1% level; ** Significant at the 5% level; * Significant at the 10% level;

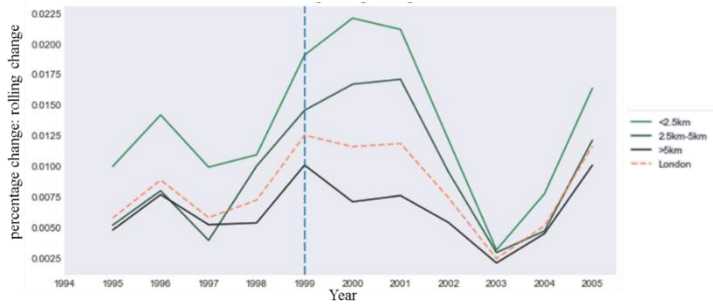
Total effect includes the impact from the current period and the stacked impacts from the lag periods. The significance of the total effect is determined by the significance of relevant coefficients;

The total effect of O₃ roadside concentration in buffer 2 fails to be estimated because there are no available data.

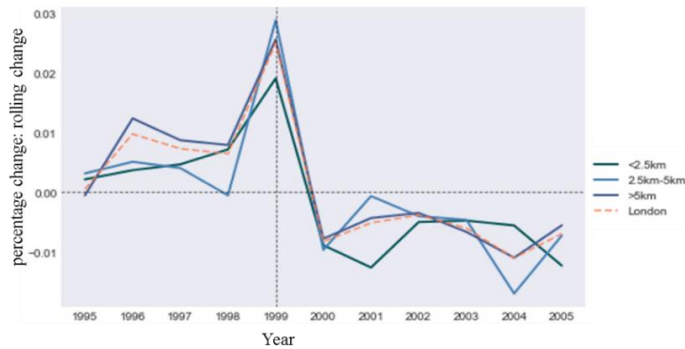
Secondly, to test the consistency of atmospheric chemical reactions, the JLE total effects on O₃, SO₂, and PM₁₀ concentrations are estimated with the baseline model, shown in Table 6. As O₃ is a secondary pollutant affected by NO_x and NO₂ (as well as meteorology), the total effect of JLE on NO₂, NO_x and O₃ are influenced by a complex set of interactions. Clapp & Jenkin (2001) illustrated the observed variation of daylight average mixing ratios of O₃, NO and NO₂ with the level of NO_x around London, which indicated a negative relationship between the roadside concentrations of O₃ and NO₂/NO_x. Therefore, the insignificant effect in O₃ roadside concentrations in buffer 1 was consistent with the corresponding effects on NO₂, NO_x concentrations. The significant decrease in O₃ roadside concentrations in buffer 3 was also consistent with the significant increases in the corresponding NO₂, NO_x concentrations. The impact on PM₁₀ roadside concentrations may have resulted from increases in transport PM₁₀ emissions from tyre and brake wear, road dust resuspension, or of diesel engine emissions. SO₂ concentrations were only significantly affected in background sites in buffer 3. Therefore, we conclude that the results of JLE impacts on O₃ are generally consistent with those for NO_x.

3.5 Explaining the results

The impacts of the JLE on air pollutant concentrations may have arisen through impacts on the population, road traffic, and modal share. Here we discuss contemporary observable trends using mid-year population estimates from the Office for National Statistics of United Kingdom (Office for National Statistics, 2017) and motor vehicle traffic flow statistics from the Department of Transport of United Kingdom (Department for Transport, 2018). Both datasets provide annual data at the London Borough level. Therefore, we assume both the population and traffic volume are homogeneous throughout each borough and estimate the population and traffic volume of each buffer area using the area fraction of each London Borough within each buffer area. We acknowledge this is an over-simplification, yet it is the only data available at the time of writing. The percentage year-on-year change in estimated population and traffic volume is illustrated in Figure 8.



(a) residential population



(b) motor vehicle traffic volume

Figure 8: Year-on-year change in (a) residential population and (b) motor vehicle traffic count in each buffer area. The vertical dashed line refers the year of the JLE.

In all buffer areas, there was an increase in residential population and motor vehicle traffic volume from 1998 to 1999. After 1999, the residential population within 5 km continued to increase, but the traffic volume in all buffer areas decreased. These are generally consistent with the estimated total impact and trend after the JLE. The population in buffer 2 started to have a higher increasing rate after 1997 and began to exceed the London average level. Buffer 2 also had the highest increasing rate in the traffic volume in 1999. It shows that there were significant changes occurring in buffer 2 around the period of JLE. These are consistent with the comparison result of NO₂ and NO_x background concentration, as population growth and traffic increases could have led to higher emissions of NO_x from transport and non-transport sources (e.g. domestic heating).

CO roadside concentrations within 2.5 km significantly decreased as a result of the JLE while the population kept increasing and traffic volume had a sharp increase from 1998-1999. As CO is mainly emitted under the cold-start condition of vehicles, one plausible explanation is that the modal share of road transport decreased around the period of JLE, leading to fewer car trips starting within this buffer area. As mentioned above, the background concentration of NO₂ and NO_x was affected to a greater degree than roadside concentrations within 2.5 km. It is plausible that the contribution of NO_x emissions from domestic heating increased due to population increases, and it may also indicate that the usage of minor roads (affecting background concentrations) increased, while the usage of major roads (affecting roadside concentrations) did not significantly change.

The pathways of the JLE effects on air pollutant concentrations are complicated. Examples of other factors which could potentially explain the mechanisms include: the increase in diesel car use and changes in spatial distribution, the change in the congestion condition and resultant changes in vehicle dynamics, and the change in the travel distances and the trip rates.

Conclusions

This paper evaluated the causal impact of the Jubilee Line extension in 1999 in London on air quality, considering the spatial heterogeneity of impacts. Estimations of the impacts on NO₂, NO_x and CO concentrations are robust in model specification and consistent in atmospheric chemistry in general. The variation in impacts on roadside concentrations and background concentrations in different buffering areas is obvious. Results indicate that the JLE generally increased the NO₂, NO_x and CO

background concentrations by 4-12%, but have insignificant or small impacts on roadside concentrations within 5 km. The supplementary analyses may imply a decrease in road transport modal share of residents living within 2.5 km. Our analysis implies that an increase in public transport supply may not necessarily lead to an improvement in air quality and suggests the provision of public transport need to be combined with policies to limit the detrimental effects potentially from induced economic activity and land use redistribution.

References

- Angel Hsu, Daniel C. Esty, Marc A. Levy & Alex de Sherbinin. (2016) *2016 Environmental Performance Index (EPI)*. Yale University.
- Beaudoin, J. & Lawell, C. C. L. (2016) Is public transit's "green" reputation deserved?: Evaluating the effects of transit supply on air quality. In: Anonymous *University of California at Davis Working Paper*. [e-book] .
- Bel, G. & Holst, M. (2015) Evaluation of the Impact of Bus Rapid Transit on Air Pollution. *Research Institute of Applied Economics*.
- Benoit, K. (2011) Linear regression models with logarithmic transformations.
- Chen, Y. & Whalley, A. (2012) Green infrastructure: The effects of urban rail transit on air quality. *American Economic Journal: Economic Policy*. 4 (1), 58-97.
- Clapp, L. J. & Jenkin, M. E. (2001) Analysis of the relationship between ambient levels of O₃, NO₂ and NO as a function of NO_x in the UK. *Atmospheric Environment*. 35 (36), 6391-6405.
- Department for Transport. (2018) *Road traffic statistics*. Available from: <https://www.gov.uk/government/collections/road-traffic-statistics> [Accessed Jan 10, 2019].
- Gendron-Carrier, N., Gonzalez-Navarro, M., Polloni, S. & Turner, M. A. (2018) Subways and urban air pollution.
- Goel, D. & Gupta, S. (2015) Delhi Metro and Air Pollution.
- Henderson, J. V. (1996) Effects of Air Quality Regulation. *American Economic Review*. 86 (4), 789-813. Available from: <https://ideas.repec.org/a/aea/aecrev/v86y1996i4p789-813.html>. [Accessed Sep 27, 2018].
- Holland, P. W. (1986) Statistics and causal inference. *Journal of the American Statistical Association*. 81 (396), 945-960.
- Imbens, G. W. & Wooldridge, J. M. (2009) Recent developments in the econometrics of program evaluation. *Journal of Economic Literature*. 47 (1), 5-86.
- King's College London. (2018) *London Air Quality Network*. Available from: <https://www.londonair.org.uk/london/asp/datadownload.asp> [Accessed Jul 21, 2018].
- Lagarde, M. (2011) How to do (or not to do)... Assessing the impact of a policy change with routine longitudinal data. *Health Policy and Planning*. 27 (1), 76-83.
- Office for National Statistics. (2017) *Estimated Resident Population Mid-Year*. Available from: <https://www.ons.gov.uk/peoplepopulationandcommunity/populationandmigration/populationestimates> [Accessed 10 Jan 2019].
- Rivers, N., Saberian, S. & Schaufele, B. (2017) Public Transit and Air Pollution.
- Rubin, D. B. (1974) Estimating causal effects of treatments in randomized and nonrandomized studies. *Journal of Educational Psychology*. 66 (5), 688.
- White, J. B. (1985) The assessment of intervention effects in time series processes.
- Wooldridge, J. M. (2015) *Introductory econometrics: A modern approach*. Nelson Education.
- Wunsch, G. (2007) Confounding and control. *Demographic Research*. 16 97-120.

2.3.9 Investigating the technological impact of European transport research and innovation towards a clean and decarbonised urban landscape

A. Tsakalidis*, K. Gkoumas, M. van Balen and F. Pekar

European Commission, Joint Research Centre (JRC), Ispra, Italy, anastasios.tsakalidis@ec.europa.eu

Introduction

Transport is one of the main sectors supporting development. Having a direct impact on the economy, the environment and the overall quality of life, a series of efforts are undertaken to maximise benefits and mitigate negative externalities. Legislation and technological advancement through targeted research and innovation (R&I) are two main levers used towards this goal. At European level, in order to address current socio-economic challenges within an ever-changing complex and competitive environment, the transport sector requires new technological developments.

One of the main fields of interest is the decarbonisation and the reduction of pollutant emissions of transport, which became increasingly prominent topics in cities across the globe. Based on the number of projects funded by European research Framework Programmes (FP) related to greenhouse gases, air quality and/or pollution within the urban context in the past decade it is observed that, over time, urban air pollution gained greater prominence in the research community (European Commission, 2017a).

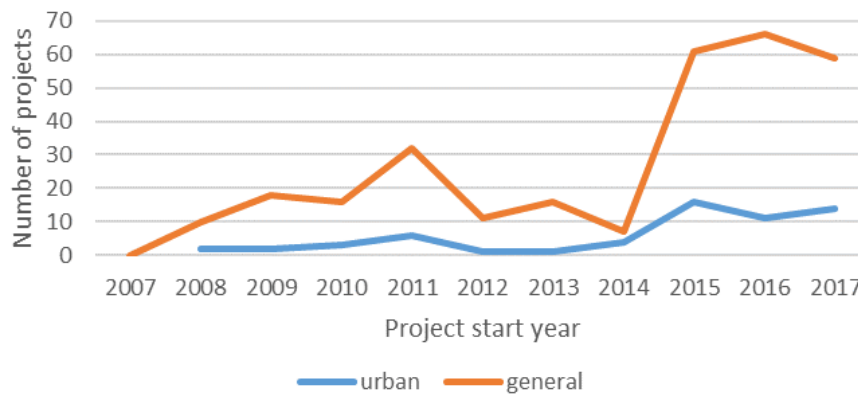


Figure 1. Evolution of projects under EU Framework Programmes in the field of emissions, urban and general.

To catalyse research innovation, the European Commission (EC) has outlined future transport R&I priorities towards the decarbonisation of the European transport sector in its Strategic Transport Research and Innovation Agenda (STRIA). The priorities were published in 2017, as part of the "Europe on the Move" package, highlighting the main transport research and innovation (R&I) areas and European Union (EU) priorities for clean, connected and competitive mobility (European Commission, 2017b, 2017c, 2015).

The STRIA has identified seven priority areas with specific actions for future R&I, that are outlined in seven roadmaps covering all transport modes and spatial levels, including urban transport: 1. Cooperative, connected and automated transport, 2. Transport electrification, 3. Vehicle design and manufacturing, 4. Low-emission alternative energy for transport, 5. Network and traffic management systems, 6. Smart mobility and services, 7. Infrastructure.

To ensure that policy makers can act upon the priorities more effectively, a monitoring and information mechanism is required. Therefore, the EC Joint Research Centre (JRC) has developed the Transport Research and Innovation Monitoring and Information System (TRIMIS) which monitors the STRIA implementation while providing policy and transport stakeholder support through a holistic assessment of technology trends, transport R&I capacities, and to publish information and data on the European transport system (Tsakalidis et al., 2018a). In this context, technologies are identified that can have the greatest impact on decarbonisation, pollutant emissions reduction and thus liveability in an urban context.

This paper focuses on the assessment of technologies relevant to urban transport with a potential impact on the decarbonisation and emissions mitigation. The analysis builds upon data retrieved from the TRIMIS database. The assessment comprises firstly the identification of technologies that could have an application within the urban environment and secondly the assessment of these technologies based on several criteria i.e. type and funding. This assessment allows the identification of technologies that are promising for further development by identifying research gaps within the different funding schemes.

Materials and methodology

The analysis draws on the TRIMIS database, which collects information on publicly funded transport research and innovation projects across Europe (Tsakalidis et al., 2018b). Currently the database contains over 6.500 projects that started between 2000 and 2019.

Projects funded by the European FPs are retrieved through an automated data interchange, while projects funded by Member States (MS) are inserted manually by national contact points. These different approaches make that the coverage of EU-funded projects is strong, while for national projects gaps exist. This paper limits the analysis to EU-funded projects between 2007 and February 2019 due to the gaps identified for MS projects, and because the most recent projects provide the best indication on technologies' state of play.

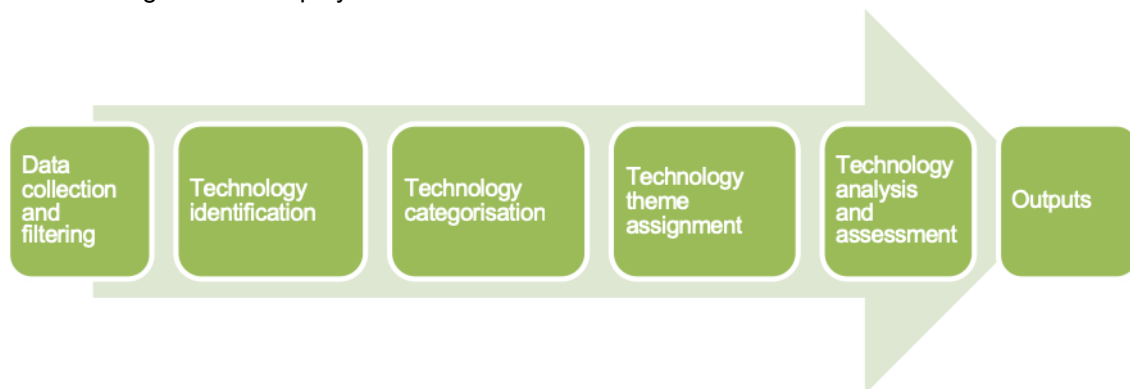


Figure 2. Technology assessment methodological steps.

A total of 1946 projects fall within the scope. Within these projects, a total of 912 technologies were identified, categorised and assigned to 62 technology themes through a Grounded Theory approach (Glaser and Strauss, 1967). The following key steps were taken:

First, the results of a study that identified technologies within European transport research projects (INTEND, 2017) were analysed by three researchers who have complementary experience in the field of transport innovation and individually assessed the technology list. Based on this review, the researchers came up with a standardised approach on what constituted a distinct technology and how to label them.

Following these discussions, all 1946 project descriptions were read and flagged when a technology was mentioned. This filtering exercise was required because EU-funded projects also cover non-technology focused projects like, for instance, those that encourage collaboration between different infrastructure managers. Once a technology was flagged in the project description, another researcher would validate the flagging and write down the technology name.

In a next step, the full list of technologies was evaluated, and the labelling of similar technologies was aligned. The labels were inspired by existing taxonomies, such as those under the Cooperative Patent Classification (CPC, 2019).

When the technology list was established, a number of overarching technology themes were defined. Themes enable a better understanding of how technologies cluster together and which fields of research receive relatively greater interest. An extensive list of themes was created and consequently reduced to the minimum number of themes under which all technologies could still be logically placed. This process led to a total of 62 themes.

In a final step, all projects were assessed on whether they focused on the urban context. If so, the associated technologies and their themes were highlighted. The funds that were associated with each technology were determined by linking them with the total project budget. If multiple technologies were researched in the project, the budget allocated to the technology of interest was determined by dividing the project budget by the number of associated technologies. The limitations of this attribution approach are acknowledged, but is considered to be transparent and appropriate in the absence of technology-budget reports.

Innovation and technologies addressed in the urban context

This section focuses on the technologies addressed in EU-funded research in the urban context. Applying a methodology developed for the creation of a taxonomy for new and emerging transport technologies and trends (Gkoumas and Tsakalidis, 2019), it is possible to assess technologies addressed within European FPs organised in a hierarchic manner. The technology map, which is structured using the hierarchic taxonomy and includes a magnitude of information for each technology, allows different visual representations in the form of tree structures, focusing on desired geographical distributions, performance indicators or other metrics. This process allows the assessment of the status and potential of transport R&I and new and emerging technologies and trends towards a clean and decarbonised urban landscape and, in the future, the assessment of the “technology innovation phase” (Gkoumas et al., 2018), based on TRL levels as identified by the European Commission (2017d).

A first assessment focuses on Horizon 2020 (H2020) projects. By limiting the projects to those related to urban, that corresponds to research with a focus on cities or metropolitan areas, it was possible to identify 22 technology themes (Figure 3). Different visualisations are possible to present the elements of the taxonomy (outer part of the circular section), linked to various attributes that can provide information in a qualitative or quantitative manner. In the specific case, the attributes shown (starting from the outer part of the circular section) are:

- “Total budget” (bars in green colour)
- “Number of projects” (bars in orange colour)

A total of EUR 504 million has been invested in the relevant H2020 projects. As can be seen in the figure, Fuel Cells and Hydrogen technologies are those primary financed within H2020 (in terms of total budget), while, information systems and electric road vehicles are researched in a high number of projects. Some further specifications are reported below for the three technology themes identified, in particular:

- The “Fuel Cells and Hydrogen” technology theme is dominated by five technologies researched within 3 projects. The two dominant projects are the JIVE and JIVE 2 projects (EUR 106,009,000 and EUR 105,987,000, co-funded from the Fuel Cells and Hydrogen Joint Undertaking (FCH JU)) that focus on the promotion of hydrogen fuel cell buses across in Europe. JIVE researches hydrogen refuelling stations and hydrogen production while JIVE 2 involves regions with experience of the technology scaling up fuel cell bus fleets and those seeking to build their knowledge and experience by demonstrating fuel cell buses in small fleets for the first time. The JIVE and JIVE 2 projects together will see the deployment and operation of nearly 300 fuel cell buses in 22 European cities/regions, thus providing a sound basis for further development of this sector.
- The “Information Systems” technology theme includes 29 projects for EUR 103,800,000. Among these, nine are Small Medium Enterprise (SME) instrument phase 1 projects that focus on novel sustainable urban mobility planning schemes. The majority of the remaining H2020 projects focus on novel sustainable urban mobility planning schemes (12 projects) and ICT support systems for multimodality (4 projects). The 3 projects with the highest budget in this theme are demonstration projects, namely:
 - the PORTIS project (EUR 17,678,000) which demonstrates and evaluates integrated sets of sustainable mobility measures in 5 major port cities across Europe;
 - the CIVITAS ECCENTRIC project (EUR 19,307,000) which will demonstrate and test the potential and replicability of integrated and inclusive urban planning approaches; and,

- the CIVITAS DESTINATIONS project (EUR 19,975,000), which will demonstrate and evaluate the effectiveness of innovative sustainable mobility solutions, including shared mobility and e-infrastructures towards zero emissions transport, in 6 tourist cities.

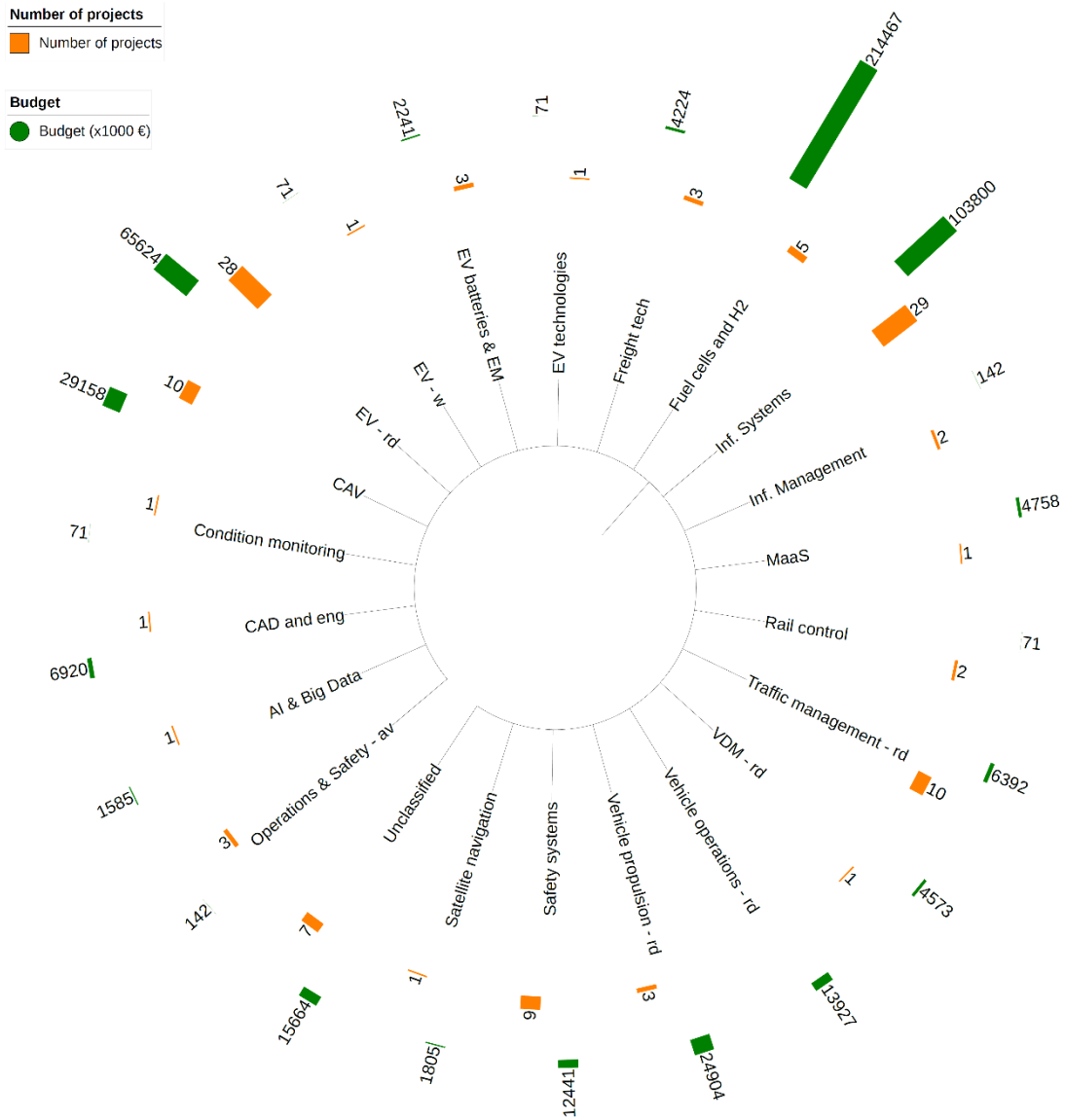


Figure 3. Technology tree for urban transport technologies with an impact on urban road transport emissions mitigation and decarbonisation.

Abbreviations: av: aviation; w: waterborne; rd: road; EV: Electric Vehicles; CAD: Computer Aided Design; AI: Artificial Intelligence; VDM: Vehicle Design and Manufacturing; MaaS: Mobility as a Service; H2: Hydrogen; EM: Energy management

- The “Electric road vehicles” technology theme includes 28 projects for EUR 65,624,000. Among these, 17 are SME instrument phase 1 projects that focus for the most part in public charging infrastructures, retrofitting systems, and electric bikes and buses. The remaining 11 projects focus on different aspects (hybrid bicycles, urban freight vehicles, buses, energy management systems, electric three-wheelers and quadricycles and stackable solutions). The project with the highest budget in this theme is the ASSURED demonstration project (EUR 47,296,000) which focuses on the integration of urban commercial vehicles with fast charging infrastructure.

From the above analyses, a multiplicity of initiatives that cover a broad spectrum of the technology development phases emerges, ranging from early stage SME instrument phase 1 research, which focuses on research and early stage market potential analysis, to large-scale projects, focusing on the demonstration and validation of more mature technologies.

Considerations and conclusions

The possibility to rely on a database of European transport related R&I projects and programmes available in TRIMIS and on specific technology assessment methodologies provides the basis for monitoring the European innovation capacities and supporting the assessment of the transport sector performance and maturity status in a wide range of transport technology areas. Regarding researched technologies that may have an impact on the urban landscape, a first analysis leads to the following conclusions:

- a. There are several large-scale demonstration and implementation projects that focus on more mature technologies. This can concern one technology, or the integration of different individual technologies as a system. Such projects are mainly found within the “Fuel Cells and Hydrogen” theme, and the “Information Systems” theme.
- b. A number of technologies are addressed under the SME instrument scheme. This is especially evident within the “Electric road vehicles” technology theme, and it is an indication that this theme attracts innovators who identify research and market gaps that need to be addressed, or who can come up with possible disruptive ideas that can further contribute to innovation. Thus, this instrument seems particularly useful for innovation in an urban context.

The main technology themes identified above support the decarbonisation and pollutant emissions reduction of transport, with a potential impact on the economy, the environment and the quality of life, especially in the urban context, where the efforts to mitigate negative externalities can have a direct impact on citizens’ life. The themes cover a broad spectrum of development phases, and include both more innovative technologies researched towards their market potential, and large-scale demonstration and validation of more mature technologies. The latter is reflected in the case of hydrogen fuel cell buses demonstration projects. It is expected that when more technologies become mature, demonstration and validation projects will be needed. At this stage, it is difficult to assess the (cost) efficiency of the R&I initiatives in terms of results versus funding or number of projects. This would require – among others - additional indicators on the possible barriers, also beyond technology, and on the actual market uptake.

The analyses are ongoing since the groundwork for the implementation of the assessment methodologies has been laid only recently. More specifically, the researched technologies are expected to be complemented with additional indicators that link the identified technologies and technology themes to technology development phases (from research to invention, demonstration and validation).

The European Commission has set its R&I priorities through STRIA and its seven roadmaps. Alternative fuels, electrification and transport infrastructure are the most relevant ones for the urban environment. Further efforts are required in order to have a more complete coverage of all technology sectors and the technologies that can have an impact on urban transport, its decarbonisation and pollutant emissions abatement. This is the case particularly for the STRIA roadmaps on cooperative, connected and automated transport, network and traffic management systems, and smart mobility and services that are underrepresented in terms of technologies in the urban context. This analysis delivers insights for future funding allocation, which can be rearranged accordingly to promote a more holistic development of R&I in Europe covering all relevant STRIA roadmaps.

Acknowledgements

The views expressed here are purely those of the authors and may not, under any circumstances, be regarded as an official position of the European Commission. The Joint Research Centre is in charge of the development of TRIMIS, and the work has been carried out under the supervision of the Directorate-General for Mobility and Transport (DG MOVE) and the Directorate-General for Research and Innovation (DG RTD) of the European Commission that are co-leading the Strategic Transport Research and Innovation Agenda (STRIA).

References

- CPC, (2019). Cooperative Patent Classification [WWW Document]. Cooperative Patent Classification. URL <https://www.cooperativepatentclassification.org> (accessed 2.26.19).
- European Commission, (2017a). TRIMIS Transport and Research and Innovation Monitoring and Information System [WWW Document]. Europa - TRIMIS Transport Research and Innovation Monitoring and Information System. URL <https://trimis.ec.europa.eu/>
- European Commission, (2017b). Towards clean, competitive and connected mobility: the contribution of Transport Research and Innovation to the Mobility package SWD/2017/0223 final. Brussels.
- European Commission, (2017c). EUROPE ON THE MOVE - An agenda for a socially fair transition towards clean, competitive and connected mobility for all COM/2017/0283 final. Brussels.
- European Commission, (2017d). Horizon 2020 Work Programme 2018-2020 - General Annexes (European Commission Decision C(2017)7124 of 27 October 2017). Brussels.
- European Commission, (2015). Towards an Integrated Strategic Energy Technology (SET) Plan: Accelerating the European Energy System Transformation C/2015/6317 final. Brussels.
- Gkoumas, K., Tsakalidis, A., (2019). A framework for the taxonomy and assessment of new and emerging transport technologies and trends,. Transport 32.
- Gkoumas, K., Tsakalidis, A., van Balen, M., Grosso, M., Haq, G., Ortega Hortelano, A., Pekar, F., (2018). Inventory, modelling and assessment of New and Emerging Technologies and Trends (NETT) in the transport sector: A methodology for the Transport Research and Innovation Monitoring and Information System (TRIMIS). Publications Office of the European Union, Luxembourg. doi:10.2760/552646
- Glaser, B.G., Strauss, A.L., (1967). The Discovery of Grounded Theory: Strategies for Qualitative Research. Aldine Transaction, New Brunswick.
- INTEND, (2017). Home - Intend Project [WWW Document]. INTEND – INtendify future Transport rEsearch NeeDs. URL <https://intend-project.eu> (accessed 2.26.19).
- Tsakalidis, A., Gkoumas, K., Pekar, F., Grosso, M., Haq, G., Marelli, L., (2018a). Towards an integrated European platform for monitoring and analysing transport research and innovation (TRIMIS), in: Proceedings of 7th Transport Research Arena TRA 2018, April 16-19, 2018, Vienna, Austria.
- Tsakalidis, A., Gkoumas, K., Pekar, F., Grosso, M., Haq, G., Marelli, L., (2018b). EU Transport Research & Innovation Status Assessment Report 2017: An overview based on the Transport Research and Innovation Monitoring and Information System (TRIMIS) database. Publications Office of the European Union, Luxembourg. doi:10.2760/331714
- Tsakalidis, A., van Balen, M., Gkoumas, K., Grosso, M., Haq, G., Pekar, F., (2018c). Towards an integrated monitoring and assessment framework for the Strategic Transport Research and Innovation Agenda - Using TRIMIS as a policy support mechanism. Publications Office of the European Union, Luxembourg. doi:10.2760/788905

2.3.10 On-road heavy-duty truck emission factors for black carbon and nitrogen oxides in China

Hui Wang¹, Shaojun Zhang¹ and Ye Wu¹

¹School of Environment, Tsinghua University, Beijing, 100084, China.

Keywords: chasing, heavy-duty trucks, emission factors

Presenting author email: hui-wang17@mails.tsinghua.edu.cn

1. Introduction

Road traffic produces air pollutants in the populous areas, and leads to substantial exposure to harmful pollutant species^{1, 2}. The primary pollutants from traffic exhaust could form substantially secondary pollutants in the atmosphere, thus leading to adverse impacts on public health³⁻⁶. In the past decades, increasingly stringent standards have been implemented to reduce vehicle emissions^{4, 7}. Laboratory measurement by using dynamometer is a fundamental technique in developing these emission standards. Nevertheless, dynamometer tests are criticized by many researchers due to the great lab-to-road discrepancy, i.e., which often provide lower results than real-world emissions^{3, 8}. Notably, real-world NO_x emissions from modern diesel vehicles could exceed the corresponding limits with dynamometer testing in many countries. After the disclosure of Volkswagen emission scandal in 2015, more real-world featured components of emission regulations have developed in many regions of the world. Real-world testing by using portable emission measurement system (PEMS) has been adopted by emissions regulations in the US, Europe and China, and on-road conformity requirements have been applied to control certain key pollutants (e.g., NO_x, particle number)⁹.

However, expensive instrument costs and lengthy set up and operation times of PEMS testing can be major limitations in the implementation, in particular to deliver a fleet-scale surveillance in the future. High emitters, despite of their small amount in the entire fleet, often contribute to a majority of total emissions of pollutants^{10, 11}. This has led to the development of more cost-effective, efficient methods, such as mobile chasing measurements^{11, 12}. The mobile chasing employs a platform, typically a vehicle equipped with rapid response pollutant analysers, to chase targeted vehicles and analyse the temporal fluctuations of plume concentrations. As the fuel-containing carbon dominantly emitted in the form of carbon dioxide (CO₂), fuel-based emission factors of individual vehicles can be estimated based on the concentration ratio of pollutant to CO₂ (i.e., carbon balance). The mobile platform provides more spatial-resolved results compared with stationary measurements. The mobile platform has recently been utilized for more useful functions, such as mapping traffic pollution.

During 2017-2018, we employed the chasing platform in various provincial regions in China (e.g. Beijing, Hebei, Sichuan, Guangdong, Shanxi, Shaanxi, etc.), in which more than one thousand HDTs (Including diesel and natural gas fuels, gross vehicle weight>4.5t) were measured on typical highways (average speeds~60 km/h).

2. On-road measurements

2.1 Description of instrumental setup

Our mobile platform was developed using a gasoline powered minivan, capable of transporting substantial weight and space of fast response instruments. Sampling inlets were mounted on body-front of the vehicle (see Fig1& Fig 2). The inlet lines were positioned above the vehicle boundary layer, and entered the vehicle through the rear window. Particulate-phase air pollutants were sampled using flexible conductive tubing while NO_x was sampled using high density Teflon tubing. Instruments were powered by two 12 volt deep-cycle storage battery/inverters, which could support up to 6 h of continuous instrument operation. Table 1 lists the monitoring instruments employed at the mobile platform. The primary objective of this study is to evaluate the accuracy of NO_x emission factors measured by plume chasing. We employed high-resolution analyzers of NO_x (nCLD66, Eco Physics AG, Switzerland), BC (AE33, Magee Scientific's, Slovenia) and CO₂ (Li-820, LI-Cor®, USA) for the mobile platform, both providing second-by-second measurements. Other on-board instruments include one GPS data logger, and one camera to collect concurrent data regarding vehicle speed, location, and front view video, respectively.



Fig 1. Field measurement

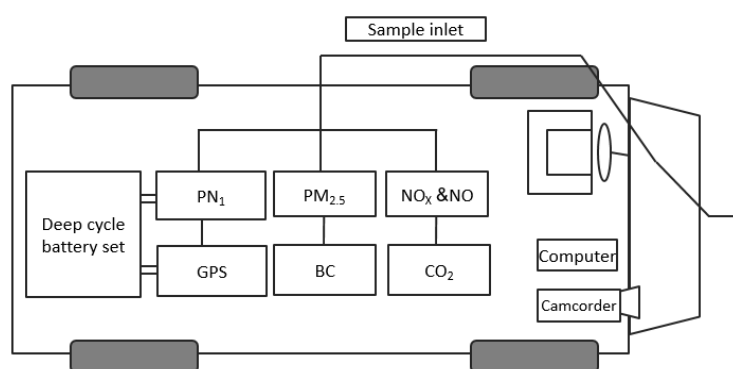


Fig 2. schematic diagram of chasing platform

Table1 The equipment of chasing platform

Pollutant	Measurement analyzer	Maximum range	Resolution	Time resolution	Standard gas concentration
CO ₂	LI-COR's Li-820 (non-dispersive infrared detector, NDIR)	20000 ppmv	<0.01 ppmv	1 s	500ppmv
NO _x	Eco Physics AG's nCLD66 (chemiluminescence detector, CLD)	50000 ppbv	<0.01 ppbv	1 s	2000ppbv
BC	Magee Scientific's AE33 (Light absorption)	100µg /m ³	<0.001 µg /m ³	1 s	/

2.2 On-road experimental procedure

Before each on-road test, the quality assurance processes included flow and zero checks of all instruments, and regular calibration of gaseous pollutant monitoring instruments. For each heavy duty truck, we repeated such chasing procedures to evaluate the emission factor.

1) Measured on-road concentrations of CO₂ and pollutants (NO_x& BC) for approximately 1 min before each chasing test when there were no other vehicles surrounding the mobile platform in order to avoid any interference from nearby vehicles.

2) Moved the mobile platform behind one HDDT. The initial timestamp of chasing started when the distance between the mobile platform and targeted HDDT was within approximately 30 m.

3) Maintained a stable distance between the mobile platform and the HDDT according to the driving speed (i.e., the faster the speed, the further the separation distance). The chasing process lasted for at least 2 mins (typically 2 to 5 mins).

4) Once the chasing duration was sufficient, the mobile platform passed the test HDDT. This moment of passing was marked the ending timestamp of chasing.

5) Conducted 1-min background measurement after completing the chasing, when the mobile platform ran in front of the test HDDT and there were no other surrounding vehicles.

2.3 Data analysis

The approach of calculating emission factors is based on the moving average ratios of [P]/[CO₂] with their road-level backgrounds determined and subtracted. Eq. 1 illustrates the calculation of specific pollutants (NO_x&BC) emission factors based on 10-s moving averages of pollutants to CO₂ concentration ratios.

$$EF_p = a \cdot W_c \cdot \frac{1}{T-9} \cdot \int_{i=1}^{t=T-9} \frac{\int_{t=i}^{t=i+9} ([P]_{mobile\ t} - [P]_{bg})}{\int_{t=i}^{t=i+9} ([CO_2]_{mobile\ t} - [CO_2]_{bg})} \quad (1)$$

where, $[P]_{mobile\ t}$ and $[CO_2]_{mobile\ t}$ are the valid concentration data for chasing measurements at moment t and T is the total valid number of 1-Hz chasing data. $[NO_x]_{bg}$ and $[CO_2]_{bg}$ are the median background concentration for pollutant NO_x and CO₂, respectively. Where, W_c is the carbon mass fraction in the diesel fuels, taken as 0.87 in this study. Where, a is the unit conversion factor, for example it is 46/12 for NO_x.

3. Results and Discussion

During 2017-2018, we employed the chasing platform in various provincial regions in China (e.g. Beijing, Hebei, Sichuan, Guangdong, Shanxi, Shaanxi, etc.), in which more than one thousand HDTs (Including diesel and natural gas fuels, gross vehicle weight > 4.5t) were measured on typical highways (average speeds ~60 km/h).

The preliminary results (partially measured vehicles) showed that Emissions of pollutants from heavy vehicles vary from region to region (see Fig 3). The NO_x emission level of Guangdong province is relatively low, which is superior to other regions. However, the BC emission in GD is higher. NO_x emission factor in the Shanxi province is higher. This may be due to different emission standards and fuel products in different provinces. We need to be more focused on high-emission Trucks.

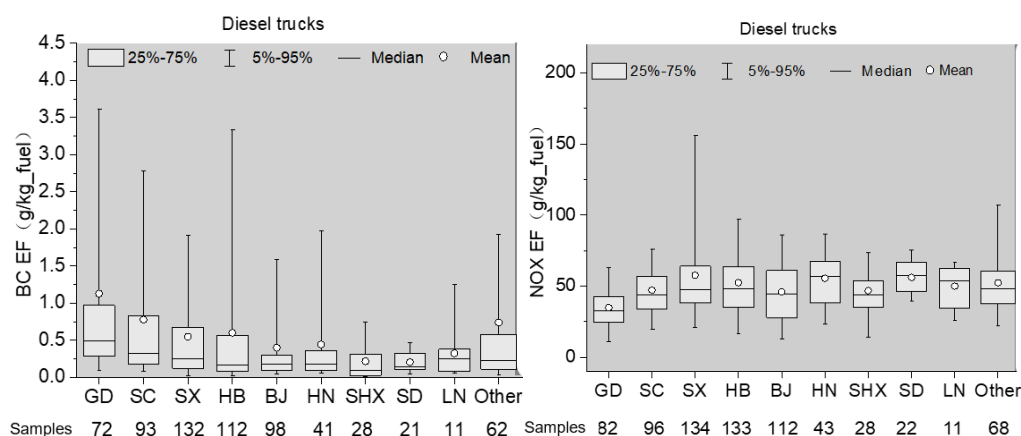


Fig 3. BC and NO_x emission factors of diesel trucks between different regions

Note: GD:Guangdong; SC:Sichuan; SX:Shanxi; HB:Hebei; BJ:Beijing; HN:Henan; SHX:Shaanxi; SD:Shandong; LN:Liaoning; CHN: China; NG truck: Natural gas truck

The plume event-specific average BC and NO_x EFs for HDTs (including 578 diesel trucks and 23 natural gas trucks) is 0.50g/kg_{fuel} and 50.67 g/kg_{fuel}, respectively. Through the license plates of chased

vehicle, we obtain parts of vehicle emission standards and the chasing test results showed that BC emissions are significantly reduced as emission standards become more stringent for heavy-duty diesel trucks (HDDTs). Heavy-duty natural gas trucks (HDNTs) emit significantly lower BC than the diesel engines. While no improvement in fleet-wide NO_x emission factors for China IV diesel trucks (claimed to have adopted selective catalytic reduction (SCR)) and HDNTs compared with China III trucks. Failure to refill urea tank and tampering of SCR are highly suspicious for the unsatisfactory performance of SCR systems.

We also evaluate the emission reduction benefit for phasing out high-emission trucks(see Fig 4& Table 2). If the Chinese government phasing out 10 % high emission HDTs of BC, the total emission of BC will be reduced 51.71%. The emission reduction benefit for phasing out 10% high NO_x emission HDTs will be 22.08%. These findings have highlighted great challenges to control NO_x emissions from modern heavy-duty fleets in China and will be useful to update road emission inventories.

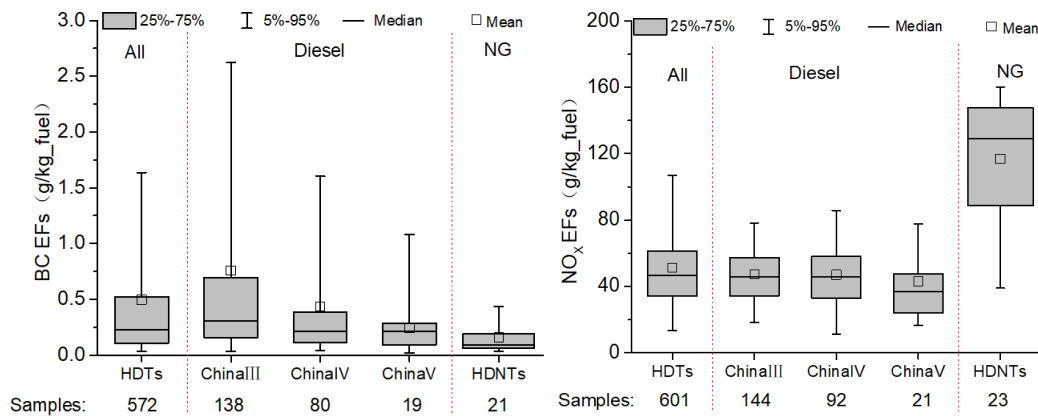


Figure 4. Emission factors of heavy-duty trucks: BC and NO_x

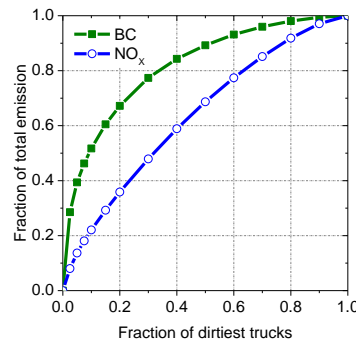


Figure 5: Cumulative distribution of HDTs emission for BC and NO_x

Table 2: Emission reduction benefit for phasing out high-emission trucks

Vehicle type	Fraction of phasing out High-emission trucks	BC emission reduction ratio	NO _x emission reduction ratio
Diesel trucks	20%	68%	35%
	40%	83%	58%

Acknowledgements

This work was sponsored by the National Key Research and Development Program of China (2017YFC0212100)

References

1. Tong, Z.; Baldauf, R. W.; Isakov, V.; Deshmukh, P.; Zhang, K. M., (2016). Roadside vegetation barrier designs to mitigate near-road air pollution impacts, *Science of the Total Environment*, 541, 920-927.
2. Zhang, K. M.; Wexler, A. S.; Zhu, Y. F.; Hinds, W. C.; Sioutas, C., (2004). Evolution of particle number distribution near roadways. Part II: the 'Road-to-Ambient' process, *Atmospheric Environment*, 38, (38), 6655-6665.
3. Anenberg, S. C.; Miller, J.; Minjares, R.; Du, L.; Henze, D. K.; Lacey, F.; Malley, C. S.; Emberson, L.; Franco, V.; Klimont, Z., (2017). Impacts and mitigation of excess diesel-related NO_x emissions in 11 major vehicle markets, *Nature*, 545, (7655), 467.
4. Grange, S. K.; Lewis, A. C.; Moller, S. J.; Carslaw, D. C., (2017). Lower vehicular primary emissions of NO₂ in Europe than assumed in policy projections, *Nature Geoscience* 10, (12), 914.
5. Jiang, B.; Liang, S.; Peng, Z.-R.; Cong, H.; Levy, M.; Cheng, Q.; Wang, T.; Remais, J. V., (2017). Transport and public health in China: the road to a healthy future, *The Lancet* 390, (10104), 1781-1791.
6. Jonson, J. E.; Borken-Kleefeld, J.; Simpson, D.; Nyíri, A.; Posch, M.; Heyes, C., (2017). Impact of excess NO_x emissions from diesel cars on air quality, public health and eutrophication in Europe, *Environmental Research Letters*, 12, (9), 094017.
7. Wu, Y.; Zhang, S.; Hao, J.; Liu, H.; Wu, X.; Hu, J.; Walsh, M. P.; Wallington, T. J.; Zhang, K. M.; Stevanovic, S., (2017). On-road vehicle emissions and their control in China: A review and outlook. *Science of The Total Environment*, 574, 332-349.
8. Wu, Y.; Zhang, S.; Li, M.; Ge, Y.; Shu, J.; Zhou, Y.; Xu, Y.; Hu, J.; Liu, H.; Fu, L., (2012). The challenge to NO_x emission control for heavy-duty diesel vehicles in China, *Atmospheric Chemistry and Physics*. 12, (19), 9365-9379.
9. Giechaskiel, B.; Clairotte, M.; Valverde-Morales, V.; Bonnel, P.; Kregar, Z.; Franco, V.; Dilara, P., (2018). Framework for the assessment of PEMS (Portable Emissions Measurement Systems) uncertainty, *Environmental research*. 166, 251-260.
10. Dallmann, T. R.; Kirchstetter, T. W.; DeMartini, S. J.; Harley, R. A., (2013). Quantifying on-road emissions from gasoline-powered motor vehicles: Accounting for the presence of medium-and heavy-duty diesel trucks, *Environmental science & technology*. 47, (23), 13873-13881.
11. Wang, X.; Westerdahl, D.; Hu, J.; Wu, Y.; Yin, H.; Pan, X.; Zhang, K. M., (2012). On-road diesel vehicle emission factors for nitrogen oxides and black carbon in two Chinese cities, *Atmospheric environment*. 46, 45-55.
12. Ježek, I.; Drinovec, L.; Ferrero, L.; Carriero, M.; Močnik, G., (2015). Determination of car on-road black carbon and particle number emission factors and comparison between mobile and stationary measurements, *Atmospheric Measurement Techniques*. 8, (1), 43-55.

2.4 Energy optimization of transportation systems

This section includes papers presented in the context of the “Energy optimization of transportation systems” session of the TAP conference. Table 5 provides an overview of these papers, as they are listed in the following sub-sections.

Table 5. Titles and authors of “Energy optimization of transportation systems” papers

	Paper Title	Authors
2.4.1	Developing Eco-Driving Strategies Considering City Characteristics	A. Monzon, J.F. Coloma, M. Garcia, Y. Wang, and A. Boggio-Marzet
2.4.2	How automation and connectivity can impact traffic flow and CO2 emissions. A microsimulation study on a highway network.	M. Makridis, K. Mattas, B. Ciuffo and G. Fontaras
2.4.3	Optimization of a bus lane with intermittent priority dynamically activated by the road traffic	A. Kampouri and I. Politis
2.4.4	Well-to-wheel emission factors for future cars in Germany with a focus on fleet composition, new technologies and emissions from energy supplies	S. Seum, S. Ehrenberger and T. Pregger
2.4.5	Has the climate benefited from EU “diesel boom”? - Assessment of CO2-eq emissions from EU’s increasing diesel car fleet	J. Leitão, E. Helmers, U. Tietge and T. Butler
2.4.6	OLYMPUS: An urban emissions model focused on the individual	A. Elessa Etuman and I. Coll

2.4.1 Developing Eco-Driving Strategies Considering City Characteristics

A. Monzon^{1*}, J.F. Coloma², M. Garcia², Y. Wang¹, A. Boggio-Marzet¹

Professor, andres.monzon@upm.es

¹Transport Research Centre, Universidad Politécnica de Madrid, Madrid, 28040, Spain.

²Betancourt Research Group. Department of Construction, Universidad de Extremadura, Caceres, 10003, Spain.

1. Introduction

One of the challenges of the developed societies is to foster low carbon mobility models, looking at social equity and fair distribution of wealth criteria. It is, in short, the challenge of sustainability. For this reason, sustainable mobility means ensuring that our transport systems respond to economic, social and environmental needs, minimizing their negative repercussions (Government of Spain, 2010).

In 2017, the transport sector contribution to EU-28 greenhouse gas emissions was 28.5 % of total. Emissions from transport in 2016 were 26 % above 1990 levels despite a decline between 2008 and 2013 (EEA, 2018a). Emissions need to fall by around two thirds by 2050, compared with 1990 levels, in order to meet the long-term 60 % greenhouse gas emission reduction target as set out in the 2011 Transport White Paper (EC, 2011). Achieving the 2030 targets will require new and expanded policies and approaches to energy efficiency in the Member States that can keep their energy consumption in check (EEA, 2018b).

Countries may act in several key areas in order to reduce transport sector GHG emissions. A comprehensive transport-sector GHG reduction strategy should at least address the following four areas:

- 1) Reducing the demand for transport: control of land uses to avoid car dependency, increasing load factors and balancing modes in mobility patterns.
- 2) Mode share: measures facilitating less GHG intensive modes such as public transport and non-motorised modes.
- 3) Fuel choice: measures aiming to use of technologies for alternative fuels and new energy sources different than petrol.
- 4) Fuel efficiency: foster efficient technologies for vehicles and traffic management, traffic congestion abatement measures and eco-driving (OECD, 2008).

In this context, eco-driving emerges as an operational decision of drivers to maximize fuel efficiency and, consequently, reduce GHG emissions (Sivak and Schoettle, 2012). The literature shows that the efficiency of eco-driving varies widely depending on the external circumstances and learning methods (Huang et al., 2018). The reduction of CO₂ emissions before and after receiving eco-driving instruction in several field trials varies from 10% to 0.5% depending on the road type, i.e., highways or urban roads (Alam and McNabola, 2014). Traffic flows and road slope as external factors have direct influence on eco-driving efficiency (Wang and Boggio-Marzet, 2018). Therefore, eco-drivers should adopt specific strategies according to different cities context and distinct road conditions and traffic volumes.

Most of the investigations done so far focus on measuring very specific impact of particular type of cars and rad. But the results from this specific case study approach are very difficult to generalize and transfer to other urban contexts.

This paper presents a research aiming to compare the impacts produced by adopting eco-driving in different cities, type of vehicles, road segments and drivers features. It intends to deepen understanding of the influence of city size and driving characteristics on the effectiveness of eco-driving. Therefore, the aim of the research is to compare the general changes in fuel consumption, CO₂ emissions and driving patterns in terms of city and road type in order to develop specific eco-driving strategies.

The field trials have been conducted in two Spanish cities (Madrid and Caceres), which in the central and the west part of the Country. 24 drivers of both gender, with different year of driving experience, drove two different fuel type of vehicles- gasoline and diesel- along roads of different characteristics at

various time periods during one month. During the experiment, drivers attended an eco-driving course. Thus, it enables to compare the impacts of eco-driving before and after the training for two cities.

After this introductory section, Section 2 presents the methodology for testing the impacts of eco-driving in both cities Madrid and Caceres. Section 3 analyses the results and compares them with previous studies. The final part includes the main conclusions and possible policy recommendations based on these results.

2. Methodology

In order to develop specific eco-driving strategies considering cities' characteristics, this paper evaluates eco-driving short-term impacts of a training programme on fuel savings and reduction of CO₂ emissions in two different cities. The methodological framework is shown in Figure 1.

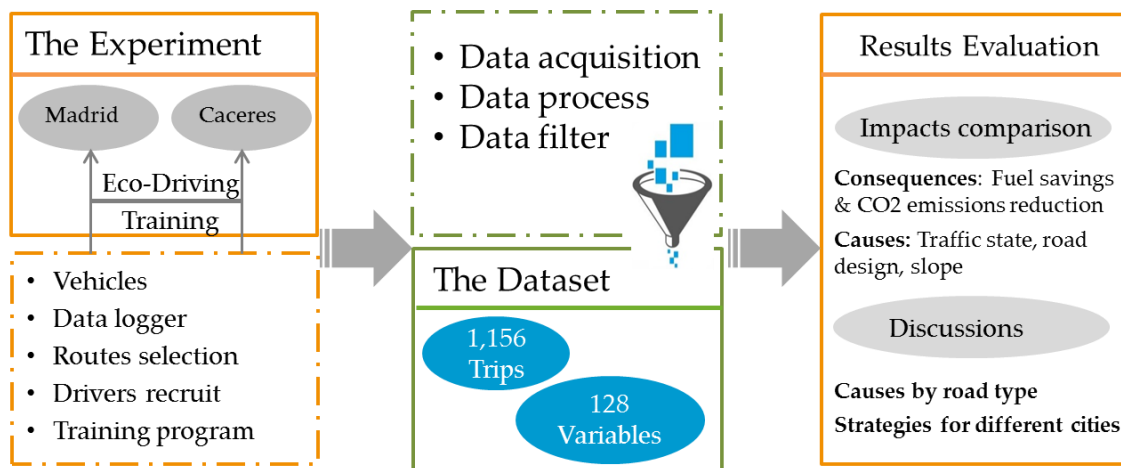


Figure 1: Research Framework.

The research is based in real life experiments, and the methodology consists of three steps: data acquisition, dataset creation through data processing and filtering, analysis of results by evaluating impacts before and after eco-driving training.

Firstly, two eco-driving case studies were carried out in parallel in two Spanish cities (Madrid and Caceres). Madrid is the capital city of Spain and has a population of 6.5 million inhabitants and a land area of 8,030 km², while Caceres is a relatively small city with 95,000 inhabitants covering an area of 30 km². As a consequence, the cities have very different road characteristics and traffic flows. The experiment consisted of 4 field trials, two in each city, two without and two with eco-driving. 24 drivers were performing the trials following pre-established routes composed by different road sections, according to infrastructure capacity and traffic conditions. The trial took place in April-May 2017 with two vehicles: a diesel-fuelled Opel Astra and a petrol-fuelled Fiat 500. The test was first performed with drivers driving normally along pre-established itineraries. Then, after drivers attended an eco-driving training, a second set of car-runs following the same itineraries of the first driving period.

Data were recorded second by second through an on-board logging device (OBD-Key) (KBM Systems Ltd., London, UK), preinstalled in each vehicle. Through this, we have been able to know the instantaneous value of GPS position of the vehicles and instantaneous values of several driving patterns during the whole test (i.e. instantaneous speed, acceleration, deceleration, engine speed.). Once collected all data recorded, the VSP-Vehicle specific power model has been applied to estimate the instantaneous fuel consumption of each vehicle (more details in part 2.4). Then, data have been processed and statistical values of them have been calculated through the software R. Through the same software and Google Geo, we were able to split each itinerary covered, into road sectors with homogeneous road section. In this terms, we could later perform the analysis of results depending on road type (Table 1, Table 3)

Thus, after the data cleaning and the data process, the sample is composed by 1,156 trips, corresponding to 8,140 km (5,959 km in period 1 and 5,232 km in period 2), each one characterized second by second by 128 different variables.

Finally, the results evaluation has been focused on the impact of eco-driving in terms of changes in fuel consumption and CO₂ emissions between Period 2 (after eco-driving training) and Period 1 (before training). Results are presented in the next section 3.

Ten different routes were selected -six for Madrid and four for Caceres- to cover different traffic and infrastructure conditions: moderate or steep slopes and congested or fluid traffic flows. Figure 2 shows the location of the field trials in both cities of Madrid and Caceres.

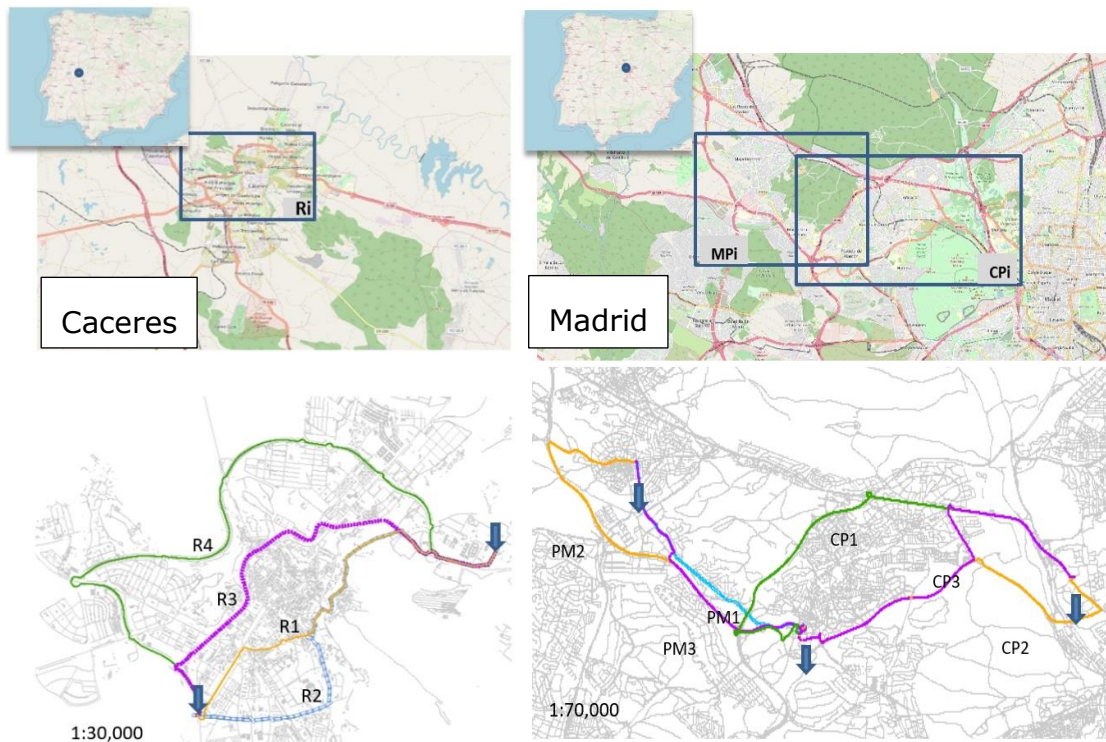


Figure 2: Monitored itineraries in the data collection campaign in Madrid and Caceres.

Roads with common characteristics are used both in Madrid and Caceres for the sake of comparative analysis. They correspond to three different road typologies: *local street*, *urban collector* and *major arterial*. The results obtained for these types of routes serve to compare the efficiency of eco-driving in both cities. Table 1 includes the main characteristics of these roads.

Table 1: Information on the common circulation routes in both cities

Road Type	Lanes	Speed Limit (km/h)
Local street	1 x 1	50
Urban collector	2 x 2 separated by barrier. Parking both sides	30/50
Major arterial	2 x 2 separated by barrier	50/80

2.1 Case study of Caceres

The city of Caceres is quite small and can be crossed from side by side in less than 15 min. Four alternative routes with different Level of Service (LOS) (U.S. Department of Transportation, 2013) were chosen to cross the city following itineraries with different characteristics and traffic volumes. They can be ordered in terms of their increasing LOS (from lowest to highest), as follows:

Route 1 (local road) runs along urban streets and passes right through the heart of Caceres city centre. It is 6.1 km long, and its travel time is around 15 min. This route has a dual carriageway with a median. Speed is limited to 50 km/h. It is regulated by traffic lights and suffers some congestion problems at peak hours.

Route 2 (urban collector road) is 6.7 km long and its travel time is about 14 min. It is one of the most important avenues in Caceres as it provides access to the bus station, conference centre, sports arena, mortuary, and hospital, leading to some traffic delays. It also has a dual carriageway with a median, but due to its urban character, the speed limit is 50 km/h and 30 km/h in several sections.

Route 3 (perimeter road) is the old bypass road, which is already integrated in the urban network. It also has a two-lane dual carriageway and a median or is demarcated by a continuous double line. The speed limit is 50 km/h. It has a length of 6.7 km and a travel time of about 13 min. It has almost no congestion.

Route 4 (Major arterial road) follows the outer city bypass. It has a length of 10.3 km and can be travelled in about 12 min. It is the longest and quickest route. It runs through the north of the city with a two-lane dual carriageway with a median. Intersections are in the form of roundabouts and pedestrian crossings regulated by traffic lights. Speed limits vary between 80 km/h and 40 km/h. Traffic is usually fluid all day.

2.2 Madrid Case Study

Two itineraries, located in the Northwest of Madrid with different road sections and alignments, were selected to guarantee a variety of driving performances and traffic characteristics in the sample. The two itineraries have a moderate slope and connect the Madrid city centre with two municipalities in the Madrid Region (Pozuelo and Majadahonda), where 92% of daily trips are made by car (Wang and Monzon, 2016).

The itineraries cover the main road types with different functionalities, including highway, major arterial road, urban collector road, and local road. With reference to the image above, (Fig. 2), itinerary CPi (Centre to Pozuelo, both directions) contains three parallel routes (i.e., CP1, CP2, and CP3) consisting of mixed highways with different levels of service. Itinerary MPi (Majadahonda to Pozuelo, both directions) also has three routes (i.e., MP1, MP2, and MP3) that combine highway with typical urban arterial roads to the suburbs, and contain several roundabouts and pedestrian crossings.

2.3 Driver Selection, Scheduling, and Eco-Driving Training

Twenty-four drivers (twelve in each city) of different sex were recruited in a wide range of ages (Mean = 30.15) and driving experience (Mean = 10.30). All of them participated in an eco-driving training in the middle of the experiment, so they could deploy these techniques during the second driving period and we could compare the results obtained with the first one.

An analysis of key performance indicators (KPI) was used to assess drivers' performance before and after the course, its relation with fuel consumption, and the ways to incentivize better performance for top decision managers.

During the driving test, six people were assigned to each vehicle, with two people taking turns to drive (driver and assistant, changing every hour) who iteratively performed trips along the selected routes. Each couple of drivers covered a driving shift and drove 4 hours a day; each day there were three different driving shift. Thus, each vehicle has been driven 12 h a day to obtain enough data on the different traffic situations (free circulation, moderate traffic, and congestion) and weather conditions (rain, fog, etc.).

2.4 Fuel consumption and emissions calculation

The value related to fuel consumption was calculated based on the VSP-Vehicle Specific Power model, which is a convenient single measure that represents road load on a vehicle, being an accredited methodology to characterize vehicles and driving profiles using real-world data (Coelho et al., 2009). Informally, it represents the ratio between the power demand of the vehicle and its mass. Knowing the instantaneous speed, acceleration and road slope, this model provides the instantaneous power demand of the vehicle according to the following formula, developed by Jimenez-Palacio in 1999.

$$\begin{aligned} \text{VSP} \left[\frac{\text{W}}{\text{kg}} \right] &= \frac{\text{Power}}{\text{Mass}} = \frac{\frac{d}{dt} (E_{\text{kinetic}} + E_{\text{potential}}) + F_{\text{rolling}} * v - F_{\text{aerodynamic}} * v}{m} = \\ &= v(1.1 * a + 9.81 * \text{grade} + 0.132) + 3.02 * 10^{-4} * v \end{aligned}$$

in which: E_{kinetic} is the kinetic energy; $E_{\text{potential}}$ is the potential energy; F_{rolling} is the rolling resistance force; $F_{\text{aerodynamic}}$ is the aerodynamic resistance force; v is the instantaneous speed (m/s); m is the mass (kg); a is the acceleration (m/s²); grade is the road grade (m/m).

Then, each second of driving has been associated to a VSP mode, each one related to a certain value of fuel consumption, according to Faria et al. (2017) it's possible to correlate every mode with fuel consumption and emissions by using the following table (Faria et al., 2017).

The value related to CO₂ emissions was converted from the value of fuel consumption using the emission factor (equal to 3.169 for both diesel and gasoline) extracted from the "Air Pollutant Emission Inventory Guidebook 2016" (EEA, 2016) for petrol and diesel light vehicles.

2.5 Impacts comparison method

The evaluation of the impact of eco-driving focuses on changes in fuel consumption and CO₂ emissions between Period 2 (after eco-driving training) and Period 1 (before training).

Effects of the training programme in terms of the type of vehicles, drivers and road type in both cities are firstly checked. Through a multiple regression analysis (Coloma et al., 2018), we concluded that, RPM, negative and positive acceleration and speed are closely associated with the fuel consumption throughout the trip. An additional variable related to traffic conditions (95th percentile of recorded speed) is also analysed in order to understand the influence of traffic on eco-driving efficiency. Table 2 presents an overview of the selected parameters, their units, and the corresponding abbreviations

Table 2: Description of the parameters selected for measuring eco-driving impacts

Parameter Type	Description	Code	Unit
Fuel consumption and emissions	Average fuel consumption	avg_fc	l/s
	Average CO ₂ emissions	avg_CO ₂	g/km
Driving performance	Average speed	avg_speed	km/h
	Average RPM	avg_rpm	rpm
	time with acceleration more than 0.83 m/s ^s	Pacc_3	s
	time with deceleration less than -0.83 m/s ^s	Pdec_3	s
traffic intensity	95 th percentile of instant recorded speed	V ₉₅	km/h

The analysis is extended then by exploring the changes in the value of the parameters in the different scenarios: specific road types with similar characteristics in both cities. These results will show the influence of the size of a city on the efficiency of eco-driving, considering not only the savings in fuel consumption and CO₂ emissions, but also the changes achieved in the driving behaviour through eco-driving.

3. Analysis of Results

This section presents the impacts of eco-driving training. First it explores the overall impacts of eco-driving training regardless the city, along with the changes in driving performance. Then, it shows the specific impacts according to the three road types selected in Madrid and Caceres to investigate the combined influence of city size and eco-driving in the different situations of the test trials.

The performance features of the driving tests in both cities aggregated are shown in Table 3, along with the experimental statistics of distances driven by route and each vehicle.

Table 3: km-driven per vehicle, road type and test period.

Road type	Non eco-driving (period 1) (trips/km)				Eco-driving (period 2) (trips/km)			
	Astra (diesel)	Fiat (gasoline)	Total trips	Total km	Astra (diesel)	Fiat (gasoline)	Total trips	Total km
Local street	467	539	1006	1035	499	480	979	985
Urban collector	114	168	282	394	126	150	276	395
Major arterial	212	241	453	1,208	241	225	439	1,096

3.1 Overall Impacts of Eco-Driving (after training course)

Figure 3 shows the reduction (%) of the different driving parameters analysed due to eco-driving in the three types of road common to the cities of Madrid and Caceres.

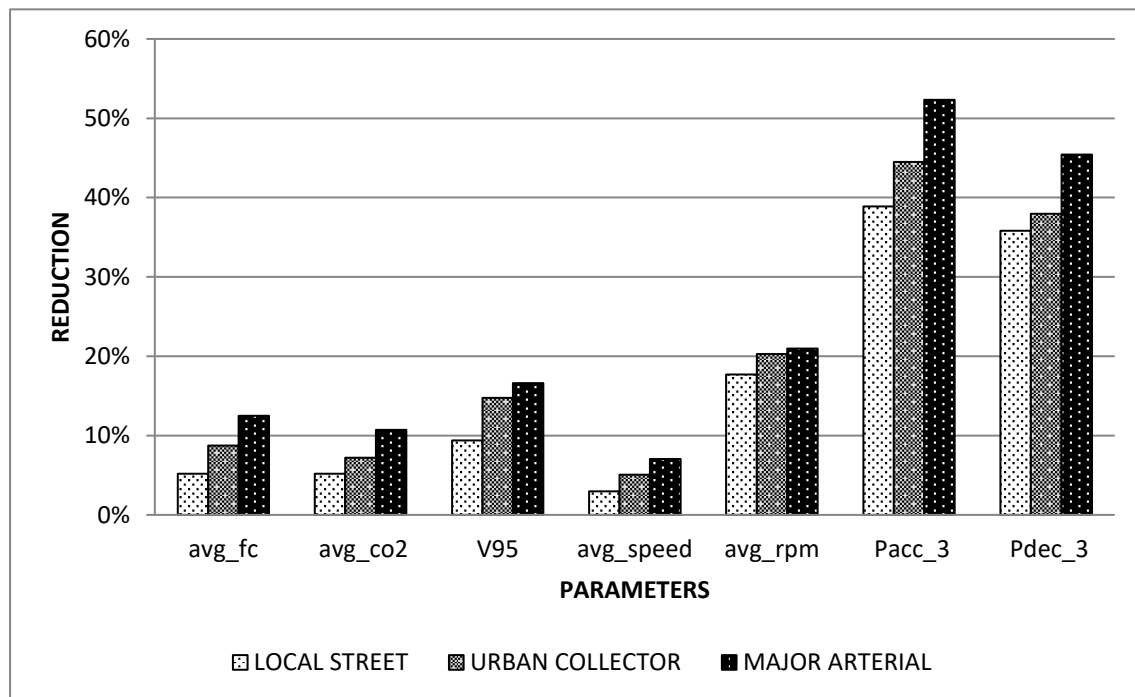


Figure 3: Eco-driving impact on traffic and emissions parameters

Fuel consumption and CO₂ emissions are always reduced with the eco-driving, with higher savings on the roads with the highest LOS (major arterial) and lower on the lower level (local street). The savings values are between 5% and 12%, being consistent with other studies values (Johansson, 1999; Andrieu and Saint Pierre, 2012).

The eco-driving produces important reductions in all the driving parameters analyzed in this research. The greatest savings are again linked to the best level of service, being "major arterial" which provides the most reduction value and "local street" the least.

Accelerations and decelerations are the parameters that produce the greatest reductions in their values (36-52%) while the average speeds are those that reduce their value less with the eco-driving (3-7%).

3.2 Impacts of Eco-driving according to city and road type.

3.2.1 Fuel Consumption and emissions

Figures 4 and 5 show the reduction in fuel consumption and CO₂ emissions produced by eco-driving in the two cities and for the three types of roads studied.

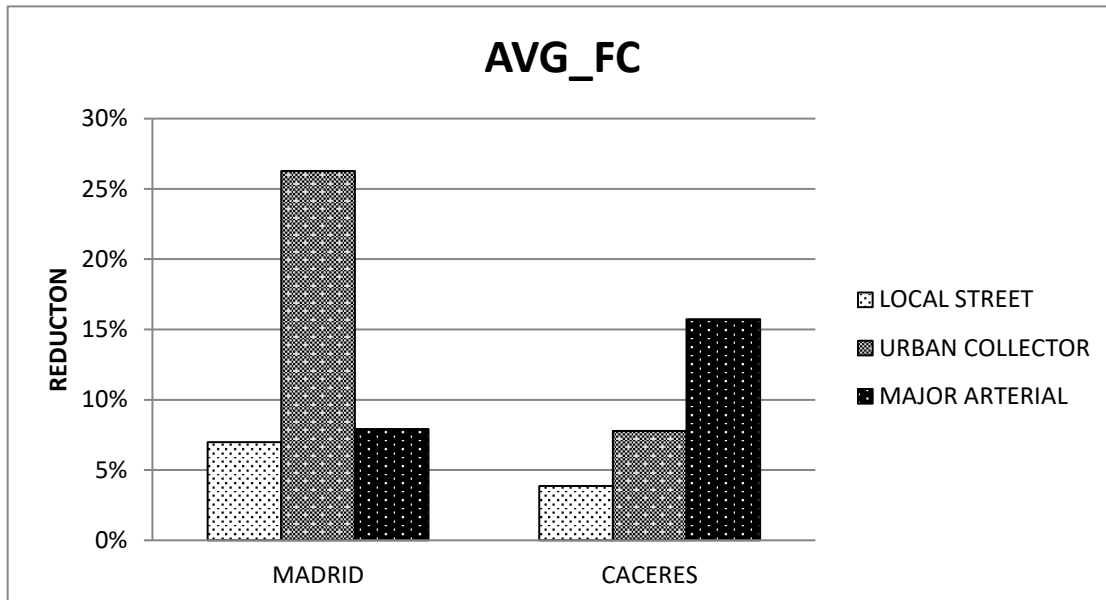


Figure 4: Average fuel consumption.

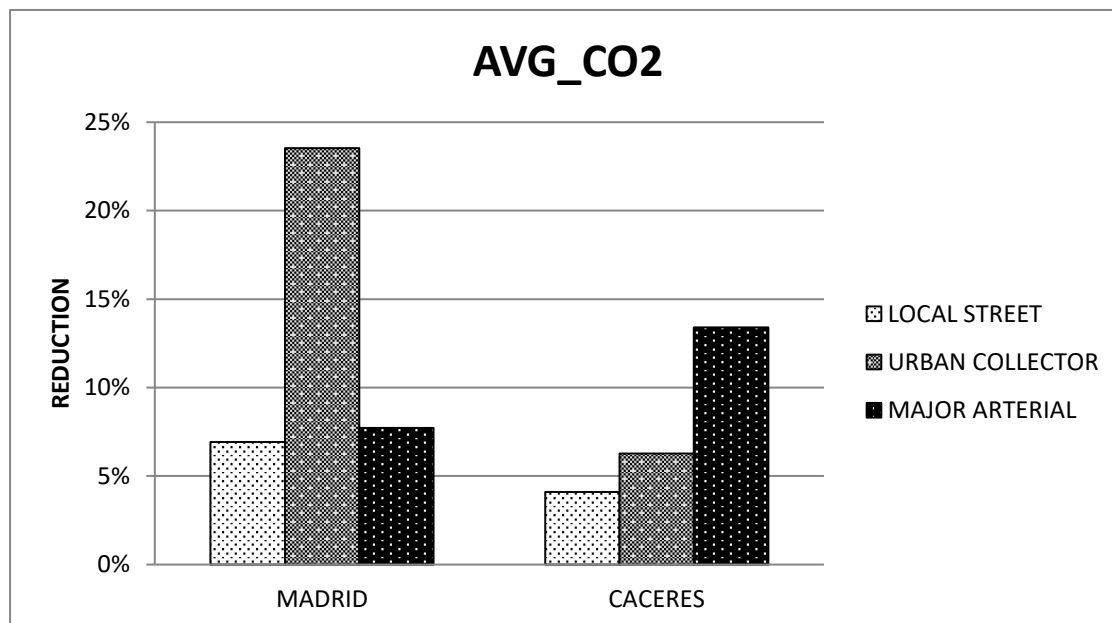


Figure 5: Average CO₂ emissions.

Caceres shows reductions in consumption and CO₂ emissions for all road types, increasing the savings with the LOS. In Madrid the result is more dispersed. Local street produces less savings, comparing with urban collector and major arterial. As known, in Madrid these type of streets is frequently congested, this suggests that eco-driving is not effective in traffic jams (congestion). This type of negative effects on saturated roads have been obtained in other studies carried out in Madrid (García-Castro and Monzon, 2014). On the other hand, the effect of duplicating a lane of circulation (urban

collectors) is very favourable in fuel consumption and CO₂ emissions for the urban collector, also observing a positive effect in the major arterial.

3.2.2 Impact on driving performance

Figures 6, 7, and 8 show respectively, the reduction that the eco-driving produces on the parameters average speed, average rpm, accelerations and decelerations, which are the parameters with the greatest influence on fuel consumption.

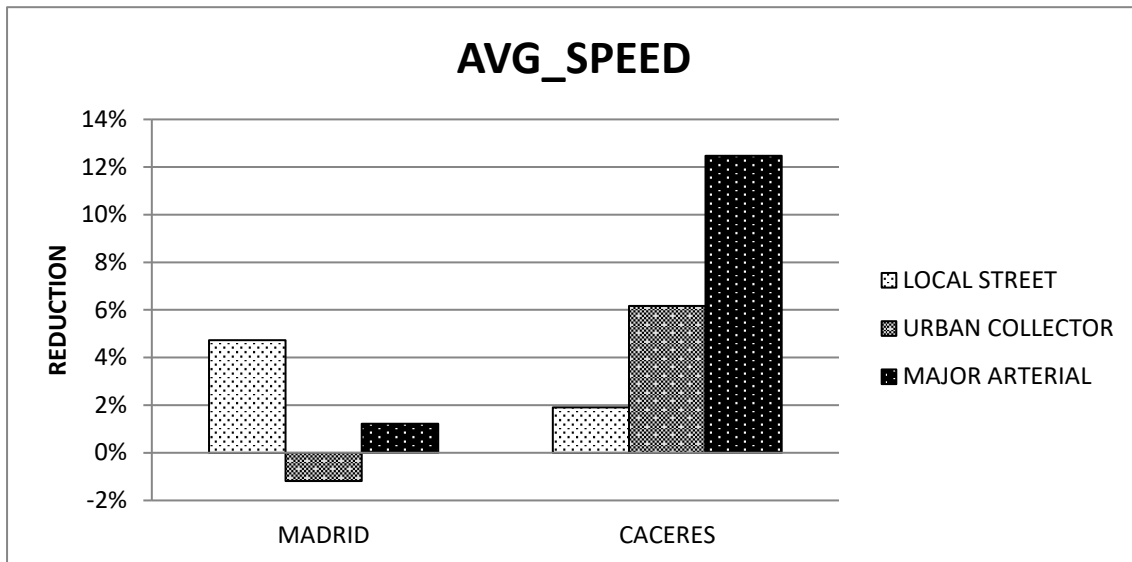


Figure 6: Changes on average speed.

The eco-driving reduces the average speed of circulation in general in all types of road. These values are much higher in the Caceres roads than Madrid, since they suffer to a lesser extent, the effects of traffic congestion.

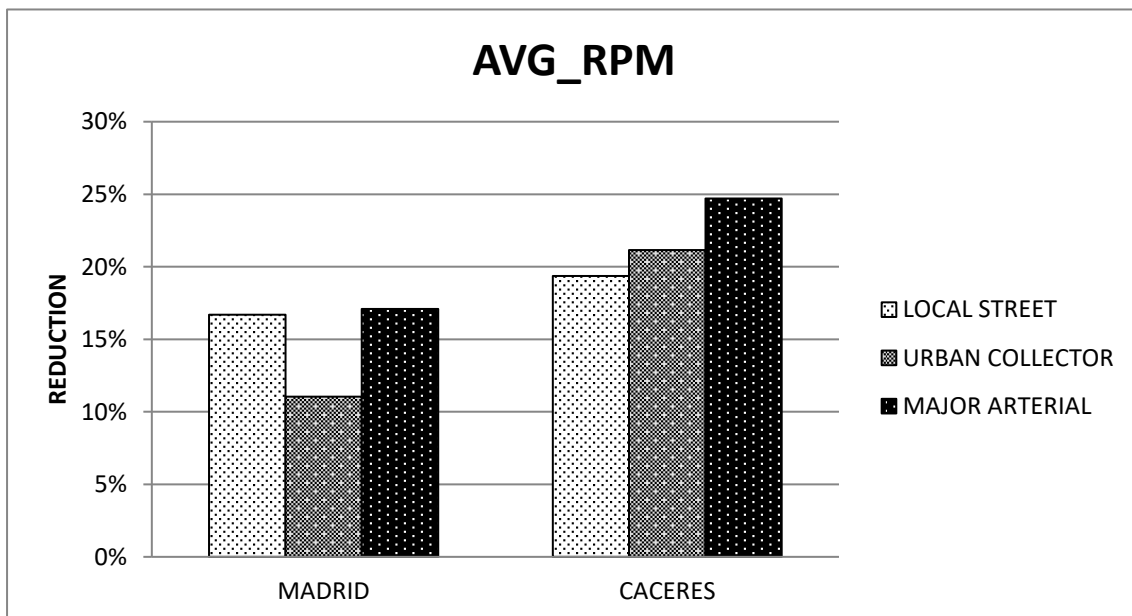


Figure 7: Changes on average RPM.

RPMs are reduced in both cities and for all types of roads with eco-driving. The reduction is also greater in the less congested city

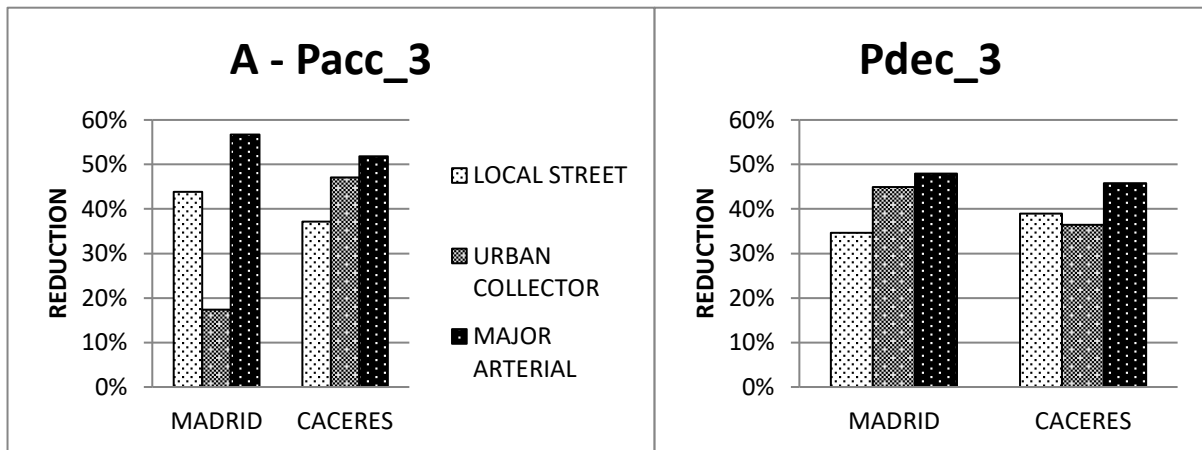


Figure 8: Reduction of time in accelerations and deceleration higher than 0.83 m/s^2 .

Eco-driving produces smoother driving that is reflected with the accelerations and decelerations that take place. In all type of road and for both cities, important reductions are produced with the savings being proportional to the LOS.

3.2.3 Impacts on traffic intensity

Figure 9 shows the reductions produced in the V_{95} with the eco-driving.

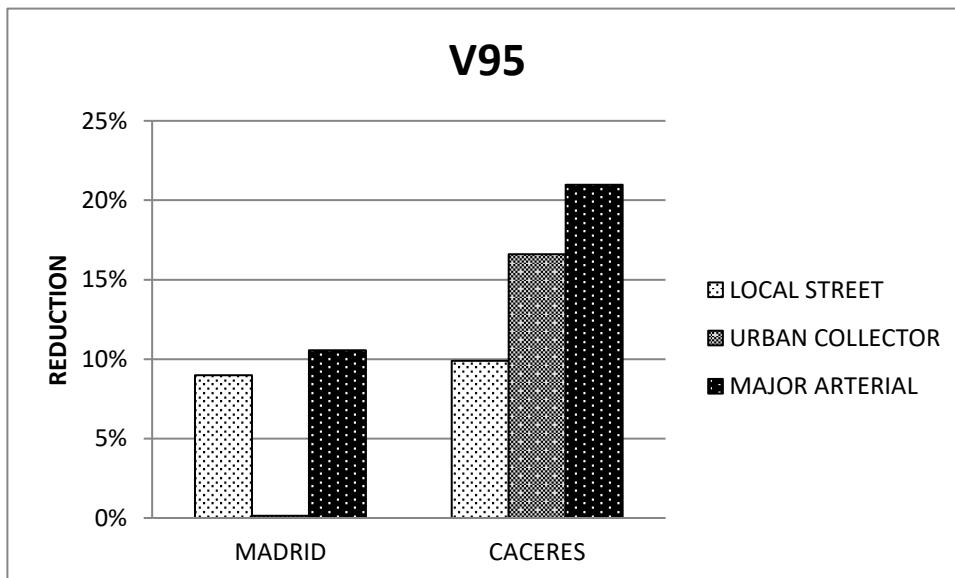


Figure 9: Speed reduction for V_{95} .

A generalized reduction of the V_{95} speed is observed for both cities, which increases with the LOS, except for urban collector that in Madrid remains constant. In our research, for each type of homogeneous road section, the 95^o percentile of the speed distribution is assumed as free flow speed characterizing the sector. Thus, results indicate that eco-driving reduces traffic speeds, being greater these reductions in the roads with higher level of service.

4. Conclusions and Policy Recommendations

4.1 Main findings

This research studies the effects of eco-driving on fuel consumption, CO₂ emissions and driving parameters in two very different cities of Spain, Madrid and Cáceres.

The results obtained show that eco-driving techniques are very effective in reducing fuel consumption and CO₂ emissions, both in large congested cities and in small cities. The savings values achieved in both cities are in a range of 5% and 12%. This efficiency grows with the road LOS and decreases with the size of the city, being the small cities not congested, the most effective in the application of these techniques. On low LOS roads, which are usually congested, the efficiency of eco-driving decreases and can even produce more congestion and increase fuel consumption.

The effectiveness of eco-driving in a large and congested city like Madrid is different. Eco-driving techniques have been found to be inefficient on local streets with one lane. However, these same roads, when the lane is duplicated (urban collector), improve the reduction of consumption and emissions. Finally, the effects of saving fuel on higher LOS roads (major arterial), are similar to those obtained in a small city such as Cáceres.

4.2 Policy recommendations

For small and non-congested cities like the city of Cáceres, it is recommended to apply the eco-driving techniques in any type of road, being more efficient the savings of fuel consumption and CO₂ emissions in roads with higher LOS.

For large cities like Madrid, it is recommended to duplicate lanes whenever it's possible, since this measure improves the LOS of the road and the efficiency in the application of eco-driving techniques. As in small cities, also in Madrid the major arterials result to be the perfect roads to perform eco-driving.

Therefore, Public Administration should encourage the use of these techniques and train the drivers from the driving schools.

4.3 Future developments

In future investigations it would be advisable to measure if the results of this study could vary when the number of eco-drivers increase. The benefits of one single eco-driver appear to be relevant for both type of cities. However, it is dubious how the impacts could change with high percentage of cars making eco-driving in the three type of road sections and city categories. If the traffic density could change as to have impact on the emissions, and which one.

Acknowledgements

This work was supported in part by the national R & D programme (Ministerio de Economía y Competitividad) under the Eco-Traffic Project "Medición y Modelización de Eco-Driving táctico y operacional". Ref TRA2016-76485-R. The authors also acknowledge the collaboration of the City of Cáceres in the data collection process

References

- Alam, M.S.; McNabola, A. (2014). A critical review and assessment of Eco-Driving policy & technology: Benefits & limitations. *Transport Policy*, 35, 42–49.
- Andrieu, C., Saint Pierre, G. (2012). Comparing effects of eco-driving training and simple advices on driving behavior. *Procedia-Social and Behavioral Sciences*, 54, 211-220.
- Coelho, M.C.; Frey, H.C.; Roupail, N.M.; Zhai, H.; Pelkmans, L. (2009). Assessing methods for comparing emissions from gasoline and diesel light-duty vehicles based on microscale measurements. *Transportation Research Part D: Transport and Environment*, 14, 91–99.
- Coloma, J. F., García, M., Wang, Y. (2018). Eco-Driving effects depending on the travelled road. Correlation between fuel consumption parameters. *Transportation Research Procedia*, 33, 259-266.

- EC, European Commission. (2011). White Paper on transport. Available online: https://ec.europa.eu/transport/sites/transport/files/themes/strategies/doc/2011_white_paper/white-paper-illustrated-brochure_en.pdf (accessed on 15 February 2019).
- EEA, European Environment Agency. (2016). Air Pollutant Emission Inventory Guidebook 2016. Available online: <https://www.eea.europa.eu/publications/emep-eea-guidebook-2016> (accessed on 15 February 2019).
- EEA, European Environment Agency. (2018a). Greenhouse gas emissions from transport. Available online: <https://www.eea.europa.eu/data-and-maps/indicators/transport-emissions-of-greenhouse-gases/transport-emissions-of-greenhouse-gases-11> (accessed on 15 February 2019).
- EEA, European Environment Agency. (2018b). Trends and projections in Europe 2018. DOI: 10.2800/931891
- Faria, M.; Farias, T.; Baptista, P. (2017). Driving behavior patterns: Impacts on emissions and safety performance. In Proceedings of the NECTAR 2017 International Conference, Madrid, Spain, 31 May–2 June 2017.
- Garcia-Castro, A.; Monzon, A. (2014). Using floating car data to analyse the effects of its measures and eco-driving. *Sensors*, 14, 21358–21374.
- Government of Spain. (2010). Estrategia Española de movilidad sostenible. Ministerio de Fomento y Ministerio de Medio Ambiente y Medio Rural y Marino. Available online: <https://www.fomento.es/estrategia-espan%CC%83ola-de-movilidad-sostenible> (accessed on 15 February 2019).
- Huang, Y.; Ng, E.C.Y.; Zhou, J.L.; Surawski, N.C.; Chan, E.F.C.; Hong, G (2018). Eco-driving technology for sustainable road transport: A review. *Renewable and Sustainable Energy Reviews*, 93, 596–609.
- Jimenez-Palacios. (1998). Understanding and Quantifying Motor Vehicle Emissions with Vehicle Specific Power and TILDAS Remote Sensing. Ph.D. Thesis, Massachusetts Institute of Technology, Department of Mechanical Engineering, Cambridge, MA, USA.
- Johansson, H. (1999). Impact of Ecodriving on Emissions and Fuel Consumption: A Pre-Study; Swedish National Road Administration: Borlange, Sweden.
- OECD, Organisation for Economic Co-operation and Development and International Transport Forum Working Group. (2008). Greenhouse Gas Reduction Strategies in the Transport Sector. Available online: <https://www.itf-oecd.org/sites/default/files/docs/10ghgtrends.pdf> (accessed on 15 February 2019).
- Sivak, M., Schoettle, B. (2012). Eco-driving: Strategic, tactical, and operational decisions of the driver that influence vehicle fuel economy. *Transport Policy*, 22, 96-99.
- U.S. Department of Transportation. (2013). Highway Functional Classification: Concepts, Criteria and Procedure. Available online: https://www.fhwa.dot.gov/planning/processes/statewide/related/highway_functional_classifications/fcauab.pdf (accessed on 15 February 2019).
- Wang, Y., Monzon, A. (2016). Economic crisis and its influences on the interaction between land use and transport in Madrid Region. *Transportation Research Procedia*, 18, 100–107.
- Wang, Y., Boggio-Marzet, A. (2018). Evaluation of Eco-Driving Training for Fuel Efficiency and Emissions Reduction According to Road Type. *Sustainability*, 10(11), 3891.

2.4.2 How automation and connectivity can impact traffic flow and CO₂ emissions. A microsimulation study on a highway network.

M. Makridis^{1}, K. Mattas², B. Ciuffo and G. Fontaras*

¹European Commission Joint Research Centre, Sustainable Transport Unit, 21027 Ispra, Italy, michail.makridis@ec.europa.eu

Abstract

The interest on the impact of automation and connectivity in future transport networks is very high both from a research and a policy perspective. Results in the literature show that many of the anticipated advantages of connected/automated vehicles on congestion and energy consumption are questionable. Many studies focus on microsimulation in order to provide quantitative and qualitative answers to the above questions. However, the car-following models used do not consider vehicle dynamics, and the estimation of emissions is based on average-speed models. This work presents the results of a microsimulation study over a highway network, based on a set of 8 scenarios. The work simulates different vehicle technologies that generate different driving behaviours with and without the simulation of vehicle dynamics. The status of the network is assessed in terms of flow and speed. Furthermore, emissions are estimated for all scenarios using both the average-speed EMEP/EEA fuel consumption factors and a generic version of the CO₂MPAS model that provides instantaneous estimations. The results show that automation can deteriorate the status of the network due to conservative driving, and that connectivity is the key for less congestion. Results show that the AVs consume more compared to the other vehicle types. Emissions-wise, the difference between manually-driven vehicles and automated or connected seems low but the instantaneous-based model captures the dynamic difference from one 10-minute period to the next with higher detail.

Introduction

The impact of automation-related technologies on traffic network conditions is a topic studied for many years now (Louwerse and Hoogendoorn, 2004),(Kesting et al., 2010). Connected and Automated vehicles (CAVs) are expected to bring significant advancements in the existing road transport systems in terms of reducing traffic congestion, energy consumption, CO₂ and pollutants emissions (Litman, 2015) (Alonso Raposo et al., 2017).

The picture looks promising, but as research on the assessment of the impacts of automation and connectivity advances, many of the anticipated advantages of CAVs are questioned in Fiori et al. (2018) presented preliminary results showing that moving from internal combustion engine vehicles (ICEVs) to plug-in electric vehicles (PEVs), the relationship between congestion and energy consumption can change with higher energy consumption connected to the free-flow test-cases. Mattas et al. (2018) presented a simulation case study on the impact of CAVs focusing on the possible benefits of connectivity. The results show that depending on the traffic demand, AVs introduction can have adverse effects on traffic flow, while CAVs may benefit the network performance, depending on their market penetration. At the same time, the tools used in impact assessment studies have known limitations that may affect the final predictions. Results in the work of Ciuffo et al. (2018) raise concerns about the capability of the existing car-following models to reproduce observed vehicles' acceleration dynamics and thus estimate vehicles emissions and energy/fuel consumption.

The prospect of CAVs in reducing the environmental impact of vehicles is of great importance. In this context, it is thus important to investigate how and to which extent CAVs technologies will affect vehicle energy use and reduce traffic emissions. On the other hand, if the technology does not deliver the expected results, it is essential to identify the correct traffic management strategies to help up reach the desired emissions reduction goals.

The scope of the present paper is to contribute to the investigation of the impact of automation and connectivity in future road transport networks based on certain assumptions regarding the vehicle technology, the supply, and the demand. In the present paper we present a microsimulation study (Aimsun environment) using scenarios that give insights regarding the impact of CAVs on the evolution of emissions over the highway network. Different technologies generate different driving behaviours that impact the network's overall congestion levels. This work tries to answer whether the different

driving behaviours produce significant differences in emissions during rush hours, and how significant is the impact of detailed vehicle dynamics simulation and instantaneous emissions in the outcome.

The network used is the ring road of Antwerp presented in (Mattas et al., 2018). Initially, we build four scenarios. Each of the four scenarios refers to 3-hour simulation with a) manually-driven vehicles, b) AVs, c) CAVs and d) CAVs with 20% increased traffic demand. Two different approaches were simulated for every vehicle type resulting in eight scenarios; a) using common car-following models for the simulation of each technology; b) introducing the simulation of vehicle dynamics on free-flow using the Microsimulation Free-flow aCceleration model (MFC) (Makridis et al., 2019) to explicitly describe the acceleration curve of the vehicles and the driving style. Consequently, assuming the same network and scenarios we analyse the impact of vehicle dynamics and driving style microsimulation in traffic flow and emissions. The assessment regarding the CO₂ estimations is based on two models, the fuel consumption and CO₂ emissions factors proposed by the EMEP/EEA guidebook, and a generic version of CO₂MPAS (Fontaras et al., 2018) similar to the one described in (Tsiakmakis et al., 2017). The EMEP/EEA guidebook methodology (“EMEP/EEA air pollutant emission inventory guidebook - 2016,” n.d.), is more widely known by its software implementation, COPERT. It foresees an average-speed model and is frequently used in most European countries in order to estimate emissions of all major air pollutants produced by different vehicle categories. CO₂MPAS is a vehicle specific simulation model recently introduced by the EU in its vehicle CO₂ certification system (Fontaras et al., 2018).

Simulations

This section describes the driver models used in order to simulate the different technologies, the models used to provide emissions estimations and finally the physical network and the different scenarios.

Driver models

The AIMSUN traffic simulation software is used in this study. Six combinations of driver and vehicle types were simulated. The first three are state of the art car-following models that have been regularly used for the simulation of manually-driven, automated, and connected and automated vehicles (CVs, AVs, CAVs). In order to simulate in detail the dynamics of the vehicle and see its impact on traffic flow and emissions, each of these models was coupled with the Microsimulation Free-flow aCceleration model (MFC) (Makridis et al., 2019), a dynamics-based model also incorporating the driver's behaviour, creating three additional models. The three new hybrid models derive from the original formulas by substituting their free-flow acceleration parts a_{ff} , with the corresponding one from the MFC model. Regarding overtaking, lane changing and giving way behaviours, the default AIMSUN models have been used, taking into account the different reaction times and deceleration capabilities for AVs and CAVs.

Conventional Vehicles (CVs): For the simulation of manually driven vehicles, the default model that is implemented in AIMSUN was used. This is a modified Gipps' car-following model (Gipps, 1981). The Gipps model can be described as follows:

$$v_n(t + \tau) = \min\left\{v_n(t) + 2.5 * a_n \tau \left(1 - \frac{v_n(t)}{V_n}\right)^{\frac{1}{2}}, b_n \tau + \sqrt{(b_n^2 \tau^2 - b_n [2[x_{n-1}(t) - s_{n-1} - x_n(t)] - v_n(t)\tau - v_{n-1}(t)^2/\hat{b}])}\right\} \quad (1)$$

Where a_n is the maximum acceleration, b_n is the most severe braking, s_n is the effective size of the vehicle, V_n is the desired speed, $x_n(t)$ and $v_n(t)$ are the location and speed of the vehicle n at time t , and τ is the reaction time. The model can be expressed in a more abstract way as:

$$v_{n,t+\tau} = v_{n,t} + \min\{a_{ff}, a_{cf}\} * \tau \quad (2)$$

Where τ is the reaction time, a_{ff} the free-flow acceleration and a_{cong} the acceleration under car-following.

Automated Vehicles (AVs): To simulate AVs, the model proposed in (Shladover et al., 2012) is used. It is a first order model representing ACC vehicle longitudinal behaviour. For the lateral movement, the

default AIMSUN model was used, according to the ACC maximum deceleration and car following deceleration functions. The acceleration under car-following for the model is described by the following equation:

$$a_{cf} = k_1(d - t_w v_{n-1}) + k_2(v_{n-1} - v_n) \quad (3)$$

Where k_1 and k_2 are constants, t_w is the desired timegap and d is the current inter-vehicle distance. For more details please refer to (Shladover et al., 2012).

The acceleration under free-flow is described as follows:

$$a_{ff} = \max(\min(k(V_n - v_n), a_n), b_n) \quad (4)$$

Where k is a constant, a_n is the maximum acceleration, b_n is the maximum deceleration, v_n is the speed of the follower and V_n is the desired speed of the follower. More abstractly we have:

$$v_{n,t+\tau} = v_{n,t} + \min\{a_{ff}, a_{cf}\} * t \quad (5)$$

Where, τ is the reaction time, a_{ff} the free-flow acceleration and a_{cf} is the acceleration under car-following.

Connected Automated vehicles (CAVs): In order to simulate the longitudinal movement of CAVs, we use the model described by (Arem et al., 2006; Talebpour and Mahmassani, 2016). The aforementioned CAV model was used when following another type of vehicle, assuming that a CAV will behave as an AV when it is not able to exchange information with its neighbouring vehicles. CAVs are also forced to obey the speed limits, in the same way as AVs. Lane changing is again modelled based on the default AIMSUN algorithm, using the CAVs particular car following deceleration model.

$$a_{ff} = k(V_n - v_n) \quad (6)$$

Where V_n is the desired speed and v_n the current speed of the follower.

$$a_{cf} = k_a a_p + k_v(v_{n-1} - v_n) + k_d(r - r_{ref}) \quad (7)$$

Where k_a , k_v , and k_d are constant factors and v_{n-1} and v_n the speed of the leader and the follower, a_p the acceleration of the leader, r and r_{ref} denote the current and reference clearance to the leading vehicle. For implementation details please refer to (Arem et al., 2006).

Finally, the model can be described in the same formula as above:

$$v_{n,t+\tau} = v_{n,t} + \min\{a_{ff}, a_{cf}\} * t \quad (8)$$

Where, τ is the reaction time, a_{ff} the free-flow acceleration and a_{cf} is the acceleration under car-following.

MFC free-flow model: The Microsimulation Free-flow aCeleration model is a vehicle dynamics-based model for the estimation of the vehicle's free-flow acceleration based on the specifications of the vehicle and the driving style of the driver.

$$a_{ff} = a_w \cdot a_{cp} \quad (9)$$

Where a_w is the willingness of the driver to accelerate and it is defined according to her driving style and a_{cp} is the acceleration potential of the vehicle based on its technical characteristics. Implementation details can be found in (Makridis et al., 2019).

Table 1 presents the values of the maximum acceleration and deceleration and reaction time parameters used with each model. The maximum parameter values reported in the table are used in AIMSUN as the means of normal distributions in the drivers' population. AVs and CAVs have stricter limits on accelerations and decelerations. These are aimed to increase passengers' comfort. Reaction times are also much lower for AVs and CAVs. But, they are not negligible. For other driving parameters, not shown in Table 1, the default values in AIMSUN were used for human-driven vehicles. Within the

AV and CAV models, the parameter values are those reported in the references, they are derived from (Shladover et al., 2012; Talebpour and Mahmassani, 2016).

Table 1 Vehicle Parameters

Vehicle type	Max Acceleration	Max Deceleration	Reaction time
Conventional	3 m/s ²	-6 m/s ²	0.8 sec
AV	2 m/s ²	-3 m/s ²	0.3 sec
CAV	2 m/s ²	-3 m/s ²	0.3 sec

Predicting models for CO₂ emissions

The two models chosen for this exercise CO₂MPAS and COPERT are systematically presented below. COPERT is an average-speed model, frequently used in most European countries in order to estimate emissions from all major air pollutants produced by different vehicle categories. It is an implementation of the emissions inventory guidebook (“EMEP/EEA air pollutant emission inventory guidebook - 2016,” n.d.), the reference instrument designed to facilitate reporting of on-road emissions in European countries, allowing for a transparent and standardized, hence consistent and comparable, emissions reporting procedure.

As mentioned in the introduction, CO₂MPAS is a vehicle CO₂ emissions and energy consumption simulator, created in order to facilitate the introduction of the WLTP test protocol in the European legislation. The core of CO₂MPAS is a longitudinal dynamics physical model simulating energy flow and losses at various components. It operates using as input information regarding the vehicle (eg mass, road loads, tyre type etc), components (eg gearbox type, ratios, number of gears), and the engine (eg max power, capacity, maximum torque output) (Fontaras et al., 2018). CO₂MPAS is an open source tool, and it is available online with all its documentation (European Commission, 2015). In this work, we use a generic version (CO₂MPAS-generic) operating in a mixed forward/backwards implementation, with the MFC driver model defining the acceleration achieved at each time-step based on the network conditions, and the CO₂MPAS generic calculating the energy flows in each vehicle following a similar approach as presented by (Tsiakmakis et al., 2017).

Network and scenarios

The case study network for the simulation experiments is the ring road around Antwerp, Belgium as depicted in Figure 1. The ring road’s specifications were extracted from Open Street Maps and refined, resulting to a network consisting of 119km of roads with 27 centroids (origin/destination points), 208 sections with variable numbers of lanes and 117 intersections. There are no traffic lights on the network. Due to the ring road shape, there are obvious paths for each O/D pair, so no distinction has been made between user equilibrium and system optimum, although this can amplify the benefits of connectivity in different situations.

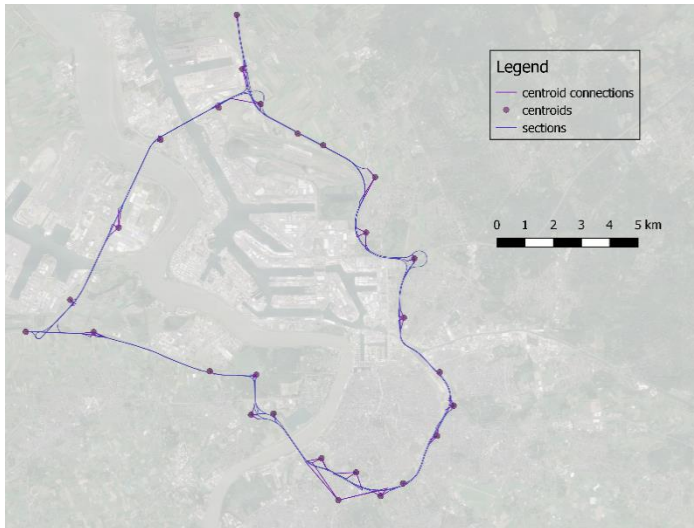


Figure 1: The ring road model of Antwerp, Belgium

Traffic count data during the morning peak hour, where utilised to produce the base scenario traffic demand. The Frank and Wolfe algorithm (Frank and Wolfe, 1956), which is available as a built-in tool in AIMSUN was used to adjust a planning O/D matrix to the observed data.

Eight scenarios have been designed to support this study on the ring road of Antwerp:

Scenario 1: Only CVs.

Scenario 2: AVs with no communication capability.

Scenario 3: CAVs with V2V communication.

Scenario 4: CAVs with V2V communication and increased traffic demand by 20%

Scenario 5: CVs using the MFC for the simulation of free-flow acceleration.

Scenario 6: AVs using the MFC for the simulation of free-flow acceleration.

Scenario 7: CAVs using the MFC for the simulation of free-flow acceleration.

Scenario 8: CAVs using the MFC for the simulation of free-flow acceleration; moreover, increased traffic demand by 20%

In all cases it is assumed that the vehicle fleet consists 100% of vehicles of the same technology et 100 conventional vehicles, 100% automated etc.

Different technologies generate different driving behaviours that impact the network's overall congestion levels. Each basic scenario (scenarios 1-4) was run twice; using the original free-flow acceleration of the model and using the proposed free-flow acceleration by the MFC vehicle dynamics-based model for an average vehicle of segment C and uniform distribution of different drivers according to the MFC driver parameters. Each run refers to three hours of simulation with the second hour being the network's peak hour. The first and the last hour are loading and unloading periods with lower demand equal to 20% of the observed peak hour demand. All different scenarios were run with the same random seed numbers in order to reduce the effect of stochasticity on the difference in the results.

Results

Data regarding the state of the network were gathered over 10 minute intervals. The results focus on three major dimensions, the impact of the vehicle/driver technology, i.e. CVs, AVs or CAVs, the impact of the simulation of vehicle dynamics, i.e. MFC and finally, the differences in the emissions estimations from EMEP/EEA and the instantaneous generic CO₂MPAS.

Figure 2 illustrates the evolution of the average harmonic speed per 10minute period over the 3-hour simulation for different vehicle types and all scenarios. During the first hour, the network is loading and the demand is quite low. Consequently, all vehicle types manage to maintain high average speeds close to the road speed limits. Since CVs do not always obey the speed limit, this behaviour is reflected in their harmonic average speed as well.

On the end of the first hour the demand is increasing to its peak value and the network starts to become saturated. When the vehicle dynamics are not simulated (Scenarios 1-4), the vehicles accelerate sharper and consequently they are able to maintain higher speeds and also offload the network quicker after the second hour. Vehicle dynamics simulation (Scenarios 5-8) leads to lower average speeds. Furthermore, increased demand (Scenarios 4 and 8) lead to the worst results in terms of speed. As expected communication between the vehicles leads to much better status for the network with average speeds that are significantly higher than the other two vehicle types (CVs and AVs).

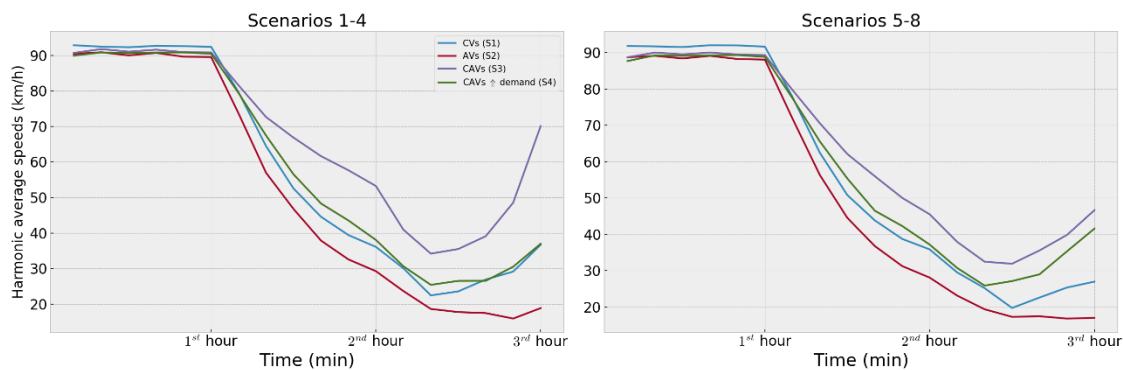


Figure 2: Harmonic average speed for CVs, AVs, CAVs and CAVs with increased demand for the eight different scenarios. On the left, the vehicle types do not include vehicle dynamics simulation. On the right, the MFC model was applied.

The introduction of vehicle dynamics in microsimulation leads to more conservative accelerations on the road. The observations in this study are aligned with the conclusions in (Makridis et al., 2019) that traditional car-following models used in simulation software tend to be overly aggressive, leading to sharp accelerations. This behaviour in some cases prevents the network from becoming saturated. However, this is an artefact as standard vehicles do not have the capability to accelerate so sharply.

In general, it has been observed that automation alone is not capable of improving the situation of the transport network. On the contrary, the driving behaviour of the AVs is more conservative with less sharp acceleration and desired speed fixed to the road limits, resulting in a more saturated network for the same demand. Connectivity seems to be the key to the reduction of congestion over the network. Connected vehicles can reduce time headways without reducing their level of traffic safety, simply because they exploit the available (though connectivity) information for the leading vehicle.

Figure 3 depicts the same results in terms of network outflow in number of vehicles per hour. It is worth noting that AVs are more conservative leading the lowest throughput when the network becomes congested. It is important to mention that AVs do not manage in our simulations to serve the requested demand like CVs and CAVs. The CAVs with increased demand, as expected, have a higher throughput, which is considered very close to the network's capacity. However, even with the normal peak demand, CAVs perform very well approaching the capacity of the network, while with the CVs but most notably with the AVs, the average throughput decreases a lot.

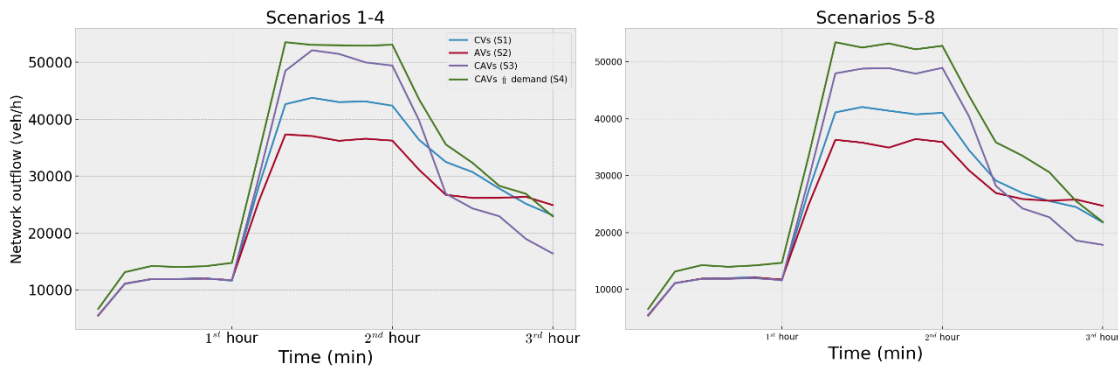


Figure 3: Network outflow for CVs, AVs, CAVs and CAVs with increased demand for the eight different scenarios. On the left, the vehicle types include vehicle dynamics simulation. On the right, the MFC model was not applied.

Local CO₂ emissions predictions

The figures below present the change in the total fuel consumption (and consequently CO₂ emissions that are directly proportional to fuel consumption) compared to those of the basic scenario of 100% conventional vehicles in the fleet. Many simulation studies provide fuel consumption estimations based on the EMEP/EEA methodology, which foresees an average speed model. However, vehicle dynamics affect a lot the instantaneous fuel consumption of each vehicle and it is interesting to see whether this instantaneous deviation is reflected in the overall results over a network. We use a generic version of CO₂MPAS to provide fuel consumption estimations for the scenarios when the MFC model is used to simulate the vehicle dynamics (Scenarios 5-8). This model cannot be used for scenarios 1-4, as it is dependent on the vehicle dynamics, which are unrealistic without the use of the MFC model (extreme accelerations observed under the standard model).

Figure 4 presents the overall results regarding the impact of the introduction of different technologies on the total fuel consumption over the 3-hour simulations. Subfigure a presents the results for the first four scenarios without the incorporation of the vehicle dynamics, subfigure b the scenarios 5-8 with the vehicle dynamics using MFC and finally subfigure c scenarios 5-8 based on the calculations of instantaneous generic CO₂MPAS model. The results presented here are relative to the estimated emissions of CVs for the corresponding scenarios.

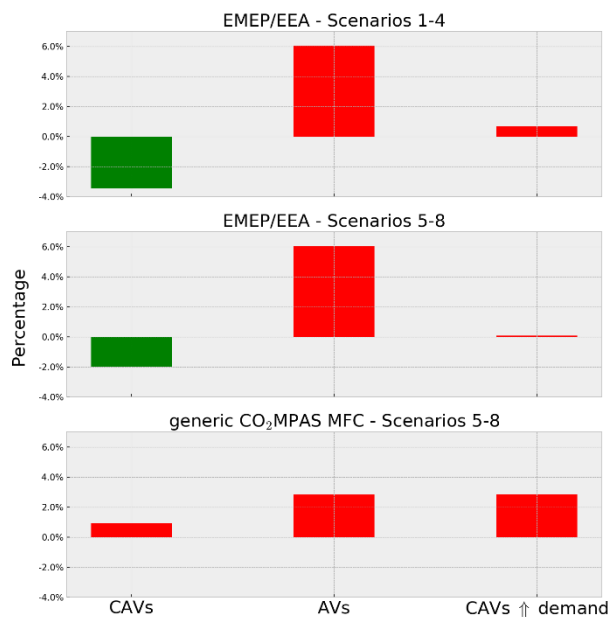


Figure 4: Impact on total fuel consumption consumed per km caused by the introduction of CAVs, AVs and CAVs with increased demand in comparison with CVs.

In all cases, the AVs seem to exhibit the highest consumption than the other vehicle-types, even in the case of CAVs with increased traffic demand. As mentioned in relevant literature (Mattas et al., 2018), automation alone is not expected to improve the situation in current transport networks, while connectivity seems very important. When looking at the overall emissions, the simulation of dynamics seems to play a small role when using the EMEP/EEA methodology, but comparing the average speed emissions factors and the instantaneously computed emissions of the generic CO₂Mpas, there are observable differences. The first seems to yield higher emissions for the AVs (6% over 2.7%) and unexpectedly low emissions of CAVs with increased demand (0.3% over 2.6%). In any case, the differences in emissions between CVs, AVs, CAVs and CAVs with increased demand do not seem significant, ranging from -3.4% to 6% for the most extreme cases. Furthermore, it is worth mentioning that according to COPERT model, CAVs produce less emissions than CVs in total while CO₂MPAS model reverses this observation by a small margin from -2% to 1% more.

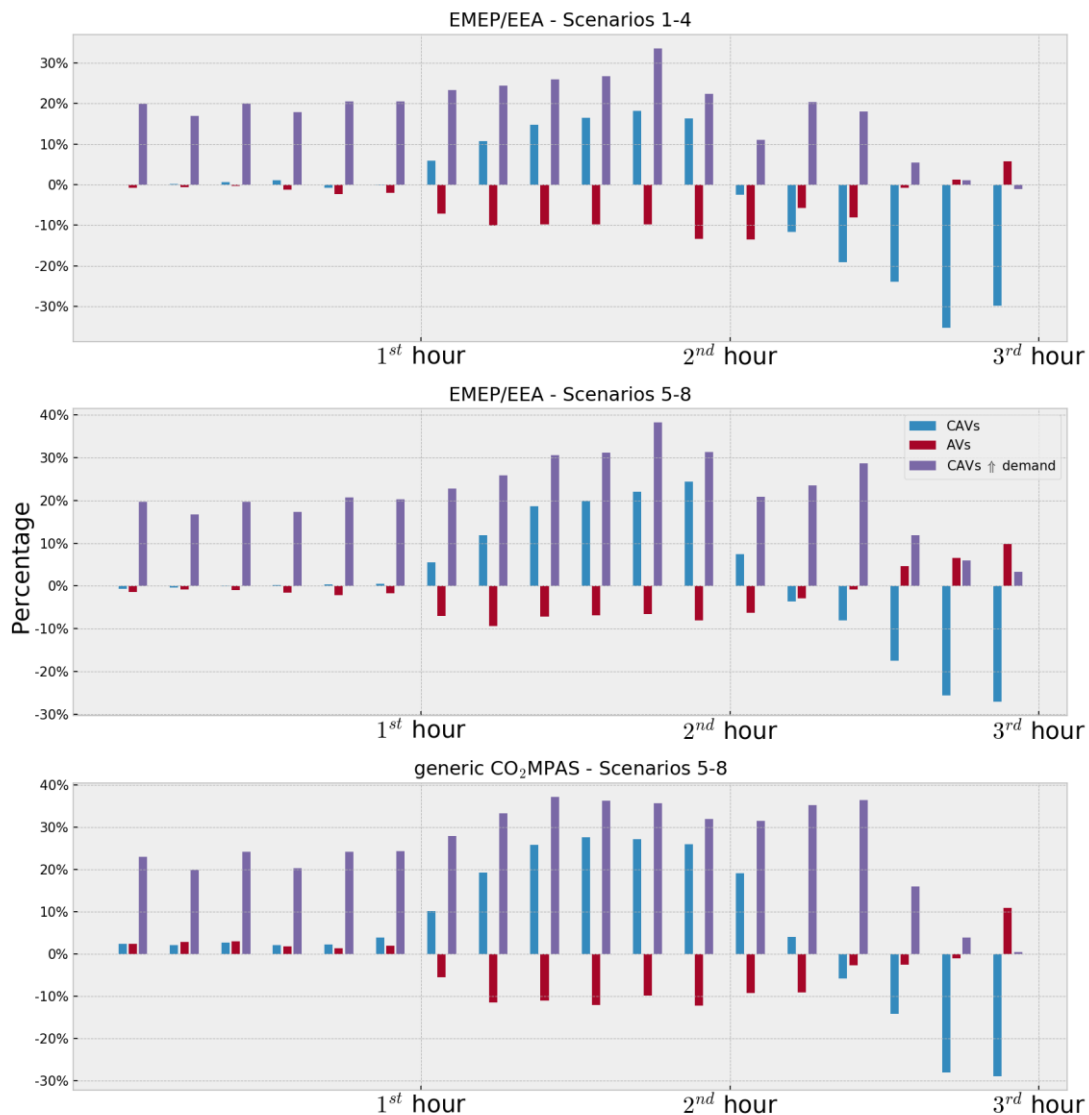


Figure 5: Fuel consumption estimations for CAVs, AVs and CAVs with increased demand in comparison with CVs.

Finally, it is interesting to observe the evolution of the total emissions produced per scenario. Figure 5, illustrates the relative results with a period of 10 minutes for the total duration of 3 hours. The reference number in this figure is the total emissions produced by CVs. As expected, the CAVs with increased demand by 20% produce much higher consumptions, yet it is interesting to note that the difference is not linearly correlated with the increase in the demand. When the network is empty, during the first hour, the increase in the demand is translated to the same increase in emissions (~20%). However, during the peak hour (2nd hour), the increase in fuel consumption seems to be related to the capacity of the network. Since more and more CAVs get into the network, the increase in the emissions reaches

almost 35%. Correspondingly, during the last hour that the network unloads, most of the demand has served and consequently the consumption drops to the values of CVs in scenario 1.

The simulation of vehicle dynamics amplifies the differences between different types of vehicles. For example, the CAVs with the generic CO₂MPAS model produce 20% more fuel consumption during the peak hour and 20% less during the last hour. This difference is not visible in the results of EMEP/EEA for scenarios 1-4, starts to become visible in the results of EMEP/EEA for scenarios 5-8 and it's clearly observable in the instantaneous estimations.

Conclusions

This work investigates the impact of automation and connectivity in future road transport networks based on certain assumptions regarding the vehicle technology, the supply and the demand. Here we present a microsimulation study using the commercial Aimsun software. The results show that among the four different basic scenarios, AVs have the highest emissions. CAVs utilize more the capacity of the network and therefore during peak hours they generate more emissions. However, looking at the total values, the differences are not considered significant. Furthermore, traditional car-following models overestimate acceleration, and therefore they unload the network quicker. The use of MFC depicts better the dynamics of the speed, flow and emissions while progressing between 10-minute periods during the entire 3-hour simulations. Finally, the instantaneous computation of emissions gives a much more detailed picture regarding emissions estimations. In addition to this the main conclusions of this work can be summarised as follows:

- Traditional car-following models that ignore the acceleration potential of the vehicle and the impact of the driver overestimate acceleration for certain speeds and therefore they artificially unload the network quicker, leading to questionable results.
- AVs have the poorest performance in terms of average speed, flow and generate the highest emissions values.
- CAVs increase the capacity of the network and therefore during peak hours they generate more emissions.
- On total values, the differences in emissions between CVs, AVs, CAVs and CAVs with increased demand do not exceed 6% and thus they are not considered significant
- The incorporation of the vehicle dynamics in the traditional car-following models using the MFC free-flow acceleration model, depicts better the dynamics of the speed, flow and emissions while progressing between 10-minute periods during the total 3-hour simulations.

References

- Alonso Raposo, M., Ciuffo, B., Makridis, M., Thiel, C., 2017. The r-evolution of driving: from Connected Vehicles to Coordinated Automated Road Transport (C-ART). Publications Office of the European Union. <https://doi.org/10.2760/666294> (ePub)
- Arem, B. van, Driel, C.J.G. van, Visser, R., 2006. The Impact of Cooperative Adaptive Cruise Control on Traffic-Flow Characteristics. *IEEE Trans. Intell. Transp. Syst.* 7, 429–436. <https://doi.org/10.1109/TITS.2006.884615>
- C. Fiori, V. Arcidiacono, G. Fontaras, M. Makridis, V. Marzano, K. Mattas, C. Thiel, B. Ciuffo, 2018. Less congestion implies less energy consumption: is it really true? Presented at the Transportation Research Board Annual Meeting, Washington, DC, USA.
- Ciuffo, B., Makridis, M., Toledo, T., Fontaras, G., 2018. Capability of Current Car-Following Models to Reproduce Vehicle Free-Flow Acceleration Dynamics. *IEEE Trans. Intell. Transp. Syst.* 1–10. <https://doi.org/10.1109/TITS.2018.2866271>
- EMEP/EEA air pollutant emission inventory guidebook - 2016 [WWW Document], n.d. . Eur. Environ. Agency. URL <https://www.eea.europa.eu/publications/emep-eea-guidebook-2016> (accessed 6.22.18).

- European Commission, 2015. CO2MPAS: Vehicle simulator predicting NEDC CO2 emissions from WLTP — CO2MPAS 2.0.0+9.g5b3144d documentation [WWW Document]. co2mpas.io. URL <https://co2mpas.io/> (accessed 9.26.18).
- Fontaras, G., Valverde, V., Arcidiacono, V., Tsiakmakis, S., Anagnostopoulos, K., Komnos, D., Pavlovic, J., Ciuffo, B., 2018. The development and validation of a vehicle simulator for the introduction of Worldwide Harmonized test protocol in the European light duty vehicle CO2 certification process. *Appl. Energy* 226, 784–796. <https://doi.org/10.1016/j.apenergy.2018.06.009>
- Frank, M., Wolfe, P., 1956. An algorithm for quadratic programming. *Nav. Res. Logist. Q.* 3, 95–110. <https://doi.org/10.1002/nav.3800030109>
- Gipps, P.G., 1981. A behavioural car-following model for computer simulation. *Transp. Res. Part B Methodol.* 15, 105–111. [https://doi.org/10.1016/0191-2615\(81\)90037-0](https://doi.org/10.1016/0191-2615(81)90037-0)
- Kesting, A., Treiber, M., Helbing, D., 2010. Enhanced Intelligent Driver Model to Access the Impact of Driving Strategies on Traffic Capacity. *Philos. Trans. R. Soc.* 368.
- Litman, T., 2015. Autonomous Vehicle Implementation Predictions: Implications for Transport Planning. Presented at the Transportation Research Board 94th Annual Meeting Transportation Research Board.
- Louwerse, W.J.R., Hoogendoorn, S.P., 2004. ADAS safety impacts on rural and urban highways, in: *IEEE Intelligent Vehicles Symposium, 2004*. Presented at the IEEE Intelligent Vehicles Symposium, 2004, pp. 887–890. <https://doi.org/10.1109/IVS.2004.1336502>
- Makridis, M., Fontaras, G., Ciuffo, B.F., Mattas, K., 2019. MFC free-flow model: Introducing vehicle dynamics in microsimulation. *TRR*.
- Mattas, K., Makridis, M., Hallac, P., Raposo, M.A., Thiel, C., Toledo, T., Ciuffo, B., 2018. Simulating deployment of connectivity and automation on the Antwerp ring road. *IET Intell. Transp. Syst.* 12, 1036–1044. <https://doi.org/10.1049/iet-its.2018.5287>
- Shladover, S., Su, D., Lu, X.-Y., 2012. Impacts of Cooperative Adaptive Cruise Control on Freeway Traffic Flow. *Transp. Res. Rec. J. Transp. Res. Board* 2324, 63–70. <https://doi.org/10.3141/2324-08>
- Talebpoor, A., Mahmassani, H.S., 2016. Influence of connected and autonomous vehicles on traffic flow stability and throughput. *Transp. Res. Part C Emerg. Technol.* 71, 143–163. <https://doi.org/10.1016/j.trc.2016.07.007>
- Tsiakmakis, S., Fontaras, G., Ciuffo, B., Samaras, Z., 2017. A simulation-based methodology for quantifying European passenger car fleet CO2 emissions. *Appl. Energy* 199, 447–465. <https://doi.org/10.1016/j.apenergy.2017.04.045>

2.4.3 Optimization of a Bus Lane with Intermittent Priority dynamically activated by the road traffic

A Kampouri¹, I. Politis²

¹Crowd Dynamics, Manchester, United Kingdom, katerina_kamp@hotmail.com

²Traffic Engineering Laboratory, Aristotle University of Thessaloniki, 54124, Thessaloniki, Greece

Abstract

The aim of this paper is the development of traffic scenarios using programming language to design a Bus Lane with Intermittent Priority (BLIP). The script of the BLIP is written via the programming language VAP in VisVap[®], an add-on module, which belongs to the PTV Vissim[®] software library. The purpose of the dynamical traffic scenarios is not only to model and optimize this bus lane, but also to evaluate if BLIP can reduce vehicle queues, air pollution and traffic congestion. The initial idea of BLIP allows the use of the bus lane by vehicles, only when there are no busses in the inspected area. Yet, in the study case area the bus frequency is high, so an alternative version of BLIP was proposed. Thus, vehicles are permitted to enter the bus lane depending on how many are traveling through the area and not by the detection of the bus. In each of the examined scenarios, vehicle queues are compared to the actual situation and the results are analysed. For the analysis of the emissions, the EnViVer[®] software is used, which compares the emissions of CO₂ from each traffic simulation.

Introduction

In order to reduce congestion in urban areas, many strategies have been proposed to improve the operational efficiency and attractiveness of public transport systems. The Dedicated Bus Lane (DBL) is perhaps one of the most popular bus priority strategies that seeks to deliver high quality transport services and improve operating speed. While DBL is able to improve the level of service of the transit system, it requires the entire bus lane to be detained and it prohibits the entry of private vehicles during a certain period, this leads to severe congestion (Eichler, 2005). To tackle this problem, an innovative priority bus approach called a bus lane with intermittent priority bus (BLIP) is suggested in a specific region of Thessaloniki, Greece. The BLIP works as follows: when a bus approaches a pavement section, the BLIP in this pavement section becomes a bus lane. Private vehicles running in front of the bus are required to leave the BLIP lane for the passing bus using variable message signals. When the bus crosses this section of the road, the BLIP lane opens again in private traffic. Private vehicles behind the bus are allowed to enter the BLIP lane at any time. BLIP is based on a series of transport infrastructures, such as automated vehicle positioning, central control system, information panel, roadway lights and bus detection (Daganzo, 2006).

Moreover, emissions are becoming more and more important in traffic studies. Using the EnViVer software, it is possible to determine vehicle emissions based on vehicle paths from PTV Vissim. Initially, the validity of vehicle speeds and accelerations are vital for the quality modelling of emissions. With PTV Vissim, these can be exported and be imported into EnViVer for further analysis. Vehicle types are used to specify additional attributes, such as fuel type or pollutant category, in each EnViVer vehicle. In EnViVer, detailed estimation of CO₂ emissions in the study area are presented in form of graphs or tables for an easy-to-understand result.

The aim of this paper is to investigate whether traffic is affected by the deactivation of the bus lane in large number of vehicles and whether it will contribute to the reduction of the air pollution. The major problem that has to be addressed is the building of the "smart" bus lane which permits the vehicles to enter and exit the bus lane dynamically. Using the PTV Vissim 11 software and the VisVap add-on module, BLIP has been modelled and then dynamical scenarios have been developed to determine whether it helps in reduce the congestion. In the following paragraphs a review of the idea on which the subject of this work is based will be analysed. Then, the study case will be presented and the reasons that set it the ideal place for study will be referred. The softwares which are used will be shown and finally the results and conclusions will be analysed.

Bus Lane with Intermittent Priority (BLIP)

Significant congestion, as well as long vehicle queues in junction sections, are a typical representation of today's urban road conditions. The research in order to minimize this phenomenon requires knowledge of the process on how the vehicle queues are formed. In addition to, it is important to obtain reliable data that will allow basic vehicle parameters, such as traffic density and average speed, to be estimated. The Bus Lane with Intermittent Priority is a dynamic bus lane that operates only when a bus is going to cross the street in which the operation is going to be applied. This paper evaluates strategies for operating buses on signal-controlled arterials using a special lane that is made intermittently available to general traffic. The advantage of special bus lanes, intermittent or dedicated, is that they release buses from traffic interference yet, their disadvantage is that they disrupt traffic.

The axis of the original BLIP idea is to divide the section of the road into a few successive sections. The length of each segment is predetermined by the geometry of the road networks, such as intersections, meaning that each section may not be equal in length. The BLIP based on the road section works as follows: when a bus approaches a pavement section, the BLIP in this pavement section becomes a bus lane. Private vehicles running in front of the bus are required to leave the BLIP lane for the passing bus using variable message signals. When the bus crosses this section of the road, the BLIP lane opens again in private traffic. Private vehicles behind the bus are allowed to enter the BLIP lane at any time (Wu, 2017).

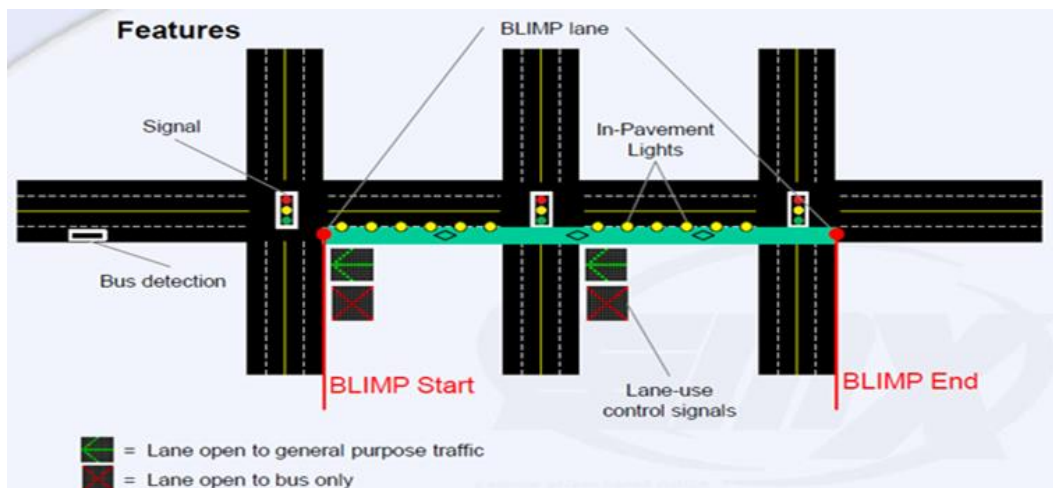


Figure 1: The way bus lane with intermittent priority works.

Numerous investigations have been carried out to investigate this idea. The implementation of the BLIP is based on a series of transport infrastructures, such as automated vehicle positioning, central control system, information panel, roadway lights and bus detection (Hu, 2014), (Smietanka, Szczypiorski, and Marcin, 2015). A simulation carried out by the US Department of Transportation reveals that BLIP reduces travel time by 14% improving queue pauses (G. Carey, 2009). This result, however, is being challenged by some other studies which BLIP has been found to contribute negatively to traffic delays and road capacity. Although many efforts have been devoted to the study of BLIP, many related challenges continue to prevent full exploitation of its potential. Finally, a comprehensive guideline for the implementation of BLIP in traffic flow and road capacity has not yet been found. (Eichler, 2005), (Daganzo, 2006) and (Todd, 2006)

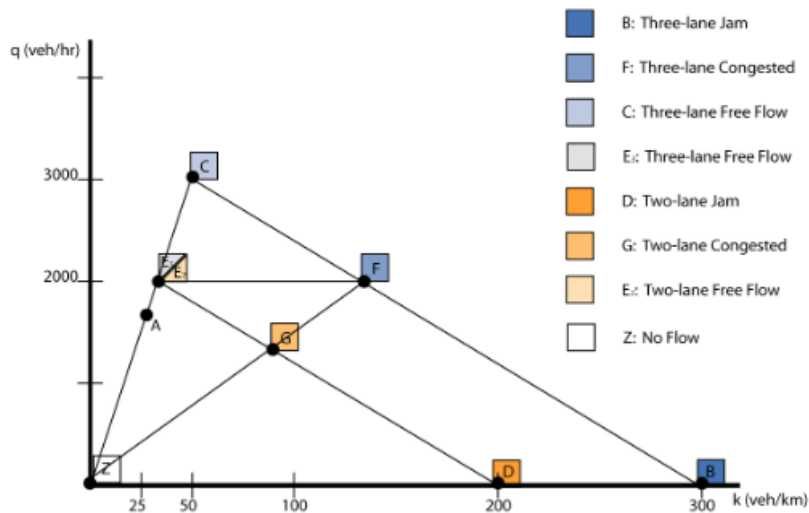


Figure 2: Flow/ Density Diagram, it represents a three-lane roadway being reduced to a two-lane roadway. (Eichler, 2005)

The diagram illustrates the following traffic states of interest: **A** = Uncongested free-flow, **B** = Full roadway jam density, **C** = Full roadway capacity, **D** = Reduced roadway jam density, **E** = Reduced roadway capacity, **F** = Congested full roadway conditions with same flow as state E, **G** = Congested reduced roadway with same speed as F. The flow at any given point on the diagram will be expressed as a q with a subscript matching the label of the point on this diagram. For example, the flow at point E will be expressed as q_E . The diagram illustrates two "curves." The first, larger curve represents the roadway at "full" capacity. The smaller of the curves represents "reduced" capacity roadway conditions, when one of the lanes has been reserved for the bus and is therefore no longer available to private vehicles. (Eichler, 2005)

Description of Study Case

Study Area

The study area is located between two intersections, the first is among Delfon Street and Vasilissis Olgas Avenue and the second lies between Themistocleous Sofouli Street and Vasilissis Olgas Avenue. The first junction has as tag reference the patisserie Terkenlis, while the second is determined by the Devido Grill Restaurant. For reasons of convenience, the streets, avenues and roads of the study case area will be renamed with reference numbers. In the following table, the reference road numbers are shown.

Table 1. Reference number of the streets, roads and avenues in the study area.

Street Name	Reference Number
Delfon Street	1
Vasilissis Olgas Avenue	2
Themistocleous Sofouli Street	3
Dimitrakopoulou Street	4
Mercuriou Street	5
Skiathos Street	6

This area is loaded daily with high traffic, as Vasilissis Olgas Avenue is one of the largest streets in the municipality of Thessaloniki. In addition to, it is of utmost importance to emphasize that the bus station, Kasa Bianca, is sited also in the study area and accepts five different bus routes throughout the day and one overnight, at a frequency of almost two (2) minutes in peak hour. Specifically, Street 2 consists of three (3) lanes, the right lane is a dedicated bus lane and it is the main street of this research. Additionally, Street 1 supplies vehicles both to Street 2 and Street 3. The two intersections operate with ninety (90) seconds traffic signal cycle. In addition, along the Street 2, there are two (2) roads that supply vehicles in its lanes, Street 5 and 6. The coordinates for the first intersection are **A (X:40.594950, Y: 22.956162)** and for the second intersection are **B (X:40.597158, Y:22.956051)**.

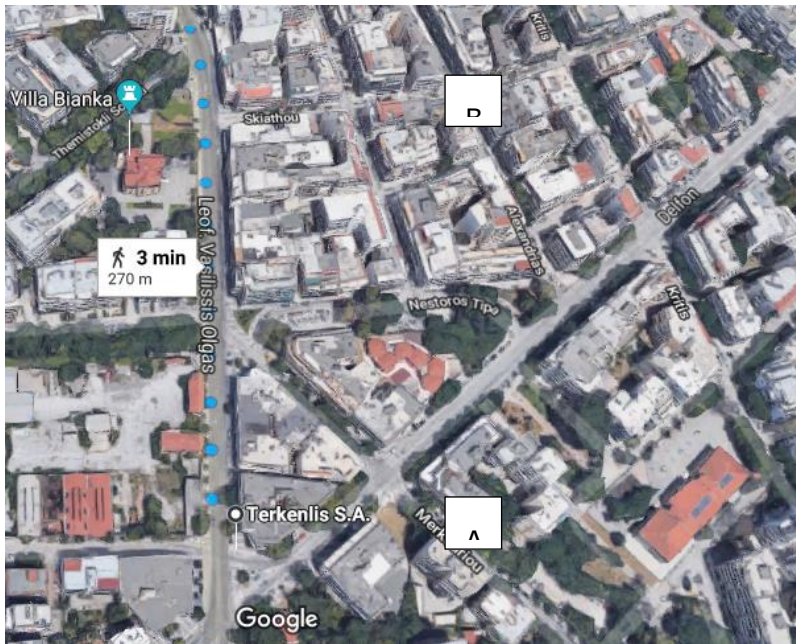


Figure 3. Map of the study case area in Thessaloniki, Greece.

Observations

In this area, congestion problem often arises due to a big number of vehicles and a high frequency of buses. Vassilissis Olgas (street 2) is one of the most crowded streets of Thessaloniki with an exclusive long-distance bus lane, this leads to a high traffic congestion. For the above reasons this area is considered one of the most appropriate choices for this research as BLIP not only proposes a direct way to reduce congestion but also tries to improve the existing situation. Prior to simulation in the PTV Vissim software, it is necessary to calculate the actual traffic load of the study area, as this would make it easier to validate the simulation. Vehicle counting is necessary in order to create a simulation model that would accurately represent the actual situation.

This process is only ensured by visiting the site on peak hours to obtain useful data and assess whether the area is suitable for the design of an intermittent bus lane. Consequently, for the measurement of traffic load, the author visited the site twice in order to plan how to record the traffic and a high-resolution digital camera was used for a total duration of 150 minutes. The chosen day was Friday, as one of the busiest days of the week, and the place where the digital camera was sited, was a spot in front of the street lights of intersection B, where the traffic could be visible. During the counting on the field, four observers were walking through the road, keeping notes and taking photos of the real situation. Long queues were formed along Street 2, this happened because of the high traffic volume and the temporary illegal parking of several heavy good vehicles that supplied the local shops with products. In addition to, it was observed that the frequency of buses was high, almost every two (2) minutes and sometimes every one-minute buses arrived in the bus stop. Finally, the people who waited at the bus stop often exceeded to ten (10) and the time interval which was required in order the bus to stop, the passengers leave or enter the bus, lasted thirty-four (34) seconds.

BLIP's logic is based on the deactivation of the bus lane and the use of the right lane by vehicles to reduce traffic load and long queue length. Activation of the bus lane starts when a bus is detected by special detectors. Specifically, once the bus is located within a few meters of the nearest detector, a signal is given to the traffic lights and the road lights are activated to inform the drivers on any length of the right lane and, if they are, to leave towards the middle lane. As soon as the bus completes its route and overtakes the detector at the end of the BLIP, the bus lane is deactivated and the vehicles can re-enter the right lane.

In the chosen study area, the bus frequency is increased so the bus lane remains permanently activated. Analytically, the bus frequency in the study case is increased and the bus lane remains permanently activated. This can be proved by the following data:

- The distance of the route is 250 m.
- The bus speed is set at twenty-five kilometers / hour (25 km / h).
- The minimum time required to stop the bus and exit / enter passengers / pedestrians is thirty-four seconds (34 seconds).
- The bus door may have a delay of three (3) seconds.
- The average estimate of the bus delay due to a red traffic signal is about twenty (20) seconds.

With the use of the equation $u = x / t$, it is easy to gain the following results:

Table 2. Delay in seconds due to red traffic light for 1 bus.

	no Red lights	1 Red light	2 Red lights
Bus	73	93	113

These values are very conservative, as they are calculated with minimum times and without the presence of a second bus. In addition, there is no added time for vehicles to change lanes, especially in the event of congestion. Finally, in the case of continuous buses, values are doubled. All of the above data creates a complex problem, which depends on too many variables, some of which do not have a fixed value. Therefore, an improved version of BLIP was proposed based on traffic load and not just on tracking of buses. The bus lane is dynamically activated depending on how many vehicles are traveling through the study area and not by the bus detection as in the original conception. The selected scenarios will examine the current situation using the BLIP variant, while the number of vehicles and buses will be increased in order to obtain results and compare them.

PTV Vissim, VisVap and Enviver

The software which is used for the simulation is Vissim and the add-on modules VisVap, and Enviver, Analytically, PTV Vissim is the leading microscopic simulation program for multimodal transport modeling and belongs to the Vision Traffic Suite software. Vissim creates the best conditions to test different traffic scenarios before they are implemented in realistic and precise detail. It is used worldwide by public sector, consulting companies and universities as it allows to simulate traffic patterns. The software offers flexibility in many attributes, such as the concepts of links and connectors, which enable users to model geometries with any level of complexity. Furthermore, the software offers a variety of attributes for behavior type and vehicle, which allows the traffic load configuration to be customized, as each user wishes to design his simulation. Also, a large number of interfaces allow the integration of other systems such as signal controllers, traffic management and emission models in Vissim. To sum up, PTV Vissim is a powerful tool for assessing and designing urban and interurban transport infrastructure. (PTV Vissim, 2018)

VisVAP

VisVap is a Vissim add-module package whose primary goal is to improve the use of freely-defined signal control logics using VAP (Programming Actuated Programming). VisVAP is a convenient tool for creating and processing logical programs through flow charts. VisVAP can be used for signaling stages as well as for signal group design. In VisVAP, program logic is defined and checked for correctness. If it is successful, it extracts the VAP file. This is how VAP files are created for the use in Vissim. (VISVAP 216 ENG, 2018)

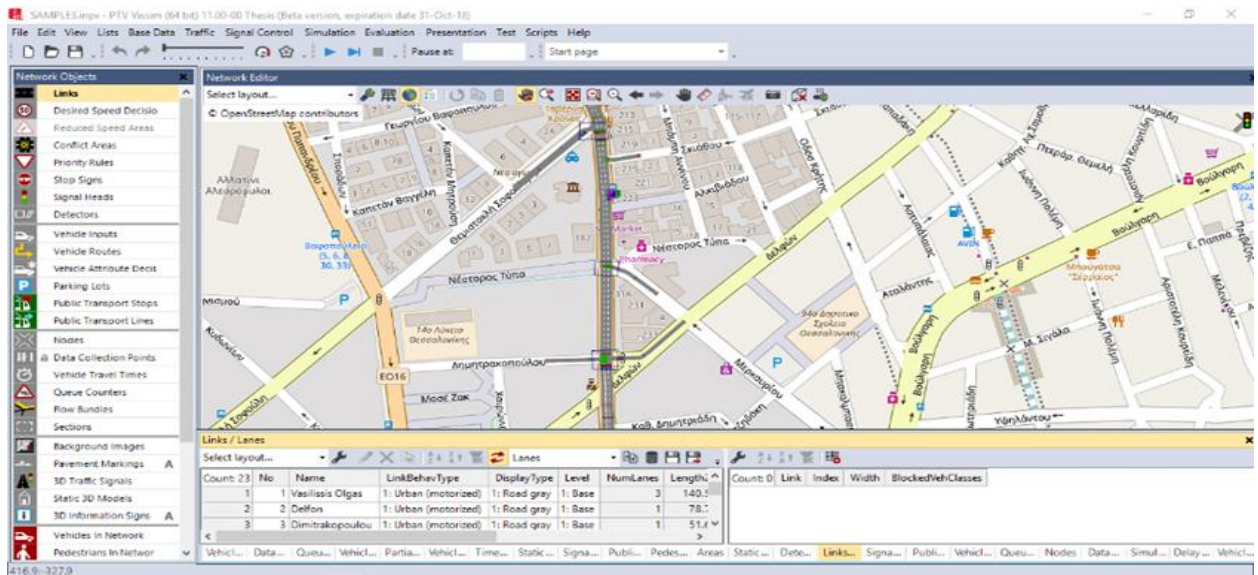


Figure 4. Vissim desktop for the study area.

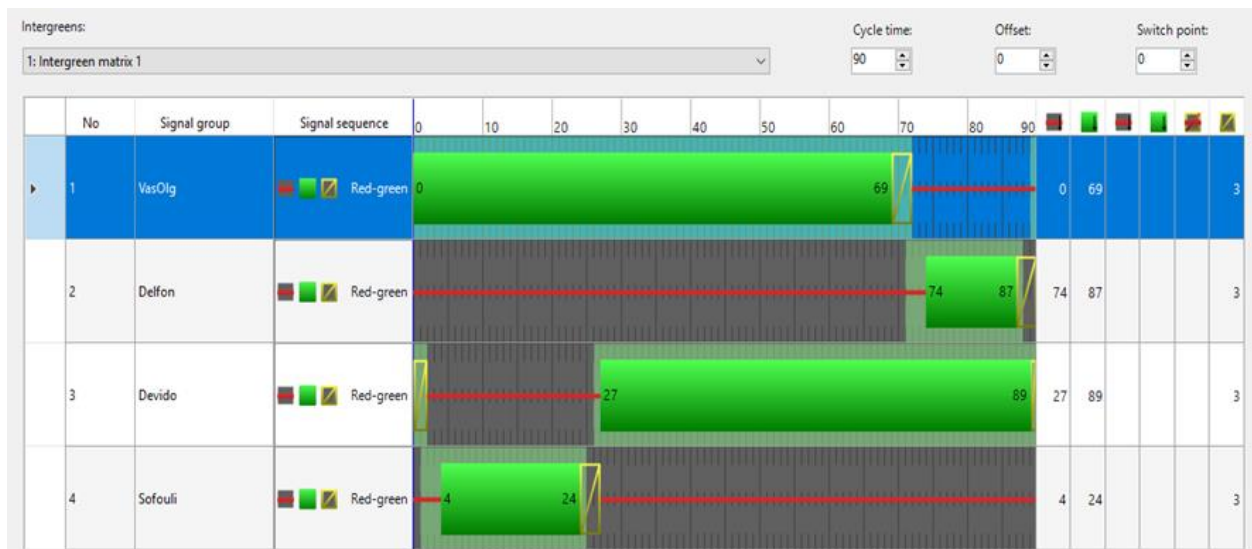


Figure 5. Vissim diagram for signal control of the study case.

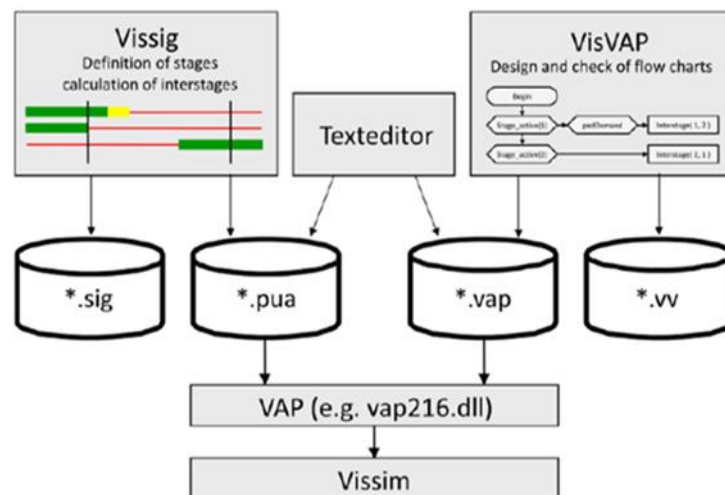


Figure 6: Operation of Vissig and VisVap in Vissim.

EnViVer

Emissions are becoming more and more important in traffic studies. In this case, total exhaust gas loads at the network level are significant. Using the EnViVer option, it is possible to determine vehicle emissions based on vehicle paths and other information from PTV Vissim. Initially, the validity of vehicle speeds and accelerations is vital for the quality modeling of emissions. With PTV Vissim, these can be exported to vehicle logs that can be imported into EnViVer for further analysis. Vehicle types are used to specify additional attributes, such as fuel type or pollutant category, in each EnViVer vehicle. In EnViVer, detailed estimates of CO₂, NO_x and PM₁₀ emissions in the area are prepared in the form of graphs or tables for an easy-to-understand result. (TNO, 2018) and (PTV GROUP, Emmissions Modeling, 2018).

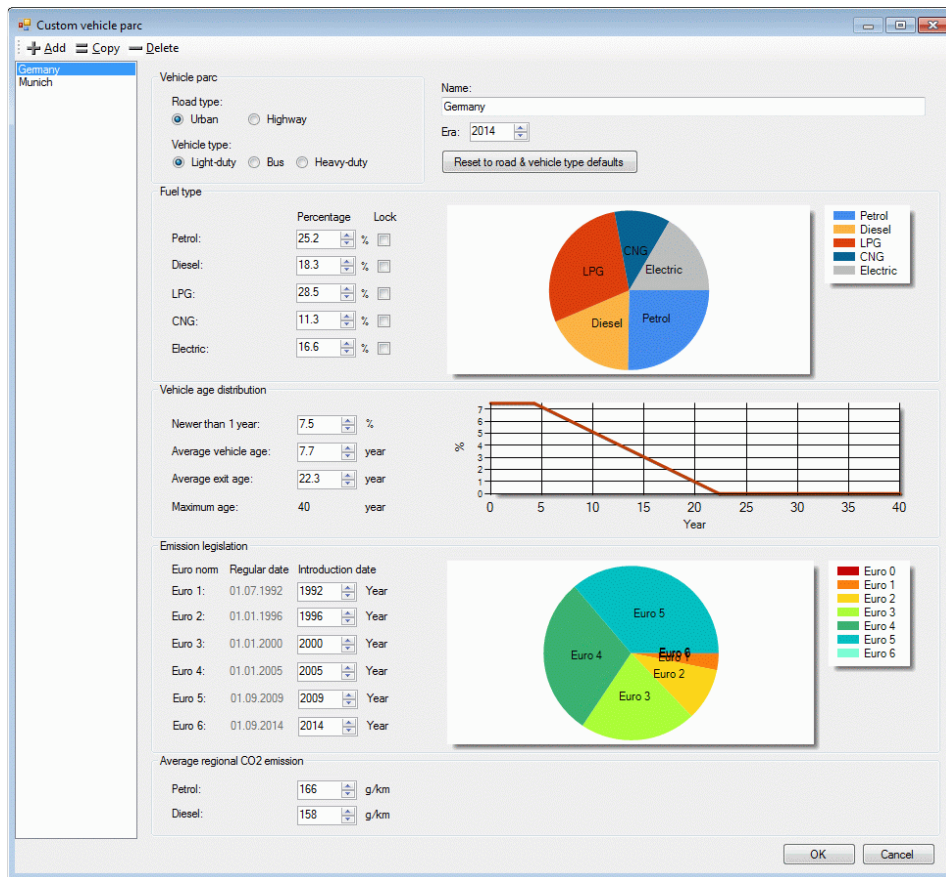


Figure 7: Default settings for the emissions.

Results

In this section, the traffic load data per quarter of the site survey is presented. In these counting the number of buses is not taken into account. The software simulation and the real data from the survey have only 6% difference in the number of vehicles, that validates that the simulation, which represents the real situation of the study area, is successful.

Table 3: Volume of Vehicles per 15 minutes in the study area (site survey).

Street	Time Interval (s)						Sum
	0-900	900-1800	1800-2700	2700-3600	3600-4500	4500-5400	
1	8	10	15	18	6	2	59
2	441	382	548	547	353	366	2637
5	26	18	33	35	33	21	166
6	2	2	9	6	3	3	25
Sum	477	412	605	606	395	392	2887

BLIP is an innovative method to improve the reliability of bus services while also promoting the efficient use of road resources. Vehicle-to-vehicle communication (V2V) is an advanced technology that can significantly improve vehicle mobility, increase traffic safety and mitigate traffic jams (Wu, 2017). It is very important that Vissim's environment is properly structured so that BLIP can work smoothly. For this reason, in-pavement lights are placed along the roadway, which will inform drivers to leave the bus-lane. The following images show the special 3D designs created / selected for the specific task. Also, Table 3 shows the scenarios which are selected for the simulations. The use of BLIP was successful, as it reduced queue lengths without deterring people from using public transport. Even in extreme urban frequency phenomena, BLIP managed to confirm the initial theories of each scenario and eventually improve congestion.



Figure 8: Three-dimensional LED traffic light for buses.

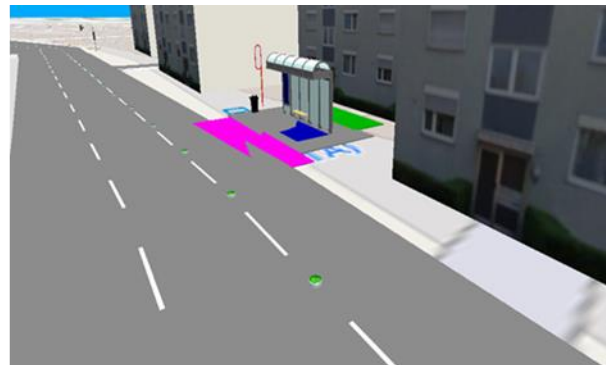


Figure 9: In-pavement lights.

It is important to emphasize that any failures which occurred during time intervals, before BLIP start to operate, happened because of random bus time positions without predetermined insertion intervals as also their completion was high. This lead to the fact that as their frequency is increased, the amount of time which a bus needs in order to stop and then start is growing. Especially, when bus frequencies are much higher than normal, their waiting times in bus stop is increased sharply. Finally, when the frequency of buses is reduced, the bus density reached 40-45 passengers on each bus (almost 50% of bus capacity).

Table 4. List of scenarios and their variables in order the study to be more understandable.

scenarios	sets	Volume (vehs)	BLIMP activation (vehs)	Bus frequency (min)
0	none	2690	no	2
1	1.1	2690	2000	2
	1.2	2690	1000	2
	1.3	2690	2500	2
2	2.1	2690	2000	1
	2.2	2690	2000	3
	2.3	2690	2000	30 secs

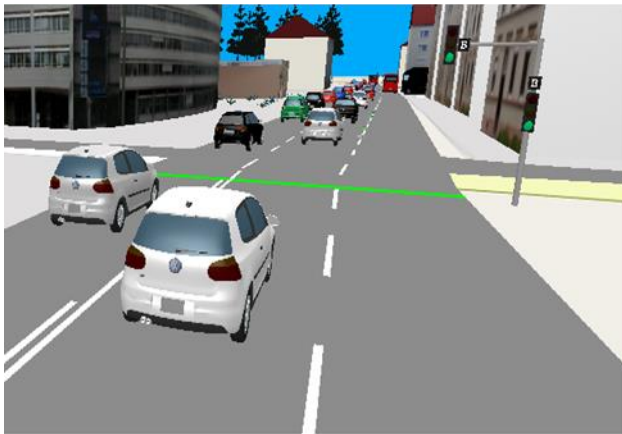


Figure 10. Vehicles are not allowed to enter the bus lane. Figure 11. Vehicle pass through the bus lane.

In the next table the emissions of CO₂ is presented, the carbon dioxide emissions are mainly reduced by the activation of the intermittent use BLIP with the exception of scenario 1.3 where activation of the BLIP occurs in high traffic load and this explains the slightly increased value. This may be due to errors during the simulation, for example some features selected in the EnViVer program might need some modifications /improvements, alternatively, the simulation in Vissim software should be improved by any bugs. However, when BLIP is used in scenarios 1.1 and 1.2 (with a calibration of 2000 and 1000 vehicles) the values are lower than the original scenario. Finally, in the cases which BLIP may not actually help in the reduce of carbon dioxide emissions, because vehicles are entering the bus lane, and this creates delay of public transport, a detailed environmental study should be carried out in order to improve directly the emissions.

In second scenario, the variable is the frequency of buses because the main focus of the research is to defend and promote the use of urban transport. The following table shows an increase in emissions, especially in the latter scenario 2.3 which the bus frequency is every 30 seconds, this happens due to the permanent occupied bus lane, in some cases the bus invades the middle lane to save time and space. Using BLIP in cases where the variable is the traffic load improves the exhaust emission, yet in cases of high frequent urban traffic the results are not as noticeable, even though there is a partial improvement.

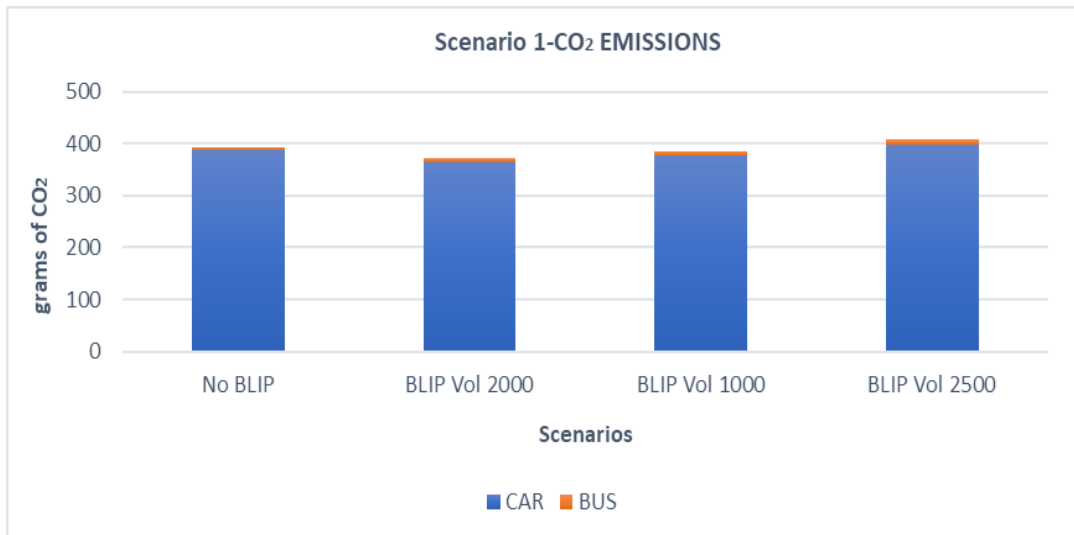


Figure 12: Graph which shows CO₂ emissions' comparison of Scenario 1.

Especially in the scenario where the urban bus frequency is every 30 seconds, the simulation encountered too many problems as waiting time and exhaust emissions were too high.

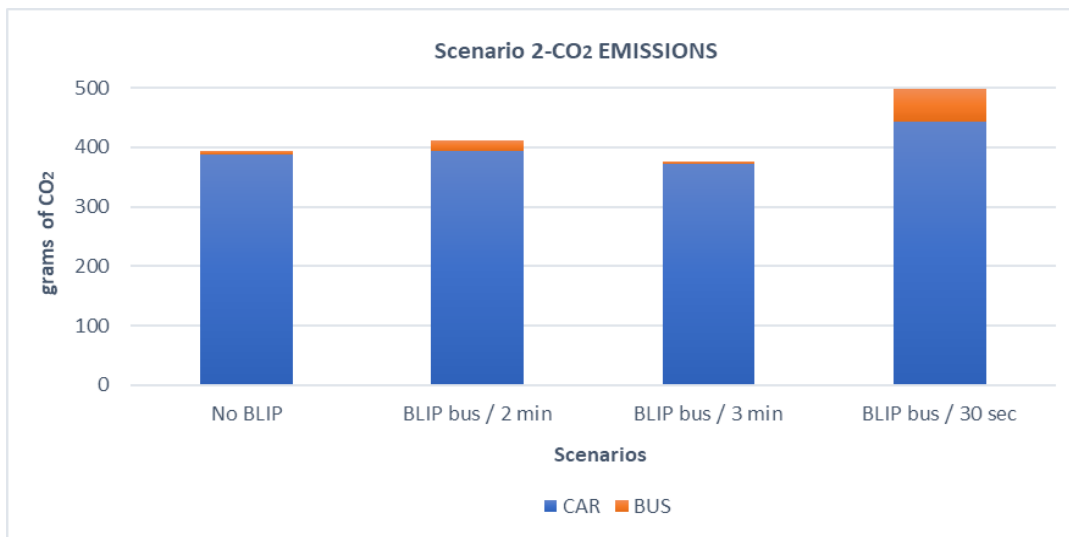


Figure 13: Graph which shows CO₂ emissions' comparison of Scenario 2.

Conclusions

Conclusion is that the intermittent use of the bus reduces congestion and the partially the emission of atmospheric gases without giving priority to private vehicle drivers. In particular, the modified proposal for the intermittent use of traffic buses, which is activated and deactivated according to traffic, does not enhance the use of private vehicles but improves a problematic situation. The results are positive, and the utility of BLIP is almost confirmed. The original concept of BLIP posed great risks of promoting the use of cars rather than the use of public transport. Unfortunately, Greece is one of the countries that suffers from a lack of good urban transport and even more from a lack of environmental consciousness and road safety. This means that most citizens choose to move by private passenger cars rather than by city buses. However, the aim of this work is to improve urban transport from all sides and at the same time to respect both the urban and the natural environment. For this reason, the BLIP was chosen to be activated only in cases of heavy traffic, which also has a high frequency in urban traffic. The interlocking of the intermittent bus lane only occurs when the urban network needs it and when the normal loads are resumed, the right lane is again converted into a bus lane. In summary, the conclusions were:

- The reduction of queue length in all cases and the decrease in some scenarios of CO₂ emissions

- In a heavily increased urban transport frequency (peak times) the road network paralyzes for a long time and the use of BLIP may aggravate the situation, yet in cases of increased movement, early activation of BLIP results in much better results and at the same time contributes to respect for the environment.
- In urban networks with a very high frequency of urban traffic the use of BLIP does not result in a reduction in the queue length of vehicles, but only offers a delay in public transport.

Limitation of study

Any simulation errors can be corrected in order the results to be improved. For example, in scenario 2.3 where the bus frequency is increased by 75%, the bus lane remains stationary from the endless bus queue. Also, a script should be developed in order to modify the signal controls and reduce the vehicle queue using BLIP concept, as well as an improvement of BLIP's code in order to minimize vehicle queues. Finally, the development of a true BLIP concept in a region with reduced urban traffic and the comparison of results with the varied version of this research should be considered.

References

- Carey T. B. (2009). *Bus lane with intermittent priority (blip) concept simulation analysis*.
- Daganzo M. E. (2006). *Bus lanes with intermittent priority: strategy formulae and an evaluation*.
- Eichler M. D. (2005). *Bus lanes with intermittent priority: assessment and design*. University of California, Berkeley.
- Hu J (2014). Transit signal priority with connected vehicle technology. Transportation Research Record.
- PTV Group. *Emmissions Modelling*. Retrieved from <http://vision-traffic.ptvgroup.com/en-us/products/ptv-vissim/use-cases/emissions-modelling/> and PTV Group. (2018). *VAP 2.16 and VisVap, User Manual*. PTV VISSION.
- Smietanka P., Szczypiorski K., Viti F., and Marcin S (2015). *Proceedings of the 18th IEEE International Conference on Intelligent Transportation Systems*.
- Szczuraszek, T. (2015). *The analysis of calculation methods of vehicle queue lengths in front of intersection inlets with traffic lights*. Bydgoszcz: Department of Road and Transportation Engineering, Construction, Architecture and Environment Faculty.
- Ritchie H (2017). *CO₂ and other Greenhouse Gas Emissions*. Retrieved from <https://ourworldindata.org/co2-and-other-greenhouse-gas-emissions>
- Todd, M. (2006). *Enhanced Transit Strategies: Bus Lanes with Intermittent Priority and ITS Technology Architectures for TOD Enhancement*. Institute of Transportation Studies.
- TNO. *EnViVer model traffic*. Retrieved from TNO: <https://www.tno.nl/en/focus-areas/traffic-transport/roadmaps/mobility-logistics-digitalisation/sustainable-mobility/improving-air-quality-by-monitoring-real-world-emissions/enviver-model-traffic-flow-and-emissions/>
- Wu, D. (2016, April 19). Evaluating Operational Effects of Bus Lane with Intermittent Priority under Connected Vehicle Environments. Retrieved from Discrete Dynamics in Nature and Society

2.4.4 Well-to-wheel emission factors for future cars in Germany with a focus on fleet composition, new technologies and emissions from energy supplies

Stefan Seum^{1*}, Simone Ehrenberger² and Thomas Pregger³

¹ Institute of Transport Research, German Aerospace Center (DLR), Berlin, Germany, Stefan.Seum@dlr.de

² Institute of Vehicle Concepts, German Aerospace Center (DLR), Stuttgart, Germany

³ Department of Energy Systems Analysis, Institute of Engineering Thermodynamics, German Aerospace Center (DLR), Stuttgart, Germany

Keywords: car emission, fleet-wide emission factors, German transport scenario, well-to-wheel, energy scenario

1. Introduction

Until today road transport remains largely fossil fuel driven and therefore significantly contributes to emissions of greenhouse gases and air pollutants, particularly nitrogen oxides and particulate matter (EEA 2015). On the other hand, new vehicle technologies are emerging and existing technologies are being improved regarding fuel efficiency and transport emissions. The assessment of technologies and their implementation with the aid of scenario analysis is an appropriate tool to evaluate effects of different development pathways. The assessment of future emissions to air needs to consider not only tailpipe emissions from engines, but also emissions associated with the generation of electricity, since transport will increasingly be electrified. In this context and with regard to the requirement to provide robust environmental assessment of transport activities this contribution addresses some of the major gaps in prospective emission estimation from future cars and vehicle fleets.

The aim of this work is to provide emission factors for future cars and fleets that allow the calculation of comprehensive emission effects in scenario analysis. This work is motivated by the project Transport and the Environment (Henning et al., 2015), in which twelve institutes of the German Aerospace Center (DLR) developed three explorative scenarios of the German transport system up to 2040. The scenarios were named *Reference*, *Free Play* and *Regulated Shift*, and Table 1 characterizes the main storylines of these long-term pathways. The scenario definitions provide consistent context settings, and societal levers were identified that affect both, the transport and the energy system. Emissions and environmental effects were calculated using a network of models, established at the DLR. Both, the transport and the energy system are included in the scenarios. The derivation of the scenarios including the setting of model parameter can be found in Seum et al. (forthcoming).

The integration of new car and fleet-wide emission factors for vehicles goes beyond scenario approaches, where improvements in technologies are only considered as relative changes. Conventional tank-to-wheel emission factors are expanded by including well-to-tank emissions derived from defined energy scenarios. This allows a non-bias comparison of different technologies. This integrated approach to develop new emission factors is presented in this article, using the example of passenger cars. The focus is on four main pollutants of road transportation, namely carbon dioxide (CO₂), carbon monoxide (CO), nitrogen oxides (NO_x), and fine particulate matter (PM₁₀).

In a first step, we modified existing tank-to-wheel emission factors to reflect the vehicle composition of future scenario fleets. Since new propulsion technologies, particularly electric drives, are swiftly appearing, we developed new tailpipe emission factors for hybrid technologies. Furthermore, for plug-in-hybrid, battery-electric, and fuel cell technologies energy consumption factors are calculated using an advanced model-based approach. The generation of electricity and the resulting emissions were considered based on long-term energy scenarios. We enhanced for this purpose a bottom-up normative energy scenario by a calibrated top-down emission forecast. The final results are well-to-wheel emission factors that include raw material processing to provide the energy for transportation. The extraction and transport of raw materials is omitted, but could be added through life cycle assessment data.

Table 1: Snapshot of the three VEU scenarios. Condensed description from Seum et al. forthcoming

Reference scenario	Free Play scenario	Regulated Shift scenario
Represents a continuation of currently existing trends, but also moderate improvements regarding the implementation of new technologies and the use of renewable energies (RE) in the transport sector.	Society follows a liberal market-economic logic. The state in this scenario takes a step back, trying to avoid hampering developments through an overburden of regulations.	Society implements more stringent regulations, combined with investments in infrastructure for public transport and financial instruments to foster the development of certain clean technologies.

2. Problem statement and approach

Together with the European legislation for limiting emissions of on-road vehicles, a set of emission modelling tools have been developed (e.g. Ntziachristos et al., 2009; Keller et al., 2017). In combination with transport demand models, such as TREMOD or REMOVE, emission models are primarily established to monitor emissions and to create national inventories. Those models allow, to a limited extent, the outlook into the future, but neglect new vehicle technologies and interdependencies with regard to technology developments. In addition, many scientific studies have been published addressing the improvement of emission factors and models for road transportation and providing data sets as basis for emission calculations (e.g., Voutsis et al., 2017; Franco et al., 2013). However, emission factors for new technologies that would allow comparative assessments are missing.

More recently, the discussion shifted to the representativeness of emission factors and model results, as evidence of increasing gaps between real-world driving emissions and emission factors emerged. Here two phenomena are observed. First, the increasing gap between real-world fuel consumption and dynamometer testbed derived values. Second, the exceedance of legal emissions limits, in particular of NO_x emissions from diesel fuelled cars. The first is due to a large leeway in the standard test procedure and particular a limited operational coverage of the old test driving cycle (NEDC – New European Driving Cycle). Fontaras et al. (2017) discusses the influencing factors for fuel consumed and evaluates the introduction of the new test driving cycle (WLTP – Worldwide harmonized Light-duty Test Procedure). The second phenomena stems from technical limits of emission control devices and manipulations that led to optimized emission figures under test conditions and often higher emissions under real driving conditions. The focus here was on NO_x emissions (e.g. Kousoulidou et al., 2013; O’Driscoll et al., 2016), which are particularly elevated with diesel cars.

The introduction of new technologies appears in a societal context and interdependencies need to be considered. The effect of societal levers (e.g. financial measures, regulation, investments) on a system level is hereby in the centre of our explorative scenario analysis. For this reason, scenario-based factor developments are an advancement to existing approaches. On the one hand, possible development pathways of vehicle concepts, their sizes and drivetrains and technology implementation need to be addressed. On the other hand, the increasing electrification of mobility in the form of battery-powered vehicles and hybrids results in well-to-tank emissions from power generation that must be taken into account in a consistent and plausible manner. Therefore, our basic approach is a coupling of scenario-based simulations of future vehicle fleets, an update and extension of emission factors for different vehicle categories, and an integration of scenario-based estimations of the future emissions from the energy supply. The following sections provide a detailed description of the approach.

The Handbook of Emission Factors (HBEFA 2017, Keller et al., 2017) provides a good starting point for developing fleet-wide emission factors for Europe. HBEFA provides emission factors for passenger cars, light and heavy duty vehicles and buses with conventional engines. The factors are split according to the propulsion systems “diesel”, “gasoline” and “gas” (CNG) and the corresponding EURO emission classes. Emission factors for passenger cars are split in engine size categories (smaller than 1.4 litre, 1.4 up to 2.0 litre and larger than 2.0 litre). Another feature of HBEFA is the distribution of vehicle-kilometre travelled on three road categories – urban, extra-urban and highway. The HBEFA Handbook offers emission factors for the years 1995 to 2030 in five year steps. The Handbook was originally developed based on emission measurements of existing vehicles and on vehicle simulations with the model PHEM. The emission factors in HBEFA are approximations of real driving emissions and fuel consumption. HBEFA was developed on behalf of the Environmental Protection Agencies of Germany, Switzerland and Austria (TU Graz, 2009). In the meantime, further countries (Sweden, Norway, and

France) as well as the JRC (European Research Centre of the European Commission) are supporting HBEFA.

In the project Transport and the Environment, we have developed three possible future explorative scenarios for Germany up to 2040 (Seum et al., 2017). In a structured approach, combining qualitative and quantitative methods, the plausible and consistent storylines of the *Reference*, the *Free Play* and the *Regulated Shift Scenario* were created (Seum et al. forthcoming). In each scenario, societal levers were identified and effects for the transport and energy system were modelled. The three scenarios affect future emissions of passenger vehicles through different evolutions of the transport system with an effect on vehicle fleets. For example, the *Reference* scenario plots a continuation of current trends with the *Free Play* and *Regulated Shift* scenarios developing in opposite directions. In the *Free Play* scenario the propulsion systems are in an unequal competition and public transit deteriorates, except for central and dense urban areas. Vice versa, the *Regulated Shift* scenario assumes policies that promote walking, biking, public transit and advanced vehicle technologies, by at the same time making private car ownership more expensive and parking less available. Thus, the vehicle fleet provided by HBEFA for the year 2030 needed to be modified according to those scenario developments and emission factors needed to be extended to the year 2040.

3. Methodology for deriving scenario-based emission factors

3.1. Passenger car size development and composition

The scenario dependent passenger car fleets were modified in two fields. First, the development of vehicle and engine size was projected. Second, the market penetration of propulsion technologies was modelled. The approach with regard to the non-technical fleet composition is presented in this section. The technical aspects are discussed in the following section.

To date there is no standard classification system for the passenger car market with regard to size and segments. Segments, however, are often used to analyse vehicle market trends. The German market for passenger cars differentiates between thirteen segments (KBA, 2016), which correspond to largely the European passenger car classes (EEC 1999) (Table 2). For the recent development, we analysed the car stock for the years 2008-2015. The largest segment is that of compact cars, which represent 26% of the vehicle in stock in 2015 (KBA, 2016). However, the fastest growing market segments are those of SUV and off-road vehicles, which nearly tripled in stock between 2008 and 2015. For our purpose to project vehicle developments according to certain scenario assumptions, we aimed to simplify the vehicle segments into three vehicle size classes: small (S), medium (M) and large (L) (see Table 2). The past decade of passenger car development is characterized by a strong growth of the segments S (+14%, 2008–2015) and L (+15%), whereas the medium size cars M only grew by 7%. Simultaneously a trend in engine downsizing by at the same time an increase in average engine power can be observed (Fontaras et al., 2017; ICCT, 2018).

Within our scenario analysis, we implemented measures that affect both, trends in vehicle size and trends in engine sizes. Since HBEFA plots the fleet performance based on the distribution of engine size in terms of cubic capacity, the allocation of engine sizes to vehicle sizes is necessary.

The data available to allocate engine sizes to passenger car segments are average displacement per KBA segment and motorization information from the ADAC database on cars (ADAC, 2016). For each segment three to four most selling cars were selected (e.g. VW Polo, Toyota Yaris, Peugeot 207 and Citroen C3 for the Supermini segment). Largest and smallest engines available for those cars were taken from the ADAC database on cars. Together with the average engine size, we applied a standard distribution of engine sizes per vehicle segment. Finally we adjusted the selection, (i.e. excluded some extreme motorization cases), in order to calibrate the engine distribution to data provided by HBEFA for 2015. The matched distribution of engines to passenger car segments is presented in Table 3.

Table 2: Classification of German passenger car stock, 2015 shares and growth 2008 – 2015 (KBA 2016)

German segments	car	EU classes	S, M, L allocation	Share in stock 2015	Growth 2008 - 2015
City car		A	S	7.0%	36%
Supermini		B	S	20.5%	8%
Small family car		C	M	27.3%	3%
Large family car		D	M	16.3%	- 15%
Executive		E	L	4.8%	- 15%
Luxury car		F	L	0.6%	20%
Compact SUV		J	M	4.2%	180%
Large 4x4		J	L	4.3%	NA
Sports car		S	L	1.9%	35%
Vans		M	M	4.6%	34%
Minibus		M	L	4.8%	16%
Utilities		M	L	3.8%	32%

Note: the category “caravans” was excluded from the analysis.

Table 3: Allocation of engine sizes to passenger car segments and S, M, L classification in 2015.

German car segments	S, M, L allocation	Engines < 1.4 l	Engines 1.4 < 2.0 l	Engines >= 2.0 l
City car	S	100%	0%	0%
Supermini	S	90%	10%	0%
Small family car	M	23%	77%	0%
Large family car	M	5%	58%	37%
Executive	L	0%	20%	80%
Luxury car	L	0%	5%	95%
Compact SUV	M	7%	88%	5%
Large 4x4	L	5%	44%	51%
Sports car	L	1%	14%	85%
Vans	M	1%	99%	0%
Minibus	L	5%	90%	5%
Utilities	L	2%	82%	16%

The setting of several assumptions provided below then led to the development of the vehicle size distribution in the three scenarios. The assumptions were calibrated by matching the *Reference* scenario engine size distribution 2030 with those of the HBEFA data for 2030. For the other two scenarios we adjusted the segment and engine distribution based on demographic and behaviour assumptions that were qualitatively set and that are consistent to the scenario storylines (Seum et al., forthcoming). The resulting trends are:

- *Reference* scenario: Trend towards small vehicles and SUV continues. S segment increases by 2%, L increases by 3%. M declines by 2%. For the engine development we assume a general downsizing trend, but with a high power trend in upscale segments. This results in 14% more engines with <1.4 l and 4% less engines with >=2.0 l cubic capacity.
- *Free Play* scenario: The comparatively low cost for private cars lead to an increased trend towards larger vehicles and SUV. S segment decreases by 40%, M increases by 10% and L increases by 30%. For the engine development we assumed a trend to higher powered vehicles that offset downsizing trends. This results in 5% less engines <1.4 l and 10% more engines with >=2.0 l cubic capacity.

- *Regulated Shift* scenario: Higher costs for private car use and an increased awareness for environmental issues lead to strong shift towards smaller cars. S segment increases by 20%, M increases by 5% and L decreases by 40%. For the engine development we assume a stronger trend towards downsizing compared to the *Reference*. This results in 50% more engines with <1.4 l and 50% less engines ≥ 2.0 l cubic capacity.

3.2. New emission factors for passenger cars

Additionally to conventional gasoline (G) and diesel (D) vehicles found in HBEFA (v3.3), we consider diesel and gasoline full hybrid electric vehicle (D-HEV and G-HEV), gasoline plug-in hybrid electric vehicles (PHEV), battery electric vehicles (BEVs) and fuel cell electric vehicles (FCEV). The emission factors for hybrid vehicles were developed using our own measurements on the DLR test-bed as well as literature reviews (EPA, 2016; Kugler et al., 2016; Suarez-Bertoa and Astorga, 2016). Furthermore, we modelled the energy demand from electric vehicles and the electrically driven proportion of plug-in hybrid vehicles. Emissions factors, which describe the mass of different emitted gases per kilometre, were developed for each type of drive-train and vehicle size within the three scenarios. As the scenarios described above illustrate the development of transport into the future, we needed to develop these emission factors for the reference years 2030 and 2040. Emission factors for 2010 were provided by HBEFA.

Energy consumption and carbon dioxide emissions were simulated with the VECTOR21 tool, (Mock, 2010) including a dedicated module for PHEV, using the world harmonized light-duty vehicle test cycle (WLTC) (Kugler et al., 2017; Schimeczek, 2015). Within this model, the energy consumption of different vehicle concepts is calculated based on the efficiency of the driving machines and gear transmission. The efficiencies are determined on the basis of simplified efficiency maps. The scenario settings as described in Table 1 and further outlined in Seum et al. (forthcoming) determine the extent of user demand on increased energy efficiency of each drive train. Based on this demand, costs for certain efficiency technologies and drive-trains evolve differently and lead to a variance in the future vehicle market. Therefore, fuel efficiency and electric energy consumption of future drive-trains diverge in the three scenarios. In case of electrified vehicles (HEV, PHEV and BEV), the efficiency technologies additionally affect the electric range and thus the absolute direct emissions and energy consumption of the vehicle in operation. For hybrid vehicles, the main influencing aspect for the energy efficiency and the share of fossil driving is the electric range. We applied this range to determine the utility factors for each vehicle. Compared to conventional vehicles, hybrid vehicles achieve a better fuel efficiency on all roads due to the permanent electric assistance of the hybrid system in addition to portions of pure electric driving in particular on urban roads (Table 4). The tank-to-wheel CO₂ emissions of the vehicles in 2030 and 2040 are directly calculated based on the resulting fuel consumption with a ratio of 2.3 kg CO₂ per litre of gasoline and 2.4 kg CO₂ per litre of diesel.

In the case of conventional gasoline and diesel vehicles, we used emission factors for air pollutants from HBEFA (v3.3) up to the reference year 2030. Emission factors for cars that use compressed natural gas (CNG) were derived from BMU (2009) and the corresponding data sets in the GEMIS database (IINAS 2017). It should be noted that data on emissions from CNG vehicles is sparse and particularly the future prospects are largely unknown. As for air pollutant emissions, in particular CO, NO_x and PM, we expect the emission factors for conventional technologies to decline in the future, i.e. beyond 2030, due to stricter regulations and controls in the upcoming years. For 2040, we assumed all vehicles would be EURO 6 compliant.

Table 4: Tank-to wheel energy consumption per drive train in MJ/km in 2040 (G = gasoline, D = diesel, G-HEV = gasoline-hybrid-vehicles, D-HEV = diesel-hybrid-vehicles, PHEV (fuel) = fossil fuel portion of plug-in-hybrid-vehicles (gasoline), PHEV (electricity) = electricity from grid portion of plug-in-hybrid-vehicles (gasoline), BEV = battery-electric-vehicles, FCEV = fuel-cell-electric-vehicles)

Drive-train	Reference			Free Play			Regulated Shift		
	S	M	L	S	M	L	S	M	L
G	1.46	1.59	3.25	1.47	1.74	2.85	1.46	1.66	3.24
D	1.30	1.51	1.61	1.30	1.62	1.75	1.28	1.42	1.76
G-HEV	1.01	1.07	1.42	1.39	1.52	1.82	1.05	1.10	1.56
D-HEV	0.80	1.00	1.49	0.96	1.22	1.79	0.94	1.07	2.13
PHEV (fuel)	-	1.51	2.09	-	1.56	2.23	1.49	1.5	2.11
PHEV (electricity)	-	0.53	0.55	-	0.54	0.58	0.52	0.52	0.56
BEV (electricity)	0.45	0.50	0.52	0.45	0.56	0.65	0.44	0.55	0.60
FCEV (hydrogen)	-	-	-	-	-	-	-	1.23	1.7

With regard to hybrid technologies, studies on HEV emissions report possible emission savings of up to 60% for particular pollutants (Fontaras et al., 2008; Alvarez and Weilenmann, 2012; Suarez-Bertoa and Astorga, 2016). As there are large uncertainties concerning the real reduction potential on the road, a conservative reduction of 10% in addition to the reduction of conventional EURO 6 vehicle was assumed. Furthermore, a 10% share of electric driving in cities was assumed for HEV as default. We recognize the large uncertainty in this assumption, but due to a lack of data on the share of electric driving of HEVs and based on estimations on energy recuperation and battery capacity, the 10% share is seen as a conservative estimation on possible electric ranges in urban driving.

The emission factors of PHEV are based on own measurements of emissions of a mid-size PHEV on the DLR vehicle dynamometer (exemplarily described in Kugler et al., 2016). These measurements delivered the emissions for the different road categories and temperatures as well as a utility factor to take into account the different electric driving shares in urban, extra-urban and highway driving situations. The utility factor implies the share of driving in the charge depletion (CD) mode and charge sustaining (CS) mode of a PHEV. In the CD mode, the battery provides sufficient energy for mainly electric driving, while in the CS mode the battery's state-of-charge (SOC) is at a low level and the vehicle is operated mainly with the internal combustion engine. For our calculation, the utility factors were taken from the WLTP standard and vary between 0.65 and 0.77, depending on vehicle size, reference year and scenario. The basic pollutant emissions are assumed to be equal for all vehicle sizes. Due to the utility factor approach, absolute CO₂ and pollutant emissions differ between the sizes.

In order to address the spatial distribution of emissions and the differences of energy consumption and emissions in different traffic situations, factors for three road categories – urban, extra-urban and highway – were applied. In case of conventional vehicles, the pollutant emission factors were taken from the HBEFA database accordingly. For energy consumption and CO₂ emissions of conventional vehicles as well as for the alternative vehicles in general, WLTC simulation and measurement data are allocated to the segments of the cycle. In a final calculation step, emissions and energy consumptions are weighted according to the shares of average driving situation in Germany, which is for the *Reference* scenario 32% urban driving, 39% of rural driving, 29% of highway driving in 2010 and 34% urban, 36% rural and 30% highway driving in 2040 (Winkler et al. 2017). Additionally, car-km travelled for the vehicle size categories per road type differs in each scenario slightly. For the electrified transport modes and vehicles we applied average emission factors from the German power generation system based on scenarios (see next section).

3.3. Emissions from electricity and fuel supply

The shift from fossil fuels to electric energy can significantly reduce transport emissions of greenhouse gases and air pollutants. Several studies have already shown that this requires a substantial shift

towards renewable energy (RE) sources and flexible infrastructures in the power system, while at the same time reducing thermal power generators based on fossil fuels (e.g., McLaren et al., 2016; Ökoinstitut, 2016; Luca de Tena and Pregger, 2018). Consistent with the socio-economic assumptions and normative political targets, we therefore assumed different developments of the power system for the three scenarios. A successful continuation of the German 'Energiewende', i.e. target-oriented RE expansion in power generation results in around 78% renewable electricity in 2040 in the *Regulated Shift* scenario. In contrast, this share is around 50% in the *Reference* case without additional politically set incentives and assumed to be only 40% in the *Free Play* scenario, equivalent to a stop of further RE expansion around the year 2020.

Consistent with the assumed political boundary conditions and the targets in transport, the scenarios differ primarily with regard to the development of renewable electricity generation, but also with regard to the demand for electricity in individual sectors due to different efficiency assumptions. Table 5 summarizes the assumptions for the German energy system. The highest renewable share of gross power generation is reached in the *Regulated Shift* scenario. Electricity demand for the sectors industry, residential, and services and commerce is derived from Schlesinger et al. (2014) for the *Reference* and the *Free Play* scenarios assuming in both cases the same efficiency path. Assumed electricity demand in the *Regulated Shift* scenario is based on normative scenarios achieving the political CO₂ emission and efficiency targets, namely the 'Target scenario' from Schlesinger et al. (2014) and the 'Long-term scenarios' from Pregger et al. (2013). All scenarios take into account decreasing intensities of the 'classical' consumers but increasing demand from implementing new technologies. These are above all heat pumps and electric boilers in the heating sector and electric vehicles in transportation, serving also as flexibility options (power-to-x) in future energy systems with high shares of variable renewable power.

The scenarios were calculated with a scenario model developed by DLR for Germany using the commercial software Mesap/PlaNet (Modular Energy System Analysis and Planning Environment, seven2one, Karlsruhe). The philosophy and basic structure of the so-called "accounting framework" were presented in Schlenzig (1999). The Mesap-based energy models were used by DLR in numerous projects for the development of normative scenarios (e.g. (Krewitt et al., 2009; Teske et al., 2018; Pregger et al., 2019).

Table 5: Main energy scenario parameters for 2040: electricity consumption and generation structure

Parameter	Base year 2010	Reference 2040	Free Play 2040	Regulated Shift 2040
Gross electricity consumption [TWh/yr]	612	574	560	560
thereof transport (incl. for hydrogen)	20	35	17	126
<u>Share of power generation:</u>				
Renewables without biomass	11%	41%	31%	65%
Biomass	5.4%	10%	9%	13%
Hard coal	18%	14%	21%	3%
Lignite	23%	18%	22%	0%
Non-biogenic waste	4%	1%	1%	1%
Oil	1%	0%	0%	0%
Natural gas	14%	16%	15%	18%

Emission factors for thermal power generators were derived from emission estimates and factors provided by the German Environment Agency (UBA, 2015), used for emission reporting. While energy models distinguish sectors and fuels, possibly with subcategories such as cogeneration, emission factors usually refer to specific plant sizes and permit requirements. Since an assignment of the emission factors could only be made on an aggregated level, we applied a top-down calibration of our emission estimation based on bottom-up calculations from official emission reporting for the energy sector (UBA, 2016a). The calibration was done for the years 2009, 2011, 2012 and 2014. Emission factors were then assumed to stay constant in the future as the further development of air pollution regulation in the future is unknown. Therefore changes in our average specific emissions from electricity supply are only due to the changing generation mix. Emission factors for the supply of fossil fuels are

own estimations representing emissions from industrial process heating, modified by the calibration. The resulting specific direct emissions for the supply of electricity and fuels referring to MJ consumed were derived from the scenario results for the refinery production, the fuel consumption in transportation and estimated emissions in the conversion sector derived from the official emission reporting (UBA, 2016b).

4. Results and discussion

In this section we compile the results of our analysis above. First, the final segment and engine size shares are presented. Second, tank-to-wheel (tailpipe) emissions and well-to-tank emissions for electricity and fuels are presented separately. Finally, we provide an overview of total emissions (well-to-wheel) by scenario and drivetrain.

Table 6: Scenario development for 2040 of passenger car segment distributions and engine sizes distribution for gasoline and diesel cars. (S = small, M = medium, L = large)

Scenario 2040	Segment	% share of segments for all technologies	Distribution of engine size for gasoline and diesel cars		
			Engines < 1.4 l	Engines 1.4 < 2.0 l	Engines >= 2.0 l
Reference	S	28.0%	28.0%	0.0%	0.0%
	M	51.3%	8.3%	37.1%	5.9%
	L	20.8%	0.7%	11.0%	9.0%
Free Play	S	16.8%	15.9%	0.8%	0.0%
	M	56.4%	8.7%	40.5%	7.2%
	L	27.0%	0.8%	13.2%	13.0%
Regulated Shift	S	33.5%	33.6%	0.0%	0.0%
	M	53.9%	13.1%	36.7%	4.1%
	L	12.5%	0.6%	8.2%	3.6%

Both the car size and the technology mix differ in the three scenarios. Table 6 presents the resulting passenger car fleet development with regard to car size, applicable for all engine technologies on the left side. On the right side of Table 6, the distribution of engine size for gasoline and diesel engines is presented. In all scenarios, the mid-size category dominates. However, in the *Free Play* scenario a clear shift to larger cars and larger engines is visible. The S car segment nearly halves compared to the *Reference* scenario and the L segment increases by one third. The engines ≥ 2.0 l are even 35% above the *Reference* level. In the *Regulated Shift* scenario the tendency to downsize engines and vehicles is clearly visible. Small cars are 20% and engines <1.4 l nearly 30% above the *Reference* levels. The M size categories are elevated in both, the *Free Play* and the *Regulated Shift* scenarios, but originating from the S or the L category respectively. Further discussed in Ehrenberger et al. (forthcoming) are changes in the fleet composition with regard to the gasoline and diesel fuelled vehicles.

Table 7 and Table 8 present the development of tank-to-wheel emission factors for cars by category for the three underlying scenarios. In the case of air pollutants, specific emissions from gasoline and diesel engines are nearly the same in all three scenarios because of identical assumptions regarding emission limits, although car segment and size shares are different. The final scenario-based CO₂ emission factors per vehicle are a combination of technological progressions in energy efficiency and in case of hybrid vehicles the increase of the electric mileage due to higher battery capacities and again increase in energy efficiency.

Due to technology improvements, the CO₂ and pollutant emissions of conventional vehicles will already decrease in all scenarios for 2040 compared to 2010. A further reduction is achieved through an increasing share of electric driving in particular in the *Regulated Shift* scenario. Political CO₂ targets directly affect the achieved energy and thus CO₂ efficiency of the vehicles. The *Free Play* scenario with the least strict regulations consequently shows the highest emissions of the three scenarios except for PHEVs. This vehicle type shows a higher degree of maturity in this scenario as more PHEVs are demanded by the market. The reverse mechanism applies for the conventional gasoline vehicles, despite of stricter CO₂ targets in the *Regulated Shift* scenario. NO_x emissions remain high for vehicles using a

diesel engine, both in the case of conventional and hybrid electric vehicles (Table 8). Thus the NO_x emission factors for an average diesel car remain approximately seven times higher compared to gasoline cars.

Table 7: Tank-to-wheel CO₂ emissions in g/km of considered vehicle categories (G = gasoline, D = diesel, G-HEV = gasoline-hybrid vehicle, D-HEV = diesel-hybrid vehicle, PHEV = plug-in-hybrid vehicle (gasoline) and CNG = compressed natural gas vehicle)

Drive-train	Base year 2010	Reference 2040	Free Play 2040	Regulated Shift 2040
G	197	127	148	131
D	184	114	125	111
G-HEV	-	87	117	94
D-HEV	-	69	79	88
PHEV	-	27	28	32
CNG	-	120	123	113

Table 8: Tank-to-wheel NO_x, CO, and PM emissions for different drive-train types in the reference scenario. (G = gasoline, D = diesel, G-HEV = gasoline-hybrid vehicle, D-HEV = diesel-hybrid vehicle, PHEV = plug-in-hybrid vehicle (gasoline) and CNG = compressed natural gas vehicle)

Drive-train	NO _x [g/km]		CO [g/km]		PM [g/km]	
	2010	2040	2010	2040	2010	2040
G	0.167	0.020	1.206	0.638	0.003	0.002
D	0.641	0.150	0.051	0.028	0.021	0.002
G-HEV	-	0.017	-	0.500	-	0.002
D-HEV	-	0.135	-	0.010	-	0.002
PHEV	-	0.003	-	0.009	-	0.001
CNG	-	0.057	-	1.442	-	0.000

Table 9 provides the derived emission factors for electricity and fuel generation by scenario. The results for power generation vary significantly depending on the assumed supply structure and for transport fuels only slightly due to the underlying structure of oil product use and generation in the energy system. For the consideration of well-to-tank emissions of hydrogen, the emission factors from electricity generation are divided by the (loss) factor 0.7. In addition, well-to-tank emissions from the gas supply for CNG vehicles were estimated using the simple methodology described above. As a result, the specific emissions 0.5 g CO₂ per MJ (based on gas consumed), 2 mg NO_x per MJ, 0.5 mg CO per MJ and 0.1 mg PM₁₀ per MJ are considered in all scenarios below.

The fleet-wide emissions are a result of tailpipe emissions (tank-to-wheel) and refinery emissions as well as the emissions originating from the electricity generation, used for transport purposes (well-to-tank).

Table 9: Calculated well-to-tank emissions from energy supply per unit of electricity respectively oil product in g/MJ

Specific emission	2010	Reference 2040	Free Play 2040	Regulated Shift 2040
CO₂				
electricity (g/MJ)	138.3	86.9	114.2	24.2
transport fuels (g/MJ)	4.6	3.7	3.6	3.8
NO_x				
electricity (g/MJ)	0.1175	0.0775	0.0922	0.0439
transport fuels (g/MJ)	0.0041	0.0036	0.0035	0.0029
CO				
electricity (g/MJ)	0.0522	0.0381	0.0439	0.0264
transport fuels (g/MJ)	0.0004	0.0004	0.0003	0.0003
PM₁₀				
electricity (g/MJ)	0.0036	0.0027	0.0032	0.0012
transport fuels (g/MJ)	0.0007	0.0005	0.0005	0.0004

Taking the above described scenario effects into consideration, different shares of tank-to-wheel and well-to-tank vehicle emissions can be identified (Figure 1). Clearly, the higher the grade of electrification, the less CO₂ is emitted per km. Due to a higher share of renewable energy in the 2040 electricity mix in the *Regulated Shift* scenario, the BEV and PHEV vehicles have the highest CO₂ benefits of all considered vehicle types. The conventional technologies develop less efficiently in the *Regulated Shift* scenario, whose framework settings strongly support the evolution of highly electrified drive-trains. Therefore, the conventional and full hybrid vehicles develop more efficient in other frameworks like the *Reference* or *Free Play* scenarios.

In case of NO_x emissions, diesel vehicles as well as the electricity production contribute most to the overall emissions. Gasoline cars have similar NO_x emissions as BEVs or PHEVs. Nevertheless, tailpipe (tank-to-wheel) NO_x emissions might have different (local) impacts on air quality and health than NO_x emissions from power plants. CO emissions remain an issue for gasoline and CNG vehicles in all scenarios, although, information on future emissions from CNG vehicles is highly uncertain. Particle emissions are critical both from indirect and direct sources and in this case, fuel production (gasoline and diesel) has considerable impact with the exception of CNG vehicles. Even in a predominantly renewable electricity supply, particle emissions are still clearly present, which is due to the emission estimate for the mostly decentralised use of biomass.

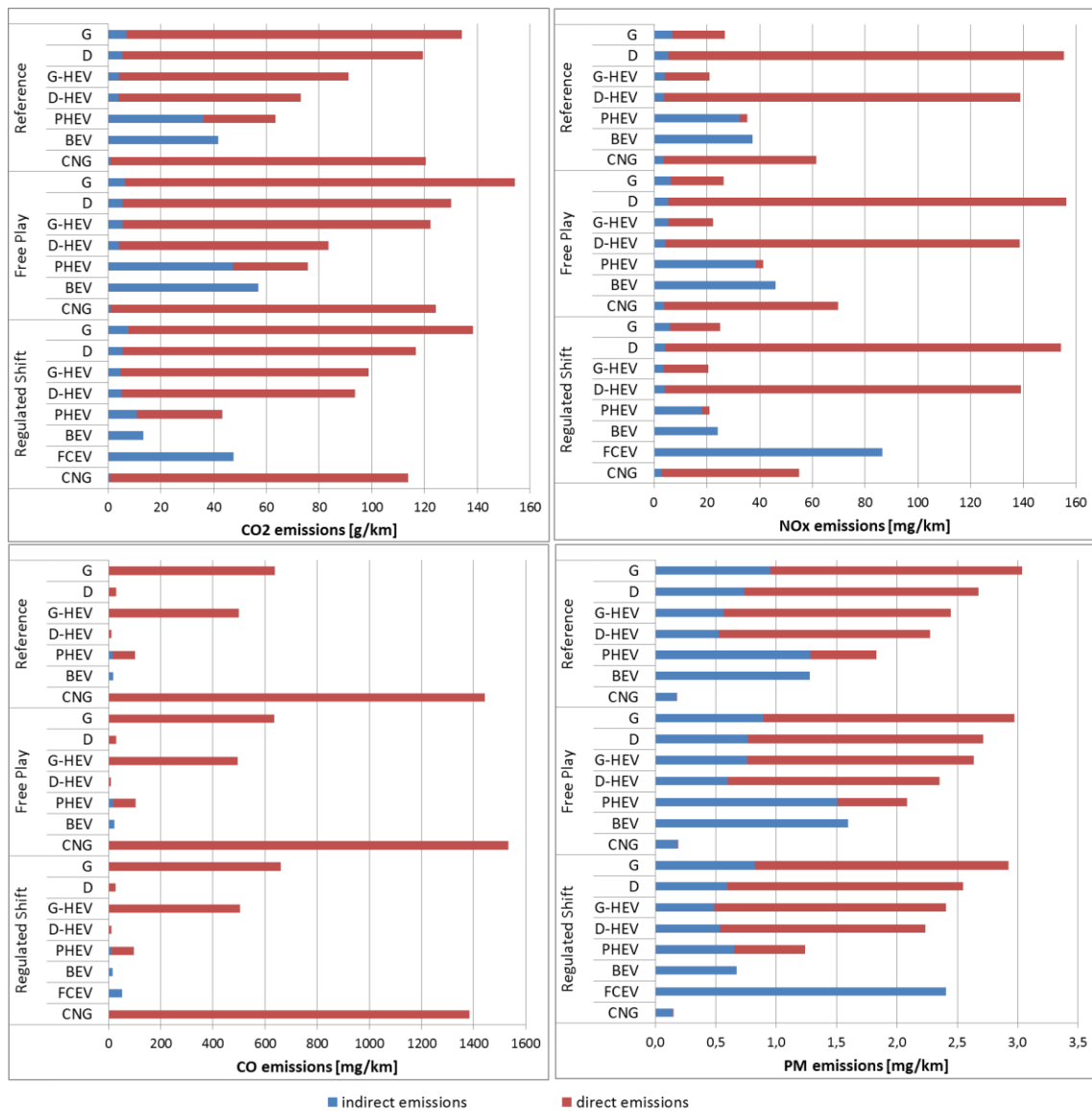


Figure 1: Calculated total indirect and direct emissions of the vehicle technologies in 2040. (G = gasoline, D = diesel, G-HEV = gasoline-hybrid vehicle, D-HEV = diesel-hybrid vehicle, PHEV = plug-in-hybrid vehicle (gasoline), BEV = battery-electric vehicle, FCEV = fuel-cell electric vehicle and CNG = compressed natural gas vehicle)

5. Conclusion

This paper highlights the importance to systematically address interdependencies of developments in the transport and energy sectors in scenario analysis, with regard to the overall emissions. The development of emission factors must take those interdependencies into account and future analyses need to build on plausible and consistent assumptions. Consistency and plausibility is best achieved in explorative scenarios, with a subsequent modelling of the effects of societal decisions on the transport and energy system. Development pathways into the future will influence car fleets, technologies and also the whole energy system. Important factors are changes in fleet composition and vehicle sizes, the market penetration of new vehicle concepts and technologies and also the future generation mix for electricity. One example of interdependence is the accelerated progress and efficiency improvements when more vehicles of an advanced technology enter the market. While general improvements can be expected with all technologies, the technologies with significant market shares will be able to improve faster than others.

The composition of vehicle fleets has a large impact on future emissions from passenger cars. For example, CO₂ emissions of gasoline vehicles vary by 17% and of diesel by 13%, purely due to

differences in vehicle and engine size (see Table 7) While generally the electrification of private passenger cars is perceived as beneficial with regard to greenhouse gas emissions, the extent largely depends on the developments of the electricity system. The operational benefits alone are small, when electricity is not predominately generated by renewable sources and high share of coal based electricity is applied. Thus, a deep decarbonization pathway needs to include the electrification of significant portions of the passenger car fleets in conjunction with a sustainable power generation structure. In addition, temporal and regional interactions between energy and transport systems are relevant with regard to load balancing, resulting infrastructure needs and future energy costs and could also further improve the assessment of well-to-tank emissions.

Furthermore, the emission reduction prospects differ from pollutant to pollutant. For example, nitrogen oxide and particulate matter emissions from power generation could still significantly contribute in the future to the overall ambient air emissions, depending on the remaining thermal generation capacities for electricity. More precise bottom-up considerations of the role and emission factors of future decentralized biomass and biogas power plants are desirable in this respect. With regard to the direct tailpipe NO_x emissions, a significant reduction is technically feasible and can be expected with all technologies. This inherits the assumption that the divergence between real-world driving emissions and test-bed emissions will diminish in the future. Furthermore, diesel fueled vehicles will have elevated tailpipe NO_x emissions, albeit at much lower levels than today.

Further research is needed regarding the effects of different scenarios for ambient air quality. Since in some scenarios the release of air pollutants is shifted from tailpipe to power plant stacks, an effect of street-level emissions and imported background emissions can be expected. Furthermore, as tailpipe particulate emissions decrease, the secondary emissions from tire and brake wear as well as from resuspension of dust become more important. This too warrants further research. Further research should also look into the life cycle aspects of fully electrified vehicles as well as resource aspects since the battery production is associated with high energy demand and emissions. Finally, the question on changes in the vehicle usage in light of emerging technologies should be investigated.

6. References

- ADAC (2016). Online database on car models: Autokatalog. Accessed April 2016. <https://www.adac.de/infotestrat/autodatenbank/autokatalog/default.aspx?ComponentId=199514&SourcePageId=287152>.
- Alvarez R., Weilenmann M. (2012). Effect of low ambient temperature on fuel consumption and pollutant and CO₂ emissions of hybrid electric vehicles in real-world conditions. *Fuel* 97, 119–124. <https://doi.org/10.1016/j.fuel.2012.01.022>.
- BMU (2009). RENEWABILITY – Stoffstromanalyse nachhaltige Mobilität im Kontext erneuerbarer Energien bis 2030. Teil 1: Methodik und Datenbasis. Endbericht an das Bundesministerium für Umwelt, Naturschutz und Reaktorsicherheit (BMU). Öko-Institut und DLR Institut für Verkehrsforschung (in German).
- EEA (2015). Evaluating 15 years of transport and environmental policy integration. TERM 2015: Transport indicators tracking progress toward environmental targets in Europe. European Environmental Agency (EEA) Report No 7/2015. ISSN 1977-8449.
- EEC (1999). Case No. COMP/M.1406 – Hyundai / Kia. Regulation (EEC) No 4064/89, merger procedure. Article 6(1)(b) NON-OPPOSITION. 17/03/1999. Commission of the European Communities. http://ec.europa.eu/competition/mergers/cases/decisions/m1406_en.pdf
- EPA (2016). Annual certification test data for light duty vehicles. United States Environmental Protection Agency.
- Fontaras G., Zacharof N.G., Ciuffo B. (2017). Fuel consumption and CO₂-emissions from passenger cars in Europe – Laboratory versus real-world emissions. In: *Progress in Energy and Combustion Science* 60 (2017) 97-131.
- Fontaras G., Pistikopoulos P., Samaras Z. (2008). Experimental evaluation of hybrid vehicle fuel economy and pollutant emissions over real-world simulation driving cycles. *Atmospheric Environment* 42, 4023–4035. <https://doi.org/10.1016/j.atmosenv.2008.01.053>
- Franco V. et al. (2013). Road vehicle emission factors development: A review. *Atmospheric Environment* 70, 2013, 84-97
- HBEFA 2017. Handbook Emission Factors for Road Transport (HBEFA), Version 3.3, released April 2017. <http://www.hbefa.net/e/index.html>
- Henning A., Plohr M., Özdemir E.D., Hepting M., Keimel H., Sanok S., Sausen R., Pregger T., Seum S., Heinrichs M., Müller S., Winkler C., Neumann T., Seebach O., Matthias V., Vogel B. (2015). The DLR transport and the

environment project - Building competency for a sustainable mobility future. DLR Deutsches Zentrum für Luft- und Raumfahrt e.V. - Forschungsberichte 2015, Januar (38), 192-198.

ICCT (2018). European vehicle market statistics. Pocketbook 2018/19. The International Council on Clean Transportation 5.12.2018. <https://www.theicct.org/publications/european-vehicle-market-statistics-20182019>.

IINAS (2016). GEMIS – Global Emission Model for integrated Systems. Version 4.93, downloaded January 2017. <http://iinas.org/gemis.html>

KBA (2016). Fahrzeugzulassungsklassen (FZ) Neuzulassungen von Kraftfahrzeugen nach Umwelt-Merkmalen. Jahr 2015. FZ 14. Kraftfahrtbundesamt Statistik. (annual statistics on vehicle registrations) (in German).

Keller M., Hausberger S., Matzer C., Wüthrich P., Notter B. (2017). HBEFA Version 3.3. Hintergrundbericht. MK Consulting, TU Graz, Infras Bern, April 25, 2017 (in German). http://www.hbefa.net/e/documents/HBEFA33_Hintergrundbericht.pdf.

Kousoulidou M., Fontaras G., Ntziachristos L., Bonnel P., Samaras Z., Dilara P. (2013). Use of portable emissions measurement system (PEMS) for the development and validation of passenger car emission factors. *Atmospheric Environment*, 64 (2013) 329-338.

Krewitt W., Teske S., Simon S., Pregger T., Graus W., Blomen E., Schmid S., Schäfer O. (2009). Energy [R]evolution 2008 - A sustainable world energy perspective. *Energy Policy*, 37 (12) 5764–5775.

Kugler U., Brokate J., Schimeczek C., Schmid S.A. (2017). Powertrain scenarios for cars in European markets to the year 2040, in: TAE Conference Proceedings - 11th International Colloquium Fuels. Presented at the 11th International Colloquium Fuels – Conventional and Future Energy for Automobiles, Stuttgart, Germany.

Kugler U., Ehrenberger S., Brost M., Dittus H., Özdemir E.D. (2016). Real-world driving, energy demand and emissions of electrified vehicles. *Journal of Earth Sciences and Geotechnical Engineering* 6 (2016) 157–172.

Mock P. (2010). Entwicklung eines Szenariomodells zur Simulation der zukünftigen Marktanteile und CO₂-Emissionen von Kraftfahrzeugen (VECTOR21). PhD thesis, Universität Stuttgart. (in German)

Luca de Tena D., Pregger T. (2018). Impact of electric vehicles on a future renewable energy-based power system in Europe with a focus on Germany. *International Journal of Energy Research* 42(8), pp. 2670-2685.

McLaren J., Miller J., O'Shaughnessy, E., Wood E., Shapiro E. (2016). Emissions Associated with Electric Vehicle Charging: Impact of Electricity Generation Mix, Charging Infrastructure Availability, and Vehicle Type. National Renewable Energy Laboratory (NREL), Technical Report, April 2016, https://afdc.energy.gov/files/u/publication/ev_emissions_impact.pdf.

Ntziachristos L., Gkatzoflias D., Kouridis C., Samaras, Z. (2009). COPERT: A European road transport emission inventory model. *Information Technologies in Environmental Engineering*. 491-504. 10.1007/978-3-540-88351-7_37.

Ökoinstitut (2016). Electric mobility in Europe – Future impact on the emissions and the energy systems. Öko-Institut e.V. and Transport & Mobility Leuven (TML). Assessing the status of electrification of the road transport passenger vehicles and potential future implications for the environment and European energy system, Specific Contract under Framework Contract EEA/ACC/13/003 <https://www.oeko.de/fileadmin/oekodoc/Assessing-the-status-of-electrification-of-the-road-transport-passenger-vehicles.pdf>

O'Driscoll R., ApSimon H.M., Oxley T., Molden N., Stettler M.E.J., Thiyagarajah A. (2016). A Portable Emissions Measurement System (PEMS) study of NO_x and primary NO₂ emissions from Euro 6 diesel passenger cars and comparison with COPERT emission factors. *Atmospheric Environment* 145 (2016) 81-91.

Pregger T., Naegler T., Weimer-Jehle W., Prehofer S., Hauser W. (2019) [forthcoming]. Moving towards socio-technical scenarios of the German energy transition – lessons learned from integrated energy scenario building. *Climatic Change*.

Pregger T., Nitsch J., Naegler T. (2013). Long-term scenarios and strategies for the deployment of renewable energies in Germany. *Energy Policy* 59 (2013) 350–360, doi:10.1016/j.enpol.2013.03.049.

Schimeczek C. (2015). Report on enhanced model algorithm and model calibration (Project deliverable No. D6.1), eMAP Project. German Aerospace Center, Stuttgart.

Schlenzig C. (1999). Energy planning and environmental management with the information and decision support system MESAP. *International Journal of Global Energy Issues*, 12 (1-6) 81–91.

Schlesinger M. et al. (2014). Entwicklung der Energiemärkte - Energiereferenzprognose, Prognos AG & Energiewirtschaftliches Institut (EWI) an der Universität zu Köln & Gesellschaft für wirtschaftliche Strukturforschung

(GWS). (in German). Available at: http://www.ewi.uni-koeln.de/fileadmin/user_upload/Publikationen/Studien/Politik_und_Gesellschaft/2014/2014_06_24_ENDBER_P7570_Energiereferenzprognose-GESAMT-FIN-IA.pdf.

Seum S., Ehrenberger S., Heinrichs M., Kuhnimhof T., Müller S., Pak H., Pregger T., Winkler C. [forthcoming]. Transport and the Environment, building three different transport scenarios for Germany until 2040. Submitted to Transport Research Part D.

Seum S., Goletz M., Kuhnimhof T. (2017). Verkehrssystemforschung am DLR - Mobil in Deutschland 2040. Teil 1: Der methodische Szenario-Ansatz im Projekt Verkehrsentwicklung und Umwelt. Internationales Verkehrswesen, 69 (1), Seiten 60-63. Trialog Publishers Verlagsgesellschaft. ISSN 0020-9511. Teil 2: Die Szenarien des VEU-Projekts. Internationales Verkehrswesen, 69 (2), Seiten 78-81. Trialog Publishers Verlagsgesellschaft. ISSN 0020-9511 (in German).

Suarez-Bertoa R., Astorga C. (2016). Unregulated emissions from light-duty hybrid electric vehicles. Atmospheric Environment 136 (2016) 134–143. <https://doi.org/10.1016/j.atmosenv.2016.04.021>.

Teske S., Pregger T., Simon S., Naegler T. (2018). High renewable energy penetration scenarios and their implications for urban energy and transport systems. Current Opinion in Environmental Sustainability 30 (2018) 89–102.

TU Graz (2009). Emission factors from the model PHEM for the HBEFA version 3. http://www.hbefa.net/e/documents/HBEFA_31_Docu_hot_emissionfactors_PC_LCV_HDV.pdf.

UBA (2015). Emissionsfaktoren für die nationale Emissionsberichterstattung (Emission factors for national emissions reporting). Umweltbundesamt (UBA), Dessau-Roßlau, Fr. Juhrich/Hr. Kotzulla, Fachgebiet I2.6 – Zentrales System Emissionen (ZSE), personal communication.

UBA (2016a). Übersicht zur Entwicklung der energiebedingten Emissionen und Brennstoffeinsätze in Deutschland 1990 – 2014 (Overview of the development of energy-related emissions and fuel use in Germany 1990 – 2014). Umweltbundesamt (UBA), Dessau-Roßlau, Fachgebiet I 2.5 - Energieversorgung und -daten (in German) <https://www.umweltbundesamt.de/publikationen/uebersicht-zur-entwicklung-energiebedingten>.

UBA (2016b). Common reporting format (CRF) tables. Germany CRF 2016 (2018). Umweltbundesamt (UBA), Dessau-Roßlau, see <https://unfccc.int/documents/65332>.

Vouitsis I., Ntziachristos L., Samaras C., Samaras Z. (2017). Particulate mass and number emission factors for road vehicles based on literature data and relevant gap filling methods. Atmospheric Environment, 168 (2017) 75–89.

Winkler C., Burgschweiger S., Mocanu T., Wolfermann, A. (2017). Modellierung des Personen- und Güterverkehrs in Deutschland als Entscheidungsunterstützung für die Politik. In: Straßenverkehrstechnik, 08 (2017) 551-558.

Supporting Information to:

Well-to-wheel emission factors for future cars in Germany with a focus on fleet composition, new technologies and emissions from energy supplies

Stefan Seum^{1*}, Simone Ehrenberger² and Thomas Pregger³

¹ Institute of Transport Research, German Aerospace Center (DLR), Berlin, Germany, Stefan.Seum@dlr.de

² Institute of Vehicle Concepts, German Aerospace Center (DLR), Stuttgart, Germany

³ Department of Energy Systems Analysis, Institute of Engineering Thermodynamics, German Aerospace Center (DLR), Stuttgart, Germany

Tables A1 to A4 contain the individual values of the bars in Figure 1 “Calculated total indirect and direct emissions of the vehicle technologies in 2040”. The following abbreviations are used:

G = gasoline vehicle

D = diesel vehicle

G-HEV = gasoline-hybrid vehicle

D-HEV = diesel-hybrid vehicle

PHEV = plug-in-hybrid vehicle (gasoline)

BEV = battery-electric vehicle

FCEV = fuel-cell electric vehicle

CNG = compressed natural gas vehicle

Table A1: List of total indirect and direct CO₂ emissions [g/km] of the vehicle technologies in 2040

	reference		free play		regulated shift	
	indirect emissions	direct emissions	indirect emissions	direct emissions	indirect emissions	direct emissions
G	7.05	126.96	6.44	147.69	7.81	130.55
D	5.44	113.96	5.51	124.55	5.67	110.98
G-HEV	4.66	87.06	5.90	116.82	4.64	94.11
D-HEV	4.14	69.24	4.61	79.37	5.09	88.61
PHEV	36.29	27.25	47.28	28.43	10.99	32.46
BEV	41.73	-	57.08	-	13.29	-
FCEV	-	-	-	-	47.64	-
CNG	0.88	119.56	0.93	123.25	0.73	113.02

Table A2: List of total indirect and direct NO_x emissions [mg/km] of the vehicle technologies in 2040

	reference		free play		regulated shift	
	indirect emissions	direct emissions	indirect emissions	direct emissions	indirect emissions	direct emissions
G	6.86	20.00	6.26	20.00	5.96	19.00
D	5.30	150.00	5.36	151.00	4.32	150.00
G-HEV	4.07	17.00	5.32	17.00	3.54	17.00
D-HEV	3.78	134.98	4.20	134.43	3.88	135.25
PHEV	32.48	2.87	38.46	2.87	18.08	2.91
BEV	37.20	-	46.11	-	24.14	-
FCEV	-	-	-	-	86.52	-
CNG	3.50	58.00	3.70	66.00	2.90	52.00

Table A3: List of total indirect and direct CO emissions [mg/km] of the vehicle technologies in 2040

	reference		free play		regulated shift	
	indirect emissions	direct emissions	indirect emissions	direct emissions	indirect emissions	direct emissions
G	0.76	638.00	0.54	634.25	0.62	658.89
D	0.59	28.00	0.46	28.62	0.45	25.92
G-HEV	0.45	500.34	0.49	493.92	0.37	503.54
D-HEV	0.42	9.52	0.36	9.41	0.40	10.05
PHEV	15.35	85.71	17.67	86.41	10.19	86.45
BEV	18.27	-	21.94	-	14.51	-
FCEV	-	-	-	-	52.02	-
CNG	0.88	1442.00	0.93	1531.93	0.73	1383.25

Table A1: List of total indirect and direct PM emissions [mg/km] of the vehicle technologies in 2040

	reference		free play		regulated shift	
	indirect emissions	direct emissions	indirect emissions	direct emissions	indirect emissions	direct emissions
G	0.95	2.09	0.89	2.08	0.82	2.10
D	0.74	1.94	0.77	1.95	0.60	1.95
G-HEV	0.57	1.88	0.76	1.88	0.49	1.92
D-HEV	0.53	1.75	0.60	1.75	0.54	1.70
PHEV	1.28	0.55	1.51	0.58	0.65	0.59
BEV	1.28	-	1.60	-	0.67	-
FCEV	-	-	-	-	2.41	-
CNG	0.18	0.00	0.19	0.00	0.15	0.00

2.4.5 Has the Climate Benefited from the EU “Diesel Boom”? – Assessment of CO₂-eq Emissions from EU’s Increasing Diesel Car Fleet

Joana Leitão^{1*}, Eckard Helmers², Uwe Tietge³, Tim Butler¹

¹ Institute for Advanced Sustainability Studies, 14467 Potsdam, Germany, joana.leitao@iass-potsdam.de

² Department of Environmental Planning and Technology, University of Applied Sciences Trier, Germany

³ The International Council on Clean Transportation, 10178 Berlin, Germany

Introduction

Climate change is one of the main environmental challenges worldwide which has already been addressed in several international protocols, starting in Kyoto in 1997 and followed by several amendments that led to the more recent Paris Agreement. The road transport sector is one of the main sources of anthropogenic emissions with a significant contribution to total greenhouse gases (GHG) and air pollutants. Emission reduction policies have not been so effective for this sector compared, for example, with energy consumption from industry or household sectors. Efforts have focussed on CO₂ reduction for newly registered cars (e.g., EEA, 2017) but in fact, presently, European GHG emissions from the transport sector are still rising. Several targets and policies implemented in the European Union (EU) have not been sufficient to reach the necessary climate mitigation goals established in international protocols. Additionally, traffic-related emissions are still the main cause for the recurrent exceedances of air quality standards in the cities which lead to high rates of premature mortality in the EU (EEA, 2016; Anenberg et al., 2017; Jonson et al., 2017). Passenger vehicles are a significant source of air pollutants such as nitrogen oxides (NO_x) and Black Carbon (BC), a component of emitted particulate matter (PM). BC has also a relevant direct contribution to climate change with a net positive radiative forcing resulting from absorption of solar radiation and an indirect impact by altering the properties and lifetime of cloud droplets and ice particles.

Emissions from vehicles are measured under idealized laboratory conditions following standardized driving cycles such as the New European Driving Cycle (NEDC). However, this has been found to not be fully representative of real-world (RW) driving conditions (Borken-Kleefeld et al., 2014; Giechaskiel et al., 2015; Degraeuwe and Weiss, 2017). Recent data from the non-governmental organisation International Council on Clean Transportation (ICCT) arising from an evaluation of approx. one million points of real-world fuel consumption data shows that, particularly after European CO₂ standards were introduced in 2008/2009, the gap between standard NEDC measurements and RW emissions has been growing for both diesel and petrol cars, reaching an average deviation of +42% for new diesel passenger cars in 2015 in Europe (Tietge et al., 2016).

Here, we present results previously published in Helmers et al. (2019) where direct real-world CO₂ emissions of newly registered cars in the EU-15, between 1995 and 2015, are evaluated for three scenarios with varying fleets: the historic fleet (which we refer to as the European “diesel boom”); percentages of diesel cars stable at the low levels from the early 1990s (no “diesel boom”); and high proportions of petrol hybrid cars and cars burning gaseous fuels (an advanced mitigation option). For the first time, real-world emission factors based on Tietge et al. (2017) are used to calculate the balance of real-world CO₂ emissions of passenger cars differentiated by diesel and petrol engines during this period.

Methodology

In order to assess the effectiveness of the European “diesel boom” as a measure to reduce the overall climate impact of the passenger car fleet, lifetime CO₂-eq emissions of all European passenger cars (use phase only) registered between 1995 and 2015 were determined and compared with two alternative scenarios (see description below). In addition to direct CO₂ emissions, also the additional radiative forcing due to primary-emitted BC was considered. To be able to compare diesel and petrol vehicles in terms of CO₂-eq emissions, the GWP100 (Global Warming Potential for a time horizon of 100 years) recommended value and respective uncertainty from Bond et al. (2013) were used, i.e., GWP100 of 100-900-1700. Other GHGs, like CH₄ and N₂O, were not considered due to their small contribution to tailpipe GHG emissions. Direct emissions by passenger vehicles have been previously estimated to be in the range of 1–2% of the GHG emissions (Defra, 2012; CDP, 2016) and their relative contribution to the total well-to-wheel GHG emissions being 1.5% in case of diesel fuel and 1.7% in case of petrol (Fritsche, 2007).

The real-world/type-approval deviation data from Tietge et al. (2017) was used to calculate the real-world CO₂ emissions of all newly registered petrol, diesel, and HEV in Europe (Fig. 1). A detailed description of the approach adopted here and data used is presented in Helmers et al. (2019) (see section 2.1 and Fig. 1 of the manuscript). Average divergence values were used to adjust type-approval CO₂-emissions of newly registered vehicles. Prior to the year 2001, the divergence between type-approval and real-world emissions for 2001, +9.0% in case of diesel and +8.0% in case of petrol cars, were used for the years 1995–2000.

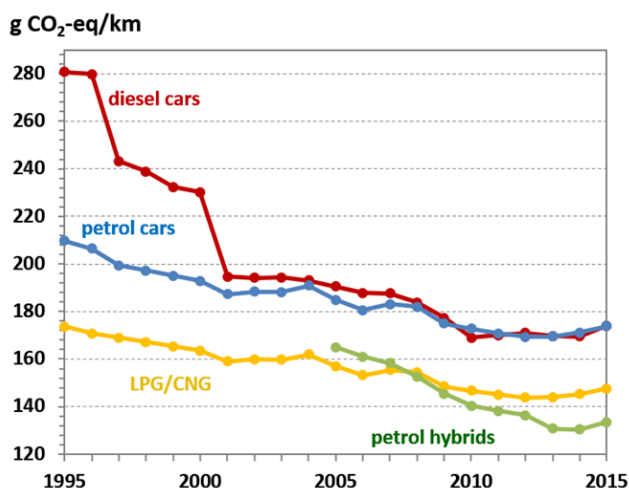


Figure 1: Total real-world CO₂-eq (CO₂+BC) emissions of new cars in Europe.

Real-world fuel consumption factors were determined from our real-world CO₂ emissions and based on the equations and default values provided by EEA (2018) (see further details in Table 1 of Helmers et al. (2019)). These estimations are subject to some uncertainty which was represented in this analysis as the standard deviation of the real-world emission factors, resulting therefore in a central value and corresponding range of lowest to highest emissions. Real-world PM emission data distinguishing between Euro standards are rare in the scientific literature. A summary of assumed PM emission factors per vehicle types and corresponding BC fractions (EEA, 2018) is shown in Table 2 of Helmers et al. (2019). Since there is a lack of detailed information on European level for the Euro class of new registered cars, here it was assumed that all cars correspond to the newest Euro standard of the respective registration year. Similarly, official data is not available concerning the number of vehicles manufactured with diesel particle filters (DPFs) before its mandatory implementation in the Euro 5 vehicles. Therefore, a linear rise of the share of diesel cars with DPFs is assumed to occur between 2000 and 2010, reaching 100% coverage around 2010 (see black in Fig. 2).

Real-world CO₂ and PM emissions for each of the considered scenarios were calculated using the COPERT v5.1.1 model (Ntziachristos et al., 2009; Emisia SA, 2018), a tool developed to facilitate the assessment of national emissions from the road transport sector. Here, this tool was used for a scenario analysis, using the above mentioned ICCT real-world fuel consumption and PM emission factors and the fleet compositions as described below. Hot exhaust emissions were determined for only one driving mode with an assumed average driving speed of 50 km/h, and yearly mileage of 12500km (Weymar and Finkbeiner, 2016). A comparison of emissions for the historical fleet using default COPERT assumptions and the real-world emission factors showed that, COPERT CO₂ emissions are lower than our RW emissions for petrol and diesel vehicles, with a negligible difference at the end of the analysed period. Nevertheless, one important finding is the high difference found in the BC values that reflect the different assumption of DPF implementation, which is not yet considered in COPERT. At the end of the analysed period, when all cars in fleet have DPFs, both calculations show similar results.

Three Vehicle Fleet Scenarios

The annual total vehicle registrations for EU-15 considered and respective market shares according to different fuel types, for each of the scenarios, are presented in Fig. 2.

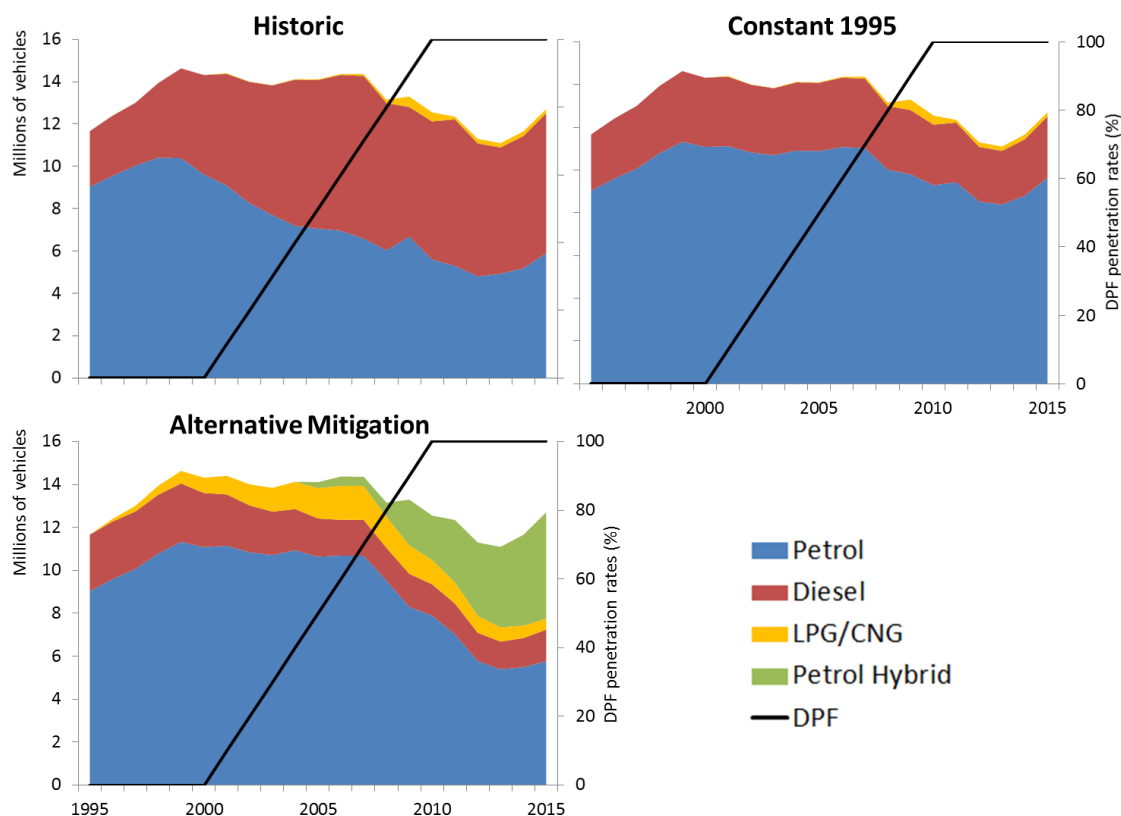


Figure 2: New passenger car registrations per fuel type in Europe (EU-15) for the three considered scenarios. Also shown assumed percentage of DPF (penetration rates in %).

The annual total vehicle registrations for EU-15 considered and respective market shares according to different fuel types, for each of the scenarios, are presented in Fig. 2.

- Historical fleet

Aiming at a reduction of CO₂ emissions, in the two decades since 1995, Europe passenger vehicles fleet has seen an overall technology change from the petrol vehicles to the diesel cars (reviewed in Cames and Helmers, 2013). From the circa 281 million cars newly registered in the EU-15 between 1995 and 2015, 122 million are diesel cars and 159 million petrol cars (ACEA, 2016). New registrations data and share of diesel vehicles used to build the historic baseline scenario was taken from ACEA (2017) (see Helmers et al. (2019) for further details).

- Constant 1995

This scenario assumes a lack of strong political support for diesel vehicles in Europe, avoiding its “diesel boom” over the past 20 years. In this case, diesel as well as petrol cars are assumed to have remained constant in terms of market shares from 1995 (22.6% and 77.4%, respectively), while all other factors evolved as in the historical case.

- Alternative mitigation

Assuming a different CO₂ mitigation strategy that could have been implemented in Europe is portrayed on this scenario. It reflects available technology during the considered time period and uses Japan as reference, a highly industrialized country with a strict regulation that successfully reduced emissions. Diesel cars are assumed to have reached a low market share of 11.6% in 2006 and remained at this value. This development is in accordance with the long-term diesel share of the European market prior to 1995 (Cames and Helmers 2013). Furthermore, assuming an encouragement of European regulators, the domestic car industry would have developed further the petrol hybrid electric vehicles (HEV) as it happened in Japan. The GHG mitigation potential of this technology was already known in the late 1990s (Cames and Helmers, 2013). Accordingly, the alternative scenario is based on the market

penetration of HEV observed in Japan, which increased from 2008 onwards (JAMA 2015, 2016). Additionally data for 2014 and 2015 have been extrapolated from change of the previous two years (ICCT, 2015). The share of LPG plus CNG cars peaked at an 11% market share in 2006, declining after 2008 to 4% in 2015 as a result from the increasing market penetration of HEV.

Results

The committed CO₂ and BC emissions over the full on-road lifetime of all new passenger cars registered in Europe (EU-15) between 1995 and 2015 are presented in Table 1, for each of the three scenarios: historic baseline, constant 1995, and alternative mitigation.

Table 1: Total committed lifetime emissions of CO₂, BC and total CO₂-eq for vehicles registered between 1995-2015, for each scenario, with respective low and high values calculated as described in text.

Scenario	Species	central estimate (Mt)	scenario range (Mt)	
			Lowest	Highest
Historical	CO ₂	10062	8327	11761
	BC (CO ₂ -eq)	483	54	913
	total CO ₂ -eq	10545	8381	12673
Constant 1995	CO ₂	10140	8395	11844
	BC (CO ₂ -eq)	360	40	680
	total CO ₂ -eq	10500	8435	12524
Alternative Mitigation	CO ₂	9892	8215	11554
	BC (CO ₂ -eq)	299	33	565
	total CO ₂ -eq	10191	8248	12119

According to the results obtained the climate impact of the European “diesel boom” between 1995 and 2015 was approx. 45 Mt CO₂-eq. Although a direct reduction in CO₂ emissions is verified when comparing the first two scenarios, there is an increase of BC emissions (mostly registered in the period in which diesel vehicles were not fitted with DPFs) that offsets the positive mitigation effect of diesel vehicles. In the case that the fleet would have varied according to assumptions of the alternative mitigation scenario the climate benefit would have been of 354 Mt CO₂-eq compared with the historic scenario. The uncertainty range in GWP100 estimates of BC has an impact of about 500 Mt CO₂-eq, which is of similar magnitude to the overall climate benefit of the alternative mitigation scenario. In this sense, all three scenarios are virtually indistinguishable from each other in terms of their total climate benefit over the period 1995 to 2015 within the ranges calculated here.

Committed CO₂ and BC emissions (and respective ranges) over the full vehicle lifetime of 200000 km, i.e. a total of 16 years (Weymar and Finkbeiner, 2016) are shown in Fig. 3 for the year in which the vehicles were first registered, in the time period of 1995 to 2015. The large scenario range for BC in the earlier years is explained by the fact that diesel vehicles were not fitted with particulate filters at the time. Despite the large ranges for both species, a downward trend is apparent in annual committed emissions. However, this downward trend is not consistent: before 2000 and after 2012, (yearly) lifetime committed emissions appear to increase slightly.

Comparing emissions with numbers of new vehicle registrations highlights indicating that the committed GHG emissions from passenger cars each year are strongly influenced by the number of new vehicle registrations in that year. Furthermore, looking at the evolution between 1995 and 1999, an increase in the number of vehicle registrations coincides with growing GHG emissions, even if real-world emission factors were declining as a result of improvements in fuel efficiency. On the other hand, the increase in the fleet during 2013 and 2015 coincided with rather constant values of real-world emission factors.

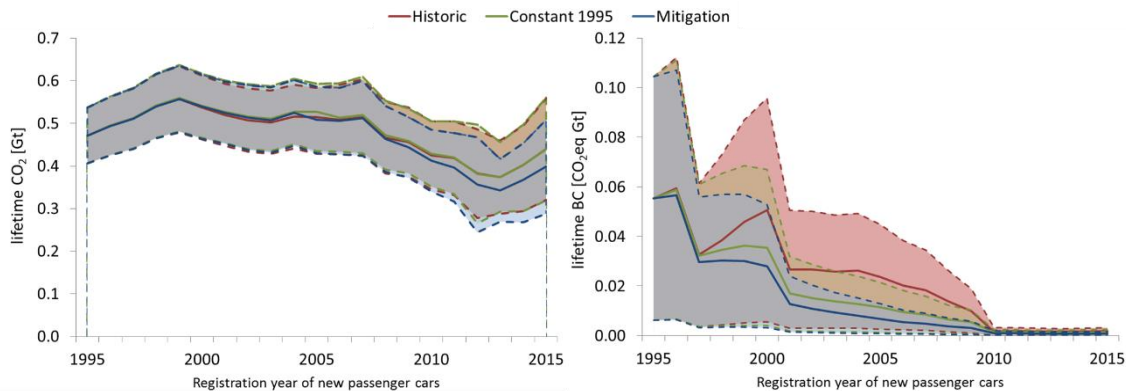


Figure 3: Annual committed GHG emissions (in Gt) for CO₂ (left pane) and BC (in CO₂-eq, right pane), for new passenger cars registered between 1995 and 2015 in the EU-15, in the three scenarios analysed in this study: Historic (red), Constant 1995 (green) and Alternative Mitigation (blue). (Solid lines are central values and shaded areas the ranges of scenarios).

Conclusion

The results of this study clearly demonstrate that the European diesel car boom that started in the mid-1990s most likely was ineffective at reducing climate warming emissions from the European transport sector, bringing in practice no climate benefit in terms of CO₂-eq emissions in the period of 1995-2015.

While before 2011 the European diesel cars still emitted much less CO₂ per-km than petrol cars, more recently (since 2001) this difference became quite negligible and diesel and petrol vehicles each produce similar real-world GHG emissions. From 1995 to 2000, when European diesel cars lacked particle filters, these vehicles were extremely unfavourable for climate mitigation. After 2000, emissions from the two competing technologies have shown similar radiative forcing effects from both CO₂ and BC. In this calculation, no deterioration (malfunction due to aging, e.g. of DPF) effects are considered. Real-world CO₂ emissions of diesel cars have not declined appreciably since 2001, whereas the values from petrol cars have been stagnant since 2012. Furthermore, when accounting also with black carbon related CO₂-eq, an even higher impact (to both climate change and air pollution) of diesel cars is found. This is especially the case in the early years when DPF was not widely implemented and resulting PM emission contributed to excessive levels of air pollution that can cause severe adverse health effects in exposed populations.

The results of the alternative scenario show that limited CO₂-eq savings would have been possible by promoting petrol hybrids instead of diesel vehicles as it has been done in Japan. However, this study also suggests that there is no fundamental climate benefit when switching from one fossil fuel to another. Real-world CO₂ emissions from European passenger cars may even be rising again due to a combination of increased annual vehicle registrations and a stagnation in real-world CO₂ emission values for all types of vehicles, including diesel, petrol, and hybrid vehicles.

From today's perspective, Europe chose the wrong alternative by promoting diesel cars instead of the other powertrains and fuels which were available at the time. This is particularly true when also considering the adverse health effects due to emissions from diesel vehicles. In 2015, annual new vehicle registrations were still lower than pre-2008 levels. If the positive trends in new vehicle registrations and the flat trend in real-world CO₂ emissions both continue, as they have since 2013, annual committed GHG emissions from newly registered European passenger vehicles will continue to rise in the coming years. In order to significantly reduce GHG emissions from the European passenger vehicle fleet, either the total size of the fleet must be decreased, or real-world CO₂ emission values must be reduced, either by more stringent CO₂ standards and better policy enforcement or by introducing a significant number of low emission vehicles, such as battery electric cars powered using electricity from renewable energy sources.

Many diesel cars as marketed in Europe in the past 20 years have much higher BC emissions as well as up to 15 times higher NO_x emissions as per g NO_x/kg fuel consumption according to real-world measurements (Chen and Borken-Kleefeld, 2014) in the direct comparison with petrol cars. Exploration

of further alternative scenarios with more detailed characterization of European (and national) fleet composition remains a source for further improvement of this analysis where air pollution impacts could also be accounted.

Acknowledgements

This work was hosted by IASS Potsdam, with financial support provided by the Federal Ministry of Education and Research of Germany (fBMBF) and the Ministry for Science, Research and Culture of the State of Brandenburg (MWFK). The authors would like to thank Erika von Schneidemesser for useful comments on earlier versions of this manuscript. The Emisia group that built COPERT is acknowledged for the tool freely distributed and used in this study, and particular gratitude is given to G. Mellios for his endless support and clarifications provided.

References

- ACEA (2016). The Automobile industry pocket guide 2016-2017, http://www.acea.be/uploads/publications/POCKET_GUIDE_2015-2016.pdf, Accessed May 9, 2017.
- ACEA (2017). New passenger car registrations breakdown by share of diesel. https://www.acea.be/uploads/statistic_documents/Share_of_diesel_in_new_cars_in_West_Europe_%281990-2017%29.xlsx, Accessed May 9, 2017.
- Anenberg S.C., Miller J., Minjares R., Du L., Henze D.K., Forrest Lacey F., Malley C.S., Emberson L., Franco V., Klimont Z., Heyes C. (2017). Impacts and mitigation of excess diesel-related NO_x emissions in 11 major vehicle markets, *Nature*, 545, 467–471, doi:10.1038/nature22086.
- Bond T.C., Doherty S.J., Fahey D.W., Forster P.M., Berntsen T., DeAngelo B.J., Flanner M.G., Ghan S., Kärcher B., Koch D., Kinne S., Kondo Y., Quinn P.K., Sarofim, M.C., Schultz M.G., Schulz M., Venkataraman C., Zhang H., Zhang S., Bellouin N., Guttikunda S.K., Hopke P.K., Jacobson M.Z., Kaiser J.W., Klimont Z., Lohmann U., Schwarz J.P., Shindell D., Storelvmo T., Warren S.G., Zender C.S. (2013). Bounding the role of black carbon in the climate system: A scientific assessment, *J Geophys Res Atmos.*, 118 (11), 5380-5552, doi:10.1002/jgrd.50171.
- Borken-Kleefeld J., Fuglestved J., Berntsen T. (2014). Mode, Load, And Specific Climate Impact from Passenger Trips, *Environ. Sci. Technol.*, 47 (14), 7608–7614, doi: 10.1021/es4003718.
- Cames M., Helmers E. (2013). Critical evaluation of the European diesel car boom – global comparison, environmental effects and various national strategies, *Environ Sci Eur*, 25(15), doi 10.1186/2190-4715-25-15.
- CDP, (2016). Guidance Methodology for Estimation of Scope 3 Category 11 Emissions for Oil and Gas Companies. 29/01/16 First Version of Guidance Methodology. <https://www.cdp.net/Documents/Guidance/2016/CDP-Scope-3-c11-Guidance-Oil-Gas-2016.pdf>, Accessed May 12, 2017.
- Chen Y., Borken-Kleefeld J. (2014). Real-driving emissions from cars and light commercial vehicles - Results from 13 years remote sensing at Zurich/CH, *Atmospheric Environment*, 88, 157-164, doi: 10.1016/j.atmosenv.2014.01.040.
- Defra, 2012. Guidelines to Defra/DECC's GHG Conversion Factors for Company Reporting. Version: 1.0, updated: 28/05/2012. https://www.gov.uk/government/uploads/system/uploads/attachment_data/file/69554/pb13773-ghg-conversionfactors-2012.pdf, Accessed May 12, 2017.
- Degraeuwe B., Weiss M. (2017). Does the New European Driving Cycle (NEDC) really fail to capture the NO_x emissions of diesel cars in Europe?, *Environmental Pollution*, 222, 234-241, doi: 10.1016/j.envpol.2016.12.050.
- EEA (2016). European Environmental Agency: Air quality in Europe — 2016 report, *EEA Report No 28/2016*, 88 pp. https://www.eea.europa.eu/publications/air-quality-in-europe-2016/at_download/file Accessed May 8, 2017.
- EEA (2017). Fuel efficiency improvements of new cars in Europe slowed in 2016, News Published 20 Apr 2017, last modified 24 Apr 2017, <https://www.eea.europa.eu/highlights/fuel-efficiency-improvements-of-new> Accessed May 7, 2017.
- EEA (2018). EMEP/EEA air pollutant emission inventory guidebook 2016. 1.A.3.b.i-iv Road transport 2018. <https://www.eea.europa.eu/publications/emep-eea-guidebook-2016/part-b-sectoral-guidance-chapters/1-energy/1-a-combustion/1-a-3-b-i/view>, Accessed July, 2018.
- Emisia SA. (2018). COPERT data. <http://www.emisia.com/utilities/copert/>, COPERT v5.1.1. downloaded on June 8 2018.
- Fritsche, U.R. (2007). Endenergiebezogene Gesamtemissionen für Treibhausgase aus fossilen Energieträgern unter Einbeziehung der Bereitstellungsvorketten. Kurzbericht im Auftrag des Bundesverbands der deutschen Gas-

und Wasserwirtschaft e.V. (BGW). http://www.iinas.org/tl_files/iinas/downloads/GEMIS/2007_thg_fossil_BGW.pdf, Accessed May 12, 2007.

Giechaskiel B., Riccobono F., Vlachos T., Mendoza-Villafuerte P., Suarez-Bertoa R., Fontaras G., Bonnel P. and Weiss M. (2015). Vehicle Emission Factors of Solid Nanoparticles in the Laboratory and on the Road Using Portable Emission Measurement Systems (PEMS), *Front. Environ.Sci.*, 3:82, doi: 10.3389/fenvs.2015.00082.

Helmers E., Leitão J., Tietge U., Butler T. (2019). CO₂-equivalent emissions from European passenger vehicles in the years 1995–2015 based on real-world use: Assessing the climate benefit of the European “diesel boom”, *Atmospheric Environment*, 198, 122-132, doi: 10.1016/j.atmosenv.2018.10.039.

ICCT (2015). Light-duty Vehicle Efficiency Standards. Fact Sheet Japan, http://www.theicct.org/sites/default/files/info-tools/pvstds/Japan_PVstds-facts_jan2015.pdf, Accessed 24 July 2017.

JAMA (2015). The motor industry of Japan 2015, Japan Automobiles Manufacturers Association, <http://www.jama-english.jp/publications/MIJ2015.pdf>, Accessed May 13, 2017.

JAMA (2016). The motor industry of Japan 2016, Japan Automobiles Manufacturers Association, <http://www.jama-english.jp/publications/MIJ2016.pdf>, Accessed May 13, 2017.

Jonson J.E., Borken-Kleefeld J., Simpson D., Nyiri A., Posch M., Heyes C. (2017). Impact of excess NO_x emissions from diesel cars on air quality, public health and eutrophication in Europe, *Environ. Res. Lett.*, 12, 094017, doi:10.1088/1748-9326/aa8850.

Ntziachristos L., Gkatzoflias D., Kouridis C., Samaras Z. (2009). COPERT: A European Road Transport Emission Inventory Model. In: Athanasiadis I.N., Rizzoli A.E., Mitkas P.A., Gómez J.M. (eds), *Information Technologies in Environmental Engineering. Environmental Science and Engineering*. Springer, Berlin, Heidelberg, doi: 10.1007/978-3-540-88351-7_37.

Tietge U., Díaz S., Mock P., German J., Bandivadekar A., Ligterink N. (2016). From laboratory to road: A 2016 update of official and “real-world fuel consumption and CO₂ values for passenger cars in Europe, white paper, <http://www.theicct.org/laboratory-road-2016-update>, Accessed May 7, 2017.

Tietge U., Mock P., Franco V., Zacharof N. (2017). From laboratory to road: Modeling the divergence between official and real-world fuel consumption and CO₂ emission values in the German passenger car market for the years 2001–2014, *Energy Policy*, 103, 212-222, doi: 10.1016/j.enpol.2017.01.021.

Weymar, E., Finkbeiner, M. (2016). Statistical analysis of empirical lifetime mileage data for automotive LCA, *Int. J. Life Cycle Assess.*, 21, 215–223, doi:10.1007/s11367-015-1020-6.

2.4.6 OLYMPUS: An urban emissions model focused on the individual

A. Elessa Etuman¹, J. Coll¹

¹ Laboratoire Interuniversitaire des Systèmes Atmosphériques (LISA), UMR CNRS 7583, Université Paris Est Créteil et Université Paris Diderot, Institut Pierre Simon Laplace (IPSL), Créteil, France

Abstract

OLYMPUS is a modeling platform based on the generation of a synthetic population and the estimation of the mobility of individuals in a city, through an activity-based travel demand approach. These data are used to simulate road traffic in the city, taking into account congestion on the road network. In parallel, the model addresses the issue of energy demand on the territory, through the estimation of energy consumption per household. Road traffic emissions, as well as emissions related to building heating, are calculated using COPERT emission factors and the European environment Agency (EEA) methodology, respectively. The comparison of these emissions with the Paris regional inventory shows overall good results, even if the lack of representation of freight transport and interurban mobility induces a slight underestimation of the total emissions.

Introduction

Air quality modeling is an approach to simulate atmospheric concentrations of pollutants that is essentially constrained by the chemistry and physics of the atmosphere. From a numerical point of view, the model solves the mass conservation equation at each computation time step and for each compound. The terms of this equation are the following: emission in the air by anthropogenic and biogenic activities, air mass mixing from horizontal and vertical movements, physical and chemical transformation processes and finally deposition processes. Although all these parameters are crucial for the determination of atmospheric pollutant concentrations, it is the control of pollutant emissions that now covers the greatest scientific and societal issues of air quality modelling. And this issue far exceeds the possible technological evolutions on pollutant emitting processes. Indeed, it is now recognized that the reduction of pollutant emissions in major cities will necessarily involve a more rational use of energy and the optimization of urban mobility practices. To meet the expectations on air quality management, the calculation of emission inventories, usually carried out upstream of the chemistry-transport models, should be based on the use of comprehensive tools capable of simulating all the activities resulting from individual uses, and which may affect ambient air. These tools must therefore be able to apprehend the urban fabric, the shape of the city, its organization, its economy and its offer of services in order to deduct the mobility of city dwellers and the spatiotemporal location of polluting activities, in different public policy scenarios.

Currently, research on the urban environment is based on highly monothematic approaches. There is therefore a strong need for an innovating multidisciplinary research, which would consider the societal drivers for pollutant emissions and offer a cross-cutting view of urban issues. The approach we have developed aims to remove the technical locks of interdisciplinarity, through the development of a modeling chain linking the urban parameters simulated by a set of disciplinary models. It is structured around the OLYMPUS tool which has been built to integrate energy transition scenarios combining public policies, technological developments and individual practices, in order to produce household activity data and calculate emissions related to combustion activities, for different urban forms. It provides input data for chemistry-transport models, for the simulation of air quality at the scale of an agglomeration.

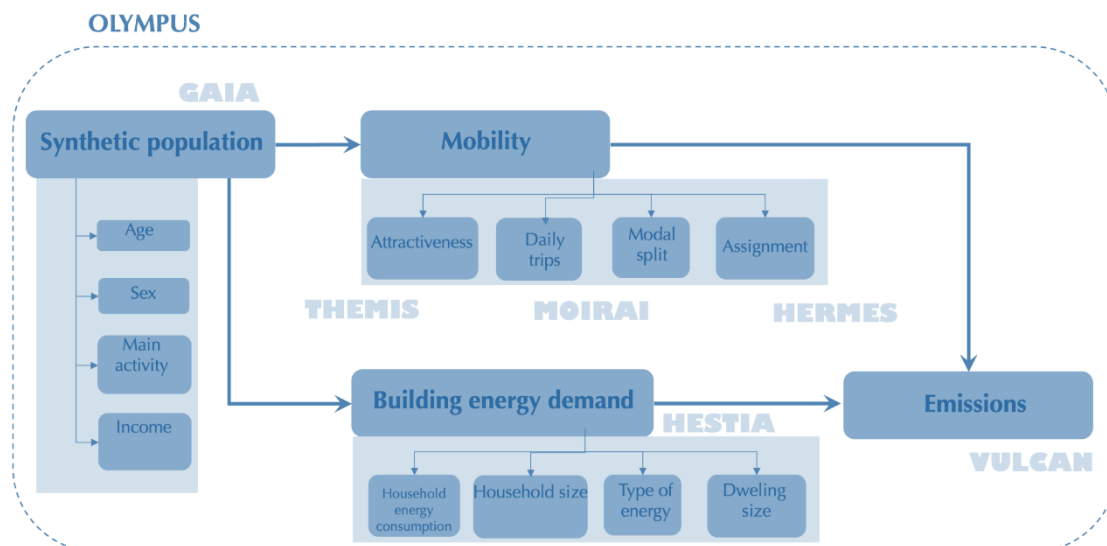


Figure 1: schematic representation of the OLYMPUS organizational chart.

Methodology

OLYMPUS is a modeling platform that aims to simulate anthropogenic air pollutant and greenhouse gas emissions from energy consumption activities in urban areas. The inputs are the socio-economic parameters (areas of employment, housing, cost of energy, etc.) as well as the urban structuring and the geographical characteristics (transport networks, urban density and types of housing by area) of the territories. From this dataset, OLYMPUS generates a synthetic urban population and then deduces mobility and energy consumption practices for households and professionals, using the theory of rationality, gravity models and conditional probabilities. Emissions of pollutants will be estimated from those activities (Elessa A. et al, 2018).

OLYMPUS relies on the 6 following modules:

- **GAIA** for the generation of a synthetic population. This step builds on existing approaches for population generation through conditional probabilities, widely described in the literature. The choice of conditional probabilities was made by taking inspiration from models such as MOBISIM (Antoni, J et al. 2010). Furthermore, GAIA integrates a socio-economic component of the properties of agents that is distributed in space. This feature makes it possible to diversify the synthetic population generated by conditional probabilities. The characteristics of the agents of the population created in OLYMPUS include notably sex, age, main activity and income. To this end, OLYMPUS feeds primarily on population census data. The use of supplementary surveys can be implemented in the model for the refinement of the synthetic population.

- **THEMIS, MOIRAI** and **HERMES** for the generation of mobility choices, mobility matrixes and road trip allocation on the road network. Road transport modeling is similar to that used in the so-called "4-step" conventional models but its calculations are performed at the agent level, which represents a much greater degree of discretization of the calculations. The 4 steps are:

- (1) generation of transport demand. It is based on the attractiveness potential of the activities in each district and comes under the THEMIS module

- (2) spatial distribution of the transport request (creation of origin-destination matrixes) and (3) identification of modal choice for each agent of the synthetic population, both provided by MOIRAI

- (4) assignment of the transport request on the network, finally carried out for each agent by HERMES.

- **HESTIA** for energy demand modeling on the territory. The modeling of the energy consumption in buildings lists combustion activities for residential, institutional and commercial heating, as well as for the production of hot water and cooking. Since average consumption data are derived from global surveys, the approach is considered a top-down approach, but the implementation of factors related to

building energy efficiency and household characteristics makes it possible to consider the implementation of energy scenarios. Moreover, the calculation is carried out in a bottom-up way, since it is discretized at the level of each household of the synthetic population.

- **VULCAN** for calculating pollutant emissions from the population activity simulated in the preceding modules. The calculations of the intensity of emissions in the OLYMPUS platform are carried out in the VULCAN module, in accordance with the recommendations of the EEA emission methodology. With regard to transport, this implies the use of emission factors from the COPERT 4 methodology. The factors proposed make it possible to discriminate the type of vehicle, the engine, the type of fuel used, but also the age of the vehicle, in order to reflect compliance with increasingly stringent European standards for emission limits.

Configuration

OLYMPUS has been implemented in the Paris megacity. The selected simulation year is 2009, due to the importance of the available data. The main information is recalled below:

- For the generation of the synthetic population, the model uses the INSEE (French National Institute for Statistics and Economic Research) census data for the year 2009. The age, sex and activity of the agents of the population was considered. Also, car and driving license owners were statistically identified. The city-center, the inner and outer suburbs are identified as 3 different environments where the distribution of the household type varies.

- Input data forcing transport modeling mainly depend on (1) job centers and their size, which are extracted from INSEE and then spatialized by a GIS to be grouped by districts, (2) the structure of the public transport network and the road network (data are from local agencies), and (3) a panel of surveys giving information such as the average cost and number of trips per day for an individual in a household.

- The parameters influencing energy demand such as the fuel consumption profile and the average energy use per unit area were derived from energy agency surveys (ARENE and CEREN). Finally, the vehicle fleets are also provided by regional surveys.

Emissions modeling of the Paris urban fabric was carried out using a supercomputer, allowing more than 40 million trips and their related emissions to be processed. The modeling platform generated the emissions of all the pollutants needed as inputs by CHIMERE: NO_x, NMVOCs, CO and particles with the speciation of the PM₁₀ and PM_{2.5} fractions. The model generates annual emissions as well as a diurnal time profile.

Results

The modeled population was compared to that of census data. The results from this comparison are detailed in [Elessa A. et al \(2018\)](#). Although the total number of individuals is constrained by the use of surveys, we can see that GAIA slightly overestimates the child population and underestimates the senior population. This bias may not have no strong impact on mobility, as these age groups do not predominantly participate in individual mobility, although the particularities of home-school trips often constrain the modal choice of adults.

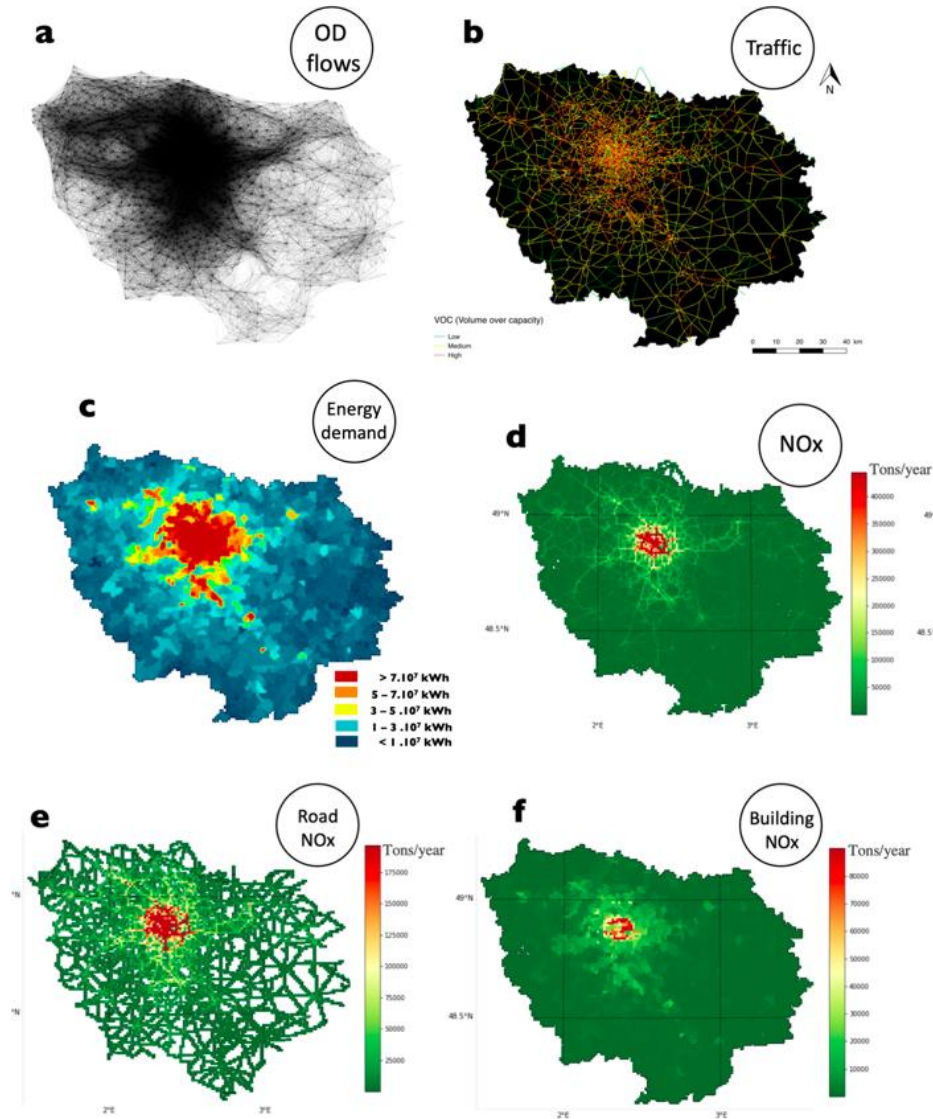


Figure 2: OLYMPUS outputs for Great Paris - (a) Origin-destination matrix (b) Daily road traffic (c) Building energy demand of Greater Paris, (d) Total NOx emissions (e) NOx road transport emissions (f) NOx emissions from the residential sector.

The validation of the transport-demand from MOIRAI was carried out by comparing the modeled mobility data with transport data from the Global Ile-de-France Transport Survey (EGT) provided by the Observatory of mobility in Ile-de-France (OMNIL). The average number of trips per individual modeled by OLYMPUS is 4.05, which represents a difference lower than 5% with the number estimated from the Global Transport Survey. The average trip length was also compared with that found in the EGT. With an average modeled trip length of 4.7 km, MOIRAI overestimates by approximately 7% the average distances actually traveled per trip, which is our largest gap with survey data. The difference in the total trip numbers between modeled data and observations is less than 1%. Finally, the modeled modal split differs only slightly from the one observed, as MOIRAI overestimates by only 2.4% the mobility by private car and the use of sustainable modes, at the expense of public transport use. Overall, we have considered these results satisfactorily represent the peculiarities of Ile-de-France mobility.

The simulated allocation of road transport was also evaluated. The paths from the origin-destination (OD) matrices were distributed on the main transport network using a “shortest path algorithm” that connects the OD pairs. The simulated data were then compared to the traffic data on the regional road

network, made available by the Institute of Urban Planning and Development (IAU). The comparison was made on the basis of the annual average daily traffic (TMJA), which represents the total annual traffic divided by 365 days. Our results show that OLYMPUS fairly well reproduces well the high densities of traffic in the ring road and in the portions of motorways connected with Paris. However, the model has difficulty to reproduce the high traffic densities on the main regional highways of the outer suburbs, and particularly in the west and southwest of the area. We assumed that the bias is due to the fact that OLYMPUS considers only the mobility of people living in the simulated territory, and misses trans-regional mobility. In addition, OLYMPUS does not consider the possibility for agents to reach for employment centers outside the region. Overall, we consider that the simplified modeling of the transport of goods can strongly contribute to an underestimation of the flows. These are points of improvement.

The energy demand of the territory was modeled using the unit energy consumption coefficients per m² of ARENE and CEREN. The final energy consumption of Île-de-France is 303 TWh in 2009 according to ARENE, the residential and tertiary sector representing more than 50% of these consumptions. The modeling of the regional energy demand (HESTIA) is quite satisfactory, as this component is very little informed by the surveys (type of heating system, practices...), and the difference observed with regional emissions is only + 9.6%.

Modeling emissions from road transport (linear structure) and from residential and tertiary heating practices (emissions per surface) was conducted by VULCAN at a temporal resolution of one hour. Surface emissions of PM_{2.5} from the residential and tertiary sector are also represented. The temporal resolution of these surface emissions is annual.

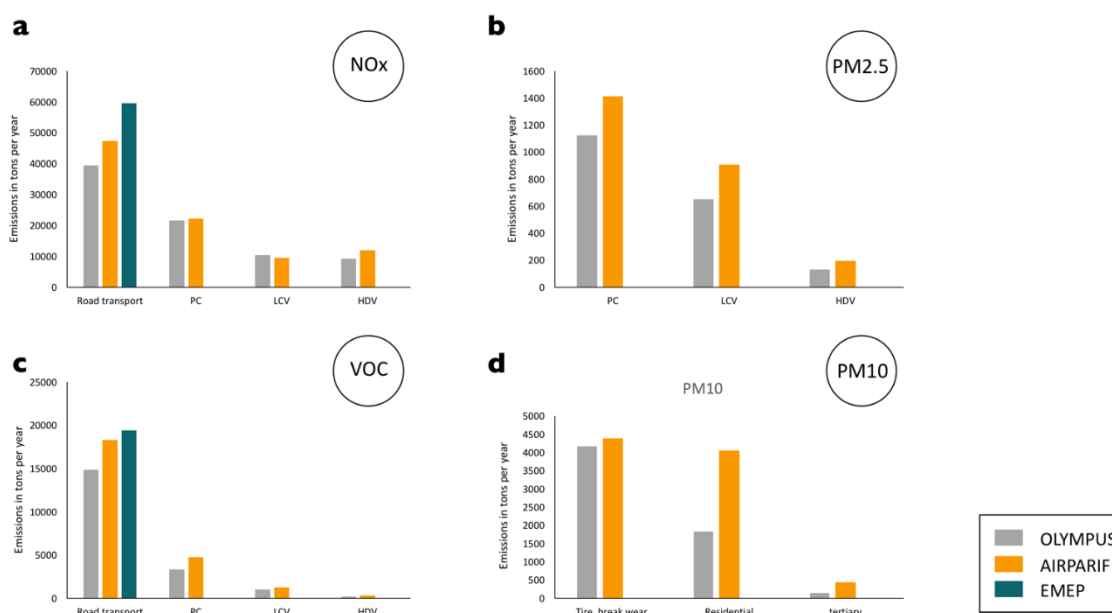


Figure 3: Comparison of OLYMPUS emissions with local and European emission inventories for a) NO_x, b) PM_{2.5} and c) VOC from total road traffic and/or specific subcategories such as private cars (PC), light commercial vehicles (LCV) and heavy-duty vehicles (HDV) – d) PM₁₀ emissions are shown for the resuspension source of traffic and for residential and tertiary heating activities.

Quantitative validation of emissions was performed by comparing the modeled emissions with the AIRPARIF and EMEP emission registries (see Figure 3). The emissions estimate produced by VULCAN is lower in the road transport sector, and higher in the residential and tertiary sectors. The differences observed with the AIRPARIF inventory for road traffic are explained by a wide variety of choices and modeling assumptions. In particular, since the modeling of the road network is simplified, the model does not include all the road traffic whose portions of trips to join the modeled transport network. Also, each inventory was developed from its own set of assumptions on the fleet composition or driving regimes. The fact that OLYMPUS underestimates emissions compared to AIRPARIF is also expected as OLYMPUS does not take into account individual interregional mobility. As for freight transport modeling, the representation of this activity remains based on simplistic assumptions, such as the application of percentages to total traffic by area or by type of road, that are specific to each inventory

process. In view of all this, the quantitative OLYMPUS-AIRPARIF comparison can be considered as quite satisfactory. To support this statement, we can rely on the study conducted in the framework of the project ANR TrafiPollu⁸ which compared the results of the COP-Cete-Heaven model with the AIRPARIF emission register and obtained differences between inventories very similar to those we obtain with OLYMPUS. Their analysis concludes that intrinsic assumptions about cold start modeling and fuel evaporation, but also variability in the composition of the vehicle fleet should induce a minimum of 20% differences on the totals and do not necessarily call into question coding or approach choices.

Lastly, the differences in the assessment of domestic and commercial heating emissions show that this activity remains an issue in the inventories. It is important to mention the fact that there is still a major lack of data on heating practices and household energy choices, so emission models must build-up on a set of assumptions to allocate emissions to households in the different urban districts. The same observation was made by the TrafiPollu when comparing this fraction of the emission inventory with AIRPARIF. However, it should be noted that the problem of wood heating is emerging and increasingly framed in France. Inventories should be able to rely on better forcing data in the near future.

Conclusions

At the end of our work of implementation and evaluation of the OLYMPUS tool on the Île-de-France region, we can conclude that our modeling approach is relevant for building road traffic emission inventories and carrying out analyzes of the impact of transport and energy policies, even if some points such as freight transport still need to be improved. In order to overcome the differences from reality and to work on the link between change of practices and evolution of emissions, it will be particularly relevant to implement OLYMPUS in several differentiated situations, representing different choices of urban mobility or public policies. for spatial planning. This will make it possible to quantify the sensitivity of the simulated emissions to the key variables of each module of the platform, and thus provide decision support on the levers of urban energy sobriety.

Acknowledgements

This work was performed using HPC resources from GENCI-CCRT (grant 2017-t2015017232). This work also received support from the French National Agency for Research (ANR-14-CE22-0013) and the Île-de-France region (DIM R2DS). We also acknowledge AIRPARIF and the LABEX Urban Futures.

References

Antoni, J., Tannier, C., Vuidel, G., and Hirtzel, J. : MobiSim: un modèle multi-agents et multi-scalaire pour simuler les mobilités urbaines, in *Modéliser la ville, Forme urbaine et politiques de transport*, edited by: Antoni, J.-P., Paris, France, 50–77, 2010.

Arthur Elessa Etuman and Isabelle Coll, OLYMPUS v1.0: Development of an integrated air pollutant and GHG urban emissions model - Methodology and calibration over Greater Paris, *Geoscientific Model Development*, 11, 5085–5111, <https://doi.org/10.5194/gmd-11-5085-2018>, 2018.

⁸ <https://sites.google.com/site/trafipollu/home>

GETTING IN TOUCH WITH THE EU

In person

All over the European Union there are hundreds of Europe Direct information centres. You can find the address of the centre nearest you at: https://europa.eu/european-union/contact_en

On the phone or by email

Europe Direct is a service that answers your questions about the European Union. You can contact this service:

- by freephone: 00 800 6 7 8 9 10 11 (certain operators may charge for these calls),
- at the following standard number: +32 22999696, or
- by electronic mail via: https://europa.eu/european-union/contact_en

FINDING INFORMATION ABOUT THE EU

Online

Information about the European Union in all the official languages of the EU is available on the Europa website at: https://europa.eu/european-union/index_en

EU publications

You can download or order free and priced EU publications from EU Bookshop at: <https://publications.europa.eu/en/publications>. Multiple copies of free publications may be obtained by contacting Europe Direct or your local information centre (see https://europa.eu/european-union/contact_en).

The European Commission's science and knowledge service

Joint Research Centre

JRC Mission

As the science and knowledge service of the European Commission, the Joint Research Centre's mission is to support EU policies with independent evidence throughout the whole policy cycle.



EU Science Hub

ec.europa.eu/jrc



@EU_ScienceHub



EU Science Hub - Joint Research Centre



Joint Research Centre



EU Science Hub



Publications Office
of the European Union

doi:10.2760/289885

ISBN 978-92-76-17328-1